

INVESTIGATIVE PHOTOCHEMISTRY: ELUCIDATING THE MECHANISM
OF THE PHOTO-FAVORSKII REARRANGEMENT

By

C2008

Kenneth F. Stensrud

Submitted to the Department of Chemistry and the Faculty of the
Graduate School of the University of Kansas in partial fulfillment of the
requirements for the degree of Doctor of Philosophy

Chairperson

Date Defended: _____

The dissertation committee for Kenneth F. Stensrud certifies
that this is the approved version of the following dissertation:

INVESTIGATIVE PHOTOCHEMISTRY: ELUCIDATING THE MECHANISM
OF THE PHOTO-FAVORSKII REARRANGEMENT

Dissertation Committee:

Chairperson

Date Approved: _____

Abstract

Kenneth F. Stensrud, Ph.D.
Department of Chemistry, April 2008
University of Kansas

The *p*-hydroxyphenacyl chromophore (pHP) is a versatile phototrigger for an assortment of biological nucleofuges, such as γ -aminobutyric acid (GABA). The photochemistry is trenchant; irradiation discharges the nucleofuge and induces rearrangement of pHP, analogous to the ground state Favorskii rearrangement.

Structure-reactivity relationships were explored with pHP GABA's. Electron donating groups lowered the release efficiency, Φ_{dis} , relative to the unsubstituted analog. Electron withdrawing carbonyl groups attenuated Φ_{dis} . Fluoro moieties modulated the pKa of pHP; protonated pHP manifested higher Φ_{dis} than their conjugate base counterparts. The reactive excited states were determined as triplets by Stern-Volmer quenching and laser flash photolysis studies. The triplet lifetimes were $\sim 10^{-9}$ s with release rate constants of 10^7 to 10^8 s⁻¹. Auxochrome substitutions lengthened the λ_{max} of pHP but lowered Φ_{dis} . Added perchlorate salts markedly improved Φ_{dis} for pHP GABA's, imputing intermediate ion-radical pairs.

Comprehensive photo-Favorskii mechanisms were posited for protonated and conjugate base forms of pHP GABA.

Acknowledgements

There have been frequent comments regarding my use of flowery, poetic words instead of those deemed appropriate for scientific writing. Though I have learned to distinguish one from the other while composing this dissertation, I find it truly risible that, at this time, words fail me when appositely expressing my gratitude to my advisor, Professor Richard Givens. Dr. Givens equanimity in dealing with my oft hair-brained ideas and digressions cannot be understated. My motivations to work long hours at solving our research problems originated from his encouragements and well considered proposals. Honestly, I shouldn't continue to indite a synopsis of his qualities, as they will present as mere platitudes. I can only state with certainty that Dr. Givens will always remain close to my heart for everything he has passed on to me both as a scientist and a man of utmost integrity.

My parents, Ken and Donna, have sacrificed more than I can fathom to ensure that their son, the opsimath, would succeed in his endeavors. I am grateful for your closeness and support. Mom and dad, my love for you will transcend this life. My brother Dan has always been there for me irrespective of the difficulty of the times. Dan, I look forward to growing old with you as both my brother and best friend.

My wife, Beth Stensrud, was the linchpin in my success as a graduate student. The single greatest event in my life was meeting you my first semester at KU. You were my foundation, my stimulus to endure time of tumult. I am dubious that I would

have persevered without you. Beth, from you I have recognized the existence of angels.

I owe a debt of gratitude to Dr. Todd Williams for his willingness to instruct me on the applications of the QQQ and furthermore permit me to utilize the instrument without restrictions over the past two years. I can honestly state that I would have completed a tenth of the amount of work if I did not have access to instrument and your exhortations. Todd, your succor will always be remembered and revered.

Professor Abraham Yousef was my antecedent in the laboratory. Your forbearance and willingness to instruct when I was maladroit will never be forgotten. Abraham, I owe much of my success in the laboratory to you, your mundane disposition was appreciated more than you can know. I hope we can stay in touch throughout the years.

To Dr. Elizabeth Cope, you were a friend and lab colleague. Beth, I will never forget the long hours and weekends we spent in the laboratory, imbued with successes, failures, and insightful talks. I appreciated this. It is eerie now when I come into lab on the weekends and I don't see you.

To Dr. Gerry Lushington, Professor Jakob Wirz, Dr. Dominik Heger and Professor Karl Kandler, thank you for your collaborative efforts. The information that you gleaned facilitated the solution of my research problems.

John Hershberger - we came in together and we will go out together. Through good and bad times, times of confusion and consumption, our experiences will never be forgotten.

Table of Contents

	page
Abstract	iii
Acknowledgements	iv
List of Figures	xi
List of Schemes	xvii
List of Tables	xxi
List of Equations	xxiv
Glossary of Chemical Compounds Studied	xxv
Introduction	1
I. Early Investigations of The Favorskii Rearrangement	1
II. Bordwell's Contributions	5
A. Rate, Isotope and Nucleofuge Studies	6
B. Substituent, LFER, Salt, Media Studies	11
C. Ramberg-Backland Analogy-Role of Orbital Overlap	17
D. Influence of α -Substituents	21
E. Evidence for a Dipolar Intermediate	29
F. Studies in Stereochemistry	32
III. Computational Investigations	37
IV. Variations to the Classical Favorskii Rearrangement	44

V. The Photochemical Version of the Favorskii Rearrangement	46
Statement of Problem	92
Results	94
I. Synthetic Methodologies	94
A. pHP GABA Series and 4-Fluorophenacyl GABA	94
B. pHP Glu Series	101
C. Other pHP Caged Amino Acids	102
D. pHP Deoxycholic Acid	104
E. pHP Diethyl Phosphonate	106
F. pHP F	106
G. 5-Acetylsalicylic Acid and Salicylamide GABA Series	107
H. 5-Acetylsalicylic Acid Alkanoyl Compounds	113
I. α -alkyl-pHP diastereomers	114
J. FITC-DOC	116
II. Exploratory Photochemistry	117
A. ^1H NMR Analysis, pHP GABA Series	119
B. ^1H NMR Analysis, α -Alkyl-pHP GABA Series	125
C. ^1H NMR Analysis, pHP Glu Series	128
D. ^1H NMR Analysis, Other pHP-Caged Amino Acids	130
E. ^1H NMR Analysis, pHP Deoxycholic Acid	131
F. ^1H NMR Analysis, pHP Diethyl Phosphonate	133
G. ^1H NMR Analysis, pHP F	133

H. ¹ H NMR Analysis, 5-Acetylsalicylic acid GABA Series	135
I. ¹ H NMR Analysis, 5-Acetylsalicylic Acid Alkanoyls	137
J. ¹ H NMR Analysis, α -Alkyl pHP Diastereomers	140
K. ¹⁹ F NMR Analysis, pHP and 5-Acetylsalicylic Acid GABA's	142
III. UV-Vis Spectroscopic Studies	145
A. pHP GABA Series and 4-Fluorophenacyl GABA	145
B. pHP Glu Series	153
C. Other pHP-Caged Amino Acids, DOC and Fluoride	154
D. 5-Acetylsalicylic Acid GABA Series and Alkanoyls	154
E. α -Alkyl-pHP Diastereomers	156
IV. Fluorescence Spectroscopic Studies	156
V. Time Correlated Single Photon Counting Studies	158
VI. Quantitative Photochemical Analysis	159
A. pHP GABA Series at 300 nm	160
B. pHP GABA Series at 350 nm	168
C. pHP Glu Series	169
D. Other pHP-Caged Amino Acids	170
E. pHP DOC and Fluoride	171
F. 5-Acetylsalicylic Acid GABA Series and Alkanoyls	171
G. α -Alkyl-pHP Diastereomers	173
VII. Stern-Volmer Quenching Studies	174
VIII. Computational Studies	176

A. ClogP Calculations	177
B. Energies and Geometries of Triplet Biradicals	179
C. Spin and Charge Density Calculations	181
IX. Laser Flash Photolysis Studies	183
Discussion	198
A. Synthetic Strategies	198
B. General Photochemistry	201
C. Preliminary Mechanistic Studies	203
D. Substituent Effects on the Photo-Favorskii Rearrangement	209
E. Miscellaneous Substituent Effects on pHP GABA Photochemistry	216
F. Substituent Effects on 5-acetylsalicylic acid GABA derivatives	221
G. Nucleofuge Effects on the Photo-Favorskii Rearrangement	221
H. Nucleofuge Effects - Linear Free Energy Relationships	223
I. Media Effects on the Photo-Favorskii Rearrangement	226
J. Salt and Ionic Strength Effects	231
K. Rationalized Mechanism of the Photo-Favorskii Rearrangement	240
L. Biological Studies	244
M. Future Studies	248
Conclusion	251
Experimental	255

List of Figures

- Figure 1.** Diphenylcyclohexanones examined in the Favorskii reaction. 6
- Figure 2.** A potential energy illustration of the semibenzilic rearrangement process, revealing relative energies (in kcal/mol) of stationary points on the reactive surface that were calculated at the HF/6-31G* level. 40
- Figure 3.** A potential energy surface diagram of the cyclopropanone rearrangement mechanism, revealing relative energies (in kcal/mol) of stationary points on the reactive surface that were calculated at the HF/6-31G* level. 43
- Figure 4.** Left: Time dependent decay profile of pHP diethyl phosphate (³**114**) band ~1600 cm⁻¹ with ns ³TR. Right: Time dependent decay profile of ³**114** band ~1600 cm⁻¹ with ns ³TR. 70
- Figure 5.** Time dependent decay profile of ³**110** at ~1600 cm⁻¹ in ns-³TR spectra. Circles indicate degassed, triangles open air, and squares oxygen. 72
- Figure 6.** Left: 1) Bottom - psTR³ spectrum of **115** in water.
2) Top - psTR³ spectrum of **115** in water.
Right: 1) Bottom - psTR³ spectrum of **115** in buffer, pH = 9.00.
2) Top - psTR³ spectrum of **115** in buffer, pH = 9.00. 75
- Figure 7.** DFT determined, optimized geometry and bond distances (Å) of ³**115** in water. 77
- Figure 8.** Stern Volmer analysis of ³**114** lifetimes as a function of water concentration, in percentage. 81
- Figure 9.** Phillips' proposed structure of unknown, **M**, as a solvation/contact ion pair complex. 84
- Figure 10.** Step-scan FTIR of **121** in CD₃CN (2% D₂O) at 50 ns (red) and 1 μs (blue) delay. 89
- Figure 11.** Plot of k_{obs} of ³**114** vs. mole fraction of deuterium in degassed, 10% aq. CH₃CN at 25°C. 90

Figure 12. Novel pHP GABA esters.	94
Figure 13. α -methyl and ethyl-pHP GABA enantiomers, (R,S)-140 and (R,S)-141 respectively.	99
Figure 14. pHP Glu derivatives, 143-145 .	101
Figure 15. Other pHP caged amino acids, 146-149 .	103
Figure 16. 5-acetylsalicylic acid and salicylate GABA derivatives, 153, 154, 157-165 .	108
Figure 17. 5-acetylsalicylate GABA compounds where the standard Pd/C protocol for debenzylation wasn't effective.	112
Figure 18. Two 5-acetylsalicylic acid alkanoyl derivatives (155 and 156).	113
Figure 19. ^1H NMR spectrum of <i>m</i> -OCF ₃ -pHP GABA (131) in D ₂ O.	120
Figure 20. ^1H NMR spectrum after 2 h photolysis of (131) in D ₂ O.	121
Figure 21. Spiking experiment with <i>p</i> -hydroxy- <i>m</i> -trifluoromethoxybenzyl alcohol (131 ₂).	122
Figure 22. Pre-photolysis ^1H NMR spectrum of <i>m</i> -OCH ₃ -pHP GABA, (134), in D ₂ O.	123
Figure 23. ^1H NMR spectrum of the photolysis mixture of 134 at 300 nm in D ₂ O.	125
Figure 24. ^1H NMR spectrum of α -methyl-pHP GABA enantiomers (R,S)-140 in D ₂ O prior to irradiation.	126
Figure 25. ^1H NMR spectrum of the product mixture after 1 h irradiation of (R,S)-140 at 300 nm, in D ₂ O.	127
Figure 26. ^1H NMR spectrum of photolysis mixture with added 2-(4-hydroxyphenyl)propanoic acid.	128
Figure 27. Pre photolysis ^1H NMR spectrum of <i>m</i> -CF ₃ -pHP Glu (145) in 1:1 D ₂ O: CD ₃ OD.	129

Figure 28.	¹ H NMR analysis of products from photolysis of <i>m</i> -CF ₃ -pHP Glu (145) at 300 nm in 1:1 CD ₃ OD:D ₂ O.	130
Figure 29.	¹ H NMR spectrum of 150 in 1:9 D ₂ O:CD ₃ OD prior to photolysis.	131
Figure 30.	¹ H NMR spectrum of the product mixture after irradiation of 150 for 4 h at 300 nm in 1:9 D ₂ O:CD ₃ OD.	132
Figure 31.	¹ H NMR analysis of 152 in 1:3 D ₂ O:CD ₃ OD prior to irradiation.	133
Figure 32.	¹ H NMR assessment of the product mixture after 1 h photolysis of 152 at 300 nm in 1:3 D ₂ O:CD ₃ OD.	134
Figure 33.	¹ H NMR spectrum of 153 in D ₂ O prior to photolysis.	135
Figure 34.	¹ H NMR analysis of the product mixture from 1 h photolysis of 153 at 300 nm in D ₂ O.	136
Figure 35.	¹ H NMR analysis of 156 in d ⁶ -DMSO prior to irradiation.	138
Figure 36.	¹ H NMR spectrum of the product mixture after irradiation of 156 in 1:9 D ₂ O:CD ₃ OD.	139
Figure 37.	¹ H NMR spectrum of a mixture of 166 and 167 in 1:1 D ₂ O:CD ₃ OD.	140
Figure 38.	¹ H NMR spectrum of the product mixture from irradiation of 166 and 167 at 300 nm in 1:1 CD ₃ OD:D ₂ O.	142
Figure 39.	¹⁹ F NMR spectrum of 129 in D ₂ O prior to photolysis.	143
Figure 40.	¹⁹ F NMR spectrum of the product mixture from photolysis of 129 at 300 nm in D ₂ O.	144
Figure 41.	Comparison of UV-Vis spectra of 123 in water (red) and pH = 8.2 buffer (pink).	148
Figure 42.	UV-Vis spectroscopic analysis of 1 mM solution of 123 in unbuffered aqueous solution.	149
Figure 43.	UV-Vis spectroscopic analysis of 5 mM 123 in 0.01 M HEPES, 0.1 M LiClO ₄ , pH = 8.2.	150

Figure 44. UV-Vis probe of the photolysis of 129 , predominantly the conjugate base in water, monitored at 3 minute intervals.	152
Figure 45. Fluorescence spectrum of 130 in 0.01 M HEPES, 0.1 M LiClO ₄ pH = 8.2, $\lambda_{\text{ex}} = 325$ nm.	157
Figure 46. TCSPC decay profile for <i>m</i> -CF ₃ -pHP GABA (130) in 0.1 M LiOH.	159
Figure 47. Stern-Volmer relationship from the photolysis of 124 in water with potassium sorbate as the quencher, Q.	175
Figure 48. Out of plane orientation of the carbonyl constituent of tetraF 117 relative to the aryl plane.	181
Figure 49. Predicted radical positions for the tetraF 117 , from MP2 calculations at the B3LYP level using the 6-31G* basis set.	183
Figure 50. Three dimensional, time resolved <i>absorption</i> contour of 122 in aqueous CH ₃ CN.	185
Figure 51. Three dimensional <i>triplet decay</i> contour of 122 in aq. CH ₃ CN.	186
Figure 52. Cross section of the three dimensional, time resolved absorption contour of 122 in aqueous CH ₃ CN.	187
Figure 53. Three dimensional, time resolved triplet decay contour of 101 in aqueous CH ₃ CN.	188
Figure 54. Triplet decay profile of 101 at 400 nm in aqueous CH ₃ CN.	189
Figure 55. Triplet decay profile of 101 at 500 nm in aqueous CH ₃ CN.	189
Figure 56. Three dimensional, time resolved triplet decay contour of 128 in aqueous CH ₃ CN.	190
Figure 57. A cross section of the three dimensional absorption contour of 128 in aqueous CH ₃ CN.	191
Figure 58. Triplet decay plot for 128 in aqueous CH ₃ CN.	192
Figure 59. Cross section of the three dimensional absorption profile of 153 in water.	193
Figure 60. Triplet decay profile for 153 in water.	194

Figure 61. Cross section of the three dimensional absorption contour of 154 in aqueous CH ₃ CN.	195
Figure 62. Cross section of the three dimensional absorption profile of 154 in aqueous CH ₃ CN.	196
Figure 63. Triplet decay profile of 154 at 416 nm in aqueous CH ₃ CN.	197
Figure 64. Photoproducts of 134 a) <i>m,m'</i> -diOCH ₃ - 115 , b) <i>m,m'</i> -diOCH ₃ - α -OH- 115 and 133 c) <i>m</i> -OCH ₃ - 115 , d) <i>m</i> -OCH ₃ - α -OH- 115 .	207
Figure 65. Plot of pK _a of fluoro pHP GABA's vs. Φ_{dis} in water (blue diamonds) and buffer pH 7.3 (pink squares).	211
Figure 66. A. Plot of rate constants for release, k_r , of pHP GABA's vs. pK _a 's in water. B. Plot of rate constants for release, k_r , of pHP GABA's vs. pK _a 's in pH 7.3 buffer.	213
Figure 67. Proposed H-bonding between the <i>o</i> -OH and ketone carbonyl of 135 .	217
Figure 68. H-bonding between meta and para-OH moieties of 136 .	218
Figure 69. Lowest energy conformations of decaged 139 and 115 by low level MM2 calculations.	219
Figure 70. A plot of rates of disappearance, (Φ_{dis}/τ) vs. the pK _a of pHP esters, establishing a Brønsted linear free energy relationship.	226
Figure 71. Titration curves obtained from ¹ H NMR analysis depicting the dependence of quantum yields for acetate appearance, Φ_{app} (Φ_p in plot) on pH for photolysis of pHP acetate 114 in 1:1 CH ₃ CN (circles).	228
Figure 72. Observed enhancements of k_{obsd} of trifluoroacetylation of 172 (R = CH ₃) as a function of [LiClO ₄].	234
Figure 73. Plot of Φ_{dis} vs. [LiClO ₄] for pHP GABA (101).	235
Figure 74. Plot of Φ_{dis} vs. [LiClO ₄] for <i>o</i> -F-pHP GABA (123).	236
Figure 75. Plot of Φ_{dis} vs. [LiClO ₄] for 2,5-diF-pHP GABA (125).	237

Figure 76. Plot of Φ_{dis} vs. $[\text{Mg}(\text{ClO}_4)_2]$ for 2,3-diF-pHP GABA (124).	238
Figure 77. Proposed coordination between Mg^{2+} and 2,3-diF-pHP GABA (124).	239
Figure 78. Amplified current as a function of photoreleased GABA from <i>m</i> -OCF ₃ -pHP GABA (131).	244
Figure 79. Population data of peak currents normalized to the maximum peak response and fitted to Hill's equation to derive EC ₅₀ values for 130 , 131 , and 134 .	245
Figure 80. Membrane currents elicited from photolysis of 131 are completely obstructed by Garbazine, indicating origin activation as the GABA _A receptor.	246
Figure 81. Reverse potential deduced from the photolysis of 131 .	246
Figure 82. Probing the effect of 131 on the holding currents or membrane input resistance.	247

List of Schemes

Scheme 1. Richard's asserted mechanism of the Favorskii rearrangement.	3
Scheme 2. McPhee's mechanism of the Favorskii reaction.	3
Scheme 3. Loftfield's mechanism of the Favorskii rearrangement.	4
Scheme 4. Dewar's proposed mechanism of the Favorskii reaction.	5
Scheme 5. The reaction of 2-bromo-4,4'-diphenylcyclohexanone (25) with CH_3O^- to corresponding intermediates.	7
Scheme 6. Disparate reaction pathways for α -chlorobenzyl methyl ketone derivatives in $\text{CH}_3\text{O}^-/\text{CH}_3\text{OH}$.	12
Scheme 7. A depiction of the Ramberg-Backland reaction.	17
Scheme 8. Delocalized (sp^2) vs. localized (sp^3) electron models.	18
Scheme 9. Anchimeric π assistance in establishing a cyclopropanone intermediate.	19
Scheme 10. Rates of bromide release from anionic α -bromo substrates.	20
Scheme 11. Reactions of α -chloro analogs in $\text{CH}_3\text{O}^-/\text{CH}_3\text{OH}$.	21
Scheme 12. Discrete mechanistic pathways for α -chlorobenzylpropiophenone (51) to the rearranged ester (44) and α -methoxyketone (45).	24
Scheme 13. Reaction courses of isomers 53 and 43 to rearranged 44 and α -methoxy ketone (45).	26
Scheme 14. Reactions of alkyl substituted α -chloro ketones with CH_3O^- .	27
Scheme 15. Product distributions from the reaction of α -chloro ketones with low concentrations of CH_3O^- .	29
Scheme 16. Proposed mechanism for the reaction of α -chloroketone, (56) with low $[\text{CH}_3\text{O}^-]$ to form the methyl ester (59).	30

Scheme 17. Suggested dipolar (oxyallyl) mechanism to indanone (61).	31
Scheme 18. Stork-Borowitz proposal for stereochemical inversion of precursors to Favorskii products.	32
Scheme 19. Reactions of α -bromo ketones (63) and cis/trans diastereomers (66) with CH_3O^- in CH_3OH .	33
Scheme 20. Bordwell's suggested reaction pathways of 63 to diastereomers (64 and 65) in CH_3O^- , directed by the oxyallyl intermediate (69).	35
Scheme 21. The proposed semibenzilic mechanism of conversion of α -chlorocyclobutanone to cyclopropane carboxylic acid through calculated stationary points.	38
Scheme 22. The Favorskii rearrangement mechanism of α -chlorocyclobutanone to cyclopropane carboxylic acid through calculated stationary points.	41
Scheme 23. Proposed mechanism of the homo-Favorskii reaction.	45
Scheme 24. Posited mechanism to account for the formation of chlorobenzene from α -chloroacetophenone derivatives.	49
Scheme 25. Posited mechanism of benzoic acid release from the <i>p</i> -methoxyacetophenone chromophore.	51
Scheme 26. Product compositions from photolysis of corresponding α -chloroketones.	53
Scheme 27. Results from photolysis of pHP ATP and pHP diethyl phosphate in aqueous media.	57
Scheme 28. Proposed mechanism for phosphate release from the pHP chromophore.	58
Scheme 29. Radical pair mechanism for the formation of dibenzyl (107) from phenacyl caged phenylacetic acid.	61
Scheme 30. Hydrogen atom transfer mechanism for substrate release.	62
Scheme 31. Singlet excited state proton transfer mechanism for acetate release.	64

Scheme 32. Concerted mechanism for acetate release from pHP.	66
Scheme 33. Proposed thermodynamic cycle of <i>p</i> -hydroxyacetophenone (115).	68
Scheme 34. Phillips proposed mechanism for excited state processes of <i>p</i> -hydroxyacetophenone (115).	78
Scheme 35. Proposed intermediate precursor to rearranged product.	83
Scheme 36. Posited mechanism for phosphate release from the pHP chromophore.	86
Scheme 37. Proposed mechanism for diethyl phosphate release from pHP.	87
Scheme 38. The synthesis of <i>m</i> -F-pHP GABA (122).	96
Scheme 39. Synthesis of the <i>o</i> -OH derivative of pHP GABA (135).	98
Scheme 40. Synthesis of α -methyl-pHP-GABA enantiomers ((R,S)- 140).	100
Scheme 41. Synthesis of 4-fluorophenacyl GABA (142).	101
Scheme 42. Synthesis of <i>m</i> -F-pHP Glu (144).	102
Scheme 43. Synthesis of pHP Gly (146).	104
Scheme 44. Synthesis of pHP DOC (150).	105
Scheme 45. Synthesis of pHP diethyl phosphonate (151).	106
Scheme 46. Synthesis of pHP F (152).	107
Scheme 47. Synthesis of 5-acetylsalicylic acid GABA (153).	109
Scheme 48. 5-acetyl salicylamide benzophenone GABA (157).	110
Scheme 49. Synthesis of 5-acetylsalicylic acid dodecanoate (155).	114
Scheme 50. Synthesis of α -methyl-pHP diastereomers (166 and 167).	115
Scheme 51. Synthesis of FITC-DOC (168).	117
Scheme 52. Preliminary mechanism of the photo-Favorskii rearrangement, with 153	205

Scheme 53. Modified version of Yousef's discrete mechanistic pathways to <i>m,m'</i> -diOCH ₃ - 115 and <i>m,m'</i> -diOCH ₃ - α -OH- 115 .	208
Scheme 54. Proposed mechanism of GABA photorelease from the conjugate base of 101 .	215
Scheme 55. Winstein's ion-pair, solvolysis mechanism with added LiClO ₄ .	232
Scheme 56. Proposed photo-Favorskii mechanism for protonated pHP GABA esters	242
Scheme 57. Proposed photo-Favorskii mechanism for the conjugate base of pHP GABA esters.	243

List of Tables

Table 1. Summary of rates of halide release, k ; isotope exchange ratios, k_H/k_D , and rate comparisons, k_{Br}/k_{Cl} for reactions of 23-26 under Favorskii conditions.	7
Table 2. Summary of hydrogen-deuterium exchange with 24, 26 , and the rearranged Favorskii esters over one half life (~ 3 h) at 0°C with $0.05\text{ M CH}_3\text{O}^-$.	9
Table 3. Results of the reactions of 28 at various $[\text{CH}_3\text{O}^-]$ and $[\text{LiClO}_4]$ in CH_3OH at various temperatures.	12
Table 4. Effect of water composition on the reaction rate, k_2 , of $\text{PhCH}_2\text{COCH}_2\text{Cl}$ (40) in $0.05\text{ M CH}_3\text{O}^-/\text{CH}_3\text{OH}$ at 0°C .	14
Table 5. Summary of observed and Favorskii rate constants and product yields in $\text{CH}_3\text{O}^-/\text{CH}_3\text{OH}$ at 0° for substituted 28 as a function of substituent.	15
Table 6. Results from the reaction of 40, 43, and 46 in varying $[\text{CH}_3\text{O}^-]$ in CH_3OH at 0°C .	22
Table 7. Summary of product yields and rates of reaction for 46, 49 and 53 as a function of CH_3O^- in CH_3OH .	28
Table 8. Results of reactions of 63 and 66 with various $[\text{CH}_3\text{O}^-]$ in CH_3OH at 0°C .	33
Table 9. Relative energies (kcal/mol) of stationary points associated with the semibenzilic rearrangement mechanism, in the gas and aqueous phases, as determined by various computational methods.	39
Table 10. Relative energies (kcal/mol) of stationary points associated with the cyclopropanone rearrangement mechanism, in the gas and aqueous phases, as determined by the connoted computational methods.	42
Table 11. Substituent effects on the photoproduct distributions from photolysis of substituted α -chloroacetophenones in ethanol, irradiated at 300 nm for 1-2 h.	50

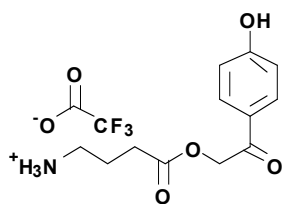
Table 12. Photoproduct % compositions from photolysis of 3% solutions of 82 a-d in degassed CH ₃ OH.	52
Table 13. Time constants for triplet decays of 116 , 114 , and 110 in mixed CH ₃ CN/H ₂ O solvents and corresponding pK _a 's of the nucleofuge.	80
Table 14. Rate constants, <i>k</i> _{obs} , for decay of triplet pHP acetate (³ 114) as a function of the D/H mole fraction, <i>n</i> , using ns-LFP in 10% aq. CH ₃ CN at 25°C.	89
Table 15. UV-Vis properties of 122-142 with corresponding pK _a values.	146
Table 16. Times for 100% conversion to photoproducts of 1 mM concentrations of 122-141 in water.	151
Table 17. UV-Vis parameters and estimated times for 100% conversion to photoproducts from irradiation at 300 nm and associated pK _a 's for 143-145 .	153
Table 18. UV-Vis parameters and 100% conversion times for 146-152 , from irradiation at 300 nm.	154
Table 19. UV-Vis parameters, 100% conversion times from irradiation at 300 nm, and % conversion after 24 h from irradiation at 350 nm for 153-165 .	155
Table 20. Fluorescence of 122-131 in 0.01 M HEPES, 0.1 M LiClO ₄ at pH 8.2.	157
Table 21. TCSPC derived fluorescence decay profiles of 101 , 122-131 in aq. 0.1 M LiOH.	158
Table 22. Quantum yields for 122-141 and the unsubstituted parent (101) in water and 0.01 M ammonium acetate buffer, pH 5.0 to 9.0	161
Table 23. Quantum yields for 122-141 and the unsubstituted parent (101) from photolysis in buffers pH 7.0 to 9.0, with and without adjusted ionic strengths	163
Table 24. Quantum yields for 122-131 , 133-134 and the unsubstituted parent (101) from photolysis in organic media and degassed aq. solution adjusted ionic strengths.	165

Table 25. Quantum yields for 122-141 and the unsubstituted parent (101) from photolysis in water with adjusted ionic strengths from 0.008 to 1.0 M LiClO ₄ .	167
Table 26. Quantum yields for 122-124 and the unsubstituted parent (101) from photolysis in water with adjusted ionic strengths and added GABA at 300 nm.	168
Table 27. Quantum yields for 122-131 in 0.01 M TRIS, 0.1 M LiClO ₄ at pH 9.0 at 350 nm.	169
Table 28. Quantum yields of 143-145 and unsubstituted parent (102) from photolysis in water, pH 7.0, pH 7.3 and pH 8.2 buffers at 300 nm.	170
Table 29. Quantum yields of 146-149 in water, pH 7.3 buffer, and water with adjusted ionic strengths.	171
Table 30. Φ_{dis} of 153 in various media from photolysis at 300 nm.	172
Table 31. The values for Φ_{dis} and Φ_{app} of 154 from photolyses at 300 nm in a variety of media.	172
Table 32. Φ_{dis} and Φ_{app} for 157-165 in 3:1 H ₂ O:CH ₃ OH at 300 nm.	173
Table 33. Parameters derived from Stern-Volmer quenching analysis for 122-131 , 137-139 , and 153 in water and 0.01 M HEPES, 0.1 M LiClO ₄ at pH = 7.3.	176
Table 34. ClogP values for GABA derivatives (unsubstituted parent (101), 122-131 , 133-134), Glu derivatives (unsubstituted parent (102) and 143-145) and the conjugate bases of 122-131 .	178
Table 35. The out of plane (OOP) contortion angles and relative energies of the oxyallyl-phenoxy triplet biradicals (117) of 122-131 .	180
Table 36. Calculated spin and charge densities for tetraF 117 .	182
Table 37. Pump probe spectroscopy results from 101 , 122 , 125 , 128-131 , and 153 in water and mixed media.	184
Table 38. Parameters of 168-171 and other pHP derivatives.	225

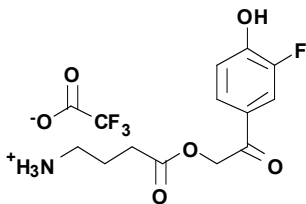
List of Equations

Equation 1	1
Equation 2	2
Equation 3	36
Equation 4	45
Equation 5	47
Equation 6	47
Equation 7	48
Equation 8	50
Equation 9	52
Equation 10	56
Equation 11	59
Equation 12	60
Equation 13	83
Equation 14	84
Equation 15	90
Equation 16	219
Equation 17	224
Equation 18	233

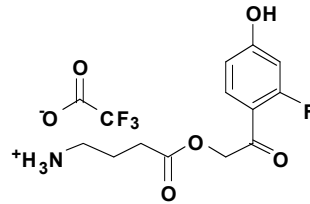
Glossary of Chemical Compounds Studied



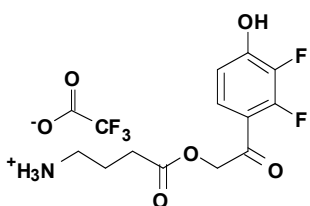
pHP GABA (101)



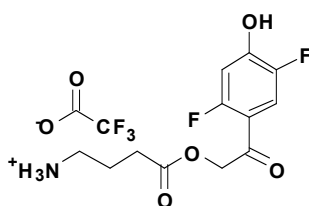
m-F-pHP GABA (122)



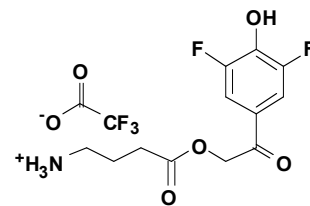
o-F-pHP GABA (123)



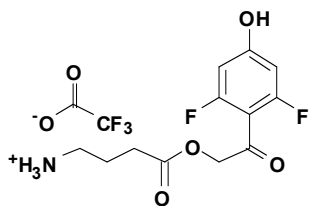
2,3-diF-pHP GABA (124)



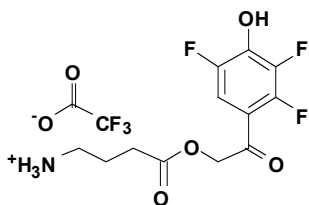
2,5-diF-pHP GABA (125)



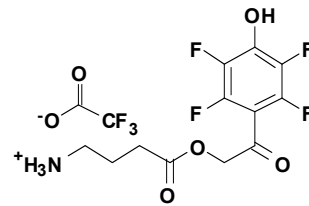
3,5-diF-pHP GABA (126)



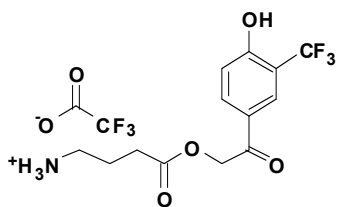
2,6-diF-pHP GABA (127)



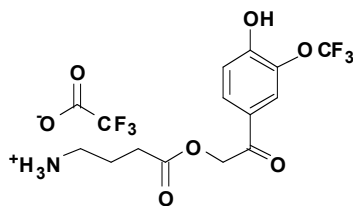
2,3,6-triF-pHP GABA (128)



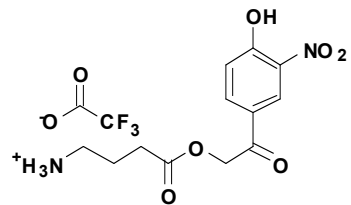
2,3,5,6-tetraF-pHP GABA (129)



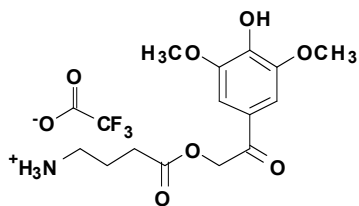
m-CF₃-pHP GABA (130)



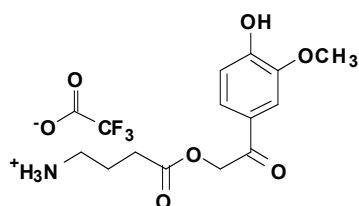
m-OCF₃-pHP GABA (131)



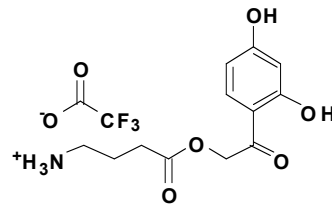
m-NO₂-pHP GABA (132)



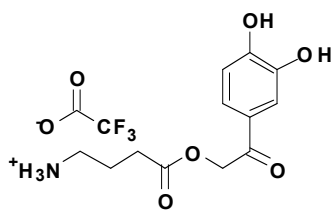
m,m'-diOCH₃-pHP GABA (133)



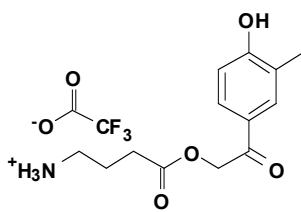
m-OCH₃-pHP GABA (134)



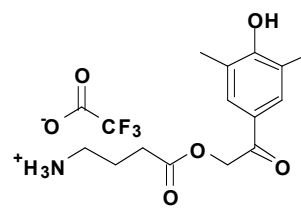
o-OH-pHP GABA (135)



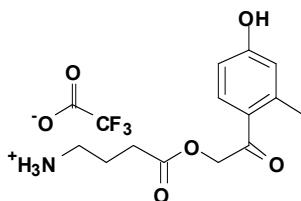
m-OH-pHP GABA (136)



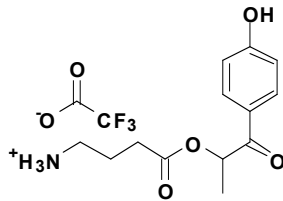
m-CH₃-pHP GABA (137)



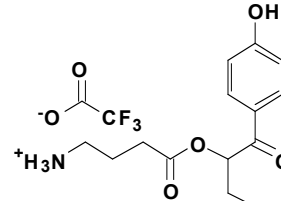
m,m'-diCH₃-pHP GABA (138)



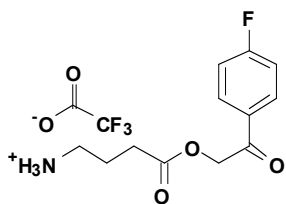
o-CH₃-pHP GABA (139)



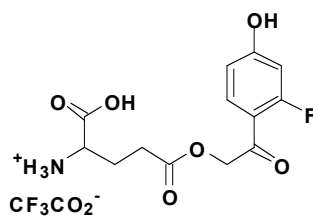
(*R,S*)- α -methyl-pHP GABA (140)



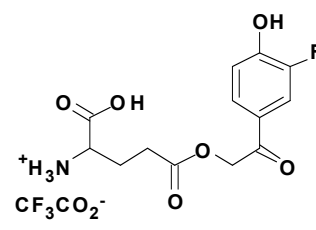
(*R,S*)- α -ethyl-pHP GABA (141)



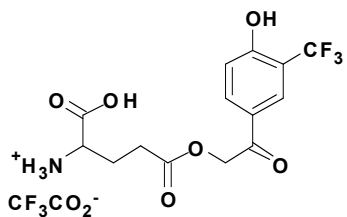
4-fluorophenacyl GABA (142)



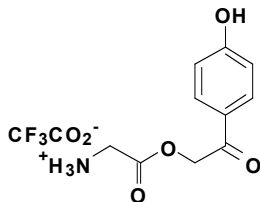
o-F-pHP Glu (143)



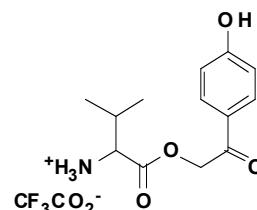
m-F-pHP Glu (144)



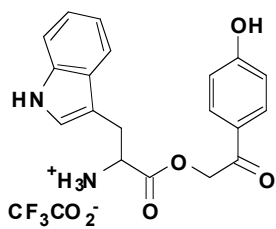
m-CF₃-pHP Glu (145)



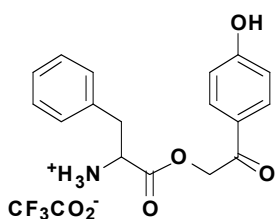
pHP Gly (146)



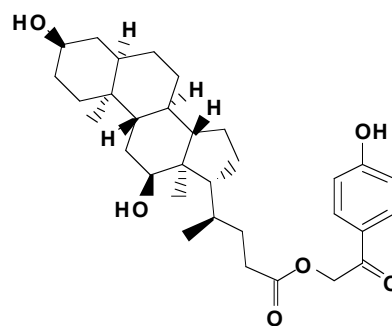
pHP Val (147)



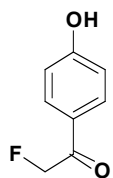
pHP Trp (148)



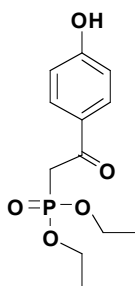
pHP Phe (149)



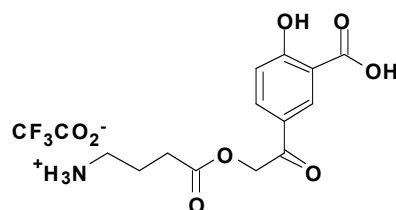
pHP DOC (150)



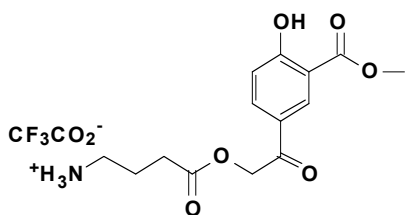
pHP F (151)



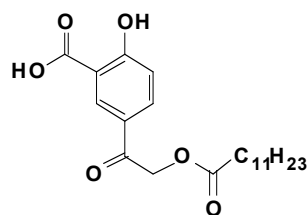
pHP diethyl phosphonate (152)



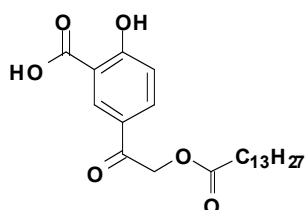
5-acetylsalicylic acid GABA (153)



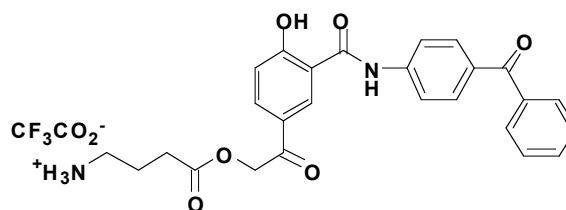
methyl-5-acetylsalicylic acid GABA (154)



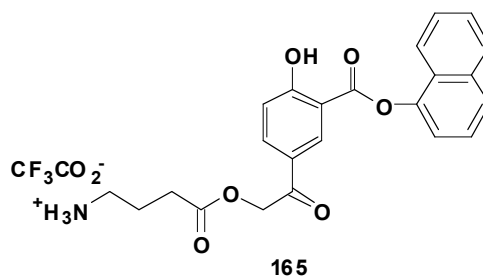
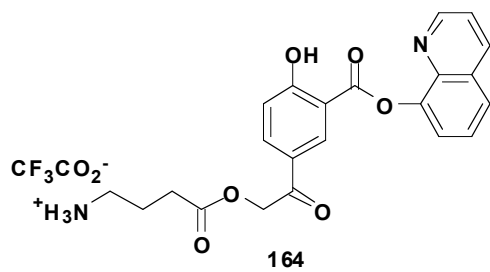
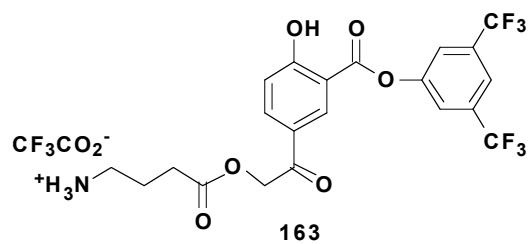
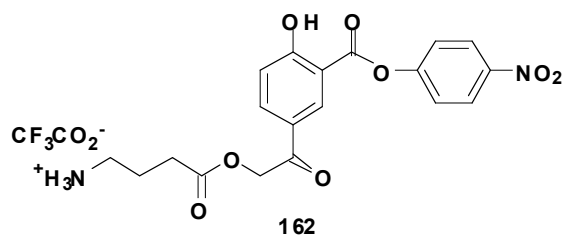
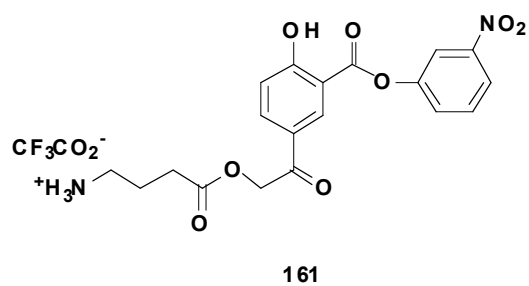
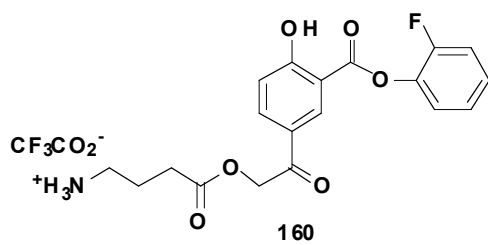
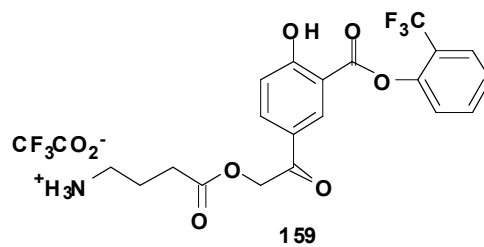
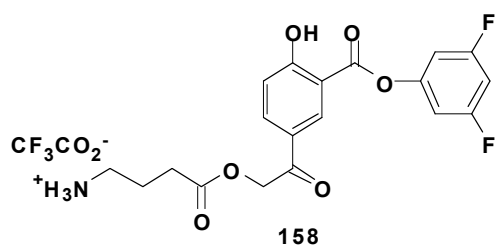
5-acetylsalicylic acid do decanoate (155)

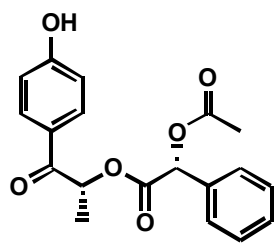


5-acetylsalicylic acid tetradecanoate (156)

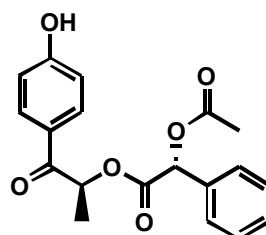


157

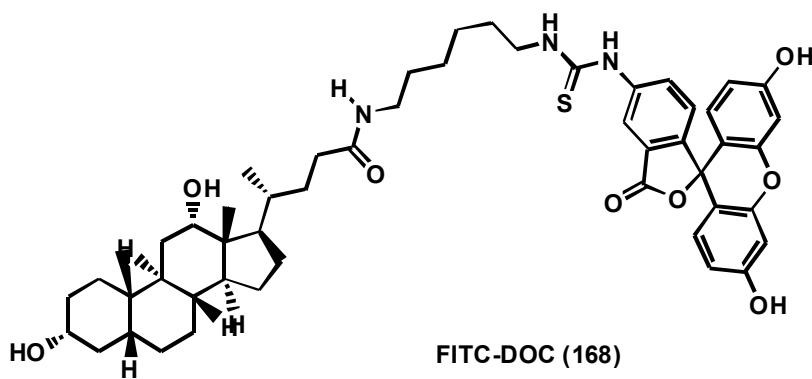




(R,R)-166



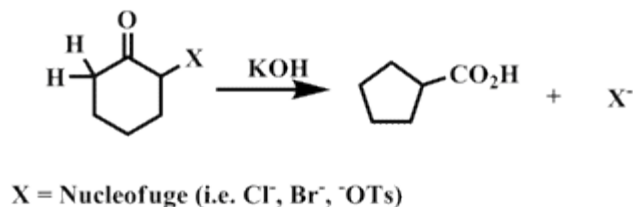
(R,S)-167



FITC-DOC (168)

Introduction

The Favorskii¹ reaction or rearrangement, though discovered over a century ago, continues to be widely exploited by synthetic chemists in the manipulation and assembly of organic molecules, such as Tricycloclavulone² and Kelsoene.³ This assertion is buttressed by the manifestation of 832 references in a SciFinder Scholar[®] search.⁴ The “classical” Favorskii rearrangement involves base-mediated rearrangement of ketones bearing α -substituents with favorable nucleofuge attributes, to produce carboxylic acids, esters, or amides (Equation 1, with KOH as the base). In equation 1, the rearrangement leads to a ring contraction and conversion of the ketone to a carboxylic acid. Further designations can be made depending on whether α -hydrogens exist to the carbonyl moiety (these will be elaborated later).

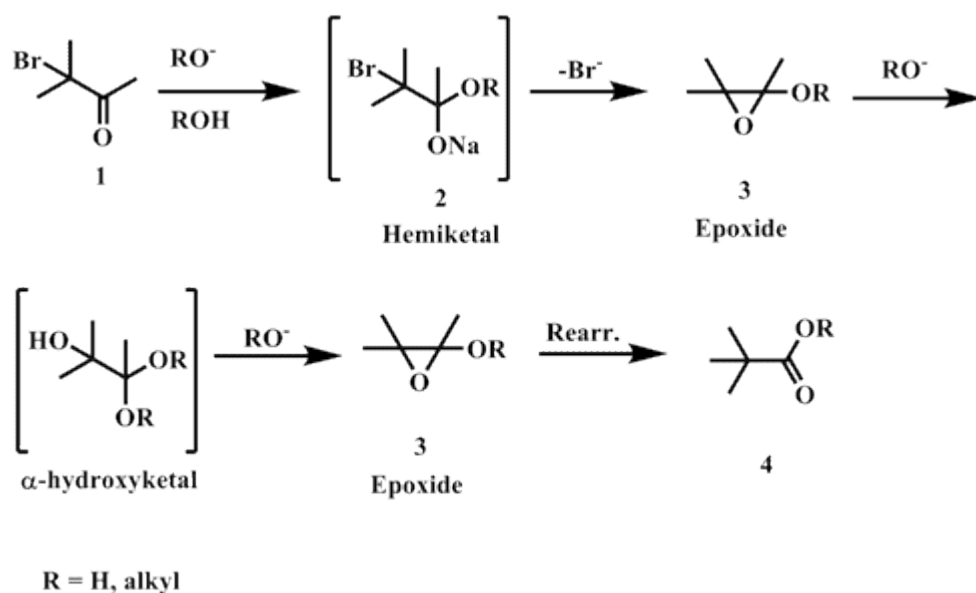


Eq. 1

I. Early investigations into the mechanism of Favorskii rearrangement.

Efforts to generate a “working” mechanism to explain classical Favorskii rearrangement have been pervasive⁵ and continuous,⁶ and have centered on four discrete pathways:⁷ a) Aston’s proposition⁸ (Equation 2) related a nucleophilic

approach by alkoxide (RO^-) to the carbonyl moiety (**2**), followed by nucleofuge (bromide) disjunction to generate an epoxyether (**3**). Rearrangement through methyl migration proceeded to the Favorskii product (**4**). An independent study by Stevens and coworkers,⁹ however, using a related set of reaction conditions, failed to find the anticipated ester products.

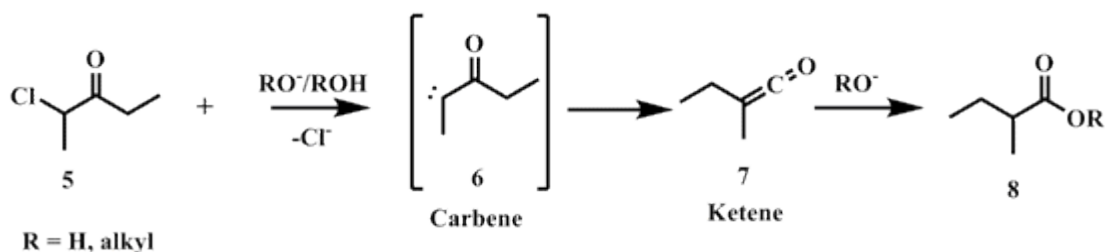


Eq. 2

From this and accompanying studies,¹⁰ the transposition of epoxyether intermediates to acids/esters (Aston's postulate) has been judged as unsuitable for Favorskii-type rearrangements. b) A second hypothesis¹¹ (Scheme 1) accentuated the formation of a ketene (**7**), initiated by base induced α -proton abstraction, then abrupt halide departure to form carbene (**6**), with a supervening "Wolff" rearrangement to

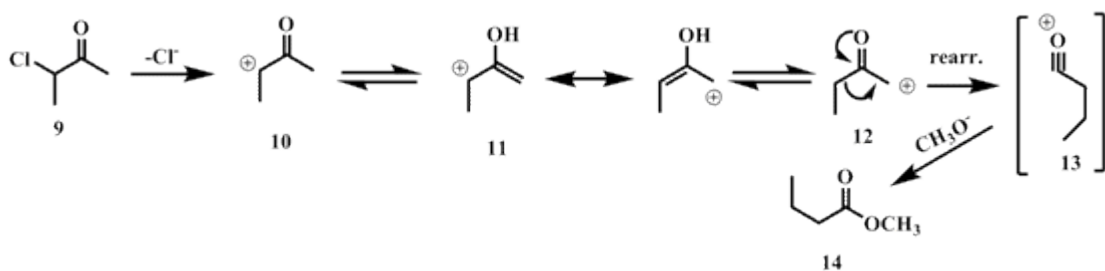
the ketene. Once formed, the ketene was promptly attacked by the nucleophilic alkoxide to produce the Favorskii ester (**8**). Several related studies evinced the direct formation

Scheme 1. Richard's asserted mechanism of the Favorskii rearrangement.



of trialkyl acids and esters from ketones,⁷ which would directly oppose a ketene precursor. c) A third proposal suggested an initial unimolecular disjunction of the

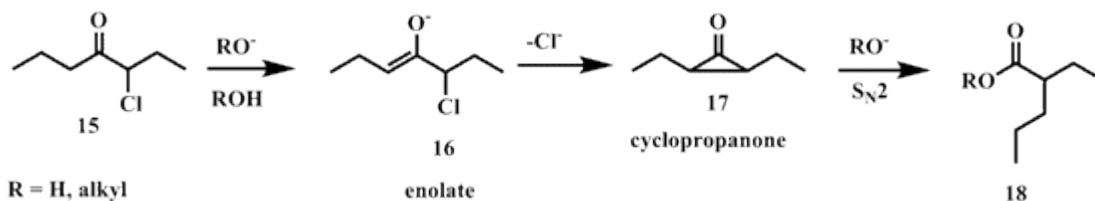
Scheme 2. McPhee's mechanism of the Favorskii reaction.



nucleofuge to afford an α -ketocarbenium ion (**10**), followed by tautomerizations **11** and **12**, acylium formation from alkyl migration (**13**) and then rearrangement to the acid/ester¹² (**14**) (Scheme 2). In this mechanism, there appeared to be a marginal role

for the base, which, in subsequent studies, was shown to be indispensable for the generation of Favorskii products. d) The most widely accepted mechanism was first proposed by Lofffield¹³ and advanced by several researchers.^{14,15,16,17} The reaction sequence has been suggested as stepwise,^{13,18,14} involving base induced deprotonation^{19,14} at the α position to the carbonyl to form an enolate (**16**) followed by intramolecular displacement and cyclization via halide disjunction to educe a cyclopropanone intermediate (**17**) then nucleophilic attack at the carbonyl to induce the signature 1,2-rearrangement product in the furnishing of Favorskii ester (**18**)

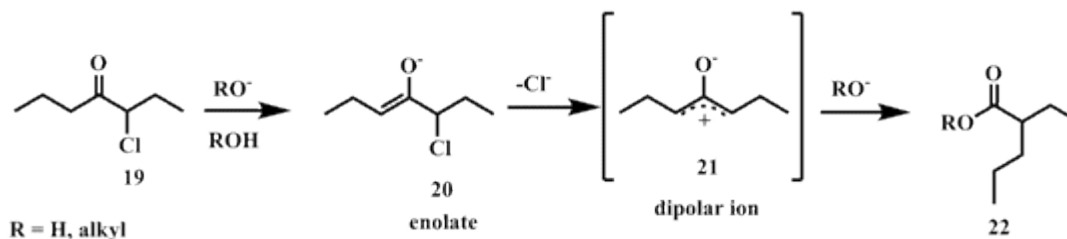
Scheme 3. Lofffield's mechanism of the Favorskii rearrangement.



(Scheme 3). Lofffield demonstrated that the preponderance of products derived only from epoxyether intermediates were generated from the α -Cl precursor and posited the rate determining step (RDS) for these analogs as the reversible, initial deprotonation. Dewar,²⁰ through computational efforts, averred that a disfavored overlap between the newly formed enolate **20** (Scheme 4) and chloro-bearing carbon would preclude cyclization by an $\text{S}_{\text{N}}2$ process and proposed a dipolar, planar oxyallyl ion **21** formed by chloride departure, followed by rearrangement to the Favorskii ester

22. This intermediate would be amenable to the formation of α -methoxyketone derivatives, which are common by-products in Favorskii rearrangements.

Scheme 4. Dewar's proposed mechanism of the Favorskii reaction.



A dipolar ion (i.e., a zwitterion) was suggested as a prominent Favorskii intermediate in subsequent studies by Bordwell (*vide infra*).²⁹ At this time, both cyclopropanone and oxyallyl intermediates are considered to be practicable intermediates in the course to Favorskii products²¹ as neither has been precluded empirically.

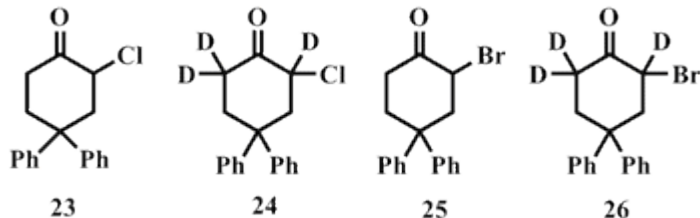
II. Bordwell's contribution to evidence for the Favorskii rearrangement.

A luminary in the study of the Favorskii rearrangement was Bordwell²², who, in a series of 11 reports, communicated the results of his all-encompassing efforts towards an improved comprehension of the mechanism: (1) rate parameters (rate determining steps, accelerating/decelerating factors),^{14,23,24} (2) substituents (structure/reactivity correlations),^{25,26} (3) neighboring groups (anchimeric assistance),²⁷ (4) nucleofuges,²³ (5) temperature,²³ (6) base concentration and ionic strength,²³ (7) intermediates,^{28,29} (8) competing mechanisms (by-products),^{25,27} and

(9) stereochemistry,³⁰ among several others. A conspectus of some noteworthy findings from his research concerning the Favorskii rearrangement is presented.

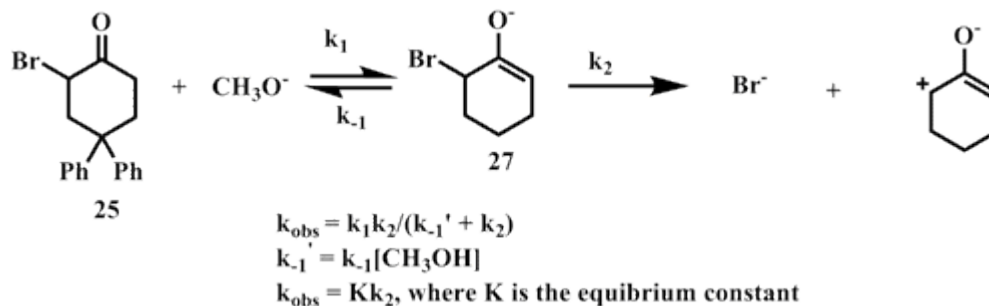
A. Rate, Isotope and Nucleofuge studies. His seminal publication¹⁴ scrutinized earlier findings by Loftfield¹³ concerning the disparate product distributions obtained with α -Br vs. α -Cl ketone precursors. In his studies, Bordwell evaluated isotope and leaving group effects on rates of halogen ion release for protonated and deuterium labeled 2-chloro and 2-bromo-4,4-diphenylcyclohexanones (**23-26**) (Figure 1) in sodium methoxide/methanol at 0°C, common conditions for the Favorskii rearrangement.

Figure 1. Diphenylcyclohexanones examined in the Favorskii reaction.



In choosing di-substitution at the 4 position, he reasoned that the axial orientation of the diphenyl groups would encumber the preferred axial position of the halogen that promotes the formation of epoxyether intermediates (precursors for side reactions) and thus optimize conditions for monitoring any of the aforementioned effects. The series of steps involved in these reactions of interest for **25** are depicted in Scheme 5 with associated steady state expressions.

Scheme 5. The reaction of 2-bromo-4,4'-diphenylcyclohexanone, **25**, with CH_3O^- to corresponding intermediates. The rates for each step are provided, along with an overall rate expression.



Preliminary results from these studies are summarized in Table 1. The lack of a 1^0 kinetic isotope effect (KIE) and a considerable rate enhancement with Br^- over Cl^- as the nucleofuge were evident and from these observations, it was asserted that the enolate formation for **25** was formed reversibly and chloride departure was rate determining.

Table 1. Summary of rates of halide release, k ; isotope exchange ratios, $k_{\text{H}}/k_{\text{D}}$, and rate comparisons, $k_{\text{Br}}/k_{\text{Cl}}$ for reactions of **23-26** under Favorskii conditions. Table adapted from ref. 14.

Substrate	k ($10^4 \text{ M}^{-1} \text{ s}^{-1}$)	$k_{\text{H}}/k_{\text{D}}$	$k_{\text{Br}}/k_{\text{Cl}}$
α -chlorocyclohexanone	40		
23	0.61		
24	0.58	1.05 (23/24)	
25	71		116 (25/23)
26	17	4.1	

The near unity ($k_H/k_D = 1.05$) for **23** suggested a rapid, possibly reversible deprotonation prior to the rate determining C-Cl ionization. The relatively low KIE ($k_H/k_D = 4.1$) for **25**, typically 13 for acetone in hydroxide at 0° C,³¹ indicated the high probability of partial deuterium exchange prior to Br⁻ departure, but was insignificant when compared to the prodigious leaving group effect ($k_{Br^-}/k_{Cl^-} = 116$) in contribution to the rate determining step, which, from this data, was posited to be proton abstraction for **25**. The rationalization for differences in the RDS of **23** and **25** reside in the relative barriers to the formation of the Favorskii intermediate, for each are expected to be similar, but that a “nucleofuge effect” preponderates; Br⁻ is a much better nucleofuge than Cl⁻.

To corroborate this proposal, assays to establish the extent of H-D exchange with **24** and **26** and the Favorskii rearrangement product (Table 2) were conducted by ¹H NMR and mass spectrometry (MS) prior to and at one half-life, $t_{1/2} \sim 3$ h, of the disappearance of reactant. It must be noted that the samples of **24** and **26** were not replete with deuterium (<3 D atoms/molecule on average); the rigors of synthesis and prolonged processing times, i.e., isolation and purifying stages, precluded the production of 100% d₃ for either target. The larger amount of deuterons for **26** vs. **24** was attributed to truncated processing times; there appears to be a connection between the degree of deuterium insertion and processing time length. In addition, some of the deuterium loss of **26** at $t_{1/2}$ was ascribed to processing.

Notably fast H-D exchange occurred during the reaction with **24**, evidenced by complete loss of deuterium in MS analysis, which revealed that nearly 96% of **24**

Table 2. Summary of hydrogen-deuterium exchange with **24**, **26**, and the rearranged Favorskii esters over one half life (~3 h) at 0°C with 0.05 M CH₃O⁻. Table adapted from ref. 14.

Substrate	Material Analyzed	Deuterons ^a	NMR ^b	Mass Spec. ^c
24	24	~2	1.8	d ₀ 3.2 d ₁ 24.7 d ₂ 60.5 d ₃ 11.6
24	24 (recovered at t _{1/2} ^c)	0	0.3	d ₀ 96.7 d ₁ 3.3
24	Rearranged Ester	0	0.05	d ₀ 94.6 d ₁ 5.4
26	26	~2.8	2.28	d ₀ 0.7 d ₁ 10.9 d ₂ 47.6 d ₃ 40.8
26	26 (recovered at t _{1/2})	1.5	1.68	d ₀ 8.0 d ₁ 33.1 d ₂ 49.5 d ₃ 9.4
26	Rearranged Ester	0.7	0.78	d ₀ 22.2 d ₁ 77.1 d ₂ 0.7

^aDeuterium atoms per molecule. ^bThe number of deuterium atoms determined by ¹H NMR. ^cDetermined by mass spectrometry.

and 95% of the rearranged ester contained no deuterons at t_{1/2}. These observations adduce a rapid pre-equilibrium with **24/23**, where k₁>>>k₂ (Scheme 5) and thus α-proton abstraction as rate determining. This phenomenon is significantly reduced for **26** based on considerable deuterium retention at t_{1/2} (1.5 deuterons from initial 2.8 deuterons). Bordwell asserted that some of this deuterium loss was not from the reaction but due to; a) processing and b) background H-D exchange that is known to occur with α-chloro and α-bromoketones in protic solvents.³² Parallel studies

involving the hydrolysis and reesterification of a partially deuterated, rearranged ester revealed virtually no H-D exchange. Thus, the presence of only 0.05 deuterons per molecule of the rearranged ester corroborates the notion of a swift pre-equilibrium for deprotonation and C-Cl ionization as the RDS.

For **26**, based on greater retention of deuterium and, above all, the prodigious $k_{\text{Br}}/k_{\text{Cl}} \sim 116$ (a typical $k_{\text{Br}}/k_{\text{Cl}}$ value for $\text{S}_{\text{N}}2$ and $\text{S}_{\text{N}}1$ reactions is 50^{33}), it was postulated that $k_2 \gg k_{-1}$ and thus k_{obs} approximated k_1 . It should be noted that the substantial yield of epoxy ether byproducts from attack of CH_3O^- at the carbonyl of unsubstituted α -bromocyclohexanone, as demonstrated by Lofffield,¹⁹ can be explained by competitive side reactions with large $k_{\text{Br}}/k_{\text{Cl}}$.³⁴ The results confirm the proposed α -deprotonation as the RDS in the Favorskii process for **26**; this also denotes a change in RDS compared to **24**. The *nature of the nucleofuge* was emphasized as a pertinent factor in determining the outcomes of Favorskii rearrangement in these studies.

Expeditive H-D exchange obviates a concerted process for the α -chlorocyclohexanones **23** and **24**. Complementary studies involving **23** and **25**, where a methyl or $-\text{C}_{20}\text{H}_{36}$ (cholestan-3-one) had been commuted with one of the phenyl moieties, demonstrated dissimilar $k_{\text{Br}}/k_{\text{Cl}}$ ratios (35 for $-\text{CH}_3$, 52 for cholestan-3-one). If the mechanism was concerted, a relatively constant, sizeable nucleofuge influence would be anticipated. This was inconsistent with the above observations and effectively precluded a concerted process for the Favorskii mechanism for **25** and **26**.

As Bordwell anticipated, the 4-substituted-2-halocyclohexanones established the prevalent formation of rearranged, ring contracted esters. For 2-chlorocyclohexanone analogs, the route to these esters was favored whether or not there existed ring substituents. In contrast to this, unsubstituted 2-bromocyclohexanone exhibited an epoxyether as the primary product, resulting from a reaction course through an epoxide intermediate. It is apparent that the 4,4' moieties effectively prevented the epoxide intermediate from forming, as no epoxyethers were reported. These studies divulged, in addition to the salient nucleofuge impact on the RDS, a *structural influence* that is pronounced for ring substitutions of α -bromocyclohexanones and that exert direct control over the outcomes of the Favorskii rearrangement.

B. Substituent Effects, Linear Free Energy Relationships (LFER's), Salt and Media effects, and Further Evidence for a Nucleofuge Effect.

In a supervening report,²³ Bordwell conveyed results from a) temperature studies; b) studies involving adjusting base [CH_3O^-] and ancillary salts [LiClO_4] (ionic strength) to discern these effects on overall yields and product distributions; c) structure-reactivity linear free energy relationships, i.e., how meta and para arene substituents impact the rates (k_{obs}) of nucleofuge release and Favorskii ester formation; d) an expansion on the nucleofuge character of the halogen, i.e., its influence on the mechanism and product outcomes. The model systems for these studies were a series

of 1-chloro-1-phenylpropan-2-ones (**28**) in CH₃OH at 0°C (Scheme 6). The results from these experiments are listed in Table 3.

Scheme 6. Disparate reaction pathways for α -chlorobenzyl methyl ketone derivatives in CH₃O⁻/CH₃OH.

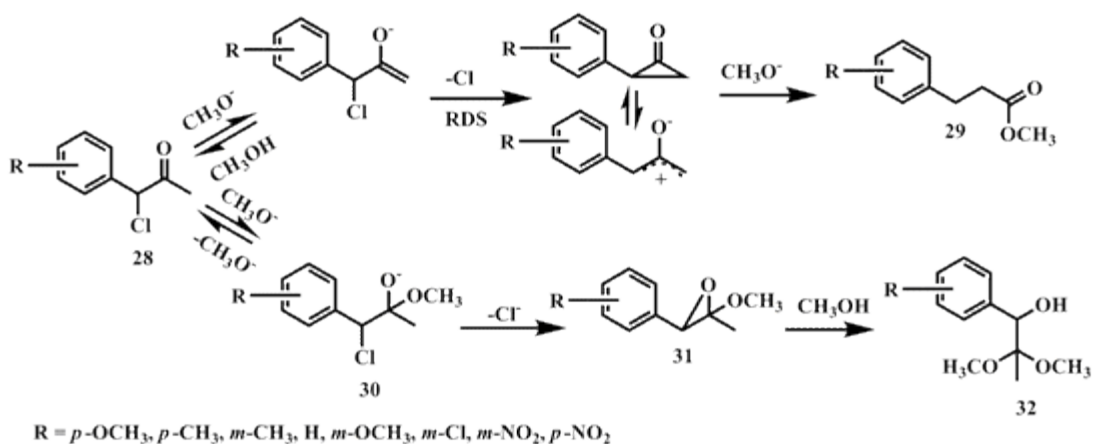


Table 3. Results of the reactions of **28** at various [CH₃O⁻] and [LiClO₄] in CH₃OH at various temperatures. Table adapted from ref. 23.

[MeO ⁻], M	T (°C)	Yield of 29 (%)	Yield of 32 (%)
Inverse addition ^a	0	9	68
0.05	0	13	81
1.00	0	17	77
2.00	0	21	70
0.05	65	37	51
2.00	65	61	35
0.05 (1 M LiClO ₄)	65	57	17
0.05 (2 M LiClO ₄)	65	63	19

^aSlow addition of 10% excess 0.05 M [CH₃O⁻] to a solution of **28**.

The enhanced yield of **29** at higher temperatures, 13% vs. 37% at 0.05 M, was attributed to the calculated 2-3 kcal/mol higher activation energy, ΔG^\ddagger , of **29** compared with hydroxy ketal **32**. This was derived from work done by Bordwell that found that ΔG^\ddagger for **28**, based on rates in 0.05 M NaOCH₃/CH₃OH between 0° and 25°C, was 17.2 kcal/mol and manifested **29** as the major product. ΔG^\ddagger for the α -methyl derivative of **28** (geminal with -Cl) was calculated to be 19.7 kcal/mol under the same conditions with the primary product being **32**. Complementary experiments with **29** and **32** in the presence of CH₃O⁻ at high temperatures evinced no reactivity.²³ Augmented yields of the Favorskii ester **29** as a function of base concentration were shown to be marginal at 0°C but improved at 65°C. Accompanying these observations was an enhancement in the yield of **29**, 37% vs. 57%, as a function of increased ionic strength from increasing the LiClO₄ concentration, i.e., a *salt effect*. It was theorized that the Favorskii reaction was impacted to a greater degree by ionic strength adjustments than the corresponding formation of **32** as evidenced by the higher yields of **29**.

A parallel study by Skrobek³⁵ divulged improved yields of the Favorskii ester from 1-chlorocyclohexyl methyl ketone in the presence of higher concentrations of CH₃O⁻ or LiClO₄ and stereochemical differences of *trans*-1-chloro-2-methylcyclohexyl methyl ketone arose from changes in [CH₃O⁻] or [LiClO₄]. No explanations, however, were proffered. Later studies²⁵ with 0.0075 M PhCH₂COCH₂Cl (**40**, pg 21, vide infra) in CH₃O⁻/CH₃OH and 0.1 M LiClO₄ at 0°C revealed a 20-30% acceleration in reaction rate and furthermore, a 100% acceleration

in 1.0 M LiClO₄. It was hypothesized that LiClO₄ imparted a stabilizing effect on the highly ionic transition state through salt-facilitated ionization of the halide. Bordwell theorized this from similar findings with *t*-butylbromide in 90% aqueous acetone and Ph₂CHCl in 80% aqueous acetone,³⁶ two S_N1 model mechanisms. No further studies, however, were conducted by Bordwell to supplement or to elaborate on the *salt effect*. Complementary to the salt effect was a boost in reaction rates for **40** (vide infra) in 0.05 M CH₃O⁻/CH₃OH at 0°C as the water content was increased (Table 4).

Table 4. Effect of water composition on the reaction rate, k_2 , of PhCH₂COCH₂Cl in 0.05 M CH₃O⁻/CH₃OH at 0°C. Table adapted from ref. 25.

Vol % H ₂ O	k_2 (10 ² , M ⁻¹ s ⁻¹)
0	2.63
5	6.23
10	13.1
25	50.3
50	289

A 110-fold acceleration in the reaction rate for **40** occurred as the water concentration increased from 0 to 50% (2.63 to 289 x 10² M⁻¹s⁻¹). A plot of the log k_2 vs. the Grunwald-Winstein Y ,³⁷ which represents quantitative measures of the effect of the “ionizing power” of the solvent on the reaction, provided an excellent correlation (slope = 0.647; R² = 0.995; standard deviation = 0.037). For **28**, a 197 fold increase in reaction rate was distinguished by increasing content of water from 0 to 50% (0.22 to 42 x 10² M⁻¹s⁻¹) and thus the slope would be expected to be even

greater. The considerable ionizing power of water ($Y = 3.56$ for ionization of $(\text{CH}_3)_3\text{C-Cl}$),³⁷ was apparent from data in Table 4. These observations further support the prior contention that heterolysis of the C-Cl possesses a high degree of ionic character in the transition state and accordingly, Cl^- departure represents the RDS. A *media effect* was clearly distinguished from these studies.

Several aryl-substituted functionalities were examined for their impacts on observed rates of halide ion release from **28**, i.e., to explore whether a linear free energy relationship existed. The data for substituents are revealed in Table 5. A modest surge in yields of **29** was observed for nearly every substituent as the base concentrations were increased from 0.05 to 1.0 M. The influences of temperature and base concentration on product distribution denoted competing reaction pathways, each of which displayed a first order dependence on $[\text{CH}_3\text{O}^-]$. The impacts of substituents on yield and k_{obs} were conspicuously related to their electron releasing and withdrawing capacities relative to -H; para-substituted, electron donating groups

Table 5. Summary of observed and Favorskii rate constants and product yields in $\text{CH}_3\text{O}^-/\text{CH}_3\text{OH}$ at 0° for substituted **28** as a function of substituent. Table adapted from ref. 23.

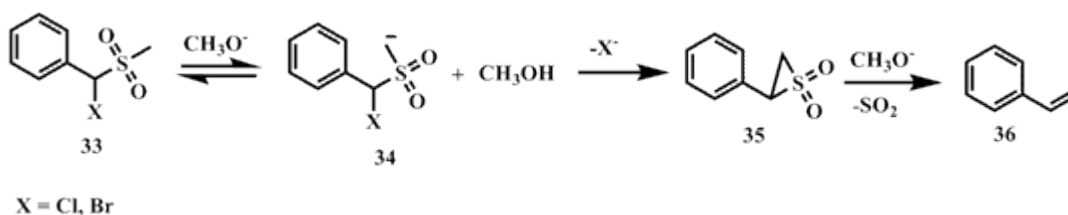
Precursor	$k_{\text{obs}}/10^3$ $\text{M}^{-1}\text{s}^{-1}$	$k_{\text{Favorskii}}/10^3$ $\text{M}^{-1}\text{s}^{-1}$	%Yield of 29		
			$[\text{MeO}^-], 0.05 \text{ M}$	$[\text{MeO}^-], 1.0 \text{ M}$	$[\text{MeO}^-], 0.05 \text{ M}$
H	3.09	0.4	13	17	81
<i>p</i> -NO ₂	5.09	ND	0	-	62
<i>p</i> -Cl	6.21	0.31	5	9	83
<i>p</i> -OMe	39.4	26.8	68	65	-
<i>m</i> -OMe	2.72	0.33	12	25	79
<i>p</i> -Me	6	1.5	25	36	56
<i>m</i> -Me	3.23	0.45	14	22	61
<i>p</i> -F	7.5	0.83	11	16	65

(-OCH₃, -CH₃) manifested elevated rates for the production of **29** while para-substituted electron withdrawing groups (-F, -Cl and NO₂) evinced preferences for **32**. Initial attempts to rationalize these phenomena through linear free energy relationships (LFER) led to poor correlations using log k_{obs} and Hammett σ substituent constants ($\rho = -1.1$; $R^2 = 0.875$; standard deviation = 0.275); ameliorated correlations were found by employing σ^+ constants ($\rho = -2.37$; $R^2 = 0.992$; standard deviation = 0.13 (5%)). The negative ρ suggested an accumulation of positive charge (carbocation character) or a loss of electron density (decreased anionic character) in the transition state of the RDS. From this, Bordwell postulated that two key steps in the mechanism leading to **31** were impacted the most by substituents. First, the reversible addition of CH₃O⁻ to **28**, the initial step in forming **31**, is estimated to have a $\rho \sim 0.8$ based on analogous studies.³⁸ Electron withdrawing groups would be expected to accelerate this process; this prediction was confirmed by the present study. Secondly, halogen departure from **30** was calculated to have a $\rho \sim -0.9$. Electron donating groups were expected to accelerate the rate of this process; results from this study were also consistent with this prediction. The electron donating or withdrawing *natures of the arene-substituted functional groups* were shown to exert a direct control over reaction pathways of **28** in forming **29** and **32**.

C. The Ramberg-Backland (R-B) analogy and role of orbital overlap.

To obtain an improved perspective on the step entailing halide ionization, Bordwell examined the Ramberg-Backland (R-B) reaction³⁹ of α -halosulfones as an alternative model (Scheme 7). The reaction is well understood and characterized by

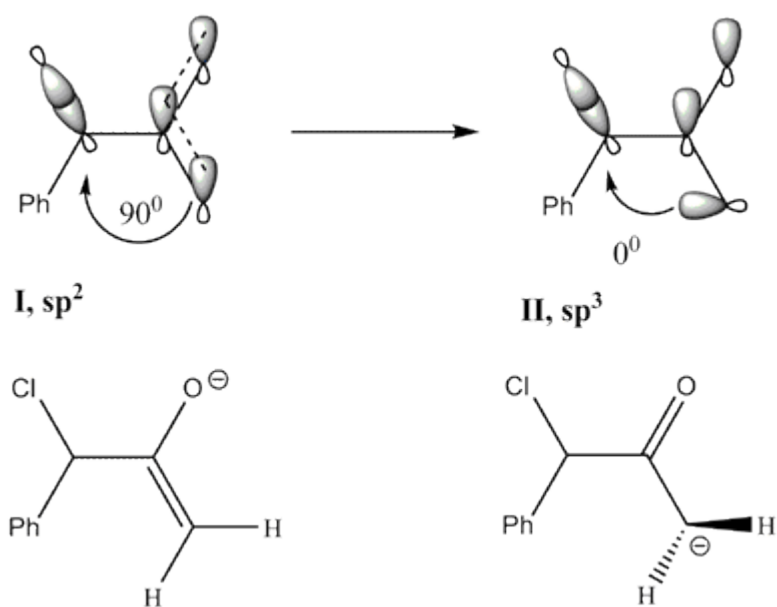
Scheme 7. A depiction of the Ramberg-Backland reaction.



swift, reversible carbanion formation **34** which mediates the rate determining departure of the halide ion to produce an episulfone **35** that readily extrudes SO_2 to form styrene **36**. A leaving group effect, $k_{\text{Br}}/k_{\text{Cl}} > 50$, though smaller than in the Favorskii reaction, nevertheless, suggested considerable C-X cleavage in the transition state of the RDS. A positive ρ value (+0.8) in 40% aqueous dioxane was determined from the rate dependence on substituents. Despite significant C-X ionic character, a positive ρ indicated that electron withdrawing groups should accelerate C-X heterolysis and required the inchoate C-C bond to be nearly completed in the transition state. This finding diverged from the Favorskii reaction; a large negative ρ -1.1 predicted that electron withdrawing groups would decelerate the rate of C-X cleavage²² and the C-C bond formation would be much less developed. Here,

mechanistic disparities in the two reactions became obvious. The negative charge afforded from hydrogen atom abstraction was localized on the carbon of the sulfone due to poor p-d π orbital overlap, whereas the carbanion was primarily a delocalized entity in the Favorskii reaction (Scheme 8); the p-orbital is held preferentially parallel

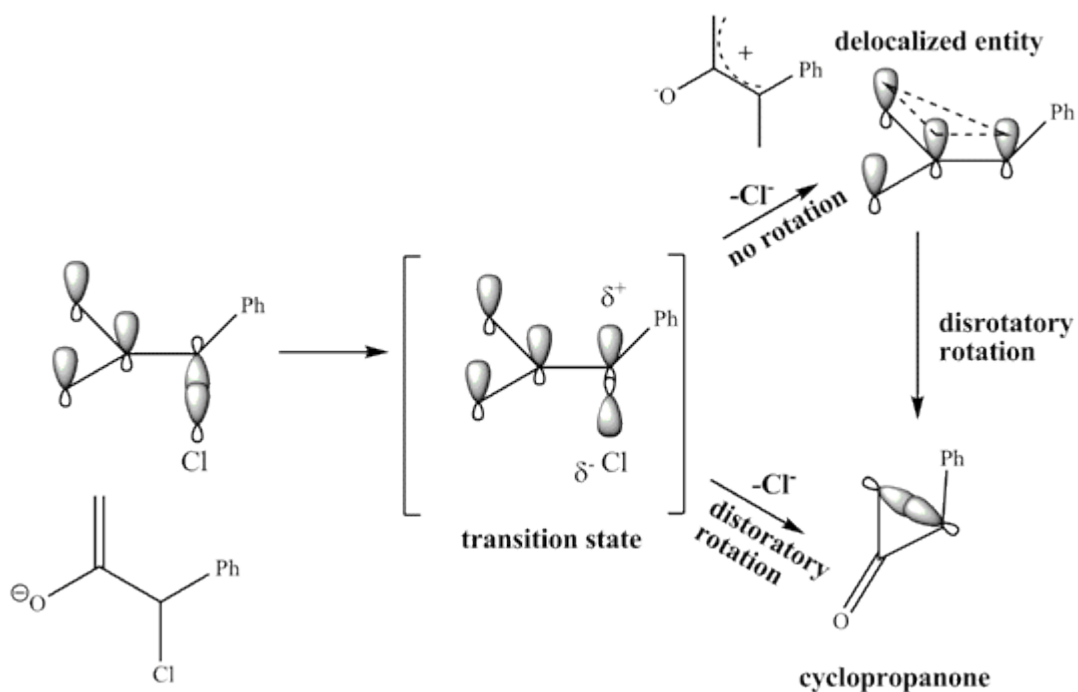
Scheme 8. Delocalized (sp^2) vs. localized (sp^3) electron models.



to the contiguous carbonyl π system (**I**). To reduce the appropriate trajectory for a S_N2 cyclopropanation, the carbanion orbitals must contort out of plane (deconjugate) with the carbonyl (**II**), localizing electron density, i.e., inducing a hybridization change from sp^2 to sp^3 and thus diminishing the feasibility of this route, at least from an

energetics perspective. Conversely, an arrangement where the C-Cl bond is held parallel to the enolate p orbital (Scheme 9) effectuates partial π overlap of the

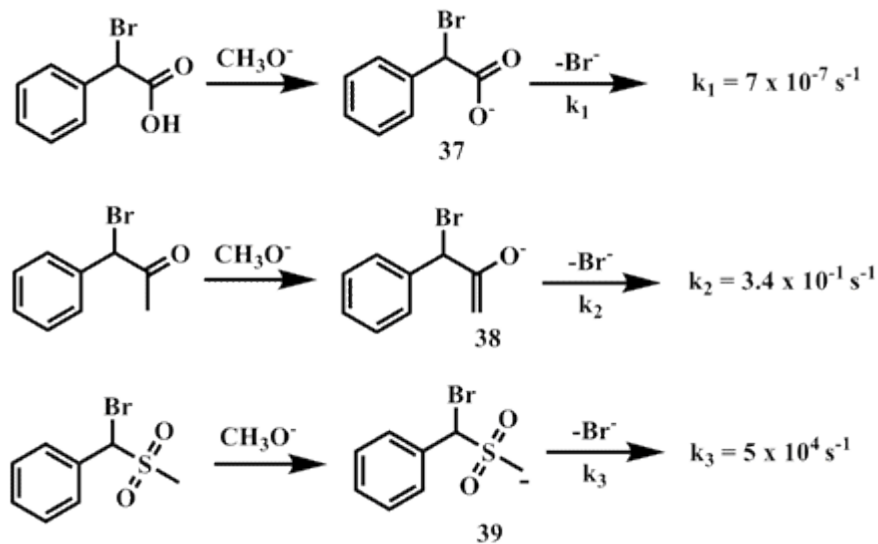
Scheme 9. Anchimeric π assistance in establishing a cyclopropanone intermediate.



developing p-orbital of the C-Cl center in the transition state, a stabilizing interaction that would promote the formation of cyclopropanone through disrotatory rotation. Energetically, anchimeric π electron participation in halide discharge to effect Favorskii precursors was perceived to be the favored route. To probe this hypothesis, Bordwell determined first order rate constants of bromide release from the base

promoted anions corresponding to three similar α -bromo substrates in 0.05 M CH_3O^- / CH_3OH at 0°C (Scheme 10). A five order of magnitude rate enhancement was

Scheme 10. Rates of bromide release from anionic α -bromo substrates.

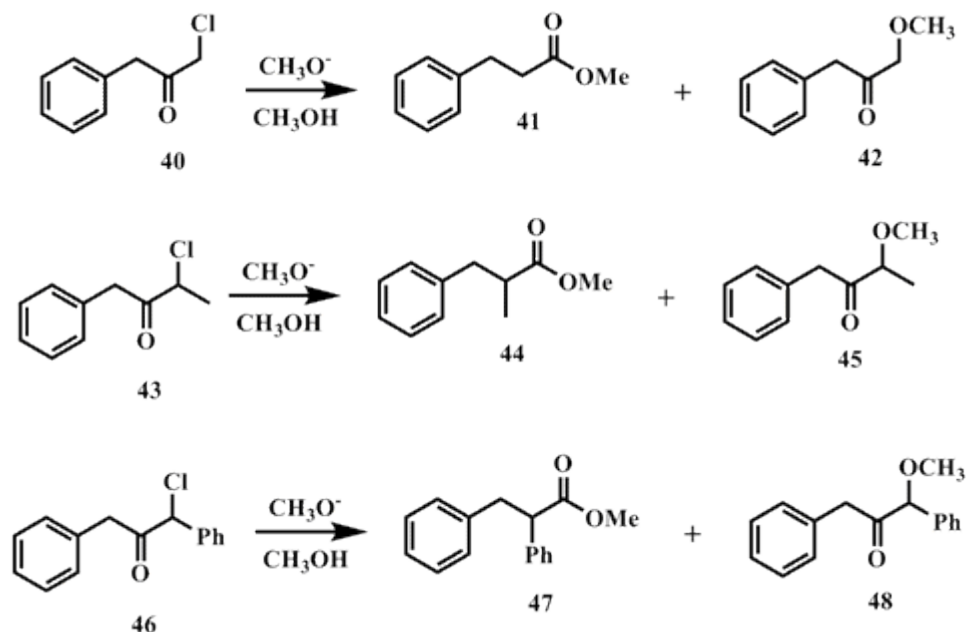


evinced by the enolate, **38**, compared to the carboxylate, **37**. An obvious neighboring group effect, anchimeric π assistance, seemed reasonable to Bordwell, as the only other feature common to both **37** and **38** was resonance delocalization. Bordwell reasoned that if resonance stabilization predominated, **37** would manifest a more rapid rate of bromide release. For **39**, as a sulfur enolate is a less important resonance contributor due to the poor p-d orbital overlap, the more *localized* carbanion displayed further a five order of magnitude increase for bromide release, imputing σ (electrons localized on a sp^3 orbital) electron participation. Bordwell inferred from

these studies that π *electron participation* was a salient feature in the mechanism of Favorskii reaction.

D. The influence of α -substituents. Earlier, it was revealed by Bordwell that both the nature and locus of the substituent in cyclohexanones strongly influenced product distributions of the Favorskii reaction, i.e. a *structure-reactivity* relationship was established. Analogous investigations were extended to linear α -haloketones, specifically the role of methyl^{27,28} and phenyl²⁶ substituents in altering parameters of the Favorskii reaction such as rates of halide departure and product yields. Previous investigations of 1-chloro-3-phenylpropan-2-one **40** (Scheme 11) in 0.05 M

Scheme 11. Reactions of α -chloro analogs in $\text{CH}_3\text{O}^-/\text{CH}_3\text{OH}$.



CH₃O⁻/CH₃OH at 0°C exhibited rapid H-D exchange and a ρ of -5.0,²³ denoting an initial, reversible deprotonation step and suggesting a high degree of C-Cl bond dissociation in the transition state. From this, Bordwell rationalized that α-methyl or phenyl substituents (e⁻ contributors) should stabilize this accumulation of positive charge and augment the rate of halide ionization, k₂. He studied the behaviors of 3-chloro-1-phenylbutan-2-one (**43**) and 1-chloro-1,3-diphenylpropan-2-one (**46**) under an assortment of conditions and compared results to those obtained for **40**.²³ Results from these examinations are displayed in Table 6. As observed earlier, a direct

Table 6. Results from the reaction of **40**, **43**, and **46** in varying [CH₃O⁻] in CH₃OH at 0°C. Table adapted from ref. 27.

	40	43	46
Relative rates ^a	1	>250	>330
Deuterium exchange	~80%	~6%	N ^b
k _{Br} /k _{Cl}	63	0.9	1.0
Hammett ρ	-5.0	1.4	1.1
Salt effect ^c	25-30%	N ^b	~7%
Products with:			
2 M NaOCH ₃	100% 41	100% 44	39% 47 , no 48 ^d
0.05 M NaOCH ₃	100% 41	61% 44 , 39% 45	15% 47 , 85% 48
10 ⁻⁵ M NaOCH ₃	100% 41	100% 45	100 % 48

^aChloride ionization. ^bN = negligible. ^c0.1 M LiClO₄. ^dAn unidentified compound was formed.

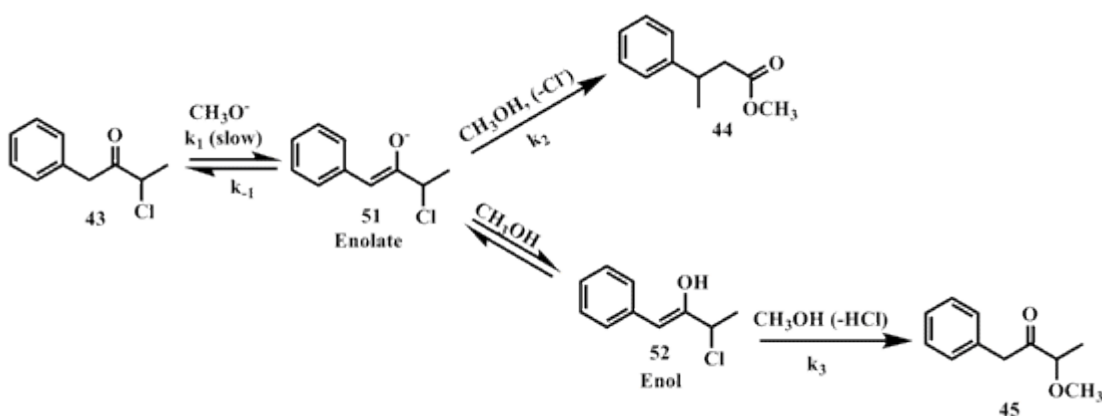
correlation was found between [OCH₃⁻] and product composition for **43** and **46**; larger quantities of OCH₃⁻ favored Favorskii product formation. No changes in product distribution as a function of [OCH₃⁻] for **40** were noticed; the Favorskii ester was the dominant product in all cases. A mechanistic interpretation will be provided later.

Control experiments were performed for validation and found that: 1) No chloride was released from **43** or **46** in the absence of CH_3O^- in CH_3OH over 24 h and 2) neither **44** nor **47** reacted in 2 M $[\text{CH}_3\text{O}^-]$ for 2 h; this ruled out degradation of these Favorskii esters to other products, which would result in false percent yields to be reported for their formation. Furthermore, it was found that the product ratios for **40**, **43** and **46** remained steady at 0°C and 70°C in 0.05 M $\text{CH}_3\text{O}^-/\text{CH}_3\text{OH}$, 61% and 39% respectively, negating a *temperature* effect. In the presence of 0.1 M LiClO_4 , a salt effect was minimal for **43** as there was essentially no change in yield and for **46** only a 7% increase was reported; a significant salt effect for **40** amounted to a ~25-30% increase in the production of Favorskii esters.

When the Br^- analogs were tested under the same conditions, the product ratios were nearly identical. However, the reaction rates for halide detachment in 10 molar excess CH_3O^- under the same conditions revealed no variation for **43** and **46** ($k_{\text{Br}}/k_{\text{Cl}} \sim 0.9$ and 1 respectively) but was pronounced for **40** (~63). This phenomenon, in itself, intimates distinct mechanisms for **40** and **43/46** to rearranged products. Corroborating these are the sizeable differences in ρ for **40** (-5.0) compared to **43** (1.4) and **46** (1.1). A substantial buildup of positive charge in the transition state of the RDS for **40** is anticipated and thus C-Cl bond breakage should possess a large degree of ionic character at the transition state. Analogous to its structural isomer (**28**) the RDS for **40** is hypothesized as chloride ionization. In contrast, positive ρ values for **43** and **46** indicate a buildup of negative charge in the transition state and adduce that the RDS is, in fact, proton abstraction. As Bordwell anticipated,

the α -methyl **43** and phenyl **46** moieties, through stabilization of the positive charge on the chloride-bearing carbon, unambiguously transposed the RDS of the Favorskii reaction to proton abstraction, comparable. From these results and those obtained from related experiments, Bordwell formulated a mechanism to account for the formation of **44** and α -methoxy ketone (**45**) (Scheme 12).

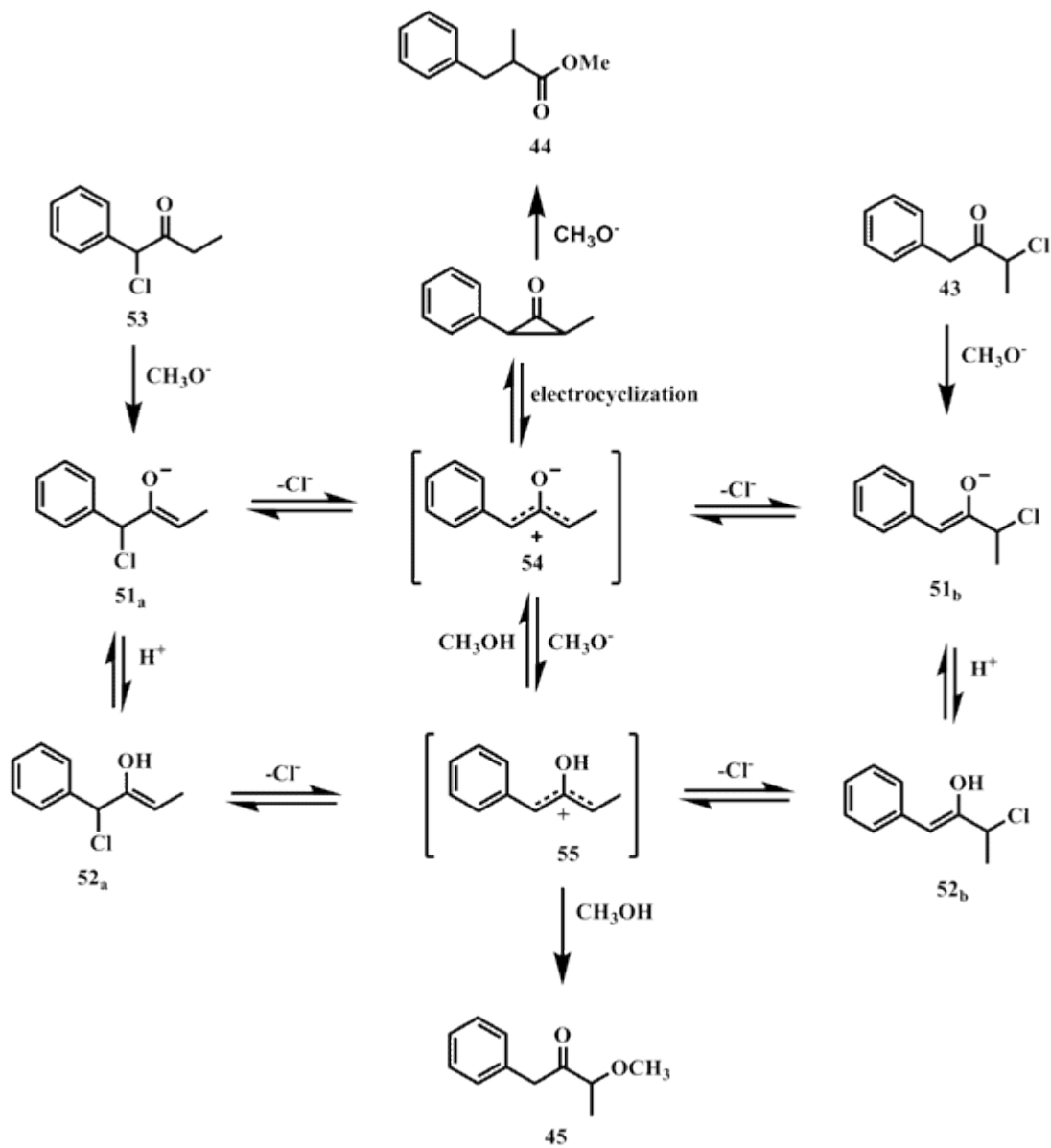
Scheme 12. Discrete mechanistic pathways for α -chlorobenzylpropiophenone **43** to the rearranged ester (**44**) and α -methoxyketone (**45**).



The RDS, as previously derived, represents k_1 , or rate of enolate formation. The rearranged ester (**44**) was engendered from the enolate intermediate (**51**) through the Favorskii rearrangement. The β -hydroxy allyl chloride (enol) intermediate (**52**) was assumed to be in rapid equilibrium with **51** and thus permitted solvolysis to occur in forming **45**. The relative magnitudes of k_2 and k_3 , along with direction of equilibrium, control the **44** to **45** ratios. When methoxide concentrations are high, enolate [**51**] is high, $k_2 > k_3$, and the formation of **44** is promoted. Conversely, when

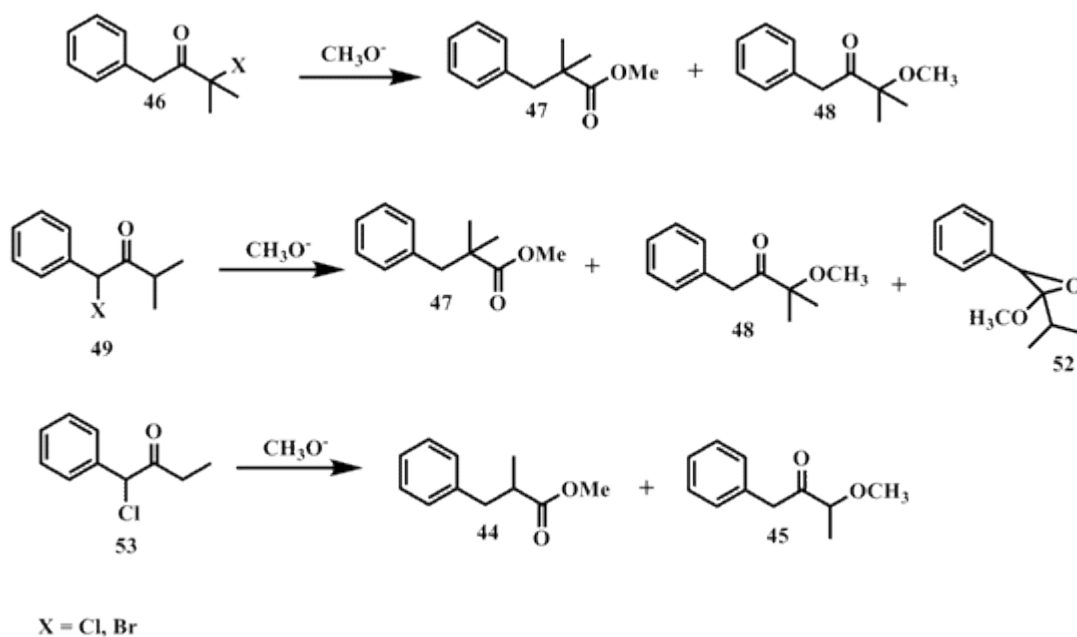
CH_3O^- concentrations are reduced, enol **[52]** is high, $k_3 > k_2$, and **45** preponderates. Bordwell estimated that the enol to enolate ratio, $[\mathbf{52}]/[\mathbf{51}] \sim 40$ at 0.05 M $[\text{CH}_3\text{O}^-]$.²⁶ The α -substituted methyl **43** and phenyl **46** groups were vital to this mechanistic change. Structure-reactivity relationships, once again, were indicated as important factors in the Favorskii reaction. Recall that the Favorskii ester is produced solely from **40** irrespective of $[\text{CH}_3\text{O}^-]$. To recapitulate the importance of $[\text{CH}_3\text{O}^-]$ in determining product outcomes of the Favorskii reaction, a side by side, detailed mechanistic depiction of the reaction pathways of **43** and its isomer **53** ($\text{R} = \text{H}$) is exhibited in Scheme 13. The primary route to **44** for each precursor, after predominant enolate (**51_a** and **51_b**) formation when concentrations of CH_3O^- were higher, was postulated to be through an oxyallyl zwitterion, **54**, which was presumed to be in equilibrium with the reactive cyclopropanone. The competing route to **45** was thought to involve the protonated oxyallyl zwitterions (**55**) when enols (**52_a** and **52_b**) preponderated at low $[\text{CH}_3\text{O}^-]$. Rearrangement to **44** was precluded from **55**, where CH_3O^- addition was favored to furnish **45**. An additional consideration in determining the pathways to **44** and **45**, though not explicitly mentioned, is the interconversion between oxyallyl intermediates **54** and **55**, i.e., a Curtin-Hammett condition. Small energy barriers for proton exchange would rapidly interconvert **54** and **55**. High $[\text{CH}_3\text{O}^-]$ would favor **54**, while low concentrations would favor **55**.

Scheme 13. Reaction pathways of isomers **53** and **43** to rearranged **44** and α -methoxy ketone (**45**).



An extension²⁸ of investigations into structure-reactivity relationships of the Favorskii rearrangement was applied to tertiary α -haloketones **46**, **49**, and **53**, each containing two substitutions on the α -position of the carbonyl (Scheme 14). Control

Scheme 14. Reactions of alkyl substituted α -chloro ketones with CH_3O^- .



experiments demonstrated the isomerization of **53** to **43** at ~20% over 6 months at ~0°C; this was accounted for in determining relevant factors pertaining to product formation. Results from these experiments are displayed in Table 7.

Table 7. Summary of product yields and rates of reaction for **46**, **49** and **53** as a function of CH_3O^- in CH_3OH . Table adapted from ref. 28.

Substrate	$[\text{CH}_3\text{O}^-]$, M	% Yield α -methoxyketone 45/48	% Yield of Favorskii ester 44/47	k ($10^3 \text{ M}^{-1} \text{ s}^{-1}$)
46 (Br)	0.05	97	3	-
	1	60	35	-
46 (Cl)	0.05	~97	~3	-
49 (Cl)	0.05	-	10	0.016
	1	-	45	-
49 (Br)	1	-	-	0.024
53 ^{a,b} (Cl)	0.05	30	70	

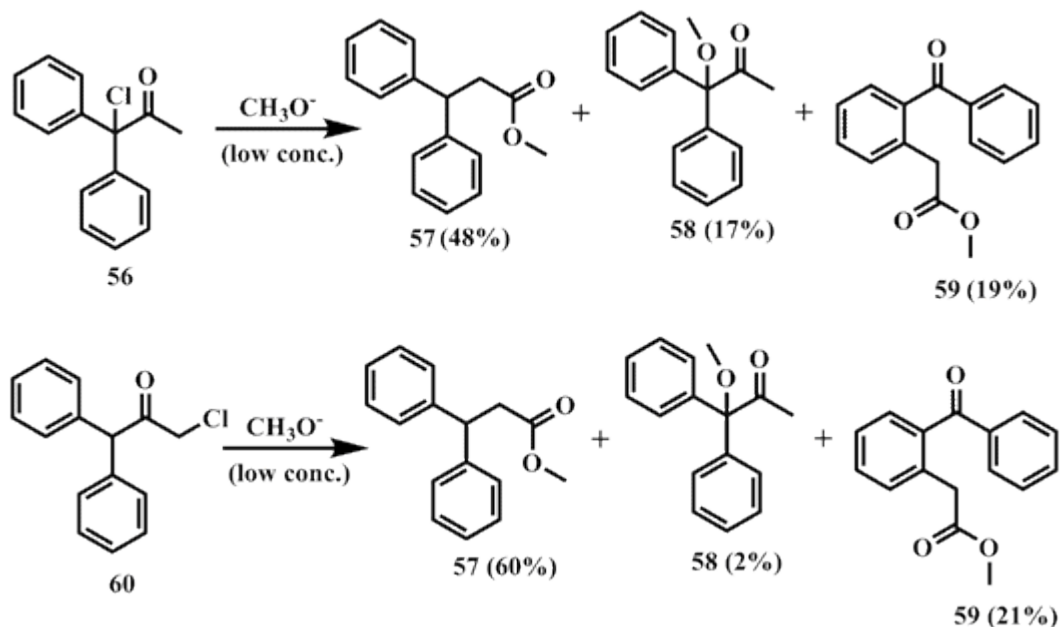
^aThe yield of Favorskii ester is 100% in 2 M NaOCH_3 . ^bAt 10^{-5} M, the α -methoxyketone was the sole product.

An improved yield of Favorskii ester as the $[\text{OCH}_3^-]$ increased was manifested. This observation seemed to bolster the plausibility of the previously posited enol/enolate mechanism in accounting for product distributions, i.e., a greater quantity of OCH_3^- (greater basicity) would shift the enol/enolate towards the enolate that promotes the rearrangement process. The lack of a halogen effect, $k_{\text{Br}}/k_{\text{Cl}} \sim 1$, for **49** was similar to previously encountered examples and signifies rate determining proton abstraction. The rate for proton abstraction of $\text{PhCH}(\text{Cl})\text{COCH}_3$, **28** (vide supra), was accelerated 35 fold compared to **49**; this phenomenon implies an *encumbering (possibly steric), effect* exerted by the methyl group in retarding the rate of proton abstraction. The RDS changes from proton abstraction to halide departure. A steric component to the Favorskii mechanism is further advanced when one compares the deprotonation rates of **53** with **46**; the former disclosed a 35 fold acceleration over the latter. The RDS for **46** was postulated as proton abstraction based on analogy with previous work.²⁵

E. Evidence for a dipolar (oxyallyl) intermediate in the Favorskii reaction.

Bordwell inadvertently provided evidence for the formation of Dewar's²⁰ proposed dipolar ion in studies²⁹ involving 1-chloro-1,1-diphenylpropanone (**56**) and 3-chloro-1,1-diphenylpropanone (**60**) in $\text{CH}_3\text{O}^-/\text{CH}_3\text{OH}$ at 0°C ; his specific aims were to probe the effects phenyl substituents on the Favorskii reaction.

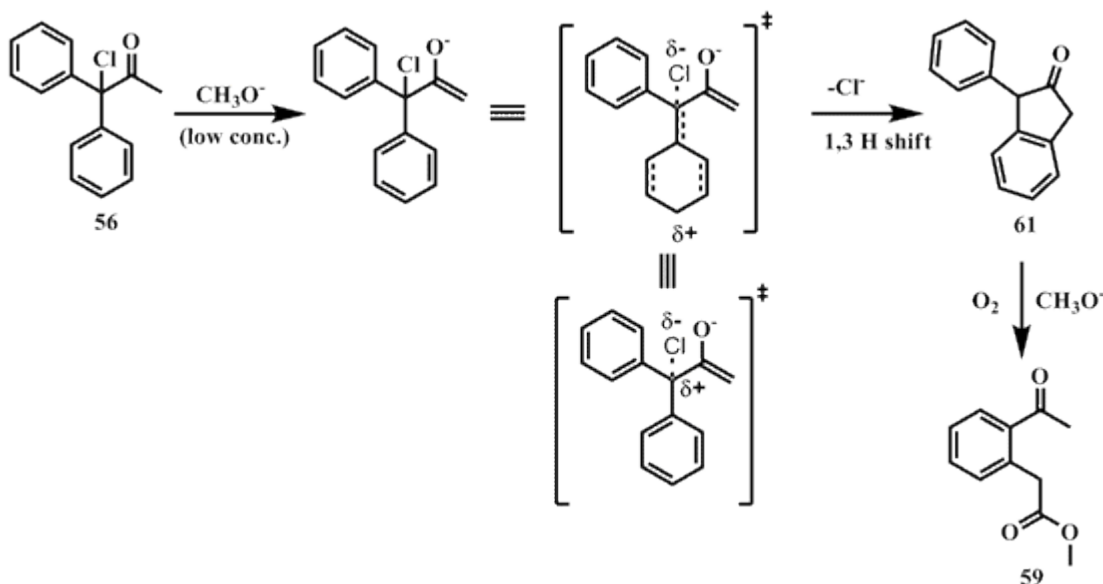
Scheme 15. Product distributions from the reaction of α -chloro ketones with low concentrations of CH_3O^- .



At 0.05 M CH_3O^- , both precursors gave the Favorskii ester (**57**) in approximately 97% yield. At lower concentrations of base, however, an array of products was obtained (Scheme 15), along with, perhaps most interestingly, **59**. Noteworthy, were the identical constituents that materialized from each precursor under Favorskii conditions, although the compositions of each product set were

discrete. It was reasoned that the emergence of **59** stemmed from low $[\text{CH}_3\text{O}^-]$, permitting the intramolecular cyclization of the enolate to engender an indanone, **61**, that thenceforth, would react with O_2 in the presence of CH_3O^- (Scheme 16). This

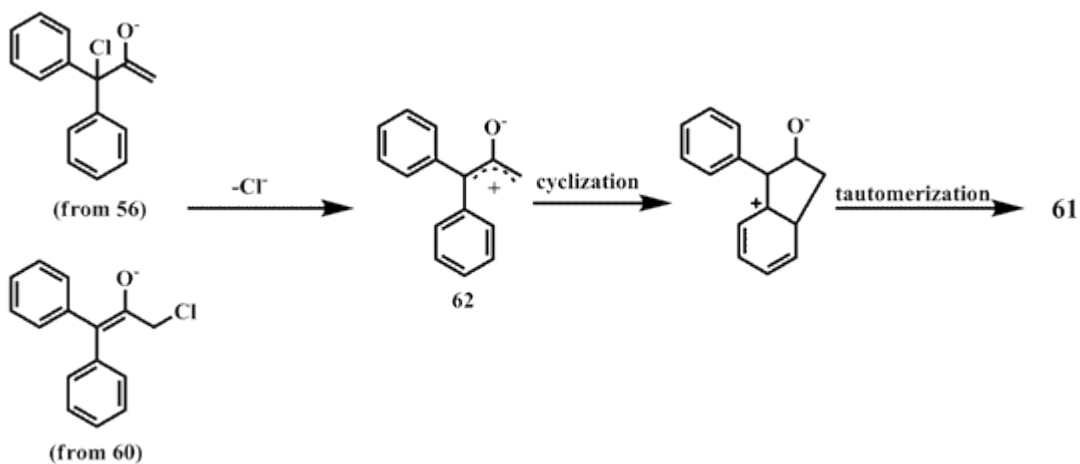
Scheme 16. Proposed mechanism for the reaction of α -chloroketone, **56**, with low $[\text{CH}_3\text{O}^-]$ to form the methyl ester, **59**.



proposed sequence was supported by an independent study from Smith⁴⁰ that demonstrated an “unknown acid, melting point 131°C ” from reaction of **61** with cold sodium hydroxide. In a supplementary study, a pure sample of **61** promptly transformed to **59** upon oxidation (O_2) in a methanolic solution of methoxide. The rate of halide ionization for **56** was estimated to be enhanced 625 fold compared to its mono-phenyl analog; this unequivocally demonstrated a stabilizing effect by the phenyl moiety. In addition, only about 11% deuterium exchange occurred with **56**.

The RDS for **56**, therefore, was posited to be deprotonation. A “dipolar-like” transition state was advanced, resulting from halide ion departure from the enolate intermediate. It was reasoned that the second phenyl group would effectively disperse the positive charge accumulation at the C-Cl center through resonance. A parallel phenomenon, though not as marked, was observed for **60**, where the rate of halide ionization was augmented 25 fold vs. its unsubstituted analog **40**. Additionally, $k_{\text{Br}}/k_{\text{Cl}}$ was found to be ~ 4 , supporting enolate formation as being rate determining. After extensive, congruent investigations using analogs of **56** and **60**, Bordwell maintained that an oxyallyl intermediate (**62**) was formed (Scheme 17).

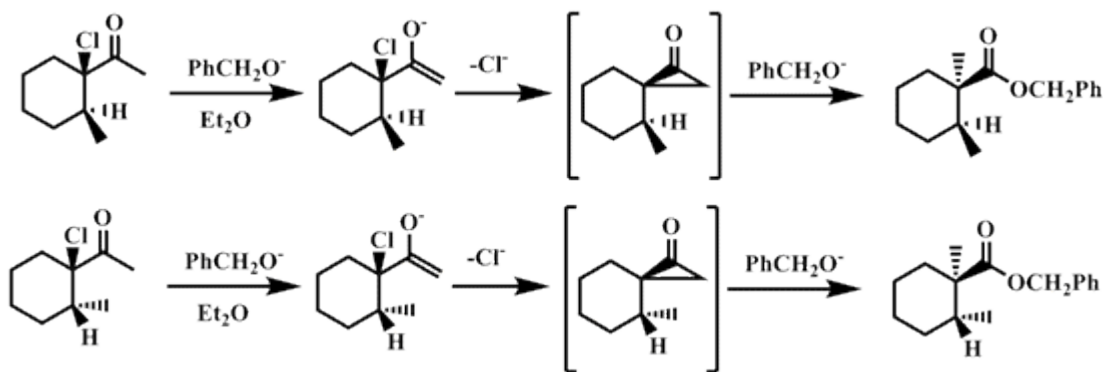
Scheme 17. Suggested dipolar (oxyallyl) mechanism to indanone (**61**).



Hoffmann⁴¹ independently determined energetic preferences (22 kcal/mol) for dipolar ions at equilibrium relative to cyclopropanone. However, Dewar⁴² and Liberles⁴³ asserted cyclopropanones to be more stable by 78 and 83 kcal/mol, respectively.

F. Studies in Stereochemistry. Stereochemical investigations of the classical Favorskii reaction have been carried out by several groups,⁶ most notably Stork and Borowitz,¹⁸ who discerned the stereospecific formation of esters from non-epimerizable ketones (Scheme 18). They suggested an operating, inversion or S_N2

Scheme 18. Stork-Borowitz proposal for stereochemical inversion of precursors to Favorskii products.



process. Solvent polarity, however, was determined to direct the stereochemical outcome; this theory was advanced by House⁴⁴ et. al., who's studies divulged the formation of inversion products only in non-polar media.

Bordwell³⁰ also explored Favorskii reactions involving stereochemical conversions, specifically 2-bromo-4-methyl-4-phenylcyclohexanone (**63**) and the *cis/trans* isomers of 2-bromo-5-methyl-5-phenylcyclohexanones (**66**) under Favorskii conditions. The reactions of **63** and **66** to generate corresponding products are outlined in Scheme 19 and results presented in Table 8.

Scheme 19. Reactions of α -bromo ketones **63** and *cis/trans* diastereomers **66** with CH_3O^- in CH_3OH .

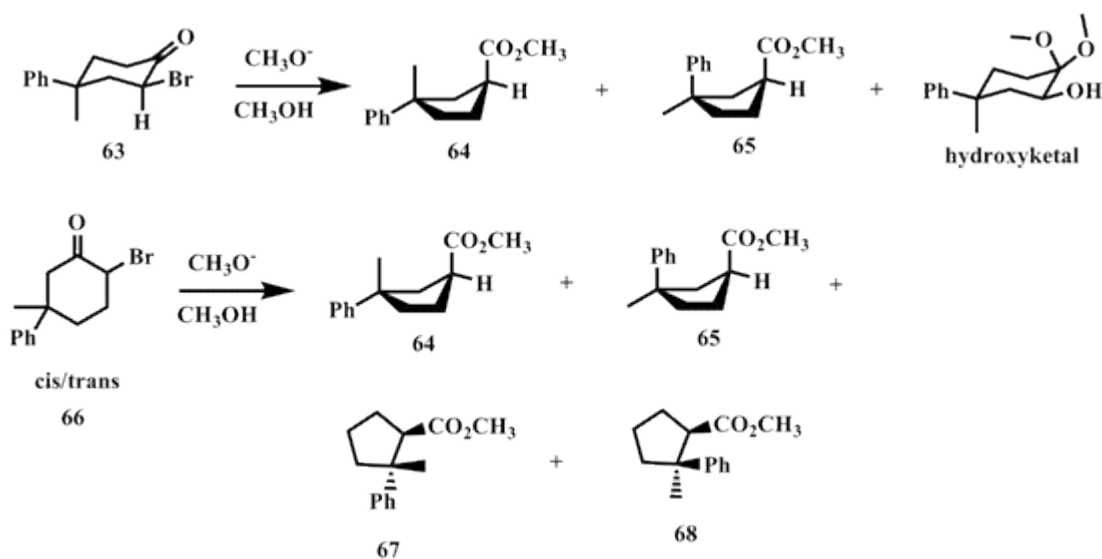


Table 8. Results of reactions of **63** and **66** with various $[\text{CH}_3\text{O}^-]$ in CH_3OH at 0°C .
Table adapted from ref. 30.

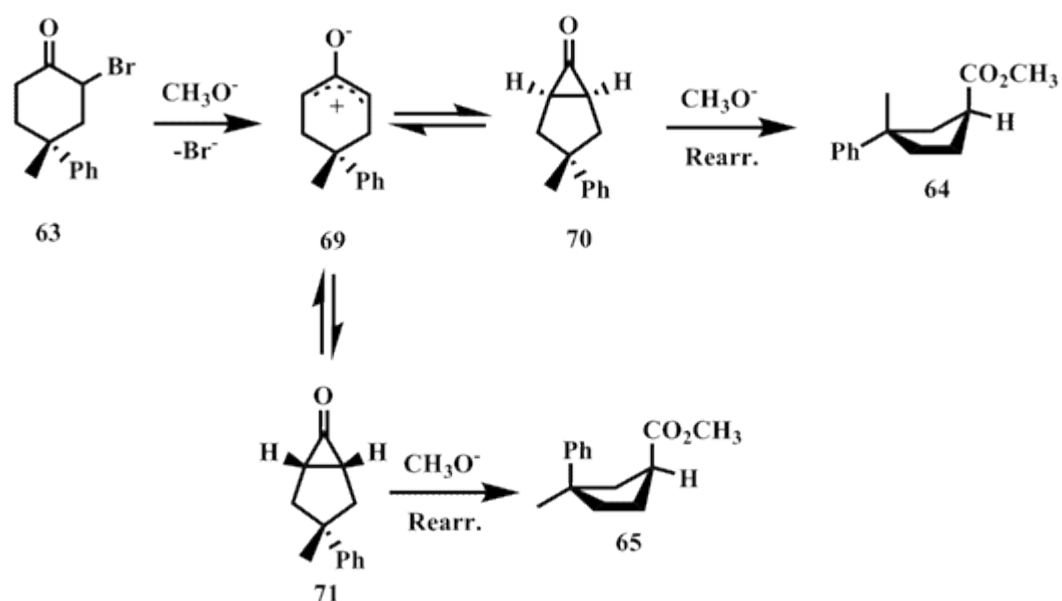
Substituent	$[\text{NaOCH}_3]$, M^a	% ester	% hydroxyketal
63	$\sim 10^{-5}$	40 (1:3, 64:65)	36
	2	55 ^a	37
66	0.05	9 (57:6:14:23, 64:65:67:68)	ND ^b
	1	22 ^a	ND
	2	69 (45:7:9:39, 64:65:67:68)	ND

^aProduct ratio not provided. ^bPercentage not given.

For both precursors, a pronounced increase in Favorskii ester yield was seen to accompany concentrated base solutions, a common occurrence for several α -haloketones previously encountered. The relatively enhanced ester yields for **63** vs. **66** was evidence for a 1,3-diaxial effect, specifically in impeding the halide from adopting the axial position, a favored orientation for epoxyether (α -methoxyketone precursor) formation. This effect was not revealed for **66**. When the reaction of **63** was conducted at low $[\text{CH}_3\text{O}^-]$, a 40% ester yield was obtained with relative *inverse* ratios of 1:3 for **64** and **65**. Reactions of **66** (either isomers) afforded **64**, **65**, and two other esters **67** and **68** with relative ratios of 57:6:14:23, respectively, in 0.05 M CH_3O^- in methanol, that changed to 45:7:9:39 for **64**, **65**, **67**, and **68**, respectively, in 2 M $[\text{CH}_3\text{O}^-]$ in methanol, and 26:24:28:22, respectively, when equilibrated (>150 h reflux). It appeared that greater base concentrations fostered the formation of **68** over **64**. It was postulated that for **63**, an internal $\text{S}_{\text{N}}2$ reaction (Lofffield's mechanism¹³) would educe an inverted product if the halide was equatorial and retention if axial. The principal ester for **63** was found to be **64**, advancing the notion that retention had occurred (presumed disjunction of an axial halide). This is not manifested with **66** (*cis*), where **65** would have been anticipated to be major product according to Lofffield's mechanism, but, in fact, demonstrated a preponderance of **64**. The uniform product distribution for *cis/trans* **66** denoted that an epimerization at the halide locus may have been operative. To furnish an $\text{S}_{\text{N}}2$ reaction, *cis/trans* **66** would have to first equilibrate and then generate the ester via the equatorial halide; an inversion step required an equatorial halide orientation for **66**. Consequently,

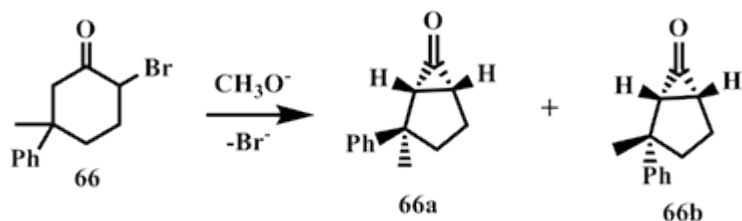
Bordwell proposed that the dipolar ion intermediate was a feasible precursor to the Favorskii ester (Scheme 20). Upon the formation of the dipolar ion, **69**, a *disrotatory* ring closure was effected, producing cyclopropanones **70** and **71**. The stereochemistry

Scheme 20. Bordwell's suggested reaction pathways of **63** to diastereomers **64** and **65** in CH_3O^- , directed by the oxyallyl intermediate (**69**).



of the products was decided following halide detachment, which adequately justified the product distributions above. Low $[\text{CH}_3\text{O}^-]$ advanced the formation of **65** over **64** but the converse at 2 M concentration. Bordwell speculated that this phenomenon was due to the more rapid formation of **71** over **70**; low concentrations of CH_3O^- permitted equilibrium to be achieved between the two cyclopropanone intermediates. The product ratios were, thus, controlled by the equilibrium position and rate

constants of reactions of cyclopropanone or corresponding hemi methylketal with CH_3O^- . The product distributions were directed by the rates in which **70** and **71** were produced. The formation of 4 esters from cis/trans **66** was reasoned to occur from two cyclopropanone intermediates, **66a** and **66b** (Equation 3), each of which reacted

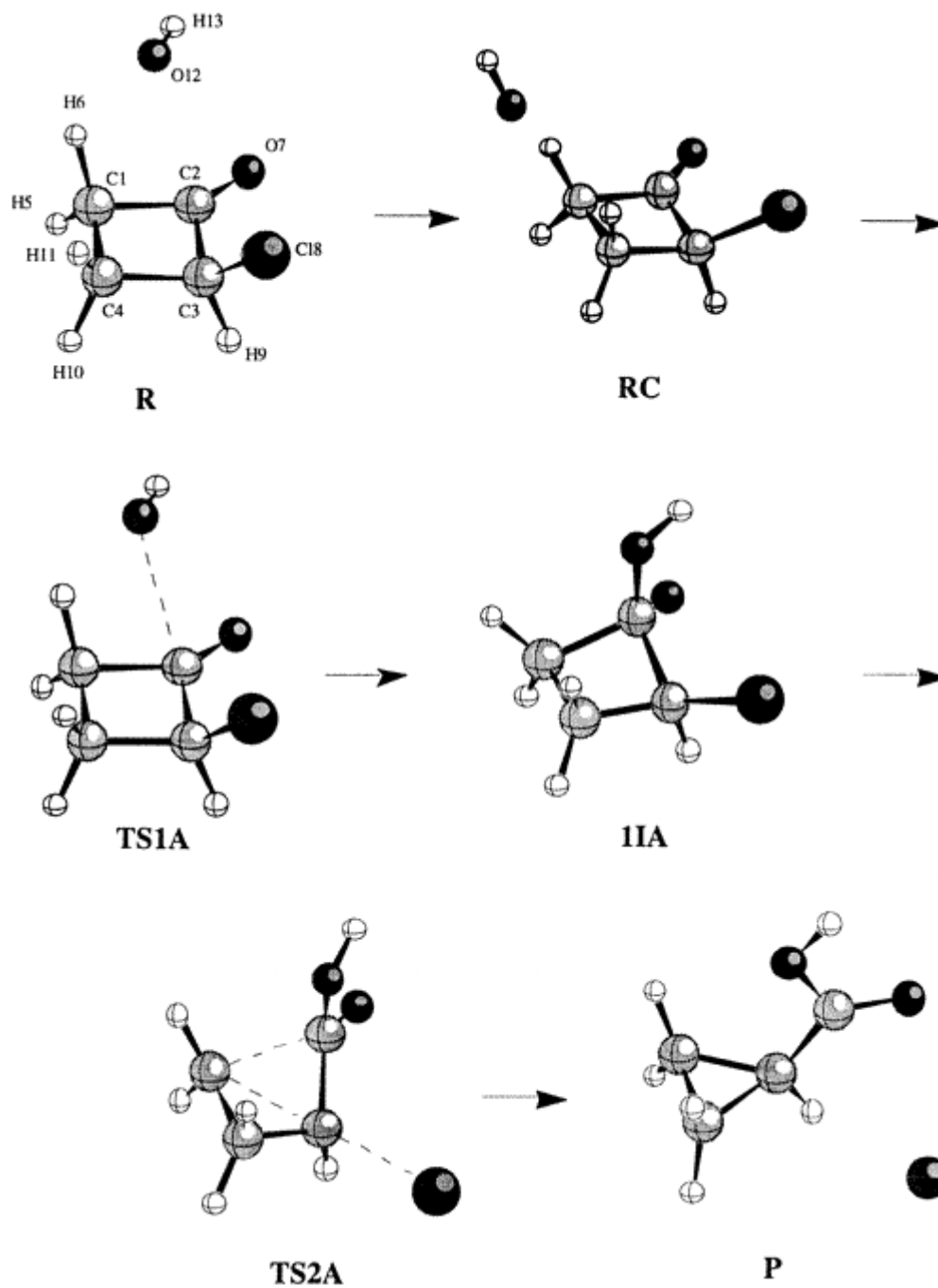


Eq. 3

with CH_3O^- in CH_3OH to bear two products; a) **66a**, which manifested the phenyl and carbonyl groups trans to each other, reacted with CH_3O^- to produce **64** and **67** and b) **66b**, which engendered **65** and **68** under the same conditions. Increasing the $[\text{CH}_3\text{O}^-]$ from 0.05 M to 2.0 M seemingly improved the yields of **66b** over **66a**, since the ratios of **65** and **68** to **64** and **67** increased. A similar explication as for the product ratios from **63** was advanced, i.e., a zwitterion intermediate first formed that underwent disrotatory ring closure in two modes to make the two cyclopropanones. In the end, however, Bordwell conceded that *further studies were required* to better comprehend the stereochemical inversions and retentions that were exhibited by the product distributions.

III. Computational Investigations. Andres⁴⁵ and coworkers recently communicated results from extensive computational investigations using *ab initio* calculations at the Hartree-Fock level of theory with 6-31G* and 6+31G* basis sets and electron correlations at the MP2/6-31G* level based DFT, BLYP/6-31G* of the Favorskii reaction mechanism. Hydroxide ion (HO⁻) mediated rearrangement of α -chlorocyclobutane to cyclopropanecarboxylic acid was utilized as a model system. Two mechanisms were accentuated in the investigations; 1) the signature Favorskii route with cyclopropanone intermediate and 2) semibenzilic path, which has been coined the “quasi”-Favorskii reaction and will be elaborated on later, in the gas and aqueous phase. For each mechanism, a series of *reactant complexes (RC)*, *transition states (TS)*, *intermediates (I)*, and *corresponding precursor (R)* and *product (P)* entities were determined along with relative energies. These were termed *stationary points*. The semibenzilic acid route showed 6 stationary points (Scheme 21).

Scheme 21. The proposed semibenzilic mechanism of conversion of α -chlorocyclobutanone to cyclopropane carboxylic acid through calculated stationary points. Reproduced with permission from the ACS, ref. 45.



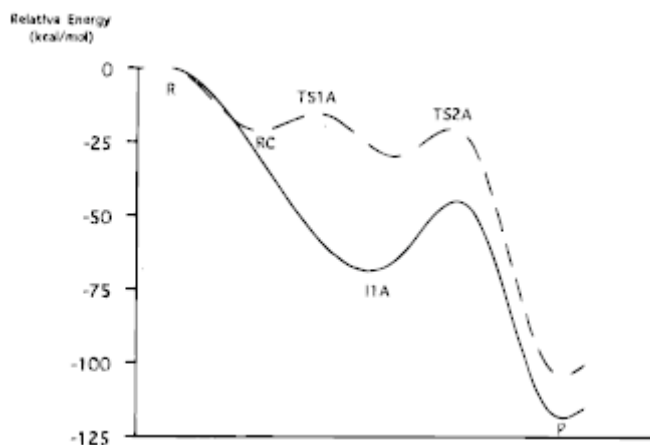
The relative energies for stationary points corresponding to the semibenzilic acid rearrangement are tabulated for gas and aqueous phases in Table 9.

Table 9. Relative energies (kcal/mol) of stationary points associated with the semibenzilic rearrangement mechanism, in the gas and aqueous phases, as determined by various computational methods. ND, not determined. Table adapted from ref. 45.

	HF/6-31G*	HF/6+31G*	MP2/6-31G*	BLYP/6-31G*
		Gas Phase		
R	0.00	0.00	0.00	0.00
RC	ND	-19.07	-36.57	-54.21
TS1A	ND	-17.58	-33.90	-45.56
I1A	-63.97	-44.86	-73.70	-75.22
TS2A	-48.55	-27.21	-62.56	-73.21
P	-115.46	-94.03	-107.07	-109.58
		Aqueous Phase		
R	0.00	ND	ND	ND
RC	-20.74	ND	ND	ND
TS1A	-15.59	ND	ND	ND
I1A	-29.60	ND	ND	ND
TS2A	-26.56	ND	ND	ND
P	-100.55	ND	ND	ND

In the gas phase, nucleophilic approach by HO⁻ was calculated to be, for the most part, barrierless; the initial interaction was manifest by strong hydrogen bonding between the anionic HO⁻ and α -hydrogen atoms to the carbonyl, leading to a stabilized **RC** complex. The **RC** complex was thought to ready HO⁻ for nucleophilic attack on the carbonyl, in assembling the intermediate **IA**, through a transition state, **TS1A**; the energy barrier to **IA** ranged from 1.5 (HF/6-31G*) to 8.6 (BLYP/6-31G*) kcal/mol; this approach was calculated to occur on the very flat region of a potential energy surface, PES, exhibited in Figure 2.

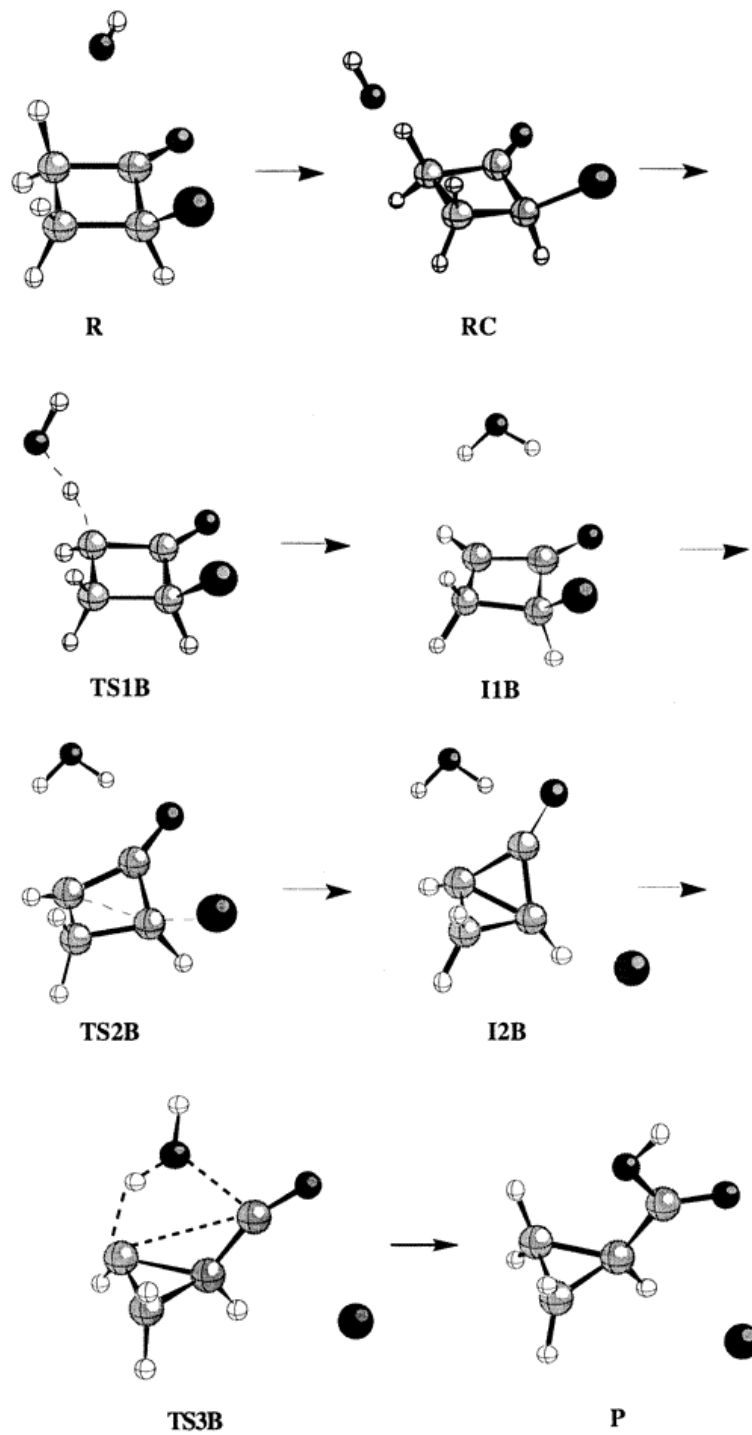
Figure 2. A potential energy illustration of the semibenzilic rearrangement process, revealing relative energies (in kcal/mol) of stationary points on the reactive surface that were calculated at the HF/6-31G* level. The broken line indicates the aqueous phase; the bold line, gas phase. Reproduced by permission of the ACS, ref. 45.



The rearrangement step (**TS2A**) displayed a diverse range of activation energies, 17.6 kcal/mol (HF/6+31G*) to 2.0 kcal/mol (BLYP/6-31G*); this was the obvious rate determining step for the reaction, as collectively, these energies were higher than those calculated for **TS1A**..

In an aqueous environment, the PES was quite disparate from the gas phase for the semibenzilic acid rearrangement. Reliable relative energies originated only from HF/6-31G* level computations. The rate determining step changes to **TS1A** (recall that it was **TS2A** in the gas phase from HF/6+31G* and MP2/6-31G* calculations) by nucleophilic attack by HO⁻ at the carbonyl; the activation barrier for this was 5.1 kcal/mol. An extensive solvation of HO⁻ by water was designated as the primary source of this observation and further impacted the relative energies of **IIA**

Scheme 22. The Favorskii rearrangement mechanism of α -chlorocyclobutanone to cyclopropane carboxylic acid through calculated stationary points. Reproduced with permission from the ACS, ref. 45.



and **TS2A** that were destabilized 34.4 and 22.0 kcal/mol, respectively. An additional solvation effect was manifest on the energy barrier for the rearrangement (**TS2A**) step, which dropped from 15.4 kcal/mol in the gas phase to 3.0 kcal/mol in solution.

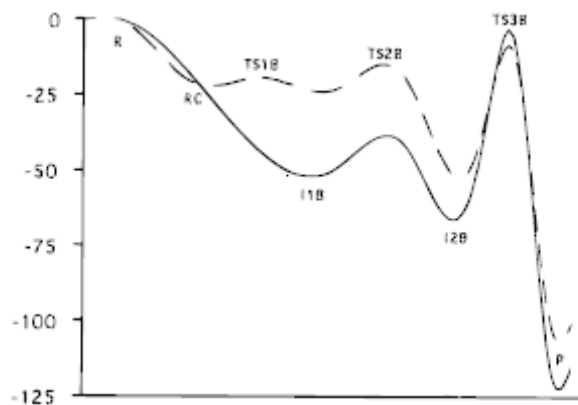
A total of 8 stationary points were determined for the Favorskii rearrangement mechanism (Scheme 22). The relative energies for associated stationary points in the gas and aqueous phases are presented in Table 10.

Table 10. Relative energies (kcal/mol) of stationary points associated with the cyclopropanone rearrangement mechanism in the gas and aqueous phases, as determined by the connoted computational methods. ND, not determined. Table adapted from ref. 45.

	HF/6-31G*	HF/6+31G*	MP2/6-31G*	BLYP/6-31G*
		Gas Phase		
R	0.00	0.00	0.00	0.00
RC	ND	-19.07	-36.57	-54.21
TS1B	ND	-15.46	-32.83	-45.66
I1B	-49.50	-31.28	-56.14	-64.35
TS2B	-42.17	-22.83	-50.05	-60.79
I2B	-47.68	-29.79	-45.49	-49.89
TS3B	-6.91	12.80	-9.18	-24.14
P	-115.15	-94.03	-107.07	-109.58
		Aqueous Phase		
R	0.00	ND	ND	ND
RC	-20.74	ND	ND	ND
TS1B	-19.36	ND	ND	ND
I1B	-23.14	ND	ND	ND
TS2B	-20.04	ND	ND	ND
I2B	-41.79	ND	ND	ND
TS3B	-11.63	ND	ND	ND
P	-100.55	ND	ND	ND

Akin to the semibenzilic mechanism, the **RC** was determined as the initial point of contact for HO⁻ and α -chlorobutanone in the gas phase. The activation barrier for proton abstraction (**TS1B**) ranged from 3.61 (HF/6+31G*) to 8.55 kcal/mol (BLYP/6-31G*), while that for the formation of cyclopropanone (**TS2B**) spanned from 3.56 (BLYP/6-31G*) to 8.45 (HF/6+31G*) kcal/mol. The rearrangement step through **TS3B** was established as the rate determining step in all methods of calculation; the energy barriers ranged from 42.59 (HF/6+31G*) to 25.77 (BLYP/6-31G*) kcal/mol. The cyclopropanation pathway for rearrangement in water manifested stationary point energies that were appreciably higher than in the gas phase, matching earlier observations for semibenzilic acid in water. A potential energy surface diagram denoting the cyclopropanone rearrangement route is provided in Figure 3.

Figure 3. A potential energy surface diagram of the cyclopropanone rearrangement mechanism, revealing relative energies (in kcal/mol) of stationary points on the reactive surface that were calculated at the HF/6-31G* level. The broken line indicates the aqueous phase; the bold line, gas phase. Reproduced with permission by the ACS, ref. 45.

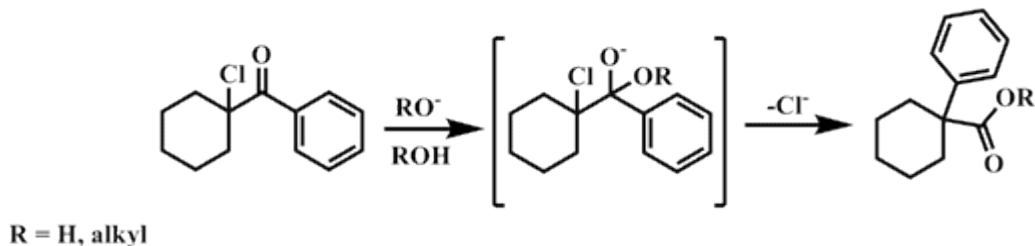


Similar to the semibenzilic mechanism above, a change in curvature of the incipient reaction steps inferred pronounced, solvation-incited encumbering effects on the reactivity of HO⁻. A very low energy barrier (**TS1B**, 1.4 kcal/mol) to forming the enolate intermediate **I1B** was manifested. The ensuing conversion to cyclopropanone through **TS2B** disclosed an energy barrier of 3.1 kcal/mol, a decline from the gas phase that was 7.2 kcal/mol. Lastly, the rearranging, rate determining step through **TS3B**, showed an energy barrier of 30.2 kcal/mol (**I2B**); this represented a steep drop compared to 40.8 kcal/mol in the gas phase. The exothermicity of the reaction was reduced by 15 kcal/mol compared to the gas phase. Akin to results for the semibenzilic mechanism, a general solvent influence on the cyclopropanone mechanism was to lower the activation barriers to intermediates and the corresponding product; this phenomenon was particularly noticeable on the PES (Figure 3). The semibenzilic mechanism appeared to be the most favored pathway to the Favorskii acid in either phase, by virtue of the drastically reduced energy barriers of rate determining steps to rearranged product. However, the inherently large *ring strain* of cyclobutanones, though not considered in the report, would be anticipated to play a substantial role in directing the preferred reactivity through the semibenzilic mechanism which requires fewer steps to the rearranged product.

IV. Variations to the classical Favorskii Reaction.

As alluded to earlier, several variations of the Favorskii reaction have been recognized and implemented in the realm of synthesis: 1) Non-enolizable ketones

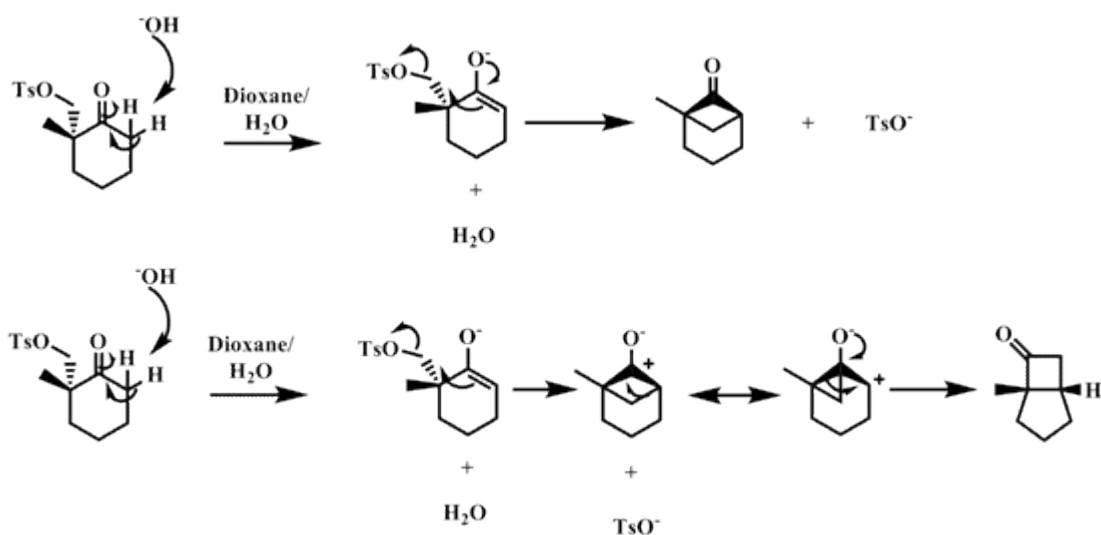
can undergo rearrangements to acids/esters in what is termed the “quasi-Favorskii” reaction⁴⁶ (Equation 4), this likened to a semibenzilic acid type of rearrangement. The primary distinction from the classical Favorskii is that no enolate or cyclopropanone intermediates are formed in the reaction course. 2) Ketones with γ -nucleofuges



Eq. 4

can undergo base-moderated rearrangements, the “homo-Favorskii” reaction⁴⁷ (Scheme 23), to produce cyclobutanones, which, being more robust than cyclopropanone homologs, are isolable.³

Scheme 23. Proposed mechanism of the homo-Favorskii reaction.

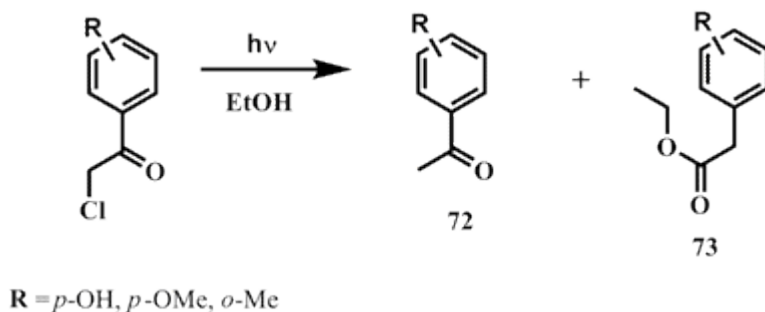


In general, reactions involving the formation of acids/esters from base facilitated rearrangements of α -nucleofuge substituted ketones can be considered the “Favorskii” sort. Up to this point, the focus has been on the ground state Favorskii reaction. The excited state complement is now presented.

V. The Photochemical Version of the Favorskii Rearrangement.

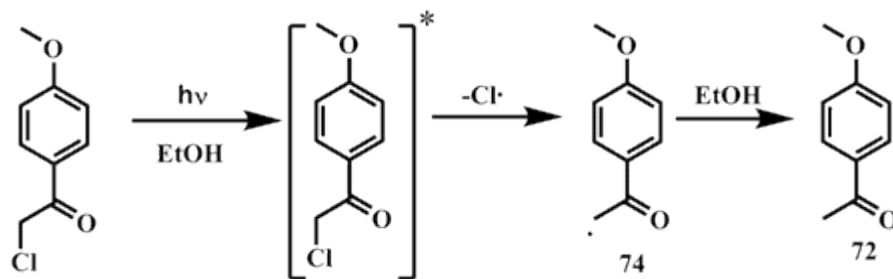
A more obscure, lesser known reaction involving rearrangements of α -substituted ketones to effect acids/esters in the excited state, the “Photo-Favorskii”, has, comparatively, received little attention.¹⁰ The earliest report of photolyses involving α -haloketones, practical antecedents for these types of rearrangements, was by Strachan et. al.,⁴⁸ where chloroacetone was irradiated either neat or in non-hydroxylic solvents at 313 nm. Although a curious array of photoproducts was conveyed, including acetone, no rearrangements were demonstrated. However, the formation of acetone as a principal photoproduct intimated homolytic C-Cl bond scission and thus radical transients, which have been posited as viable precursors to Favorskii products. Though not broached in this report, it can be surmised that the excited state pathway for chloroacetone photolysis to photoproducts was through the triplet, as acetone is known to intersystem cross with an efficiency of near unity.⁴⁹ Multiplicities will become a prominent interest later in this thesis. The seminal publication for the photo-Favorskii reaction was by Anderson and Reese⁵⁰ almost 50 years ago and involved UV irradiation of 1% α -chloroacetophenone derivatives in ethanol over a 1-2 hour time span. With certain substituents ($R = p\text{-OH}$, $p\text{-OCH}_3$, and

o-OMe) two major products, acetophenone (**72**) and ethyl 2-phenylacetate (**73**) were obtained, the latter in abundance (Equation 5).



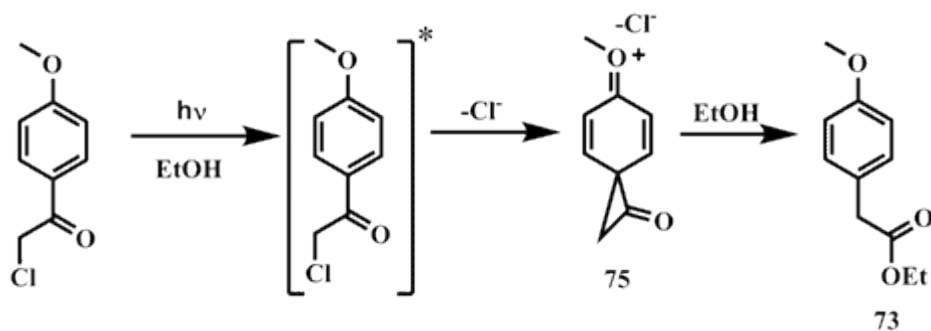
Eq. 5

The pathway to **72**, as depicted in Equation 5, was hypothesized to occur by the homolytic cleavage of the C-Cl bond, yielding an α -keto radical (**74**) which would then abstract a hydrogen atom from ethanol, effecting **72**. The provenience of this stemmed from the aforementioned Strachan⁴⁸ studies and is presented in Equation 6 with the *p*-OCH₃ derivative. To obtain **73**, the authors rationalized the intermediacy



Eq. 6

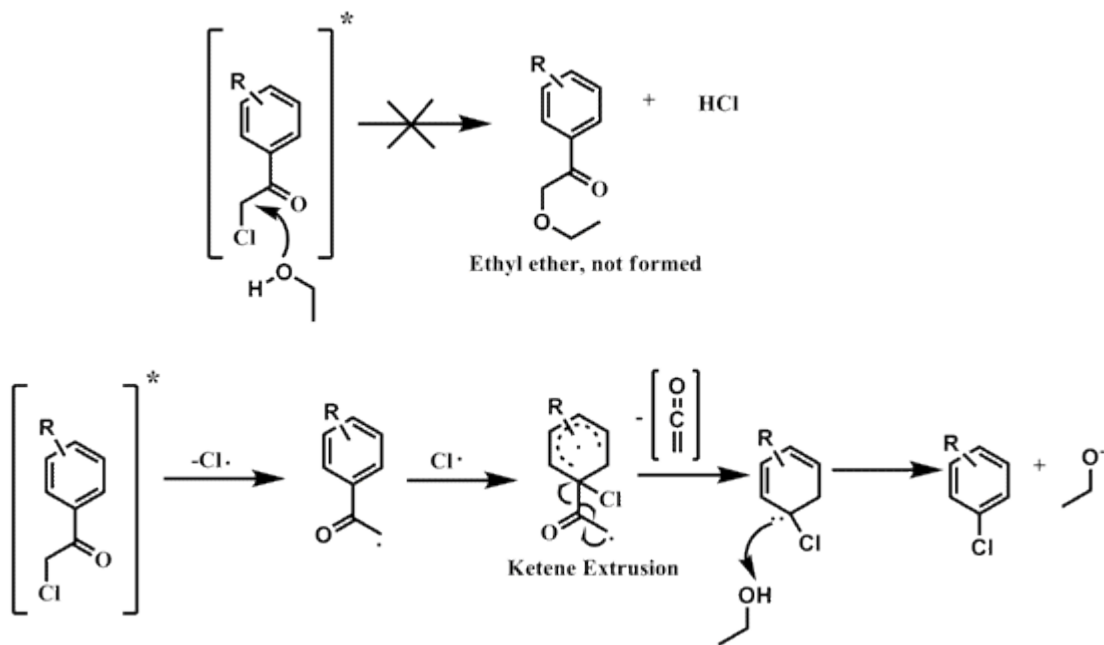
of a spiro-cyclopropanone (**75**), with subsequent attack by EtOH at the carbonyl and, lastly, a ring-opening, 1,2-aryl shift, affording **73** that effectively amounted to a Favorskii rearrangement (Equation 7). Other intermediates were proposed, but no mechanistic explorations were related nor appeared subsequently in the literature. A



Eq. 7

potential ethyl ether substituent product, envisaged by the attack of EtOH at the methylene locus with concomitant chloride disjunction, was not reported, though precursor decay, presumably through ketene extrusion to chlorobenzene was formed as a minor product (Scheme 24).

Scheme 24. Posited mechanism to account for the formation of chlorobenzene from α -chloroacetophenone derivatives.

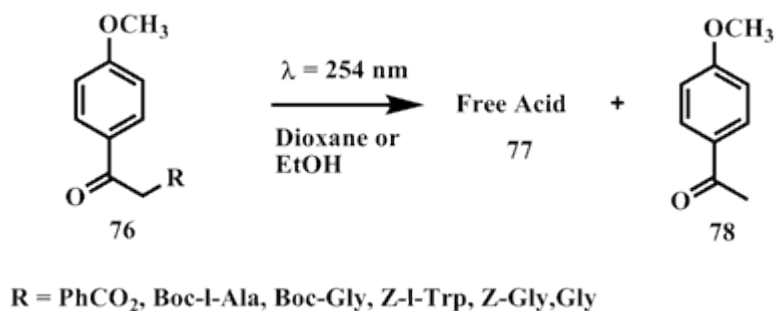


The electronic and positional influences of several substituents were discerned and are disclosed in Table 11. Strong electron donors, i.e., *p*-OH, *o*-OMe, *p*-OMe evinced the highest yields of Favorskii rearrangement product (**73**) while moderate donating (-Cl, -Me), generated none, except for, curiously *o*-Me (4%). In addition, electron withdrawing moieties (-CO₂Me) failed to reveal **73**.

Table 11. Substituent effects on the photoproduct distributions from photolysis of substituted α -chloroacetophenones in ethanol, irradiated at 300 nm for 1-2 h. Table adapted from ref. 50.

Substituent (X)	%Yield, acetophenone, 72	%Yield, ethyl phenylacetate, 73
<i>p</i> -OH	26	32
<i>p</i> -OMe	30	32
<i>o</i> -OH	3	0
<i>o</i> -OMe	16	32
<i>o</i> -Me	58	4
H	53	0
<i>p</i> -CO ₂ Me	48	0
<i>p</i> -Cl	55	0
<i>o</i> -Cl	45	0
<i>m</i> -OMe	15	0

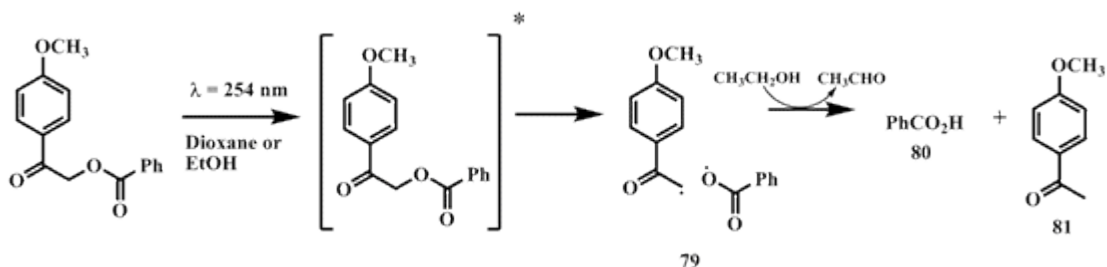
Since this seminal report, a paucity of research has been reported regarding the photo-Favorskii reaction. Sheehan⁵¹ investigated the use of the *p*-methoxyphenacyl chromophore as a phototrigger for carboxylic acids. This entity had previously been shown by Anderson and Reese to be a precursor for rearranged products and substrate release after irradiation (Equation 8). However, after irradiation at 254 nm in 1,4-dioxane or ethanol for 5-17 h, they reported that **76** was converted to free acid (**77**) and *p*-methoxyacetophenone (**78**).



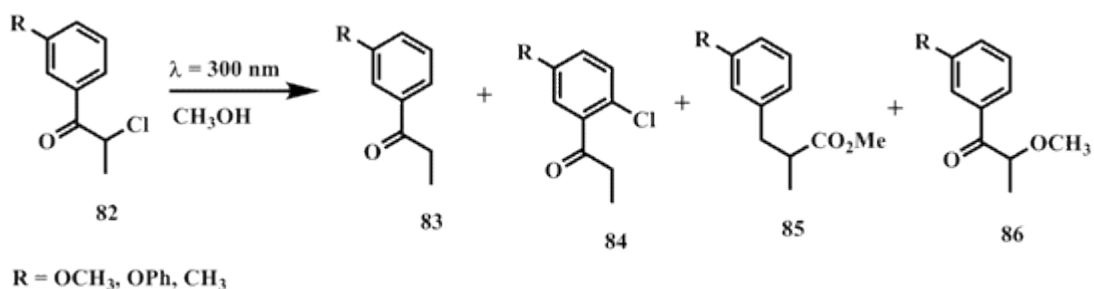
Eq. 8

The theorized mechanism to explain the formation of photoproducts (Scheme 25) is in accord with those previously addressed,^{48,50} where upon irradiation, C-O bond

Scheme 25. Posited mechanism of benzoic acid release from the *p*-methoxyacetophenone chromophore.



homolysis occurs producing geminate radicals **79** that are posited to readily abstract H atoms from the solvent, yielding primary photoproducts **80** and **81** and products from solvent oxidation (e.g. acetaldehyde). Unlike Anderson and Reese's earlier results, no Favorskii rearrangement esters were reported. The disparate results suggested a nucleofuge effect, but this premise was not further substantiated. Sonawane⁵² et. al., recognized the versatility of this method in the practical synthesis of useful phenylacetic acids. An early report concentrated on the nature and position of the substituent on the chromophore in determining photolysis products of α -chloropropiophenone derivatives (Equation 9).⁵³



Eq. 9

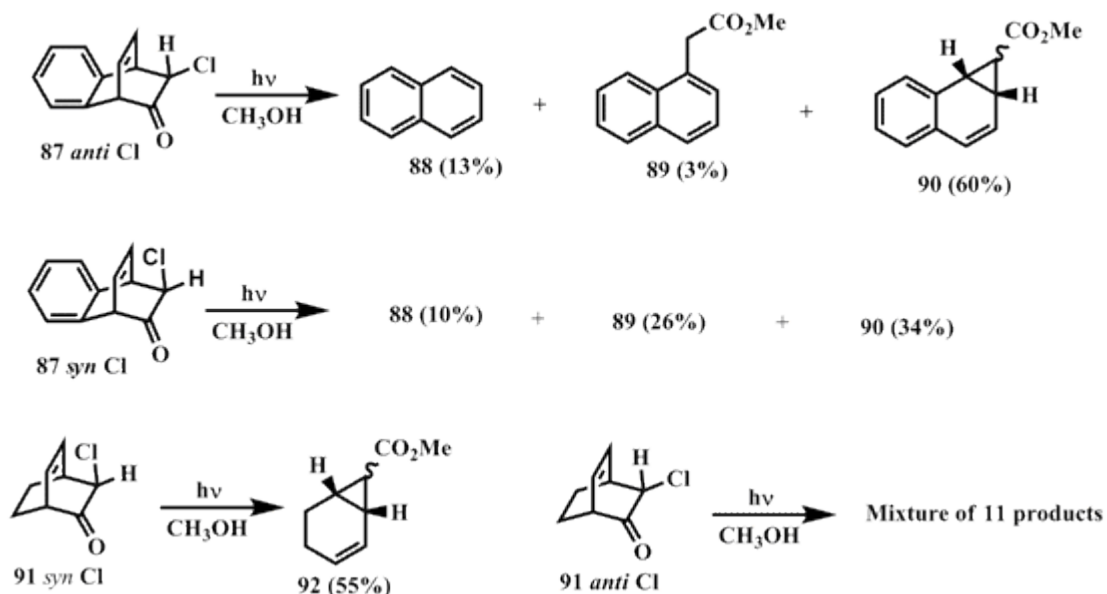
The principal photoproducts generated from 300 nm irradiation of a 3% solution of **82** in degassed methanol for 6 h were propiophenone (**83**) the *o*-chloropropiophenone, (**84**) the Favorskii ester (**85**) and the methylether (**86**). It was revealed that the substituent locus and electronic characteristics profoundly affected the product ratios (Table 12). Notably, both *p* and *m*-methyl derivatives of **82c** (methyl as a mild electron donor) produced **85** as the primary product while the *p*-OCH₃ (stronger electron donor) **82a** and *m*-OCH₃ (electron withdrawing) each afforded an exiguous amount of **85**, the latter consistent with the previous findings of Anderson and Reese.

Table 12. Photoproduct % compositions from photolysis of 3% solutions of **82a-d** in degassed CH₃OH. Table adapted from ref. 53.

Compound	R	Product Compositions, %			
		83	84	85	86
82a	(<i>m</i> -OCH ₃)	13	68	0	19
	(<i>p</i> -OCH ₃)	12	0	8	70
82b	(<i>m</i> -OPh)	70	21	8	0
82c	(<i>m</i> -CH ₃)	33	0	66	0
	(<i>p</i> -CH ₃)	8	0	76	0
82d	(<i>m</i> -NO ₂)	100	0	0	0

Since the late 1960's, Givens and coworkers⁵⁴ have gained considerable insight by studying photo-induced extrusion and rearrangement reactions, though those amenable to the photo-Favorskii rearrangement are the most recent among their studies. Early studies⁵⁵ were aimed at comprehending stereoelectronic effects, i.e., the role of the nucleofuge (e.g., halogen, carboxylate, phosphate, and others) in determining the outcomes of photolyses of α -substituted chromophores, such as isomers of 2-chloro bicyclo[2.2.2.]octanone (Scheme 26). These were not tailored

Scheme 26. Product compositions from photolysis of corresponding α -chloroketones.



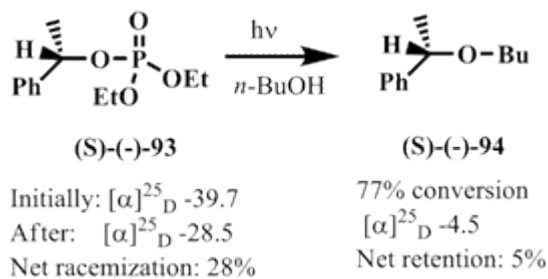
specifically to investigate the photo-Favorskii rearrangement, that is, products derived from 1,2 migrations or cyclopropanone/oxyallyl intermediates. Nevertheless, a

detailed understanding of the rearrangement process that afforded esters, acids, or amides provided a stimulus for future endeavors with the ‘less-than-familiar’ Favorskii rearrangement. Photolysis of *syn* and *anti* 2-chlorobenzobicyclo[2.2.2]octadien-3-one isomers of **87** in methanol was shown to generate esters **89** and **90**, though in dissimilar ratios. The compound *syn*-2-Chlorobicyclo[2.2.2]octenone, **91**, produced the ester **92** as the major photoproduct, while from corresponding *anti*-**91** isomer emerged a complex assortment of products. Rearrangements had occurred to produce esters, though a Favorskii-like, 1,2-aryl migration was not discerned in these systems. Additionally, a salient impact of the chloride orientation was demonstrably a determinant in the product compositions. It was assumed that the initial step in these reactions involved carbon-chloride bond scission,⁴⁸ though whether through homolysis⁵⁶ that would engender a geminate radical pair, or heterolysis⁵⁰ to form chloride ion and an α -carbenium ion was speculative. A number of plausible radical and ionic intermediates were surmised and, ultimately, through sets of supplementary experiments, a conflation of radical/ion attributes for the intermediates was proposed to account for product distributions.⁵⁷ The singlet was determined to be the reactive excited state in these reactions. Experiments involving triplet quenching with piperylene failed to divulge any vicissitudes in product yields and those involving triplet sensitization with acetophenone manifested marked declines in quantum yields, 0.03 for **87** (*anti* Cl) and 0.09 **87** (*syn* Cl), than those from direct irradiation, 0.35 and 0.32, respectively.

The use of benzoin (desyl) as an α -keto phototrigger, originally established by Sheehan and Wilson⁵⁸ for caging phosphates,^{59,60} was explored principally for its longer wavelength absorption ($\lambda_{\text{max}} > 350$ nm), efficacious quantum yields ($\Phi > 0.28$) for substrate release or “decaging”, and trenchant photochemistry; the primary photoproducts were the released substrate and benzofuran, derived from an internal benzoin photocyclization.

Despite its obvious utility as a phototrigger, the mechanism for substrate release and cyclization doesn't abide by a “Favorskii-like” process, i.e., no cyclopropane intermediates nor 1,2-migrations were borne and would not warrant further discussion except for one salient feature. The triplet state preponderated and as such a plausible *α -keto carbocation intermediate*⁶¹ appeared to be viable to product formation; a similar *α -keto carbocation intermediate* is thought to be a possible precursor to the cyclopropanone intermediate in the Favorskii rearrangement. Independent studies^{55,62} reported a Hammett correlation of $\rho = -0.9$ vs. σ , imputing positive charge buildup (carbocation character) in the transition state. Indirect evidence for an α -aryl carbocation intermediate was obtained by Givens and Matuszewski⁵⁹ through ¹⁸O labeling experiments with corresponding arylmethyl phosphate esters. These studies disclosed that expeditive oxygen exchange between benzylic and phosphoryl units had occurred by, presumably, an ion-pair species. The same report⁵⁹ revealed an observed photostereoisomerization of (S)-(-)-**93** in *n*-butanol, shown in Equation 10, that competed with the substitution reaction to

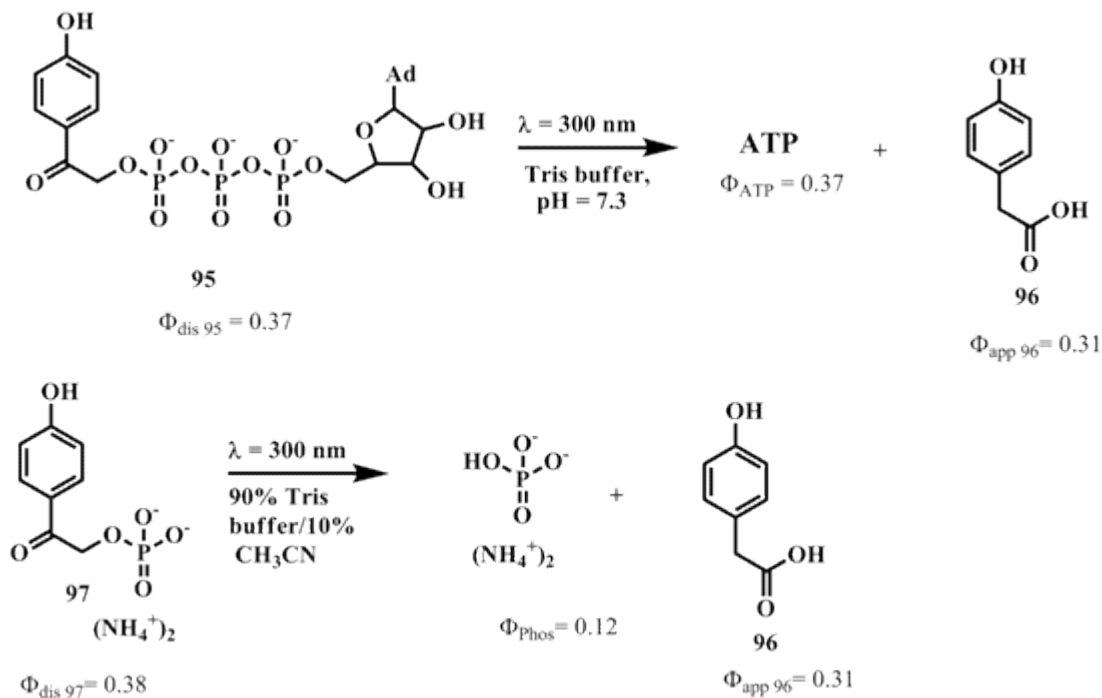
produce (S)-(-)-**94**, which itself was formed with a slight, net retention; the phenomenon strongly suggested the intermediacy of ion-pairs.



Eq. 10

Givens' seminal photo-Favorskii report⁶³ concerned the *p*-hydroxyphenylacyl chromophore as a cage for ATP (pHP ATP, **95**) and for inorganic phosphate (pHP phosphate, **97**) (Scheme 27). Photolysis of **95** and **97** at 300 nm in Tris buffer efficiently produced ATP and inorganic phosphate, $\Phi_{\text{app1}} = 0.37$ and $\Phi_{\text{app3}} = 0.12$, respectively, as well as the rearranged (Favorskii) *p*-hydroxyphenylacetic acid (**97**, $\Phi_{\text{app2}} = 0.31$). The process was shown to originate from the triplet surface by studies on the Stern-Volmer (S-V) quenching using 2-naphthalenesulfonate by the decline in Φ_{dis} as the concentration of 2-naphthalenesulfonate was increased. The slope of the resulting linear dependence (K_{SV}) provided an indirect measure of the triplet lifetime and a rate constant for fragmentation, $k_{\text{obs}} = 6.0 \times 10^8 \text{ s}^{-1}$.

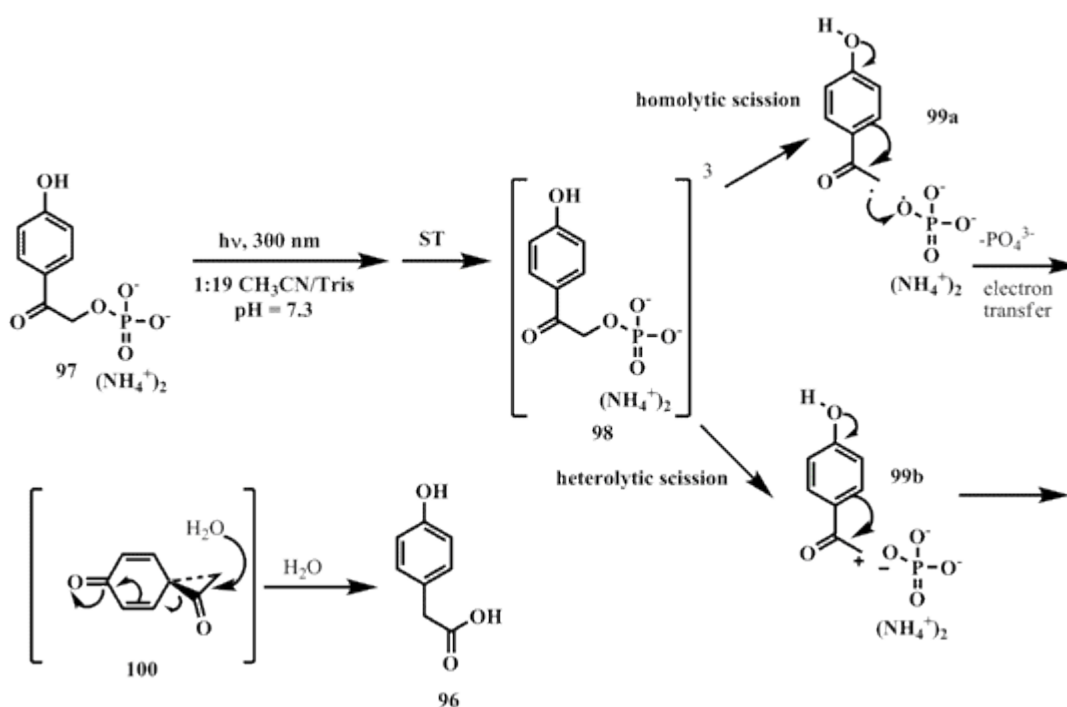
Scheme 27. Results from photolysis of pHP ATP and pHP diethyl phosphate in aqueous media. The quantum yields for these processes are included.



Unlike unsubstituted or *m*-substituted phenacyl esters studied by Anderson and Reese⁵⁰ and Givens⁶⁴ which primarily generated reduced acetophenones or radical-based products upon photolysis in aqueous media, *p*-hydroxyphenylacetate esters and acids (**96**) were the predominant products of photolysis of *p*-hydroxyphenacyl cages. The putative mechanism (Scheme 28) was derived from several consonant studies^{65,66} involving photo-induced solvolyses of benzhydryl chlorides, and involved a sequence beginning with prompt intersystem crossing to the triplet (**98**) followed by homolytic or heterolytic bond scission to generate geminate radical (**99a**) or ion pairs (**99b**). For the reduced pair, a neighboring group assisted,

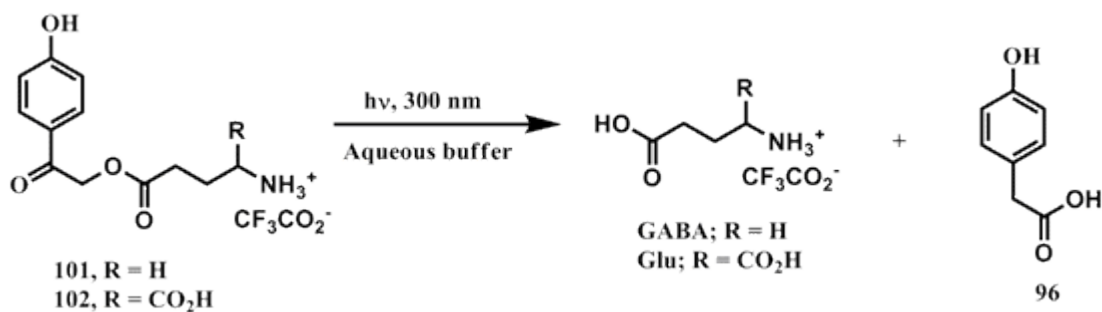
electron transfer was a possible supervening step before or after the Favorskii dienedione (**100**) and release of inorganic phosphate. These discrepancies were the subject of extensive investigations by Givens, Wirz, Wan and Corrie, Phillips and others and will be a major theme of the study reported here.

Scheme 28. Proposed mechanism for phosphate release from the pHP chromophore.



Lastly, solvent mediated cyclopropanone ring opening was proposed to occur to generate the Favorskii rearrangement product, *p*-hydroxyphenylacetic acid (**96**). The relatively high efficacy for photo-stimulated substrate release from the pHP chromophore with accompanying Favorskii rearrangement provided the thrust for Givens, et. al.,^{67,68,78} not only to investigate the utility of the reaction as an effective

phototrigger for biologically relevant substrates, but also to experiment with the design of better analogs and ultimately, to understand the mechanistic features of this reaction. A follow up report⁶⁷ concerned the photochemistry of pHP-caged neurotransmitters, γ -aminobutyric acid (GABA) and *l*-glutamate (Glu), as depicted in Equation 11. Photolysis of pHP GABA (**101**, $\Phi = 0.35$) or pHP Glu (**102**, $\Phi = 0.12$) in aqueous buffer at $\lambda = 300$ nm cleanly released the neurotransmitter with the rearranged **96**. Stability studies revealed that **101** and **102** resisted hydrolysis for



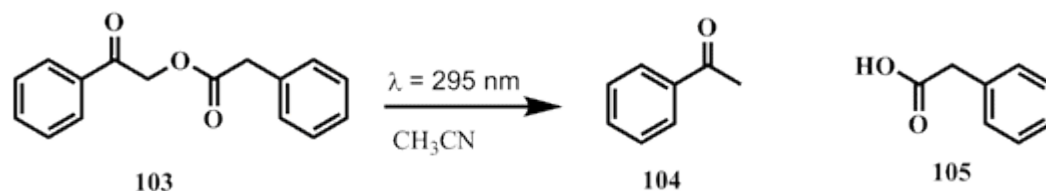
Eq. 11

more than 24 h when placed in aqueous media, an important feature for application as a phototrigger. The mechanism was posited to resemble that delineated in Scheme 27.

These findings served to expand the utility of pHP as a phototrigger for carboxylates as well as phosphates and unequivocally demonstrated an operative photo-Favorskii process, i.e., the discrete nucleofuge characteristics did not alter the photorelease pathway. This phenomenon, as will be demonstrated later, is

inconsistent for nucleofuges whose conjugate acids are weaker than phenols. Other biologically significant carboxylic acids such as the oligopeptide bradykinin⁶⁸ and the dipeptide (Al-Al)⁶⁸ were caged by pHP and demonstrated consistent release efficiencies through the photo-Favorskii route. In addition, pHP was shown to be an effective and precise delivery agent for Glu⁶⁷ and bradykinin⁶⁸ in biochemical neuronal function assays. These excitatory neurotransmitters evoke $[Ca^{2+}]$ increases in sensory neurons. This effect was probed by Ca^{2+} sensitive dyes, FURA-2⁶⁷ and indo-1,⁶⁸ that are loaded into the neurons prior to the assay. An enhancement in the fluorescence intensity of these dyes as a function of $[Ca^{2+}]$ indicates neurotransmitter action at the sensory neuron. Caged pHP bradykinin and Glu are silent in this regards, i.e., they effectuate no significant changes in $[Ca^{2+}]$ as demonstrated by no significant variations in the fluorescence intensity of the dye. However, upon irradiation, abrupt fluorescence from the dyes was observed, indicating the neuronal release of augmented $[Ca^{2+}]$ in response to the newly liberated bradykinin or *l*-glutamate.

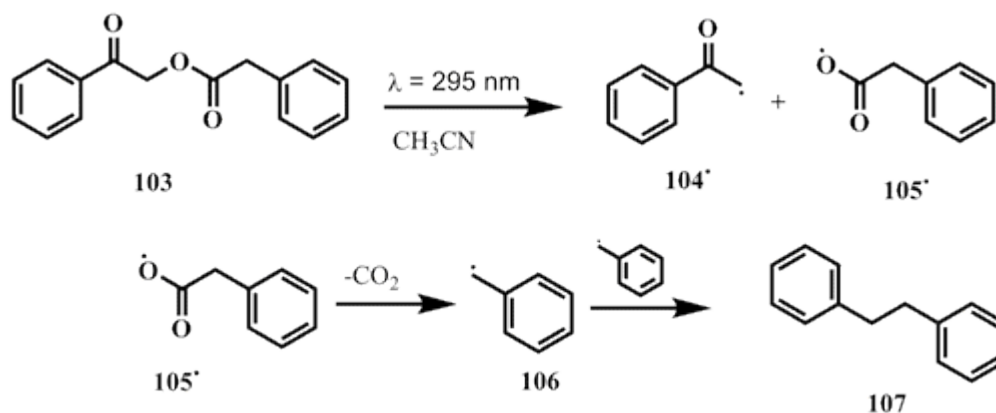
Falvey⁶⁹ was among the first to introduce an alternative photo-Favorskii mechanism to account for photosolvolysis products he observed when conducting LFP studies with phenacyl phenylacetate **103** in CH_3CN (Equation 12).



Eq. 12

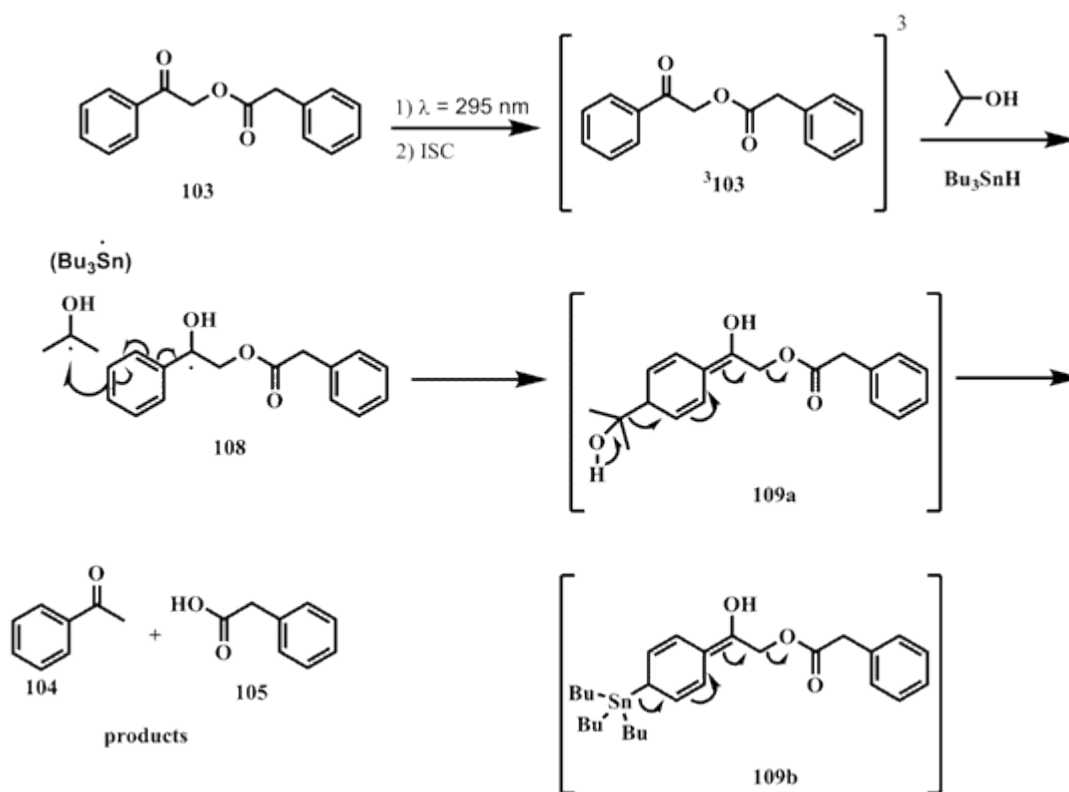
It was anticipated that if the presumed mechanism initiated with bond homolysis (Scheme 29) the phenylacetoxy radical (**105**) would rapidly decarboxylate to form the benzyl radical (**106**),⁷⁰ then dimerize to 1,2-diphenylethane (**107**). However, **107** was detected only in minute amounts (<0.5%) by HPLC analysis after photolysis.

Scheme 29. Radical pair mechanism for the formation of dibenzyl (**107**) from phenacyl caged phenylacetic acid.



Photolysis conditions for **103** were modulated with isopropanol, a H atom donor, or the H atom donor tributyltin hydride, each of which divulged markedly improved quantum yields for disappearance. A complex, hydrogen atom transfer 2-hydroxypropyl (or stannyl) radical addition mechanism was posited (Scheme 30).

Scheme 30. Hydrogen atom transfer mechanism for substrate release.



A transient absorption spectrum was obtained that indicated the presence of a triplet species ($^3\mathbf{103}$), which was further characterized by O_2 quenching and the likeness of the LFP absorption spectrum ($\lambda_{\text{max}} = 340 \text{ nm}$ with a lifetime $\tau = 5.5 \text{ ns}$) to acetophenone's known triplet ($\lambda = 330\text{-}350 \text{ nm}$, depending on solvent composition).⁷¹ It was hypothesized that the triplet state would abstract a hydrogen atom from isopropanol or tributyltin hydride to generate a ketyl radical transient ($\mathbf{108}$). Evidence for this came again from a transient absorption spectrum that exhibited a longer lived species with a $\lambda_{\text{max}} = 310 \text{ nm}$, corresponding nicely to known ketyl radicals obtained from other acetophenone derivatives.⁷¹ The triplet $\mathbf{108}$ was then

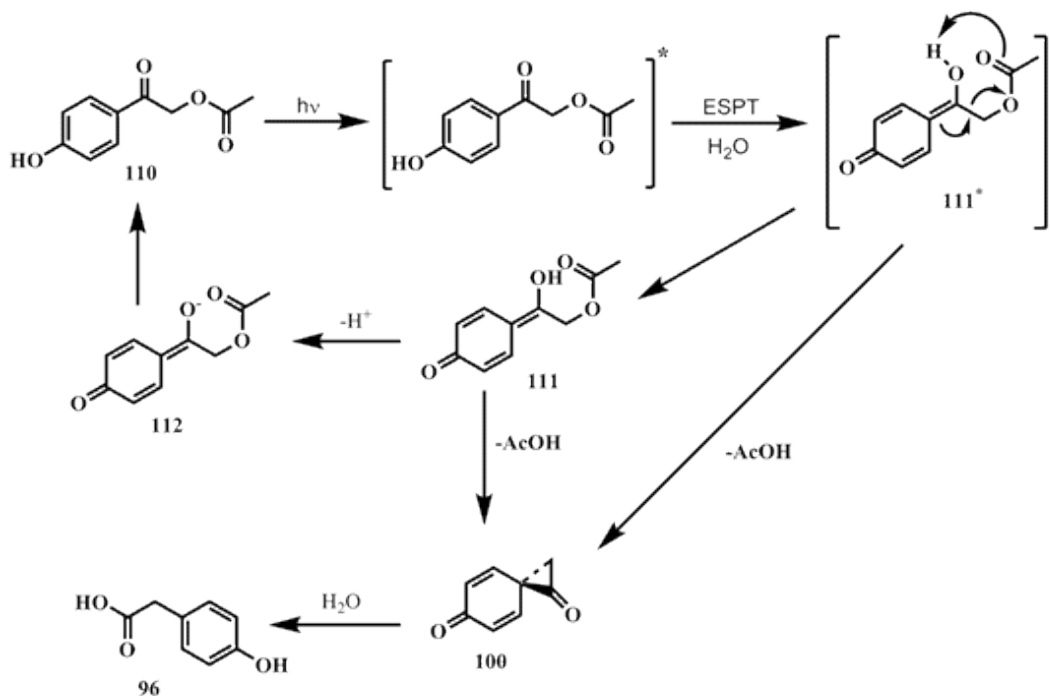
observed to decay to a transient with a lifetime, τ , of > 1 ms and a $\lambda_{\text{max}} \sim 330$ nm; this entity was tentatively assigned **109a** or **109b**, dependent on the H-atom source and termed a metastable, “light absorbing transient” (LAT).⁷² LAT promptly disintegrated to **104** and **105**. Favley’s experiments explicitly demonstrated the importance of hydrogen atom abstraction to initiate events leading to the formation of fragmentation products from α -substituted acetophenone derivatives.

Wan and Corrie⁷³ conducted a series of photolyses with the analogous *p*-methoxyphenylacyl chromophore, specifically gauging the photorelease of a series of carboxylic acids. A noteworthy discovery, however, was made in that no photolysis was seen to occur with *p*-methoxyphenyl acetate in 1:1 D₂O/CD₃CN after protracted irradiation times. Earlier studies carried out by Givens⁶² had shown that photosolvolysis of *p*-methoxyphenylacyl phosphate esters readily occurred after short irradiation times in mixed organic media. The nucleofuges (acetate and phosphate) were the only significant differences in these studies. It follows that the nucleofuge character seemed to have a significant impact on the photochemistry of *p*-methoxyphenyl derivatives, akin to Bordwell’s earlier findings with ground state reactions. Dissimilar to “photo-inertness” of the *p*-methoxyphenyl acetate, the *p*-hydroxy analog revealed a photosolvolysis and rearrangement to the *p*-hydroxyphenylacetic acid with a high efficiency in 1:1 H₂O/CH₃CN, $\Phi = 0.41$. The discrepancy in photolysis behavior asserts *the pertinence of the phenolic O-H* in photosolvolysis of these precursors. It was reasoned, then, that initial homolytic scission was obviated by the assumption that the excited state electronic differences

between the -OH and -OCH₃ moieties were negligible and hence would not be expected to evoke such drastic changes in the product distribution.

Wan and Corrie went on to suggest a singlet excited-state proton transfer (ESPT) mechanism to describe the photo-Favorskii rearrangement of pHP acetate (Scheme 31).

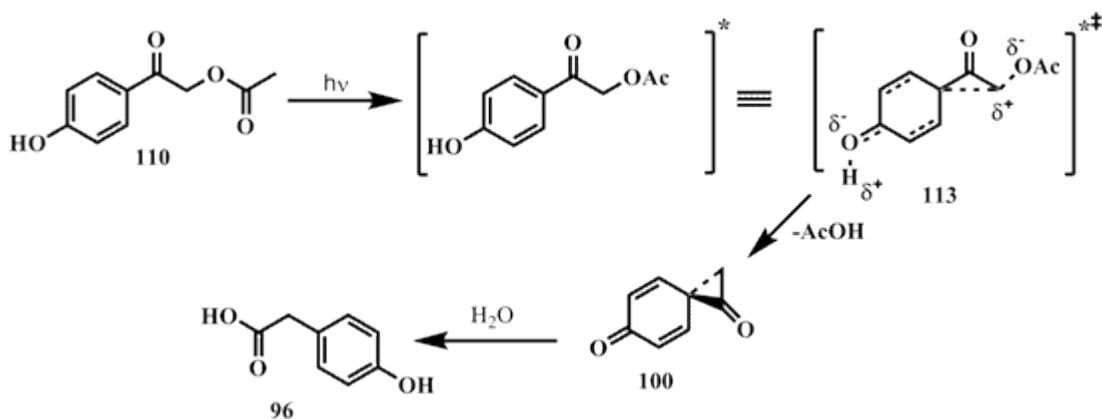
Scheme 31. Singlet excited state proton transfer mechanism for acetate release.



Cogent evidence for this mechanism was empirically derived and included: (1) Insignificant declines in the quantum yields for decay of **110** in 1:1 H₂O/CH₃CN in the presence of known triplet quenchers piperylene and sodium sorbate, signaling the

singlet state as the reactive excited state. These findings were in direct contradiction to the previously mentioned report by Givens,⁶³ where pHP ATP (**95**) imparted, unequivocally, a significant decline in Φ_{dis} in the presence of the triplet quencher, 2-naphthylsulfonate. (2) A singlet excited state correlation with solution pH ($\text{pK}(\text{S}_1) \sim 1$) and quantum yield for acetate formation, Φ_{p} , in 1:1 $\text{H}_2\text{O}/\text{CH}_3\text{CN}$ was observed for pHP acetate. This phenomenon was ascribed to ESPT based on consistencies with other $\text{pK}(\text{S}_1)$ studies.⁷⁴ (3) From laser flash photolysis studies, a strong absorption band appeared at $\lambda_{\text{max}} = 330$ nm that was not quenched by O_2 . Absorption decay profiles indicated two transients, one shorter lived (**112**, $k_{\text{d}} = 6.3 \times 10^6 \text{ s}^{-1}$)⁷⁵ and one longer (**111**, $k_{\text{d}} = 1.8 \times 10^5 \text{ s}^{-1}$)^{76,77} with similar λ_{max} values (~ 330 nm). When excited, **110** underwent rapid, adiabatic ESPT to generate **111**^{*}. This then abided two decay routes; one through solvent mediated deprotonation, restoring **110**, while the other decayed by intramolecular proton transfer and acetate dissociation to generate **100**, and subsequent solvolysis to **96**. One additional, concerted mechanism was proposed, which entailed phenol deprotonation coupled with acetate departure through transition state **113** directly to **96** (Scheme 32).

Scheme 32. Concerted mechanism for acetate release from pHP.

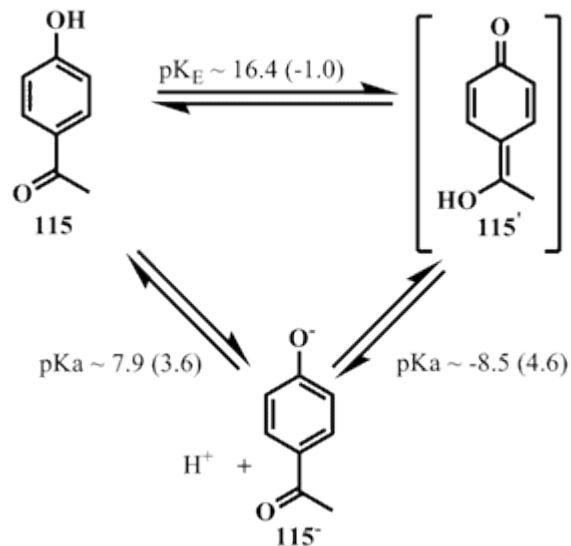


Results from a comprehensive study into the identification of triplet excited state transients of pHP diethylphosphate were communicated by Givens and Wirz,⁷⁸ employing both direct laser flash photolysis and indirect S-V quenching methods of analysis. Photolysis of *pHP diethyl phosphate* (**114**) in wet CH₃CN ($\geq 5\%$ water) disclosed only the production of **96**, contrasting the product mixture reported in dry CH₃CN. The photoreaction was accelerated 5-fold in the presence of H₂O, while air saturation or 0.5 mM piperylene, a triplet quencher, educed a 4-fold deceleration. The quantum yield of diethyl phosphate release from **114**, Φ_{dis} , in wet CH₃CN, was conveyed as 0.94 from laser flash photolysis studies, which dwindled to 0.37 with 10 mM piperylene. To understand and interpret the laser flash photolysis results from **114**, *p*-hydroxyacetophenone (**115**) was employed as a model system, lacking a leaving group. Triplet *p*-hydroxyacetophenone (**³115**) underwent singlet-triplet crossing with a rate constant, $k_{\text{ISC}} \sim 2.7 \times 10^{11} \text{ s}^{-1}$, identified by signature $\lambda_{\text{max}} = 370$ nm triplet-triplet absorption band in dry CH₃CN that was red-shifted to $\lambda_{\text{max}} = 395$ nm

in wet CH₃CN. The acidity of the triplet excited *p*-hydroxyacetophenone was registered by rapid protonation of bromophenol blue, suggesting a pK_a ~ -1.0 for the phenolic OH. The triplet energy of ³**115** as determined to be 70.5 kcal/mol⁷⁹ by phosphorescence and accordingly was observed to transfer energy to added naphthalene, which has a triplet energy E_T = 62 kcal/mol.⁷⁸ The equilibrium constant for enolization of **115** with the hydroxyquinomethylene (**115'**), pK_E, was calculated to be 16.4 by DFT, and subsequent dissociation constant for **115'**, K_a = -8.5, forming **115⁻**. Ionization of ³**115'** was shown to be suppressed in dry CH₃CN, but occurred adiabatically in 50% aq. CH₃CN to generate ³**115⁻**, with k_{ion} = 9.6 x 10⁶ s⁻¹ (pK_a 4.6); ³**115⁻** showed absorption bands similar to ³**115**, λ_{max} = 405 nm and a weaker band at λ = 500 nm.

Excitation of ground state **115⁻** at λ = 308 nm in 0.1 M NaOH manifested bands at λ = 405 nm and λ = 500 nm, signifying that these were due to ³**115⁻**. Corresponding studies in acidic solutions demonstrated that ³**115⁻** underwent rapid *protonation* with a k_{H⁺} ~ 4 x 10¹⁰ M⁻¹s⁻¹ from the decay of the band at λ_{max} = 350 nm. The enol protonated form was denoted as ³**115'** based on the lack of naphthalene quenching and supporting DFT calculations that suggested a triplet energy of approximately 38.4 kcal/mol. These aforementioned results were assimilated into a thermodynamic cycle for the triplet manifold that parallels the ground state (Scheme 33).

Scheme 33. Proposed thermodynamic cycle of *p*-hydroxyacetophenone (**115**). Adapted from ref. 78.



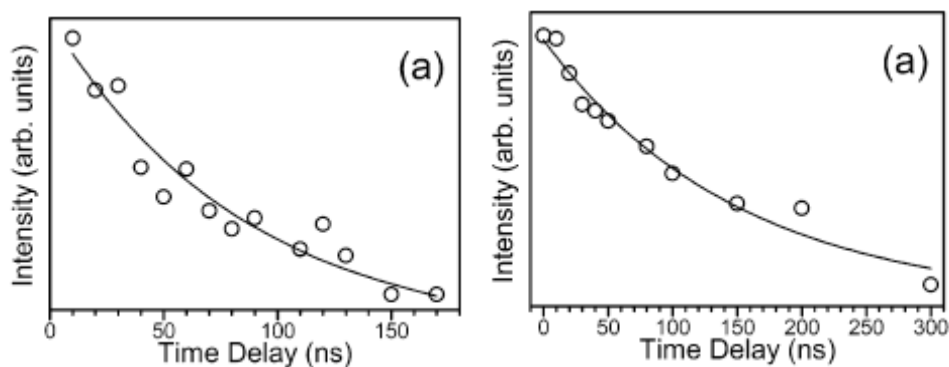
The thermodynamic cycle of the triplet state proton tautomerization, determined from the laser flash photolysis studies of **115** and DFT modeling, was subsequently applied to pHP diethyl phosphate **114**. An intense absorption band at $\lambda = 395$ nm appeared in dry CH_3CN , which was ascribed to its corresponding triplet **³114** based on observed energy transfer to added naphthalene with a rate $k_{ET} \sim 7.8 \times 10^9 M^{-1}s^{-1}$ and phosphorescence spectra at 77 K in a solid matrix of ethyl ether, isopropanol, and isopentane (5:2:2). The self-quenching of **³114** accelerated with increasing concentrations of **114**, by a second order decay, $k_{sq} = 8.5 \times 10^8 M^{-1}s^{-1}$. The decay rate of **³114** was accelerated by the addition of air or oxygen; $k_q = 3.0 \times 10^9 M^{-1}s^{-1}$, a 2.8 fold increase in oxygen or $0-1.25 \times 10^{-2} M$ piperylene that revealed $k_q \sim 4.5 \times 10^9 M^{-1}s^{-1}$, a 1.9 fold increase. The rate constant for phosphate release from **114**

increased exponentially with water through 5% H₂O, $k_{\text{dis}} \sim 2.8 \times 10^7 \text{ s}^{-1}$. Above 5%, the rate was too fast to be measured by the LFP system utilized. A good correlation between the influence of piperylene on the steady state lifetime and the time resolved laser flash photolysis parameters adduced a reactive triplet state for release of diethyl phosphate from **114**. The ratio of lifetimes of ³**114** in 10 mM piperylene quencher (Q) in 5% aq. CH₃CN were $\tau_q/\tau_o = k_{\text{obs}}/(k_{\text{obs}} + k_q[\text{Q}]) = 0.38$. The quinomethylene (³**114'**) was monitored by acid titration with HClO₄ (0.1 - 10 mM) at half-protonation, 4.0 mM HClO₄. In accord with Wan's findings⁷³, Φ_{dis} of ³**114** declined with increasing [H⁺], due to protonation of ³**114**⁻ to form ³**114'**. Collectively, these findings adduced the triplet as the reactive state of *p*-hydroxyacetophenone (³**115**) for the photo-Favorskii rearrangement.

The lack of detail in the mechanistic interpretations, the easily synthesized pHP ester and the available TR³ spectrometer for detailed vibration spectra of triplet and other sufficiently long-lived intermediates, attracted Phillips and coworkers to enter the research arena of the pHP photoremovable protecting group. A series of empirical and theoretical investigations further probed the decay mechanism of pHP. Their first report⁸⁰ examined the excited state structures of pHP diethyl phosphate (**114**) and *p*-hydroxyacetophenone (**115**) in N₂ purged CH₃CN, employing picosecond (ps) and nanosecond (ns) Time Resolved Resonance Raman spectroscopy (TR³). No bands were observed in the 0-2 ps vibrational spectrum of **115** and **114**. After 10 ps, however, a band at 1600 cm⁻¹ was discerned for each, and its decay monitored on the nanosecond timescale. The inception of this band was established as 5.3 and 6.7 ps,

respectively, with a growth rate of 86 and $150 \times 10^9 \text{ s}^{-1}$, respectively, and completely disappeared after $\sim 200 \text{ ns}$ (Figure 4). The decay rates for transients of **114** and **115** were hastened in air, implying *excited triplets* ($^3\mathbf{114}$, $^3\mathbf{115}$). This supposition was corroborated by Kerr-gated, time-resolved fluorescence (KGTRF) measurements of pHP-diethylphosphate (**114**) and *p*-hydroxyacetophenone (**115**) which decayed with rate constants $k_{\text{ISC}} \sim 5 \times 10^{11} \text{ s}^{-1}$ that correlated with $\sim 3.8 \times 10^{11} \text{ s}^{-1}$ for Givens.⁷⁸ Perhaps more importantly, however, was that this value was congruent with the ps growth of the 1600 cm^{-1} band seen by TR³ above and attributed to the triplet state of **114** and **115**. The pump $\lambda = 267 \text{ nm}$ was consistent with the high energy absorption band of **114** and **115**, stemming from a S_0 - S_3 , $\pi\pi^*$ transition. Excitation wavelengths near 300 nm were characterized by S_0 - S_1 , $\pi\pi^*$ transitions. KGTRF data suggested

Figure 4. Left: Time dependent decay profile of $^3\mathbf{114}$ band $\sim 1600 \text{ cm}^{-1}$ with ns ^3TR . Right: Time dependent decay profile of $^3\mathbf{114}$ band $\sim 1600 \text{ cm}^{-1}$ with ns ^3TR . Reproduced with permission from ACS, ref. 80.

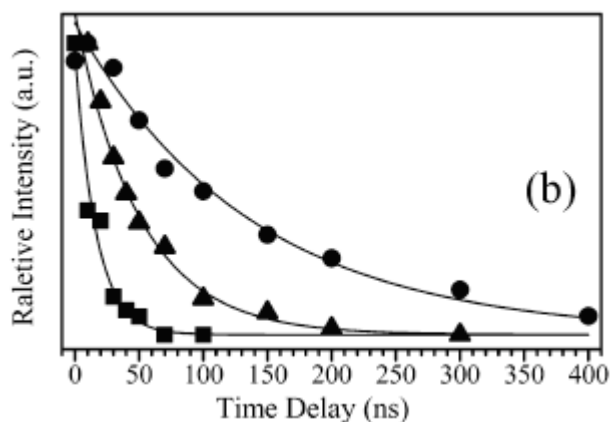


that intersystem crossing for both **114** and **115** adhered to the $n\pi^*$ S₁ to $\pi\pi^*$ T₁ pathway in both 1:1 CH₃CN:H₂O and neat CH₃CN. The similar decay attributes of triplet pHP diethyl phosphate (³**114**) and triplet *p*-hydroxyacetophenone (³**115**) gleaned from ns-TR³ and KGTRF analyses, and pHP acetate (³**110**)⁸¹ in neat CH₃CN, inferred that photophysical processes of **115** were thus independent of the nucleofuge. This disposition, however, was reversed in a later TR³ study⁸² with **114** and **115** in aqueous CH₃CN that disclosed a strong correlation between the triplet lifetime and nature of the nucleofuge. Energies of ³**115** were computed by DFT to be 69 kcal/mol (cp. experimental ~70.5 and Wirz⁷⁸ ~69.6) and for ³**114**, 67 kcal/mol (cp. experimental ~ 70.6⁷⁴). TR³ spectra provided conformational analyses of ³**115** and ³**114**; DFT applications were consistent with the TR³ results. TR³ spectra suggested that the carbonyl of ³**115** was distorted ~16⁰ out of plane (OOP) of the ring, in contrast to ground state, where the chromophore is planar. Similarly, a ~21⁰ OOP orientation of the carbonyl relative to the aryl ring was found for ³**114**, compared to ~2⁰ OOP for the ground state. From the planarity of the carbonyl and attached groups, the sp² nature of the carbonyl for the triplet species was thought to be preserved.

A second report that year⁸¹ detailed a similar set of TR³, KGTRF, and DFT studies for pHP acetate (**110**), akin to Corrie and Wan's model.⁷³ Coincident ps and ns TR³ spectra were obtained to those of **114** and **115** (Figure 5). No activity was observed after initial excitation (0-2 ps), after which a time-dependent band at 1601 cm⁻¹ emerged at ~50 ps. The decay of this, analogous to **114** and **115**, revealed a

good fit to a single exponential growth and a decay function by least squares analysis; time constant for growth was 12 ps and 137 ns for decay in N₂ purged CH₃CN, (Figure 5).

Figure 5. Time dependent decay profile of ³110 at ~1600 cm⁻¹ in ns-³TR spectra. Circles indicate degassed, triangles open air, and squares oxygen. Reproduced with permission from the ACS, ref. 81.



In the presence of air, the decay constant decreased to 50 ns, and in oxygen to 16 ns, consistent with a likely triplet excited state. Once again, the decay summary of ³110 was consonant with triplet diethyl phosphate (³114) and triplet *p*-hydroxyacetophenone (³115) and was consistent with previous work with ³110. Additionally, the nanosecond rate of deactivation, as indicated by the disappearance of bands associated with ³110, was seen to accelerate as a function of pHP concentration. This observation was consistent with earlier studies⁷⁸ and was ascribed to self-quenching from head-tail hydrogen abstraction by the carbonyl from a neighboring phenolic OH. To support the assignment of triplet state reactivity, KTRF

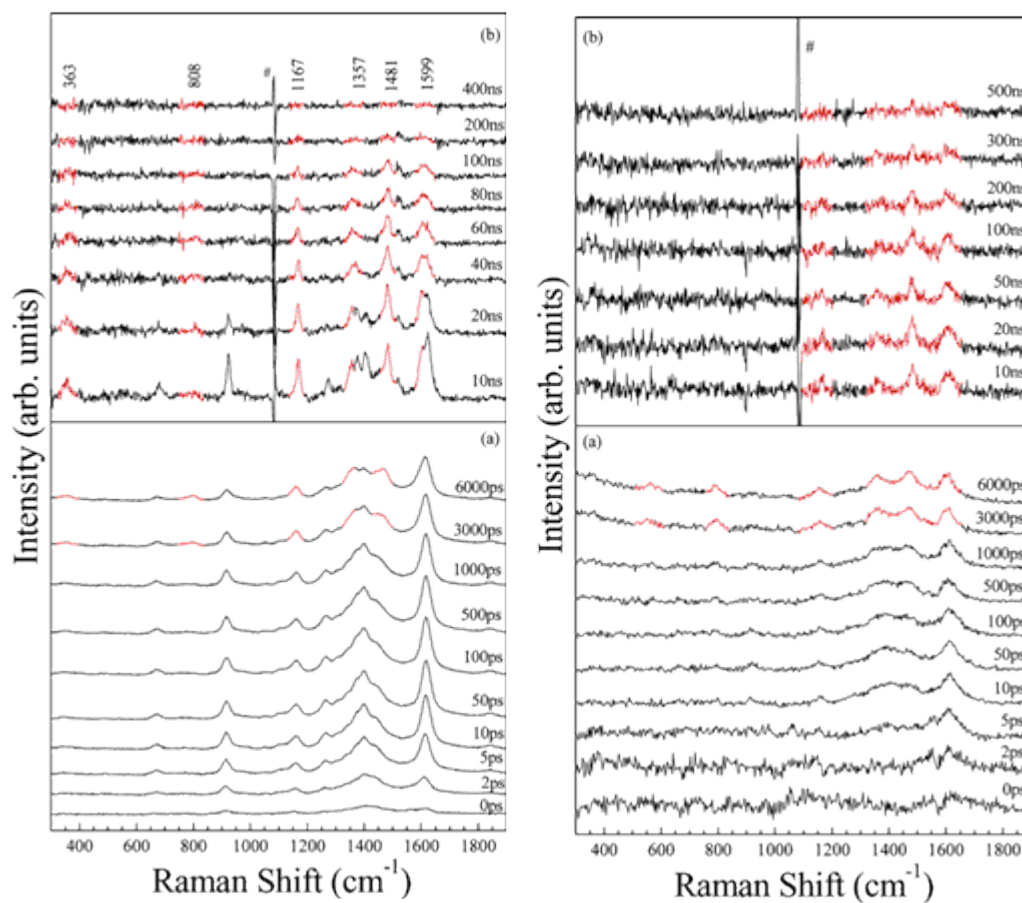
studies on **110** gave $k_{ISC} \sim 5.0 \times 10^{11} \text{ s}^{-1}$ that were congruous with the rapid growth of the $\sim 1600 \text{ cm}^{-1}$ band seen in ^3TR spectra and assigned to the carbonyl triplet as well as the results of previous studies.^{74,75} This result was divergent from the $1.1 \mu\text{s}$ triplet lifetime of **110** that Corrie and Wan⁷³ reported. It was believed that Corrie and Wan's value was obtained in thoroughly O_2 purged conditions and that residual O_2 was believed to be the cause of a shortened, 137 ns lifetime of $^3\text{110}$ in Phillips' study.

A fluorescence decay of 2 ps was detected that conflicted with the 12 ps growth of the $^3\text{110}$ described earlier. Phillips, therefore, concluded that some other process early in the ps time regime must be active in developing the triplet TR^3 spectrum. This was designated as triplet relaxation of surplus energy brought forth by efficient intersystem crossing to an unrelaxed, upper triplet. Evidence for this assertion originated from frequency changes in the band centered at 1600 cm^{-1} up to 200 ps ; a band shift from 1570 cm^{-1} at 4 ps to 1601 cm^{-1} at 50 ps was observed. In addition, band widths were reported to narrow during this time, an indication of excess energy relaxation. The implications for this were as follows: The lowest triplet of **110** was considered to be much lower in energy than the corresponding singlet. The energy gap between $^1\text{n}\pi^*$ and $^3\text{n}\pi^*$ had been determined to be $\sim 1800 \text{ cm}^{-1}$ for acetophenone;⁸³ this corresponds to $^3\text{n}\pi^*$ and $^3\pi\pi^*$ energy gap of analogous *p*-hydroxyacetophenone,⁷⁹ $\sim 2500 \text{ cm}^{-1}$. Phillips reasoned that these values and the similarity of energies of $^1\pi\pi^*$ and $^1\text{n}\pi^*$ for **110**, as determined by ground state UV absorption, would provide some insights into the $\pi\pi^*$ triplet energy. Several empirical studies reported a near degeneracy in lowest $\text{n}\pi^*$ and $\pi\pi^*$ triplet states of

acetophenone.^{84,79,83} Hence, the triplet state is thought to be easily perturbed by environmental changes, such as substituents, phase (gas, liquid, solid), solvent polarity, H-bonding, etc. For example, the lowest triplet energy of acetophenone is considered to be $n\pi^*$ in the gas phase⁸⁵ and in non-polar solvents,⁷⁹ and $\pi\pi^*$ in polar solvents and in the solid phase.⁷⁹ Most *p*-substituted acetophenones including *p*HP diethyl phosphate (**114**), are believed to have a lowest $\pi\pi^*$ triplet both in polar and non-polar media.⁷⁹ TR³ measurements for **110** revealed close similarities to **114**, as did the corresponding phosphorescence profiles. These attributes, as well as the likeness of their triplet lifetimes, led Phillips to conclude that ³**110** is $\pi\pi^*$ in character. A triplet energy of 67 kcal/mol was calculated for *p*HP acetate (**110**) by DFT that was in agreement with previous studies.⁷⁸ Conformational analysis imparted by DFT revealed a $\sim 20^\circ$ OOP contortion of the carbonyl relative to the aromatic ring for ³**110** compared to a planar ground state, also consistent with other *p*HP analogs.

To discern the initial steps of substrate photorelease from *p*HP and concomitantly reconcile two disparate assertions regarding reactive state multiplicities, Phillips⁸⁶ employed his psTR³ and nsTR³ methods for the analysis of *p*-hydroxyacetophenone (**115**) in aqueous media. The focus of this study was on the solvent-assisted deprotonation of **115**, believed to be crucial in the rearrangement process. This investigation derived from results of an analogous study⁸⁷ of the *p*-methoxy derivative of **115** in water, which substantiated a water-stimulated modification in properties of the triplet state vs. dry CH₃CN. Dynamics of **115** from ps-TR³ analysis in water are depicted in Figure 6. Contrary to earlier results in dry

Figure 6. Left: 1) Bottom - psTR³ spectrum of **115** in water. 2) Top - psTR³ spectrum of **115** in water. Right: 1) Bottom - psTR³ spectrum of **115** in buffer, pH = 9.00. 2) Top - psTR³ spectrum of **115** in buffer, pH = 9.00. Reproduced with permission from the ACS, ref. 86.



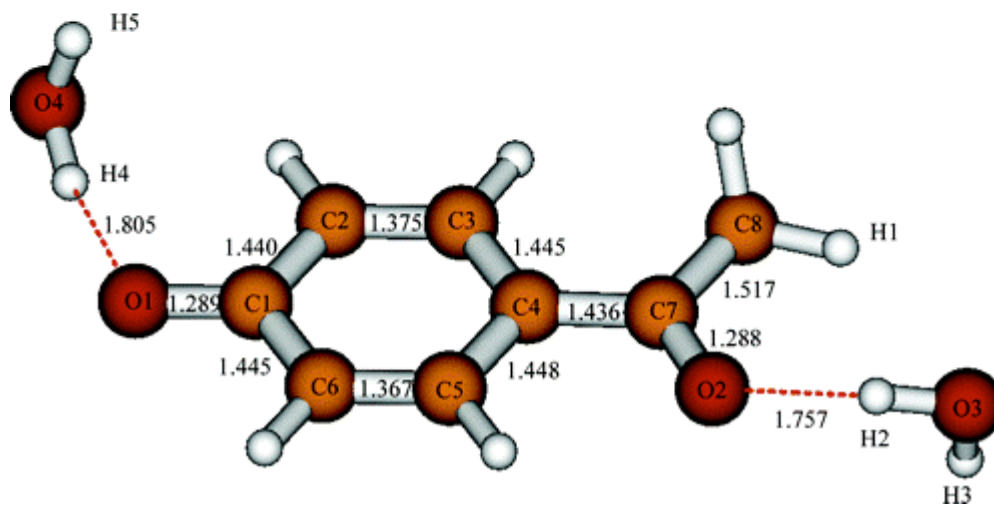
CH₃CN⁸⁰ that evinced one transient species, two short-lived transients were conspicuous in the spectra: (1) one conveyed a band at 1600 cm⁻¹ that correlated with previous studies⁸⁰ in dry CH₃CN, emerging at 2 ps and decaying within ~10 ns, (2) another showed bands at 1599, 1481, 1357, and 1167 cm⁻¹ that decayed within 95 ns. When measured in N₂ purged water, the decay of bands associated with the second transient lengthened to 140 ns, a clear indication of O₂ quenching and evidence for a

triplet reactive state. The new transient was ascribed to H-bonding between the solvent and ${}^3\mathbf{115}$, not evidenced in aprotic CH_3CN , and now distinguished as ${}^3\mathbf{115}'$. Results of ps-TR³ analysis of $\mathbf{115}$ in buffer, pH = 9.00 (Figure 6) revealed that the formation of the new entity was faster than in neutral water, and was the sole entity that emerged in the ns spectrum. It was deduced that this species was the triplet *p*-hydroxyacetophenone anion (${}^3\mathbf{115}'$). The direct excitation of a ground state anion of $\mathbf{115}$ under these conditions was precluded on the basis of its very low ϵ at the pump λ = 267 nm, and probe wavelengths of 400 and 415 nm. Control experiments in basic solutions with $\mathbf{115}'$ as the conjugate base tautomer and using a pump wavelength of λ = 341 nm, produced parallel spectra that had similar triplet decay dynamics, thus supporting the likelihood of ${}^3\mathbf{115}'$ as the intermediate. Full Raman spectral assignments of bands associated with ${}^3\mathbf{115}'$ and the corresponding protonated tautomer (${}^3\mathbf{115}$) manifested salient differences that were reproduced by DFT model calculations.

The kinetic profile of ${}^3\mathbf{115}$ was shown to be a good fit for a two-exponential function comprised of a growth, 90 ns, and decay constant, 200 ns. Control TR³ experiments with $\mathbf{115}$ in acidic media (pH = 1) demonstrated the presence of only this entity. A similar transient was observed from Wirz and Givens⁷⁸ at low pH, and was tentatively designated as a quinoid enol triplet ($\mathbf{115}'$) (Scheme 32). From this comprehensive study, it was inferred that an excited state deprotonation step was plausible for pHP, and ${}^3\mathbf{115}'$ a likely precursor to nucleofuge release. An optimized

conformation from DFT fit of TR³ spectra for triplet *p*-hydroxyacetophenone ³**115** in water is depicted in Figure 7.

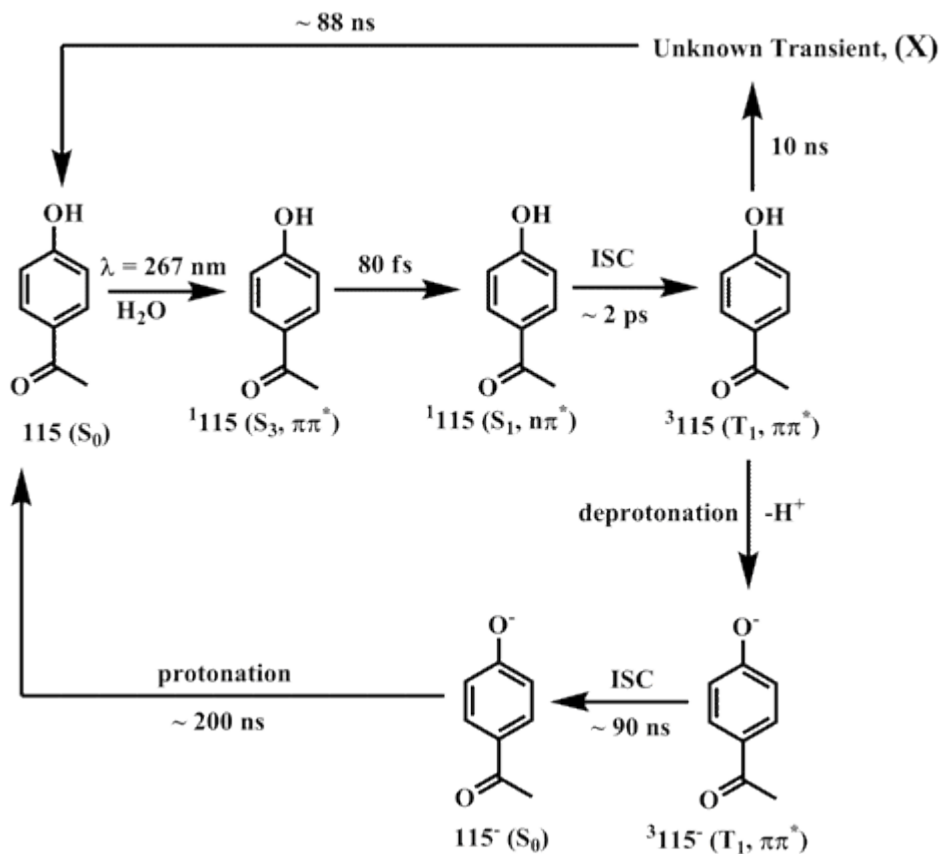
Figure 7. DFT determined, optimized geometry and bond distances (Å) of ³**115** in water. Reproduced with permission by the ACS, ref 86.



The results depicted extensive hydrogen bonding between water and ³**115**. Two water molecules associated with the phenolic O-H, affording 14.8 kcal/mol of stabilization energy; one water molecule interacted with the carbonyl moiety, affording 6.8 kcal/mol of stabilization energy. H-bonding with the phenolic O-H was thought to preface water-mediated deprotonation of triplet *p*-hydroxyacetophenone (³**115**) to the corresponding the triplet anion, ³**115**⁻. This event seemed plausible by the increased acidity of the phenolic proton of **115** in the triplet state, pK_a = 3.6, compared to the ground state, pK_a = 7.6.⁷⁸ TR³ analysis disclosed an unspecified transient (termed **X**) that emerged contemporaneously with ³**115**⁻; this entity exhibited

a decay constant of 88 ns, similar to 95 ns for $^3\mathbf{115}^{\cdot-}$. UV measurements of the $\mathbf{115}$ after TR³ analysis manifested no significant degradation, leading Phillips to conclude that \mathbf{X} rapidly deactivates back to ground state $\mathbf{115}$. No further efforts were conducted to identify \mathbf{X} . TR³ and DFT results were assimilated to propose a decay and deprotonation mechanism for $\mathbf{115}$ (Scheme 34). This mechanism deviated from

Scheme 34. Phillips proposed mechanism for excited state processes of *p*-hydroxyacetophenone ($\mathbf{115}$).



Wirz and Givens' (Scheme 32), chiefly in regards to the identification of **X**. Givens and Wirz assigned this to the triplet enol ($^3\mathbf{115}'$) formed from a step involving solvent-induced protonation of $^3\mathbf{115}^-$. The aforementioned TR³ measurements of **115** in water manifested concomitant formation of $^3\mathbf{115}^-$ and **X** that represented the decay of $^3\mathbf{115}$. Experiments conducted in acidic media, where a reprotonation step is obviated, indicated a direct decay route of $^3\mathbf{115}$ through **X**. Having elucidated the sequence of photophysical and reaction events leading up to substrate release from pHP, Phillips turned to mechanism of substrate release, the heart of the photo-Favorskii reaction.⁸⁸

As before, ps and ns-TR³ spectroscopy were employed along with femtosecond transient absorption (fsTA) spectroscopy, for the investigations of pHP diethyl phosphate (**114**) and pHP diphenyl phosphate (**116**) in dry and 1:1 CH₃CN:H₂O (aq. CH₃CN) solutions. Results from fsTA analysis of **114** in both solvents revealed the formation of a strong absorption band at ~400 nm while one at ~320 nm decayed rapidly; one exponential function fit the simultaneous growth and decay components, with a time constant of 2.5 ps. This value matched the ISC constant derived previously⁸⁰ and implied a rapid ISC to the triplet state. Pronounced changes in shape of the 400 nm band from 4 to 35 ps were observed in aq. CH₃CN *but not in neat CH₃CN*; the band was wide and structureless earlier than 4 ps, but better defined later. Phillips ascribed this occurrence to specific solvent-solute interactions, such as H-bonding. Investigations with fsTA of *p*-hydroxyacetophenone (**115**) in aq. CH₃CN exhibited no such shifts in the band shape at 400 nm. Concerning

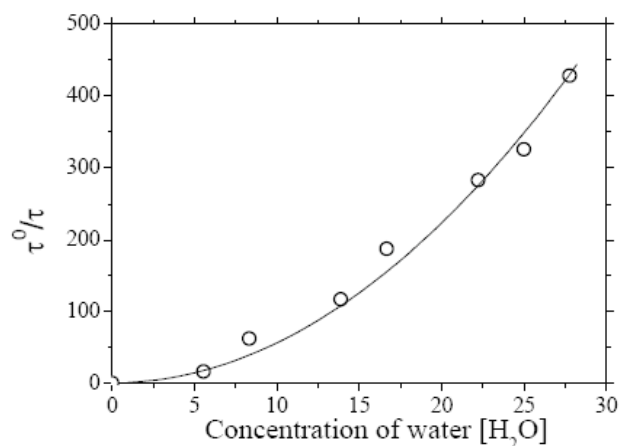
116, fsTA measurements were congruent with **114**, imputing structurally similar triplet reactive states. The triplet lifetimes of these, however, proved to be different, as determined by TR³ analysis; ³**114** exhibited ~ 150 ns lifetime in CH₃CN and ~350 ps in aq. CH₃CN. Those for ³**116** were ~27 ns in CH₃CN, ~150 ps in aq. CH₃CN. A synopsis for decay profiles of pHP diethyl phosphate (³**114**) and pHP diphenylphosphate (³**116**) as a function of water concentration are presented in Table 13, with pHP acetate (³**110**) for comparison.⁸² Hydrogen ion dissociation constants, pK_a, for the nucleofuges were included; these directly correlate with the respective anion stabilities in aqueous media as well as relative leaving group ability in the context of heterolysis in aqueous media. A higher pK_a indicates a more stabilized, anionic leaving group. A noticeable trend was observed between the pK_a and triplet lifetime; ³**116**, with the lowest nucleofuge pK_a of 0.4, manifested the shortest triplet lifetime, 150 ps in aq. CH₃CN, while for ³**110** with a pK_a of 4.76, one order of magnitude longer at 2.130 ns.

Table 13. Time constants for triplet decays of **116**, **114**, and **110** in mixed CH₃CN/H₂O solvents and corresponding pK_a's of the nucleofuge. Table adapted from ref. 88.

H ₂ O % (vol)	triplet decay (τ_1 , ps)						10%	pK _a
	75%	50%	40%	30%	25%	15%		
pHP diphenyl phosphate, ³116		150					830	0.4
pHP diethyl phosphate, ³114	290	350	530	800	1280	2400	9000	1.39
pHP acetate, ³110		2130						4.76

A correlation between water concentration and triplet lifetime was also apparent; the lifetime of $^3\mathbf{114}$ progressively shortened as the water content increased, with initial pronounced changes (10%-30% 11.2-fold, 30-50%, 2.2-fold, and 50-75%, 1.2-fold) and later leveling off as water was added. The same was observed for $^3\mathbf{116}$, though not to the same caliber. Stern-Volmer analysis of $\mathbf{114}$ and $\mathbf{116}$ evinced a curved, near quadratic dependence on water concentration (Figure 8). Presupposing that water addition influences heterolysis in a non-linear fashion,⁸⁸ the S-V results indicated a likely, triplet heterolytic dissociation route for phosphates from excited state $\mathbf{114}$ and $\mathbf{116}$. The salient influence of water concentration asserts that water is not only involved in early pHP deprotonation but also in the rearrangement (solvolysis) step. These studies adduce a 2nd order dependence of the triplet lifetime on water.

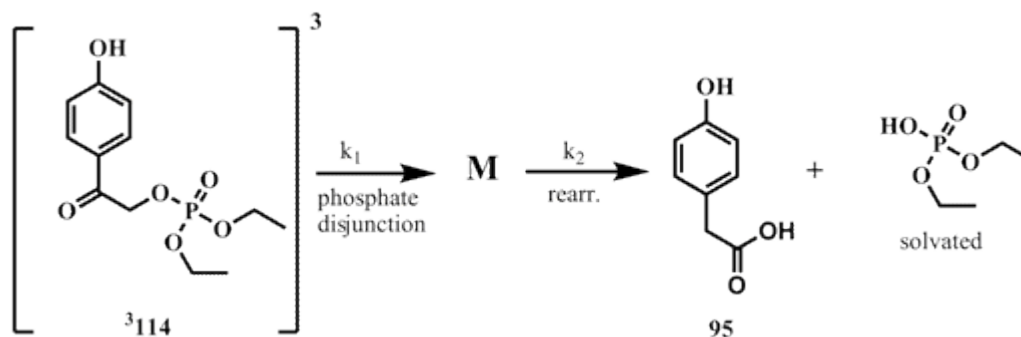
Figure 8. Stern Volmer analysis of $^3\mathbf{114}$ lifetimes as a function of water concentration, in percentage. Reproduced with permission by the ACS, ref. 88.



Solvation of the nucleofuge, as well as the pHP chromophore, was considered to be an important constituent in the correlation between triplet decay dynamics and leaving group ability, demonstrated in Table 9. The double bonded oxygen of phosphate, like the carbonyl, has strong basic character and hence would be expected to interact strongly with water as an H-bond acceptor. The effect of this interaction is an electrophilic pull towards ionization. Acidic and basic sites of the pHP chromophore and nucleofuge are anticipated to be strongly solvated by water. To corroborate this “concerted” solvation premise, fsTA studies were performed with **114** in DMSO, a H-bond acceptor but poor donor, and trifluoroethanol (TFE), an H-bond donor but poor acceptor. In DMSO, the fsTA spectrum, denoting the triplet decay profile, was akin to that obtained in dry CH₃CN and demonstrated a triplet lifetime > 200 ns with an accompanying low quantum yield (<0.01). In TFE, a slightly shorter triplet lifetime was reported, as well as a low quantum yield (no data was provided for this). However, a 1:1 combination of DMSO/TFE revealed a significantly shortened lifetime for triplet pHP diethyl phosphate (³**114**) and a quantum yield of 0.17 for phosphate release. These findings seem to support a general requirement for “concerted” solvation of the pHP chromophore and nucleofuge for efficient nucleofuge release from the excited state pHP chromophore. A comparison of spectra obtained from psTR³ analysis of **114** and an authentic sample of rearranged *p*-hydroxyphenylacetic acid photoproduct (**95**) (pump λ = 267 nm, probe λ = 200 nm) in 1:1 CH₃CN:H₂O was carried out to inspect the formation dynamics of **95**. The formation and growth of bands following excitation of **114** were

undeniably associated with the formation of **95**. A first order exponential curve fit resulted in a time constant of ~1100 ps. When comparing this to the triplet delay for **114** (~350 ps), a discrepancy was ostensible between the rearrangement reaction and triplet decay. The triplet decay was associated with nucleofuge (phosphate) disjunction; hence, to account for the delay time (~750 ps) between the triplet decay and formation of *p*-hydroxyphenylacetic acid (**95**), an intermediate (**M**) was proposed in Scheme 35 and thought to be produced immediately after nucleofuge disjunction but before the appearance of **95**. An evasive, but accepted intermediate in the Favorskii reaction is cyclopropanone (**100**) which, as of yet, has not been detected. Thus, **M**, was perceived as a likely fit for **100**, but necessitated corroborating data.

Scheme 35. Proposed intermediate precursor to rearranged product.



A formula was proposed to describe the formation of **95** from ³**114** (Equation 13).

$$[\mathbf{95}] = \{[\mathbf{3121}]/(k_2 - k_1)\} * [k^2(1 - e^{-k_1 t}) - (k^1(1 - e^{-k_2 t}))]$$

Eq. 13

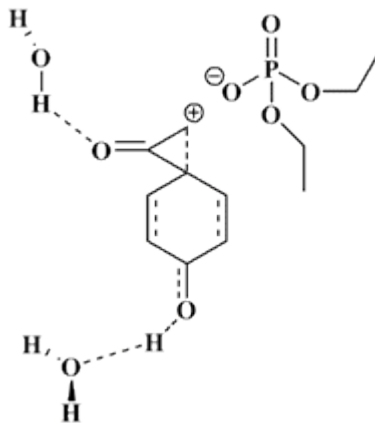
The rate for phosphate detachment and decay of $^3\mathbf{114}$ to \mathbf{M} , k_1 , was deemed to be much faster than k_2 . Efforts were concentrated on determining the rate of rearrangement, k_2 , through psTR³ measurements in CH₃CN with various water at pump $\lambda = 267$ nm, probe $\lambda = 200$ nm. From exponential fits of the spectra, k_2 was determined to be $1.69 \times 10^{-9} \text{ s}^{-1}$ ($k_2 = 1/\tau_2$, $t_2 \sim 470$ ps) and was found to be *insensitive to the water concentration*. To quantify the formation of \mathbf{M} , as a model system, equation 14, derived directly from equation 13, was applied. Though not empirically

$$[\mathbf{X}] = [^3\mathbf{114}]^* \left[\frac{k_1}{(k_2 - k_1)} (e^{-k_1 t} - e^{-k_2 t}) \right]$$

Eq. 14

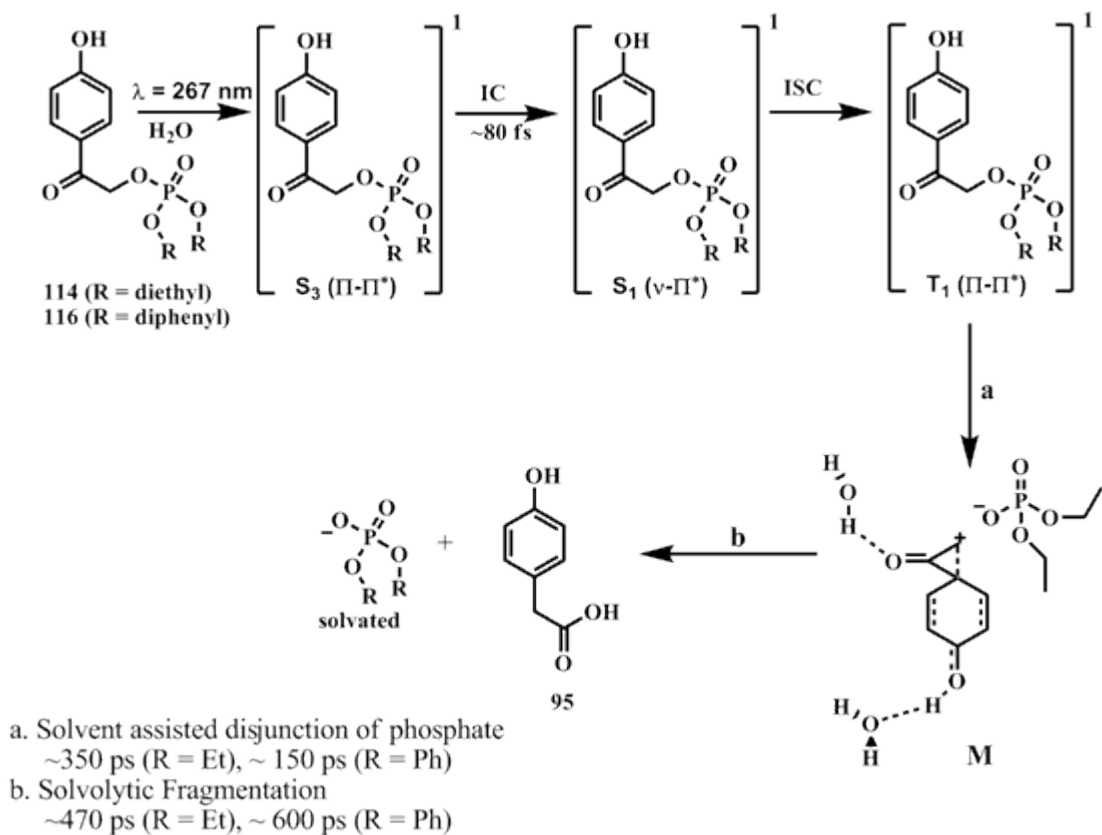
confirmed, a solvent assisted, “push-pull” neighboring group⁸⁹ stimulus from the H-bonded solvent was postulated to afford \mathbf{M} as a solvated complex containing features

Figure 9. Phillips’ proposed structure of unknown, \mathbf{M} , as a solvation/contact ion pair complex.



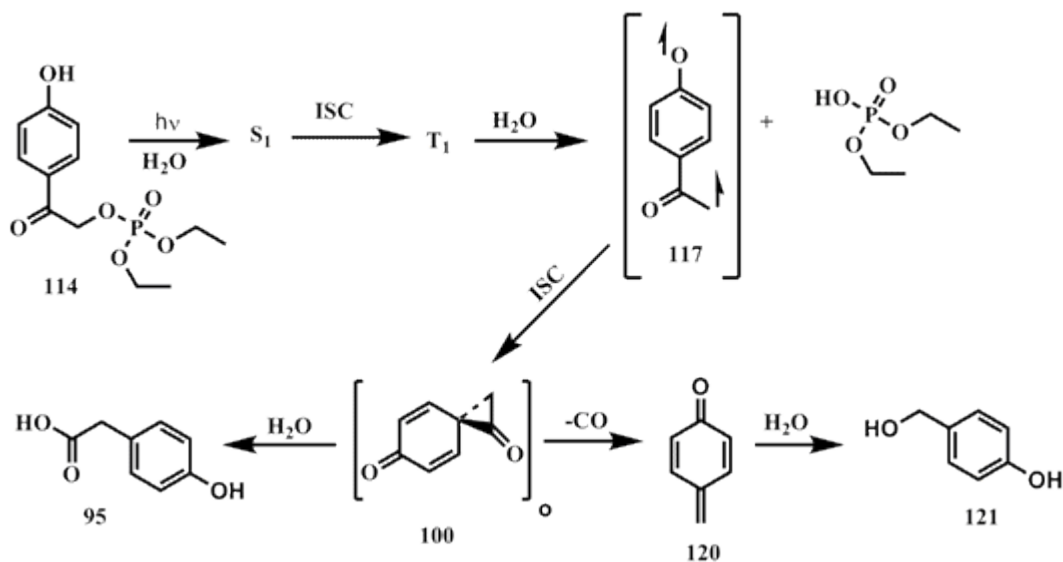
of a contact ion pair of α -protonated cyclopropanone (**100**) and liberated phosphate anion (Figure 9, with **114**). Calculations with DFT at the random phase approximations (RPA) of **100** indicated an electronic transition with a large oscillator strength at $\lambda \sim 274$ nm, which was consistent with a spectral band at $\lambda = 274$ nm associated with **M**. Further empirical attempts to bolster this structural hypothesis, such as Kerr gated ps-TR³ were ineffectual, probably due to the relatively low concentration of **M** expected when $k_2 \gg k_1$ (steady state condition) as well as the lack of a strong absorption band between 300 to 700 nm when probed by fsTA. Incorporation of the mechanistic features acquired from these studies compelled Phillips⁸⁸ to propose a new, detailed photo-Favorskii rearrangement to account for the formation of **95** (Scheme 36). The salient attributes of this mechanism are: (1) The rate of (a) is largely dependent on the water content and nature of the nucleofuge; (2) The rate of (b) is dependent on the nature of the nucleofuge but mainly independent of water concentration. Phillips conveyed two more comprehensive, though theoretical, investigations concerning the excited state photochemistry of pHP acetate (**110**)⁹⁰ and the role of water in assisting the nucleofuge disjunction/solvolytic rearrangement steps of the photo-Favorskii rearrangement for ³**114** and ³**116**.⁹¹ Information gleaned from these studies served to corroborate hypotheses derived from earlier, empirical data,⁸⁰ and are beyond the scope of this introduction.

Scheme 36. Posited mechanism for phosphate release from the pHP chromophore.



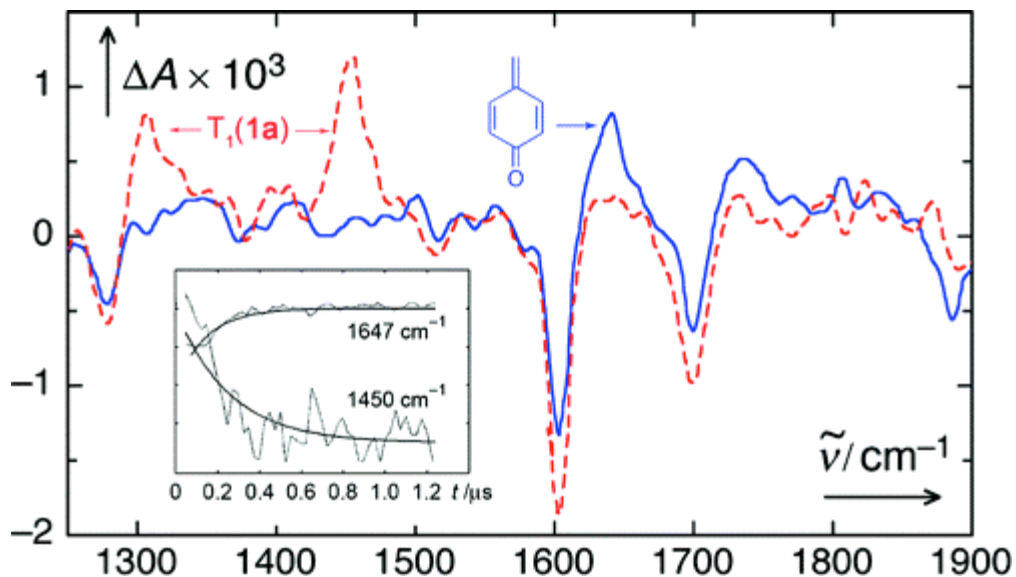
In the latest installment of the ongoing exploration of the photo-Favorskii rearrangement, Givens and Wirz,⁹² reported the detection of an anionic pHP triplet biradical (**117**) in the reaction course of excited pHP diethyl phosphate (**114**), pHP tosylate (**118**) and pHP mesylate (**119**) from time resolved IR and UV studies. An amended, generalized mechanism was proposed and represented in Scheme 37.

Scheme 37. Proposed mechanism for diethyl phosphate release from pHP.



It was revealed that the lifetime of $^3\mathbf{114}$ reduced from ~ 0.4 ns in 50% aq. CH_3CN ⁸⁸ to ~ 100 ps in 87% aq. CH_3CN and ~ 63 ps in 100% H_2O . Transient absorption spectra for **118** and **119** were consistent with **114**. Decay kinetics of $^3\mathbf{114}$ accorded with those reported by Phillips.⁸⁰ However, new transient absorption bands were detected at 445 and 420 nm, and were assigned to triplet biradical (**117**) based on the likeness of shape, location, and weak intensity of analogous phenoxy radicals.⁹³ MP2 calculations predicted the carbonyl of **117** to be contorted 27° out of plane from the aromatic ring. TDFT and open shell PPP SCF CI⁹⁴ calculations failed to detect the singlet analog of **117**, implying an expeditive cyclization to **100** after ISC. Efforts to detect **100** by step scan FTIR, anticipated to be found at ~ 1880 cm^{-1} ⁹² were ineffectual (Figure 10).

Figure 10. Step-scan FTIR of **114** in CD₃CN (2% D₂O) at 50 ns (red) and 1 μs (blue) delay. Reproduced with permission from the ACS.



However, bands at 1450 and 1300 cm^{-1} were immediately discerned after excitation and promptly decayed (first order) with a coincident emergence of another band at 1647 cm^{-1} , $k \sim 8.5 \times 10^6 \text{ s}^{-1}$ (2% D₂O in CD₃CN). This rate of appearance was accelerated with additional water at the expense of band amplitude. This was tentatively designated as the *p*-quinone methide (**120**) and was congruent with results from recent work by Kresge⁹⁵ et. al., in the photolysis of *p*-hydroxybenzyl acetate. Nanosecond LFP evaluation of pHP diethyl phosphate (**114**) in wet CH₃CN supported the configuration of this transient; excitation of ³**114**, $\lambda = 395 \text{ nm}$, produced an absorbing species, $\lambda = 276 \text{ nm}$, which was relatively long-lived ($k \sim 0.01 \text{ s}^{-1}$ in 5% H₂O, 0.05 s^{-1} in 10% H₂O) and waned with increasing water content. Kresge⁹⁵ reported a rate constant of 3.3 s^{-1} in 100% water. These observations provided strong

support for the triplet biradical (**117**). Low temperature ^1H NMR, (-25°C , 2.5% D_2O in CD_3CN) of **114** conveyed the abrupt emergence of peaks associated with **120** upon irradiation. The likely route to the formation of **120** is through CO extrusion of spirodiendione (**100**). To further elucidate the role of water in the photoreaction, SKIE were probed with pHP acetate (**114**) using ns-LFP (degassed, 10% aq. CH_3CN , 25°C), with a particular focus on the decay kinetics of $^3\text{114}$. In addition, a secondary photoproduct, *p*-hydroxybenzyl alcohol (**121**), was asserted from the putative *p*-quinone methide (**120**), derived from solvent kinetic isotope studies (SKIE) using laser flash photolysis (ns-LFP) in 87% aq. CH_3CN (Table 14).

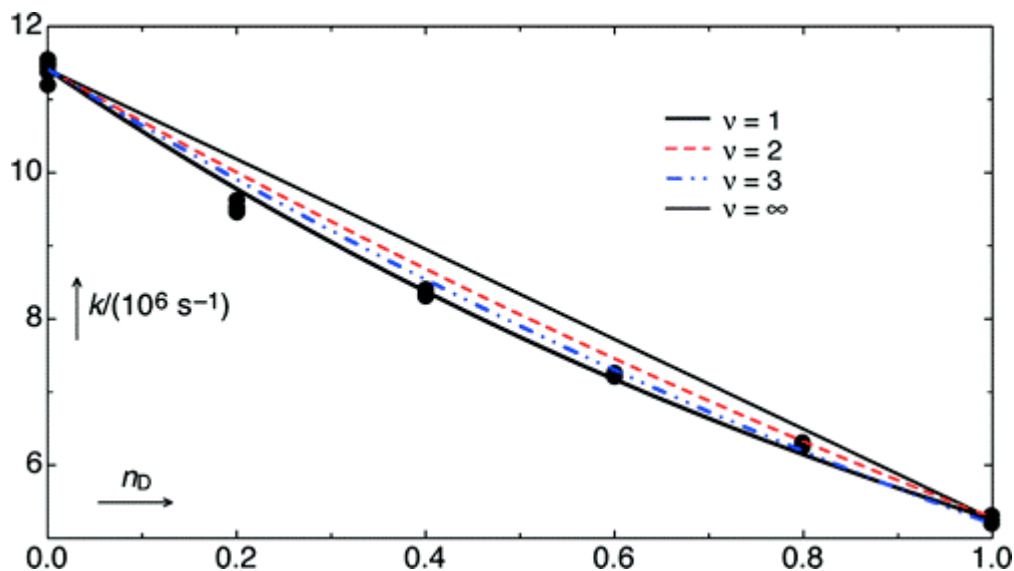
Table 14. Rate constants, k_{obs} , for decay of $^3\text{114}$ as a function of the D/H mole fraction, n , using ns-LFP in 10% aq. CH_3CN at 25°C . Table adapted from ref. 92.

n^a	average k_{obs} (10^6 s^{-1})	$k_{\text{H}}/k_{\text{n}}$
0.00	11.4 ± 0.14	1.00
0.20	9.53 ± 0.07	1.20
0.40	8.36 ± 0.04	1.36
0.60	7.24 ± 0.03	1.57
0.80	6.29 ± 0.03	1.81
1.00	5.25 ± 0.06	2.17

^a n = mole fraction = $n_{\text{D}}/(n_{\text{D}} + n_{\text{H}})$.

By employing the *proton inventory* method⁹⁶ of analysis the total SKIE was determined to be 2.17. Decay constants for $^3\text{114}$, k_{obs} , were then plotted against

Figure 11. Plot of k_{obs} of $^3\mathbf{114}$ vs. mole fraction of deuterium in degassed, 10% aq. CH_3CN at 25°C . The black line signifies the expected correlation for a single site isotope effect ($v = 1$), see equation 4. The lower line indicates a multisite, general solvation ($v = \infty$). The central two lines represent a two site effect (red, $v = 2$), and a three site effect (blue, $v = 3$). Reprinted with permission from the ACS.



deuterium mole fractions, n_D , depicted in Figure 11. An appropriate comparison (Equation 15) was exploited to model the solvent kinetic isotope results where n is the mole fraction and v represents the number of isotope effect sites on $^3\mathbf{114}$.

$$k_n/k_H = (1 - n + n[k_H/k_D]^{-1})^v$$

Eq. 15

When $v = 1$, the entire isotope effect ($k_H/k_D = 2.17$, Table 10) is realized at one site.

When $v = 2$, two sites are equally affected, as in conterminous, two-proton transfer ($k_H/k_D = 2.17^{1/2} = 1.47$). When $v = 3$, three sites are uniformly impacted, ($k_H/k_D =$

$2.17^{1/3} = 1.30$), and when $v = \infty$ a general solvation condition at multiple sites by water is effected.⁹⁶ The plot clearly exhibited a curved line, precluding a one site effect, while advancing a minimum of two site H-bonding between triplet pHP acetate **3114** and the solvent. The phenolic proton of **3114** was calculated to be more than 4 orders of magnitude more acidic than **114**, whereas, the carbonyl moiety is more basic.⁷⁸ Two site SKIE results were in good agreement with these properties; a) one site, a robust H-bond donation of the phenolic proton to the enveloping water molecules and b) the other site, H-bond accepting of the carbonyl with the surrounding water molecules *with concomitant phosphate departure*. These results confirm that hydration is a *sine qua non* for the photo-Favorskii reaction, as previously asserted by Wan,⁷³ Givens,⁷⁸ and Phillips.^{80,81,82, 86,87,88,89}

A prodigious quantity of information has been gleaned over the past decade with respect to the photo-Favorskii rearrangement. This has advanced a number of appropriate mechanisms to account for the steps leading to formation of the signature, rearranged phenylacetic acid (ester) photoproduct. Further studies are warranted, however, to further improve the overall comprehension of the photo-Favorskii rearrangement, much the same as Bordwell's pervasive studies on the ground state Favorskii rearrangement, such as the impacts of *substituents*, *added salt (ionic strength)*, and *media* among others, which have received little or no attention.

Statement of Problem

The *p*-hydroxyphenacyl (pHP) chromophore has received a considerable amount of attention over the past decade as a versatile photoremovable protecting group for a wide variety of substrates. The intriguing rearrangement of pHP that accompanies photoinduced substrate release has been equated with the well known, ground state Favorskii rearrangement. This excited state process, therefore, has been termed the “photo-Favorskii” rearrangement. Several working mechanisms for this process have been posited, primarily from theoretical and spectroscopic studies.

These mechanistic studies, though useful in bringing together preliminary details on the rearrangement of the pHP chromophore, are narrowly restricted in scope, which emphasize only a small pool of pHP derivatives and photolysis conditions. A number of programmed modifications of the photo-Favorskii substrates and conditions would add immeasurably to our understanding and would further elucidate the mechanistic picture of this rearrangement: 1) Would electron donating or withdrawing substituents on pHP impact the photorelease of substrates? 2) Is there a positional effect expressed by the substituents? If so, what are its origins? Fluorine, from its inherently high electronegativity and lipophilicity, is an attractive substituent for pHP for the investigation of electronic effects on the photochemistry, solvent and solubility property effects, and spectroscopic characteristics. 3) The λ_{max} of pHP at 280 nm extends slightly past 300 nm at 1 mM, a concentration that is typical for photolysis reactions. One goal of this research has

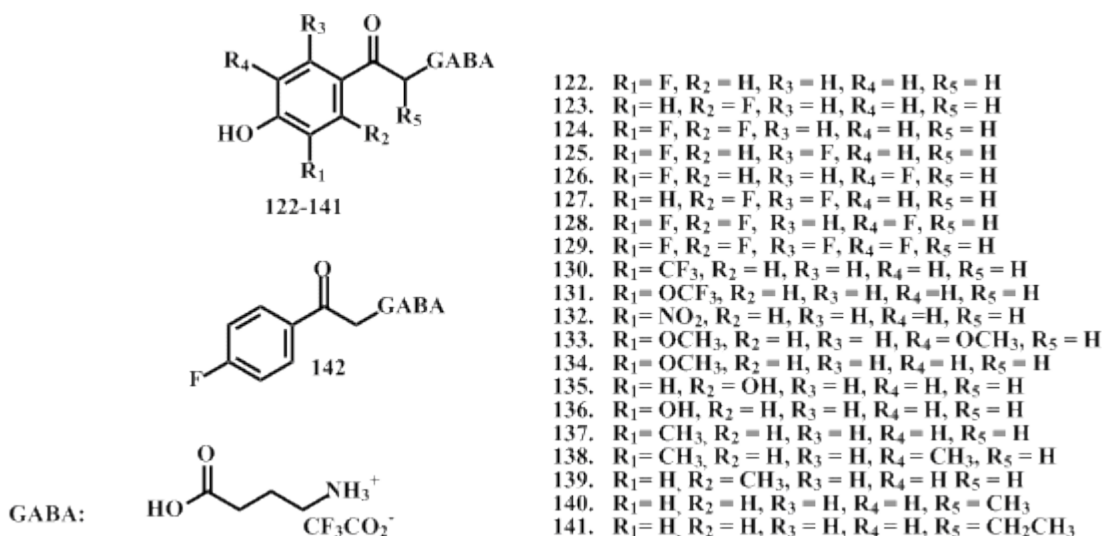
been to extend the absorption profile of pHP beyond 350 nm, making it more amenable for biological studies. The *m*-methoxy moiety has been the sole auxochrome investigated at this time; other groups and additional approaches addressing this goal could provide favorable efficiencies and extended λ_{max} . 4) The range of leaving groups or nucleofuges examined in mechanistic studies of the photo-Favorskii reaction has also been confined. An expansion of substrates, especially to establish the limiting parameters of the nucleofuge and the determination of correlations between the nature of the nucleofuge and photorelease parameters, would be useful. 5) Lastly, the majority of studies tailored for the investigation of the mechanism of the photo-Favorskii rearrangement have employed water and/or aqueous acetonitrile as the media. The variations of standard physical organic parameters related to the media, such as ionic strength, pH, water content, and lipophilicity, that influence the photoreactivity and product outcomes of pHP caged compounds have not been established and would certainly improve our mechanistic understanding of the photo-Favorskii rearrangement.

Results

I. Synthetic Methodologies

A. **pHP GABA series (122-141) and 4-fluorophenacyl GABA (142).** The novel pHP GABA esters that were synthesized along with 4-fluorophenacyl GABA are depicted in Figure 12.

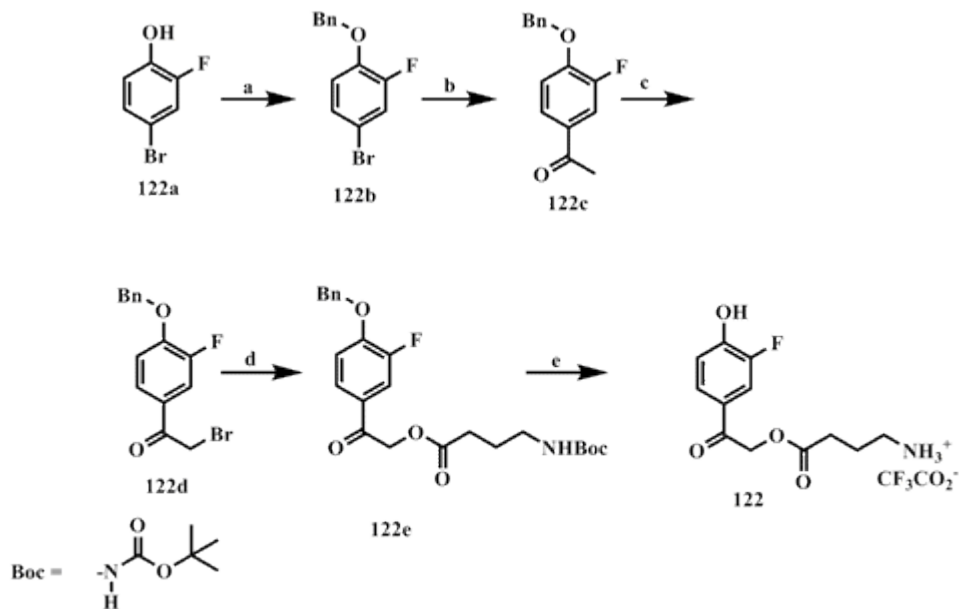
Figure 12. Novel pHP GABA esters.



1) **Synthesis of 4-(2-(3-fluoro-4-hydroxyphenyl)-2-oxoethoxy)-4-oxobutan-1-aminium 2,2,2-trifluoroacetate, (*m*-F-pHP GABA, 122).** The synthesis of **122** (Scheme 38) was initiated with commercially available 4-bromo-2-fluorophenol, (**122a**), which was reacted with benzyl bromide to produce the benzyl protected **122b** in high yield. Protection of the phenol was required prior to the supervening, acetylation step. The benzyl moiety is robust to severe conditions and easily removed

when appropriate; thus it was a logical choice as a protecting group. Stille conditions, entailing the use of tributyl-1-ethoxy(vinyl)stannane and Pd(0) in an inert atmosphere were then applied to **122b**, effectuating **122c** in 89% yield. This approach to acetylation has received very little attention, in fact none for preparing *p*-hydroxyacetophenones from phenol precursors. We have refined this methodology to the point where we routinely obtain >80% yields of targeted compounds. The supervening step entailed α -bromination of **122c** through reaction with dioxane-dibromide at 0°C, furnishing **122d** in ~95% yield as estimated by ¹H NMR. Prudence was required to prevent α,α' -dibromination from occurring; the reaction was generally halted before complete conversion and the yield was estimated by GC/MS or ¹H NMR. Separation of **122d** from **122c** was cumbersome and not essential to the subsequent, caging step; thus, in subsequent studies, no purification was attempted. The procedures through the α -bromination step were routinely used for all pHP and 5-acetylsalicylic acid derivatives. The penultimate step, arguably the most critical, encompassed the “caging” or coupling of GABA with the pHP chromophore. Specifically, **122d** underwent a facile S_N2 reaction with the carboxylic acid terminus of N-Boc protected GABA (Boc, *tert*-butoxycarbonyl) at room temperature in the presence of potassium carbonate, to afford the fully carbamate protected pHP-ester, **122e** in 89% yield. This substrate coupling procedure was commonly used for all carboxylic acid containing substrates, such as GABA, Glu, and long chain alkanes. Complete deprotection, i.e., the removal of the Boc and benzyl moieties of **122e** was effected with distilled trifluoroacetic acid (TFA), 0°C to room temperature, over a 24

Scheme 38. The synthesis of *m*-F-pHP GABA (**122**).



a. BnBr, K₂CO₃, CH₃CN, 16 h, 93%. b. Pd(PPh₃)₄, tributyl(1-ethoxyvinyl)stannane, PhCH₃, 100°C, 18 h, 89%. c. DDB, CH₂Cl₂, 0° to rt, 1 h, 95%. d. N-Boc GABA, K₂CO₃, CH₃CN, rt, 24 h, 89%. e. TFA, 0°C to rt, 24 h, 78%

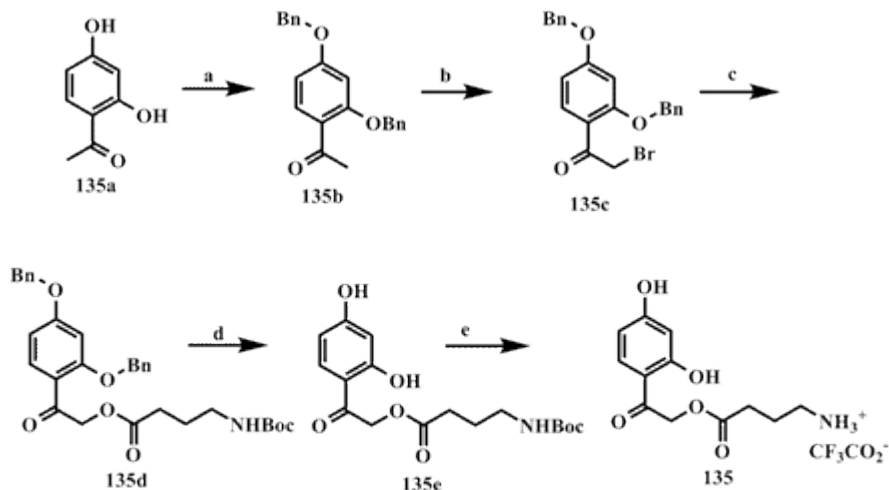
h period. After lyophilization, **122** was produced in 78% yield. The fabrication of **123-132** followed a congruent set of steps as **122**.

The synthetic sequence for **133-139** was initiated with commercially available *p*-hydroxyacetophenones. The *m,m'*-OCH₃-pHP GABA (**133**) and *m*-OCH₃-pHP GABA (**134**) were assembled following the procedure in a prior report.⁹⁷ A modified synthetic procedure for **135-139** was utilized compared to **133** in efforts to achieve a better overall yield.

2) Synthesis of 4-(2-(2,4-dihydroxyphenyl)-2-oxoethoxy)-4-oxobutan-1-aminium-2,2,2-trifluoroacetate, (*o*-OH-pHP GABA, **135).** The synthetic strategy for **135** is

depicted in Scheme 39. To ensure that complete benzylation of commercially available 1-(2,4-dihydroxyphenyl)ethanone (**135b**) was achieved, 3 equivalents of benzyl bromide and 4 equivalents of potassium carbonate were used and reacted for 36 h under mild conditions. After purification, **135b** was furnished in 97% yield. Bromination to **135c** was accomplished under standard conditions in ~94% yield by ¹H NMR. The coupling of N-Boc GABA with **135c** was achieved under standard conditions, though exhibited lower yields than other pHP's giving, **135d** in 48% yield. The diminished yield for this step may originate from a steric effect of the *o*-benzyl group. One additional step involving the facile removal of the benzyl constituent of **135d** was used. The method entailed dissolving **135d** in ethyl acetate, adding activated Pd/C (30% w/w), and then plugging the reaction vessel with a septum. While lightly stirring, hydrogen gas (H₂) was suffused into the reaction vessel by balloon through a long needle positioned near the surface of the solution. A short needle was added as an outlet to permit gas to escape; thus the atmosphere becomes saturated with H₂ generally after one full balloon, at which time the short needle is removed to prevent air from entering the vessel. Prudence was required in the handling of the reaction not only due to the heightened flammability imparted by H₂ but also Pd/C, which itself is extremely flammable. After H₂ addition, the reaction was monitored closely by TLC to prevent undesired reduction of the carbonyl moiety. Complete conversion was achieved after 4 h. Following workup and drying, **135e** was afforded in 97% yield. The last step differed slightly from that used for **122-131**. **135e** was immersed in 1:1 mixture of a TFA:CH₂Cl₂ solution at room temperature.

Scheme 39. Synthesis of the *o*-OH derivative of pHP GABA (**135**).



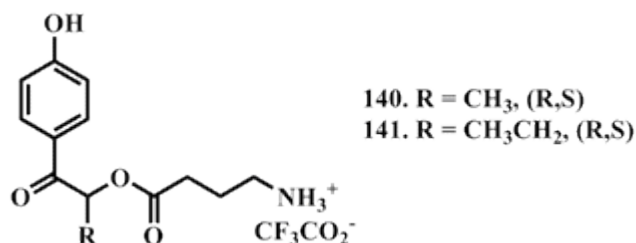
a. BnBr, K₂CO₃, CH₃CN, 36 h, 97%. b. DDB, CH₂Cl₂, 0° to rt, 1 h, ~94%. c. N-Boc GABA, K₂CO₃, CH₃CN, rt, 24 h, 48%. d. Pd/C, H₂, EtOAc, 4 h, 97%. e. TFA:CH₂Cl₂, 1:1, 15 min, rt, 85%.

Significant effervescence was observed from the degradation of the Boc group to CO₂ and isobutylene; the reaction proceeded for ~15 min, and following lyophilization, effected **135** in 85% yield.

Compounds **136-139** were generated in a manner analogous to **135**. When necessary, very slight variations and concentrations in the methodology were used. The yields in each step did not diverge significantly excepting the N-Boc coupling step. Here, yields of **136d-139d** were much improved (>80%); presumably, no *o*-substituent of the magnitude of benzyl ether (**135d**) encumbered the substitution process.

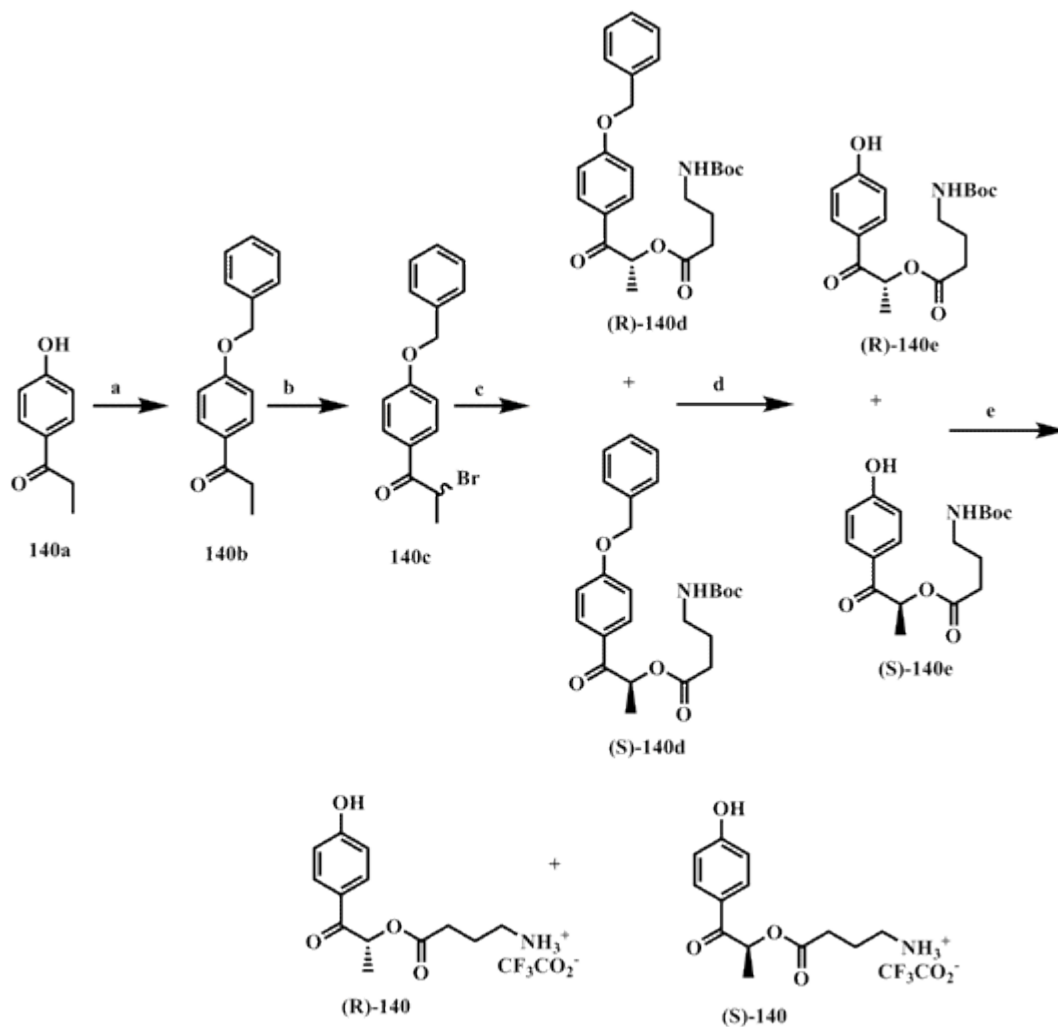
Compounds **140** and **141** represented enantiomeric mixtures of α -methyl and ethyl-pHP GABA analogs (α -methyl and ethyl-pHP GABA, Figure 13).

Figure 13. α -methyl and ethyl-pHP GABA enantiomers, **(R,S)-140** and **(R,S)-141** respectively.



The synthetic procedure to **(R,S)-140** is outlined in Scheme 40. The reaction series commenced with commercially available *p*-hydroxypropiophenone (**140a**) which was then benzylated to **140b**, α -brominated to racemic **140c** and coupled with N-Boc GABA to furnish **(R,S)-140d** as a racemate. Resolution of these using normal phase flash chromatography with various eluents and HPLC was unsuccessful. Subsequent benzyl deprotection to **(R,S)-140e** also defied resolution as did the products after Boc deprotection to generate **(R,S)-140**. Further efforts to isolate these enantiomers from one another were unsuccessful. The α -ethyl analogs, **(R,S)-141**, were synthesized by the same procedure as above and were not successfully resolved either.

Scheme 40. Synthesis of α -methyl-pHP GABA enantiomers, (R,S)-140.

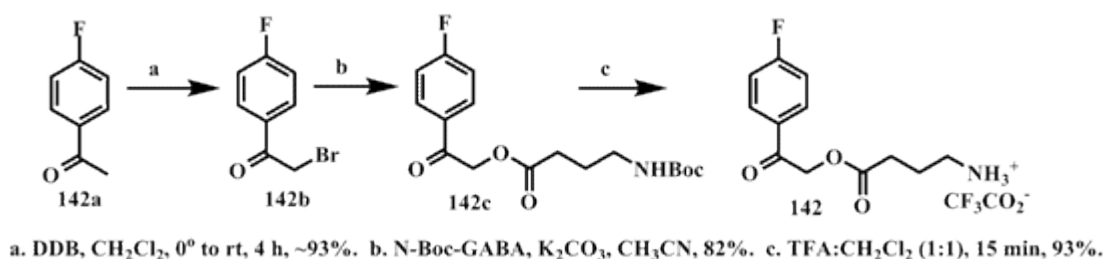


a. BnBr, K_2CO_3 , CH_3CN , 24 h, 96%. b. DDB, CH_2Cl_2 , 0° to rt, 2 h, ~92%. c. N-Boc GABA, K_2CO_3 , CH_3CN , rt, 24 h, 91%. d. Pd/C, H_2 , EtOAc, 4 h, 99%. e. TFA: CH_2Cl_2 , 1:1, 15 min, rt, 90%.

3) Synthesis of 4-(2-(4-fluorophenyl)-2-oxoethoxy)-4-oxobutan-1-aminium 2,2,2-trifluoroacetate, (4-fluorophenacyl GABA, 142). The preparation of 4-(2-(4-fluoro-phenyl)-2-oxoethoxy)-4-oxobutan-1-aminium-2,2,2-trifluoroacetate (**142**) patterned closely after the sequence to generate **135** (Scheme 41); the starting

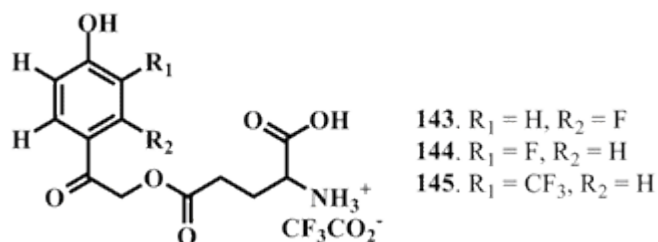
material consisted of 4-fluoroacetophenone (**142a**). The objective in preparing **142** was to examine the π electron donating ability of fluorine, a mimic of hydroxyl, in assisting the photorelease of GABA.

Scheme 41. Synthesis of 4-fluorophenacyl GABA (**142**).



B. pHP-caged *l*-Glu series. A small suite of pHP *l*-glutamate (Glu) compounds were synthesized; these are listed in Figure 14.

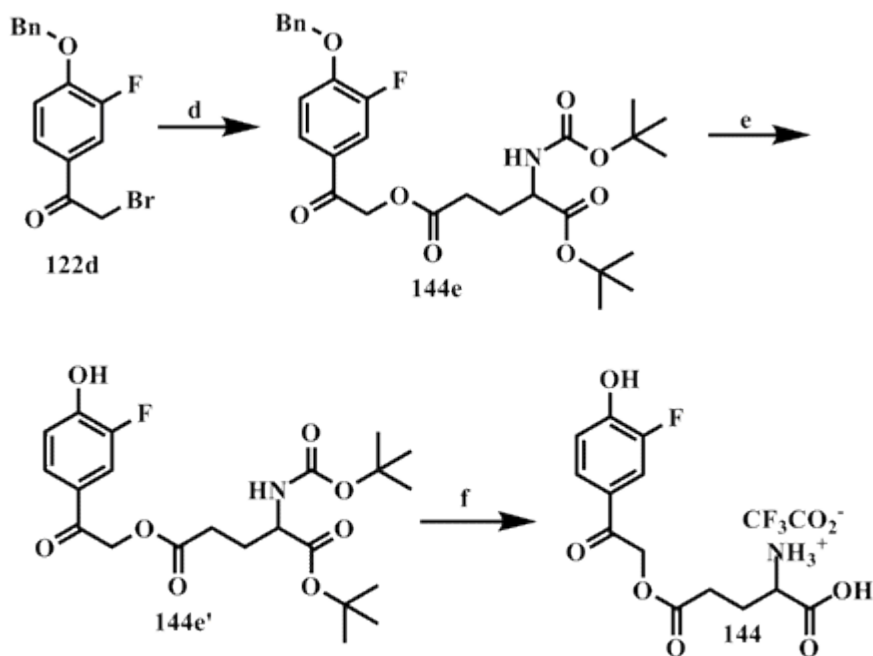
Figure 14. pHP Glu derivatives, **143-145**.



The synthesis of pHP *l*-glutamate derivatives (pHP Glu, **143-145**) involved a congruent set of steps with that of **122**; the yields for corresponding intermediates

were equable with those for **122** as well. A minor alteration for Glu, however, was an additional *tert*-butyl moiety that served to protect the ancillary carboxylic acid (Scheme 42). The effective removal of both the *N*-Boc and *tert*-butyl ester from Glu required extra reaction time in TFA:CH₂Cl₂ (1:1), approximately 2 h at room temperature.

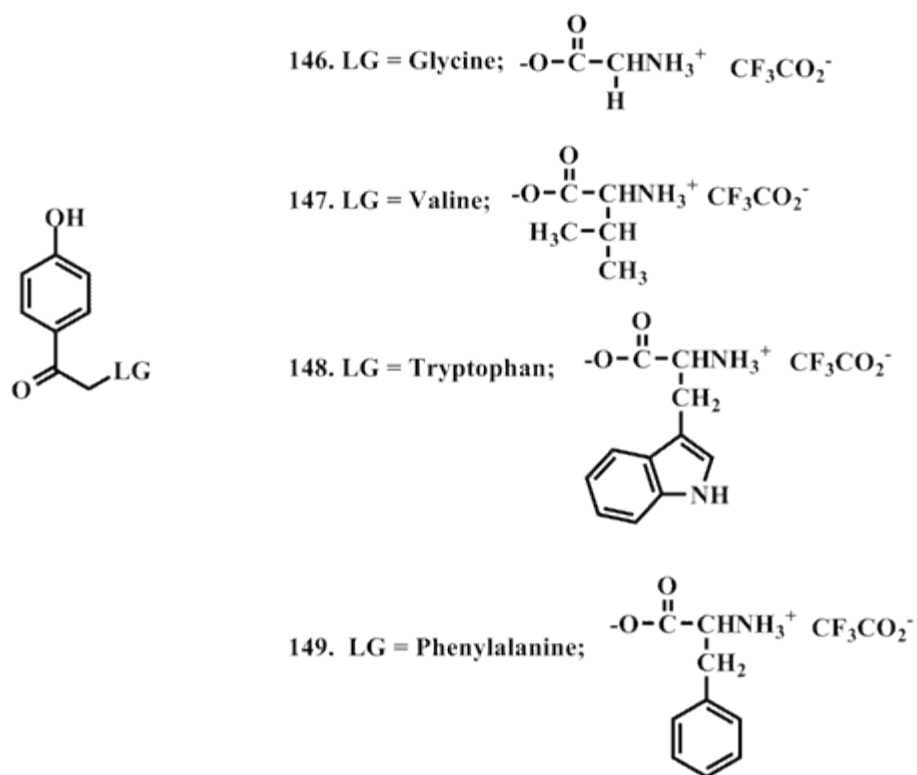
Scheme 42. Synthesis of *m*-F-pHP Glu (**144**).



d. *N*-Boc Glu-*Or*Bu, K₂CO₃, CH₃CN, rt, 24 h, 82%. e. Pd/C, H₂, EtOAc, rt, 94%.
f. TFA:CH₂Cl₂ (1:1), rt, 2 h, 84%

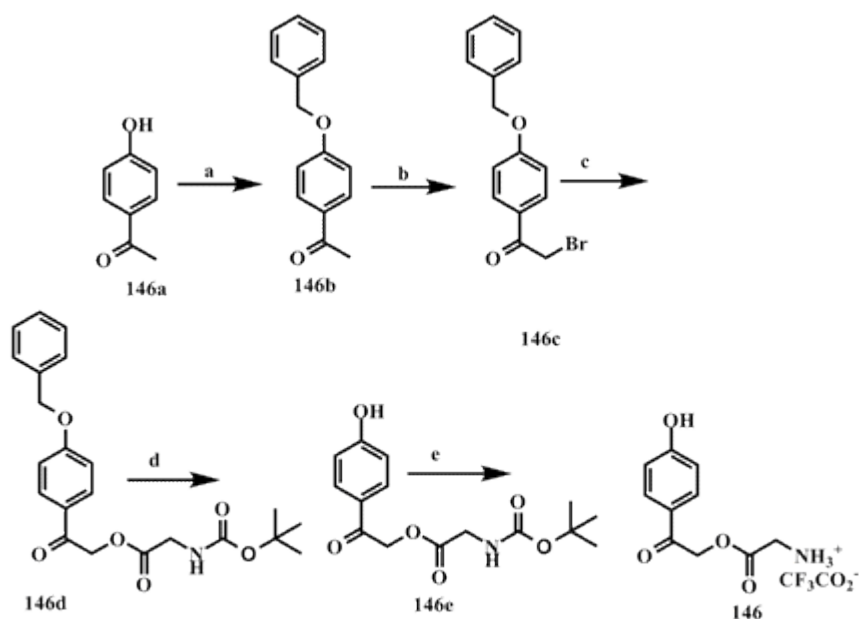
C. Other pHP caged amino-acids. Four additional amino acids were caged to the pHP chromophore (**146-149**). These compounds are listed in Figure 15.

Figure 15. Other pHP caged amino acids, 146-149.



1) **Synthesis of 2-(2-(4-hydroxyphenyl)-2-oxoethoxy)-2-oxoethanaminium 2,2,2-trifluoroacetate, (pHP Gly, 146).** The synthetic progression of steps towards pHP Gly (**146**), are depicted in Scheme 43 and are similar to the sequence for pHP GABA. The sequence commenced with the benzylation of *p*-hydroxyacetophenone using standard conditions, affording **146b** in 98%. Bromination with DDB efficaciously generated **146c** in ~95% yield as indicated by ^1H NMR. The supervening coupling of **146c** with a slight excess of N-Boc Gly in the presence of potassium carbonate, afforded **146d** in 95% yield, which, subsequently underwent Pd catalyzed debenylation to form pHP *N*-Boc Gly (**146e**) in 94%. The last short step was routine

Scheme 43. Synthesis of pHP Gly (**146**).



a. BnBr, K₂CO₃, CH₃CN, 14 h, 97%. b. DDB, CH₂Cl₂, 0° to rt, 1 h, ~95%. c. N-Boc Gly, K₂CO₃, CH₃CN, rt, 24 h, 95%. d. Pd/C, H₂, EtOAc, 4 h, 94%. e. TFA:CH₂Cl₂, 1:1, 15 min, rt, 79%.

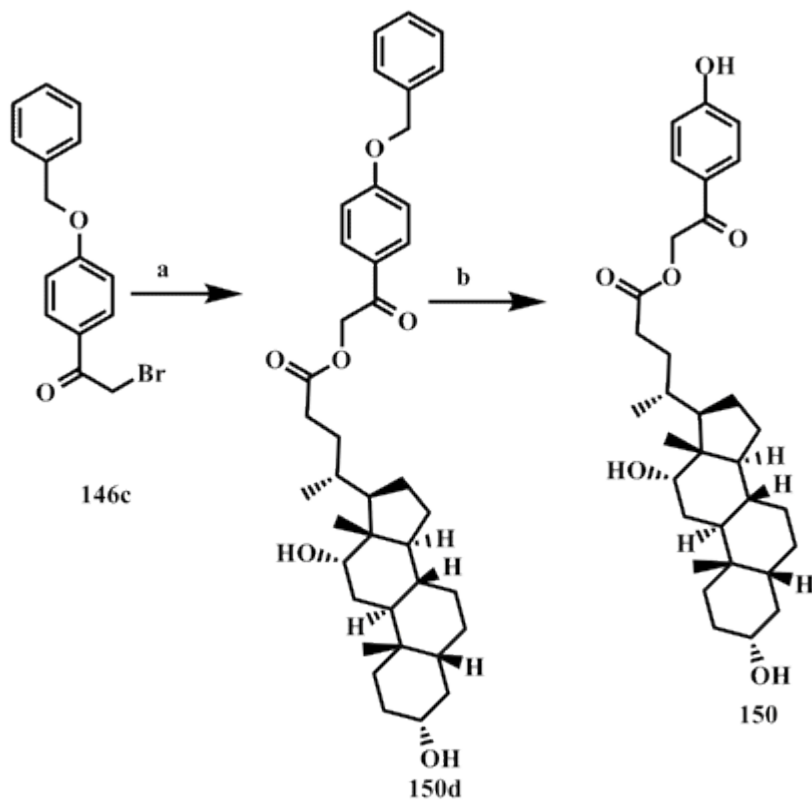
Boc removal to furnish **146** in 79% yield. The assembly of **147-149** paralleled that for **146**. The other amino acids all possessed Boc-protected amine functionalities, akin to Gly; accordingly they were caged to pHP through their carboxylate termini.

D. pHP Deoxycholic acid. The bile acid, deoxycholic acid (DOC), was caged to the pHP chromophore.

1) The synthesis of (4R)-2-(4-hydroxyphenyl)-2-oxo-ethyl-4-((3R,5R,8R,10S,12S,13R,17R)-3,12-dihydroxy-10,13-dimethylhexadecahydro-1H-cyclopenta[a]phenanthren-17-yl)pentanoate, (pHP DOC, **150**). The construction of (4R)-2-(4-hydroxyphenyl)-2-oxoethyl-4-((3R,5R,8R,10S,12S,13R,17R)-3,12-dihydroxy-

10,13-dimethyl-hexadeca-hydro-1H-cyclopenta[a]phenanthren-17-yl)pentanoate (**150**) is illustrated in Scheme 44. The caging step of DOC was similar to **122e**.

Scheme 44. Synthesis of pHP DOC (**150**).



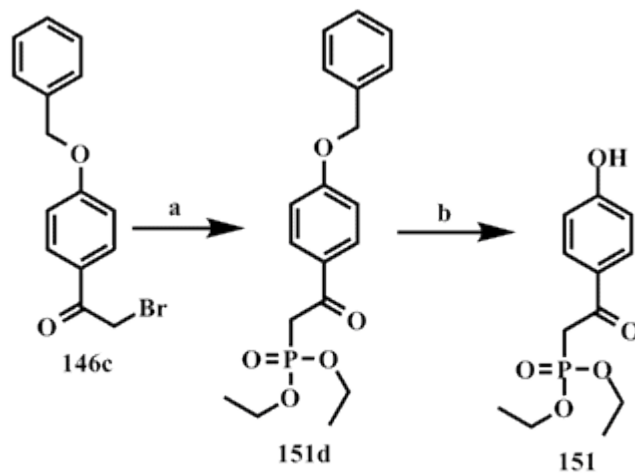
a. DOC, K_2CO_3 , DMF, 22 h, 84%. b. Pd/C, H_2 , EtOAc, 6 h, 93%.

but DMF was employed instead of CH_3CN for solubility reasons, producing **146d** in 84% yield. Reductive hydrogenation of **146d** followed under standard conditions and afforded **150** in 93% yield.

E. pHP Diethyl phosphonate. A diethyl phosphonate moiety was tethered to the pHP chromophore.

1) Synthesis of diethyl 2-(4-hydroxyphenyl)-2-oxoethylphosphonate, (pHP diethyl phosphonate, 151). The preparation of 2-(4-(hydroxyphenyl)-2-oxoethylphosphonate (**151**) to explore the nucleofuge ability of the phosphonate moiety, is displayed in Scheme 45. The initial reaction involved the Michaelis-Arbuzov protocol;⁹⁸ **146c** was heated to 100°C in dry triethylphosphite for 17 h, effectuating **151d** in 86% yield. Catalytic debenzoylation of **151d** then afforded **151** in 96% yield.

Scheme 45. Synthesis of pHP diethyl phosphonate (**151**).



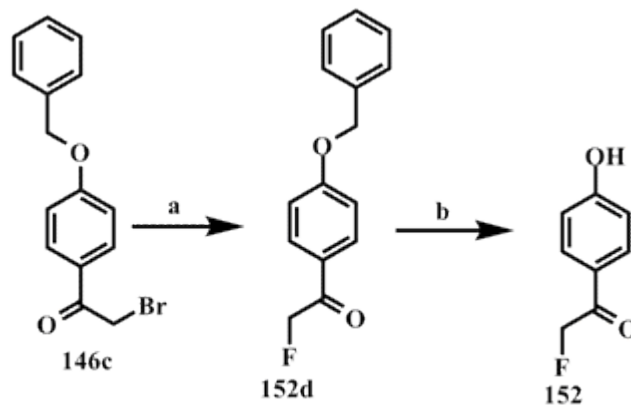
a. Triethylphosphite, 100°C, 17 h, 86%. b. Pd/C, H₂, EtOAc, 2 h, 96%.

F. pHP F. Fluoride was caged by the pHP chromophore.

1) Synthesis of 2-fluoro-1-(4-hydroxyphenyl)ethanone, pHP F 152.

The short series of chemical transformations to make 2-fluoro-1-(4-hydroxy-phenyl)-ethanone (**152**) was a study on the efficacy of fluoride release and is represented in Scheme 46. A facile S_N2 reaction between cesium fluoride and **146c** in refluxing CH_3CN for 3 h quantitatively produced **152d** by GC/MS analysis, 90% isolated yield. This was followed by a standard Pd/C reduction protocol to debenzoylation of **152d**, engendering **152** in 92% isolated yield.

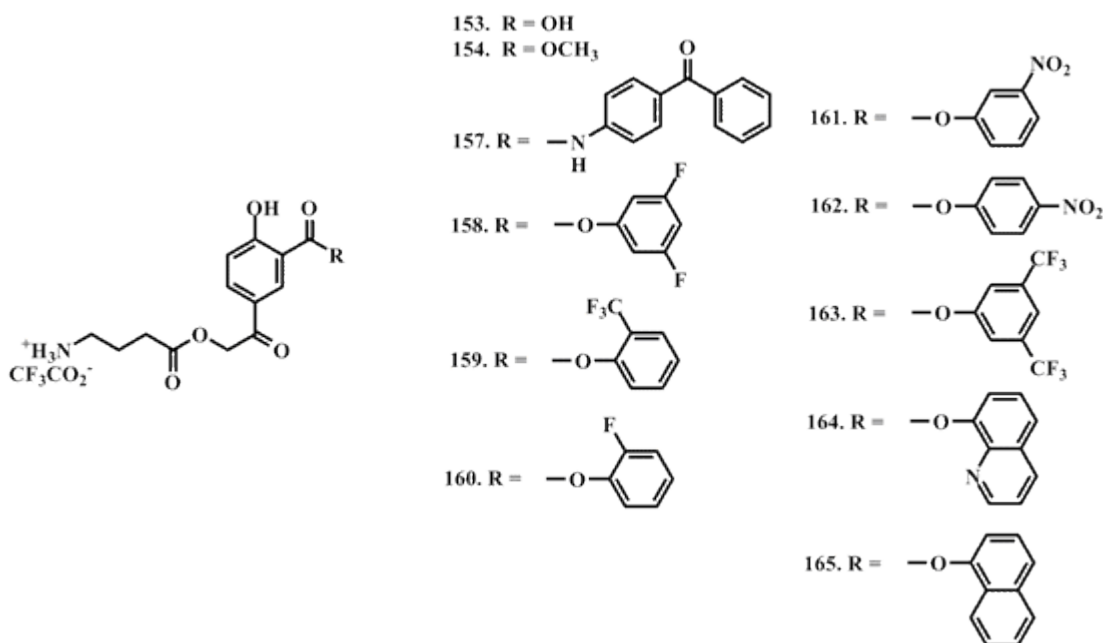
Scheme 46. Synthesis of pHP F (**152**).



a. CsF , CH_3CN , reflux, 3 h, 90%. b. Pd/C , H_2 , $EtOAc$, 6 h, 92%.

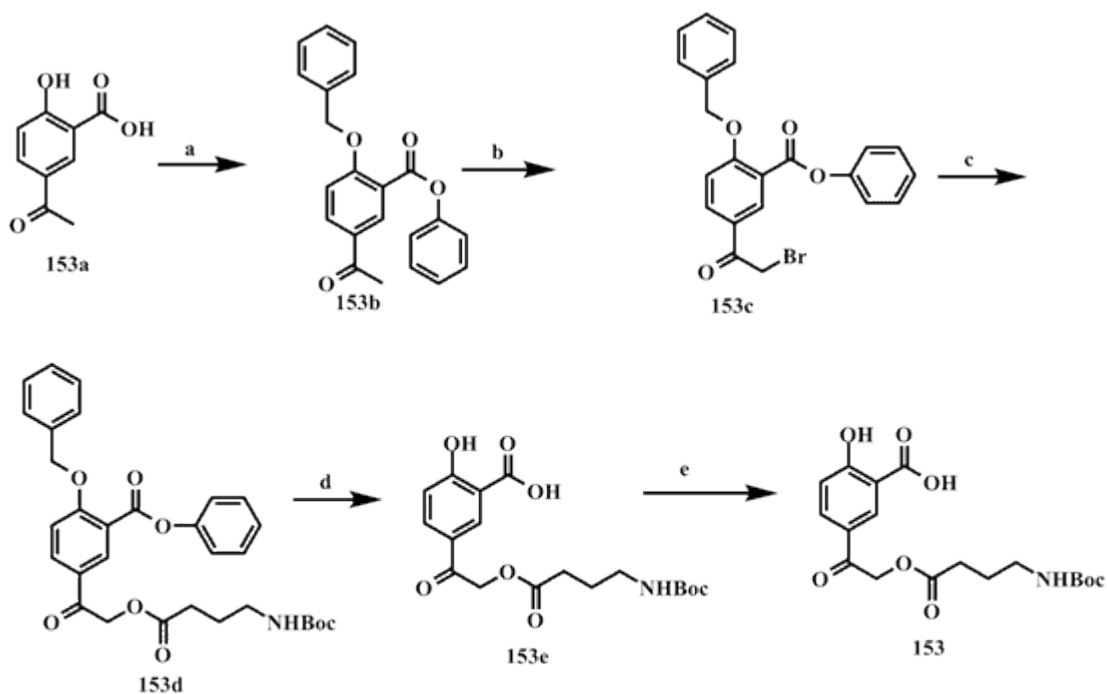
G. 5-acetylsalicylate and salicylamide GABA's. An array of novel 5-acetylsalicylate GABA and alkyl esters and one 5-acetylsalicylamide were assembled to distinguish possible antennae effects on GABA release. These, **153**, **154**, and **157-165** are represented in Figure 16. Compounds **155** and **156**, which possess alkanoyl substrates in place of GABA, will be introduced later.

Figure 16. 5-acetylsalicylic acid and salicylate GABA derivatives, **153**, **154**, **157-165**.



1) Synthesis of 4-(2-(3-carboxy-4-hydroxyphenyl)-2-oxoethoxy)-4-oxobutan-1-aminium-2,2,2-trifluoroacetate, (5-acetylsalicylic acid GABA, **153).** The synthetic approach to 4-(2-(3-carboxy-4-hydroxyphenyl)-2-oxoethoxy)-4-oxobutan-1-aminium-2,2,2-trifluoroacetate (**153**), for a substituent effect study on GABA release, is manifest in Scheme 47. The precursor, 5-acetylsalicylic acid (**153a**) was reacted with a surfeit of benzyl bromide and potassium carbonate, the same approach to generate **135b**, to provide the dibenzylated analog; the ensuing string of steps to produce **153** were analogous to those previously described for GABA coupling and complete deprotection. The starting material utilized in the preparation of **154** was the methyl ester of **153a**; an ordinary sequence of steps was followed for the coupling of GABA and subsequent deprotection.

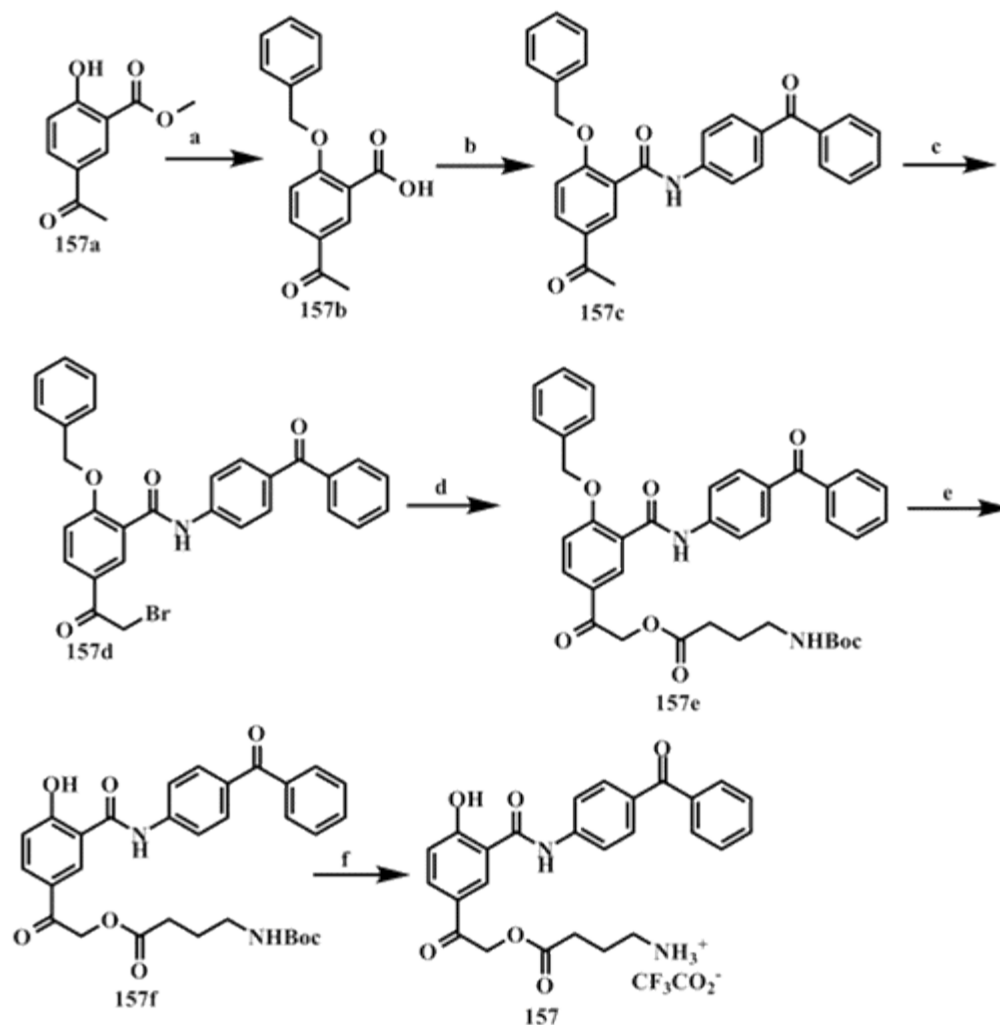
Scheme 47. Synthesis of 5-acetylsalicylic acid GABA (**153**).



a. BnBr, K₂CO₃, CH₃CN, 98% b. DDB, CH₂Cl₂, 0°C to rt, 2 h, ~ 95%.
 c) N-Boc GABA, K₂CO₃, CH₃CN, 24 h, 75%.
 d. Pd/C, H₂, EtOAc, 96%. e. TFA:CH₂Cl₂ (1:1), 15 min, 94%.

2) Synthesis of 4-(2-(3-(4-benzoylphenylcarbamoyl)-4-hydroxyphenyl)-2-oxoethoxy)-4-oxobutan-1-aminium 2,2,2-trifluoroacetate, (5-acetyl salicylamide benzophenone GABA, **157**). The procedure to compose **157** is divulged in Scheme 48. The initial step involved the benzyl protection of commercially available **157a** under standard conditions that was then hydrolyzed in 6 M KOH for 2 h at room temperature generating benzyl protected 5-acetylsalicylic acid (**157b**) in 98% yield after workup with conc. HCl. The second step involved concerned a Steglich esterification,⁹⁹ whereby **157b** was reacted with DCC and 4-aminobenzophenone in

Scheme 48. 5-acetyl salicylamide benzophenone GABA (**157**).

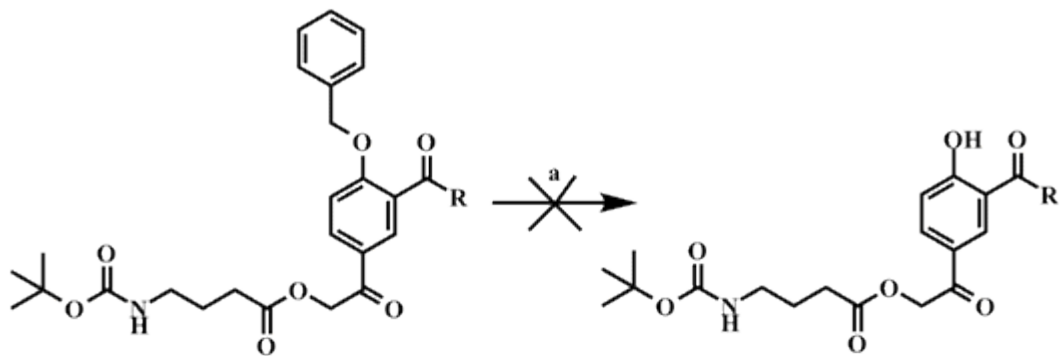


the presence of DMAP at 0°C for 12 h. After filtration to remove dicyclohexylurea (DCU), a byproduct of the reaction, and purification, **157c** was generated in 74% yield. Subsequent conversion to the α -bromo analog (**157d**) was facile by standard procedure. N-Boc GABA coupling to **157d** proved to be challenging. The reaction

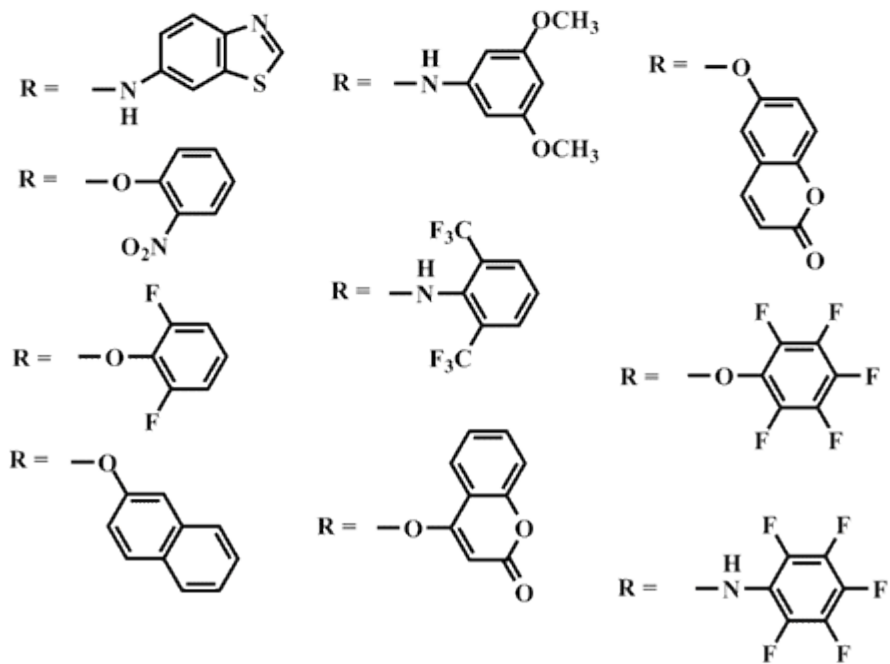
was attempted several times; the number of equivalents of N-Boc GABA was altered from 1.3 to 2.5 and reaction times from 24 to 48 h. TLC did not provide sufficient evidence to determine the extent of conversion and hence was abandoned. The reaction yields hovered around 46% irrespective of changes in conditions. At this time no explanation can be provided to account for the relatively low yields. Standard deprotection procedures converted **157d** to **157** in relatively high yield. The same protocol was utilized to assemble **158-165**.

The limiting step in the succession proved to be Pd-mediated hydrogenation to restore the phenol functionality, i.e., *step c*. Due to the reduction prospect of the carbonyl moiety, the reaction was assiduously monitored by thin layer chromatography. Compounds **153-165** exhibited discrete retentions in a variety of eluent mixtures and hence permitted the reaction to be followed until completion. However, at least a half dozen other analogs were synthesized that contained a Boc-GABA tethered constituent but evinced unchanged retentions between the benzylated and free phenol forms in all eluent mixtures. These compounds are listed in Figure 17. In these instances, the reaction progress could not be followed; highly variable product mixtures resulted from “guesses” of reaction times. The segregation of these products was cumbersome as these reactions were conducted on very small scales. The relatively labile carbamate and ester linkages possessed by the precursors precluded other common approaches to debenylation, such as TFA, TMSI, or AlCl₃. Several iterations with minor changes in conditions, such as solvent, Pd/C content,

Figure 17. 5-acetylsalicylate GABA compounds where the standard Pd/C protocol for debenzoylation wasn't effective.



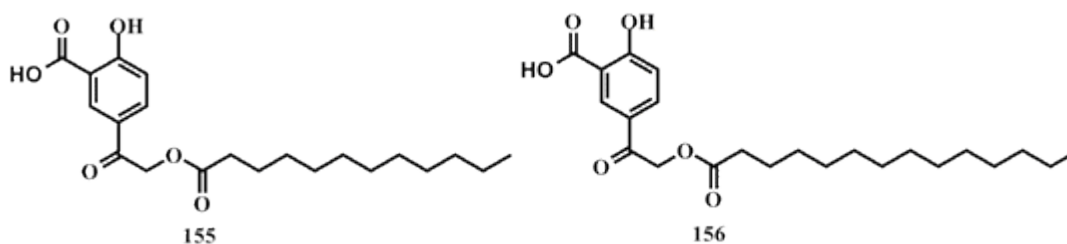
a. Pd/C, H₂, EtOAc or THF



etc. were ineffectual. Hence, a new strategy is required to educe improved conversions for this step or simply the use of a different protecting group. These derivatives were not studied further.

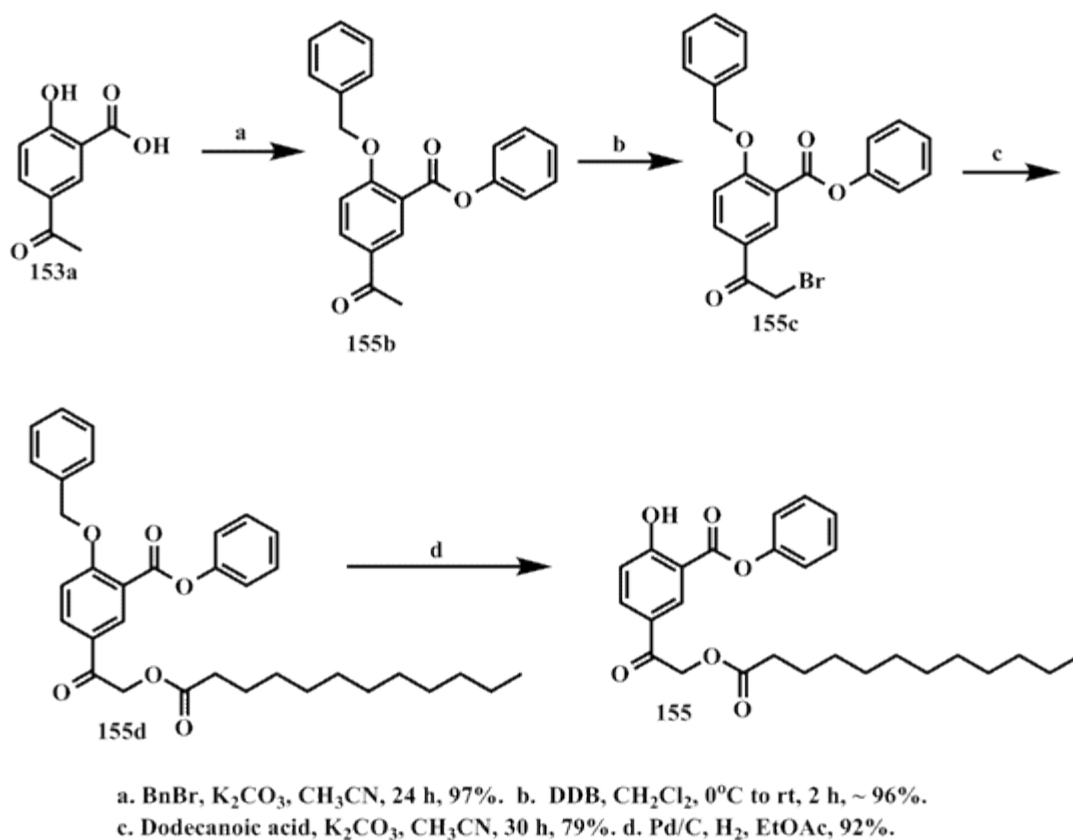
H. 5-acetylsalicylic acid alkanoyl compounds. Two 5-acetylsalicylic acid alkanoyl compounds were synthesized, **155** and **156** (Figure 18).

Figure 18. Two 5-acetylsalicylic acid alkanoyl derivatives, **155** and **156**.



1) Synthesis of 5-(2-(dodecanoyloxy)acetyl)-2-hydroxybenzoic acid, (5-acetylsalicylic acid dodecanoate, 155). The synthesis of 5-(2-(dodecanoyloxy)acetyl)-2-hydroxybenzoic acid (**155**) was completed to study its utility as a photocleavable surfactant¹⁰⁰ (Scheme 49). The short series of steps commenced with 5-acetylsalicylic acid (**153a**). The same benzylation protocol was utilized as for the assembly of **153b** but without the hydrolysis phase, to afford **155b** in high yield. Standard bromination conditions were used to furnish **155c** in high yield. The subsequent reaction of **155c** with a 2 molar excess of dodecanoic acid in a standard coupling method generated **155d** in 71% yield. Lastly, **155** was produced under common debenylation conditions in high yield. The same procedure was adhered to in generating 2-hydroxy-5-(2-(tetradecanoyloxy)acetyl)benzoic acid (**156**).

Scheme 49. Synthesis of 5-acetylsalicylic acid dodecanoate (**155**).

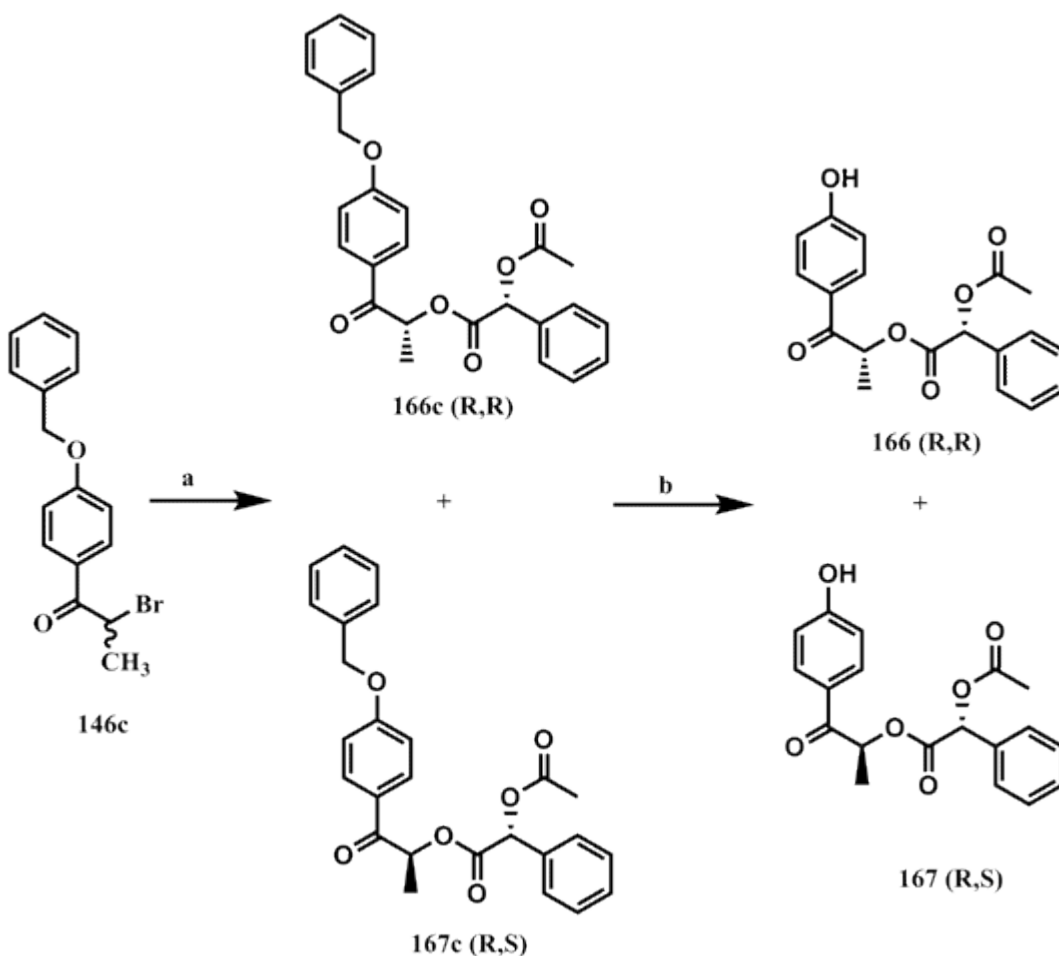


I. α -alkyl-pHP diastereomers. Two α -alkyl-pHP diastereomers were synthesized.

1) Synthesis of ((R)-((R)-1-(4-hydroxyphenyl)-1-oxopropan-2-yl) 2-acetoxy-2-phenylacetate, **166**) and ((R)-((S)-1-(4-hydroxyphenyl)-1-oxopropan-2-yl) 2-acetoxy-2-phenylacetate, **167**). The synthetic strategy for the construction of diastereomers (R)-((R)-1-(4-hydroxyphenyl)-1-oxopropan-2-yl) 2-acetoxy-2-phenylacetate (**166**) and (R)-((S)-1-(4-hydroxyphenyl)-1-oxopropan-2-yl) 2-acetoxy-2-phenylacetate (**167**), is outlined in Scheme 50. The starting material for the sequence consisted of racemic 1-(4-(benzyloxy)phenyl)-2-bromopropan-1-one (**140c**)

which underwent a S_N2 reaction with (*R*)-2-acetoxy-2-phenylacetic acid in the presence of potassium carbonate to afford a mixture of **166a** and **167a** in 94% overall yield. Efforts to segregate these diastereomers were ineffectual. Standard debenzylation

Scheme 50. Synthesis of α -methyl-pHP diastereomers (**166** and **167**).



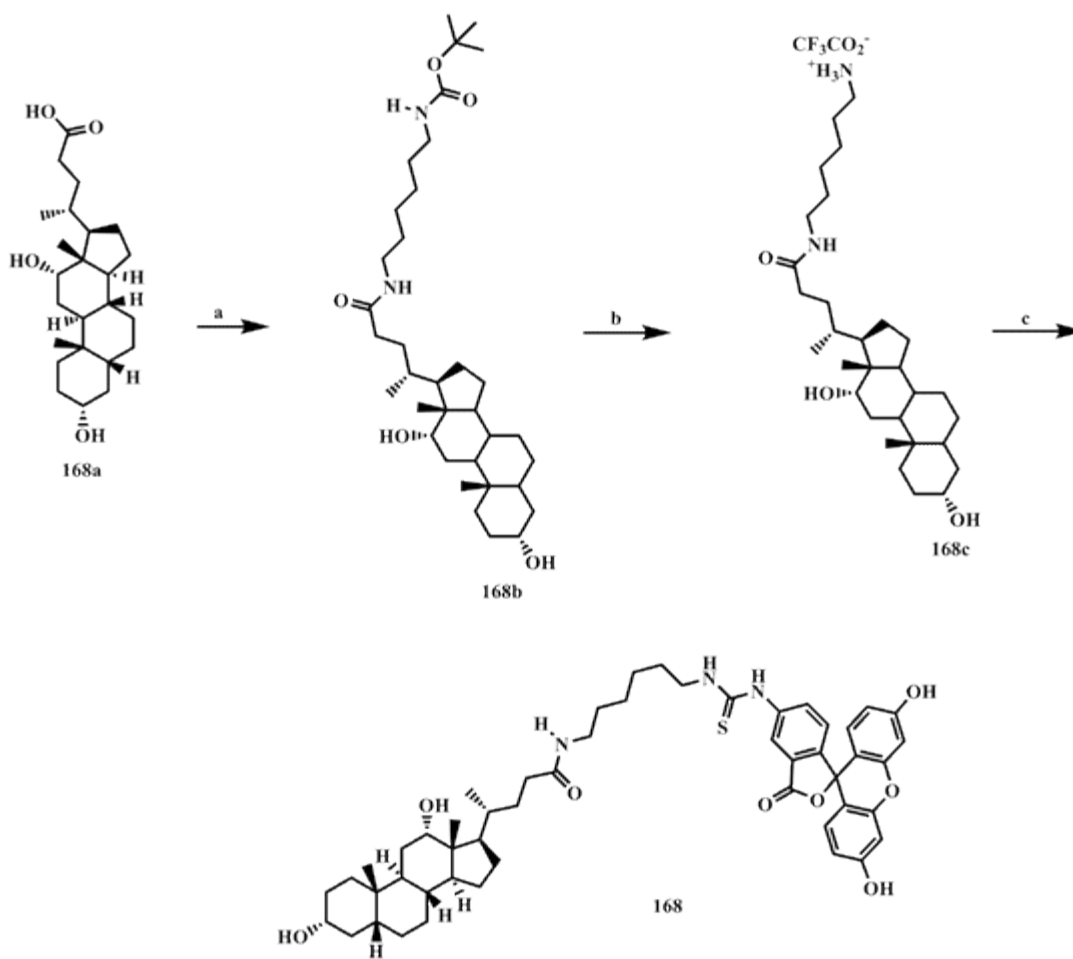
a. (*R*)-2-acetoxy-2-phenylacetic acid, K_2CO_3 , CH_3CN , 94%. b. Pd/C, H_2 , EtOAc, 99%.

conditions permitted **166a** and **167a** to be converted to **166** and **167**, respectively, in 99% yield. Attempts to separate these diastereomers by normal phase silica chromatography and reverse phase HPLC were unsuccessful. Further work on this series is expected upon completion of the thesis.

J. FITC-DOC. A molecule derived from fluorescein isothiocyanate and deoxycholic acid was constructed and given to collaborators for use in biological assays. Details from these assays will be provided in the *Discussion* section.

1) Synthesis of (R)-4-((3R,5R,8R,9S,10S,12S,13R,14S,17R)-3,12-dihydroxy-10,13-dimethylhexadecahydro-1H-cyclopenta[a]phenanthren-17-yl)-N-(6-(3-(3',6'-dihydroxy-3-oxo-3H-spiro[isobenzofuran-1,9'-xanthene]-5-yl)-thioureido)-hexyl)-pentanamide, (FITC-DOC, 168). The process for the fabrication of **168** is exhibited in Scheme 51. The series commenced with a modified Steglich esterification,¹⁰¹ where deoxycholic acid, **168a**, was reacted with 1-ethyl-3-(3-dimethyl aminopropyl) carbodiimide hydrochloride (EDCI) modified *N*-Boc-1,6-hexaneamine with *N*-hydroxybenzotriazole as an initiator to furnish **168b**. This compound was not isolated but further reacted with 4 M HCl in 1,4-dioxane for a short time to induce *N*-Boc degradation and form the ammonium trifluoroacetate species (**168c**) in good yield. The last step involved base (triethylamine) assisted, nucleophilic addition of **168c** to fluorescein isothiocyanate (FITC) to afford **168** in moderate yield.

Scheme 51. Synthesis of FITC-DOC (168).



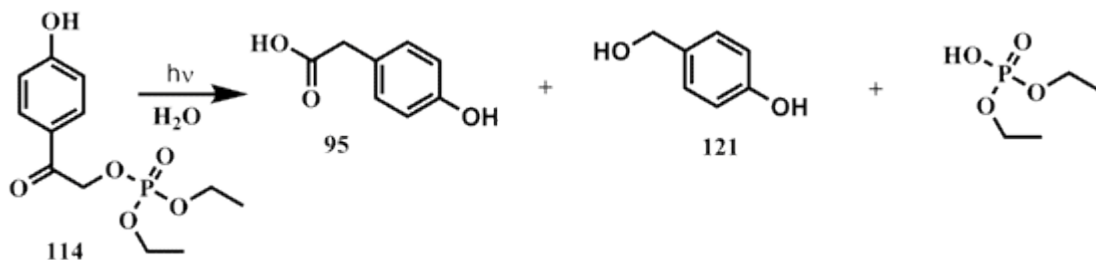
a. EDCI, HOBT, N-Boc-1,6-hexanediamine, DMF, 24 h, then b. 4M HCl in 1,4-dioxane, 1 h, 75%.
c. FITC, CH₃OH, slow addition of TEA, 0° C, 16 h, 53%.

II. Exploratory Photochemistry

As discussed in the *Introduction*, photolysis of the pHP caged complexes in aqueous media generally results in facile substrate release and concurrent precursor

rearrangement to the major *p*-hydroxyphenylacetic acid chromophore and minor *p*-hydroxybenzyl alcohol (abbreviated Scheme 37, *Introduction*).

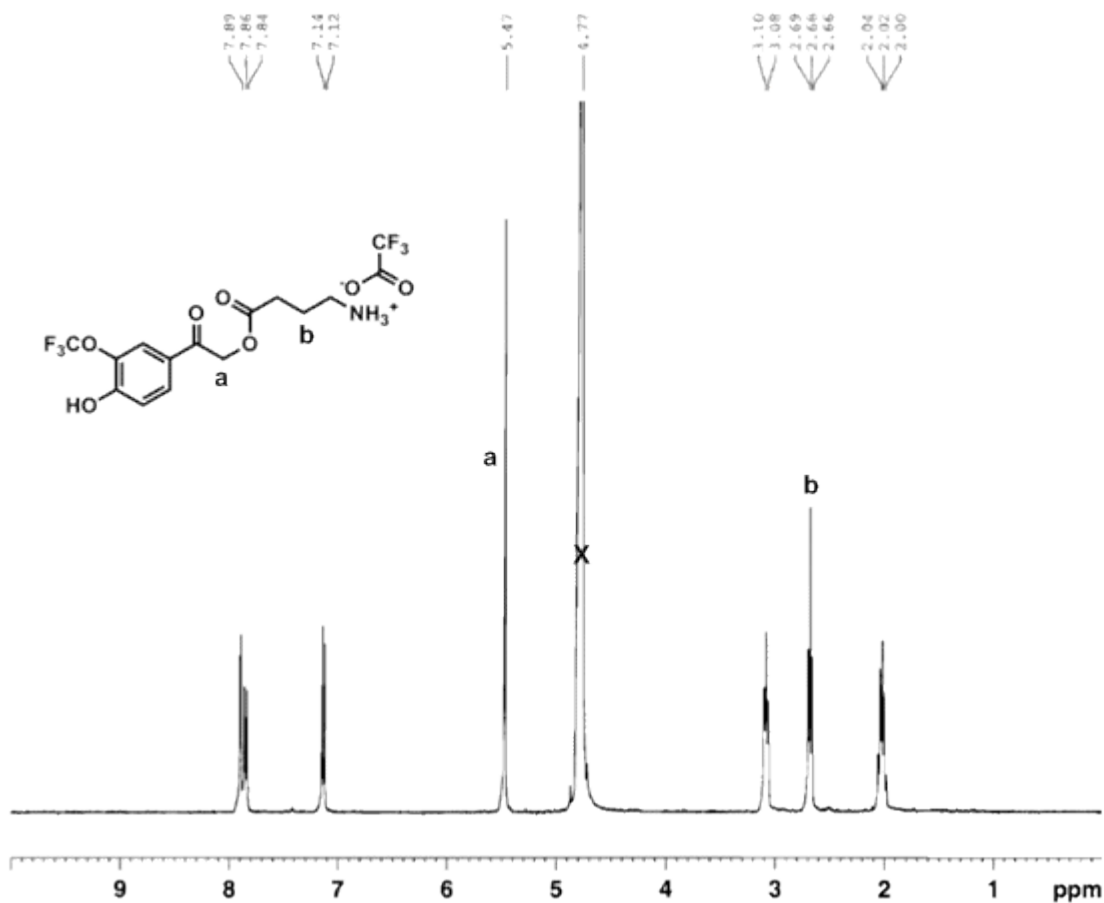
Scheme 37. (from the *Introduction*) Photolysis of *p*-hydroxyphenacyl diethyl phosphate (**114**) in water.



The formation of *p*-hydroxyphenylacetic acid (**95**) and *p*-hydroxybenzyl alcohol (**121**), a newly discovered minor product, are easily discerned by ^1H NMR analysis when pHP caged compounds are dissolved in deuterium labeled hydroxylic solvents, as D_2O , then irradiated. The methylene unit of **95** has a characteristic chemical shift, $\delta = 3.6$ ppm and that corresponding to **121**, $\delta = 4.5$ ppm. The peaks corresponding to the methylene constituents of pHP GABA precursors, **95** and **121**, being conspicuous indicators of a photochemical reaction, are denoted as *signature* peaks. To investigate whether this phenomenon is consistent with caged pHP derivatives **122-167**, preliminary photolyses monitored by ^1H NMR were conducted in aqueous media under standard (non degassed, room temperature) conditions in NMR tubes.

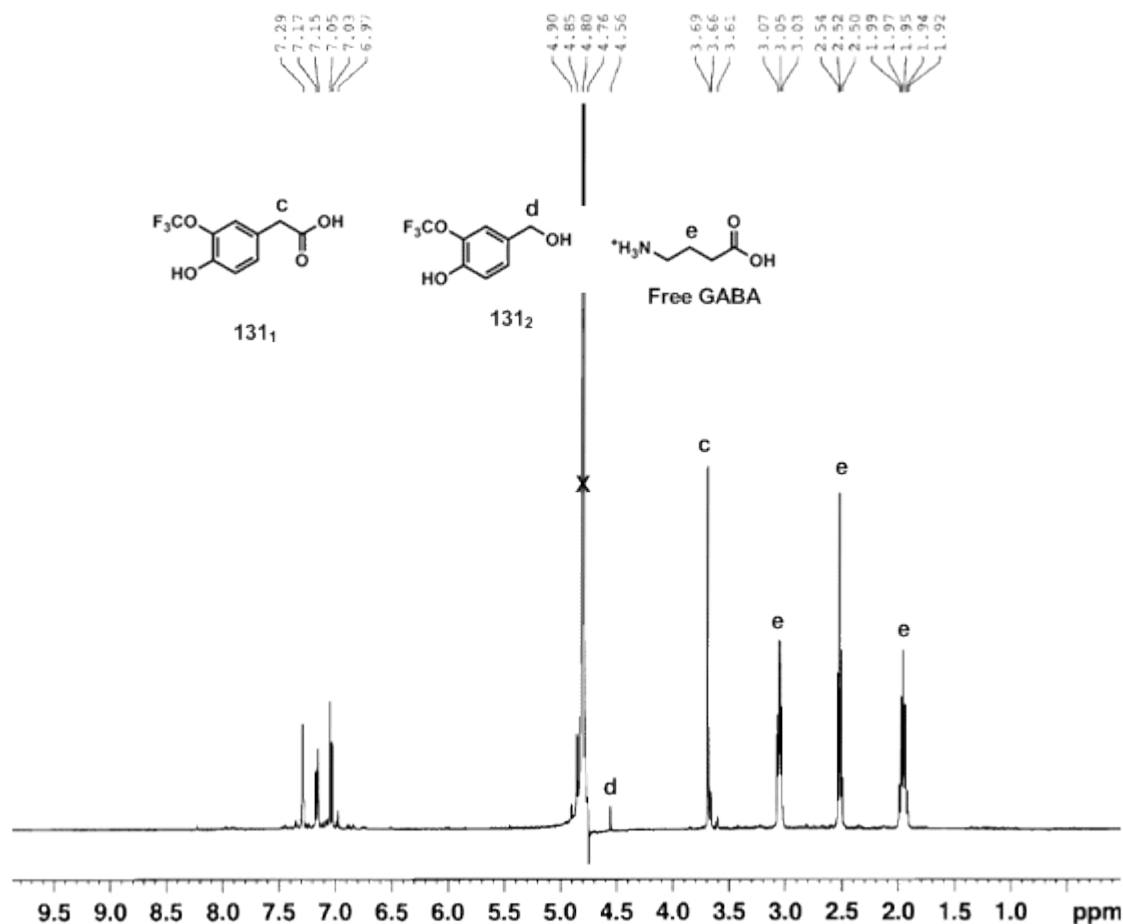
A. pHP GABA and 4-fluorophenacyl GABA ester investigations employing ^1H NMR spectroscopy. Irradiation at 300 nm of 1-10 mM concentrations of pHP GABA esters (**122-142**) in D_2O were followed up to 2 h. ^1H NMR analysis was implemented to identify the constituents of the mixture. A number of pHP GABA derivatives manifested an inertness to photolysis; these included, *m*- NO_2 -pHP GABA (**132**), *o*-OH-pHP GABA (**135**), *m*-OH-pHP GABA (**136**) and 4-fluorophenacyl GABA (**142**). Protracted irradiation times up to 24 h at 254, 300, and 350 nm produced no detectible *p*-hydroxyphenylacetic acids, as determined from the lack of characteristic chemical shifts, and only small amounts of hydrolysis products, i.e., α -hydroxyl (acyloin) acetophenones, presumably resulting from the thermal, ground state reaction. Compounds **122-131** and **137-141** evinced clean photorelease of GABA, with *p*-hydroxyphenylacetic acids as the major products estimated to be $\geq 95\%$ and *p*-hydroxybenzyl alcohol as the minor product estimated to be $\leq 5\%$. *No other photoproducts from these precursors were observed by ^1H NMR.* An example of this is illustrated with ^1H NMR spectra associated with photolysis of 0.02 M *m*- OCF_3 -pHP GABA (**131**) in D_2O (Figures 19-23). Prior to photolysis, **131** manifested two signature sets of signals; the methylene component, labeled **a** at $\delta = 5.47$ ppm, and the tethered GABA region in the aliphatic region, assigned **b**. The large signal at $\delta \sim 4.80$ ppm represents HOD, which will be commonly seen in all spectra where D_2O was utilized as the primary solvent. After 2 h of irradiation, pronounced vicissitudes in

Figure 19. ^1H NMR spectrum of *m*-OCF₃-pHP GABA (**131**) in D₂O.



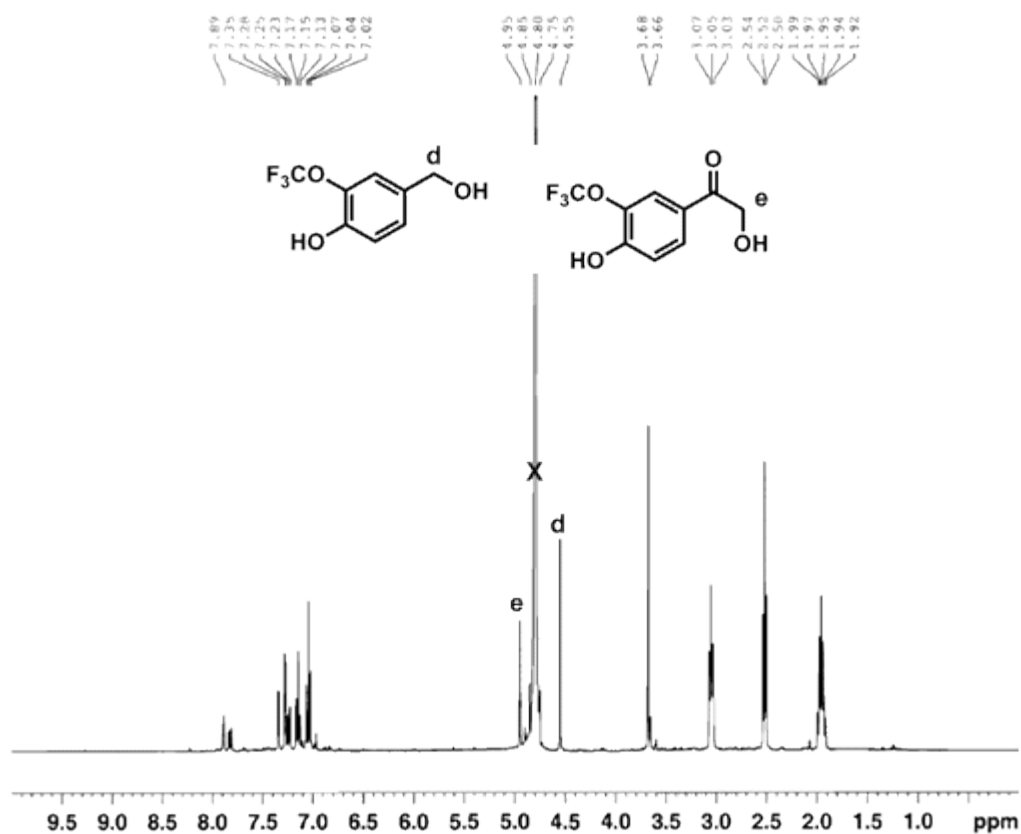
the ^1H NMR spectrum was evident (Figure 20). The signal associated with **a** is absent and two new peaks have materialized; the signal labeled **c** at $\delta = 3.66$ ppm represents the methylene unit of *p*-hydroxyphenylacetic acid (**131**₁) and the small peak labeled **d** at $\delta = 4.56$ ppm that corresponds to the methylene group of *p*-hydroxybenzyl alcohol (**131**₂). The bands that are assigned **e** correlate with free GABA, which divulge subtle differences in chemical shifts compared to caged GABA. The peak at **c** is incontrovertibly linked to the methylene of **131**₁ based on

Figure 20. ^1H NMR spectrum after 2 h photolysis of **131** in D_2O .



spiking experiments with an *authentic sample*; this entailed adding a pure sample of *p*-hydroxyphenylacetic acid to the photolysis mixture. Supervening ^1H NMR analysis manifested increases in intensities of peaks linked to this entity. In addition, to corroborate the assignment of **d** to **131₂**, *p*-hydroxy-*m*-trifluoromethoxybenzyl alcohol was independently synthesized and the authentic sample was then added into the photolysis mixture for ^1H NMR analysis, shown in Figure 21. The ^1H NMR band

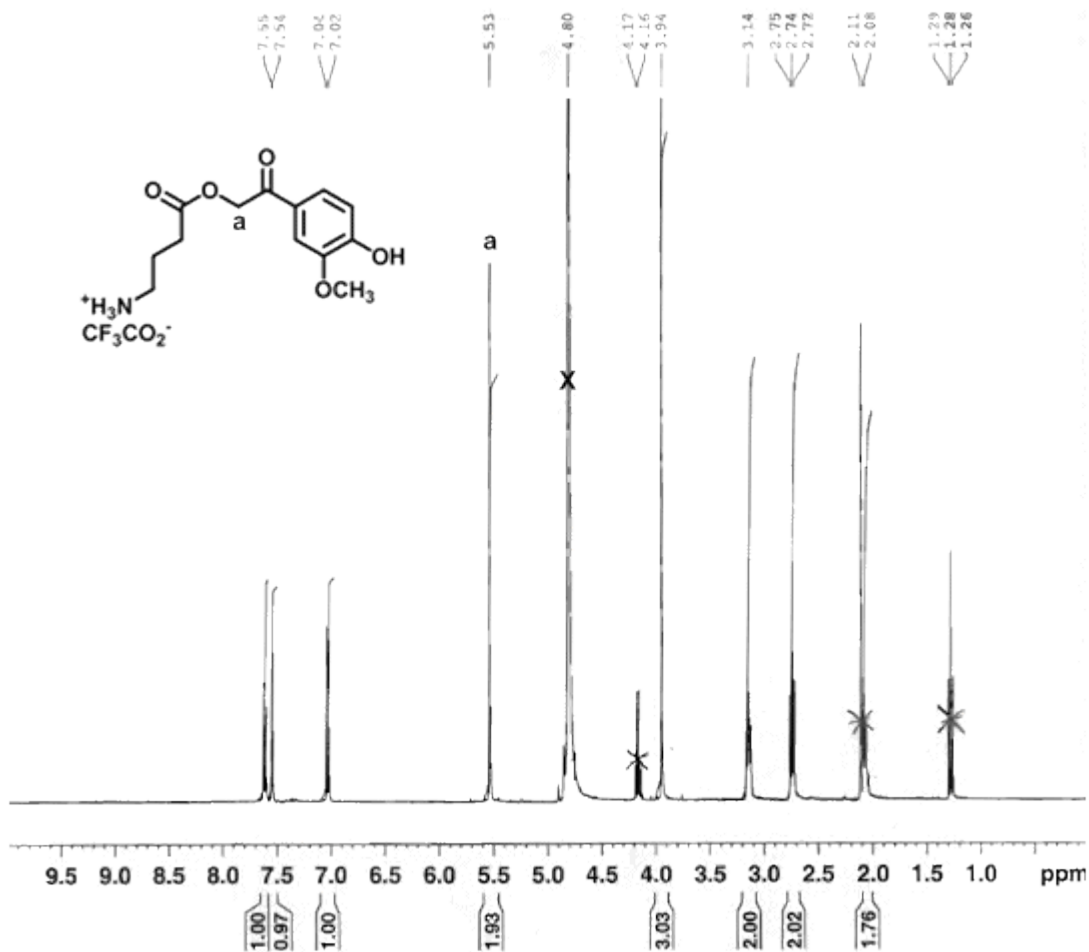
Figure 21. Spiking experiment with *p*-hydroxy-*m*-trifluoromethoxybenzyl alcohol (**131**₂).



intensity of **d** at $\delta = 4.55$ ppm is pronounced and is associated with the increase in the concentration of **131**₂, unequivocally confirming the presence of the benzyl alcohol. It should be noted that the peak near $\delta = 4.90$ ppm could constitute another variant, the acyloin **131**₃. Another, authentically synthesized sample of the *m*-OCF₃-acyloin was prepared and added to the sample to discern whether it was a photoproduct; the appearance of a new signal at **e** with $\delta = 4.95$ ppm next to the 4.90 ppm signal clearly demonstrated the absence of **131**₃, precluding the acyloin as a photoproduct. Likewise, ¹⁹F NMR's were examined where spiking experiments bolstered the ¹H

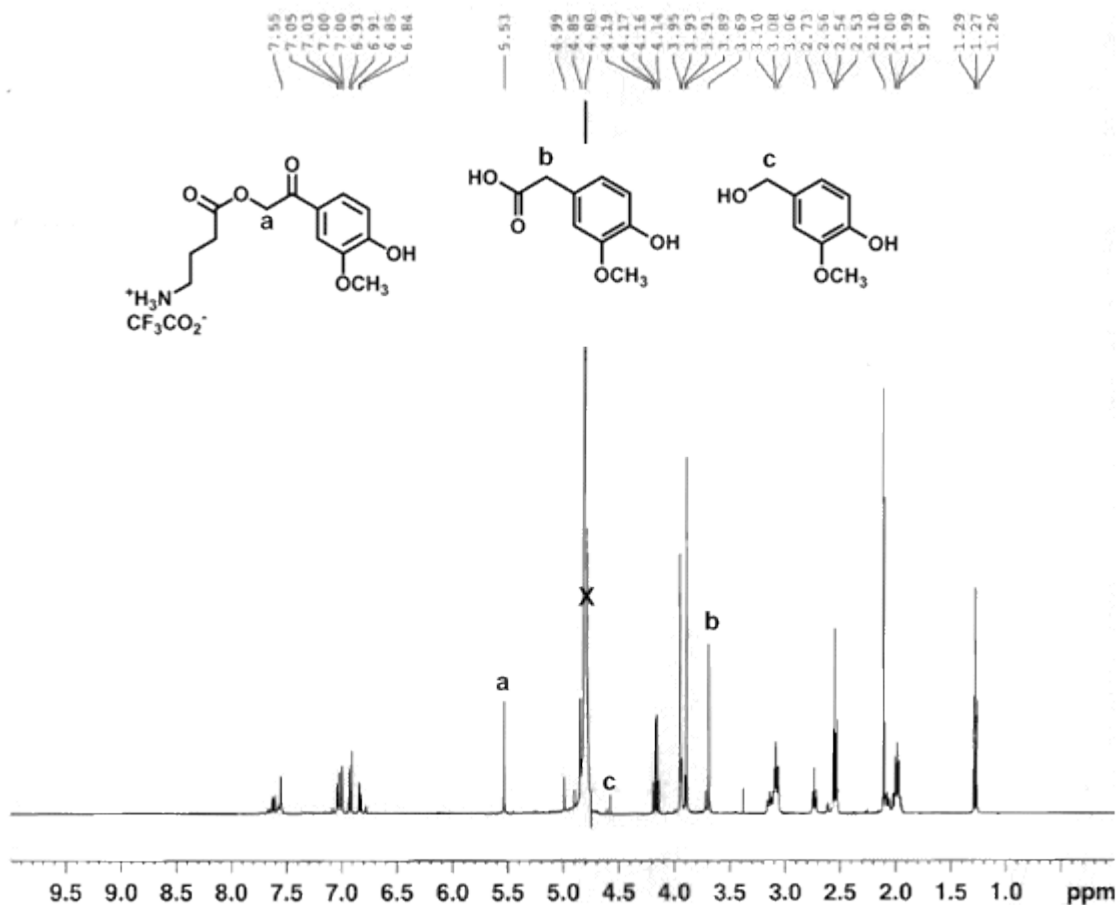
NMR results. The results of photolyses of *m*-OCH₃-pHP GABA (**134**) and *m,m'*-diOCH₃-pHP GABA (**133**) were also investigated by ¹H NMR analysis. These had been reported to exhibit preponderant GABA release pathways that were not related to pHP rearrangement at 300 nm.⁹⁷ A 0.03 M solution of **134** in D₂O was prepared (Figure 22 the signature band is designated **a**, the methylene protons at δ = 5.53 ppm)

Figure 22. Pre-photolysis ¹H NMR spectrum of *m*-OCH₃-pHP GABA (**134**) in D₂O.



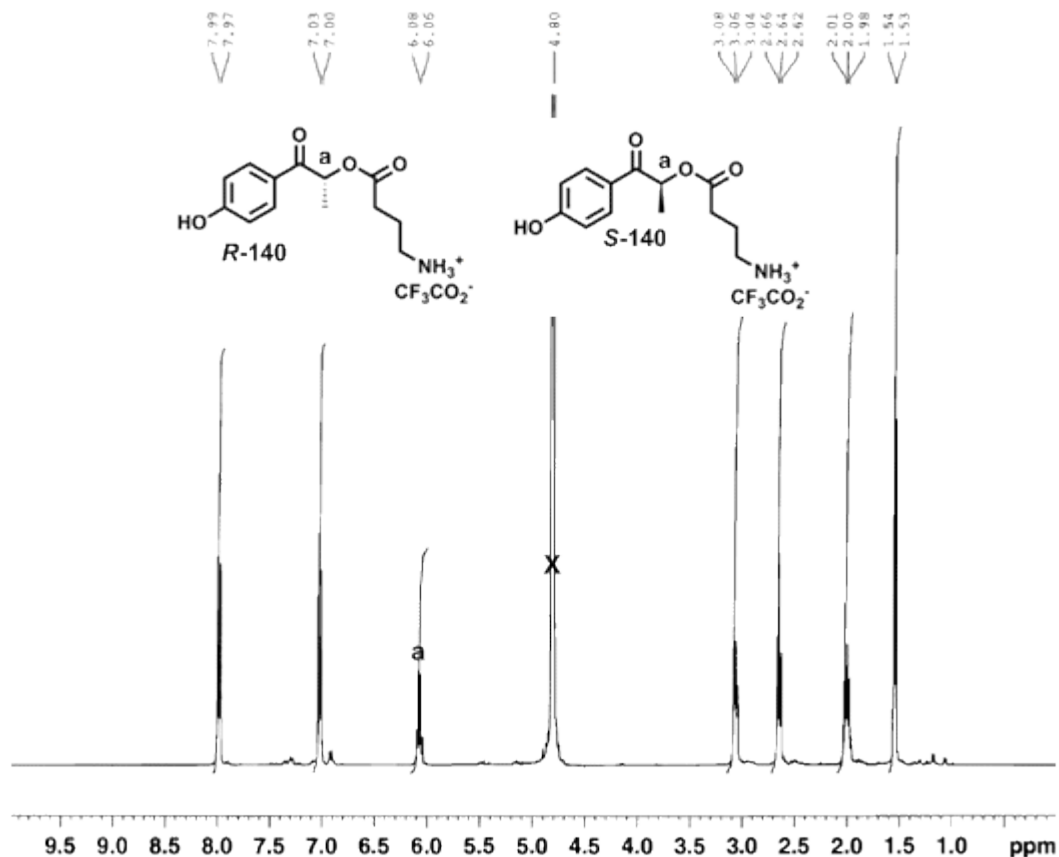
and then irradiated for 90 min at 300 nm (Figure 23). The salient chemical entity in the photolysis mixture was unmistakably unreacted starting material; it held true to the reported very low quantum efficiency for conversion. The major photoproduct, however, was the rearranged *p*-hydroxy-*m*-methoxyphenylacetic acid, its signature resonance band for methylene protons labeled **b** $\delta = 3.69$ ppm. In addition, a band labeled **c** at $\delta = 4.5$ ppm, likely to be associated with the methylene protons of *p*-hydroxy-*m*-methoxybenzyl alcohol, was apparent. There were a few minor signals due to the presence of other photoproducts which were not identified. The photolysis of nearly the same concentration of *m,m'*-diOCH₃-pHP GABA (**133**) in D₂O with 300 nm lamps for 90 minutes produced new bands at $\delta = 3.67$ and $\delta = 4.56$ ppm; the former probably indicated the *p*-hydroxyphenylacetic acid analog of **133** and the latter the *p*-hydroxybenzyl alcohol. The primary chemical species in the mixture was unreacted **133**. It is noteworthy to point out the significant disparities in photochemical behavior of *m*-OCF₃-pHP GABA (**131**) and *m*-OCH₃-pHP GABA (**133**); the former manifests a much higher efficacy for chromophore rearrangement and GABA release. The primary structural deviations are fluorine moieties in **131** that commute with hydrogens in **133**; the provenience will be discussed later in the *Discussion* section.

Figure 23. ^1H NMR spectrum of the photolysis mixture of **134** at 300 nm in D_2O .



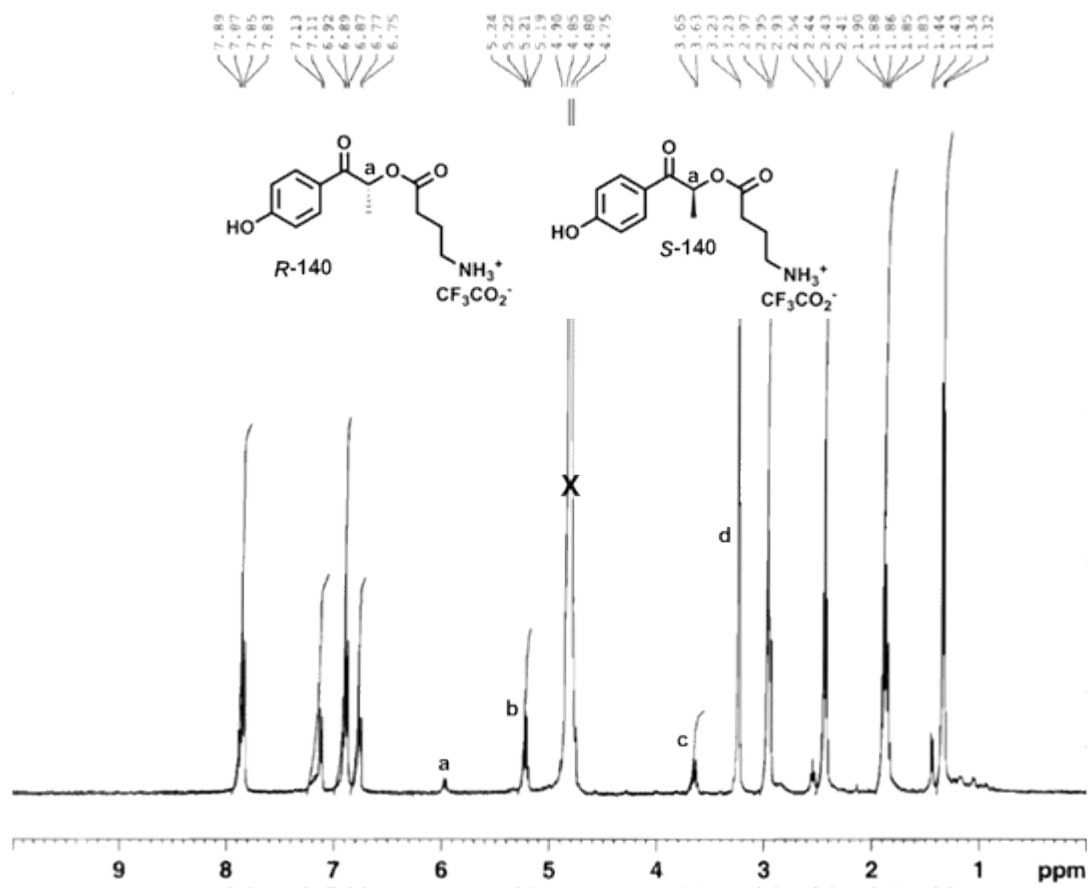
B. ^1H NMR examination of α -alkyl-pHP GABA esters. Compounds (**R,S**)-**140**, α -methyl-pHP GABA enantiomers, and (**R,S**)-**141**, α -ethyl-pHP GABA enantiomers, exhibited uncomplicated and complete photoconversions under similar conditions as described above. For example, a 0.05 M solution of a racemic mixture of (**R,S**)-**140** in D_2O (Figure 24) was irradiated for 1 h with two 300 nm lamps (Figure 25) and showed nearly complete conversion to photoproducts by diminutive **a** with $\delta = 6.08$

Figure 24. ^1H NMR spectrum of α -methyl-pHP GABA enantiomers (**R,S**)-140 in D_2O prior to irradiation.



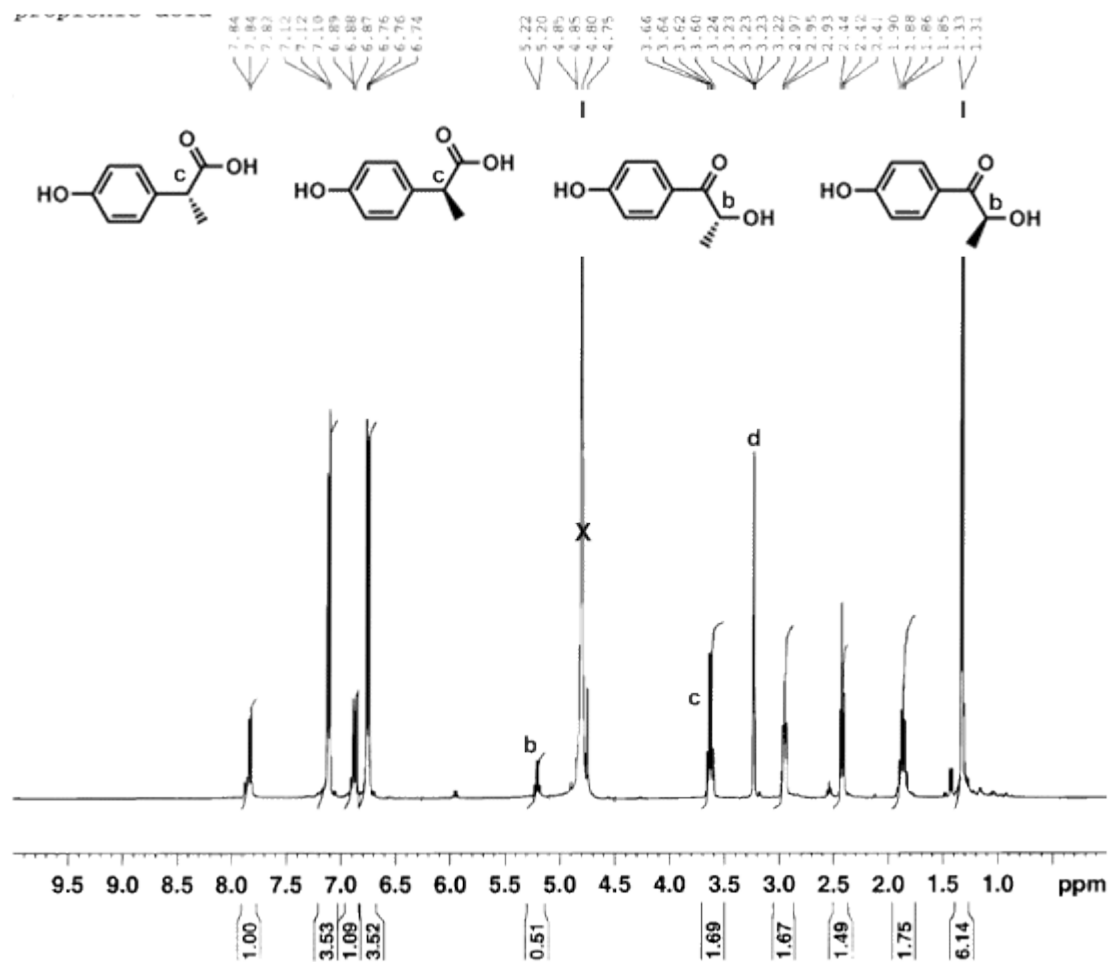
ppm and new bands for free GABA and photoproducts with resonance bands at **b** $\delta = 5.22$ ppm, **c** $\delta = 3.63$ ppm and **d** $\delta = 3.23$ ppm. A spiking experiment with 2-(4-hydroxyphenyl)propanoic acid (Figure 26) revealed an enhanced band intensity at **d** with $\delta = 3.63$, the identity of the *p*-hydroxyphenylpropionic acid photoproduct. The signals at **b** are tentatively assigned to the methine protons of α -hydroxy (acyloin) ketone of pHP based on the downfield chemical shift of aromatic hydrogen atoms

Figure 25. ^1H NMR spectrum of the product mixture after 1 h irradiation of (**R,S**-**140**) at 300 nm, in D_2O .



i.e., $\delta = 7.89$ ppm, that are similar to **140** and impute a ketone moiety. The resonance band at **d** could not be identified.

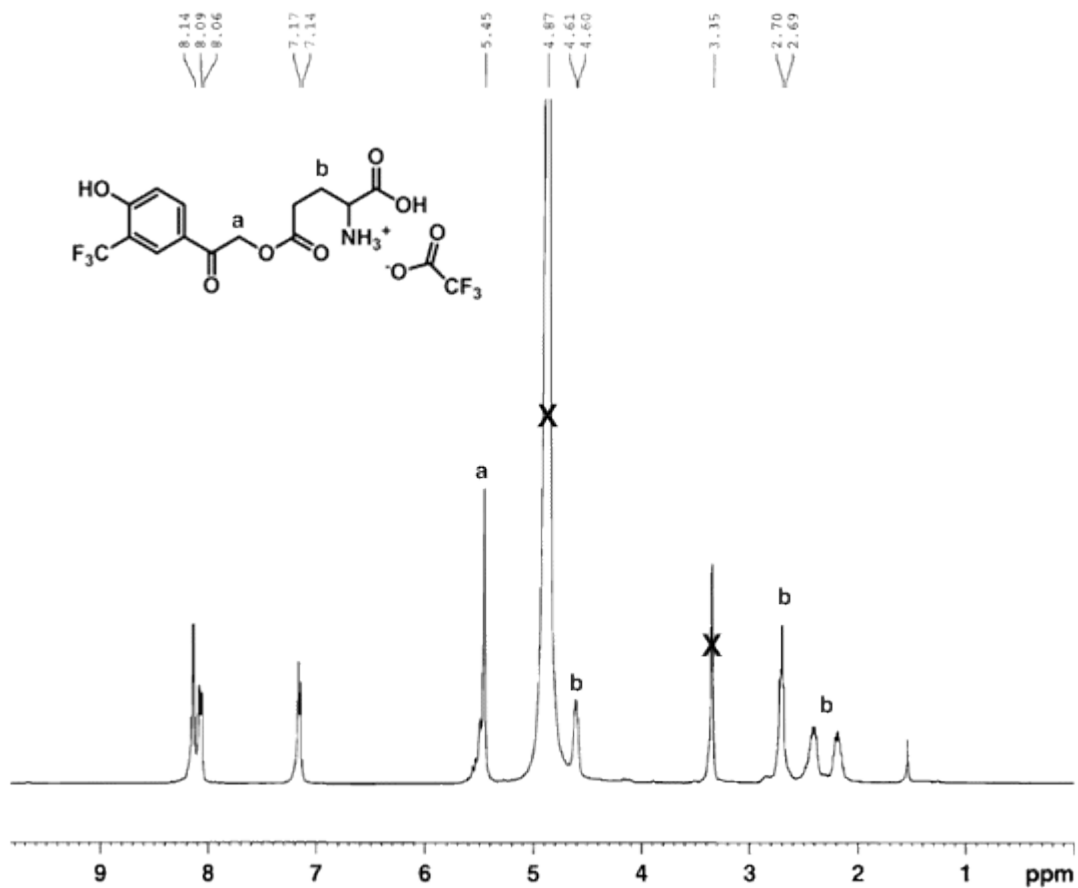
Figure 26. ^1H NMR spectrum of photolysis mixture with added 2-(4-hydroxyphenyl)propanoic acid. The enhanced peak intensity of **c** confirms the structure of the photoproduct.



C. Examinations of pHP-*l*-glutamate derivatives (143-145) by ^1H NMR analysis.

The photochemistry of pHP Glu derivatives, *o*-F-pHP Glu (**143**), *m*-F-pHP Glu (**144**), and *m*-CF₃-pHP Glu (**145**) was congruent with the corresponding GABA analogs **122**, **123** and **130**, respectively, employing identical photolysis conditions. Free *l*-glutamate along with rearranged *p*-hydroxyphenylacetic acids were released as major

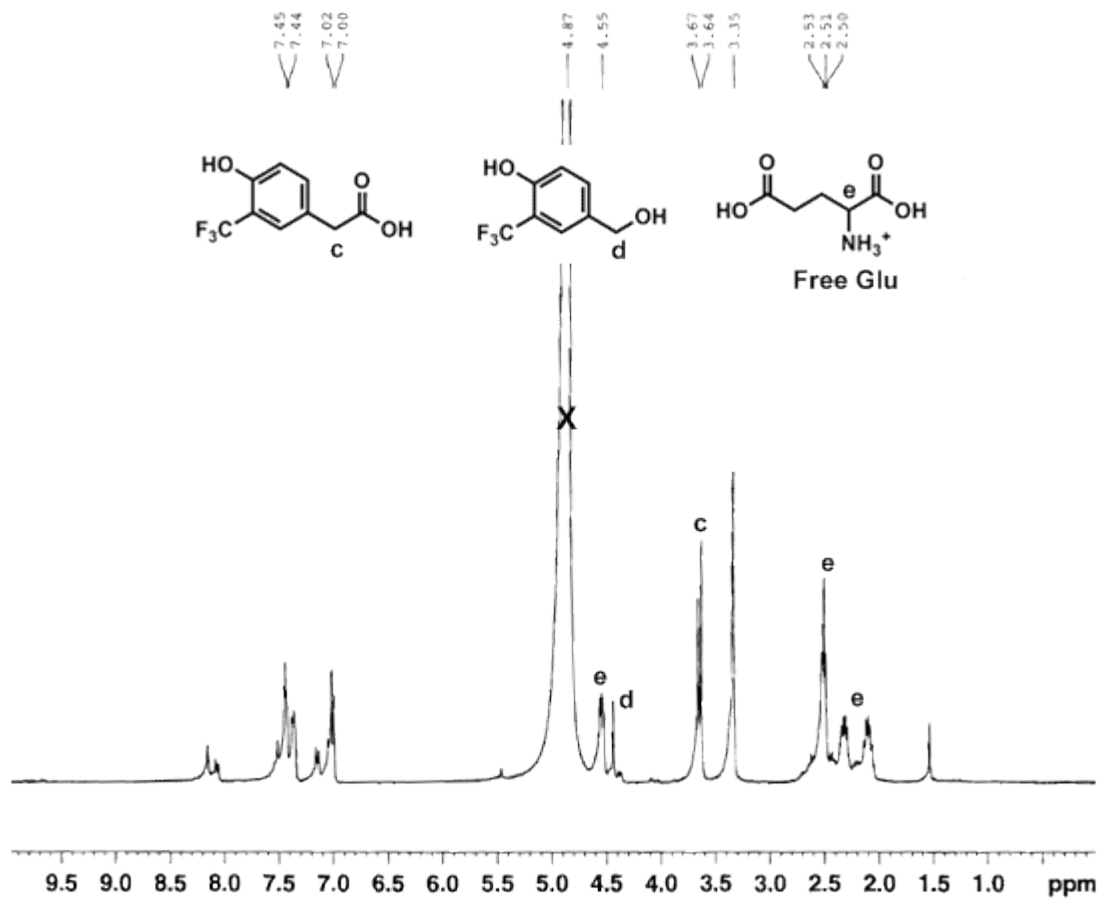
Figure 27. Pre photolysis ^1H NMR spectrum of *m*-CF₃-pHP Glu (**145**) in 1:1 D₂O: CD₃OD.



products; the sole minor products were *p*-hydroxybenzyl alcohols. For example, ^1H NMR analysis of 0.01 mM of **145** in 50% aq. CD₃OD (Figure 27) that was photolyzed for 1 h at 300 nm (Figure 28) revealed the complete disappearance of the signature methylene bands labeled **a** at $\delta = 5.45$ ppm and Glu labeled **b**, with appearance of bands that correspond to methylene protons of *p*-hydroxy-*m*-trifluoromethylphenylacetic acid, labeled **c** at $\delta = 3.66$ ppm and *p*-hydroxy-*m*-

trifluoromethylbenzyl alcohol, labeled **d** at $\delta = 4.55$ ppm, as well as free Glu (bands labeled **e**).

Figure 28. ^1H NMR analysis of products from photolysis of *m*-CF₃-pHP Glu (**145**) at 300 nm in 1:1 CD₃OD:D₂O.

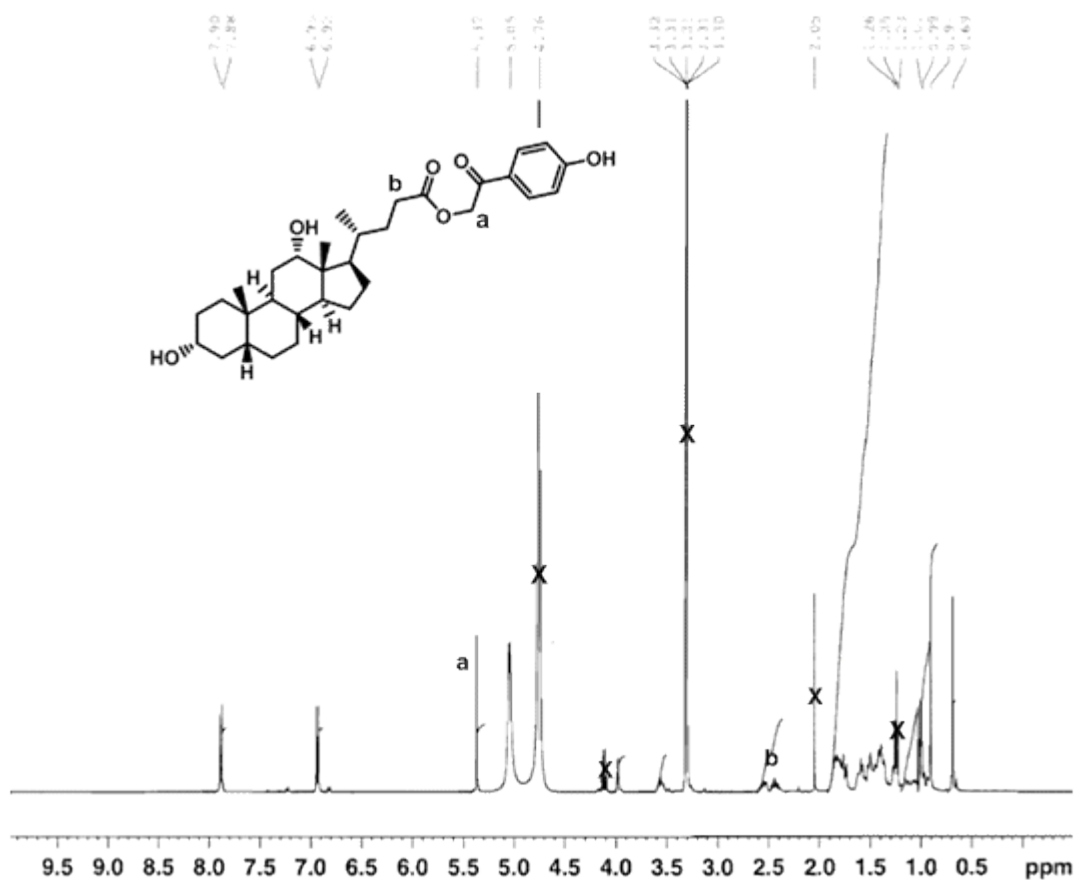


D. Investigations of pHP-caged amino acids (146-148) by ^1H NMR analysis. The photochemistry of pHP caged glycine (**146**), valine (**147**), tryptophan (**148**) and phenylalanine (**149**) paralleled that of GABA under the same photolysis conditions.

Clean transformations to *p*-hydroxyphenylacetic acid and *p*-hydroxybenzyl alcohol, along with substrate release, were observed.

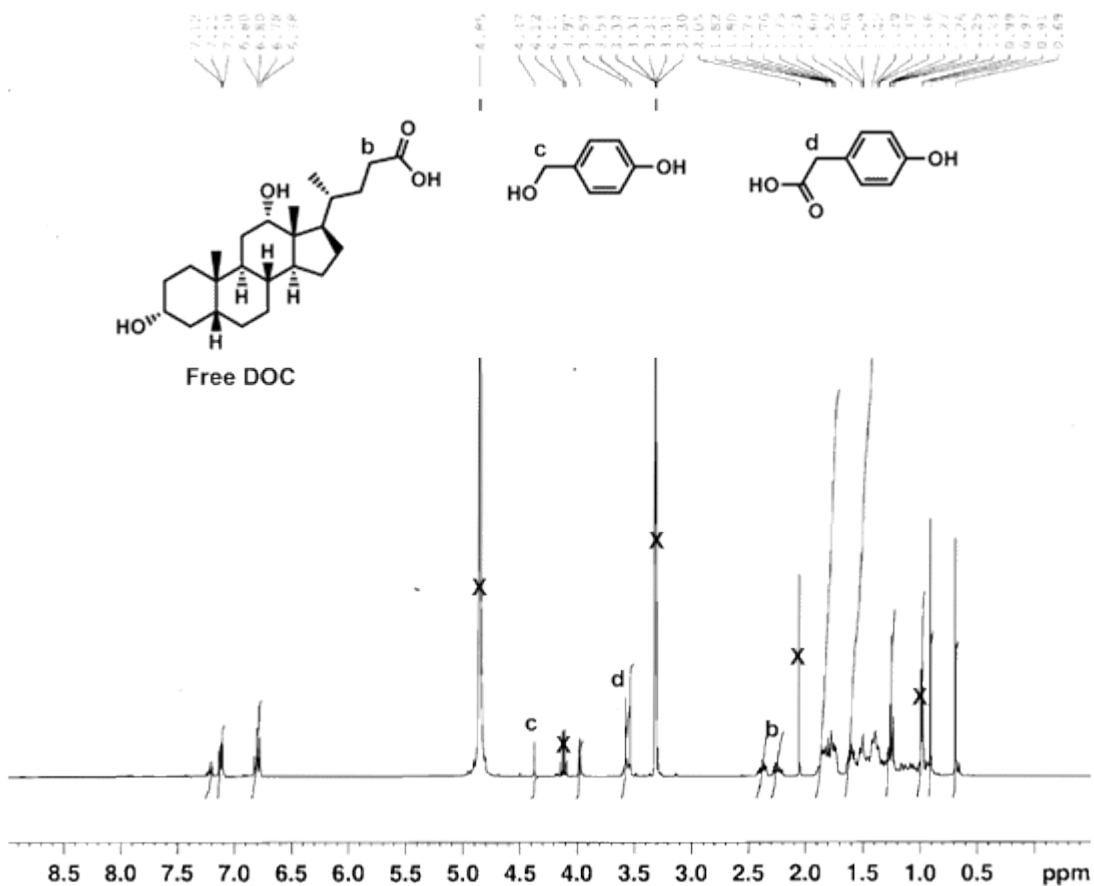
E. ^1H NMR analysis for the photolysis of pHP deoxycholic acid, (pHP DOC, **150).** A sample of 0.009 M pHP DOC (**150**) in 1:9 $\text{D}_2\text{O}:\text{CD}_3\text{OD}$ was prepared (Figure 29, the signature band is denoted **a** for methylene protons at $\delta = 5.37$ ppm and

Figure 29. ^1H NMR spectrum of **150** in 1:9 $\text{D}_2\text{O}:\text{CD}_3\text{OD}$ prior to photolysis.



b for methylene protons at $\delta = 2.49$ ppm) and was irradiated at 300 nm over 4 h (Figure 30); complete disappearance of precursor was divulged by the absence of **a**. New bands appeared at **b** with $\delta = 4.37$ ppm and **c** at $\delta = 3.57$ ppm which are posited to represent the methylene protons of rearranged *p*-hydroxyphenylacetic acid and *p*-hydroxybenzyl alcohol entities respectively. Additionally, free DOC was observed from signature resonance bands **b** at $\delta = 2.38$ ppm.

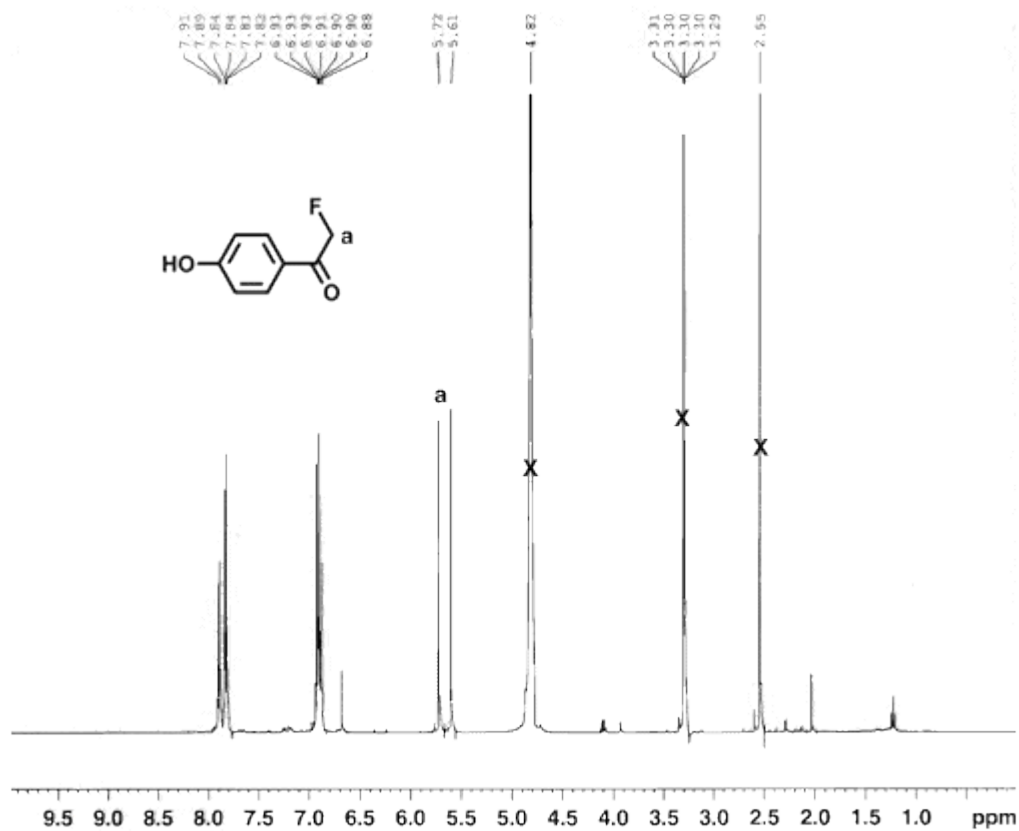
Figure 30. ^1H NMR spectrum of the product mixture after irradiation of **150** for 4 h at 300 nm in 1:9 $\text{D}_2\text{O}:\text{CD}_3\text{OD}$.



F. ^1H NMR exploration of pHP diethyl phosphonate (151). Irradiation of 0.02 M of **151** in D_2O for 2, 4, 16, and 36 h at 300 nm lamps failed to disclose any photolysis products. Additional photolysis studies with 0.015 M **151** in D_2O at 254 nm over 12 h evinced no photoproducts.

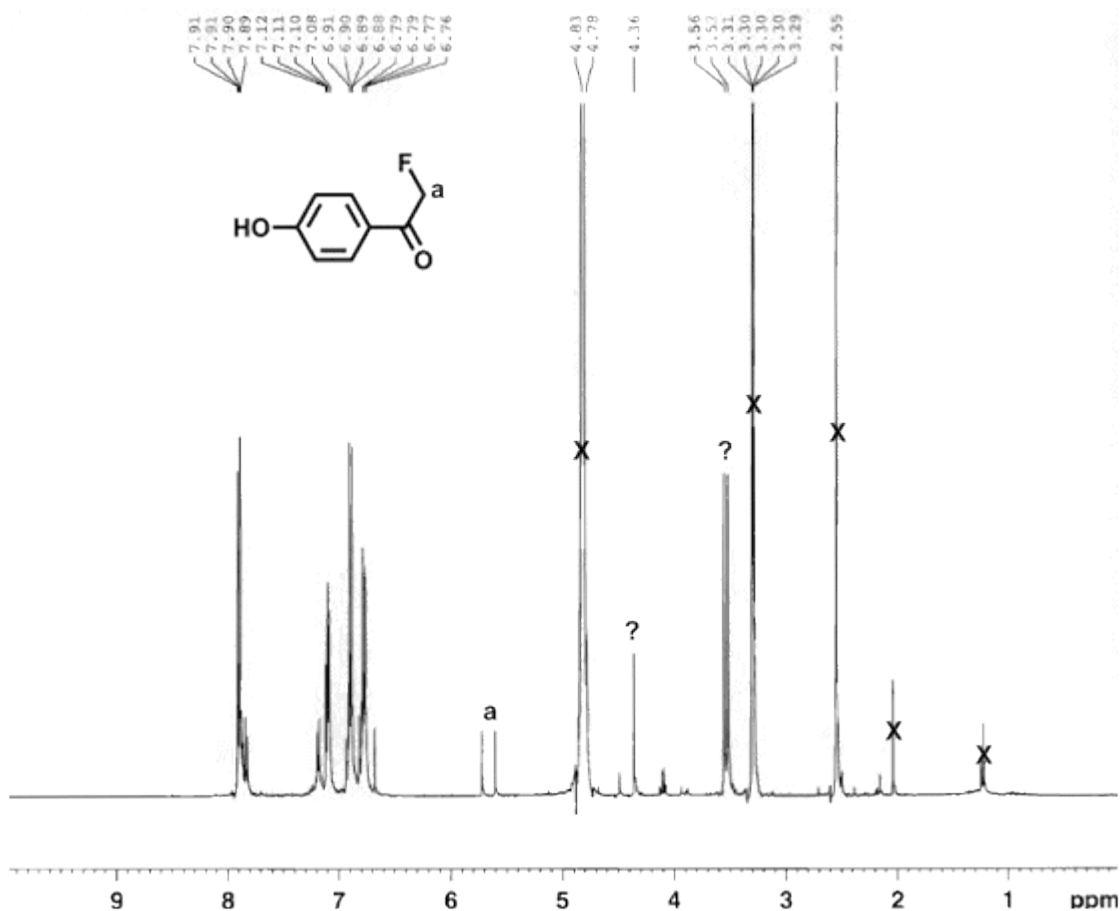
G. ^1H NMR analysis of pHP F (152). A 0.01 M sample of **152** in 1:3 $\text{D}_2\text{O}:\text{CD}_3\text{OD}$

Figure 31. ^1H NMR analysis of **152** in 1:3 $\text{D}_2\text{O}:\text{CD}_3\text{OD}$ prior to irradiation.



(Figure 31, with signature, discrete signals for each the methylene group alpha to the ketone **a** at $\delta = 5.72$ and 5.61 ppm respectively) was irradiated at 300 nm for 1 h (Figure 32). Noticeably, the bands at **a** were significantly diminished in intensity. Prominent new signals were also observed at $\delta = 3.56$ and 3.52 ppm. These are located at a similar position in the spectrum as the methylene protons of *p*-hydroxyphenylacetic acid; the exhibition of two signals in this spectrum, however, differs with the acid, which typically reveals only one resonance band. A second

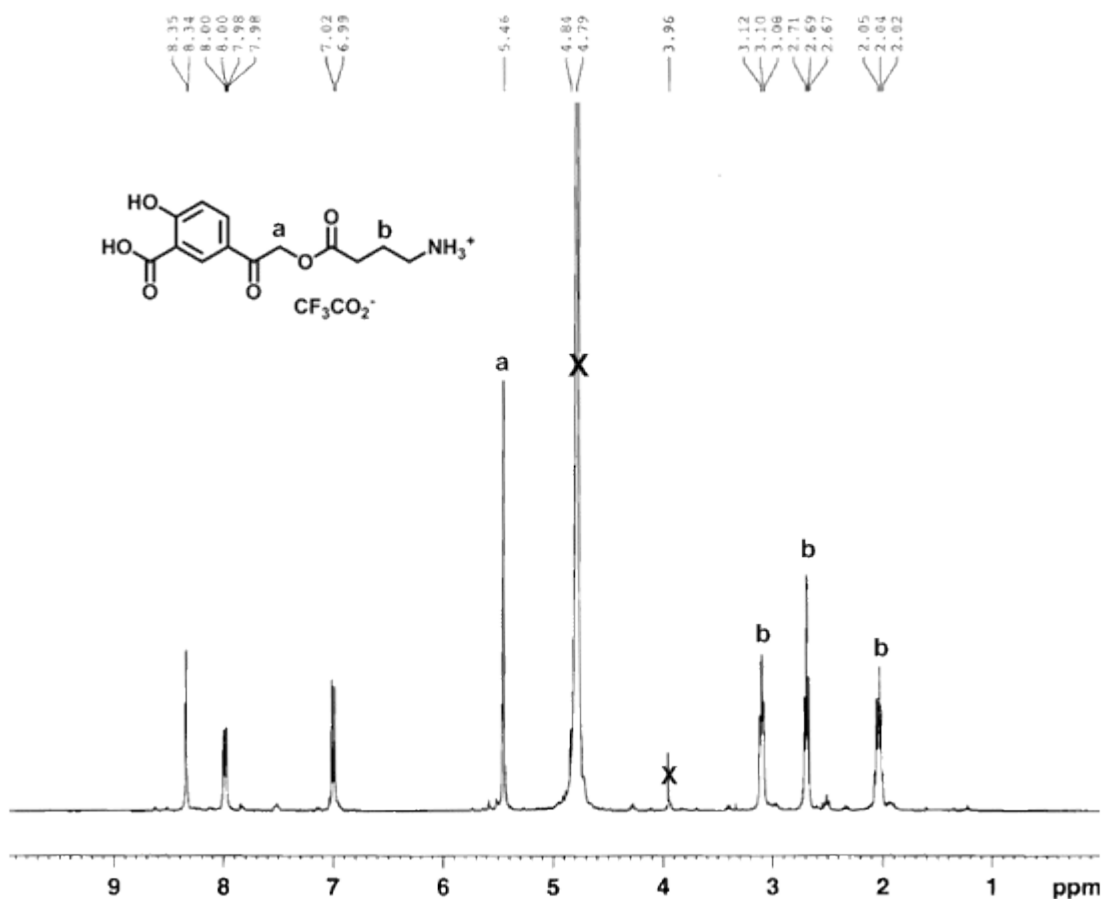
Figure 32. ^1H NMR assessment of the product mixture after 1 h photolysis of **152** at 300 nm in $1:3$ $\text{D}_2\text{O}:\text{CD}_3\text{OD}$.



prominent signal is conveyed at $\delta = 4.36$ ppm and could not be identified. Further studies are required to better understand the photochemistry of pHP F (**152**).

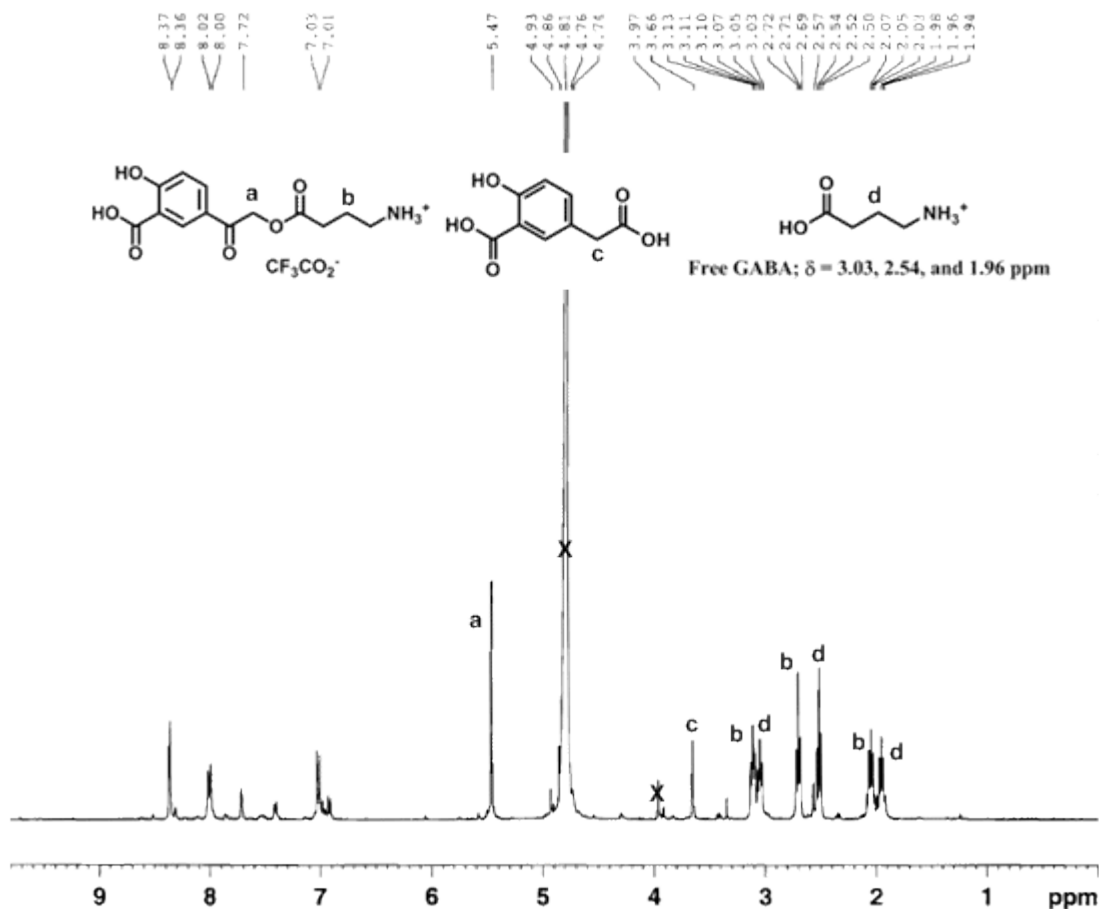
H. ^1H NMR evaluation of 5-acetylsalicylic acid (153**) and salicylate GABA derivatives (**154**, **157-165**).** A 0.18 M solution of 5-acetylsalicylic acid GABA (**153**) in D_2O (Figure 33, with signature methylene bands **a** at $\delta = 5.46$ ppm and GABA

Figure 33. ^1H NMR spectrum of **153** in D_2O prior to photolysis.



alkyl bands **b** at $\delta = 3.10, 2.69$ and 2.04 ppm) was irradiated for 1 h at 300 nm (Figure 34) manifesting the clean photorelease of GABA, **d**. This was evidenced by the

Figure 34. ^1H NMR analysis of the product mixture from 1 h photolysis of **153** at 300 nm in D_2O .

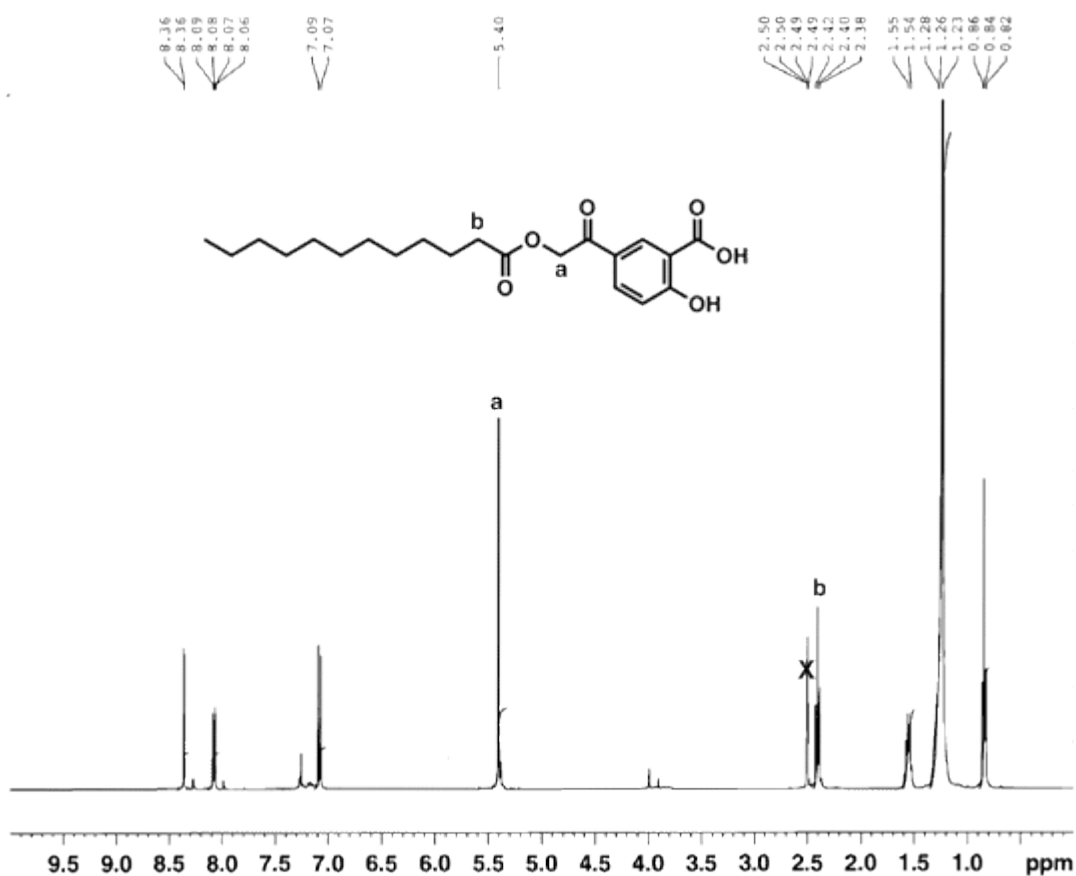


appearance of resonance bands associated with free GABA at $\delta = 3.03, 2.54,$ and 1.96 ppm, which are slightly offset in the spectrum from caged GABA. A considerable amount of starting material, **153**, remained due to the relatively short irradiation time.

A new, prominent signal at $\delta = 3.66$ ppm suggests the presence of rearranged phenylacetic acid analog labeled **c**, analogous to the previously assigned derivatives. Salicylic esters and amide derivatives of **153**, compounds **154** and **157-165**, exhibited congruent photochemical behaviors with **153**. Several of these exhibited limited water solubilities and required, first, dissolution in a CD₃OD or CD₃CN, followed by dilution with D₂O.

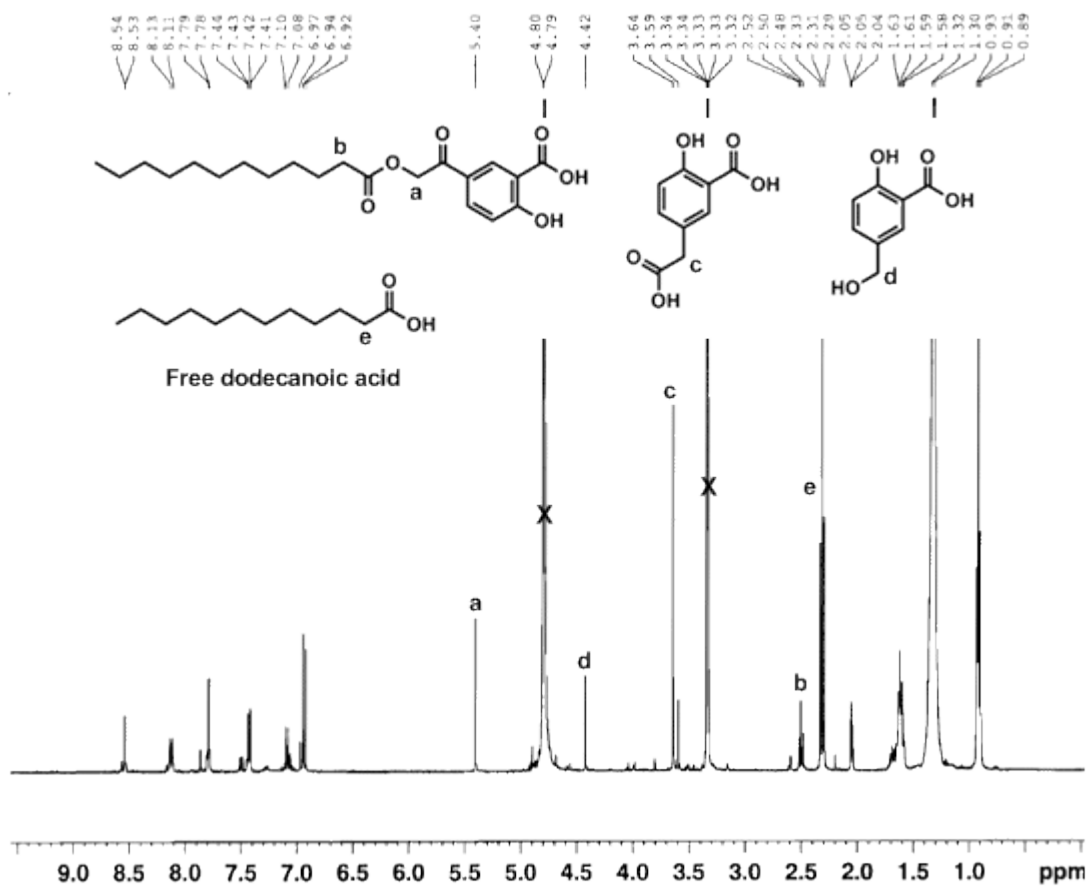
I. ¹H NMR studies of (5-(2-(dodecanoyloxy)acetyl)-2-hydroxybenzoic acid, 155) and (2-hydroxy-5-(2-(tetradecanoyloxy)acetyl)benzoic acid, 156). The photochemical behavior of model photocleavable surfactants **155** and **156** were investigated in 1:9 D₂O:CD₃OD. Similar to antennae compounds **157-165**, water solubility was a restriction. However, it was found that this was obviated by dissolution in basic buffer, which will be elaborated on later. An ¹H NMR study of

Figure 35. ^1H NMR analysis of **155** in d^6 -DMSO prior to irradiation.



155 consisted a 0.03 M solution in 1:9 $\text{D}_2\text{O}:\text{CD}_3\text{OD}$ (Figure 35), with methylene protons labeled **a** at $\delta = 5.40$ ppm and **b** at $\delta = 2.40$ ppm, was irradiated for 1 h at 300 nm (Figure 36) to give three new resonance signals centered at $\delta = 4.42$ (**d**), 3.64 (**c**), and 3.59 ppm (**e**). A significant amount of **155** was retained, evidenced by the band at **a**. It was deduced that dodecanoic acid was released from the 5-acetylsalicylic acid chromophore from the appearance of new bands at **e** at $\delta = 2.31$ ppm,

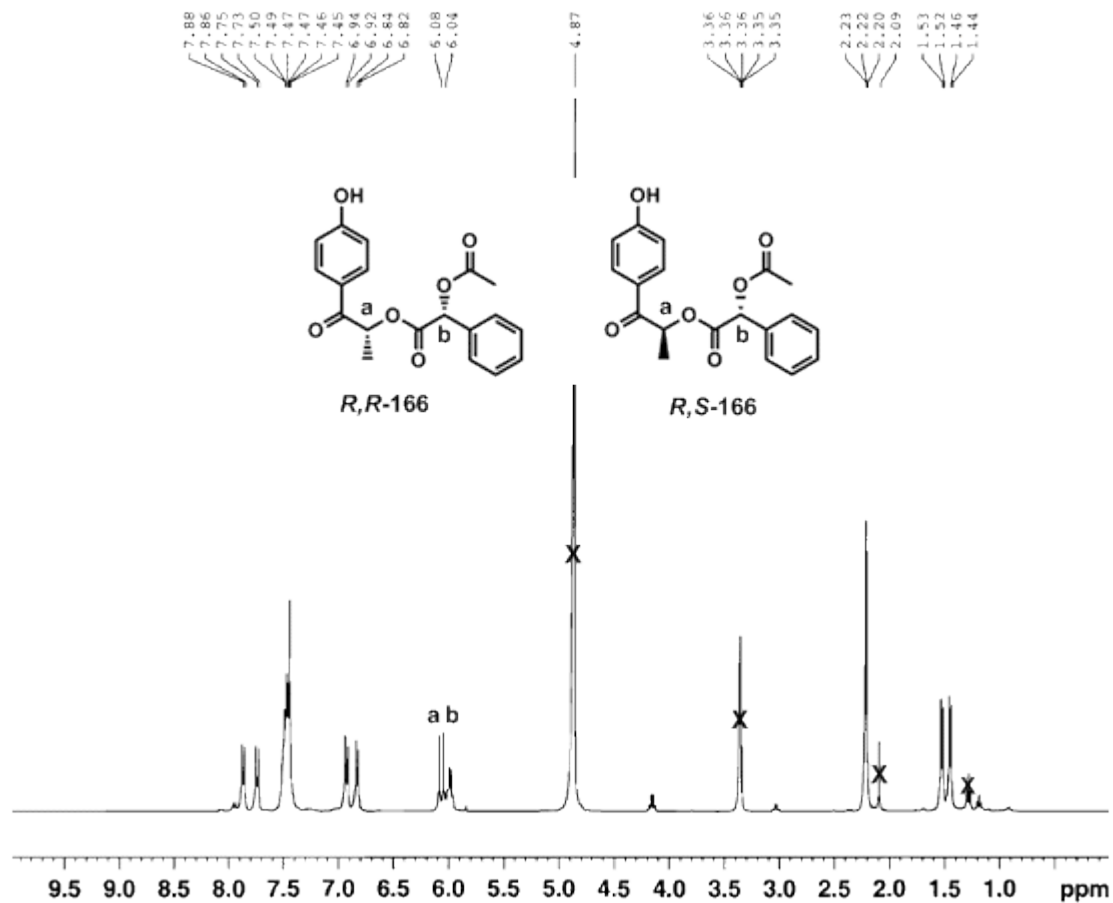
Figure 36. ^1H NMR spectrum of the product mixture after irradiation of **155** in 1:9 $\text{D}_2\text{O}:\text{CD}_3\text{OD}$.



corresponding to free dodecanoic acid, which were slightly offset from the caged analog. The chemical shifts of other products indicate that **b** might represent the methylene protons of the *p*-hydroxyphenylacetic acid derivative, and **c** or **d** correspond to methylene protons of *p*-hydroxybenzyl alcohol derivative.

J. ^1H NMR investigations of ((R)-((R)-1-(4-hydroxyphenyl)-1-oxopropan-2-yl) 2-acetoxy-2-phenylacetate, **166**) and ((R)-((S)-1-(4-hydroxyphenyl)-1-oxopropan-2-yl) 2-acetoxy-2-phenylacetate, **167**). A 0.05 M solution of a mixture of pHP

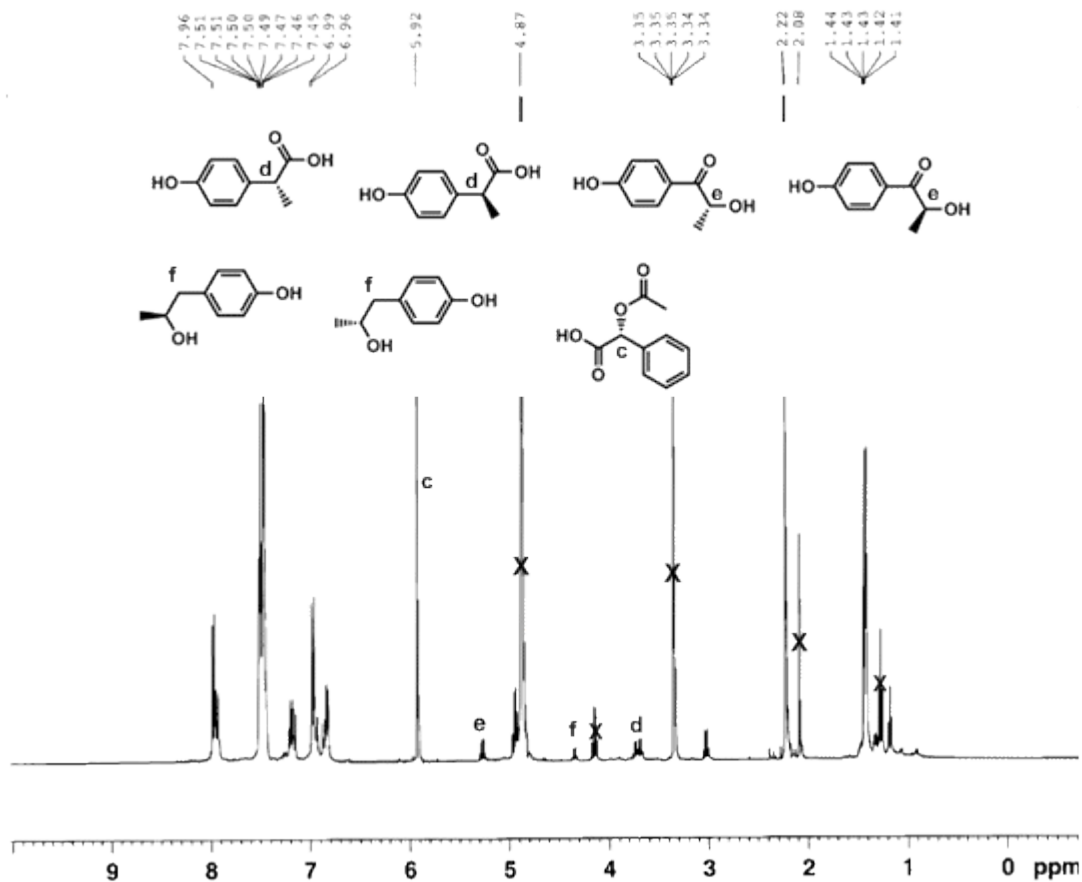
Figure 37. ^1H NMR spectrum of a mixture of **166** and **167** in 1:1 $\text{D}_2\text{O}:\text{CD}_3\text{OD}$.



phenylacetate diastereomers (**166** and **167**) in 1:1 $\text{D}_2\text{O}:\text{CD}_3\text{OD}$ (Figure 37) with signature methine protons for each at **a** and **b** that overlap at $\delta = 6.08$ and 6.04 ppm was irradiated with at 300 nm lamps for 2 h. Complete conversion of precursors (Figure 38) were apparent from the absence of signals corresponding to **a** and **b**. New

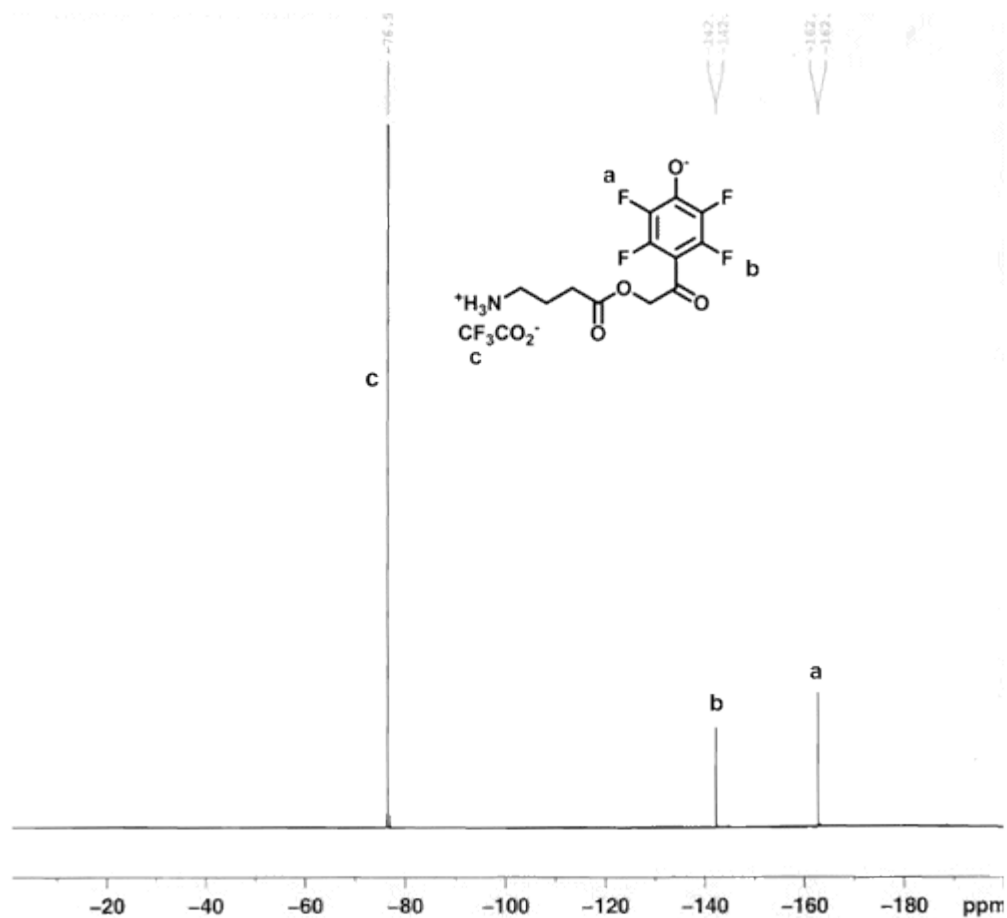
resonance signals were manifested at **c** with $\delta = 5.92$ ppm that corresponded to the released (*R*)-2-acetoxy-2-phenylacetic acid with resonance signals at 5.27, 4.34, 3.71 and 3.67 ppm. Comparing these to those obtained from the product mixture of **(R-S) 140** above, the bands at $\delta = 5.27$ ppm are posited as the methine protons of the α -hydroxy (acyloin) derivative **d**; those at $\delta = 3.71$ and 3.67 ppm likely represent the methylene protons of rearranged *p*-hydroxyphenylacetic acid derivative **e**, which had been confirmed previously from spiking experiments. In addition, the small resonance bands labeled **f** at 4.34 ppm could represent the methylene protons of *p*-hydroxybenzyl alcohol analogs.

Figure 38. ^1H NMR spectrum of the product mixture from irradiation of **166** and **167** at 300 nm in 1:1 $\text{CD}_3\text{OD}:\text{D}_2\text{O}$.



K. ^{19}F NMR analysis of fluoro pHP and 5-acetylsalicylic derivatives. ^{19}F NMR spectroscopy provided a useful technique to assess the progress of photoreactions of certain pHP derivatives. The compounds that were anticipated to manifest the most conspicuous changes in ^{19}F resonance band positions

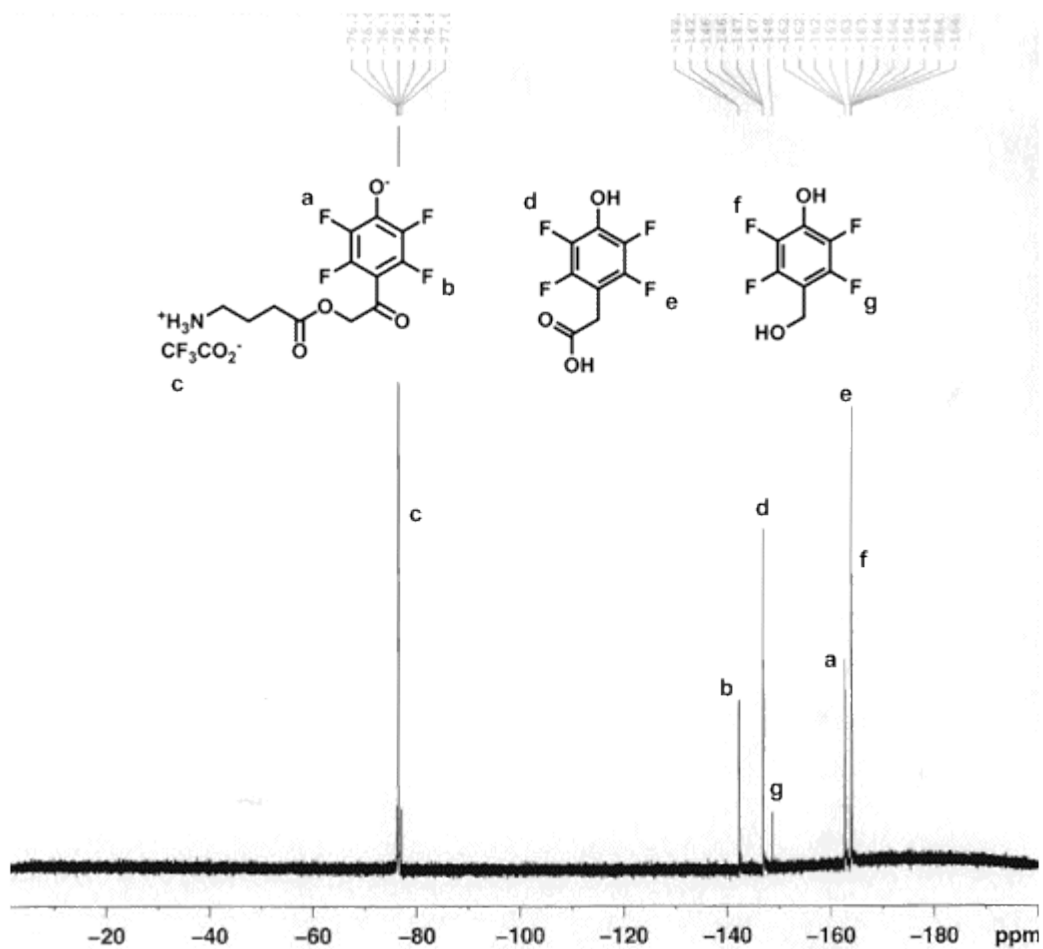
Figure 39. ^{19}F NMR spectrum of 2,3,5,6-tetraF-pHP GABA (**129**) in D_2O prior to photolysis.



were those that possessed an *o*-fluoro moiety; the powerful inductive effect imparted by the carbonyl of pHP ketone on the *o*-fluoro atom is quite disparate from the corresponding *p*-hydroxyphenylacetic acid, where this effect is obtunded by a more remote and modified carboxylate functionality. For example, a 0.03 M D_2O solution of 2,3,5,6-tetrafluoro-pHP GABA (**129**) (Figure 39) with signature ^{19}F NMR bands for the *m*-fluoro moieties labeled **a** ($\delta = -162$ ppm), the *o*-fluoro moieties labeled **b** (δ

-142 ppm), and the trifluoro constituent of the trifluoroacetate anion labeled **c** ($\delta = -76$) ppm) was photolyzed for 15 min with at 300 nm (Figure 40). Incomplete

Figure 40. ^{19}F NMR spectrum of the product mixture from photolysis of **129** at 300 nm in D_2O .



conversion to the rearranged *p*-hydroxy-2,3,5,6-tetrafluorophenylacetic acid, with resonance signals assigned **d** for *o*-fluorines ($\delta = -147$ ppm) and **e** for *m*-fluorines ($\delta = -164$ ppm), and *p*-hydroxy-2,3,5,6-tetrafluorobenzyl alcohol, with resonance signals

assigned **f** for *o*-fluorines ($\delta = -147$ ppm) and **g** for *m*-fluorines ($\delta = -164$ ppm) are clearly discernible with respect to those from **129**. The intensity of the band **e** is greater than **f**, which is expected, as the former is the major product. The corresponding ^1H NMR studies divulged that the major photoproduct of **129** was rearranged *p*-hydroxy-2,3,5,6-tetrafluorophenylacetic acid and thus the ^{19}F intensities would be major at $\delta = -147$ (**d**) and at $\delta = -164$ ppm (**e**). The *p*-hydroxy-2,3,5,6-tetrafluorobenzyl alcohol product, exiguously formed, would be identified with signals at lower intensities, i.e., **f** and **g**. A sizeable upfield shift in the *o*-fluoro resonance band, **a** to **d** of -5 ppm for the phenylacetic acid and **a** to **g** -6 ppm for the benzyl alcohol, is due to the loss of deshielding from the carbonyl. Additionally, minor vicissitudes in chemical shifts of *m*-fluoro moieties were perceived; 1 ppm for **b** to **e** and **f**, respectively, were due to the loss of the resonance and inductive withdrawing contribution of the carbonyl. The resonance and inductive bearing of the carbonyl ketone is underscored by these chemical shift changes.

III. UV-Vis Spectroscopic Studies.

A. pHP and *p*-fluorophenacyl GABA esters 122-142 in water and buffers, pH = 7.3 and 8.2. UV-Vis spectroscopic analysis of compounds **122-142** in water and pH = 8.2 buffer were completed and results presented in Table 15.

Table 15. UV-Vis properties of **122-142** with corresponding pKa values.

Cmpd	$\lambda_{\max}/\text{nm} (\log \varepsilon[\text{M}^{-1}\text{cm}^{-1}])^{\text{a}}$	$\lambda_{\max}/\text{nm} (\log \varepsilon[\text{M}^{-1}\text{cm}^{-1}])^{\text{b}}$	$\lambda_{\max}/\text{nm} (\log \varepsilon[\text{M}^{-1}\text{cm}^{-1}])^{\text{c}}$	pKa ^d
122	274 (4.00), 335 (2.97)	330 (4.06)	351(3.67), 328(3.96)	6.5
123	271 (3.97)	322 (3.87), 284 (3.91)	328(3.90), 319(3.91)	7.2
124	272 (4.09), 328 (3.04)	323 (4.10)	323 (4.07)	5.9
125	278 (3.26), 326 (3.92)	328 (4.06)	326 (4.12)	5.7
126	331 (4.14)	331 (4.12)	330 (4.14)	5.3
127	274 (4.00)	313 (4.03)	313 (4.06)	6.8
128	324 (4.05)	324 (4.11)	323 (4.01)	4.5
129	316 (3.95)	317 (4.08)	316 (4.10)	3.9
130	328 (4.11)	325 (4.02)	328 (4.10)	5.5
131	274 (4.20), 331 (3.54)	328 (4.22)	329 (4.18), 322 (4.18)	6.7
132	400 (3.08), 332 (3.65), 254 (3.92)	397 (3.20), 334 (4.14)	399 (3.22), 335 (4.20)	5.2
133 ^e	303 (3.90), 355 (3.55)	ND	ND	7.8
134 ^e	279 (3.97), 307 (3.90)	ND	ND	7.9
135	334 (3.77), 318 (3.59), 276 (3.85)	ND	ND	7.8
136	309 (3.97), 279 (3.86)	ND	ND	8.0
137	284 (3.84)	283 (3.77), 307 (3.65)	356 (3.75), 334 (3.97)	8.1
138	304 (3.79), 287 (3.96)	316 (3.40), 305 (3.81), 287 (3.88)	362 (3.91), 348 (4.05)	8.2
139	287 (4.06)	303 (3.45), 287 (3.98)	343 (3.86), 328 (4.10)	8.0
140	281 (4.10)	329 (3.98), 284 (3.92)	333 (4.02)	7.9
141	282 (4.07)	328 (3.96), 284 (3.94)	334 (4.12)	7.9
142	273 (3.57), 267 (3.89), 248(4.12)	ND	ND	-
^a In water. ^b In 0.01 M HEPES, 0.1 M LiClO ₄ , pH = 7.3. ^c In 0.01 M HEPES, 0.1 M LiClO ₄ , pH = 8.2.				
^d Determined for the corresponding p-hydroxyacetophenones, see Experimental for details.				
^e See reference 1				

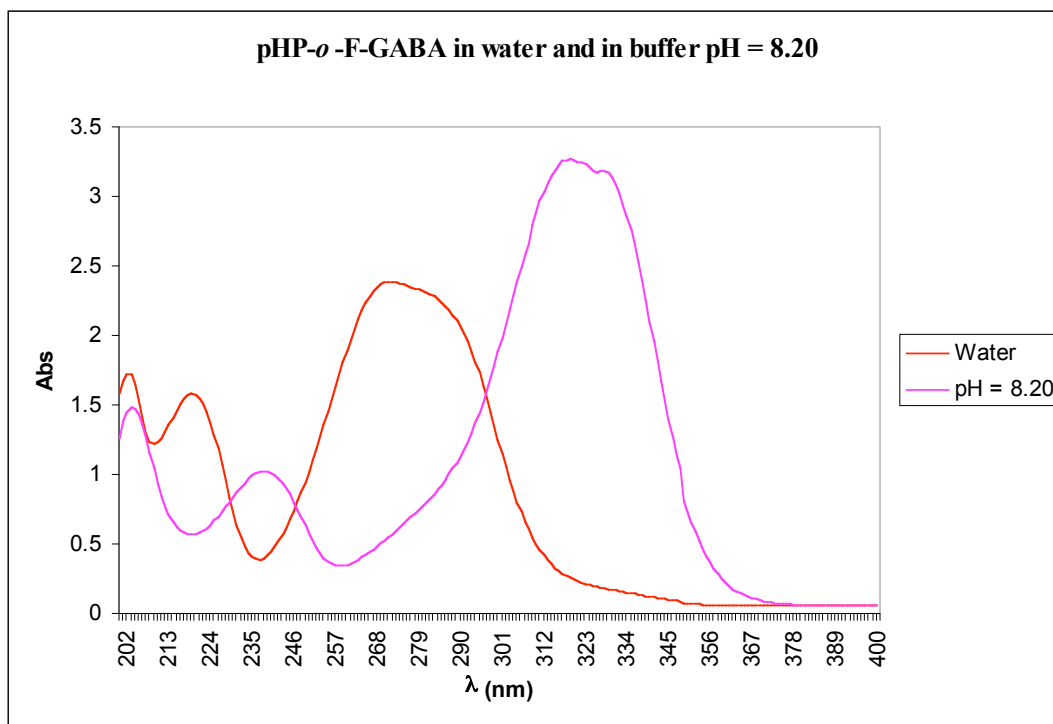
The impetus for spectral investigations in buffers relates to the protonated versus conjugate base forms of the pHP chromophore, i.e., to discern whether the conjugate bases manifest disparate photophysical properties to their protonated counterparts.

Several other buffers of identical concentration and adjusted ionic strengths were utilized; these included TRIS pH 7.5, tetrasodium pyrophosphate pH 7.4, sodium phosphate pH 7.0, ammonium acetate, pH = 7.0 and HEPES pH = 7.2 with 0.1 M LiCl. The UV-Vis parameters for these were consistent with those obtained

with HEPES, pH = 7.3, shown in Table 15. The pKa of the phenol influenced the UV-Vis spectra for all pHP esters; many derivatives manifested two or more absorption bands in unbuffered, aqueous media, resulting from the equilibrium between the protonated and conjugate base concentrations of the phenol. In HEPES buffered solution at pH = 8.2 the conjugate bases of all pHP esters dominated. The long wavelength maxima were bathochromically shifted by ~50 nm compared with the protonated form. For example, *o*-F-pHP GABA (**123**) revealed a $\lambda_{\text{max}} = 271$ nm in water, signifying the protonated form; in HEPES buffer, pH = 8.2, the λ_{max} shifts to 328 and 319 nm (Figure 41), respectively, a clear indication of the conjugate base. The photophysical parameters that influence substrate release depend on the nature of the protonated and conjugate base of the pHP chromophore and will be discussed later.

By manipulating the pH of the photoreaction media and the lamps for the Rayonet reactors (300 and 350 nm), the photoreactivity of the two forms of **122-141** allow the accurate quantization of quantum yields and rate constants for each form individually. In water, **122-141** exist dually as a mixture which makes the analysis complex (two competing photoreactions). Furthermore, as the reaction progresses, two additional changes are occurring. The pH of the aqueous solution will change, since the Favorskii rearrangement both releases an acid as the leaving group and generates a phenylacetic acid, each have different pKa's than the phenol. The second factor is a consequence of this change in that the absorption spectrum will shift to represent a higher proportion of the original protonated form of the caging

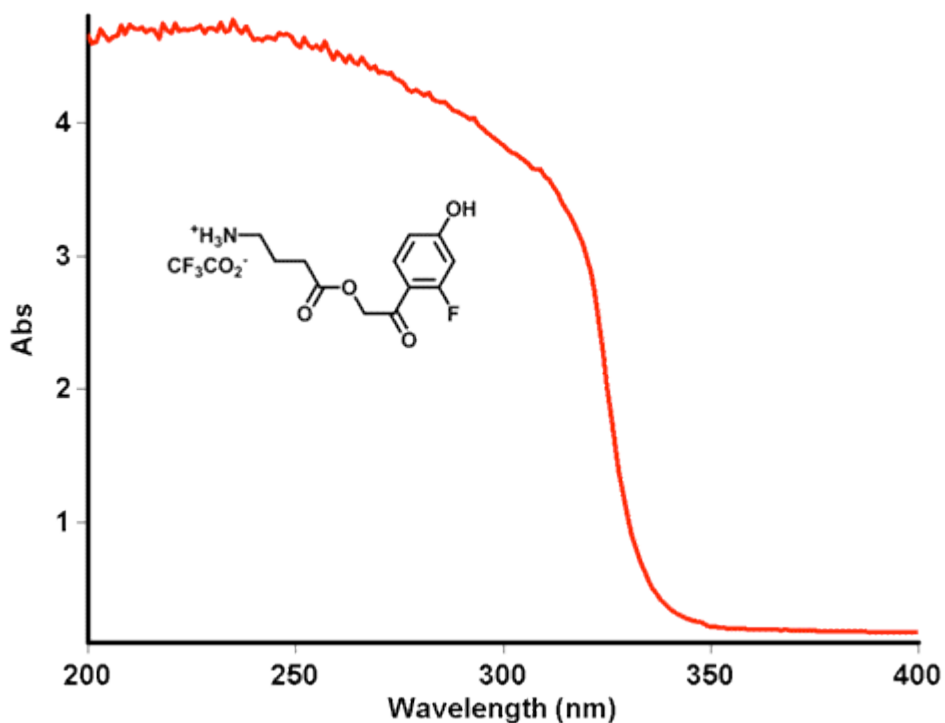
Figure 41. Comparison of UV-Vis spectra of **123** in water (red) and pH = 8.2 buffer (pink).



chromophore. For example, *o*-F-pHP GABA (**123**) revealed a λ_{max} of 271 nm (Figure 41) at low concentrations (10^{-5} M) in water, with a tapering off at 320 nm. At 1 mM concentrations, an extended absorbance profile used for photolysis was manifested (Figure 42) and reached the baseline at 350 nm. The cutoff was at 350 nm for excitation of the protonated forms of **122-132** and **135-141** in water (the *m*-methoxy compounds **133** and **134** extended past 370 nm at 5 mM concentrations). Such was not the case for the corresponding conjugate bases of pHP chromophores **122-141** (Table 15). Congruent with their protonated counterparts, saturation UV-Vis profiles of 5 mM concentrations of **122-141** conjugate bases, all or nearly all of the light was

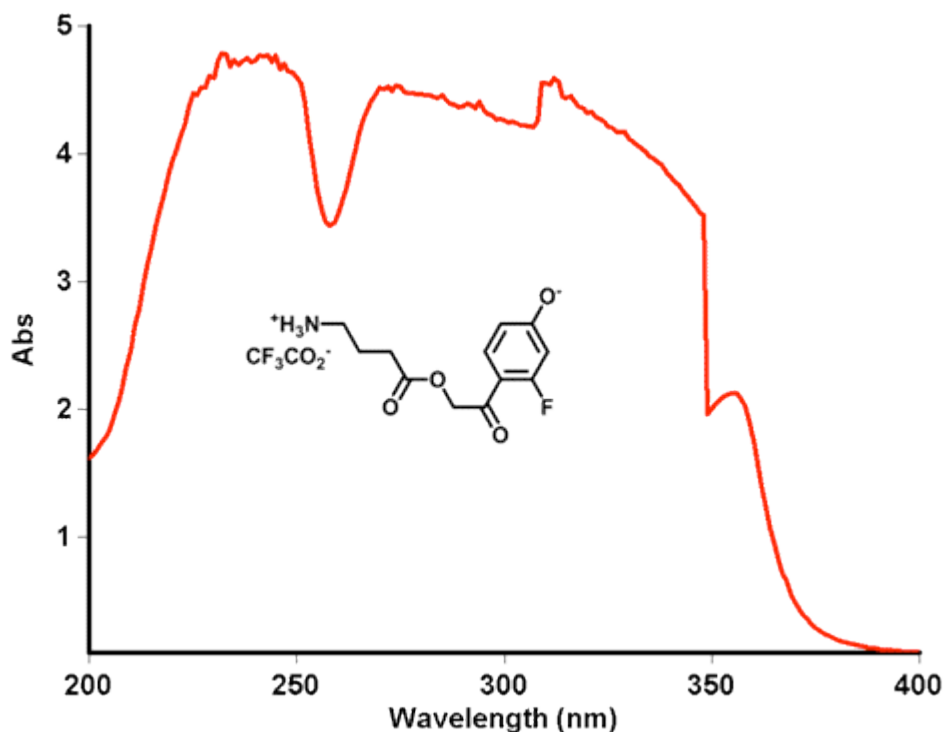
being absorbed at wavelengths up to 400 nm and therefore the 350 nm lamps would seem to be amenable for photorelease. For example, when probed at 5 mM in 0.01 M

Figure 42. UV-Vis spectroscopic analysis of 1 mM solution of **123** in unbuffered aqueous solution. The spectrum indicates a saturation condition.



HEPES, 0.1 M LiClO₄, pH = 8.2, **123** showed absorbances that extended past 350 nm (Figure 43), with a cut off nearer to 370 nm.

Figure 43. UV-Vis spectroscopic analysis of 5 mM **123** in 0.01 M HEPES, 0.1 M LiClO₄, pH = 8.2. The conjugate base predominates. The spectrum signifies a saturation condition.



The photo-conversion process of pHP GABA esters **122-141** was probed by UV-Vis spectroscopy. Recall the *p*-fluorophenacyl GABA **142** demonstrated photo-inertness at $\lambda = 254$ and 300 nm as determined by ¹H NMR and thus was not examined. All of the caged GABA derivatives were converted to products with a high efficiency when irradiated as 2 mM aqueous solutions at 300 nm (light output, 0.01 mE/mol) where complete transformation to photoproducts occurred within 20 min (Table 16). This was verified by HPLC (UV-detection) through analysis of

Table 16. Times for 100% conversion to photoproducts of 1 mM concentrations of **122-141** in water.

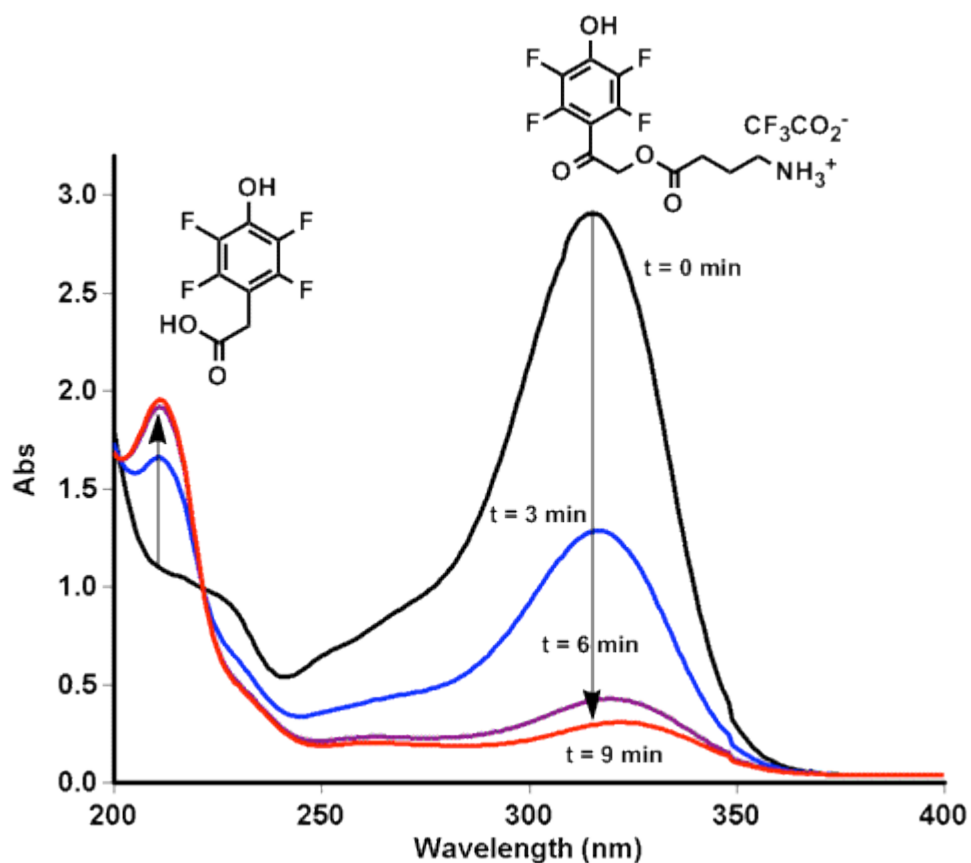
Compound	Time ^a (min)	Time ^b (min)	Time ^c (min)	Time ^d (min)
122	7	9	70	>8h
123	5	6	45	>8h
124	6	12	40	>8h
125	6	12	60	>8h
126	10	10	80	>8h
127	8	9	40	>8h
128	13	15	70	>8h
129	9	9	20	>8h
130	6	9	40	>8h
131	12	13	60	>8h
132^e	-	-	-	-
133^f	ND	ND	ND	ND
134^f	ND	ND	ND	ND
135^g	-	-	-	-
136^g	-	-	-	-
137	8	7	50	>8h
138	9	7	50	>8h
139	12	10	70	>8h
140	20	24	90	>8h
141	20	24	90	>8h
142^g	-	-	-	-

^aTwo 300 nm lamps, in water, estimated by HPLC/UV analysis in water. ^bTwo 300 nm lamps, in 0.01 M HEPES, 0.1 M LiClO₄, pH = 7.3, estimated by HPLC/UV analysis. ^cTwo 300 nm lamps, in 0.01 M HEPES, 0.1 M LiClO₄, pH = 8.2, estimated by HPLC/UV analysis. ^d16 350 nm lamps, in 0.01 M HEPES, 0.1 M LiClO₄, pH = 8.2, estimated by HPLC/UV analysis, overnight irradiation. ^eNo photolysis was observed. ^fNot determined.

aliquots every 30 seconds. For **122-141** in 0.01 M HEPES buffer with 0.1 M LiClO₄ at pH = 8.2 (Table 15), the conjugate bases were irradiated with two 300 nm lamps over longer time periods also achieved complete conversion to photoproducts. Exposure of the conjugate bases to sixteen 350 nm lamps (0.09 mE/min) led to

complete conversion to photoproducts but at much longer times, i.e., >8 hours. An illustration of a typical photolysis, as probed by UV-Vis spectroscopy, is shown in Figure 44. Here, a 10^{-4} M sample of 2,3,5,6-tetrafluoro-pHP GABA (**129**) in water was irradiated with at 300 nm and analyzed at 3 minute intervals to complete conversion at 9 min. For **129**, the absorption decrease at $\lambda \sim 316$ nm was

Figure 44. UV-Vis probe of the photolysis of **129**, predominantly the conjugate base in water, monitored at 3 minute intervals.



accompanied by an increase at $\lambda \sim 220$ nm due to the principal photoproduct, *p*-hydroxy-2,3,5,6-tetrafluorophenylacetic acid (pHP Acid). An isosbestic point at 225 nm further validates that *p*-hydroxy-2,3,5,6-tetrafluorophenylacetic acid is the primary photoproduct of **129**.

B. pHP *l*-glutamate derivatives (143-145) in water and buffer pH = 8.20. As anticipated, the UV-Vis analysis of pHP Glu derivatives (**143-145**) paralleled the UV-Vis profiles in water and buffer of their GABA counterparts **123**, **122**, **130** respectively. Corresponding λ_{\max} values, times for complete conversions (at 300 nm) in water, and pKa's of **143-145** are shown in Table 17.

Table 17. UV-Vis parameters and estimated times for 100% conversion to photoproducts from irradiation at 300 nm and associated pKa's for **143-145**.

Cmpd	λ_{\max}/nm ($\log \epsilon$ [$\text{M}^{-1}\text{cm}^{-1}$]) ^a	λ_{\max}/nm ($\log \epsilon$ [$\text{M}^{-1}\text{cm}^{-1}$]) ^b	time (min) ^c	time (min) ^d	pKa
143	272 (4.01)	323 (4.02)	7	60	7.2
144	274 (4.02), 302 (3.46)	348 (3.66), 330 (3.99)	7	70	6.5
145	328 (4.09)	326 (4.05)	6	30	5.5

^aMeasured in water. ^bMeasured in 0.01 M HEPES, 0.1 M LiClO₄, pH = 8.20. ^cIn water, estimated by HPLC/UV-Vis analysis. ^dIn 0.01 M HEPES, 0.1 M LiClO₄, pH = 8.20, estimated by HPLC/UV-Vis analysis.

C. Other pHP amino acids (glycine (146), valine (147), tryptophan (148), phenylalanine (149)), deoxycholic acid (150), diethyl phosphonate (151) and fluoride (152). The UV-Vis profiles for 146-152 in water and buffered media paralleled those

Table 18. UV-Vis parameters and 100% conversion times for 146-152 from irradiation at 300 nm.

Cmpd	λ_{\max}/nm ($\log \epsilon [\text{M}^{-1}\text{cm}^{-1}]$) ^a	λ_{\max}/nm ($\log \epsilon [\text{M}^{-1}\text{cm}^{-1}]$) ^b	time (min) ^c	time (min) ^d	pKa
146	280 (4.09)	330 (3.94), 282 (3.89)	7	5	7.9
147	279 (4.07)	327 (3.89), 281 (3.76)	7	6	7.9
148	272 (4.12), 300 (3.89), 310 (3.67)	ND	15	13	7.9
149	282 (4.09)	328 (3.98), 282 (3.91)	7	6	7.9
150	279 (4.00) ^e	ND	20 ^e	ND	7.9
151 ^f	280 (4.03)	ND	-	-	7.9
152	282 (4.12) ^g	331 (3.65), 282 (4.05) ^h	12	10	7.9

^aMeasured in water. ^bMeasured in 0.01 M HEPES, 0.1 M LiClO₄, pH = 7.3. ^cIn water, estimated by HPLC/UV-Vis analysis. ^dIn 0.01 M HEPES, 0.1 M LiClO₄ pH = 7.3, estimated by HPLC/UV-Vis analysis. ^eMeasured in 5% aq. CH₃OH. ^fNo photoreaction occurred. ^g50% aq. CH₃OH. ^h20% aq. CH₃OH.

for GABA analogs 140 and 141 above except for pHP Trp (148). The tryptophan moiety contributes to the absorptivity of the caged derivative. The nucleofuges for each, however, were quite distinct, resulting in variable conversion times. UV-Vis parameters and times for complete conversion are depicted in Table 18.

D. 5-acetylsalicylic acid and salicylate GABA and alkanoyl derivatives, 153-165.

UV-Vis spectra were obtained for compounds 5-acetylsalicylic acid GABA and alkanoyl analogs 153, 155-156, and 5-acetylsalicylate/amide GABA derivatives 154,

157-165. The parameters associated with these, along with times for complete conversion of 2 mM concentrations of precursor in water to photoproducts at 300 and

Table 19. UV-Vis parameters, 100% conversion times from irradiation at 300 nm, and % conversion after 24 h from irradiation at 350 nm for **153-165**.

Compound	λ_{\max}/nm ($\log \epsilon$ [$\text{M}^{-1}\text{cm}^{-1}$]) ^a	time (min) ^b	% conversion ^c
153	280 (3.90), 310 (3.58)	12	25
154^d	272 (4.09), 310 (3.22), 330 (3.94)	12	ND
155^e	282 (3.96)	20	20
156^e	281 (4.00)	20	20
157^f	340 (3.76), 310 (3.92), 274 (4.15)	25	50
158^g	343 (2.61), 320 (3.16), 300 (3.36), 271 (3.80)	13	50
159	305 (3.52), 269 (3.92)	22	33
160	306 (3.46), 269 (3.96), 229 (4.17)	21	33
161	308 (3.36), 271 (3.88), 233 (4.16)	16	33
162	310 (3.70), 272 (4.08)	21	25
163	307 (3.38), 271 (3.82), 234 (4.11)	13	25
164^g	312 (3.52), 273 (3.89)	17	25
165^f	313 (3.64), 273 (3.95), 227 (4.20)	11	50

^aMeasured in water. ^bTwo 300 nm lamps, estimated by HPLC with UV-Vis detection in a gradient of methanol/water. ^cSixteen 350 nm lamps, estimated by ¹H NMR analysis after 24 h, in 1:1 CD₃OD:D₂O. ^dPreviously determined. ^e90% aq. CH₃OH. ^f75% aq. CH₃OH. ^g95% aq. CH₃OH.

350 nm are illustrated in Table 19. The pKa's for these were not determined. The principal intentions for synthesizing **157-165** were: a) To lengthen the λ_{\max} of the chromophore towards 350 nm and b) to construct and evaluate a potential for an energy relay (antennae) system from the added auxochrome to enhance the photochemical efficiency. Most of the entities manifested higher molar absorptivities at 300 nm rather than at 350 nm. The full transformations to photoproducts at 300 nm, however, were markedly longer than the pHP analogs lacking the auxochrome.

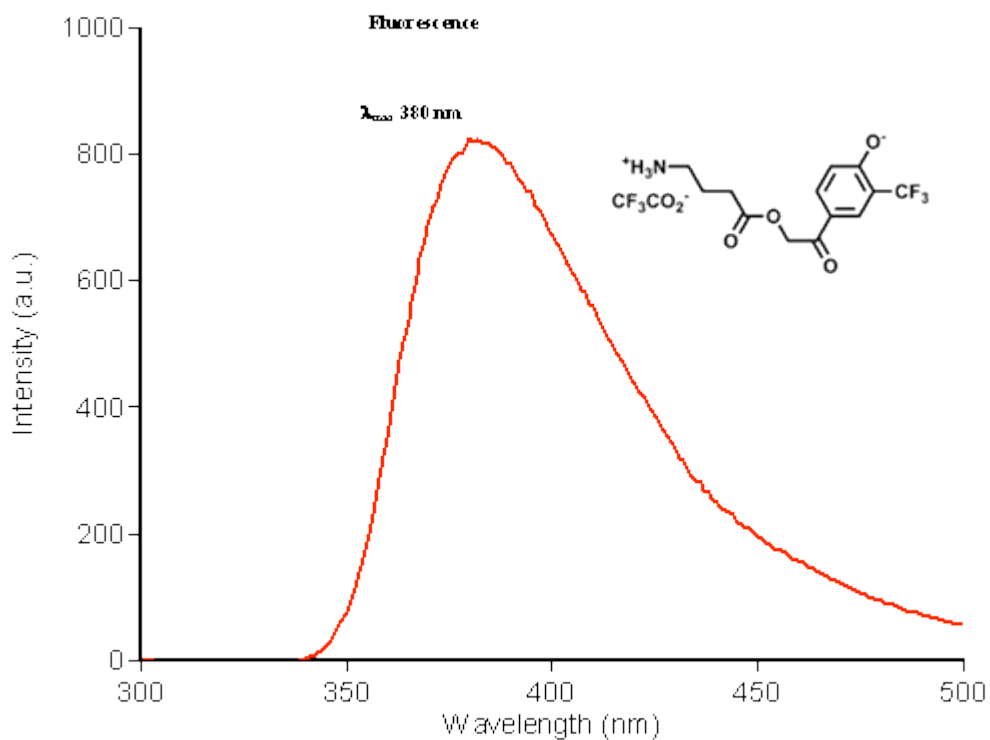
Excitation at 350 nm effectuated only marginal substrate release and necessitated more than 24 h for sufficient substrate release.

E. α -Alkyl pHP diastereomers (R,R)-166, and (R,S)-167. UV-Vis assessment of (R,R) 166 and (R,S) 167 produced an absorbance summary akin to 101 above. Exposure to two 300 nm lamps in 50% aq. CH₃OH conveyed complete conversion to photoproducts at 10 minutes for (R,R)-166 and 11 minutes (R,S)-167, as determined by HPLC/UV-Vis analysis.

IV. Fluorescence Spectroscopic Studies

The pHP chromophore does not fluoresce sufficiently for detection on a conventional, benchtop Varian Eclipse® spectrofluorimeter. The corresponding conjugate bases were weakly fluorescent. An example of fluorescence from *m*-CF₃-pHP GABA (**130**) in 0.01 M HEPES, 0.1 M LiClO₄ at pH = 8.2 is shown in Figure 45. The excitation wavelength was 325 nm, which produced a single, broad emission signal λ_{em} at 380 nm that tailed out past 500 nm. Examinations of the fluorescence properties of pHP GABA derivatives, **122-131** and the unsubstituted parent in the

Figure 45. Fluorescence spectrum of **130** in 0.01 M HEPES, 0.1 M LiClO₄ pH = 8.2, $\lambda_{\text{ex}} = 325$ nm.



same media as **130** gave the same results as **130** and are reported in Table 20.

Table 20. Fluorescence of **122-131** in 0.01 M HEPES, 0.1 M LiClO₄ at pH 8.2.

Compound	λ_{em} (nm)
122	395
123	382
124	390
125	385
126	399
127	374
128	392
129	384
130	380
131	395
Parent (101)	382

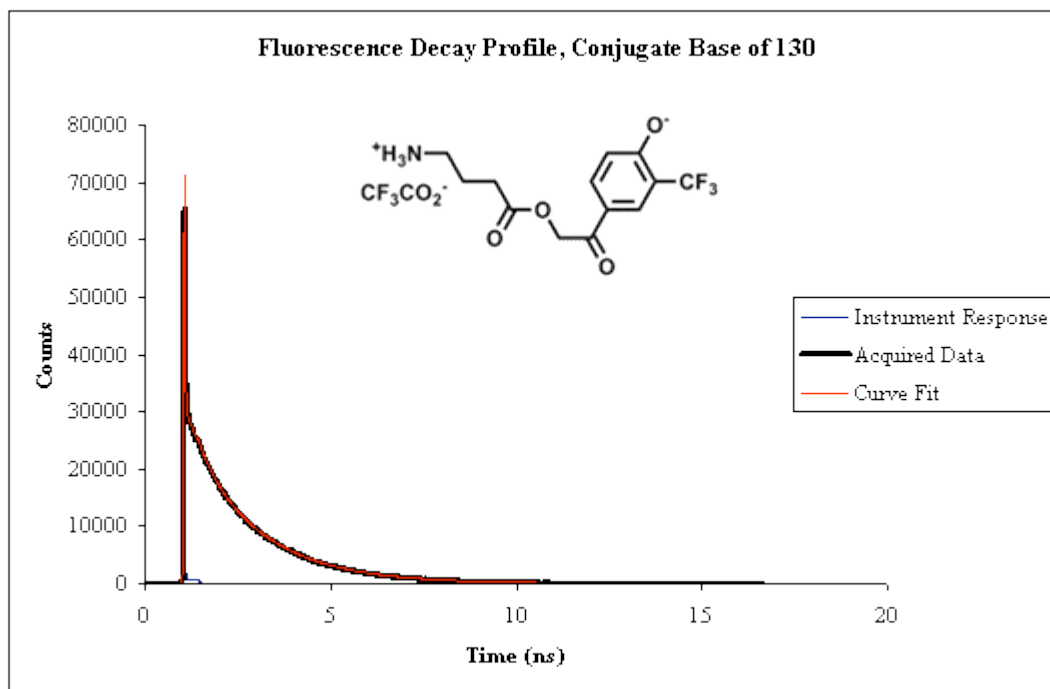
V. Time correlated single photon counting, TCSPC. TCSPC (see experimental), studies were carried out to obtain the fluorescence lifetimes for conjugate bases of **122-131**. Exponential decay profiles and the fluorescence lifetimes were obtained (Table 21). The transients were determined by the Maximum Entropy Method.

Table 21. TCSPC derived fluorescence decay profiles of **101**, **122-131** in aq. 0.1 M LiOH.

Compound	# transients	t ₁ (ns)	t ₂ (ns)
101 (parent)	2	0.106	
122	2	0.129	
123	2	0.115	
124	2	0.156	
125	1	0.197	
126	2	0.099	
127	3	0.145	0.492
128	3	0.189	0.422
129	2	0.257	
130	3	0.039	1.803
131	2	0.013	

An illustration of a TCSPC decay profile is provided in Figure 46 for a 0.1 mM solution of **130** in 0.1 M LiOH. In this example, a curve fitting application (red) correlated the fluorescence decay (black) to a single exponential best fit with a lifetime of 1.80 ns respectively.

Figure 46. TCSPC decay profile for *m*-CF₃-pHP GABA (**130**) in 0.1 M LiOH.



VI. Quantitative Photochemical Analysis

The quantum yields, Φ , equal the ratio n_x/n_p , where n_x depicts the number of photochemical or photophysical occurrences x , effectuated by light absorbed, p , by the precursor at a particular wavelength λ .¹⁰² The value can be considered as a percentage; for example, a Φ of 0.20 for pHP GABA disappearance signifies that 20% of the excited state pHP GABA molecules decayed by substrate release. It follows that the higher the quantum yield, the greater efficacy for the overall photochemical process. Quantum yields were determined for those compounds **122-167** that conveyed substrate photorelease from preliminary ¹H NMR studies; these included reactant disappearance (Φ_{dis}), substrate appearance (Φ_{app}), and appearance of

p-hydroxyphenylacetic acids (Φ_{acid}). The quantum yields of the minor *p*-hydroxybenzyl alcohols were not quantified. Analyses were accomplished by HPLC/UV and LC/MS/MS techniques and were done in triplicate.

A. Quantum yields of pHP GABA derivatives 122-141 from photolysis at 300

nm. The determination of quantum yields, Φ_{dis} , Φ_{app} , Φ_{acid} for 1-10 mM of **122-141** and the unsubstituted parent (**101**) at 300 nm were determined in an assortment of media. The principal objectives for these studies were to distinguish any pronounced variations in the quantum yields as a function of the media, i.e., effects due to buffer, pH, added salts, and changes from organic to aqueous solvent ratios. Initial photolysis studies involved the use of water buffered by 0.01 M ammonium acetate that spanned from pH 5.0 to pH 9.0. Not all precursors were probed in these media. The results are presented in Table 22. Blank spaces indicate “not determined”. In all cases, the quantum yields for precursor disappearance, Φ_{dis} , were commensurate with those for the emergence of GABA, Φ_{app} . The quantum yields for appearance of *p*-hydroxyphenylacetic acids, Φ_{acid} , were always slightly reduced; this phenomenon was expected from a competing pathway to the minor product, *p*-hydroxybenzyl alcohol. As such, Φ_{dis} will be emphasized from this point on with the assumption that Φ_{app} and Φ_{acid} do not diverge significantly from Φ_{dis} .

In general, values for Φ_{dis} were optimum in water or 0.01 M ammonium acetate solutions at pH 5.0. At pH 6.0, the values for some are lower; for example, *m*-F-pHP GABA (**123**) exhibited a $\Phi_{\text{dis}} = 0.28 (\pm 0.02)$ at pH 5.0 and $0.22 (\pm 0.01)$.

Table 22 Quantum yields for **122-141** and the unsubstituted parent (**101**) from photolyses in water and 0.01 M ammonium acetate buffer, pH 5.0 to pH 9.0.

Cmpd	pKa	Water ^a			pH 5.0 ^b			pH 6.0 ^b			pH 7.0 ^b			pH 8.0 ^b			pH 9.0 ^b					
		Φ_{dis}	Φ_{app}	Φ_{acid}	Φ_{dis}	Φ_{app}	Φ_{acid}	Φ_{dis}	Φ_{app}	Φ_{acid}	Φ_{dis}	Φ_{app}	Φ_{acid}	Φ_{dis}	Φ_{app}	Φ_{acid}	Φ_{dis}	Φ_{app}	Φ_{acid}			
Parent (101)	7.9	0.20	0.19	0.16	0.21	0.20	0.18	0.21	0.21	0.20	0.20	0.21	0.20	0.20	0.20	0.20	0.20	0.18	0.09	0.08	0.07	
122	6.5	0.16	0.15	0.15	0.24	0.23	0.23	0.12	0.11	0.10	0.10	0.12	0.11	0.11	0.11	0.11	0.09	0.09	0.09	0.02	0.02	<0.01
123	7.2	0.28	0.27	0.26	0.28	0.27	0.26	0.25	0.24	0.22	0.21	0.21	0.19	0.19	0.19	0.23	0.21	0.21	0.21	0.06	0.05	<0.01
124	5.9	0.24	0.24	0.22	0.16	0.16	0.15	0.10	0.09	0.09	0.09	0.11	0.10	0.10	0.10	0.07	0.07	0.07	0.07	0.02	0.02	<0.01
125	5.7	0.22	0.21	0.20	0.07	0.07		0.11	0.10	0.07	0.11	0.10	0.10	0.10	0.08	0.06	0.06	0.06	0.04	0.02	0.02	<0.01
126	5.3	0.11	0.11	0.10	0.08	0.07	0.07	0.05	0.04	0.05	0.05	0.05	0.04	0.04	0.04	0.03	0.03	0.03	0.03	0.01	0.01	<0.01
127	6.8	0.16	0.16	0.15	0.14	0.13	0.11	0.15	0.14	0.13	0.10	0.10	0.09	0.08	0.08	0.07	0.07	0.07	0.05	0.04	0.04	0.02
128	4.5	0.08	0.07	0.06	0.07	0.06	0.04	0.06	0.04	0.04	0.06	0.06	0.05	0.04	0.04	0.05	0.04	0.04	0.02	0.03	0.03	<0.01
129	3.9	0.11	0.10	0.10	0.08	0.07	0.09	0.09	0.07	0.05	0.10	0.09	0.09	0.08	0.08	0.09	0.08	0.08	0.06	0.09	0.08	0.06
130	5.5	0.17	0.16	0.14	0.18	0.18	0.16	0.17	0.17	0.16	0.12	0.11	0.11	0.09	0.09	0.10	0.09	0.09	0.06	0.08	0.08	0.05
131	6.7	0.09	0.09	0.07	0.07	0.05	0.04	0.07	0.06	0.04	0.05	0.05	0.05	0.03	0.03	0.03	0.03	0.02	0.02	0.02	0.02	<0.01
133	7.8	0.03	0.03																			
134	7.9	0.07	0.06																			
137	8.1	0.15	0.14	0.13																		
138	8.2	0.15	0.14	0.13																		
139	8.0	0.11	0.10	0.10																		
140	7.9	0.05	0.04																			
141	7.9	0.06	0.06																			
^a 18 M Ω , ^b 0.01 M Ammonium Acetate																						

This downward trend continued at pH 7.0; only the unsubstituted parent displayed unchanged yields from pH 5.0 to pH 7.0 ($\Phi_{\text{dis}} = 0.20 (\pm 0.01)$) to 7.0 ($\Phi_{\text{dis}} = 0.20 (\pm 0.01)$). At pH 9.0, Φ_{dis} for **122-141** were minimal; the conjugate base forms of **122-141** prevail in this medium. This important trend correlating the pKa's of **122-141** with solution pH will be analyzed further in the Discussion section.

A series of studies with **122-141** were performed in several other, commonly used buffers including TRIS, HEPES, and sodium phosphate, ranging in pH from 7.0 to 9.0. In some cases, salts were added to control the ionic strength. The findings from these are depicted in Table 23. Blank spaces indicate “not determined”. Collectively, Φ_{dis} were relatively uniform in neutral pH ~ 7 media, regardless of the buffer type or modified ionic strength. A slightly enhanced Φ_{dis} was observed when added LiClO_4 was used instead of LiCl in HEPES buffer. When photolyses were conducted in HEPES buffer pH = 8.2, the efficiencies universally declined; for example, the unsubstituted parent (**101**) manifested a Φ_{dis} of 0.21 (± 0.01) in 0.01 M HEPES and 0.1 M LiClO_4 at pH 7.3, which plummeted to 0.09 (± 0.01) under identical conditions at pH 8.2. Additionally, when photolyses were executed in 0.01 M TRIS buffer with 0.1 M LiClO_4 at pH 9.0, where the conjugate bases are the sole species, most precursors evinced low quantum yields (>0.05). The declines in Φ_{dis} of the conjugate bases were congruent with the results of the ammonium acetate buffers.

Another assemblage of photolysis experiments involved the use of organic media and mixed aqueous organic solvents. Degassing before photolysis with argon was also examined for O_2 effects on the quantum yields. The former studies

Table 23 Quantum yields for **122-141** and the unsubstituted parent from photolysis in buffers pH 7 to pH 9, with and without adjusted ionic strengths

Cmpd	pKa	pH 7.3 ^a			pH 7.2 ^b			pH 7.0 ^c			pH 7.5 ^d			pH 8.2 ^e			pH 9.0 ^f				
		Φ_{dis}	Φ_{app}	Φ_{acid}	Φ_{dis}	Φ_{app}															
Parent	7.9	0.21	0.20	0.20	0.18	0.17	0.14	0.26	0.25		0.23	0.22	0.20	0.09	0.09	0.06	0.10	0.09	0.06	0.10	0.09
122	6.5	0.12	0.12	0.11	0.08	0.08	0.06	0.08	0.07		0.08	0.08	0.08	0.02	0.02	<0.01	0.02	0.02	<0.01	0.02	0.02
123	7.2	0.21	0.20	0.19					0.07					0.06	0.06	0.03	0.04	0.03	0.04	0.03	0.03
124	5.9	0.11	0.11	0.09										0.05	0.05	0.04	0.02	0.02	0.04	0.02	0.02
125	5.7	0.10	0.09	0.09	0.08	0.07	0.05	0.08	0.08	0.06	0.13	0.12	0.11	0.02	0.02	<0.01	0.02	0.02	<0.01	0.02	0.02
126	5.3	0.05	0.05	0.04	0.02	0.02	<0.01	0.02	0.02	<0.01	0.04	0.04	0.04	0.02	0.02	<0.01	0.03	0.02	<0.01	0.03	0.02
127	6.8	0.10	0.09	0.08										0.04	0.04	0.02	0.04	0.02	0.04	0.04	0.03
128	4.5	0.06	0.06	0.04										0.02	0.02	<0.01	0.05	0.05	<0.01	0.05	0.05
129	3.9	0.10	0.10	0.08				0.06	0.05					0.09	0.09		0.06	0.06		0.06	0.06
130	5.5	0.12	0.11	0.10	0.10	0.09	0.07	0.09	0.09		0.10	0.09	0.09	0.08	0.08		0.08	0.07		0.08	0.07
131	6.7	0.06	0.06	0.05										0.02	0.02	0.01	0.06	0.05	0.01	0.06	0.05
133	7.8	0.03	0.03											0.02	0.02						
134	7.9	0.06	0.05											0.03	0.02						
137	8.1	0.15	0.16	0.13										0.08	0.08	0.06					
138	8.2	0.17	0.17	0.15										0.11	0.11	0.09					
139	8.0	0.10	0.09	0.08										0.07	0.07	0.06					
140	7.9	0.04	0.03																		
141	7.9	0.05	0.04																		

^a0.01 M HEPES, 0.1 M LiClO₄, pH = 7.3. ^b0.01 M HEPES, 0.1 M LiCl, pH = 7.2. ^c0.05 M Sodium Phosphate, pH = 7.0.

^d0.01 M TRIS, 0.1 M LiClO₄, pH = 7.5. ^e0.01 M HEPES, 0.1 M LiClO₄, pH = 8.2. ^f0.01 M TRIS, 0.1 M LiClO₄, pH = 9.0.

were performed to determine whether hydroxylic solvents, excepting water, were sufficient to induce substrate photorelease from pHP caged compounds. Of particular note, all pHP GABA esters displayed full solubility in 1-pentanol and perhaps more remarkably, in 1-octanol. The results are provided in Table 24. Blank spaces indicate “not determined”.

Reasonable Φ_{dis} values were observed for nearly all precursors in 1-pentanol and 1-octanol, though in general these were lower than in water. Exceptions to this were 2,3,6-triF-pHP GABA (**128**) where Φ_{dis} were essentially the same as in water (0.09 (± 0.01) and 0.08 (± 0.008) respectively) and *m,m'*-diOCH₃-pHP GABA (**133**) which displayed a pronounced improvement compared to water from ($\Phi_{\text{dis}} = 0.07$ (± 0.003) to 0.03 (± 0.005) respectively). In 25% aq. CH₃CN, marginal differences were observed for Φ_{dis} compared to water. However, 3,5-diF-pHP GABA (**126**) and 2,3,5,6-tetraF-pHP GABA (**129**) conveyed marked improvements (0.16 (± 0.01) vs. 0.11 (± 0.01) for the former, 0.14 (± 0.01) vs. 0.10 (± 0.01) for the latter).

Nearly all precursors manifested low quantum yields in DMSO; the fact that substrate photorelease occurred at all in this aprotic media is noteworthy. Interestingly, **128** exhibited an enhanced quantum yield in DMSO compared to water (0.12 (± 0.01) and 0.08 (± 0.008), respectively); this was further ameliorated in 10% aq. DMSO to $\Phi_{\text{dis}} = 0.15$ (± 0.02). Several other pHP GABA derivatives manifested slightly augmented yields in 10% aq. DMSO compared to water, including 2,5-diF-pHP GABA (**125**, 0.27 (± 0.01) and 0.24 (± 0.01), respectively), **126** (0.14 (± 0.01) and

Table 24 Quantum yields for 122-131, 133-134 and the unsubstituted parent from photolysis in organic media and degassed aq. solution.

Cmpd	1-pentanol		1-octanol		CH ₃ CN ^a		DMSO		DMSO ^b		Degassing ^c	
	Φ_{dis}	Φ_{app}	Φ_{dis}	Φ_{app}	Φ_{dis}	Φ_{app}	Φ_{dis}	Φ_{app}	Φ_{dis}	Φ_{app}	Φ_{dis}	Φ_{app}
Parent	0.11	0.11	0.12	0.11	0.18	0.18	0.06	0.06	0.19	0.19	0.16	0.15
122	0.13	0.12	0.07	0.06	0.15	0.15	0.04	0.03	0.18	0.17		
123	0.21	0.21	0.11	0.10	0.22	0.22	0.06	0.05	0.21	0.20		
124	0.18	0.18	0.08	0.07	0.19	0.18	0.07	0.06	0.27	0.26		
125	0.15	0.15	0.11	0.10	0.21	0.21	0.06	0.05	0.23	0.21		
126	0.08	0.08	0.11	0.10	0.16	0.16	0.06	0.06	0.14	0.13		
127	0.09	0.08	0.07	0.07	0.16	0.15	0.03	0.03	0.08	0.08		
128	0.09	0.08	0.12	0.11	0.10	0.10	0.12	0.10	0.15	0.12		
129	0.08	0.08	0.06	0.05	0.14	0.14	0.06	0.05	0.18	0.17		
130	0.14	0.14	0.14	0.13	0.15	0.14	0.04	0.03	0.10	0.10	0.18	0.17
131	0.06	0.05	0.10	0.09	0.10	0.10			0.12	0.12	0.09	0.07
133	0.07	0.06					0.03	0.02				
134	0.04	0.04										

^a25% aqueous. ^b10% aqueous. ^cArgon purge for 45 minutes.

0.11 (± 0.01), respectively), **129** (0.18 (± 0.01) and 0.11 (± 0.01) respectively), and *m*-OCH₃-pHP GABA (**131** (0.12 (± 0.01) and 0.09 (± 0.01) respectively)).

Degassing, that entailed purging the aqueous solution of the pHP GABA derivative for 45 minutes with argon, failed to change the quantum yields.

Photolyses of **122-141** were conducted in water with modified ionic strengths to distinguish whether a *salt effect* would be reflected in Φ_{dis} . The first set of experiments focused on LiClO₄ as the ancillary salt, ranging from 0.008 to 1.0 M (Table 25). Remarkably, nearly *all* pHP derivatives manifested enhancements in quantum yield at 1.0 M LiClO₄ in water. For example, a $\Delta\Phi_{\text{dis}}$ of 0.14, from 0.16 (± 0.01) to 0.30 (± 0.02) or a 94% increase for **122** was observed. Several pHP derivatives evinced improved quantum yields in 0.01 M LiClO₄ relative to water as well, such as **126** with a $\Delta\Phi_{\text{dis}} = 0.07$, from 0.11 (± 0.008) in water to 0.18 (± 0.01) in 0.01 M LiClO₄.

Other ancillary salts (NaClO₄ and Mg(ClO₄)₂) were explored for similar influences on a few pHP GABA derivatives, including the parent, **122**, **123**, and **124**. In addition, experiments involving the addition of free GABA (1 and 10 equivalents) to aqueous solutions of these four pHP-GABA precursors were performed to discern any changes in Φ_{dis} due to a *common ion effect*.¹⁰³ The findings from these studies are depicted in Table 26. Each of the precursors gave increased quantum yields in 1.0 M NaClO₄ and Mg(ClO₄)₂ relative to water, consistent with the results in LiClO₄. A curious observation, however, was the marked decline in Φ_{dis} at low concentrations of Mg(ClO₄)₂. For example, a decline in Φ_{dis} was observed for the 2,3-diF-pHP GABA

Table 25. Quantum yields for 122-141 and the unsubstituted parent from photolyses in water with adjusted ionic strengths from 0.008 to 1.0 M LiClO₄.

Cmpd	0.008 M ^a		0.01 M ^a		0.025 M ^a		0.05 M ^a		0.1 M ^a		0.5 M ^a		1.0 M ^a	
	Φ_{dis}	Φ_{acid}	Φ_{dis}	Φ_{acid}	Φ_{dis}	Φ_{acid}	Φ_{dis}	Φ_{acid}	Φ_{dis}	Φ_{acid}	Φ_{dis}	Φ_{acid}	Φ_{dis}	Φ_{acid}
Parent	0.22	0.20	0.23	0.21	0.25	0.23	0.26	0.24	0.28	0.21	0.28	0.21	0.31	0.28
122			0.23	0.21			0.24	0.22	0.26	0.24	0.29	0.27	0.30	0.28
123			0.31	0.28			0.31	0.28	0.33	0.30	0.35	0.32	0.38	0.34
124	0.26	0.24	0.30	0.28	0.31	0.28	0.32	0.30	0.31	0.29	0.25	0.22	0.30	0.25
125			0.27	0.25			0.26	0.22	0.31	0.29	0.27	0.23	0.29	0.27
126			0.18	0.15			0.19	0.17	0.20	0.18	0.21	0.19	0.21	0.19
127											0.12	0.10	0.24	0.22
128											0.06	0.04	0.10	0.09
129	0.07	0.05	0.05	0.03	0.05	0.02	0.06	0.04	0.06	0.04	0.07	0.05	0.14	0.12
130			0.17	0.15									0.26	0.25
131													0.15	0.13
133													0.06	0.04
134													0.09	0.08
137													0.17	0.15
138													0.19	0.16
139													0.15	0.14
140													0.08	0.07
141													0.10	0.09
						^a LiClO ₄								

Table 26. Quantum yields for **122-124** and the unsubstituted parent (**101**) from photolysis in water with adjusted ionic strengths and added GABA at 300 nm.

Cmpd	1.0 M ^a		0.01 M ^b		1.0 M ^b		GABA (1eq)		GABA (10eq)	
	Φ_{dis}	Φ_{acid}	Φ_{dis}	Φ_{acid}	Φ_{dis}	Φ_{acid}	Φ_{dis}	Φ_{acid}	Φ_{dis}	Φ_{acid}
Parent	0.30	0.28	0.10	0.08	0.32	0.30	0.20	0.18	0.22	0.19
122	0.25	0.24	0.08	0.06	0.25	0.23	0.17	0.16	0.16	0.15
123	0.35	0.32	0.14	0.13	0.34	0.31	0.29	0.27	0.30	0.27
124	0.31	0.28	0.12	0.10	0.32	0.29	0.25	0.23	0.26	0.24
				^a NaClO ₄ . ^b Mg(ClO ₄) ₂ .						

(**124**), from 0.24 (± 0.02) in water to 0.12 (± 0.01) in 0.01 M Mg(ClO₄)₂. At 1.0 M Mg(ClO₄)₂, however, Φ_{dis} increased to 0.31 (± 0.02). Added GABA imparted no change in Φ_{dis} relative to solutions without added GABA.

B. Quantum yields of pHP-GABA derivatives, 122-131, from photolysis at 350 nm. The quantum yields for 1-10 mM concentrations of **122-131** in 0.01 M TRIS, 0.1 M LiClO₄ at pH 9.0 were determined by photolyses at 350 nm (Table 27), where the conjugate bases preponderate.

Table 27. Quantum yields for **122-131** in 0.01 M TRIS, 0.1 M LiClO₄ at pH 9.0 at 350 nm.

Cmpd	Φ_{dis}	Φ_{app}
Parent (101)	0.0041	0.0038
122	0.0086	0.0083
123	0.0046	0.0045
124	0.0017	0.0013
125	0.0029	0.0024
126	0.0019	0.0018
127	0.0037	0.0035
128	0.0042	0.0035
129	0.0069	0.0067
130	0.0081	0.0074
131	0.0058	0.0054

Conspicuously, the quantum yields were substantially diminished in contrast to those obtained with 300 nm lamps.

C. Quantum yields for pHP-*l*-glutamate derivatives, 143-145, determined by photolysis at 300 nm. The quantum yields of **143-145** and unsubstituted parent (**102**) were ascertained from photolysis of 1-10 mM in water, 0.01 M ammonium acetate, 0.01 M HEPES buffers with 0.1 M LiClO₄ at pH 7.3 and pH 8.2 (Table 28) at 300 nm. The determination of Φ_{dis} , Φ_{app} (Glu) and Φ_{acid} were consistent with those from pHP GABA's. Only Φ_{dis} will be discussed. No significant variations were observed in Φ_{dis} in water and with neutral pH ~ 7 buffers, apart from **145**, which gave lower Φ_{dis} in pH 7.3 buffer (0.11 (\pm 0.01) versus 0.18 (\pm 0.01) in water). All showed declined Φ_{dis} in pH 8.2 buffer, associated with conjugate bases, and coherent to findings from those pHP GABA derivatives.

Table 28. Quantum yields of **143-145** and unsubstituted parent (**102**) from photolysis in water, pH 7.0, pH 7.3 and pH 8.2 buffers at 300 nm.

Cmpd	water ^a			pH 7.0 ^b			pH 7.3 ^c			pH 8.2 ^c		
	Φ_{dis}	Φ_{app}	Φ_{acid}	Φ_{dis}	Φ_{app}	Φ_{acid}	Φ_{dis}	Φ_{app}	Φ_{acid}	Φ_{dis}	Φ_{app}	Φ_{acid}
Parent	0.16	0.16	0.12	0.16	0.15	0.13	0.17	0.16	0.14	0.10	0.09	0.08
143	0.15	0.15	0.12	0.18	0.16	0.13	0.16	0.15	0.14	0.08	0.08	0.06
144	0.16	0.15	0.13	0.14	0.14	0.12	0.17	0.16	0.16	0.10	0.10	0.08
145	0.18	0.18	0.15	0.17	0.17	0.15	0.11	0.11	0.09	0.07	0.07	0.05
^a 18 M Ω . ^b 0.01 M Ammonium Acetate. ^c 0.01 M HEPES, 0.1 M LiClO ₄												

D. Quantum yields of pHP caged amino acids glycine, valine, phenylalanine, and tryptophan, 146-149, at 300 nm. The quantum yields (Φ_{dis} and Φ_{acid}) associated with **146-149** at 300 nm at 1-10 mM concentrations in water and 0.01 M HEPES with 0.1 M LiClO₄ at pH 7.3 were determined. In addition, salt effects were explored for **149** (0.1 and 1.0 M LiClO₄ aqueous solutions). The findings from these studies are summarized in Table 29. No noteworthy variations were discerned for Φ_{acid} and Φ_{dis} under any conditions. In HEPES buffer pH 7.3, an enhancement in the quantum yields was observed for **146-148**. Added salts did not significantly improve Φ_{dis} .

Table 29. Quantum yields of **146-149** in water, pH 7.3 buffer, and water with adjusted ionic strengths.

Cmpd	water ^a		pH 7.3 ^b		0.1 M ^c		1.0 M ^c	
	Φ_{dis}	Φ_{acid}	Φ_{dis}	Φ_{acid}	Φ_{dis}	Φ_{acid}	Φ_{dis}	Φ_{acid}
146	0.17	0.14	0.22	0.18				
147	0.17	0.13	0.22	0.17				
148	0.16	0.15	0.20	0.16				
149	0.10	0.08	0.09	0.08	0.13	0.11	0.12	0.10
^a 18 M Ω . ^b 0.01 M HEPES, 0.1 M LiClO ₄ . ^c LiClO ₄								

E. Quantum yields of pHP DOC (150) and pHP F (152) at 300 nm. Photolysis of 1-5 mM of **150** in 5% aq. CH₃OH produced Φ_{dis} of 0.06 (± 0.007) and Φ_{acid} of 0.04 (± 0.006) at 300 nm. For **152**, Φ_{dis} was determined to be 0.10 (± 0.01) at 1 mM in 50% aq. CH₃OH at 300 nm.

F. Quantum yields of 5-acetylsalicylic acid derivatives 153-165 at 300 nm. The quantum yields for disappearance, Φ_{dis} , of 1-10 mM of 5-acetylsalicylic acid GABA (**153**) in an assortment of media at 300 nm are listed in Table 30. The quantum yields for appearance of GABA were found as the same Φ_{dis} . The quantum yields were relatively uniform, regardless of the nature photolysis medium, though slightly enhanced in aqueous 1.0 M LiClO₄ and 1.0 NaClO₄ solutions. In a previous report,¹⁰⁴ the Φ_{dis} of the *m*-carbomethoxy derivative of 5-acetylsalicylic acid GABA (**154**) was given as 0.31 from photolysis in water at 300 nm; this diverges significantly from Φ_{dis}

Table 30. Φ_{dis} of **153** in various media from photolysis at 300 nm.

	water ^a	pH 7.2 ^b	pH 7.3 ^c	pH 7.0 ^d	pH 9.0 ^e	0.01M ^e	0.05M ^e	0.1M ^e	0.5M ^e	1.0M ^e	0.1M ^f	1.0M ^f
Cmpd	Φ_{dis}											
153	0.09	0.08	0.09	0.09	0.11	0.09	0.10	0.10	0.11	0.12	0.10	0.12
^a 18 M Ω . ^b 0.01 M HEPES, 0.1 M LiCl. ^c 0.01 M HEPES, 0.1 M LiClO ₄ . ^d 0.05 M Sodium Phosphate. ^e LiClO ₄ . ^f NaClO ₄ .												

= 0.09 (\pm 0.01) for **153**. The quantum yields for **154** were re-evaluated at 300 nm in an assortment of media. The results are depicted in Table 31. Evidently, the quantum

Table 31. The values for Φ_{dis} and Φ_{app} of **154** from photolyses at 300 nm in a variety of media.

	water ^a		pH 7.3 ^b		pH 9.0 M ^b			1.0 M ^c
Cmpd	Φ_{dis}	Φ_{app}	Φ_{dis}	Φ_{app}	Φ_{dis}	Φ_{app}	Φ_{dis}	Φ_{app}
154	0.08	0.07	0.09	0.08	0.11	0.10	0.08	ND
^a 18 M Ω . ^b 0.01 M HEPES, 0.1 M LiClO ₄ . ^c LiClO ₄ .								

yields for **154** are consistent with those determined for the parent and substantially lower than the $\Phi_{\text{dis}} = 0.31$ previously reported. Additionally, insignificant variations in these values were observed in all solvents tested.

The quantum yields for the disappearance (Φ_{dis}) of 5-acetylsalicylic acid dodecanoyl (**155**) and tetradecanoyl (**156**) esters were determined to be 0.04 (\pm 0.005) and 0.06 (\pm 0.006) respectively, from photolyses at 300 nm in 5% aqueous CH₃OH.

Additionally, Φ_{dis} in 0.01 M HEPES, 0.1 M LiClO₄, at pH 8.2 were 0.10 (± 0.01) and 0.09 (± 0.01) respectively, consistent with the GABA caged **153**.

The quantum yields for the disappearance (Φ_{dis}) of **157-165** “antennae” derivatives of 5-acetylsalicylic acid GABA, and appearance (Φ_{app}) of GABA were determined in 3:1 H₂O:CH₃OH at 300 nm (Table 32). The values were slightly irregular and except for **157** ($\Phi_{\text{dis}} = 0.01$ (± 0.002)), **159** ($\Phi_{\text{dis}} = 0.02$ (± 0.002)), and **162** ($\Phi_{\text{dis}} = 0.04$ (± 0.006)), did not vary appreciably from the parent **153** ($\Phi_{\text{dis}} = 0.09$ (± 0.01)). When irradiated at 350 nm in water and 0.01 M HEPES, 0.1 M LiClO₄ at pH 8.2, **157-165** gave very low Φ_{dis} and Φ_{app} values (< 0.01).

Table 32. Φ_{dis} and Φ_{app} for **157-165** in 3:1 H₂O:CH₃OH at 300 nm.

Cmpd	Φ_{dis}	Φ_{app}
157	0.01	< 0.01
158	0.08	0.07
159	0.02	< 0.01
160	0.06	0.05
161	0.08	0.07
162	0.04	0.04
163	0.11	0.11
164	0.07	0.06
165	0.12	0.11

G. Quantum yields of α -alkyl-pHP caged diastereomers (R,R) 166 and (R,S) 167 at 300 nm. The quantum yields for a mixture of (R,R) **166** and (R,S) **167** diastereomers was determined from photolysis at 300 nm of 5 mM concentrations of

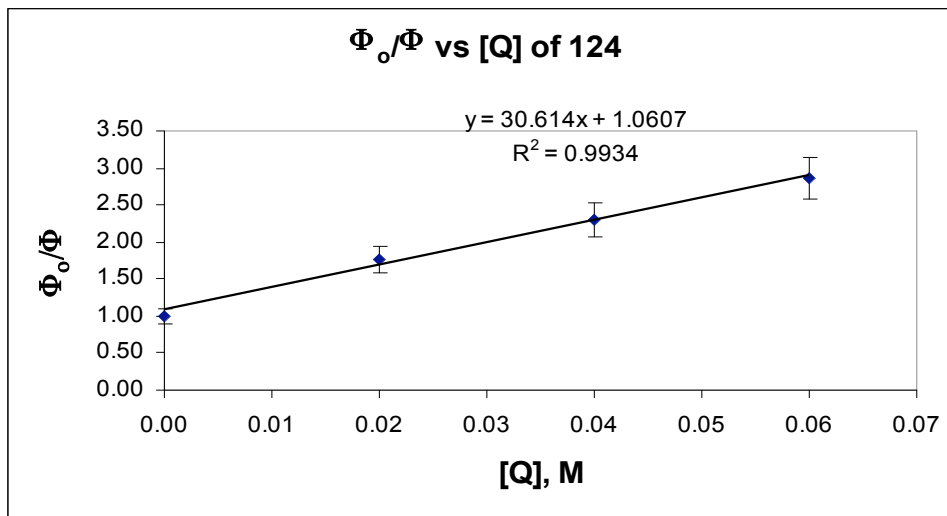
precursor in 50% aq. CH₃OH; these were found to be $\Phi_{\text{dis}} = 0.18 (\pm 0.01)$ and $\Phi_{\text{acid}} = 0.16 (\pm 0.01)$, consistent with unsubstituted pHP-GABA, 0.20 (± 0.01) and 0.16 (± 0.01) respectively.

VII. Determination of Rate Constants for Substrate Release by Stern-Volmer Quenching

The Stern-Volmer (S-V)⁷⁸ quenching method to indirectly determine the rate constants for substrate release was employed for GABA esters of **122-131**, **137-139**, and **153**. One to five mM of each was prepared in water or buffer, photolyzed at 300 nm and Φ_{dis} determined. Potassium sorbate, a triplet quencher **Q**, was added in increments and Φ_{dis} determined. Using linear regression analysis, plots of the ratios Φ_0 (quantum yield without **Q**)/ Φ (quantum yield with **Q**) vs. [**Q**] gave linear S-V plots with K_{SV} as the slope. For example, a 5 mM aqueous solution of 2,3-diF-pHP GABA (**124**) was photolyzed at 300 nm lamps along with three other solutions containing 20 mM, 40 mM, and 60 mM of potassium sorbate. A plot of corresponding Φ_0/Φ vs. [**Q**] values is illustrated in Figure 47. The slope, K_{SV} , is shown as the product of the diffusion rate, k_q , of the quencher in water (estimated to be $7.4 \times 10^9 \text{ M}^{-1}\text{s}^{-1}$)¹ and the triplet lifetime of chromophore, τ^3 . The rate of sorbate quenching is assumed to be diffusion controlled, i.e., $k_{\text{diff}} = k_q$. From the plot, τ^3 was calculated to be 4.14×10^{-9} s or 4.14 ns, and the rate of GABA release, $k_r = 5.75 \times 10^7 \text{ s}^{-1}$. Congruent analyses were completed for the other pHP GABA derivatives and

153 in water and 0.01 M HEPES, 0.1 M LiClO₄ at pH = 7.3. The results are listed in Table 33.

Figure 47. Stern-Volmer relationship from the photolysis of 2,3-diF-pHP GABA (**124**) in water with potassium sorbate as the quencher, Q.



$$\Phi_o/\Phi = 1 + K_{SV}[Q]$$

$$\text{Slope} = K_{SV} = 30.61$$

$$k_{diff} = k_q = 7.4 \times 10^9 \text{ s}^{-1}$$

$$K_{SV} = k_q \times \tau^3$$

$$\tau^3 = 4.14 \times 10^{-9} \text{ s}$$

$$k_r = \Phi_o/\tau^3 = 5.75 \times 10^7 \text{ s}^{-1}$$

	Φ	Φ _o /Φ	[Sorbate], M
Initial (Φ_o)	0.24	1.00	0.00
Series #1	0.14	1.76	0.02
Series #2	0.11	2.30	0.04
Series #3	0.08	2.86	0.06

The rate constants for GABA release spanned about 1 order of magnitude, from $k_r = 2 \times 10^7 \text{ s}^{-1}$ for *m*-OCF₃-pHP GABA (**131**), to $k_r = 1.58 \times 10^8 \text{ s}^{-1}$ for *o*-F-pHP GABA (**123**), in water. An overall decline in the rate constants was observed when the

solvent was changed to 0.01 M HEPES pH 7.3, except for 2,6-diF-pHP GABA (**126**) and 2,3,5,6-tetraF-pHP GABA (**129**), which evinced a near doubling of rate constants (4.7 to 8.9 and 2.7 to 5.5 x 10⁷ s⁻¹, respectively).

Table 33. Parameters derived from Stern-Volmer quenching analysis for **122-131**, **137-139**, and **153** in water and 0.01 M HEPES, 0.1 M LiClO₄ at pH = 7.3.

Cmpd	water ^a			pH 7.3 ^b		
	K _{SV} (M ⁻¹)	τ ³ (10 ⁻⁹ s)	k _r (10 ⁷ s ⁻¹)	K _{SV} (M ⁻¹)	τ ³ (10 ⁻⁹ s)	k _r (10 ⁷ s ⁻¹)
101 (parent)	24 ± 1 ^c	3.2 ± 0.4	6.8 ± 0.4	26 ± 1	3.6 ± 0.4	5.5 ± 0.1
122	28 ± 2	3.8 ± 0.2	4.2 ± 0.2	23 ± 1	3.1 ± 0.3	3.6 ± 0.2
123	13 ± 0.2	1.9 ± 0.1	15.8 ± 0.1	19 ± 1	2.5 ± 0.1	8.4 ± 0.2
124	44 ± 2	6.0 ± 0.6	4.0 ± 0.4	39 ± 1	5.3 ± 0.4	2.1 ± 0.3
125	15 ± 0.8	2.1 ± 0.1	10.7 ± 0.1	51 ± 2	6.9 ± 0.2	1.6 ± 0.1
126	29 ± 0.8	4.0 ± 0.1	2.5 ± 0.1	32 ± 1	4.3 ± 0.1	1.1 ± 0.2
127	25 ± 0.5	3.3 ± 0.1	4.7 ± 0.1	8 ± 1	1.1 ± 0.1	8.9 ± 0.1
128	34 ± 2	4.6 ± 0.4	1.8 ± 0.1	36 ± 1	4.8 ± 0.2	1.3 ± 0.2
129	30 ± 0.5	4.1 ± 0.1	2.7 ± 0.1	14 ± 1	1.9 ± 0.3	5.5 ± 0.3
130	20 ± 2	2.7 ± 0.3	7.4 ± 0.7	30 ± 2	4.1 ± 0.5	3.0 ± 0.4
131	33 ± 0.7	4.4 ± 0.2	2.0 ± 0.1	29 ± 2	4.0 ± 0.3	1.4 ± 0.3
137	17 ± 1	2.2 ± 0.2	6.7 ± 0.3			
138	23 ± 0.8	3.1 ± 0.5	4.9 ± 0.7			
139	15 ± 1	2.1 ± 0.3	5.2 ± 0.4			
153	11 ± 0.5	1.4 ± 0.4	6.6 ± 0.3			

^a18 MΩ. ^b0.01 M HEPES, 0.1 M LiClO₄. ^cStandard deviation.

VIII. Computational Studies with analogs of pHP GABA (**122-131**) and pHP Glu (**143-145**).

Several computational studies were conducted with derivatives of pHP GABA (**122-131**, **133-134**) and pHP Glu (**143-145**) in order to provide insights into relevant

parameters of solubility (ClogP), correlations between structure and relative energies, and electronic parameters such as spin densities and charge densities.

A. Determination of calculated logP (ClogP)¹⁰⁸ values for 122-131, 133-134 and 143-145. The *log* of the partition coefficient for 1-octanol versus water, **P**, which represents the ratio of the concentration of a particular substance **S** in 1-octanol (o) and water (w) ($P = [S]_o/[S]_w$) is a commonly employed indicator of compound hydrophobicity.¹⁰⁵ This criterion is particularly important in predicting the biological compatibility of the compound, e.g., solubility in lipids, metabolism, receptor interaction, and bioavailability, among others.¹⁰⁵ 1-Octanol has been traditionally the preferred organic constituent because of its likeness to lipids and its easy access. A positive ClogP value indicates a greater lipophilic bearing, i.e., a higher concentration of the substance in the 1-octanol layer versus the water layer. Using the CLogP® software package, version 3.4¹⁰⁶ implemented in SYBYL 7.3,¹⁰⁷ which models these values for ClogP, were calculated for **122-131**, **133-134** and **143-145**. In addition, ClogP values were determined for the conjugate bases of **122-131**, since these play a prominent role in many of the substituted pHP derivatives. These are displayed in Table 34. Within this series of compounds, *m*-CF₃-pHP GABA (**130**) evinced the

Table 34. ClogP values for GABA derivatives (**101**, **122-131**, **133-134**), Glu derivatives (**102**, **143-145**) and the conjugate bases of pHP GABA's **122-131**.

Cmpd	ClogP	ClogP	
		(conjugate base)	
Parent (101)	1.19		
122	1.06	-2.71	R ₁ = F
123	0.81	-3.15	R ₂ = F
124	0.73	-2.82	R ₁ , R ₂ = F
125	0.8	-2.75	R ₁ , R ₃ = F
126	1.05	-2.3	R ₁ , R ₄ = F
127	0.55	-3.2	R ₂ , R ₃ = F
128	0.76	-2.44	R ₁ , R ₂ , R ₄ = F
129	0.66	-2.52	R ₁ , R ₂ , R ₃ , R ₄ = F
130	2.02	-1.9	R ₁ = CF ₃
131	1.93	-1.59	R ₁ = OCF ₃
133	-3.81		R ₁ , R ₄ = OCH ₃
134	-3.38		R ₁ = OCH ₃
		Glu	
Parent (102)	-0.03		
143	-0.21		R ₂ = F
144	0.04		R ₁ = F
145	0.99		R ₁ = CF ₃

highest ClogP value at 2.02 while the *m,m'*-di-OCH₃-pHP GABA (**133**) the lowest at -3.81; the implications from these data are that **130** is the most lipophilic and **133** the least lipophilic in the series. The extra carboxylic acid moiety that distinguishes *l*-Glu

from GABA was shown to impart drastic hydrophilic changes in the ClogP values; 1.06 to 0.04 for *m*-F-pHP, 0.81 to -0.21 for *o*-F-pHP, and 2.02 to 0.99 for *m*-CF₃-pHP. The conjugate bases, as anticipated from their charges, demonstrated sharp declines in ClogP values in reference to the protonated **122-131**.

B. Energies and Geometries of Oxyallyl-Phenoxy Triplet Biradicals. Previous studies by Givens and Wirz⁷⁸ and Phillips⁸² revealed a significant role for hydroxylic component of water in the photo-Favorskii reaction. Specifically, water is thought to accept the phenolic proton from the triplet excited state of pHP, which helps drive the detachment of the hydrated nucleofuge, tantamount to a photosolvolysis process for the leaving group release and an extrusion process for the chromophore. In order for these processes to obey the Wigner spin conservation rule, if it were an overall single step for a concerted process, these coupled steps generate at least one product that possesses unpaired spins, here the a phenoxy-oxyallyl triplet biradical (**117**) is the likely candidate. A posited requirement for nucleofuge departure in this process is an out of plane (OOP) contortion of the acetate moiety relative to the planar, phenoxy ring. This generates an oxyallyl-phenoxy biradical as the extended triplet fragment. To investigate the energetics of the OOP contortions thus determine the associated relative stabilization energies of the variety of substituted triplet oxyallyl biradicals (**117**), Gaussian 03[®] MP2 calculations with 6-31G* basis set were performed for the biradical component **117** generated from **122-131**.¹⁰⁸ Additionally, the relative energies were determined for spirodienediones (**100**) that emerged after intersystem

crossing of the biradical triplet to a fleeting singlet followed by collapse to **100**. The geometries of both the spirodienone **117** and the **100** are composed of nearly orthogonal oxyallyl and phenoxy constituents. The results from these calculations are listed in Table 35. In all cases, the triplet biradical (**117**) was calculated to be substantially more stable than the corresponding spirodienone by at least 78 kcal/mol. In addition, all precursors displayed an OOP contortion of at least 22°. The

Table 35. The out of plane (OOP) contortion angles and relative energies of the oxyallyl-phenoxy triplet biradicals (**117**) of **122-131**.

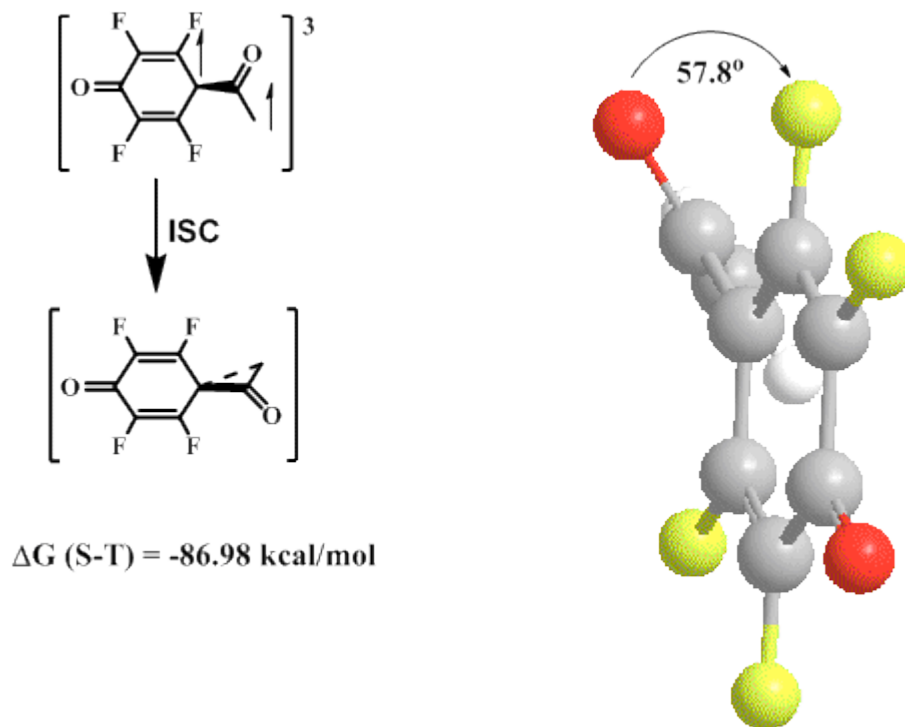
Cmpd	Singlet^a	Triplet^b	$\Delta(T-S)^c$	$\Delta(T-S)^c$	Triplet
	(Hartrees)	(Hartrees)	(Hartrees)	(kcal/mol)	Twist Angle
122	-554.847	-554.970	-0.124	-78.068	22.0
123	-554.848	-554.973	-0.125	-78.392	26.4
124	-653.685	-653.812	-0.126	-79.252	25.3
125	-653.677	-653.811	-0.134	-83.997	47.5
126	-653.690	-653.816	-0.125	-78.578	22.3
127	-653.678	-653.813	-0.137	-86.091	57.2
128	-752.528	-752.654	-0.126	-79.197	25.0
129	-851.346	-851.485	-0.139	-86.984	57.8
130	-791.614	-791.741	-0.127	-79.895	22.8
131	-866.474	-866.602	-0.128	-80.280	23.1

^aSpirodienodione. ^bOxyallyl-phenoxy biradical.

^cEnergy difference between the triplet and singlet species.

oxyallyl-phenoxy biradical associated with 2,3,5,6-tetrafluoro-pHP, **tetraF 117**, exhibited the greatest OOP contortion at 57.8° (Figure 48).

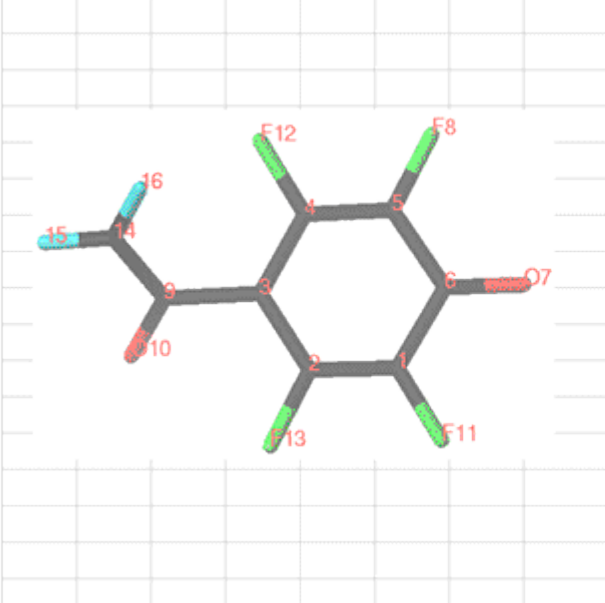
Figure 48. Out of plane orientation of the biradicals of **tetraF 117**, fluorine (yellow), oxygen (red), carbon (gray), and white (hydrogen).



C. Spin and Charge Density Calculations. The spin and charge densities of the oxyallyl-phenoxy transients were also obtained. The spin density is the amount of unpaired electron density¹⁰⁹ at specific atoms in the radical.⁹ The spin and charge densities were determined by from Gaussian 03[®] at the B3LYP level using the 6-31G* basis set of the oxyallyl-phenoxy biradicals transients of the *p*-hydroxyphenacyl analogs of **122**, **129-131**, **134**, and **154** and are represented by **tetraF 117**, the

oxyallyl-phenoxy triplet biradical from **129**, in Table 36. The carbonyl carbon, C9, evinced the lowest spin density (-0.171987) i.e., the atom with the lowest probability on which one of the unpaired electrons would dwell. In contrast, the alpha carbon to

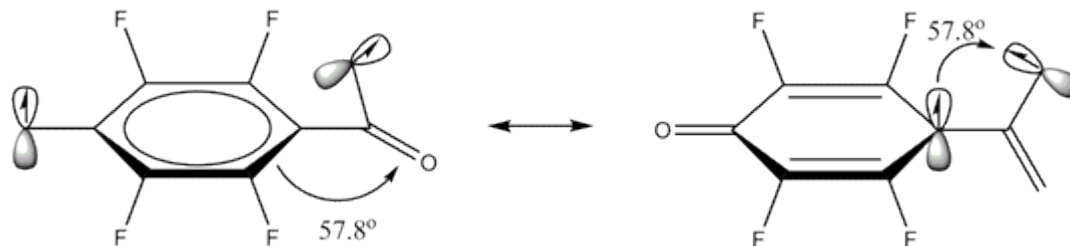
Table 36. Calculated spin and charge densities for tetraF **117**.



Atom	Type	Spin D	Charge D
1	C	0.25365	0.286447
2	C	-0.149423	0.305392
3	C	0.379063	-0.100035
4	C	-0.14822	0.287707
5	C	0.265947	0.290756
6	C	-0.087923	0.305876
7	O	0.409811	-0.440011
8	F	0.03294	-0.239243
9	C	-0.171987	0.408392
10	O	0.419314	-0.409834
11	F	0.031952	-0.23914
12	F	-0.006142	-0.271304
13	F	-0.009262	-0.251713
14	C	0.85803	-0.312481
15	H	-0.039206	0.194389
16	H	-0.038543	0.184801

the carbonyl, C14, manifested the highest spin density (0.85803). The oxygen atoms O10 (0.419314) and O7 (0.409811) conveyed nearly equivalent, significant probabilities for the location of an unpaired electron. The most favored (lowest energy) biradical distribution would place one electron at C14 and the other electron at O10 or O7 or at C3 and O10 (Figure 49).

Figure 49. Predicted radical positions for the **tetraF 117**, from MP2 calculations at the B3LYP level using the 6-31G* basis set.



IX. Laser Flash Photolysis Studies of pHP GABA derivatives (**101**, **122**, **125**, **128-131**), 5-acetylsalicylic acid GABA (**153**), and 5-acetyl-methylsalicylate GABA (**154**).

To obtain excited state parameters for **122**, **125**, **128-131**, the unsubstituted parent **101**, and **153**, such as transient absorptions and rates of decay, laser flash photolysis (LFP) studies were conducted through a long standing collaboration with the Wirz group at the University of Basel.¹¹⁰ By pump-probe optical spectroscopy with a pump wavelength of 266 nm (see *Experimental*), bands at 320, 420, and 440 nm were manifested for some derivatives and assigned to the appearance of the triplet oxyallyl phenoxy biradical (Table 37). The rate constants for intersystem crossing for all derivatives were consistently $\sim 10^{11} \text{ s}^{-1}$, and the triplet decay rate constants clustered around, $\sim 10^8 \text{ s}^{-1}$. The time to reach maximum absorption for the triplet state, however, was variable (5 ps for 2,3,5,6-tetraF-pHP GABA (**129**) to 174 ps for *m*-OCF₃-pHP GABA (**131**) in water). Three dimensional, time dependent full spectral profiles for

excitation and decay from LFP *m*-F-pHP GABA (**122**) in aqueous CH₃CN are illustrated in Figures 50 and 51.

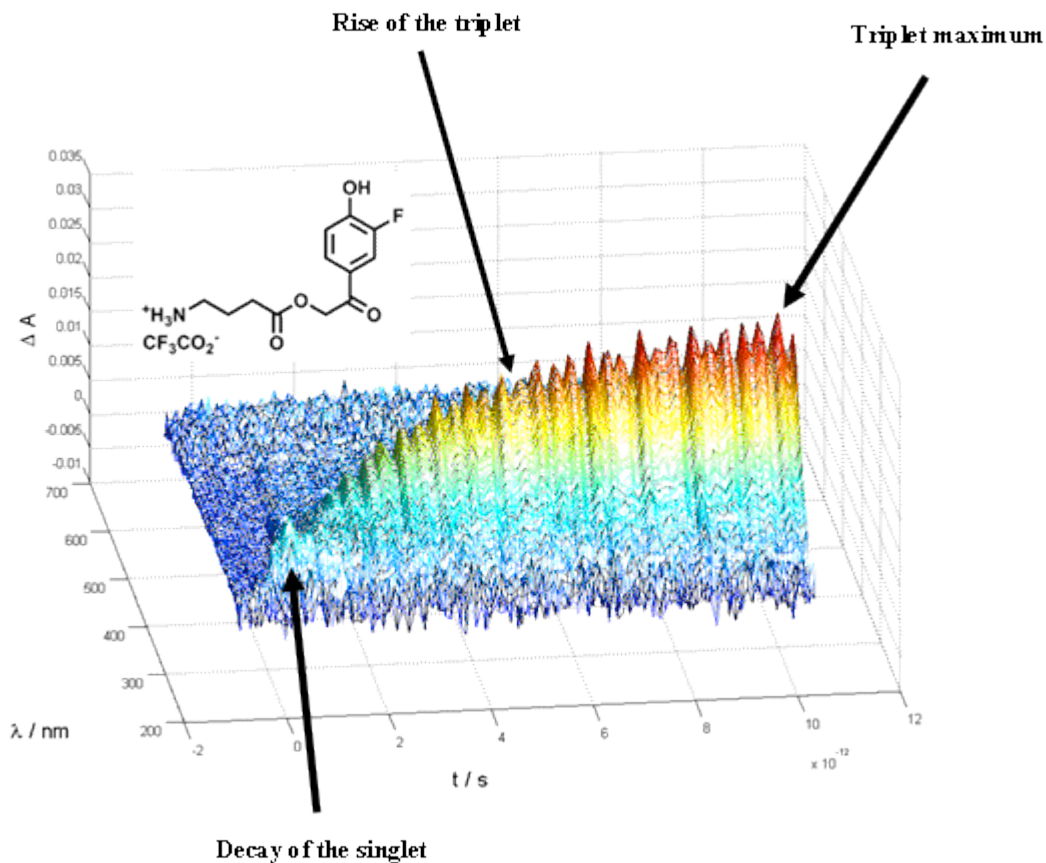
Table 37. Pump probe spectroscopy results from **101**, **122**, **125**, **128-131**, and **153** in water and mixed media.

Cmpd	k ₁	k ₂	k _r (τ ³ decay x	340 nm decay	τ ³ max.	τ ³	Biradical
	(ISC, s ⁻¹) ^a	(τ ³ decay, s ⁻¹) ^b	Φ _{dis} , s ⁻¹) ^c	(s ⁻¹) ^d	(ps) ^e	λ _{max} (nm) ^f	decay (s ⁻¹) ^g
101 ^h	4.4E+11	2.90E+09	5.8E+08	1.3E+08	70	400, 510	6.4E+08
122 ⁱ	3.6E+11	1.60E+09	2.6E+08	1.6E+08	100	394	
125 ^h		2.60E+09	5.7E+08		73		
125 ⁱ		1.60E+09	3.5E+08	4.0E+07	89	400	
128 ^h		8.30E+08	6.6E+07		73		
128 ⁱ	3.9E+11	9.00E+08	7.2E+07		80	398, 391	
129 ⁱ		3.40E+09	3.7E+08		5	410, 400	
130 ^h		2.60E+09	4.4E+08		90	405	
130 ⁱ	3.0E+11	2.60E+09	4.4E+08		60		
131 ^h		2.20E+09	2.0E+08				2.1E+08
131 ⁱ		1.40E+09	1.3E+08	6.5E+06	174	397	6.5E+06
153 ^h		9.90E+08	9.9E+07				
153 ⁱ	2.1E+11	7.00E+08	7.0E+07	1.0E+06		422	
154 ^h		1.30E+09	1.30E+08				
154 ⁱ	3.2E+11	1.30E+09	1.30E+08	1.0E+06	140	407	

^aIntersystem crossing. ^bTriplet decay. ^cRate constant for GABA release
^dRate of unknown transient decay. ^eTime to reach triplet λ_{max}. ^fTriplet
^gDecay at 420 and 445 nm. ^hWater. ⁱWater with unknown amount of CH₃CN

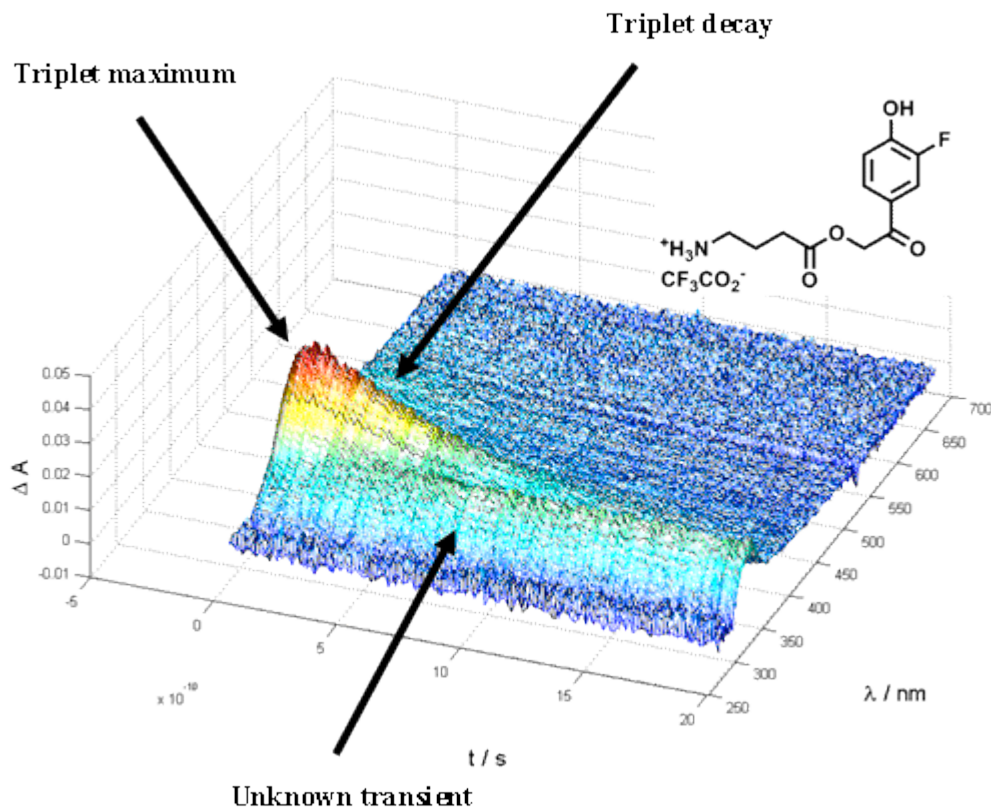
Following excitation, the initially formed singlet at 319 nm rapidly undergoes intersystem crossing to the triplet as observed by the decay of the singlet band at 319 nm within 3 ps (the singlet maximum was observed at ~ 1 ps). The rise of the triplet band at 394 nm, reaches its maximum at ~10 ps. The triplet decay occurs with a rate constant of 1.6 x 10⁹ s⁻¹. In some instances a transient is detected at λ = 340 nm that

Figure 50. Three dimensional, time resolved *absorption* contour of **122** in aqueous CH₃CN.



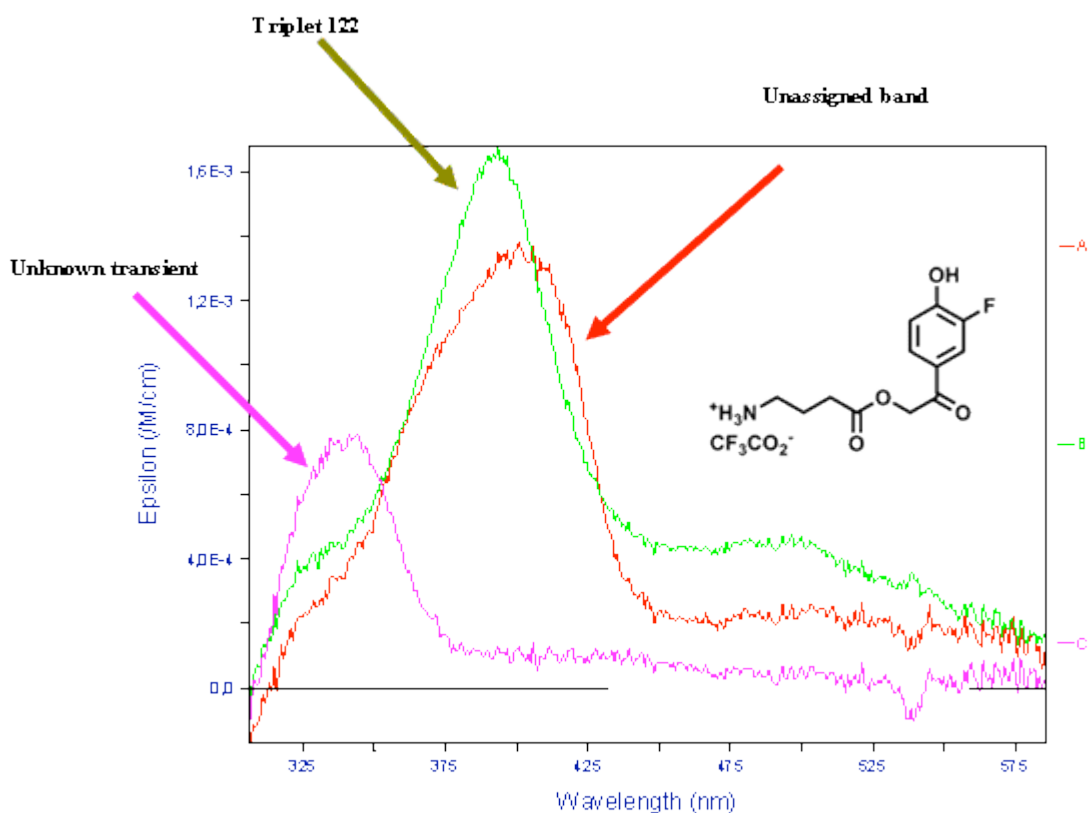
reaches a maximum at 20 ns and subsequently decays with a rate constant, $1.6 \times 10^8 \text{ s}^{-1}$. A part of this transient has tentatively also been assigned to the triplet oxyallylphenoxy biradical, *m*-F **117**. Other absorptions of transients at 420 and 440 nm were revealed for several other precursors and were also assigned to the transient **117**. Further elaboration of these findings can be found in the Discussion section.

Figure 51. Three dimensional *triplet decay* contour of **122** in aqueous CH₃CN.



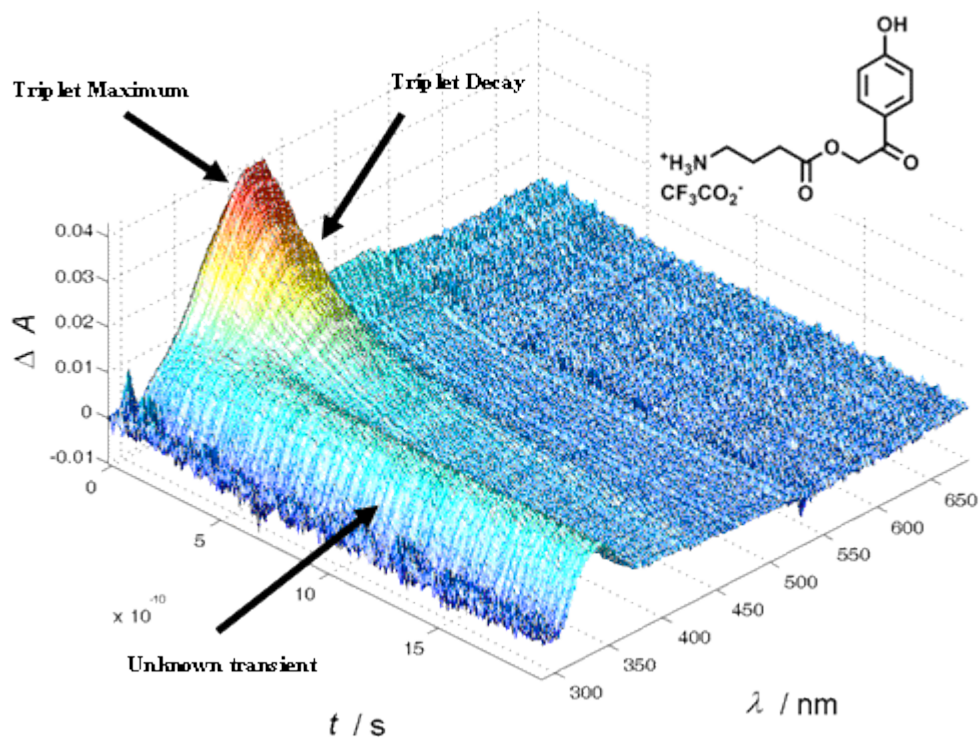
A cross section of this diagram demonstrates the triplet of **122** at 394 nm (green), an unassigned band at 420 nm (red), and unknown transient at 340 nm (violet) (Figure 52).

Figure 52. Cross section of the three dimensional, time resolved absorption contour of **122** in aqueous CH₃CN.



Triplet decay parameters for **101** were also obtained from LFP in aqueous CH₃CN. The three dimensional contour is presented in Figure 53. The triplet displayed two λ_{max} at 400 nm and 500 nm, the former much stronger than the latter, which reached their maximum absorption maxima at 8 ps and decayed with rate constants of $2.6 \times 10^9 \text{ s}^{-1}$.

Figure 53. Three dimensional, time resolved triplet decay contour of **101** in aqueous CH₃CN.



Consistent with **122**, the emergence of a band at 340 nm was observed, which decayed with a rate constant of $1.3 \times 10^8 \text{ s}^{-1}$. Corresponding one dimensional plots represent triplet decays at both wavelengths, 400 nm in Figure 54 and 500 nm in Figure 55. The curve fit is represented by the green line, derived from data points that are in red.

Figure 54. Triplet decay profile of **101** at 400 nm in aqueous CH₃CN.

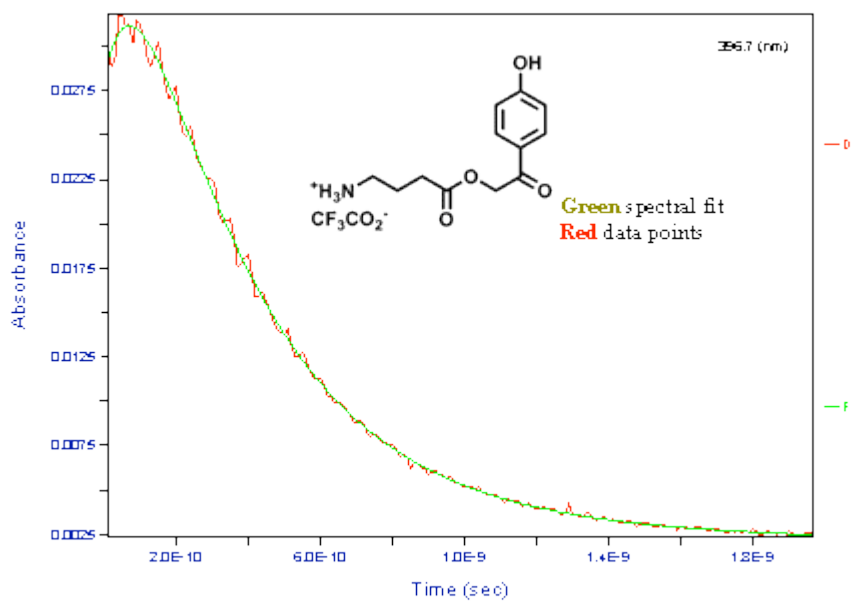
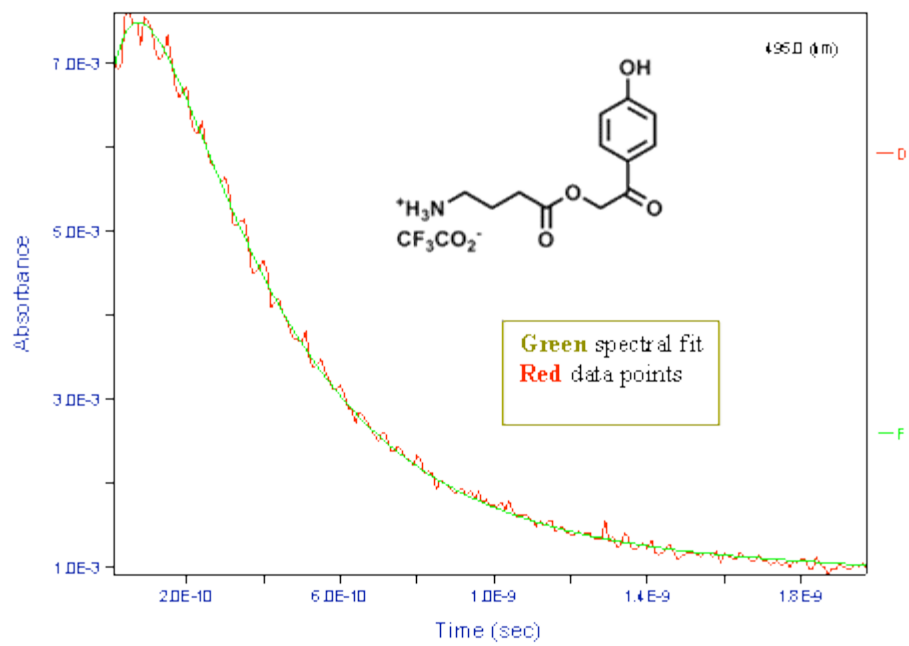
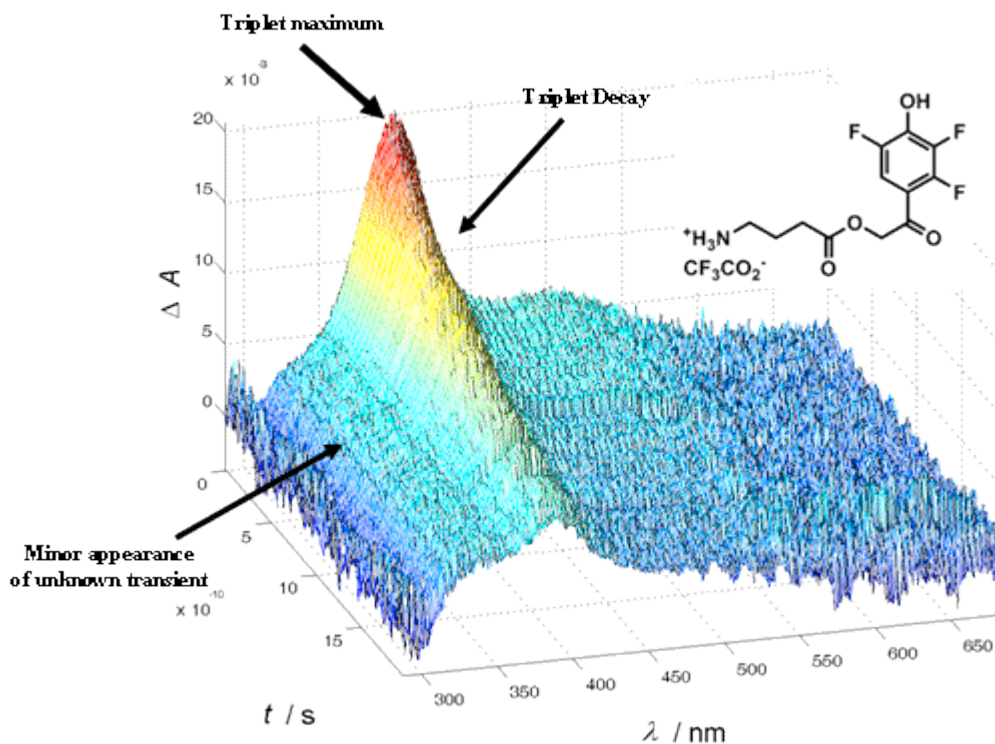


Figure 55. Triplet decay profile of **101** at 500 nm in aqueous CH₃CN.



For comparison, the triplet decay profiles of 2,3,6-trifluoro-pHP GABA (**128**) from LFP in aqueous CH₃CN are included. The three dimensional contour of **128** is shown in Figure 56. Evidently, the band at 340 nm is significantly diminished compared to other pHP GABA derivatives.

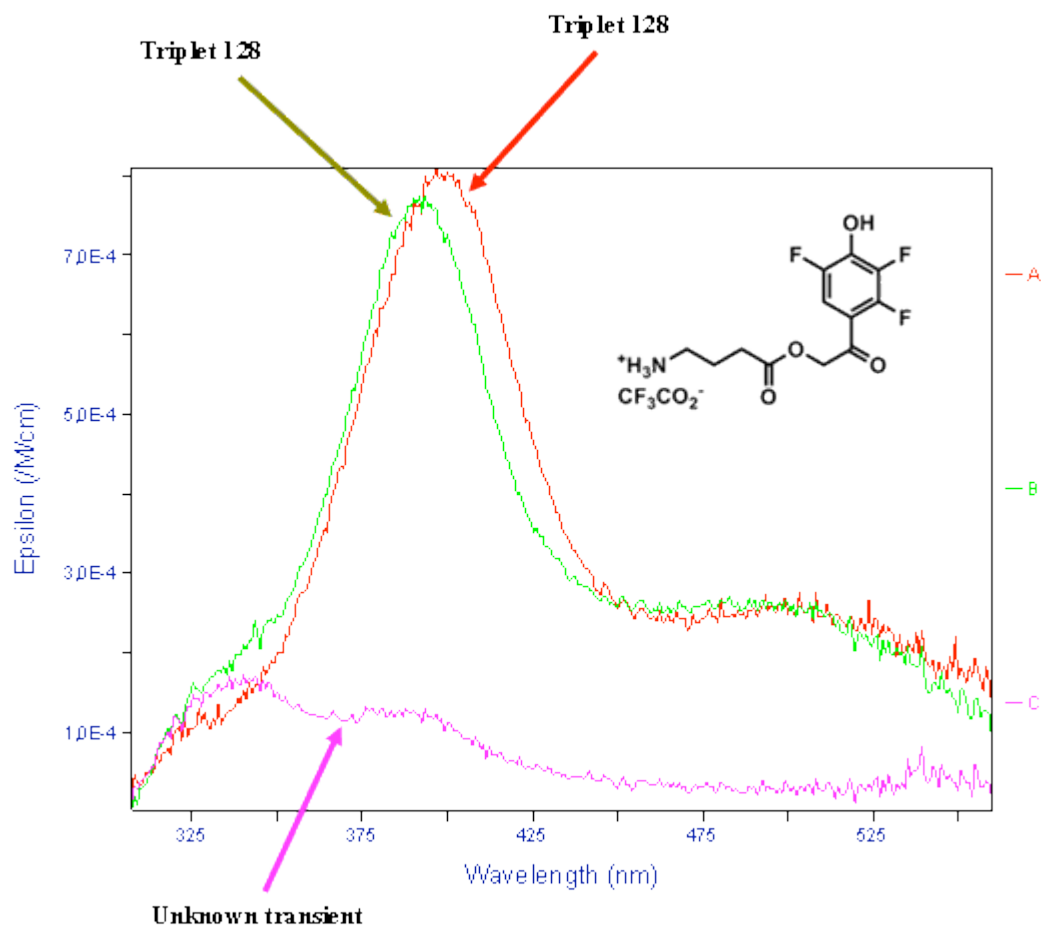
Figure 56. Three dimensional, time resolved triplet decay contour of **128** in aqueous CH₃CN.



Two triplet wavelengths were determined at 391 and 398 nm, the former much stronger in intensity than the latter, which reached their maximum absorbance at 80 ps and decayed with a rate constant of $8 \times 10^8 \text{ s}^{-1}$. A cross section of this triplet decay plot is exhibited in Figure 57. In this representation, the unknown transient at with

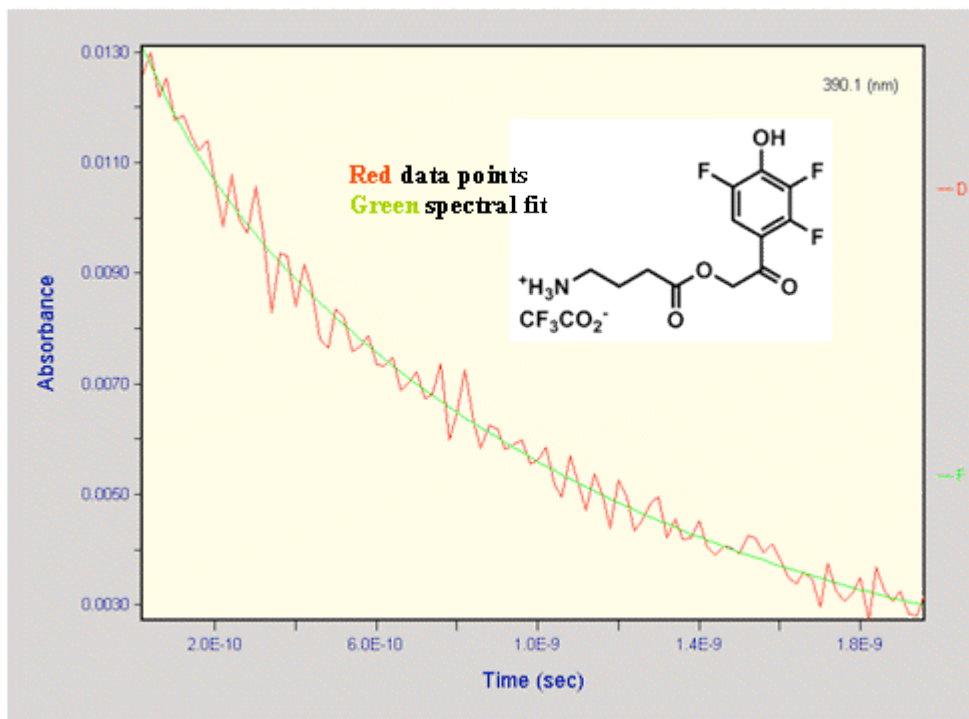
λ_{max} at 340 nm is readily apparent. Both triplet bands at 391 and 398 nm are clearly depicted as well. The corresponding one dimensional triplet decay of the band at 391

Figure 57. A cross section of the three dimensional absorption contour of **128** in aqueous CH_3CN .



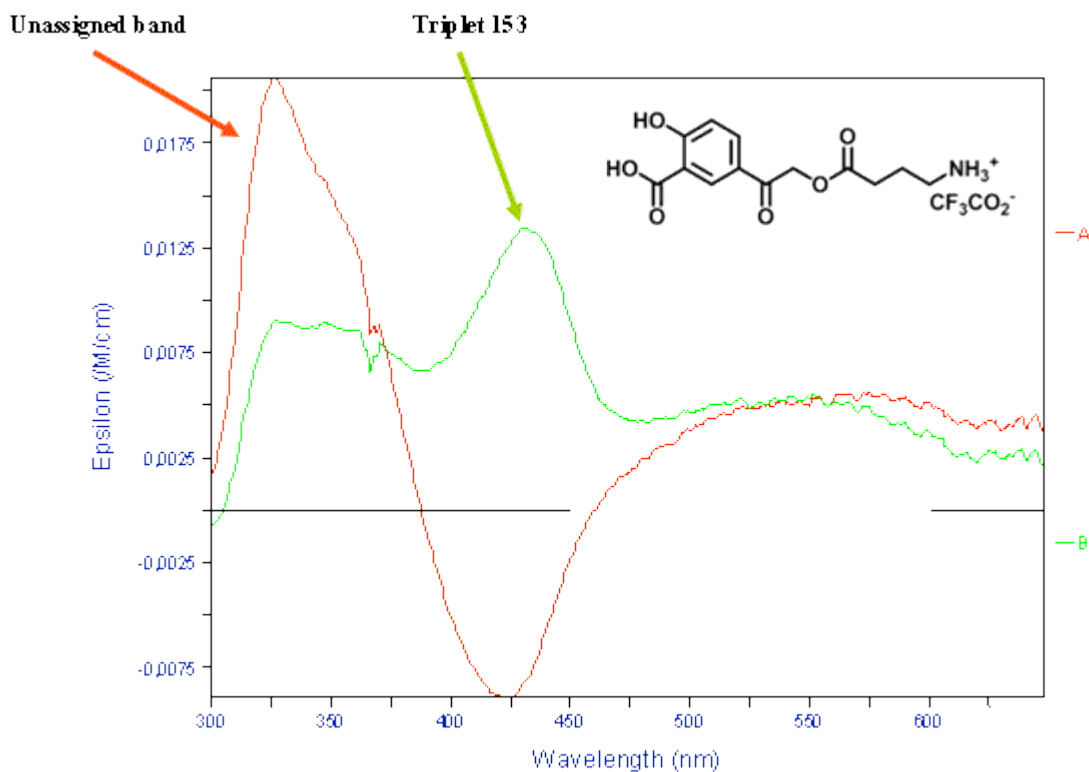
nm is presented in Figure 58. The green line represents the curve fit of the data points, which are in red.

Figure 58. Triplet decay plot of **128** in aqueous CH₃CN.



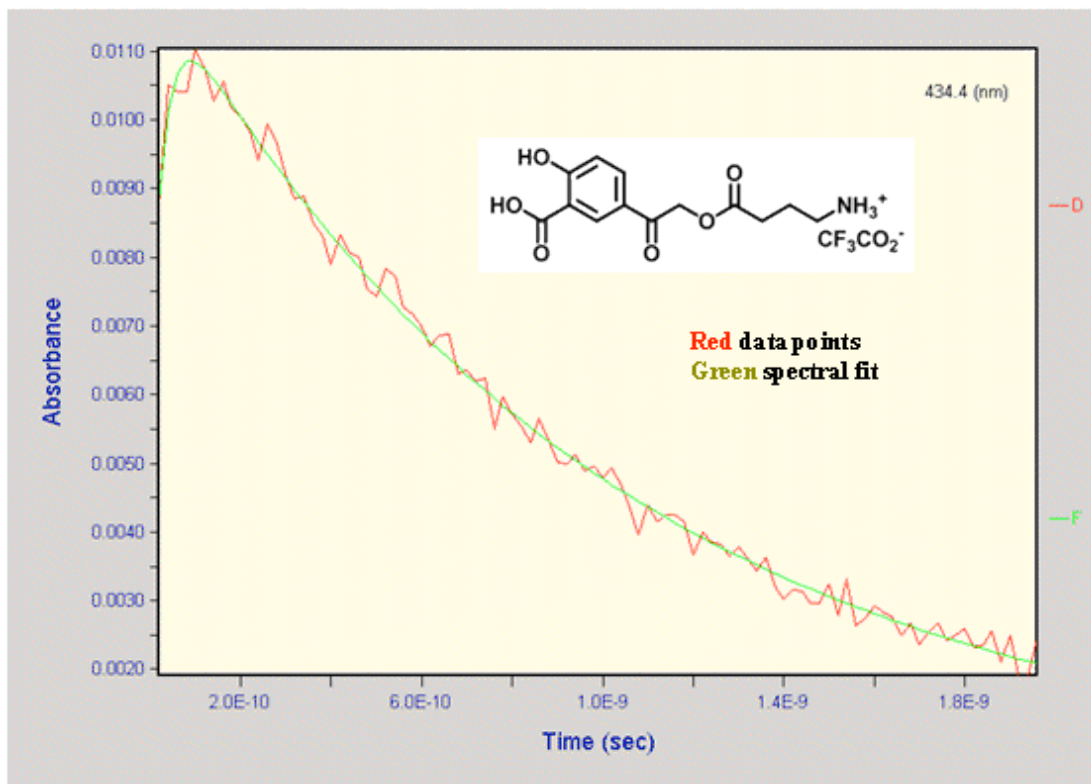
The triplet decay profiles for 5-acetylsalicylic acid GABA (**153**) in water were obtained by LFP. A cross section of the three dimensional plot is represented in Figure 59.

Figure 59. Cross section of the three dimensional absorption profile of **153** in water.



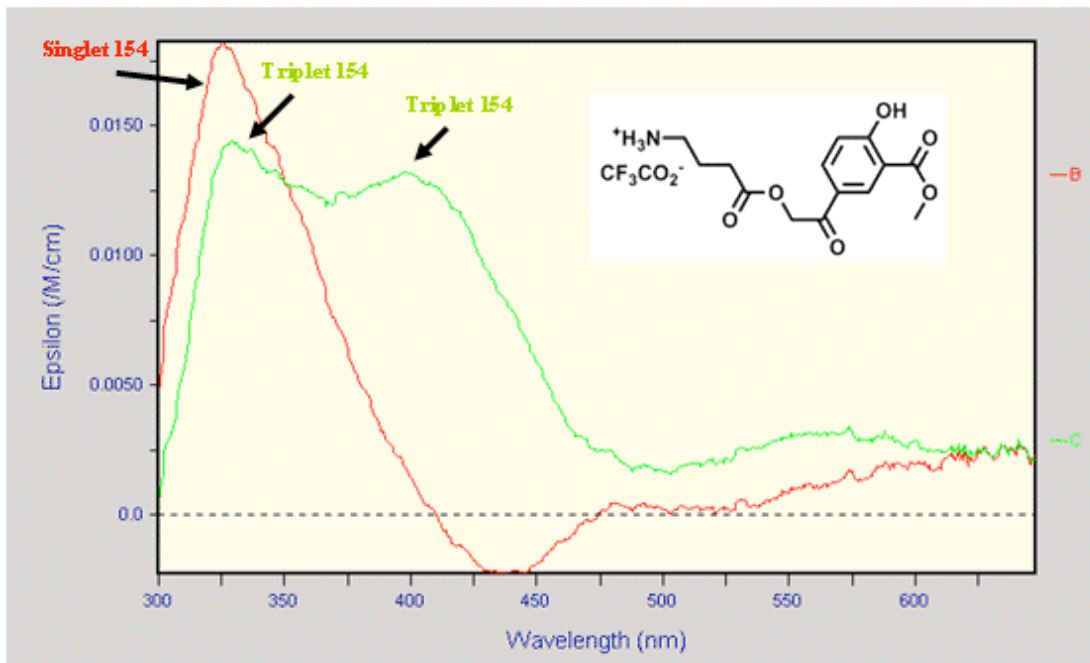
The triplet at 422 nm reaches its maximum absorption at 100 ps and decays with a rate constant of $6.0 \times 10^8 \text{s}^{-1}$. Similar to the pHP GABA esters, a band emerges at 340 nm that decays, however, with a markedly decelerated rate constant, $1.0 \times 10^6 \text{s}^{-1}$, versus unsubstituted pHP GABA, $1.3 \times 10^8 \text{s}^{-1}$, a 2 order of magnitude difference. The corresponding one dimensional triplet decay profile for **153** in water is depicted in Figure 60.

Figure 60. Triplet decay profile of **153** in water.



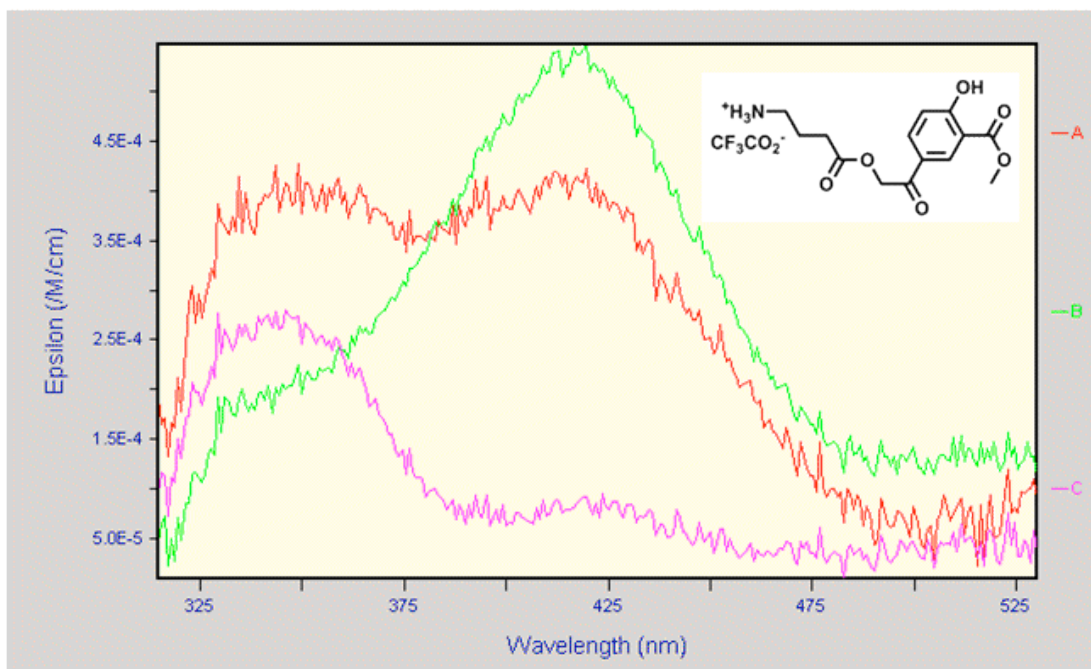
LFP studies were carried out with the 5-acetyl-methylsalicylate GABA (**154**) in aqueous CH₃CN. The absorption profile (Figure 61) revealed the singlet (red) at 326 nm which was seen to decay to two triplet bands at 330 and 396 nm.

Figure 61. Cross section of the three dimensional absorption contour of **154** in aqueous CH₃CN.



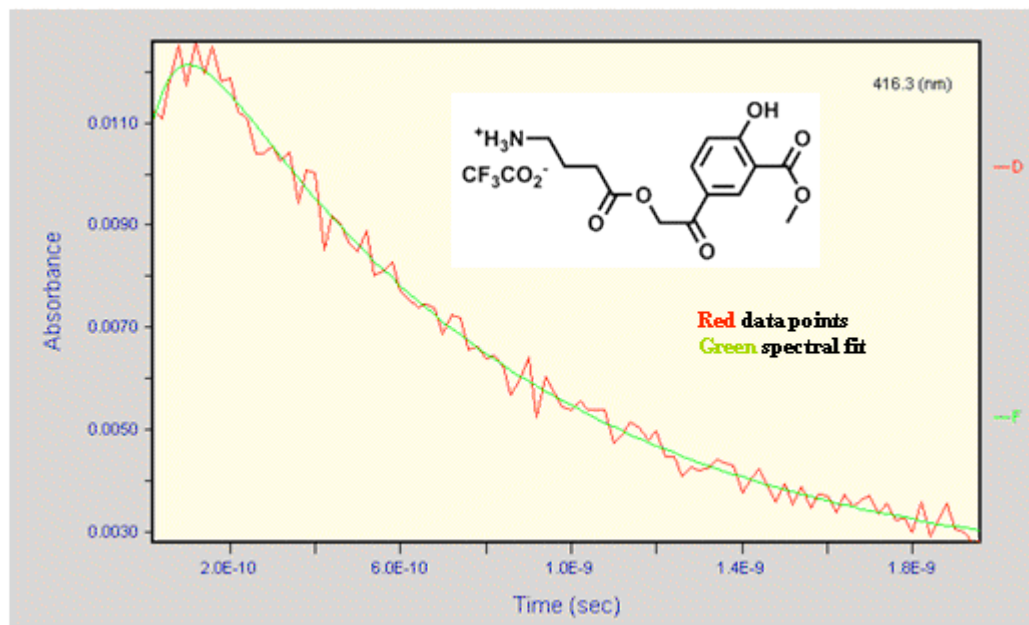
A short time later, a cross section (Figure 62) revealed the emergence of the commonly detected 340 nm band (violet), an unassigned band (red), and the triplet of **154** at 416 nm, which reaches its maximum at 140 ps.

Figure 62. Cross section of the three dimensional absorption profile of **154** in aqueous CH₃CN.



Lastly, a one dimensional decay plot of the triplet at 416 nm (Figure 63) displayed the rate of decay as $1.3 \times 10^9 \text{ s}^{-1}$.

Figure 63. Triplet decay profile of **154** at 416 nm in aqueous CH₃CN.

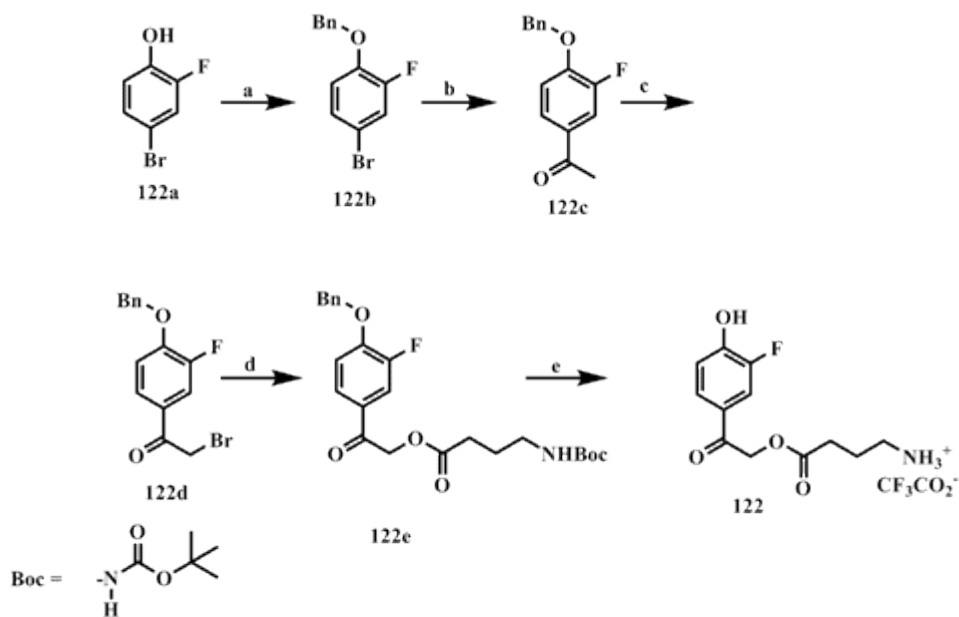


Discussion

A. Synthetic Strategies

The methodology used to synthesize pHP GABA esters **122-131** was outlined

Scheme 38. (*Introduction*) The synthesis of *m*-fluoro pHP GABA (**122**).



a. BnBr, K₂CO₃, CH₃CN, 16 h, 93%. b. Pd(PPh₃)₄, tributyl(1-ethoxyvinyl)stannane, PhCH₃, 100°C, 18 h, 89%. c. DDB, CH₂Cl₂, 0° to rt, 1 h, 95%. d. N-Boc GABA, K₂CO₃, CH₃CN, rt, 24 h, 89%. e. TFA, 0°C to rt, 24 h, 78%

in Scheme 38 (*Introduction*) with *m*-F-pHP GABA **122**. Briefly, the commercially available 4-bromo-2-fluorophenol (**122a**) was benzylated with benzyl bromide in an excess of potassium carbonate to afford **122b** that then underwent a transmetallation

reaction with a slight excess of tributyl(1-ethoxyvinyl)tin (1.1 equivalents), catalyzed by Pd(0), to afford the acetylated derivative (**122c**).

It should be noted that heretofore, this Stille protocol for acetylation had not received any use with phenols. In our study, the Stille coupling is an essential step in the synthesis of ketones **122-131**. Several other acylation procedures were initially attempted, including Friedel Crafts acylation with acetyl chloride and aluminum trichloride, the Fries rearrangement with an acetyl-substituted phenol in the presence of aluminum trichloride, and lastly, transmetallation with *n*-butyl lithium followed by addition of acetyl chloride. None of these methods provided yields of acetylated targets in excess of 20%.

Several modifications of the Stille protocol were made to improve the acetylation. Palladium (0) as the tetrakis(triphenylphosphine) complex, replaced the Pd(II) bischlorotriphenylphosphine complex (we thank Professor Helena Malinakova for this suggestion as well as advice on Stille protocols). The former is air sensitive and oxidizes rapidly, whereas the latter is stable. Presumably, when the latter is dissolved, prompt reduction to Pd (0) occurs from chloride departure, activating palladium for oxidative addition with the aryl bromide. When employed for this purpose with **122**, for example, the color turned from yellow to black within 15 minutes, even after 30 minutes of solution degassing, and the yields of **122c** never surpassed 10%. Palladium black, as it is commonly known, is an inactive form of palladium.

Another modification involved the addition of saturated aqueous KF to the solution mixture after acetylation. The byproduct of transmetallation, tributyltin bromide, is a liquid that proved difficult to separate from the target compound. Column chromatography with a broad range of eluents failed to completely remove this material. However, in the presence of KF, fluoride exchange readily occurred with bromide to generate tributyltin fluoride, a white, insoluble precipitate that was easily removed by filtration and did not react with the target. The use of Pd(0) as the catalyst for acetylation and fluoride for purification permitted the yields of **122-131c** to routinely surpass 80%.

Once **122c** (Scheme 38) was synthesized, supervening α -bromination was accomplished with dioxane-dibromide, DDB, in 1 h to afford **122d** in high yield that subsequently underwent facile S_N2 substitution with N-Boc protected GABA to generate **122e**. At this point, two divergent approaches were used. Early synthetic strategies, including the preparation of the *p*-hydroxyphenacyl GABA's, utilized distilled TFA over 24 h to eliminate both the benzyl and Boc protecting groups. Though this approach was effective in generating the fluorinated targets **122-131**, oftentimes, wet, adhesive precipitates resulted that necessitated drying under reduced pressure for more than a week. A later strategy was to first debenzylate with Pd/C and H₂ in ethyl acetate, which was quick (2 to 4 h) and efficient (>95% without the need for further purification), followed by Boc deprotection with TFA:CH₂Cl₂ (1:1) for 10-15 minutes. After lyophilization the products were generally flaky, white precipitates.

The synthetic approach for pHP GABA esters (**132-141**), 4-fluorophenacyl GABA (**142**), pHP DOC (**150**), and α -alkyl-pHP diastereomers (**166** and **167**) were patterned after that for **122** but did not require the use of the Stille protocol, as the corresponding *p*-hydroxyacetophenones and 4-fluoroacetophenone (**142**) were commercially available. In the cases where there were no protecting groups on the substrate, such as DOC for **150** and enantiomers for **166** and **167**, the last step in the sequence involved Pd/C mediated hydrogenation.

The highlight for the synthesis of pHP diethyl phosphonate (**151**) entailed the Arbuzov reaction. Here, the benzyl protected, α -brominated **146c** was refluxed neat in triethylphosphite over 17 hours to afford the phosphonate that was easily reduced to the corresponding phenol **151** via Pd/C mediated hydrogenation.

The key step in the synthesis of pHP F (**152**) consisted of a S_N2 reaction between **146c** and CsF in refluxing acetonitrile for 3 h to afford **152** after deprotection.

B. General photochemistry of pHP and 5-acetylsalicylic acid caged derivatives

The general photochemistry of pHP caged compounds was summarized in Scheme 37 in the *Introduction*.

The results from photolysis of pHP GABA and Glu esters, the pHP caged amino acids, deoxycholic acid, and diastereomers at 300 nm in aqueous media were consistent with past studies; the only photo products observed were liberated

substrate and rearranged *p*-hydroxyphenylacetic acids as major products, along with minor *p*-hydroxybenzyl alcohols.

The *p*-hydroxybenzyl alcohols had been overlooked previously. In current studies, however, a small, signature band at $\delta \sim 4.5$ ppm was universally discerned in the ^1H NMR spectra following photolysis and was verified in several cases by spiking the product mixture with an authentic sample of the corresponding *p*-hydroxybenzyl alcohol. Certain derivatives were found to be unreactive, however. These will be discussed later.

The photochemistry of *m*-methoxy derivatives **133** and **134** were re-examined. The photoproducts from these, in addition to GABA, had been reported to be predominantly *m*-methoxy-*p*HP-acyloin and *m*-methoxy-*p*-hydroxyacetophenones. The rearranged *p*-hydroxyphenylacetic acid was said to be minor or non-existent. When re-evaluated, the primary photoproduct obtained for each was, in fact, the rearranged *p*-hydroxyphenylacetic acid; this was evidenced by the intense ^1H NMR signal at $\delta \sim 3.7$ ppm (see Figure 22 in *Results*). The acyloin and acetophenone byproducts were also observed at $\delta = 4.99$ and $\delta = 2.60$ ppm, respectively, however only as minor photoproducts, along with the recently discovered *p*-hydroxybenzyl alcohol at $\delta = 4.60$ ppm. Nevertheless, the discrepancies in photoproduct distributions for **133**, **134**, and a few others were the first indicators of possible substituent-directed mechanistic changes in substrate photorelease from *p*HP.

The photochemistry of 5-acetylsalicylic acid GABA (**153**), 5-acetyl-methylsalicylate GABA (**154**), 5-acetylsalicylic acid alkanoyl acids (**155** and **156**),

and antennae compounds (**157-165**) produced primary photoproducts, besides the liberated substrate, that were consistent in chemical shift with the corresponding *p*-hydroxyphenylacetic acid ($\delta = 3.64$ ppm, Figure 35 in *Results*). In addition, minor resonance signals were generally observed at $\delta \sim 4.50$ ppm that approximated those for *p*-hydroxybenzyl alcohol.

C. Preliminary Mechanistic Studies

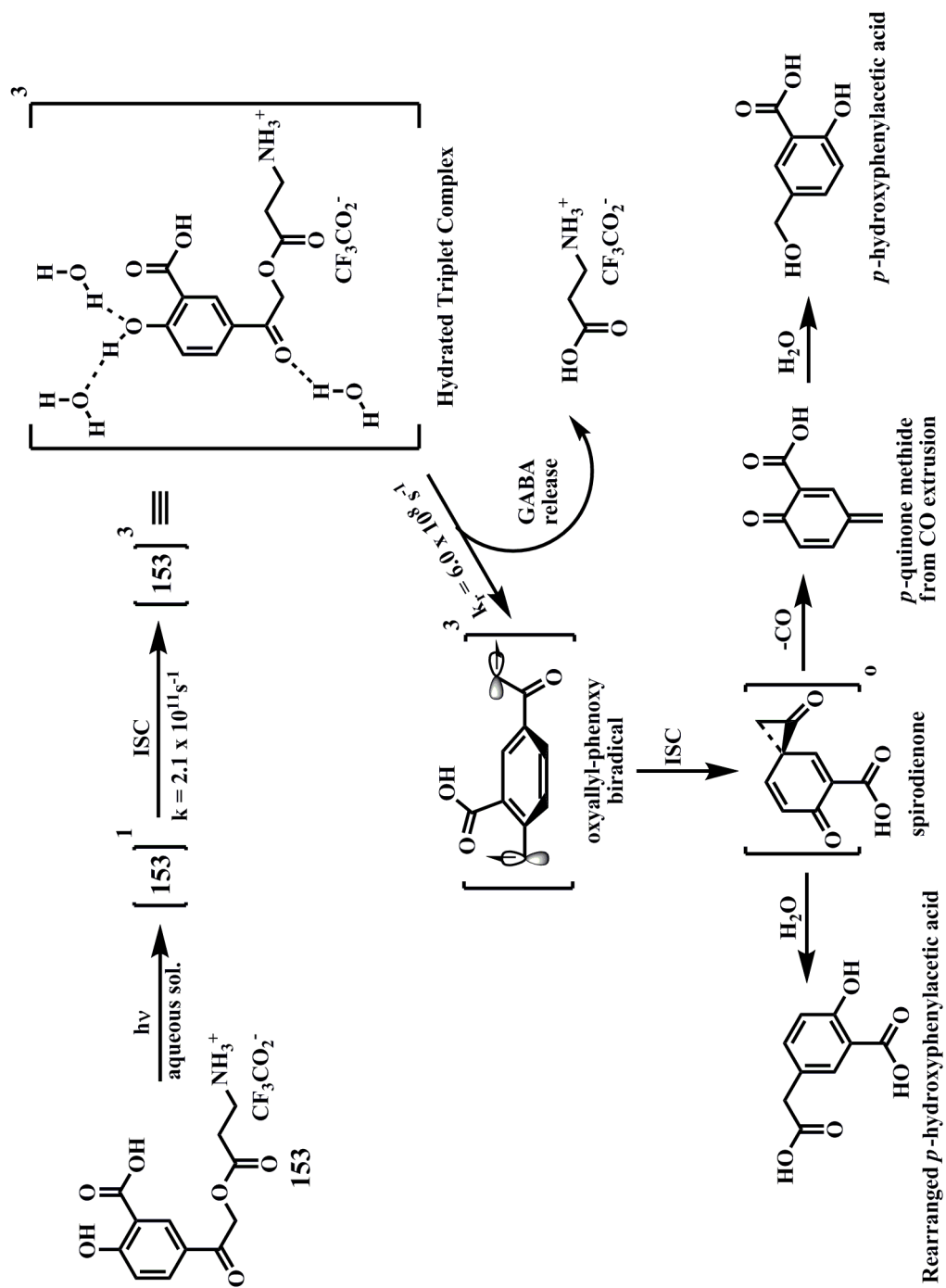
1) Excited state assignments for pHP GABA esters. Stern-Volmer quenching studies were conducted with 1-10 mM of pHP GABA esters (**101**, **122-131**, and **137-139**) using 0-100 mM of potassium sorbate as a triplet quencher in water, in pH 7.3 buffer and the reactions were analyzed by HPLC (see Table 33 and Figure 46 in *Results*). Significant drops in the quantum efficiencies were observed with increasing sorbate concentration regardless of the medium, providing good empirical evidence for a reactive triplet excited state for all of these pHP derivatives. The *m*-methoxy and *m,m'*-dimethoxy pHP GABA derivatives (**134** and **133**, respectively) had been analyzed previously^{97,111} and manifested a prevalent reactive triplet state.

In addition to S-V quenching, LFP studies were conducted on the fluorinated pHP GABA esters in both aqueous CH₃CN and water. Absorbance profiles revealed rapid intersystem crossing from the singlet to triplet states ($\sim 10^{11}$ s⁻¹) with efficiencies near unity. Degassing experiments failed to manifest any changes in the quantum efficiencies, due to the rapid decay rate (10^7 - 10^9 s⁻¹) of the pHP triplet and the inherently low concentration of O₂ in water (1.28 mM).¹¹²

In accord with previous findings by Givens and Wirz,^{78,92} and Phillips,^{80-82,86-88,99,91} the reactive excited state for these pHP GABA esters is unequivocally the triplet. In 2008, Givens and Wirz⁹² suggested the possibility of an adiabatic nucleofuge disjunction (Scheme 37) from the observation of a series of new bands at 330, 420 and 445 nm derived from LFP of pHP diethyl phosphate, mesylate, and tosylate, in aqueous CH₃CN. An oxyallyl-phenoxy triplet biradical was assigned to the transient intermediate based on these absorptions. The same bands were consistently revealed for the other LFP probed pHP GABA esters, suggesting a common triplet oxyallyl-phenoxy biradical intermediate to the entire series.

2) Excited state assignments for 5-acetylsalicylic acid GABA and its esters. The sole compound probed by S-V quenching analysis and LFP studies was 5-acetylsalicylic acid GABA (**153**). The carbomethoxy analog (**154**) was analyzed by LFP studies and was reported previously as exhibiting an operative triplet state.¹¹³ As shown in the *Results* section, **153** was readily quenched by potassium sorbate in water, manifesting a linear S-V correlation constant, K_{SV} . LFP studies in both water and aqueous CH₃CN confirmed this and clearly showed the singlet rapidly crossing to the triplet, $k = 2.1 \times 10^{11} \text{ s}^{-1}$. The triplet maximum occurred at $\lambda = 422 \text{ nm}$ within 100 ps and decayed with a rate constant of $6.0 \times 10^8 \text{ s}^{-1}$. These findings confirm the triplet as the reactive state. Additionally, short-lived absorption bands at 330, 420, and 445 nm further substantiated an triplet oxyallyl-phenoxy biradical intermediate. The remaining 5-acetylsalicylic acid derivatives (**155-165**) were not probed by S-V quenching or LFP, but, nonetheless, are anticipated to react from the triplet state.

Scheme 52 Preliminary mechanism of the photo-Favorskii rearrangement, with **153**

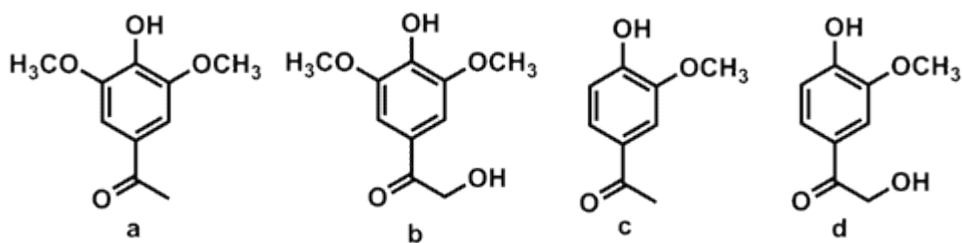


3) A preliminary photo-Favorskii mechanism. Integrating the empirical data obtained from ^1H NMR photochemical analyses in D_2O , which revealed the rearranged *p*-hydroxyphenylacetic acid and released substrates as major products in near quantitative yields and a trace amount of *p*-hydroxybenzyl alcohol, with the S-V quenching and LFP established functional triplet state and a probable oxyallyl phenoxy triplet biradical that leads to the rearranged and decarbonylation product, a preliminary photo-Favorskii mechanism is posited (Scheme 52, with **153**).

The process is as follows: Initial excitation of **153** to the singlet excited state is followed by rapid ($2.1 \times 10^{11} \text{ s}^{-1}$) intersystem crossing to the triplet, (**153**³). Significant H-bonding interactions with water assist the complex in skewing the carbonyl OOP with respect to the ring, a necessary stereoelectronic arrangement for facile substrate release. In this manner, the triplet undergoes solvent assisted deprotonation of the phenol with concomitant substrate departure ($6.0 \times 10^8 \text{ s}^{-1}$), forming a triplet oxyallyl-phenoxy biradical that has an orthogonal OOP orientation. DFT calculations of **101**, **122-131** (Table 35, *Results*) confirmed the OOP geometry of biradical and also predicted this to be much lower in energy than the corresponding ground state spirodieneone. Once formed, the biradical then rapidly relaxes with intersystem crossing and collapses to the spirodienedione. The completion of the route to the major, *p*-hydroxyphenylacetic acid product is through water-mediated fragmentation of the spirodienedione; the minor *p*-hydroxybenzyl alcohol is formed by an initial CO extrusion from the spirodienedione to form the *p*-quinone methide, which then undergoes conjugate addition of H_2O .

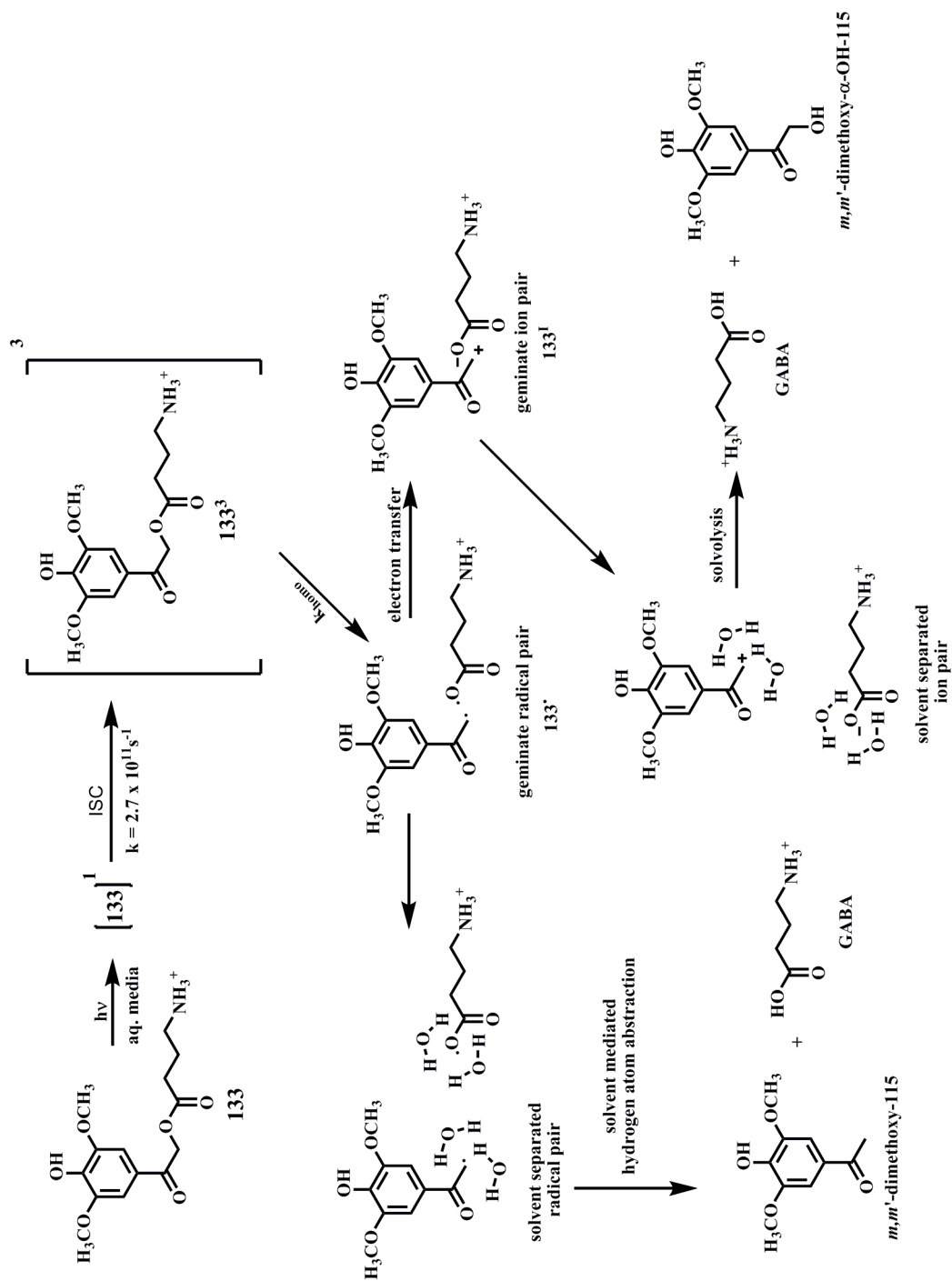
4) **Alternative mechanisms and photoproducts** The *m*-methoxy and *m,m'*-dimethoxy pHP GABA derivatives (**134** and **133**, respectively) were the only derivatives of pHP that manifested other exiguous photoproducts, such as *p*-hydroxyacetophenone (**115**) and α -hydroxy acetophenone, an acyloin derivative (α -OH-**115**) (Figure 64). It is obvious that divergent mechanisms are operative in these.

Figure 64. Photoproducts of **134** a) *m,m'*-diOCH₃-**115**, b) *m,m'*-diOCH₃- α -OH-**115** and **133** c) *m*-OCH₃-**115**, d) *m*-OCH₃- α -OH-**115**.



Yousef¹¹¹ previously explored the photochemistry of **134** in aqueous media and had noted the appearance of these photoproducts. His mechanistic interpretations were congruent with results from disparate studies of Sheehan,⁵¹ and Pincock¹¹⁴ (Scheme 53 with **133**). The photoconversion course is proposed as follows: Initial excitation of **133** to the singlet state is followed by rapid ISC, $k = 2.7 \times 10^{11} \text{s}^{-1}$ to the triplet (**133**³), which undergoes homolytic scission to produce the geminate radical pair (**133**[•]). The geminate radical pair can recombine to reproduce **133**, or can diverge into two disparate mechanisms. 1) Electron transfer occurs between the radicals to generate a geminate ion pair (**133**[±]), which can regenerate **133** by recombination (not

Scheme 53 Modified version of Yousef's proposed discrete mechanistic pathways to *m,m'*-diOCH₃-115 and *m,m'*-diOCH₃- α -OH-115



shown) or solvent separate and hydrolyze to afford GABA and *m,m'*-diOCH₃- α -OH-**(115)**. Pincock¹¹⁴ demonstrated this route was feasible from photolyses of a series of arylmethylacetates in methanol. 2) A second possible mechanism manifests solvent incited separation of the geminate radical pair to engender a solvent separated radical pair, which H atom abstracts from the mixture, analogous to Sheehan's⁵¹ suggested mechanism, from photolysis with *p*-methoxyphenacyl benzoates in EtOH, to furnish *m,m'*-diOCH₃-**115** and GABA.

D. Substituent effects on the photo-Favorskii rearrangement

1) Quantum Efficiencies of Fluoro-pHP GABA's: The role of the conjugate base. The position and extent of fluoro substitution on the pHP chromophore was found to manifest stark changes in the quantum yields for GABA release, Φ_{dis} , in aqueous solutions. The quantum yields, determined at 300 nm, for GABA and *p*-hydroxyphenylacetic acid appearance were nearly identical to Φ_{dis} in all cases, thus Φ_{dis} will be principally considered. In water (Table 22, *Results*), *m*-F-pHP GABA (**123** ($\Phi_{\text{dis}} = 0.28$)), 2,3-diF-pHP GABA (**124** ($\Phi_{\text{dis}} = 0.24$)), and 2,5-diF-pHP GABA (**125** ($\Phi_{\text{dis}} = 0.22$)) were the only derivatives that demonstrated improved yields relative to the unsubstituted parent (**101** ($\Phi_{\text{dis}} = 0.20$)), and *o*-F-pHP GABA (**122** ($\Phi_{\text{dis}} = 0.16$)) and 2,6-diF-GABA (**127** ($\Phi_{\text{dis}} = 0.16$)) were nearly the same as **101**. The common factor for these five was the $\lambda_{\text{max}} \sim 280$ nm which indicated the protonated pHP dominated. In contrast, 3,5-diF-GABA (**126** ($\Phi_{\text{dis}} = 0.11$)), 2,3,6-triF-GABA (**128** ($\Phi_{\text{dis}} = 0.08$)), and 2,3,5,6-tetraF-GABA (**129** ($\Phi_{\text{dis}} = 0.11$)), evinced

the predominant conjugate base of the chromophore, which absorbs at $\lambda_{\text{max}} > 300$ nm. In buffer pH 7.3 (Table 23, *Results*) all fluoro pHP derivatives manifested predominant conjugate bases, except **123**, which exhibited both the conjugate base and protonated forms with absorptivities nearly the same. Accordingly, Φ_{dis} at this pH were lower for all fluoro pHP GABA esters, e.g., **124** ($\Phi_{\text{dis}} = 0.11$) and **125** ($\Phi_{\text{dis}} = 0.10$), while that for **123** dipped only slightly, ($\Phi_{\text{dis}} = 0.21$).

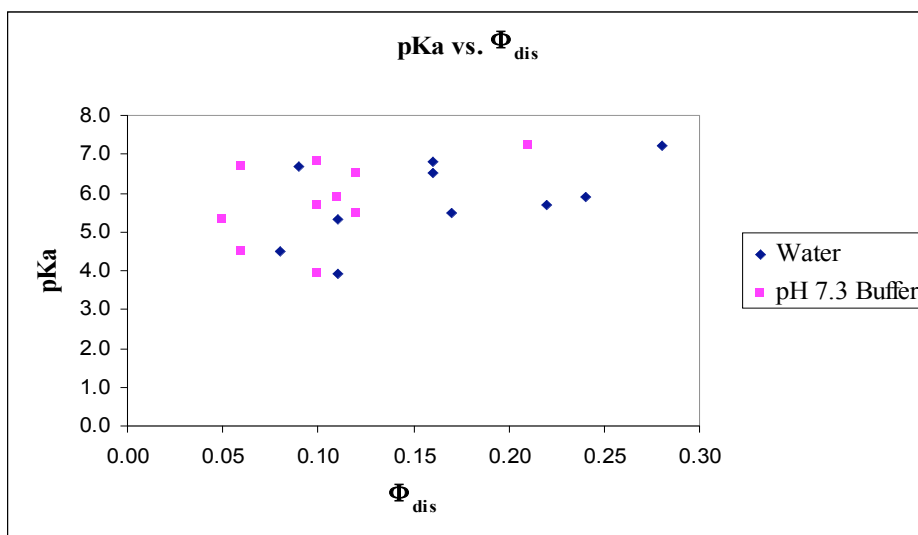
The unsubstituted parent, **101**, which was predominantly protonated, evinced a constant $\Phi_{\text{dis}} = 0.21$. At pH 8.2, *all* fluoro pHP GABA's were conjugate bases and *all* manifested low Φ_{dis} . Conspicuously, the pH of the media impacts the efficiency of photoconversion **122-131** by controlling the equilibrium between the conjugate bases and protonated forms; *thus, there exists a clear correlation between the pKa of the pHP and Φ_{dis}* . In water, pH = 6.5, those derivatives with pKa's 5.5 and lower (Table 15 *Results*) **126**, **128**, **129**, **130**, conveyed the preponderant conjugate base, with accompanying lower Φ_{dis} . Those with pKa's between 5.5 and 6.7 showed both forms, i.e., **122**, **124**, **125**, **131**, while those with pKa's 6.8 and higher, **123**, and **127**, predominantly the protonated form.

Two interesting trends are noticeable from comparisons of fluoro pHP GABA's to the unsubstituted pHP GABA (**101**). First, those with a single ortho fluorine, i.e., **123**, **124**, and **125** with pKa's 7.2, 5.9, and 5.7 respectively, exhibited higher Φ_{dis} than unsubstituted **101** in water, with no control on the pH. A sufficient explanation for this *ortho-effect* is not available. Second, the Φ_{dis} for *m*-OCF₃-pHP GABA (**131** (0.09)) was double that of its proton counterpart *m*-OCH₃-pHP GABA

(**134** (0.04)). A possible rationalization for this might be due to the reduced electron donating capacity of the $-\text{OCF}_3$ vs. $-\text{OCH}_3$, an influence that Givens, et. al., had previously reported.¹⁰⁴

Attempts to discern linear correlations between pKa and Φ_{dis} in water (blue) and Φ_{dis} at pH 7.3 (pink) (Figure 65) showed little difference between the two sets of data. However, the notion of discrete differences in the branching between decay of the excited state and progress towards release for the protonated versus conjugate

Figure 65. Plot of pKa of fluoro pHP GABA's vs. Φ_{dis} in water (blue diamonds) and buffer pH 7.3 (pink squares). Unsubstituted pHP GABA (**101**) is included for comparison.

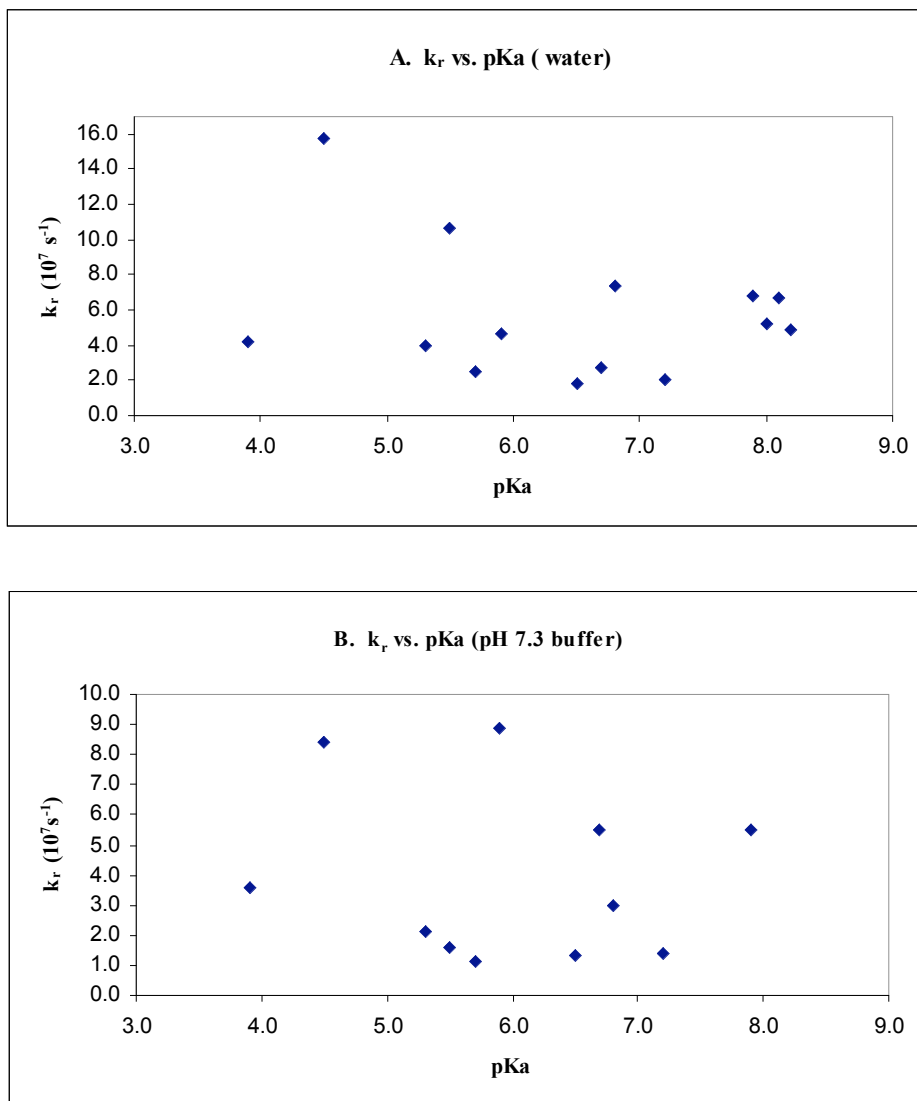


bases is consistent with our earlier conclusion. The efficiency for photorelease is apparently independent of the pKa of the chromophore within the narrow range exhibited in this fluorinated pHP GABA series.

The singlet excited state of the conjugate base also rapidly intersystem crosses to the triplet state, $k_{ISC} = 3.0 \times 10^{11} \text{ s}^{-1}$. A small fraction of the singlet also deactivates by fluorescence (*Results*, Table 20). The triplet deprotonation step, deemed to be crucial in initiating the photo-Favorskii rearrangement, is obviated from the singlet. These two distinctions separate the conjugate base pathways from the triplet reaction of the protonated pHP. However, a rapid deprotonation of the singlet excited protonated pHP is precluded as there is no fluorescence observed from this species. The diminished Φ_{dis} for the conjugate bases must result from a more efficient decay pathway. Since the products are the same, an operative photo-Favorskii rearrangement mechanism is the likely pathway.

2) Rate Constants of Fluoro pHP GABA esters. The rates constants, k_r , obtained from S-V quenching for GABA release, disclosed marginal differences in aqueous media. From Table 33, k_r spanned from $1.8 \times 10^7 \text{ s}^{-1}$ for 2,3,6-trifluoro-pHP GABA (**128**) to $1.6 \times 10^8 \text{ s}^{-1}$ for *o*-F-pHP GABA (**123**) in water and $1.1 \times 10^7 \text{ s}^{-1}$ for 3,5-diF-pHP GABA (**127**) to $8.9 \times 10^7 \text{ s}^{-1}$ for **123** in pH 7.3 buffer. These essentially identical rapid rates parallel the nearly constant quantum efficiencies. The lack of change in the rate constants as might be anticipated in other linear free energy relationships such as Hammett σ - ρ correlation militates against an ionic charge buildup in the transition state for the release of the substrate. At first pass, the result might appear implausible since the fragmentation step for covalent bond breaking results in the release of the carboxylate ion rather than a carbonyl radical. The latter has been ruled

Figure 66. A. Plot of rate constants for release, k_r , of pHP GABA's vs. pKa's in water. B. Plot of rate constants for release, k_r , of pHP GABA's vs. pKa's in pH 7.3 buffer.



out due to the absence of radical decarboxylation processes in the photo-Favorskii reaction (see *Introduction*). Attempts to correlate k_r with corresponding pKa's in water and pH 7.3 buffer demonstrated no association (Figure 66).

3) Comparisons of the Stern-Volmer derived rate constants with the LFP values. Rate constants obtained independently from LFP (Table 37) were, in general, higher by up to one order or magnitude relative to those obtained by S-V quenching studies. The triplet lifetimes obtained by LFP are accordingly shorter than those obtained by S-V quenching with sorbate. The origin of this effect may be due to the method, i.e., the nature of the quencher and estimated rate of diffusion used in calculation of the rate constants. For example, Givens and Wirz,⁹² and Phillips⁸¹ showed that added organic solvents greatly increase the lifetime of the pHP triplet. The diffusion rate constant may be an overestimate. As sorbate is added in a S-V run, the “organic nature” of the solvent will increase, lengthening the lifetime of pHP triplets. This renders them more susceptible to bimolecular quenching and gives the appearance of a slower competing rate for the reaction out of the triplet manifold. A second factor may be the relative protonation state of the pHP chromophore. A slower quenching diffusion rate for the conjugate base will have a corresponding effect on the S-V constant, K_{SV} , which will consequently result in a lower estimated lifetime of its triplet.

4) The role of H₂O. As shown previously by Givens⁷⁸ and Phillips,⁴⁵ the triplet pHP ester is influenced by water, primarily assisting in the removal of the phenolic proton but also in assisting the concomitant loss of the leaving group, GABA, through

solvation. Added organic quenchers will negatively influence the solvation and deprotonation processes causing a decrease in the triplet reactivity.

5) Other sources of variance. An additional difference lies in the excitation source. For Stern-Volmer quenching, analyses were conducted with 300 nm, RPR phosphor coated lamps that span a range from 250 to 350 nm. Both the phenol and its conjugate base, if present, will be excited at longer wavelengths near 300 nm. In contrast, the pump probe spectroscopy studies were conducted with a monochromatic laser excitation of 266 nm having a dynamic range of ± 5 nm. This wavelength would predominantly excite the protonated forms (the absorptivities are very low at 266 nm for the conjugate bases).

6) Photochemistry of the conjugate bases. Photolysis of **122-131** at 350 nm in 0.01 M TRIS pH 9, where the conjugate bases predominate, evinced Φ_{dis} that were well below 0.01, ranging from 0.001 (**124**) to 0.008 (**130**). These low values indicate that other deactivation pathways are more efficient than GABA photorelease.

7) Proposed mechanism for conjugate base. An alternative mechanism is proposed for the conjugate bases of pHP (Scheme 54, *vide supra* with the conjugate base of pHP GABA (**101**)). Red values highlighted in this mechanism are the result of this work and may differ from the mechanism for protonated pHP GABA.

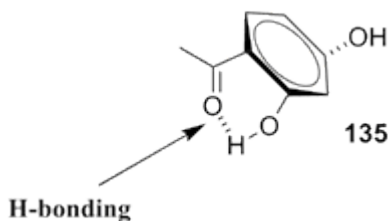
E. Miscellaneous substituent effects on pHP GABA ester photochemistry

Several other substituents were explored for their effects on the photochemistry.¹¹⁵ The nitro group is notorious for its deleterious effects on ketone

photochemistry, frequently shutting down all photoluminescent and photochemical activity. On the other hand, in an *o*-nitrobenzyl motif, the hydrogen abstraction photochemistry is the key step for this most popular photo-removable protecting group.¹⁰⁴ For nitro substituted pHP, *m*-NO₂-pHP GABA (**132**), the -NO₂ moiety extended the π - π^* absorption past 400 nm, but did not lead to GABA release when photolyzed between 254-350 nm in water. Here, the nitro group served as a deactivator.

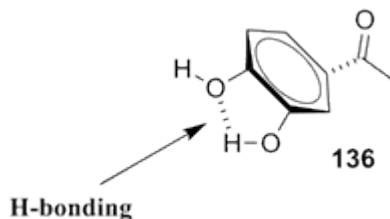
Ortho and *m*-OH-pHP GABA's (**135** and **136**, respectively) effectively quenched the photorelease of GABA as well. Hydrogen bonding with the excited ketone carbonyl for the ortho OH, a stabilizing interaction, could hinder the stereoelectronic alignment to the necessary OOP rotation angle of the carbonyl for substrate release (Figure 67).

Figure 67. Proposed H-bonding between the *o*-OH and ketone carbonyl of **135**.



The *m*-OH isomer also failed to effect GABA photorelease in water. H-bonding with the *p*-OH moiety could interfere with the crucial proton transfer step of the substrate release (Figure 68).

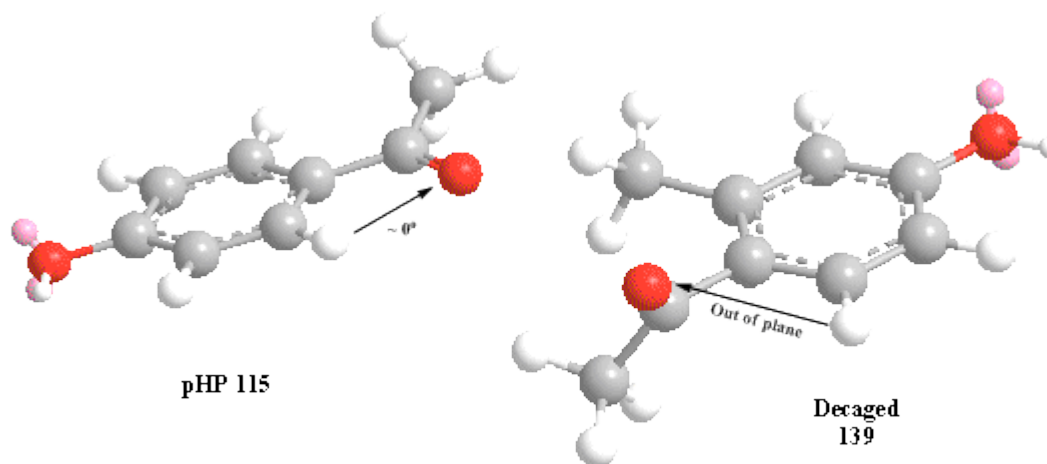
Figure 68. H-bonding between meta and para-OH moieties of **136**.



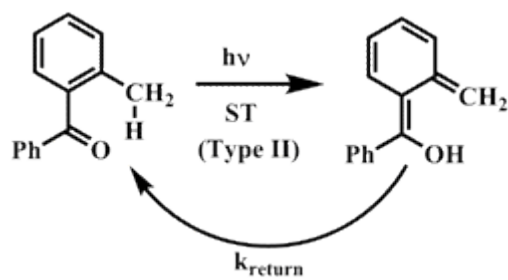
The meta-methyl substituted pHP GABA's manifested Φ_{dis} in water of 0.15. A small absorbance band shift to $\lambda_{\text{max}} = 304$ nm for **138** (24 nm) vs. pHP GABA did not change the Φ_{dis} , 0.15 and 0.20 respectively. At pH 8.2, Φ_{dis} drop to 0.08 and 0.11, respectively, congruent with declines previously seen with conjugate bases of all the derivatives.

Interestingly, the *o*-CH₃-pHP GABA (**139**) evinced a 45% decline in Φ_{dis} (0.11) compared to the unsubstituted analog (**101**) (0.20) and a 26% decline compared to meta isomer (0.15). Although the origins of this were not examined, two effects, one steric effect and the other a reversible Norrish Type II hydrogen atom abstraction may interfere with GABA release. The steric effect of CH₃ may force the acetyl moiety to adopt a conformation that is less amenable to GABA release. Low level MM2 calculations¹¹⁶ predicted the carbonyl of decaged **139** to adopt an OOP orientation with the ring (angle not specified), whereas the unsubstituted analog **115** was planar (Figure 69). The reversible nature of *o*-arylmethyl ketone photochemistry has been well documented¹¹⁷ and has been pictured

Figure 69. Lowest energy conformations of decaged **139** and **115** by low level MM2 calculations. The OOP twist angle was not determined.

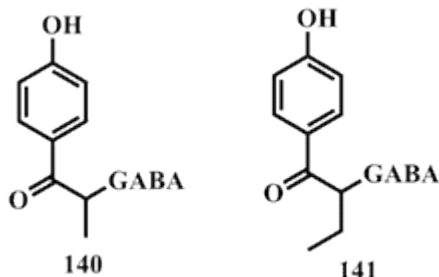


as an “energy wasting” mechanism, much the same as the alkene cis-trans isomerization process (Equation 16).



Eq. 16

The α -methyl and ethyl substituted pHP GABA's **140** and **141**, respectively, showed



low Φ_{dis} , 0.05 and 0.06, respectively. These are secondary α -centers to the ketone, which may alter the stability of the initially formed radical intermediates. The photoproducts included released GABA and the analogous, rearranged *p*-hydroxyphenylacetic acid.

The impetus for the synthesis and subsequent probing of the photochemistry of 4-fluorophenacyl GABA (**142**) was based on the well documented π electron donation of fluorine to the aromatic system of aromatic fluorine compounds.¹¹⁸ It was reasoned, then, that the *p*-fluoro moiety may be a surrogate for the *p*-OH group in inducing photorelease of GABA and rearranging to the corresponding 4-fluorophenylacetic acid. However, this compound proved to be inert at irradiation wavelengths of 254 and 300 nm.

F. Substituent effects on 5-acetylsalicylic acid GABA derivatives (154, 157-165).

The quantum yield of methyl 5-acetyl-salicylate GABA (**154**) at 300 nm spanned from $\Phi_{\text{dis}} = 0.08$ to 0.11 between pH 7 to 9, respectively, and the rate constants for GABA release, $k_r = 1.3 \times 10^8 \text{s}^{-1}$ were equable. These were consistent with 5-acetylsalicylic acid GABA (**153**). Replacing the methyl with auxochromes (**157-165**) gave quantum yields between 0.01 and 0.12. Though all of these compounds demonstrated strong absorbances at $\lambda = 350$ nm at 1 mM in water, when irradiated at 350 nm in water, they gave Φ_{dis} well below 0.01. An energy threshold for efficient GABA release from the pHP and 5-acetylsalicylic acid phototriggers may have been reached when the triplet energy of the system drops from 70 kcal/mol (pHP) to that effectuated by the auxochrome.

G. Nucleofuge effects on the photo-Favorskii rearrangement. The primary research objectives were on comprehending substituent, pH and media effects on the photo-Favorskii rearrangement. Another crucial aspect, however, concerns the nature of the nucleofuge. Carboxylic acids were emphasized in studies presented in this thesis, i.e., γ -aminobutyric acid, *l*-glutamic acid, glycine, tyrosine, phenylalanine, valine, deoxycholic acid, and alkanoyl acids.

1) *l*-Glutamate. The *l*-glutamate nucleofuge exhibited the same behavior as GABA.

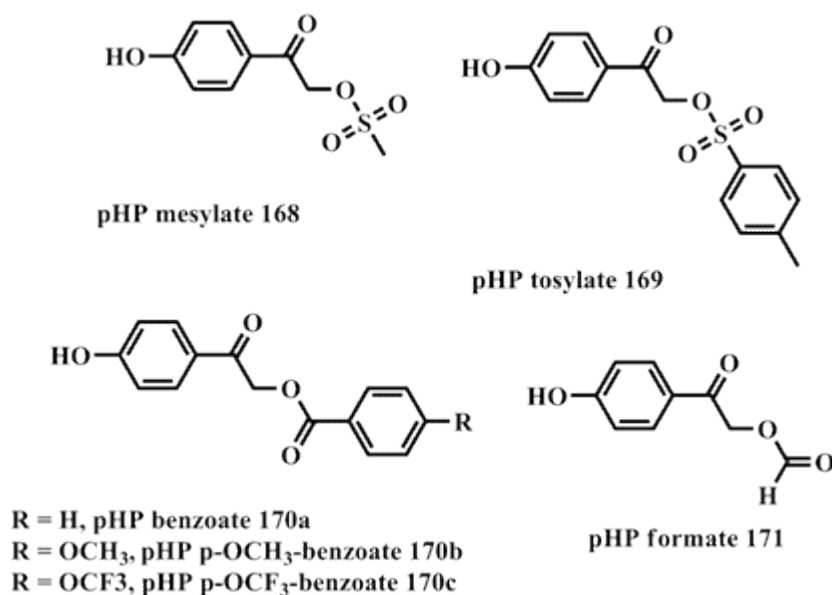
2) Other amino acids. The amino-acids glycine, valine, phenylalanine, and tryptophan manifested the same behavior as GABA.

3) Deoxycholic acid. The quantum yield for the disappearance of pHP DOC (**150**) was determined to be 0.06 in 5% aq. CH₃OH. DOC is highly lipophilic, contrary to the hydrophilic GABA salt. Solvent assistance, primarily through H-bonding with the nucleofuge, is considered to be central to nucleofuge departure. Though CH₃OH can hydrogen bond, it is much less efficient than water; less effective solvation could complicate nucleofuge departure, which would direct deactivation to other pathways. However, the rearranged *p*-hydroxyphenylacetic acid was observed, suggesting that the operative mechanism is the “photo”-Favorskii pathway.

4) Alkanoyl acids. The nucleofuge capacities of dodecanoic and tetradecanoic acids were probed as substrates caged to the 5-acetylsalicylic acid chromophore (**155** and **156**, respectively). The motivation here involved the application of these as photocleavable surfactants. Caprioli¹⁰⁰ and coworkers had synthesized structurally similar compounds to **155** and reported successful cell membrane protein extraction, improved ionization efficiencies and resolution of these proteins by MALDI analysis and facile surfactant removal by photolysis. Only a handful of photocleavable surfactants have been reported in the literature. The water solubility of **155** and **156** was low. The photolysis of 1 mM solutions of each in 5% aqueous CH₃OH at 300 nm evinced Φ_{dis} of 0.04 and 0.06, respectively. However, **155** and **156** promptly dissolved in 0.01 M HEPES with 0.1 M LiClO₄ at pH = 8.2, suggesting the carboxylic acid was deprotonated. Irradiation of 1 mM of each in this buffer divulged Φ_{dis} that were 0.10 and 0.09, respectively, *commensurate with the GABA derivative*. The improved quantum yields in buffer, substantiate water-assisted substrate

disjunction, i.e., higher water content promotes substrate disjunction because of a higher degree of solvation. This observation corroborates the hydrated triplet complex depicted in Scheme 52. Though the photocleavable surfactant properties of **155** and **156** seem favorable, i.e., each are soluble in pH 8.2 buffered media and exhibit efficient photodegradation, their biological assessments have not been determined.

H. Nucleofuge effects - linear free energy relationships. Most nucleofuges studied for this thesis were carboxylic acids. Dr. Cope, a recent graduate of the Givens group,¹¹⁹ explored the how the nature of nucleofuge impacts the photo-Favorskii rearrangement by synthesizing and probing the photochemistry of pHP mesylate (**168**), tosylate (**169**), benzoate (**170a**), *p*-OCH₃-benzoate (**170b**), *p*-CF₃-benzoate (**170c**) and formate (**171**). Through a combination of Stern-Volmer quenching and



LFP studies, a Brønsted β_{LG} (nucleofuge), linear free energy relationship (LFER) was determined.

The nucleofuge capacity has also been determined to correlate with the log of the reaction rate constant (Equation 17), where β_{LG} signifies the response of the rate constant to the nucleofuge acidity.

$$\log(k) = \beta_{LG}(\text{pKa}) + \log(C) \quad \text{Eq. 17}$$

The nucleofuge capacity is enhanced by a decrease in pKa; thus a negative β_{LG} would signify favorable nucleofuge properties. Applied to a linear free energy setting, β_{LG} indicates the degree of bond breaking (nucleofuge departure) in the rate determining step.¹²⁰ The rate determining step in the photo-Favorskii is believed to be nucleofuge disjunction, so the acquisition of a β_{LG} value is key to an improved comprehension of this step. Parameters of other esters and sulfonates with those of pHP GABA, pHP *p*-CN-phenolate¹²¹ and pHP-phenolate¹²¹ (for comparison), derived in aqueous CH₃CN, are presented in Table 38.

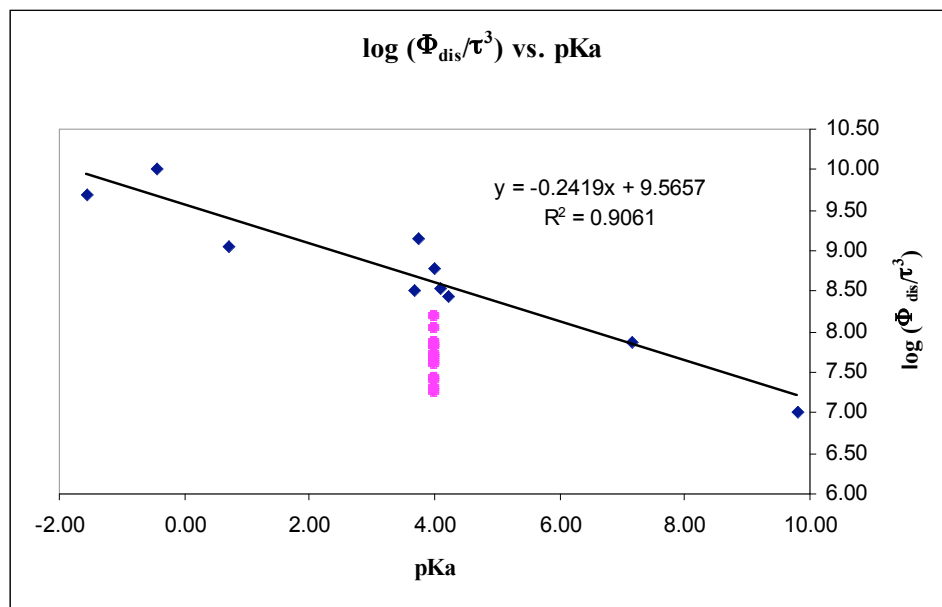
Table 38. Parameters of **168-171** and other pHP derivatives. Adapted and modified from ref.119.

pHP derivative	LG pK _a	Φ_{dis}	$k_{\tau 3 \text{ decay}} (\text{s}^{-1})$	τ^3 (ns)	$\log (\Phi_{\text{dis}}/\tau^3)^{\text{a}}$
Mesylate 168	-1.54	0.932	8.5×10^9	0.118	9.70
Tosylate 169	-0.43	1.04	9.6×10^9	0.104	10.0
Diethyl Phosphate 114	0.71	0.40	2.9×10^9	0.345	9.06
pCF ₃ Benzoate 170c	3.69	0.201	1.6×10^9	0.625	8.51
Formate 171	3.75	0.94	1.5×10^9	0.667	9.15
pOCH ₃ Benzoate 170b	4.09	0.288	1.2×10^9	0.833	8.54
Benzoate 170a	4.21	0.316	8.6×10^8	1.16	8.44
GABA 101	4.00	0.21	2.9×10^9	0.345	8.78
pCN Phenolate	7.17	0.11	6.9×10^8	1.45	7.88
Phenolate	9.8	0.04	2.6×10^8	3.85	7.02

$$^{\text{a}}\log k_r = \log(\Phi_{\text{dis}}/\tau^3)$$

The logs of the rates of disappearance, k_r , were plotted against the pK_a of the conjugate acid of the nucleofuge to obtain a slope (β_{LG}) that was -0.2419^{121} (Figure 70). A good correlation between log of k_r and nucleofuge pK_a's was observed, $R^2 = 0.9061$. The moderate, negative value for β_{LG} , indicates that some bond scission between pHP and the nucleofuge occurs in the transition state of the rate determining step. The pK_a of the nucleofuge, one direct measure of leaving group ability, is shown to be a significant factor on determining the rate of nucleofuge detachment. The data points in pink originate from the fluoro pHP GABA's; these demonstrate that substituent effects are operative in modifying k_r .

Figure 70. A plot of rates of disappearance, $(\Phi_{\text{dis}}/\tau^3)$ vs. the pKa of pHP esters, establishing a Brønsted linear free energy relationship. The values in pink represent the fluoro pHP GABA series.



I. Media effects on the photo-Favorskii rearrangement.

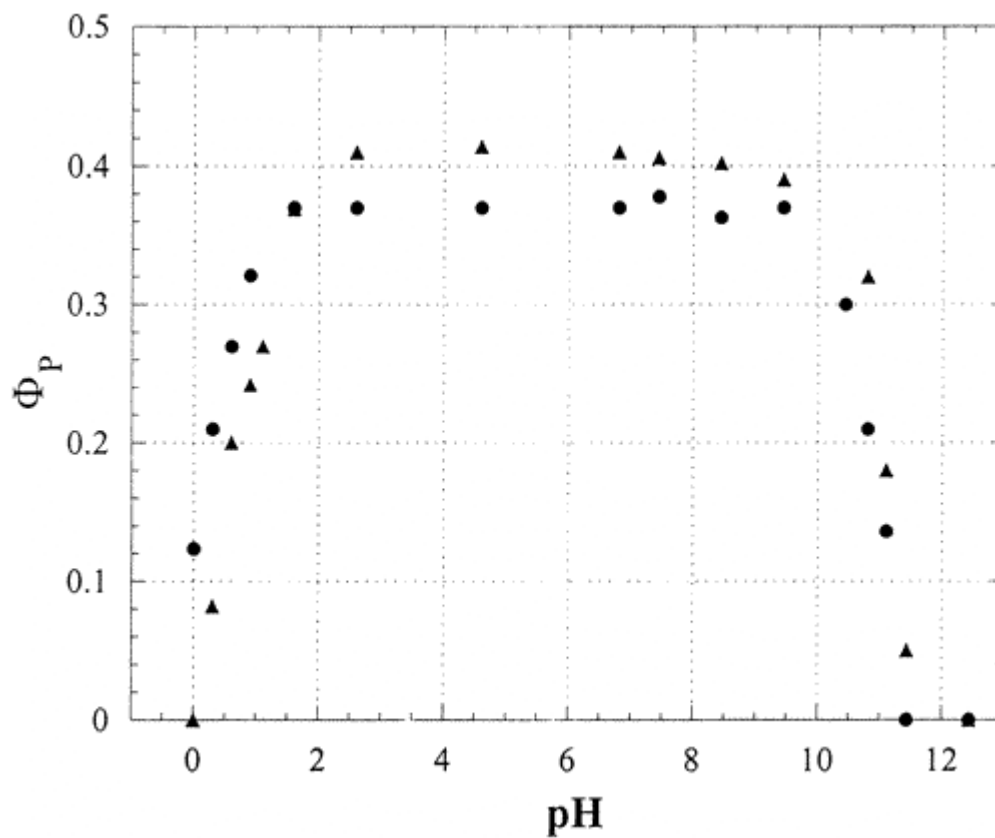
1) Background. The media in which pHP cages are photolyzed is crucial to the efficiency of the photo-Favorskii rearrangement. Wan and Corrie,⁷³ Givens and Wirz,^{78,92} and Phillips^{86,88} conveyed the pertinence of water to induce the release of phosphate and acetate from the pHP chromophore. Phillips,⁸⁸ accentuated the importance of both the hydrogen bond donor and acceptor nature of water in his modeling of the photo-Favorskii reaction. For example, in 1:1 H₂O:CH₃CN, Φ_{dis} for pHP diethyl phosphate (**114**) was 0.40. When measured in 1:1 DMSO:CF₃CH₂OH, a solvent mixture with a hydrogen bond acceptor (DMSO) and a hydrogen bond donor (CF₃CH₂OH), Φ_{dis} reduced to 0.17 but was still efficient. However, when measured

in neat DMSO or CF₃CH₂OH, the reaction did not occur. Phillips⁸⁸ demonstrated a correlation between triplet lifetime, ³τ, of pHP diethyl phosphate (**114**) and the water content in CH₃CN (Table 13); from neat CH₃CN, where ³τ was 150 ns,⁸⁰ the triplet lifetime progressively attenuated to less than 290 ps in 75% aq. CH₃CN, a factor of 517 decreases in ³τ. Likewise, the ³τ of pHP acetate **110** dropped to a more modest extent, from 137 ns in neat CH₃CN to 2.1 ns in 50% aq. CH₃CN, a factor of 65.

The triplet lifetimes are directly related to the rates of substrate release by the equation $k_r = (\Phi_{\text{dis}}/\tau)$. High Φ_{dis} have been communicated even at very low concentrations of H₂O.^{78, 119} Wan and Corrie⁷³ ascertained Φ_{dis} for pHP acetate (**110**) as 0.41 in 1:1 H₂O:CH₃CN pH 7 and revealed a correlation between media pH and Φ_{dis} (Figure 71). At low pH (0-1), Φ_{dis} for **110** spanned from 0.12 to 0.32, respectively. At pH 10.5 to 12.5, Φ_{dis} spanned from 0.30 to 0 (no acetate appearance), respectively. Earlier, a media pH dependence on Φ_{dis} was underscored for fluoro pHP GABA's **122-131**, where the ratios of protonated vs. conjugate bases altered the Φ_{dis} . Despite solvent modulated triplet lifetimes of pHP, Φ_{dis} appeared to remain steady. For example, Givens and Wirz⁷⁸ reported a Φ_{dis} for pHP diethyl phosphate (**114**) of 0.40 in 5% aq. CH₃CN with a triplet lifetime of ~ 9 ns.⁸⁸ Phillips⁸⁸ reported a Φ_{dis} of 0.40 for the same compound 1:1 H₂O:CH₃CN, though the triplet lifetime shortened to 0.350 ns. From the equation, $k_r = (\Phi_{\text{dis}}/\tau)$, the rate constants for nucleofuge disjunction change as a function of triplet lifetime. One plausible explanation is that though k_r vary according to water content, they remain

fast enough to predominate as a major triplet deactivation pathway for pHP versus other deactivation pathways.

Figure 71. Titration curves obtained from ^1H NMR analysis depicting the dependence of quantum yields for acetate appearance, Φ_{app} (Φ_p in plot) on pH for photolysis of pHP acetate (**114**) in 1:1 CH_3CN (circles). The circles represent *p*-methoxyphenacyl acetate. Reproduced with permission from the ACS, ref. 73.



2) Organic and mixed organic media. The quantum yields for disappearance, Φ_{dis} , of pHP GABA's were assessed in 25% aq. CH_3CN , DMSO, 10% aq. DMSO, 1-pentanol, and 1-octanol at 300 nm (Table 24).

a) In 25% aq. CH₃CN, the Φ_{dis} for **101**, **122-125** and **127-131** were unchanged from those for 100% water, except the marked increase for 2,6-diF-pHP (**126**) (0.16 vs. 0.11 in H₂O). UV-Vis analysis of **126** in this media revealed two absorbance bands, one at 277 nm and the other at 325 nm, reflecting the presence of both the protonated phenol and conjugate base. Recall that **126** in H₂O, only the conjugate base was manifested, at $\lambda_{\text{max}} = 331$ nm. The implication from these findings is that 25% H₂O is sufficient to effectively solvate and consequently promote GABA release and pHP rearrangement as if in H₂O. Further, the CH₃CN-H₂O mixture forces the protonation equilibrium away from the conjugate base and toward the more reactive protonated pHP form.

b) DMSO-H₂O. In accord with Phillips findings⁸⁸ with pHP diethyl phosphate (**114**), the quantum yields, Φ_{dis} , for **101**, **122-128**, **130-131** were considerably lower than with those in 100% H₂O. However, 2,3,6-triF-GABA (**128**) expressed a Φ_{dis} of 0.12, an increase vs. H₂O (0.08). Congruent with 25% aq. CH₃CN above, the Φ_{dis} for most pHP GABA derivatives in 10% aq. DMSO were similar to those in H₂O. Marked increases, however, were observed for 2,3,6-trifluoro-pHP GABA (**128** (0.15 vs. 0.08 in H₂O)) and 2,3,5,6-tetraF-GABA (**129** (0.18 vs. 0.11 in H₂O)). All pHP GABA's revealed absorbances in this medium at ~280 nm, the expected absorption for the predominantly protonated phenol; **128** and **129** have the lowest pK_a's (4.5 and 3.9, respectively) and therefore consist predominantly of the deprotonated form at higher H₂O concentrations. The results here represent Φ_{dis} for protonated **128** and **129**.

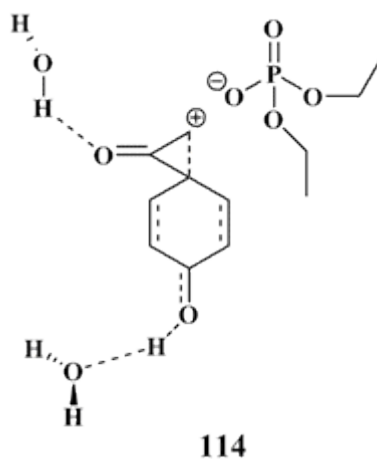
c) 1-pentanol. 1-pentanol is a model solvent for pHP GABA esters, employed here to test the relevance of the calculated ClogP's to their photorelease efficacy in lipophilic solvents. The calculated ClogP values for **101**, **122-131**, **133-134** revealed only *m*-CF₃-pHP GABA (**130** (2.02)) and *m*-OCF₃-pHP GABA (**131** (1.93)) (Table 34 *Results*) to be larger (more lipophilic) than pHP GABA (**101** (1.19)). The ClogP's of the remaining fluoro pHP GABA's **122-129**, though less than for **101**, were, nonetheless, more positive. In contrast, the *m*-methoxy pHP derivatives had ClogP values of -3.81 and -3.38, respectively. Nevertheless, 1 mM solutions of **133** and **134** in 1-pentanol were prepared without difficulty. The Φ_{dis} values were reduced by 25-50% compared to H₂O. The rest were unchanged within experimental error.

d) 1-octanol. The quantum yields in 1-octanol were consistent with 1-pentanol. Photolysis experiments of a 1mM sample of *m*-OCF₃-pHP GABA (**131**) in 1-octanol with ¹⁹F NMR analysis revealed complete disappearance after 30 minutes at 300 nm, evidenced from the lack of signal at -59.68 ppm. New bands were seen at -59.49 and -59.24 ppm, the former much larger than the latter. Spiking with an authentic sample of *p*-hydroxy-*m*-OCF₃-benzyl alcohol produced a new signal at -59.09 ppm, ruling this out as a photoproduct. Spiking with an authentic sample of *p*-hydroxy-*m*-trifluoromethoxy-acetophenone effected a substantial increase in the signal at -59.49 ppm, identifying this as the major, reduced photoproduct and comparable to the results from photolysis of *m*-OCH₃-pHP GABA (**134**) in H₂O. A radical mechanism is imputed for the photorelease of GABA in 1-octanol, the same as shown in Scheme 53.

J. Salt and ionic strength effects.

1) Background. Phillips⁸⁸ first broached the notion of contact ion pair recombination (Figure 9, *Introduction*) as a possible way to reestablish the pHP. In this example, the intimate or contact spiroketone-diethyl phosphate ion pair, formed prior to deprotonation of the phenol, was posited to either recombine to pHP diethyl phosphate as one triplet decay mechanism or completely separate to allow intersystem crossing and solvolysis in forming the rearranged *p*-hydroxyphenylacetic

Figure 9. Phillips' proposed structure of unknown, **M**, as a solvation/contact ion pair complex.



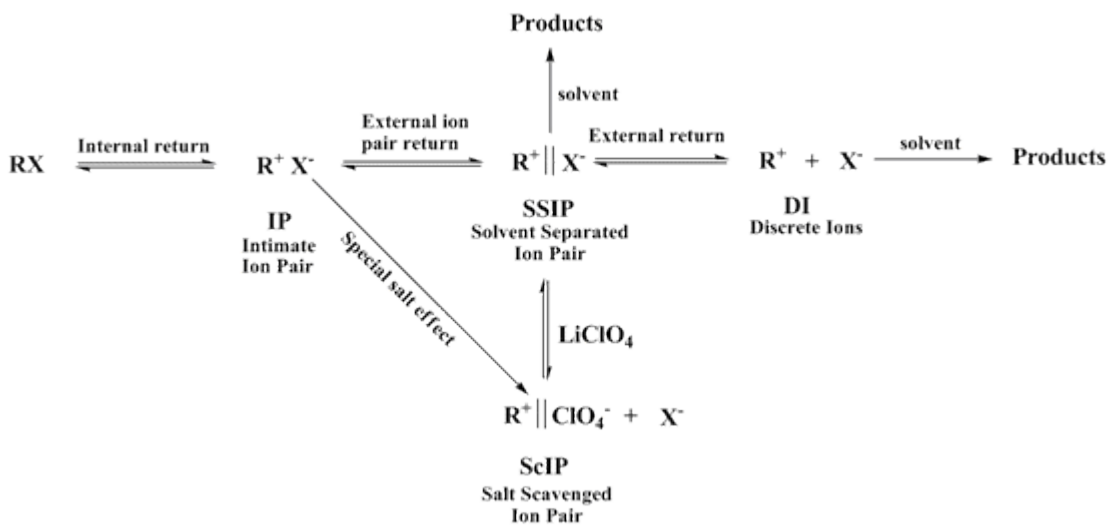
acid. A direct result of ion-pair recombination is a lower Φ_{dis} , and hence this process represents one pathway for triplet deactivation.

A conceivable method to attenuate this ion recombination is to adjust the ionic strength of the solution by adding a photostable, non-nucleophilic salts, e.g., Li^+ , Na^+ ,

or $\text{K}^+ \text{ClO}_4^-$, which could intercede between the contact ion pair and hinder substrate return.

Winstein¹²² suggested that “salt effects” could enhance observed rates of solvolysis.^{123,124,125} The Winstein ion-pair mechanism (Scheme 55) is often applied to $\text{S}_{\text{N}}1$ solvolysis reactions to demonstrate ion pair return. Initial ionization of RX

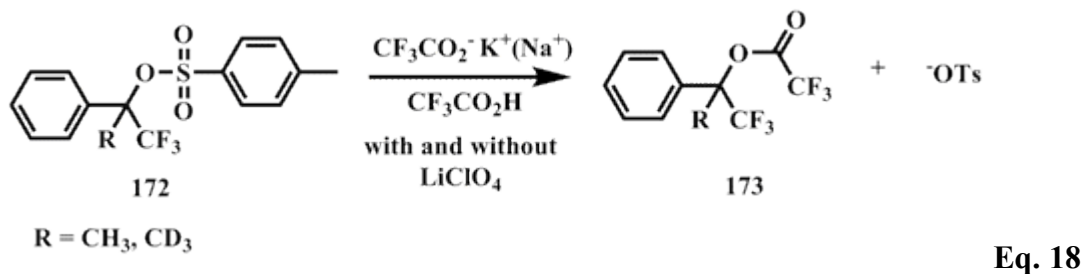
Scheme 55. Winstein’s ion-pair, solvolysis mechanism with added LiClO_4 .



produces an intimate ion pair (IP) that can recombine (internal return) or further solvate through solvent insertion to form the solvent separated ion pairs (SSIP). The SSIP can also recombine to IP or progress on to the solvolysis products. Further stages of solvent separation to unpaired discrete ions (DI) may intervene and these can recombine to SSIP. In the presence of added salts, the increased ionic strength

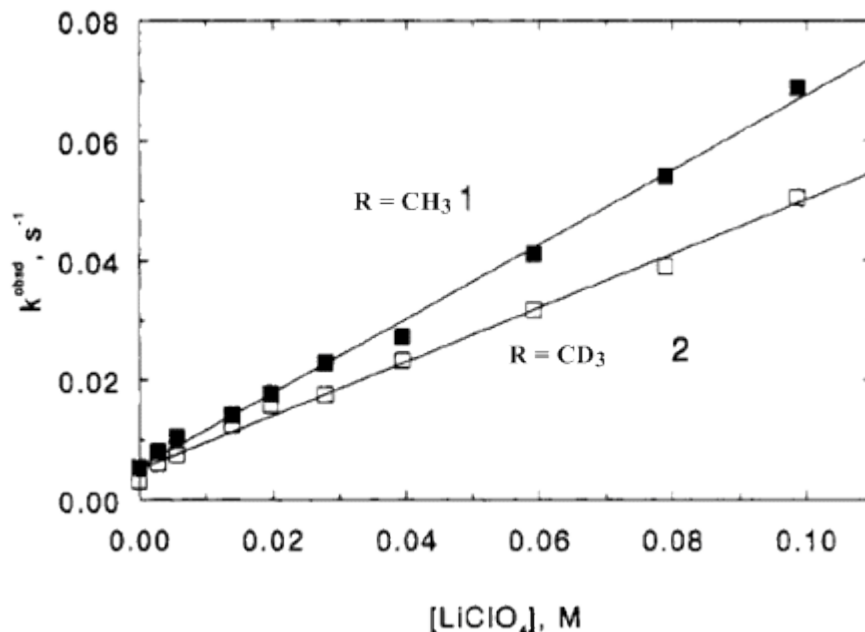
encourages the separation of the ions. Normally, these added salts do not affect the intimate ion pair dissociation. However, LiClO_4 is an exception. It is particularly effective at dissociating SSIP by Li^+ coordination with the nucleofuge through a salt scavenged pair (ScIP) that prevents external ion pair return from occurring, generally resulting in *ameliorated rates of solvolysis*. Furthermore, in certain instances, it has been shown to intercept IP and is the origin of the “special salt effect”.

Tidwell¹²⁶ and coworkers recently reported results from examinations of added LiClO_4 on the rates of trifluoroacetolysis of 1,1,1-trifluoro-2-phenylpropan-2-yl 4-methylbenzenesulfonate (**172**) (Equation 18).



A positive linear correlation between the unimolecular rates of trifluoroacetolysis of **172** (1) with NaO_2CCF_3 in $\text{CF}_3\text{CO}_2\text{H}$ and $[\text{LiClO}_4]$ was observed (Figure 72), suggesting that LiClO_4 effectively scavenges or further separates SSIP and thus hinders external ion pair return, resulting in augmented rates of trifluoroacetolysis.

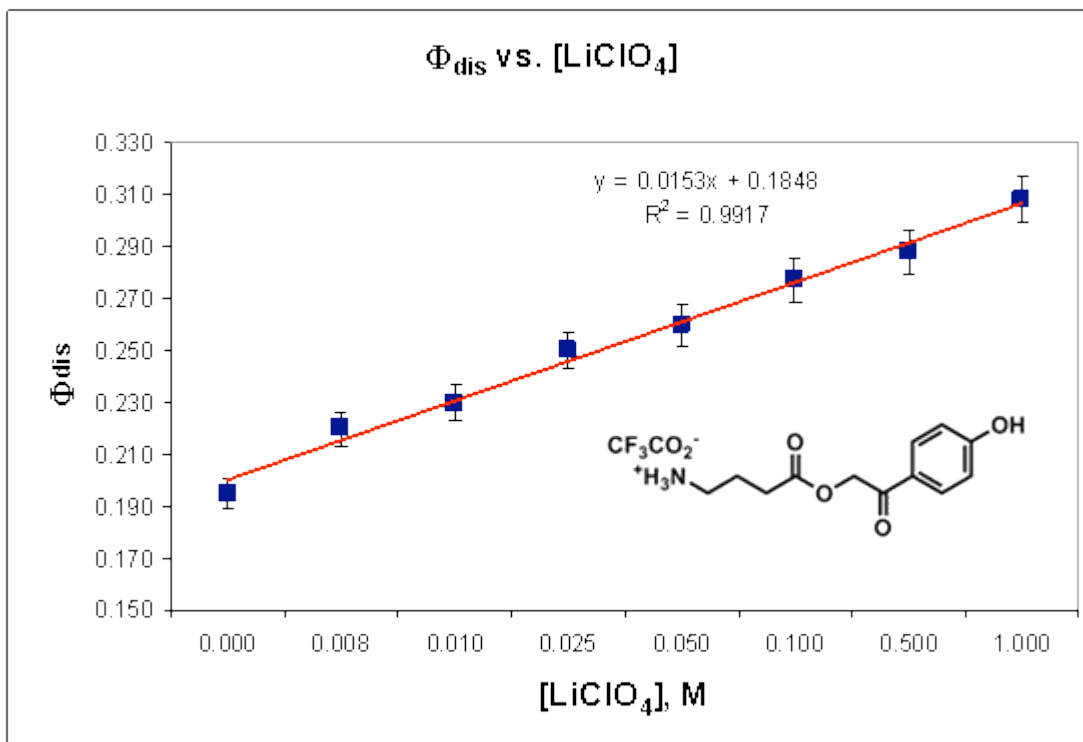
Figure 72. Observed enhancements of k_{obsd} of trifluoroacetylation of **172** ($R = \text{CH}_3$) as a function of $[\text{LiClO}_4]$. Reproduced with permission from the ACS, ref. 126.



2) Effects of added LiClO_4 on the quantum yields. Quantum yields at 300 nm were determined in the presence of $[\text{LiClO}_4]$ from 0 to 1.0 M. It was reasoned that added salt would influence any pHP GABA ionization processes including any recombination events. An increased Φ_{dis} could be evidence for a contact ion-radical pair of the triplet biradical and the nucleofuge. Conversely, if GABA departure occurred prior to phenol deprotonation of pHP, a triplet ion pair intermediate would be obtained. UV-Vis analysis of all pHP esters indicated the prevalence of protonated pHP in the ground states. Nearly all pHP GABA's, excepting the *m*-methoxy pHP derivatives (**133** and **134**) evinced enhancements in Φ_{dis} with added LiClO_4 (Table

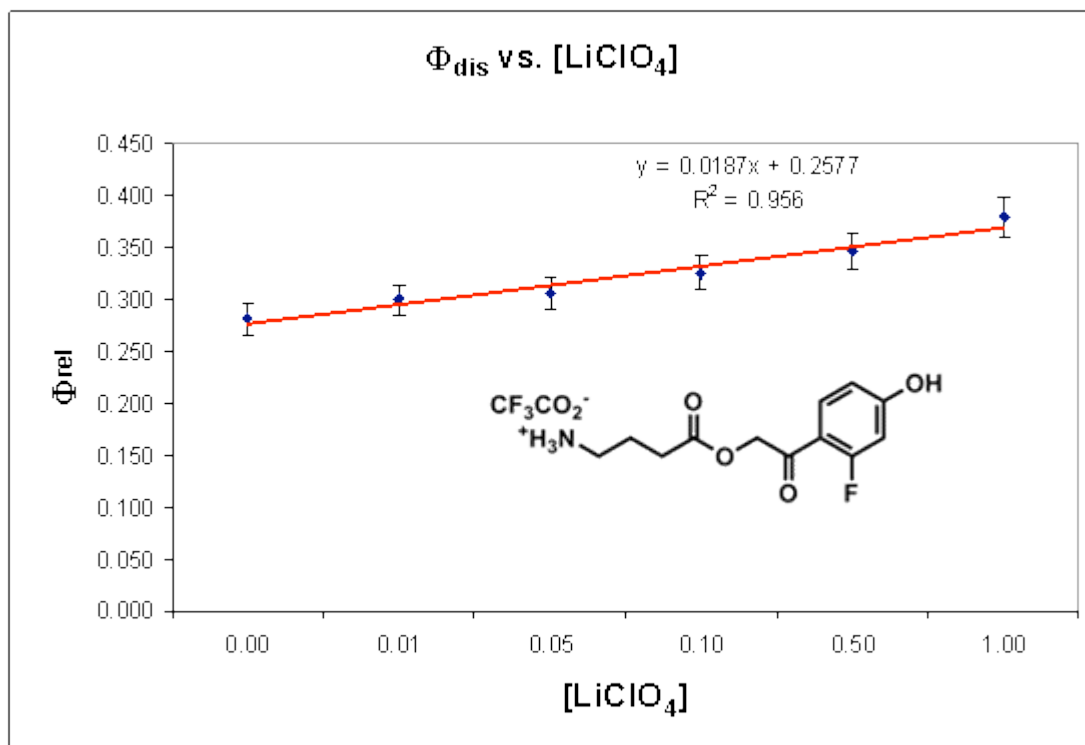
24). One example, pHP GABA (**101**), revealed a linear increase Φ_{dis} with an increase in $[\text{LiClO}_4]$ between 0 to 1.0 M (Figure 73) and a slope of 0.0153 M^{-1} or 15.3 mM^{-1} .

Figure 73. Plot of Φ_{dis} vs. $[\text{LiClO}_4]$ for pHP GABA (**101**).



This was also obtained with 2,3-difluoro pHP GABA (**123**), which disclosed a linear relationship with a slope 0.0187 M^{-1} (18.7 mM^{-1}) (Figure 74). Note that units are not bimolecular rate constants because quantum yields are in mM/Ein and are not rates.

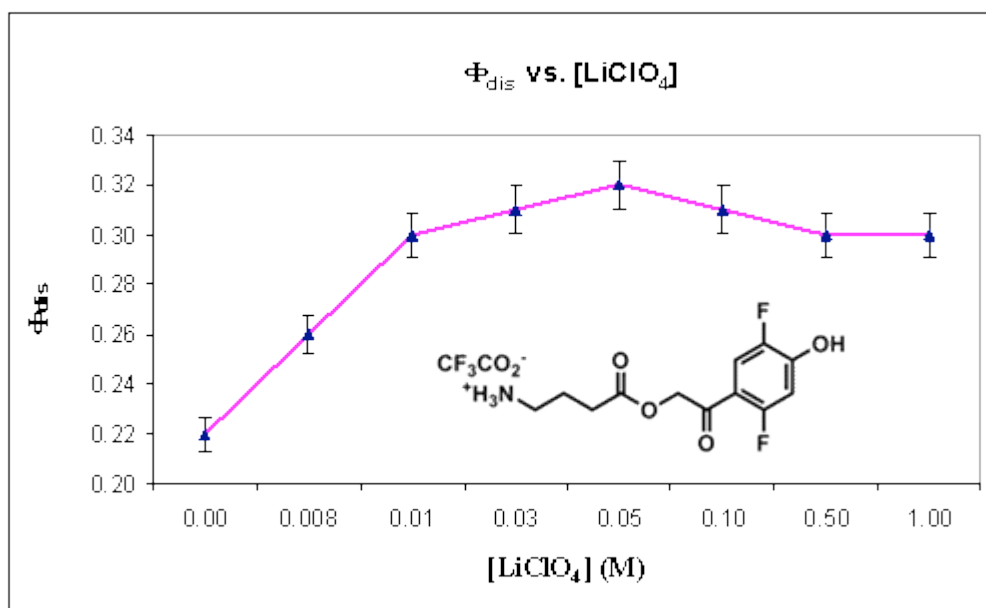
Figure 74. Plot of Φ_{dis} vs. $[\text{LiClO}_4]$ for *o*-F-pHP GABA (**123**).



In contrast to these findings, other derivatives showed an early rise in the increased efficiency dependence in LiClO_4 concentration followed by a change in slope, such as 2,5-diF-pHP GABA (**125**) (Figure 75). Initially, a special salt effect was considered. This is characterized by rapid changes induced at low concentrations of exclusively LiClO_4 as the added salt, followed by a leveling off at higher concentrations. However, a similar result was observed with NaClO_4 , which precluded the “special salt” effect associated with Li^+ . The form of the quantum yield

dependence on the concentration of LiClO₄ for **125** is similar to a saturation curve which would be expected for the ionic strength effect on quantum yields.

Figure 75. Plot of Φ_{dis} vs. [LiClO₄] for 2,5-diF-pHP GABA (**125**).

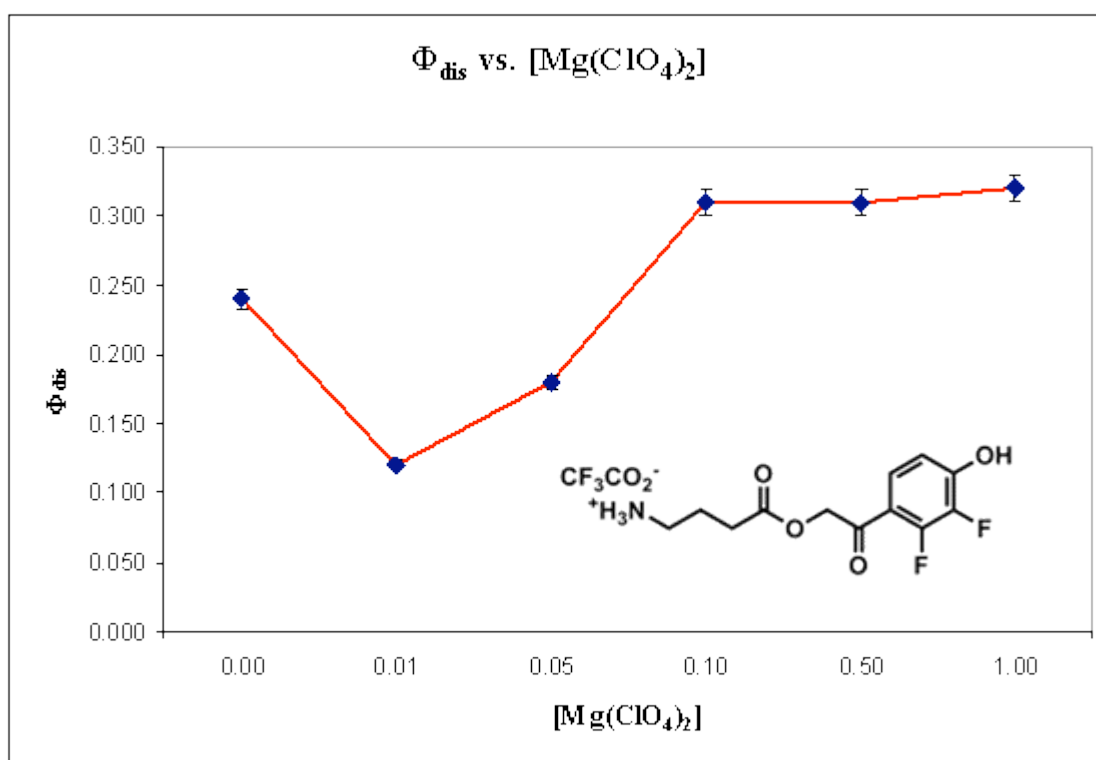


No salt effects were observed for pHP Trp (**149**), which exhibited a Φ_{dis} of 0.12 in 1.0 M LiClO₄ vs. 0.10 in water.

Other perchlorate salts, as NaClO₄ and Mg(ClO₄)₂, were probed for influences on Φ_{dis} for 2,3-diF-pHP GABA (**124**) and 2,5-diF-pHP GABA (**125**). For **125**, concentrations up to 1.0 M NaClO₄ produced a correlation that differed with LiClO₄. A logarithmic fit ($R^2 = 0.99$) was revealed that possibly signifies saturation effect. Similarly, **124** manifested a logarithmic correlation ($R^2 = 0.95$) between Φ_{dis} and

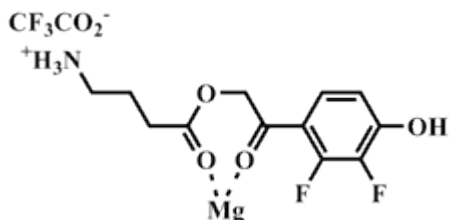
[NaClO₄]. When assessed in KClO₄, **125** manifested a logarithmic correlation ($R^2 = 0.99$) that paralleled that with LiClO₄. When assessed in Mg(ClO₄)₂, significant drops in Φ_{dis} were observed at low concentrations, but increased at 1.0 M Mg(ClO₄)₂. For example, 2,3-diF-pHP GABA (**124**) divulged a drop in Φ_{dis} from 0.24 in H₂O to

Figure 76. Plot of Φ_{dis} vs. [Mg(ClO₄)₂] for 2,3-diF-pHP GABA (**124**).



0.12 at 0.01 M Mg(ClO₄)₂ that augmented to 0.31 at 0.1 M and remained constant up to 1.0 M (Figure 76). The distinction that the doubly charged Mg²⁺ vs. singly charged Li⁺ or Na⁺ attenuates the Φ_{dis} could be through stabilizing interactions with GABA and the ketone compared to the ClO₄⁻ influence at low concentrations (Figure 77).

Figure 77. Proposed coordination between Mg^{2+} and 2,3-diF-pHP GABA (**124**).



The rate constants and lifetimes measured by LFP for the triplet excited state prior to rearrangement were also examined to discern an effect of LiClO_4 on pHP mesylate (**168**) in water and 0.66 M aqueous LiClO_4 . This was accomplished by LFP and found to cause no change in the rate for intersystem crossing, $3.4 \times 10^{11} \text{s}^{-1}$ vs. $3.9 \times 10^{11} \text{s}^{-1}$, the rate for triplet decay, $1.6 \times 10^{11} \text{s}^{-1}$ and $1.1 \times 10^{11} \text{s}^{-1}$ or the rate for the decay of the triplet biradical (**117**), $1.4 \times 10^9 \text{s}^{-1}$ and $2.0 \times 10^9 \text{s}^{-1}$. The results suggest that (1) either the ion radical recombination is occurring in those instances that show an increased Φ_{dis} with added LiClO_4 or (2) a delicate balance or compensation between the increase in the rate of rearrangement relative to the rate of triplet pHP GABA decay that does not alter the sum of these two processes is occurring. The yields of triplet (ISC vs. singlet decay) are not likely to be a factor here since Φ_{ISC} and k_{ISC} values are already maximal.

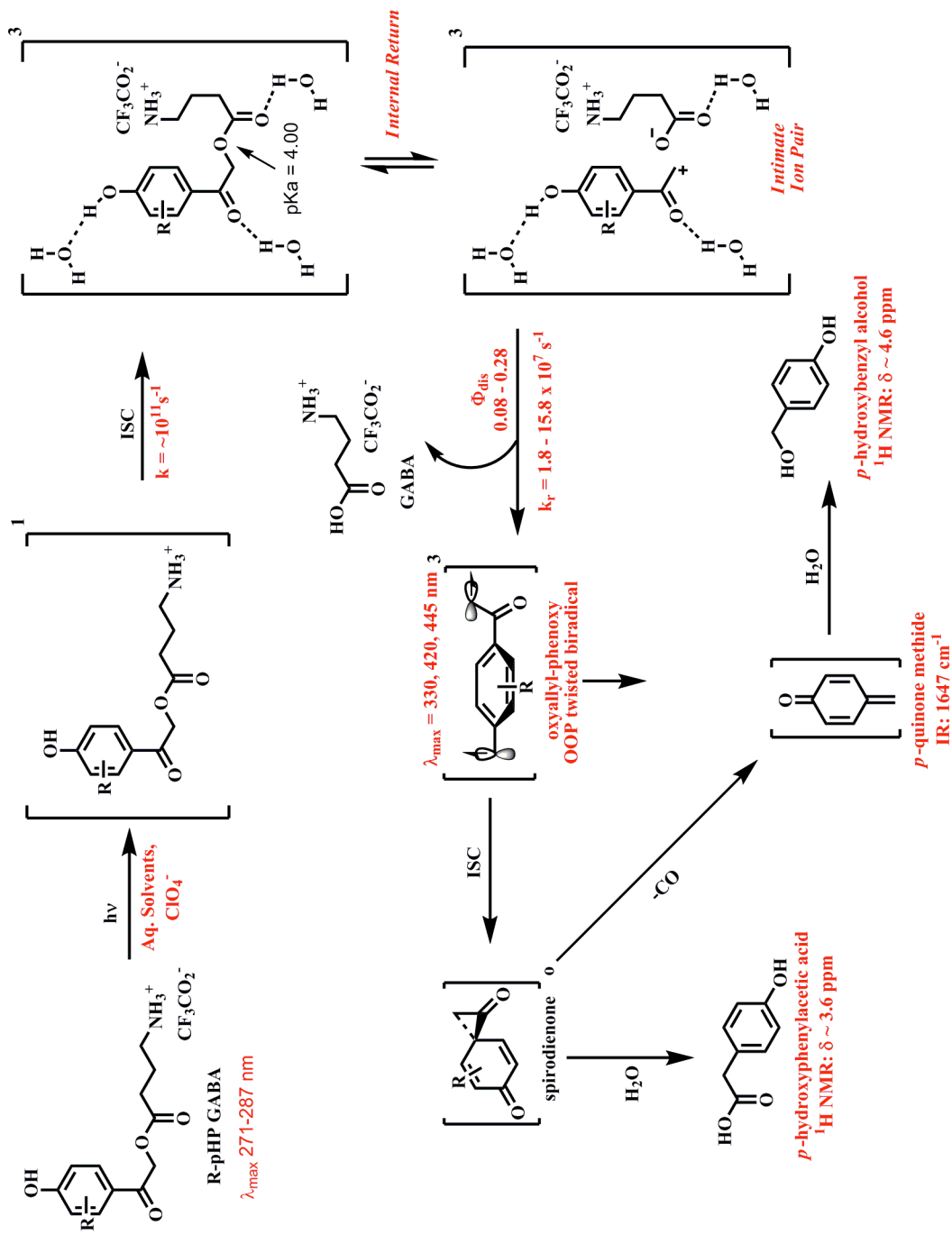
3) Common ion effect. As noted above, the recombination of the released GABA and either the protonated or unprotonated triplet biradical may serve as pathways for the decreased efficiencies in the absence of LiClO_4 . This suggests that a “common

ion-like effect”¹²⁵ might also operate here. In reference to Scheme 58, added X^- , the common ion serves to enhance the recombination steps for SSIP and DI to regenerate RX, the consequence of which is a reduced apparent rate of solvolysis. It was rationalized that added GABA would reduce Φ_{dis} by recombination of GABA with either the protonated or the conjugate base triplet pHP. However, addition of 1 to 10 equivalents of GABA (Table 26) made no significant changes on Φ_{dis} . This observation could be due to the lack of intervention at the SSIP or IP stages. It might also result from rather poor nucleophilicity of GABA. A larger quantity of GABA or better nucleophilic trapping agent, such as azide N_3^- , may be needed to reduce recombinations reflected in Φ_{dis} .

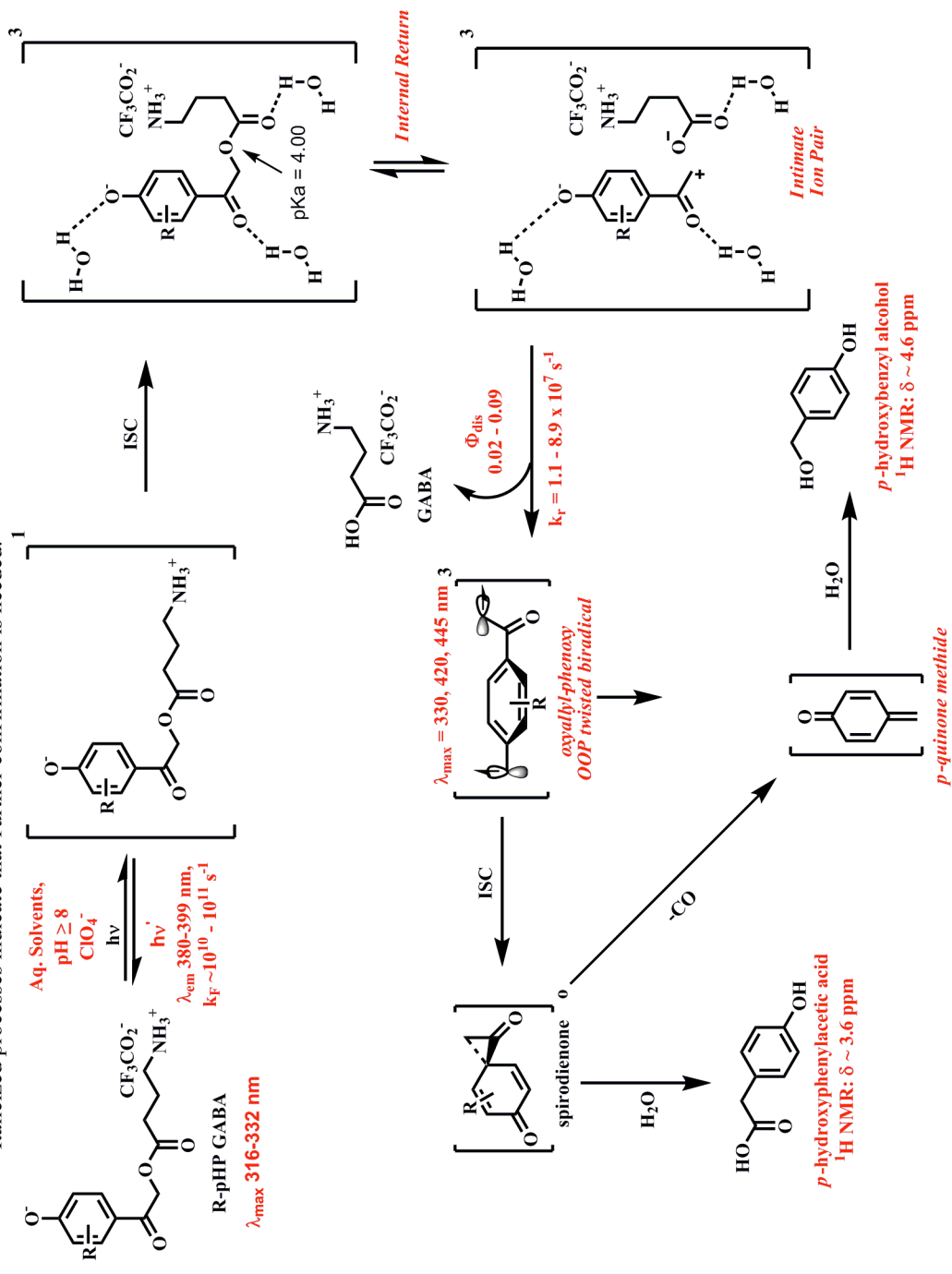
K. Rationalized mechanism of the photo-Favorskii rearrangement. A summary of the findings from studies reported here; a) the singular formation of *p*-hydroxyphenylacetic acid and *p*-hydroxybenzyl alcohol photoproducts from the pHP chromophore determined by ^1H NMR and HPLC analysis; b) a discrete deactivation pathway for the protonated pHP ($\lambda_{\text{max}} \sim 280$ nm, marginal fluorescence); c) a different, less efficient pathway for the pHP conjugate base ($\lambda_{\text{max}} \sim 330$ nm, $\Phi_{\text{dis}} \leq 0.10$, fluorescence $\lambda_{\text{em}} > 382$ nm, $k_F 10^{10}\text{s}^{-1}$); d) a narrow range for all GABA release efficiencies (Φ_{dis}) from 0.08 to 0.28, as well as for 5-acetylsalicylic acid caged carboxylic acids (GABA, *l*-Glu, Gly, etc.) at 300 nm; e) a narrow range for the Stern-Volmer and LFP derived rate constants for intersystem crossing, ($k_{\text{ISC}} \sim 10^{11}\text{s}^{-1}$) and GABA release ($k_r \sim 10^7\text{-}10^8\text{s}^{-1}$); f) the confirmatory and diagnostic absorbance bands

for the transient intermediate, a triplet biradical (330, 420 and 445 nm); g) the DFT derived, out of plane (OOP) motion of the carbonyl during formation of the oxyallyl phenoxy triplet biradical to the ring; h) a reinforcement of the recently discovered Brønsted K_{β} linear free energy relationship for the rate of nucleofuge release versus the pKa of the nucleofuge; i) a measure of the change in the reactivity of the pHP photorelease process when solvents such as organic alcohols (1-pentanol and 1-octanol) elicit GABA release at reasonable efficiencies and j) a dramatic salt effect from added LiClO_4 and related salts that improve Φ_{dis} , possibly signifying intimate ion pairs. These results are summarized by representative mechanisms for the photo-Favorskii rearrangement in Scheme 56 for protonated pHP GABA and Scheme 57 for corresponding conjugate base.

Scheme 56. Proposed photo-Favorskii mechanism for protonated pHP GABA esters. Red indicates findings from current studies. Italicized processes indicate that further confirmation is needed.



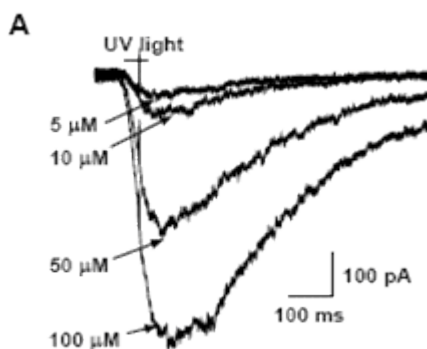
Scheme 57. Proposed photo-Favorskii mechanism for the conjugate base of pHP GABA esters. Red indicates findings from current studies. Italicized processes indicate that further confirmation is needed.



L. Biological studies.

1) Neuronal assays. Neuronal studies were conducted by the Kandler Groups at the University of Pittsburgh.¹²⁷ To test the biological activity of pHP GABA esters, *m*-CF₃-pHP GABA (**130**) *m*-OCF₃-pHP GABA (**131**) and were assessed in neurons of cortical sections of mice using patch clamp recordings.¹²⁸ Confined photolysis with 10-50 ms UV pulses through a narrow optical fiber generated whole cell inward currents. Increasing concentrations of photolyzed **131** effectuated membrane currents of sizeable amplitudes and long durations (Figure 78). To compare the sensitivity of

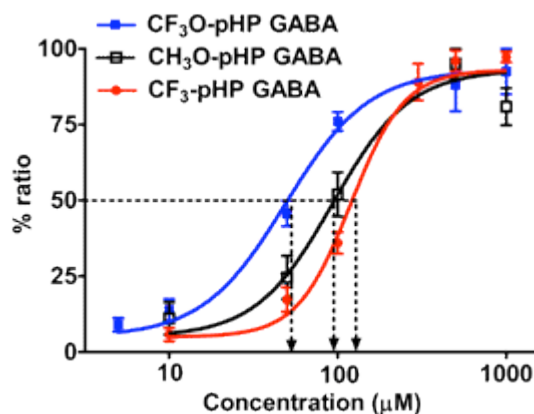
Figure 78. Amplified current as a function of photoreleased GABA from *m*-OCF₃-pHP GABA (**131**).



photolyzed **130** and **131** with previously studied *m*-OCH₃-pHP GABA (**134**),⁹⁷ concentration response curves for neurons subjected to **130**, **131**, and **134** were generated by fixing the responses to Hill's equation¹²⁸ with subsequent

determinations of half maximal effective concentration, EC_{50} , values of 49 μM , 120 μM and 93 μM , respectively, for **131**, **134**, and **130**, respectively (Figure 79). The

Figure 79. Population data of peak currents normalized to the maximum peak response and fitted to Hill's equation to derive EC_{50} values for **130**, **131**, and **134**.



data disclosed an enhanced GABA response for **131** ($\Phi_{\text{dis}} = 0.09$) versus **134** ($\Phi_{\text{dis}} = 0.04$) and, surprisingly, showed **130** ($\Phi_{\text{dis}} = 0.17$) as being the least effective.

The specific activation of the $GABA_A$ receptor antagonist SR 95531 (Garbazine; Tocris, Ellisville, MI) was probed with *m*-OCF₃-pHP GABA (**131**). Photolysis of **131** produced membrane currents that were completely blocked by Garbazine (Figure 80), signifying that the response is governed by activation of the $GABA_A$ receptor. Additionally, the current-voltage relationships of the responses divulged a reverse potential of -14.2 ± 2.9 mV (Figure 81), which is near the

Figure 80. Membrane currents elicited from photolysis of **131** are completely obstructed by Gabazine, indicating the activation origin as the GABA_A receptor.

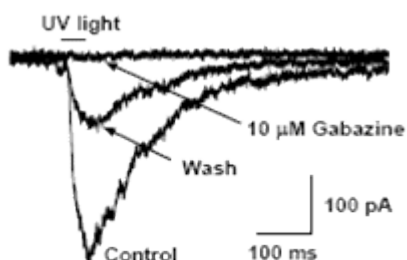
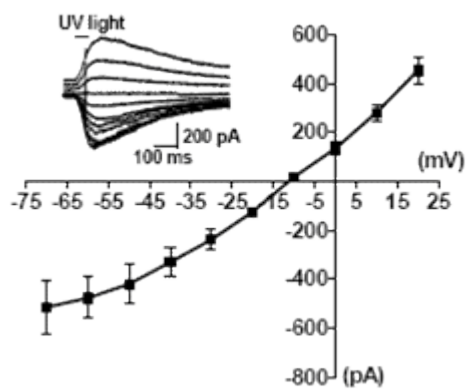


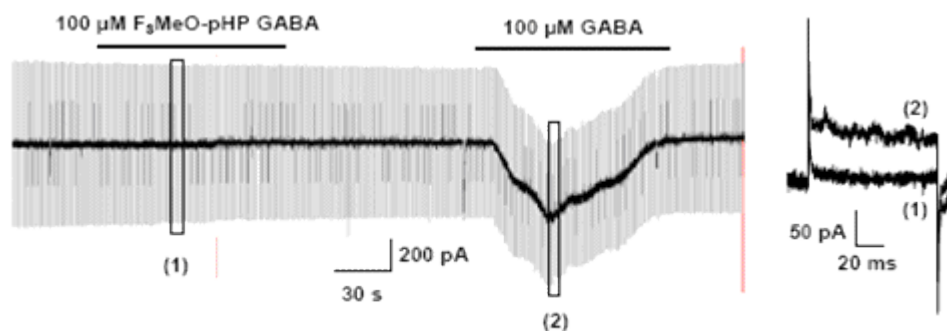
Figure 81. Reverse potential deduced from the photolysis of **131**.



theoretical potential of -20 mV, as determined from the Nernst equation for chloride concentration between the internal (60 mM) and external (133 mM) solution. Collectively, membrane currents evoked from photolysis of **130** and **131** are moderated by *activating the GABA_A chloride receptor channel*.

To determine whether caged GABA could function as an agonist for the GABA_A receptor, **130** and **131** were examined for their effects on membrane input resistance by monitoring the current responses with short command steps from a holding potential of -70 mV to step potential of -65 mV during 100 ms in the presence and absence of GABA (100 μM) or **130** and **131** (100 μM). Neither **130** nor **131** altered the holding current (Figure 82) or reduced the membrane input resistance.

Figure 82. Probing the effect of **131** on the holding currents or membrane input resistance. No effect was noticed.



However, the employ of GABA on the same neurons educed inward currents and decreased membrane resistance due to activation of GABA_A chloride channels. Thus, only photoreleased GABA and not caged GABA can activate the GABA_A chloride channels.

2) FITC-DOC. FITC-DOC was synthesized and distributed to the Picking group¹²⁹ for use. The crux of their research involves the *Shigella flexneri* organism,

specifically the induction mechanism to bacillary dysentery in humans. Bacillary dysentery is a debilitating and potentially fatal affliction educed by this organism and is common in the third world. The type III secretion system (TTS) is a crucial apparatus for infection in this organism. Among other constituents of TTS, a surface needle is protuberant. The far terminus of the needle manifests a ‘tip complex’ that consists of an invasion plasmid antigen D (IpaD), a regulatory body for TTS and necessary for the engagement and organization of the translocator protein IpaB at the needle tip in the presence of deoxycholate (DOC) or other bile salts. Until recently, the role of DOC in IpaB recruitment to the TTSA needle tip was unknown. However, current studies revealed that IpaD specifically binds to FITC-DOC, specifically at the N-terminal-domain of IpaD at its central coiled-coil, a locus that also may be involved in needle-tip interactions.¹³⁰

M. Future Studies. Substituent and nucleofuge influences on the photo-Favorskii rearrangement have been probed. The pKa’s of substituted pHP’s and variation of the nucleofuge play key roles in the efficiencies and rates of nucleofuge release. Time resolved resonance Raman, TR³, and laser flash photolysis, LFP, studies have provided a wealth of information concerning the structure and reactivity of excited state of pHP and the corresponding transient intermediates. Assimilating these data into detailed mechanisms for the photo-Favorskii rearrangement of the pHP chromophore and its substituted derivatives are condensed into Schemes 56 and 57.

Nevertheless, there are several studies that are essential for further elucidation of these processes.

1) Organic and mixed organic media. The preliminary studies reported here conveyed nucleofuge release in 10% aq. DMSO, 1-pentanol and 1-octanol, but the minor the photoproducts in the latter two studies have not been identified. The overall effects of organic or mixed organic media on the photo-Favorskii reaction would be useful information, especially with regard to future studies related to highly lipophilic, biologically relevant nucleofuges and media.

2) Salt effects. Added perchlorate salts clearly manifested enhanced Φ_{dis} for nearly all pHP GABA's. The preliminary interpretation of these effects involve an influence of salts possibly on intimate ion-radical pairs, paralleling Winstein's $S_{\text{N}}1$ solvolyses.¹²⁵ However, further investigations are required to probe the origin of the effects, particularly focusing on rates of release. Although LFP studies on pHP mesylate showed no changes in either the rates of ISC or triplet decay with 0.66 M LiClO_4 , this experiment was the only one tested and involved a superb nucleofuge, where return is expected to be minimal. Expanded LFP studies on other pHP derivatives are necessary.

3) Chiral nucleofuge. A photochemical investigation of **(R,R)-166** or **(R,S)-167** would have been useful for following the configurational changes at a stereocenter that is intimately involved in the cyclopropanone formation and collapse during the photo-Favorskii rearrangement. Measurements at partial conversion to photoproducts could test for ion-radical return as well. This could be strong evidence for the

intermediacy of an intimate ion pair prior to the triplet biradical formation. A suggested a stepwise nucleofuge departure and phenol deprotonation instead of the currently posited concomitant process may emerge.

4) Structurally similar entities to pHP. Yousef¹¹ reported low Φ_{dis} for a series of substituted 1,4 and 2,6 naphthols despite favorably lengthening the λ_{max} . Nitrogen analogs of pHP, such as 4-aminoacetophenone were briefly studied but gave radical products.¹³¹ Some structurally analogous entities to pHP should be investigated.

Conclusion

The *p*-hydroxyphenacyl (pHP) chromophore is an efficacious phototrigger for the temporal, spatial and concentration control over substrate release. The release mechanism is underscored by an intriguing rearrangement of pHP that resembles the well known Favorskii reaction. Previous quenching and spectroscopic studies with various pHP cages were effective in providing an early mechanistic picture of the photo-Favorskii rearrangement, including a) the clean photoconversion, b) favorable quantum efficiencies for release (~ 0.2 and higher) at 300 nm, c) the triplet reactive excited state, d) the dependence of the triplet lifetime on the water content of the solvent, e) the pertinence of water in inducing substrate release and proton abstraction from pHP, f) the rapid rates (10^7 - 10^9 s⁻¹) of substrate release and g) very limited structure-reactivity explorations.

However, the expanded studies reported here are essential for a more detailed, mechanistic comprehension. These include 1) distinguishing nucleofuge influences, 2) media effects (pH, buffer, mixed solvents and added salts), 3) structure-reactivity relationships (electron withdrawing and electron donating groups) and 4) modulating the pKa of the phenol to discern pH induced changes in, for example, the quantum yields for substrate release. The pHP chromophore suffers from a low molar absorptivity at $\lambda > 300$ nm, which limit its usefulness in the biological arena because of possible secondary photodegradations and the paucity of inexpensive lasers that

utilize wavelengths between 300-320 nm. Extending the λ_{max} of pHP by substitution with auxochromes is a plausible motive to overcome these deficiencies.

Several pHP GABA derivatives were specifically designed and synthesized to probe structure-reactivity relationships, primarily between the nature of the substituent and quantum yield for GABA release, Φ_{dis} . Electron donating groups, such as methoxy and hydroxy, appeared to attenuate Φ_{dis} (relative to the unsubstituted parent) or completely quench GABA photorelease. Electron withdrawing, *m*-substituted carbonyl moieties also reduced Φ_{dis} by half. The rate constants for GABA release, k_r , did not vary significantly from the unsubstituted parent.

Several fluoro pHP GABA esters were designed and synthesized to explore how modulating the pKa of pHP would result in pH induced changes by the media on Φ_{dis} and k_r . The pH of the media was found to directly control the equilibrium between the protonated and conjugate bases of these fluoro pHP derivatives as evidenced by a) λ_{max} values (<300 nm for protonated and >300 nm for conjugate bases) and b) the quantum yields for GABA release at 300 nm ($\Phi_{\text{dis}} > 0.15$ for protonated, $\Phi_{\text{dis}} < 0.10$ for conjugate bases). Stern-Volmer and LFT studies determined rate constants for release that narrowly spanned from 10^7 to 10^8 s⁻¹. At 350 nm, the conjugate bases revealed Φ_{dis} that were less than 0.01. The conjugate bases are fluorescent and the fluorescent lifetimes of 1-10 ns for these were obtained. A mechanism for GABA release from the conjugate bases of pHP was posited.

A series of 5-acetylsalicylate GABA's with UV absorbing appendages (antennae compounds) were generated in efforts to lengthen the λ_{max} of pHP. Though

this objective was accomplished, the Φ_{dis} were low at 300 nm (0.01 to 0.11) and very low (<0.01) at 350 nm.

The quantum efficiencies at 300 nm of several pHP GABA's in aqueous DMSO and CH₃CN were determined to be commensurate with those in water. However, GABA photorelease was quenched in neat DMSO. Additionally, photolyses of these compounds were conducted in 1-pentanol and 1-octanol, which disclosed reasonable efficiencies (~0.1), though the primary photoproducts were the reduced *p*-hydroxyacetophenone, signifying an alternate mechanistic pathway than the photo-Favorskii rearrangement.

When perchlorate salts were added, significant increases in Φ_{dis} were observed for nearly all pHP GABA's. A corollary from this was a proposed transient, solvent separated, triplet pHP and GABA radical or ion pair. This phenomenon suggests a possible nucleofuge ionization step prior to proton abstraction from the pHP phenol, a pathway contrary to the currently accepted concerted process.

Laser flash photolysis on several pHP GABA's revealed time resolved absorption bands at 330, 420, and 445 nm, which were ascribed to a triplet oxyallyl-phenoxy biradical, a consequence of adiabatic nucleofuge disjunction. DFT calculations of the triplet oxyallyl-phenoxy biradical determined the radicals to be contorted out of plane from 22° to 58° depending on the substituents and their position on the aryl ring. Additionally, the triplet biradicals were calculated to be at least 78 kcal/mol lower in energy than their singlet spirodienedione counterparts. Time resolved FTIR spectroscopy was conducted with pHP diethyl phosphate and

disclosed a band at 1647 cm^{-1} that was consistent with a transient *p*-quinone-methide, a suitable precursor to the minor *p*-hydroxybenzyl alcohol.

Finally, studies on biological processes that are initiated by release of an active substrate such as the neurotransmitter GABA have shown the power of spatial and concentration control in neuronal preparations. These studies were performed with three pHP GABA derivatives, which demonstrated the pHP chromophore as being an effective phototrigger for facile release of GABA in neuronal stimulation.

In summary, previous work and the studies reported here have provided a clearer understanding of the photochemical and photophysical processes of the *p*-hydroxyphenacyl chromophore. The photochemical details of the Favorskii rearrangement have been shown to include a transient oxyallyl-phenoxy triplet biradical, formed during the release of the conjugate base as substrate. The role of H₂O, solvents, pH and added salts on the photochemistry and photophysics as well as substituent effects on the chromophore have supported the general mechanistic schemes presented here.

Experimental

Methods

Melting points were conducted with open ended capillary tubes using a non-calibrated Thomas-Hoover melting point apparatus. Lyophilization was performed using a Labconco FreezeZone device set at $-52\text{ }^{\circ}\text{C}$ and 0.04 mbar. Solution pH values were determined using a Fisher Science pH 510 meter calibrated with certified Fisher buffer solutions of pH 4, 7, and 10. Products of all reactions were assessed for purity using the following instrumental techniques: For ^1H , ^{13}C , and ^{19}F NMR, Bruker DRX 400 and DRX 500 MHz spectrometers were utilized with trifluoroacetic acid as an internal standard ($\delta = -76.55\text{ ppm}$). GC/MS analysis was done on an Agilent 6890N Network GC System equipped with a Quattro Micromass Triple Quadrupole Electron Impact mass spectrometer. Exact masses were performed on a Quattro Micromass Triple Quadrupole Electro Spray Ionization mass spectrometer. UV/Vis data was obtained on a Carey Bio100 instrument using 1.5 ml quartz cuvettes. Fluorescence data were acquired on a Carey Eclipse Fluorescence Spectrophotometer using a 10 mm quartz cell. IR data were obtained using a Shimadzu FT-IR 8400 S instrument with pressed potassium bromide (KBr) pellets or a prefabricated sodium chloride (NaCl) chloroform cell for solid phase analysis, and NaCl prefabricated plates for oil analysis. Ground state $\text{p}K_{\text{a}}$'s were determined through sample titration with increasing amounts of 0.0461 M NaOH (standardized with potassium hydrogen phthalate), correlating pH vs. $[\text{OH}^-]$, and ascertaining the half equivalence point as the $\text{p}K_{\text{a}}$.

Product separation was achieved by flash chromatography using EM Science silica gel and gradient hexanes/ethyl acetate as eluting solvents. All reactions were run under ambient conditions unless otherwise stated. ^1H NMR spectroscopy was utilized to monitor the progress of photolysis of all new pHP cages. In general, a 1-10 millimolar sample of pHP-caged GABA was prepared in 2 ml D_2O , approximately 2 ml was placed in an NMR tube. This was positioned in a photoreactor equipped with two 15 W, 3000 Å Rayonet lamps and a merry-go-round. Irradiation for 30 min generally led to 100% conversion as judged by the absence of the ester proton signals. Photoproduct identification was achieved through spiking the samples of the irradiated mixture with authentic samples of the resolved GABA. Quantitative photolysis conditions for determination of quantum yields and Stern-Volmer quenching constants (K_{SV}) were as follows: The lamp light output (in mEinsteins/min) was established using the potassium ferrioxalate method.⁷ Milligram quantities of caged compounds and caffeine or acetamidophenol were weighed out on a Fisher brand Microbalance and dissolved in 4 ml of 18 MΩ ultrapure water, salt solutions of various concentrations, buffers with or without adjusted ionic strengths, or purified organic solvents were then added to a quartz tube and vortexed, resulting in a homogenous solution of the caged compound and internal standard. Concentrations of the caged compounds ranged from 1-9 mM. These tubes were then placed in a carousel within a Rayonet Photochemical Reactor equipped with two 3000 Å, 15 W Rayonet Photochemical Reactor RPR3000 Mercury Lamps as light sources.

100 μl samples were removed at 30 s intervals up to 5 minutes using a 250 μl Hamilton micro-syringe and diluted to 1 ml with water using 1 ml volumetric flasks.

Picosecond Pump-probe Spectroscopy

Picosecond transient absorption was measured with the pump–supercontinuum probe technique using a Ti/Sa laser system (Clark MXR CPA-2001; 775 nm, pulse energy 0.9 mJ, full width at half maximum 150 fs, operating frequency 426 Hz). Part of the beam was fed into a Clark MXR NOPA. The output at 532 nm was frequency-doubled by a β -barium borate (BBO) crystal to 266 nm and, after compression, provided pump pulses with an energy of 1 μJ and <150 fs pulse width. A probe beam continuum was produced by focusing the 775-nm beam in front of a CaF_2 of 4 mm path length. The pump and probe beams were focused to a 0.04 mm^2 spot on the sample that was flowing in an optical cell of 0.3 mm thickness. The absorbance was in the range of 0.3–1, depending on the solubility of the compound. The probe beam and a reference signal (passing the solution besides the pump beam) were spectrally dispersed and registered with two photodiode arrays (512 pixels). Transient absorption spectra were calculated from ratio of the two beams. Spectra recorded with time delays ranging from 0 to 1.8 ns (to observe the triplet decay) were typically recorded with 20 ps steps, those ranging from 0–8 ps (to observe ISC) with 80 fs steps. The shorter measurements were corrected for chirp using a program (SPAN) kindly provided by Prof. N. Ernstring, Berlin. To improve the signal-to-noise ratio, the

data were averaged over multiple pump-probe scans (3-6 scans with 400 shots per temporal point).

Quantum Efficiency Determinations

Quantitative analysis was achieved by HPLC/UV or HPLC/MS/MS. The LC/MS/MS instrument was a Waters 2695 Liquid Chromatographer equipped with a Quattro Micromass Triple Quadrupole Electro Spray Ionization Mass Spectrometer, outfitted with an autosampler. UV-Vis detection consisted of a Waters 2497 type with a dual wavelength detector set at 220 and 240 nm. The reservoirs used were as follows: A) 99% water, 1% methanol, 10 mM ammonium formate and 0.06% formic acid. B) 99% methanol, 1% water, 10 mM ammonium formate, and 0.06% formic acid. The column was a reverse-phase (C18), 4 μm mesh Altech Altima, 50 mm in length. Injections of 100 μl were made with an automated sampler for each run for a total of 3 injections per vial. A mobile phase gradient was utilized to optimize compound separation. The flow rate was set at 300 $\mu\text{l}/\text{min}$. Data analysis was performed by Mass Lynx Ultima software and Microsoft Excel. Smoothing functions were used for peak analysis of the chromatographic peaks. Calibration curves to obtain R values from linear least-squares regression were determined at concentrations of the reactants and products in photolyses by systematic increases of pHP-caged GABA, free GABA, and *p*-hydroxyphenylacetic acid concentrations to determine correlations with internal standards caffeine or 4-acetamidophenol. The quantum efficiencies

were then calculated from the ratio of the reactant or product concentrations to the photons absorbed using the actinometer values obtained as indicated above.

Lifetime and Rate Measurements

The Stern–Volmer quenching method¹³² was employed to determine the triplet lifetimes of pHP derivatives. Potassium sorbate served as the quenching agent. Solutions of pHP-GABA, 0.001–0.01 M, were diluted with sorbate solutions of increasing concentration (0–0.1 M), and photolyzed under the aforementioned conditions to ascertain the change in quantum efficiencies of GABA release. Φ_0/Φ vs. [Q], and the Stern–Volmer constant, K_{SV} , were determined. To determine the triplet lifetime, τ^3 , the rate of quenching, k_q , was assumed to be the rate of bimolecular diffusion, $k_{diff} \sim 7.2 \times 10^9 \text{ s}^{-1}$ (water). The rates of photorelease, k_r , were then computed as $k_r \sim \Phi_{rel} * \tau^3$.

Calculations

The atom coordinates for each molecule were introduced into SYBYL¹³³ for molecular mechanics optimization using the Tripos Force Field.¹³⁴ The ensuing structures withstood full geometric optimizations in Gaussian 03¹³⁵ at the B3LYP¹³⁶ level using the 6-31G* basis set¹³⁷, soliciting the lowest energy triplet state in each case. The triplet stabilization energy was determined by comparing the final energy of optimized structure of each compound to that of the lowest energy singlet state at the triplet-optimized geometry. In order to examine differences in the carbonyl out-of-

plane angles generated by the B3LYP calculation (vs. the MP2-level models reported elsewhere), a subset of these triplet-state species were geometrically optimized at the MP3 level¹³⁸ in Gaussian using the 6-31G* basis set.

Time Correlated Single Photon Counting Fluorescence

The experiments were conducted on a custom built instrument using a mode-locked, cavity-dumped Mira Optima 900f Ti:Sapphire system pumped by a 10W Verdi Laser from Coherent, Inc. (Santa Clara, CA) as the excitation source. The pulses were frequency tripled using an Inrad harmonic separator. The excitation wavelength was 281 nm and the fluorescence emission was measured at the emission maximum determined with a fluorescence spectrophotometer. The detection system was fitted with Oriel 27320 polarizers set to the magic angle (54.7) for fluorescent lifetime measurements, single-pass Scientech 9030 monochrometers, and Hamamatsu microchannel plate PMTs. Sample temperature was regulated using a Peltier thermoelectric temperature controller from Quantum Northwest (Spokane, WA). Data collection was performed using an SPC-630 PCI card from Becker and Hickl GmbH (Berlin, Germany). Data was collected to at least 60,000 peak counts for all of the decays. The fluorescent lifetimes were fit using the maximum entropy method implemented in Pulse5T (Maximum Entropy Data Consultants, Inc.). The analysis used 200 logarithmically spaced exponentials with a maximum of 15 ns. Discrete fitting was performed using standard iterative reconvolution techniques written in

Microsoft Excel. Samples were prepared by dissolving requisite quantities of precursors in 25 ml of 0.1 M LiOH to furnish ~ 1 mM concentrations.

Materials

All starting materials were obtained from Aldrich or Matrix Scientific, unless otherwise indicated. Solvents were distilled prior to use, employing phosphorus pentoxide (P₂O₅) and stored in flame-dried, argon purged round-bottom flasks containing activated molecular sieves. Ultrapure (18 MΩ) water was used in all instances.

Syntheses

1-(benzyloxy)-4-bromo-2-fluorobenzene, 122b. The general method of Freché, et al.¹³⁹ was followed. A solution of 4-bromo-2-fluorophenol (**122a**, 3.83 g, 20.0 mmol), benzyl bromide (2.38 ml, 20.0 mmol) and potassium carbonate (6.91 g, 50.0 mmol) in CH₃CN (30 ml) was stirred at room temperature for 15 h. The solution was diluted with 50 ml CH₂Cl₂, washed with water (3 × 30 ml), dried (magnesium sulfate), and concentrated to give 5.24 g (93%) of 1-(benzyloxy)-4-bromo-2-fluorobenzene, **122b**, as a white precipitate: Mp: 65–67 °C; IR (CHCl₃): 3020, 2987, 2684, 2304, 1498, 1421, 1265, 1217, 1051, 896, 738, 695 cm⁻¹; ¹H NMR (400 MHz, CDCl₃) δ 7.41 (m, 5H), 7.27 (dd, *J* = 6.36, *J* = 2.28, 1H), 7.26 (dt, *J* = 4.37, *J* = 2.00, 1H), 6.89 (t, *J* = 8.76, 1H), 5.13 (s, 2H); ¹³C NMR (125 MHz, CDCl₃) δ 154.23, 151.73, 146.06, 136.02, 128.88, 127.73, 120.14, 117.23, 115.86, 113.02, 71.90; ¹⁹F NMR (376 MHz,

CDCl₃ + drop CF₃CO₂H) δ -130.78; HRMS (EI): Calc'd for C₁₃H₁₀FBrO: 279.9899. Found: 279.9905.

1-(benzyloxy)-3-fluorophenyl)ethanone, 122c.¹⁴⁰ The general method of Kosugi, et al.¹⁴¹ was used. The experimental procedure is described with **129** (vide infra). White ppt., 89%, Mp: 79–81 °C; IR (CHCl₃): 3053, 2987, 1679, 1610, 1514, 1498, 1421, 1265, 1217, 1052, 896, 738, 696 cm⁻¹; ¹H NMR (400 MHz, CDCl₃) δ (ppm), 7.74 (dd, *J* = 11.33, *J* = 2.38, 1H), 7.69 (dd, *J* = 9.04, *J* = 1.59, 1H) 7.44, (m, 5H), 7.04 (t, *J* = 8.44, 1H), 5.23 (s, 2H), 2.55, (s, 3H); ¹³C NMR (125 MHz, CDCl₃) δ 196.05, 153.66, 151.16, 135.82, 130.92, 128.95, 127.57, 125.76, 116.36, 114.22, 71.25, 26.52; ¹⁹F NMR (376 MHz, CDCl₃ + drop CF₃CO₂H) -133.02; HRMS (M + H): Calc'd for C₁₅H₁₃FO₂: 245.0978. Found: 245.0951.

1-(4-(benzyloxy)-3-fluorophenyl)-2-bromoethanone, 122d. The general method of Paul, et al.¹⁴² was followed. A solution of **122c** (700 mg, 2.86 mmol) in 20 ml CH₂Cl₂ was cooled to 0 °C in an ice bath. Dioxane dibromide (773 mg, 3.15 mmol) was added and the resulting mixture stirred for 30 min. The ice bath was removed with continued stirring for another 60 min. GC/MS indicated the reaction to be complete. The solution was washed with water and CH₂Cl₂, the aqueous layer removed, and the residual layer dried with anhydrous MgSO₄, filtered, and evaporated under reduced pressure to yield an orange precipitate, 900 mg (2.58 mmol). Purification was cumbersome and unnecessary for completion of the supervening step, and hence was not pursued. ~95%. IR (CHCl₃): 3055, 2988, 1679, 1615, 1511, 1498, 1417, 1267, 1219, 1050, 891, 748, 696 cm⁻¹; ¹H NMR (400 MHz, CDCl₃) δ (ppm), 7.77 (dd, *J* =

10.00, $J = 2.38$, 1H), 7.72 (dd, $J = 7.05$, $J = 2.78$, 1H), 7.42 (m, 5H), 7.07 (t, $J = 8.43$, 1H), 5.24 (s, 2H), 4.37 (s, 2H); ^{19}F NMR (376 MHz, CDCl_3 + a drop $\text{CF}_3\text{CO}_2\text{H}$) δ (ppm), -133.12.

2-(4-(benzyloxy)-3-fluorophenyl)-2-oxoethyl-4-(tert-butoxycarbonyl-amino)-

butanoate, 122e. The general method of Hiyama, et al.¹⁴³ was utilized. A solution of 1-(4-(benzyloxy)-3-fluorophenyl)-2-bromoethanone, (**122d**, 900 mg, 2.78 mmol), potassium carbonate (1.15 mg, 8.35 mmol), 4-(tert-butoxycarbonylamino)butanoic acid (N-Boc-GABA, 678 mg, 3.33 mmol) in 50 ml of CH_3CN was stirred for 24 h at room temperature. The solution was washed with EtOAc, water, the aqueous phase discarded, and the resulting phase evaporated under reduced pressure. Flash column chromatography (5:1 Hexanes/EtOAc) afforded a white precipitate, 1.10 g (89%). Mp: 97-99 °C; IR (KBr): 3300, 3100-2800, 1742, 1701, 1600, 1517, 1437, 1400 1309, 1200, 1165, 953, 750, 700, 668 cm^{-1} ; ^1H NMR (400 MHz, CD_3CN) δ (ppm), 7.80 (dd, $J = 7.05$, $J = 2.47$, 1H), 7.78 (dd, $J = 7.05$, $J = 1.99$, 1H), 7.47 (dd, $J = 4.45$, $J = 1.78$, 1H), 7.42 (m, 5H), 5.31 (s, 2H), 5.25 (s, 2H), 2.97 (t, $J = 6.79$), 2.45 (t, $J = 7.59$ Hz, 2H), 1.76 (m, 2H), 1.40 (s, 9H); ^{13}C NMR (125 MHz, d^6 -DMSO) δ (ppm), 190.67, 172.51, 155.60, 152.30, 150.80, 135.82, 128.39, 128.14, 127.68, 126.93, 125.60, 115.28, 114.82, 77.45, 70.36, 66.12, 39.64, 30.63, 28.22, 24.96; ^{19}F NMR (376 MHz, CD_3CN + drop $\text{CF}_3\text{CO}_2\text{H}$) δ (ppm), -133.44; HRMS (M + Na): Calc'd for $\text{C}_{24}\text{H}_{28}\text{FNO}_6\text{Na}$: 468.1798. Found 468.1796.

4-(2-(3-fluoro-4-hydroxyphenyl)-2-oxoethoxy)-4-oxobutan-1-aminium-2,2,2-

trifluoroacetate, 122. The general method of Marsh, et al.¹⁴⁴ was followed. In a

flame-dried, 50 ml round bottomed flask containing 2-(4-(benzyloxy)-3-fluorophenyl)-2-oxoethyl-4-(tert-butoxy-carbonylamino)-butanoate, (**122e**, 850 mg, 1.91 mmol) was added 20 ml of freshly distilled TFA. Stirring continued for 24 h at room under ambient conditions. The solution was evaporated under reduced pressure and washed with EtOAc/water. The water layer was then extracted, frozen, then lyophilized, affording an adhesive precipitate, 550 mg (78%). IR (KBr): 3434, 3269, 3100-2800, 1741, 1693, 1610, 1553, 1420, 1201, 1050, 823, 759, 719 cm^{-1} ; ^1H NMR (400 MHz, D_2O) δ (ppm), 7.70 (d, $J = 9.03$, 2H), 7.12 (t, $J = 9.94$, 1H), 5.50 (s, 2H), 3.09 (t, $J = 7.59$, 2H), 2.66 (t, $J = 7.08$, 2H), 2.05 (m, 2H); ^{13}C NMR (125 MHz, MeOD) δ (ppm), 190.05, 172.06, 161.60, 152.27, 151.07, 150.33, 126.03, 125.33, 117.30, 115.33, 65.95, 38.54, 30.02, 22.48; ^{19}F NMR (376 MHz, D_2O) δ (ppm), -133.58; HRMS (M^+): Calc'd for $\text{C}_{12}\text{H}_{15}\text{FNO}_4$: 256.0985. Found 256.0977.

The methodology for generating compounds 123–132 was analogous to that for 122 unless otherwise indicated; the yields were consistent, as well, unless stated otherwise. Only spectroscopic data are included for each intermediate and the final caged derivatives.

1-(4-benzyloxy)-2-fluorophenyl)ethanone, 123c. **123b** is commercially available. White ppt., 90%, Mp: 97-99 $^\circ\text{C}$; IR (CHCl_3): 3056, 2992, 1701, 1616, 1510, 1487, 1415, 1275, 1207, 1055, 881, 728, 683 cm^{-1} ; ^1H NMR (400 MHz, CDCl_3) δ (ppm), δ 7.93 (t, $J = 7.76$, 1H), 7.40 (m, 5H), 6.85 (dd, $J = 8.96$, $J = 2.49$, 1H), 6.72 (dd, $J = 13.25$, $J = 2.39$, 1H), 5.15 (d, $J = 4.98$, 2H), 2.70 (s, 3H); ^{13}C NMR (125 MHz, CDCl_3) δ (ppm), 198.76, 165.25, 159.13, 135.54, 132.70, 128.78, 127.75, 118.13,

115.45, 114.03, 103.11, 70.96, 31.08; ^{19}F NMR (376 MHz, CDCl_3 + drop $\text{CF}_3\text{CO}_2\text{H}$) δ (ppm), -104.64; HRMS (M + H): Calc'd for $\text{C}_{15}\text{H}_{14}\text{FO}_2$: 245.0978. Found: 245.0962.

1-(4-(benzyloxy)-2-fluorophenyl)-2-bromoethanone, 123d. Oil, ~92%; IR (NaCl): 3058, 2990, 1711, 1621, 1510, 1486, 1413, 1265, 1227, 1063, 890, 725, 680 cm^{-1} ; ^1H NMR (400 MHz, CDCl_3) δ (ppm), δ 7.95 (t, $J = 8.84$, 1H), 7.40 (m, 5H), 6.89 (dd, $J = 8.84$, $J = 2.31$, 1H), 6.73 (dd, $J = 13.36$, $J = 2.50$, 1H), 5.15 (s, 2H), 4.49 (d, $J = 4.49$, $J = 2.50$, 2H); ^{13}C NMR (125 MHz, CDCl_3) δ (ppm), 189.31, 165.37, 159.17, 135.51, 132.68, 128.80, 127.75, 115.66, 115.45, 114.03, 102.99, 71.01, 35.73; ^{19}F NMR (376 MHz, CDCl_3 + drop $\text{CF}_3\text{CO}_2\text{H}$) δ (ppm), -104.68; HRMS (M + H): Calc'd for $\text{C}_{15}\text{H}_{13}\text{FO}_2\text{Br}$: 323.0083. Found: 323.0101.

2-(4-(benzyloxy)-2-fluorophenyl)-2-oxoethyl-4-(tert-butoxycarbonyl-amino)-butanoate, 123e. White ppt., 86%, Mp: 105–107 $^\circ\text{C}$; IR (KBr): 3303, 3100-2800, 1742, 1701, 1614, 1437, 1408, 1309, 1203, 1167, 955, 747, 700, 668 cm^{-1} ; ^1H NMR (400 MHz, $\text{d}^6\text{-DMSO}$) δ (ppm), δ 7.85 (t, $J = 8.94$, 1H), 7.40 (m, 5H), 7.10 (dd, $J = 13.59$, $J = 2.30$, 1H), 7.01 (dd, $J = 8.86$, $J = 2.42$, 1H), 6.88 (t, $J = 5.70$, 1H), 5.24 (s, 2H), 5.22 (d, $J = 3.25$, 2H), 2.98 (t, $J = 6.81$, 2H), 2.42 (t, $J = 7.60$, 2H), 1.70 (m, 2H), 1.38 (s, 9H); ^{13}C NMR (125 MHz, $\text{d}^6\text{-DMSO}$) δ (ppm), 188.97, 172.17, 164.26, 162.13, 155.60, 135.85, 131.75, 128.53, 127.96, 127.50, 115.05, 112.37, 102.82, 77.45, 70.04, 68.32, 39.30, 30.78, 28.22, 24.93; ^{19}F NMR (376 MHz, CD_3CN + drop $\text{CF}_3\text{CO}_2\text{H}$) δ (ppm), -106.01; HRMS (M + Na): Calc'd for $\text{C}_{24}\text{H}_{28}\text{FNO}_6\text{Na}$: 468.1798. Found: 468.1787.

4-(2-(2-fluoro-4-hydroxyphenyl)-2-oxoethoxy)-4-oxobutan-1-aminium-2,2,2-trifluoro-acetate, 123. Adhesive solid. IR (KBr): 3434, 3244, 3100-2800, 1741, 1693, 1610, 1523, 1421, 1400, 1309, 1269, 1198, 1166, 1050, 824, 800, 760, 720. cm^{-1} ; ^1H NMR (400 MHz, D_2O) δ (ppm), δ 7.85 (t, $J = 7.58$, 2H), 6.73 (d, $J = 9.09$, 1H), 5.40 (d, $J = 3.03$, 2H), 3.10 (t, $J = 7.64$, 2H), 2.64 (t, $J = 7.12$, 2H), 2.09 (m, 2H); ^{13}C NMR (125 MHz, D_2O) δ (ppm), 189.35, 172.10, 165.34, 165.02, 163.13, 133.68, 113.65, 113.39, 102.58, 68.71, 38.60, 30.06, 22.48; ^{19}F NMR (376 MHz, D_2O) δ (ppm), -106.45; HRMS (M^+): Calc'd for $\text{C}_{12}\text{H}_{15}\text{FNO}_4$: 256.0985. Found 256.0976.

1-(benzyloxy)-4-bromo-2,3-difluorobenzene, 124b.¹⁴⁵ Oil, 94%; IR (CHCl_3): 3058, 2982, 1600, 1510, 1465, 1250, 1202, 1050, 835, 740, 695 cm^{-1} ; ^1H NMR (400 MHz, CDCl_3) δ (ppm) 7.42 (m, 5H), 7.19 (dt, $J = 8.05$, $J = 2.50$, 1H), 6.90 (dt, $J = 8.00$, $J = 1.82$, 1H), 5.16 (s, 2H); ^{13}C NMR (125 MHz, CDCl_3) δ (ppm) 161.58, 149.74, 147.53, 135.60, 128.75, 127.50, 126.39, 117.38, 113.62, 101.35, 72.09; ^{19}F NMR (376 MHz, CDCl_3 + drop $\text{CF}_3\text{CO}_2\text{H}$) δ (ppm) -129.51, -154.65; HRMS (EI): Calc'd for $\text{C}_{13}\text{H}_9\text{F}_2\text{OBr}$: 297.9805. Found: 297.9822.

1-(4-(benzyloxy)-2,3-difluorophenyl)ethanone, 124c. White ppt., 88%, Mp: 96–98 $^\circ\text{C}$; IR (KBr): 3055, 2990, 1695, 1614, 1464, 1448, 1380, 1275, 1202, 1051, 880, 725, 680 cm^{-1} ; ^1H NMR (400 MHz, CDCl_3) δ (ppm) 7.69 (dt, $J = 9.39$, $J = 2.24$, 1H), 7.39 (m, 6H), 6.90 (dt, $J = 8.00$, $J = 1.82$, 1H), 5.26 (s, 2H), 2.71 (d, $J = 5.38$, 3H); ^{13}C NMR (125 MHz, CDCl_3) δ (ppm) 198.21, 160.44, 141.88, 140.59, 134.96, 128.75, 127.46, 118.93, 116.46, 113.62, 109.67, 71.67, 30.86; ^{19}F NMR (376 MHz,

CDCl₃ + drop CF₃CO₂H) δ (ppm) -132.74, -158.39; HRMS (M + H): Calc'd for C₁₅H₁₃F₂O₂: 263.0884. Found: 263.0887.

1-(4-(benzyloxy)-2,3-difluorophenyl)-2-bromoethanone, 124d. Oil, ~96%; ¹H NMR (400 MHz, CDCl₃) δ (ppm) 7.71 (dt, *J* = 8.44, *J* = 2.38, 1H), 7.41 (s, 5H), 6.92 (dt, *J* = 7.80, *J* = 1.90, 1H), 5.27 (s, 2H), 4.46 (d, *J* = 2.48, 2H); ¹³C NMR (125 MHz, CDCl₃) δ (ppm) 198.61, 160.37, 153.65, 140.38, 135.11, 128.93, 125.60, 117.97, 113.44, 109.93, 71.96, 31.02; ¹⁹F NMR (376 MHz, CDCl₃ + drop CF₃CO₂H) δ (ppm), -132.93, -158.06.

2-(4-(benzyloxy)-2,3-difluorophenyl)-2-oxoethyl-4-(tert-butoxycarbonyl-amino)-butanoate, 124e. White ppt., 84%, Mp: 115–117 °C; IR (KBr): 3300, 3100–2800, 1742, 1701, 1664, 1619, 1436, 1406, 1200, 1169, 1136, 955, 749, 700, 670, cm⁻¹; ¹H NMR (400 MHz, d⁶-DMSO) δ (ppm) 7.71 (dt, *J* = 8.38, *J* = 2.22, 1H), 7.41 (m, 5H), 7.29 (dt, *J* = 8.22, *J* = 1.57, 1H), 6.88 (t, *J* = 5.76, 1H), 5.34 (s, 2H), 5.25 (d, *J* = 2.82, 2H), 2.96 (t, *J* = 6.85, 2H), 2.44 (t, *J* = 7.55, 2H), 1.67 (m, 2H), 1.37 (s, 9H); ¹³C NMR (125 MHz, d⁶-DMSO) δ (ppm) 188.76, 172.13, 155.60, 152.08, 149.66, 142.12, 141.00, 139.04, 128.60, 128.02, 124.86, 116.21, 110.59, 72.91, 69.81, 69.72, 40.79, 32.09, 29.01, 26.49; ¹⁹F NMR (376 MHz, CD₃CN + drop CF₃CO₂H) δ (ppm) -158.62, -133.05; HRMS (M + Na): Calc'd for C₂₄H₂₇F₂NO₆Na: 486.1704. Found: 486.1689.

4-(2-(2,3-difluoro-4-hydroxyphenyl)-2-oxoethoxy)-4-oxobutan-1-aminium 2,2,2-trifluoroacetate, 124. Adhesive ppt., 92%; IR (KBr): 3435, 3246, 3100–2800, 1739, 1694, 1610, 1525, 1420, 1400, 1310, 1269, 1200, 1165, 1049, 825, 800, 759, 720.

cm⁻¹; ¹H NMR (400 MHz, D₂O) δ (ppm) 7.43 (d, *J* = 6.57, 1H), 6.75 (d, *J* = 9.34, 1H), 5.18 (d, *J* = 2.64, 2H), 3.04 (t, *J* = 6.81, 2H), 2.60 (t, *J* = 7.53, 2H), 1.97 (m, 2H); ¹³C NMR (125 MHz, D₂O) δ (ppm) 191.36, 173.96, 163.08, 151.57, 140.64, 138.70, 128.71, 119.79, 117.47, 113.20, 68.83, 38.34, 30.09, 21.61; ¹⁹F NMR (376 MHz, D₂O) δ (ppm) -133.71, -162.58; HRMS (M⁺): Calc'd for C₁₂H₁₄F₂NO₄: 274.0891. Found: 274.0884.

1-(benzyloxy)-4-bromo-2,5-difluorobenzene, 125b. White ppt., 91%, Mp: 58–60 °C; IR (CHCl₃): 3002, 2943, 1618, 1508, 1419, 1406, 1375, 1334, 1188, 1170, 1039, 840, 748, 702; ¹H NMR (400 MHz, CDCl₃) δ (ppm), 7.37 (m, 5H), 7.29 (dd, *J* = 6.64, *J* = 3.82, 1H), 6.82 (dd, *J* = 7.19, *J* = 2.68, 1H), 5.12 (s, 2H); ¹³C NMR (125 MHz, CDCl₃) δ (ppm), 154.82, 150.45, 148.49, 147.28, 135.96, 129.35, 128.03, 120.47, 104.54, 98.93, 72.22; ¹⁹F NMR (376 MHz, CDCl₃ + drop CF₃CO₂H) δ (ppm), -111.53, -137.66; HRMS (EI): Calc'd for C₁₃H₉F₂BrO: 297.9805. Found: 297.9833.

1-(4-(benzyloxy)-2,5-difluorophenyl)ethanone, 125c. White ppt., 89%, Mp: 89–91 °C; IR (CHCl₃): 3060, 3002, 2943, 1681, 1625, 1508, 1411, 1398, 1375, 1334, 1186, 1159, 1039, 744, 702; ¹H NMR (400 MHz, CD₃CN) δ (ppm), 7.60 (dd, *J* = 6.88, *J* = 4.78, 1H), 7.43 (m, 5H), 7.00 (dd, *J* = 6.73, *J* = 5.93, 1H), 5.20 (s, 2H), 2.54 (d, *J* = 5.18, 3H); ¹³C NMR (125 MHz, CD₃CN) δ (ppm), 194.65, 159.45, 158.50, 148.92, 136.38, 130.69, 129.43, 118.88, 117.28, 115.01, 104.46, 72.74, 31.59; ¹⁹F NMR (376 MHz, CD₃CN + drop CF₃CO₂H) δ (ppm), -110.97, -140.38; HRMS (EI): Calc'd for C₁₅H₁₂F₂O₂: 262.0805. Found: 262.0791.

1-(4-(benzyloxy)-2,5-difluorophenyl)-2-bromoethanone, 125d. Oil ~94%; IR (NaCl): 3055, 3008, 2942, 1691, 1624, 1511, 1406, 1395, 1357, 1332, 1181, 1150, 1039, 790, 744, 702; ¹H NMR (400 MHz, CDCl₃) δ (ppm), 7.70 (dd, *J* = 6.69, *J* = 4.59, 1H), 7.43 (m, 5H), 6.78 (dd, *J* = 6.50, *J* = 5.73, 1H), 5.22 (s, 2H), 4.46 (d, *J* = 2.89, 3H).

2-(4-(benzyloxy)-2,5-difluorophenyl)-2-oxoethyl-4-(*tert*-butoxycarbonyl-amino)butanoate, 125e. White ppt., 92%, Mp: 118–120 °C; IR (KBr): 3303, 3100-2800, 1741, 1701, 1657, 1623, 1512, 1437, 1407, 1203, 1165, 1144, 953, 897, 750, 699, 667, cm⁻¹; ¹H NMR (400 MHz, d⁶-DMSO) δ (ppm), 7.69 (dd, *J* = 6.66, *J* = 4.91, 1H), 7.43 (m, 6H), 6.89 (t, *J* = 5.62, 1H), 5.32 (d, 2H), 5.23 (d, *J* = 3.33, 2H), 2.97 (t, *J* = 6.79, 2H), 2.44 (t, 2H), 1.68 (m, 2H), 1.38 (s, 9H); ¹³C NMR (125 MHz, d⁶-DMSO) δ (ppm), 188.50, 172.14, 159.73, 155.59, 151.91, 149.05, 147.12, 135.26, 128.48, 128.10, 115.36, 114.11, 103.96, 77.46, 70.96, 68.25, 38.97, 30.61, 28.22, 24.92; HRMS (M + Na): Calc'd for C₂₄H₂₇F₂NO₆Na: 486.1704. Found: 486.1702.

4-(2-(2,5-difluoro-4-hydroxyphenyl)-2-oxoethoxy)-4-oxobutan-1-aminium-2,2,2-trifluoroacetate, 125. Adhesive ppt., 75%; IR (KBr): 3440, 3246, 3100-2800, 1736, 1695, 1610, 1525, 1422, 1398, 1310, 1269, 1200, 1167, 1049, 825, 800, 760, 718. cm⁻¹; ¹H NMR (400 MHz, MeOD) δ (ppm), 7.62 (dd, *J* = 6.40, *J* = 4.73, 1H), 6.81 (d, *J* = 6.75, 1H), 5.26 (d, *J* = 3.54, 2H), 3.10 (t, *J* = 7.59, 2H), 2.67 (t, *J* = 7.08, 2H), 2.05 (m, 2H); ¹³C NMR (125 MHz, MeOD) δ (ppm), 188.62, 172.02, 160.69, 158.70, 152.48, 149.40, 147.48, 115.53, 113.04, 104.71, 68.77, 38.55, 29.99, 22.48; ¹⁹F NMR

(376 MHz, MeOD) δ (ppm), -110.81, -141.90; HRMS (M⁺): Calc'd for C₁₂H₁₄NF₂O₄: 274.0891. Found: 274.0878.

2-(benzyloxy)-5-bromo-1,3-difluorobenzene, 126b. Oil, 98%; IR (NaCl): 3091, 2948, 1595, 1581, 1494, 1454, 1382, 1220, 1190, 1037, 840, 750, 696; ¹H NMR (400 MHz, CDCl₃) δ (ppm), 7.41, (m, 5H), 7.08 (d, *J* = 7.70, 2H), 5.17 (s, 2H); ¹³C NMR (125 MHz, CDCl₃) δ (ppm), 155.74, 136.37, 134.91, 129.60, 118.28, 116.52, 113.03, 109.48, 66.85; ¹⁹F NMR (376 MHz, CDCl₃ + drop CF₃CO₂H) δ (ppm), -125.93; HRMS (EI): Calc'd for C₁₃H₉F₂BrO: 297.9805. Found: 297.9815.

1-(4-(benzyloxy)-3,5-difluorophenyl)ethanone, 126c. Oil, 91%; IR (NaCl): 3033, 2927, 1689, 1616, 1577, 1508, 1454, 1433, 1360, 1197, 1041, 975, 750, 696; ¹H NMR (400 MHz, CD₃CN) δ (ppm), 7.49 (dd, *J* = 9.24, 2H), 7.41 (m, 5H), 7.36 (d, 1H), 5.30 (s, 2H) 2.57 (s, 3H); ¹³C NMR (125 MHz, CD₃CN) δ (ppm), 194.88, 156.50, 154.11, 135.99, 131.77, 128.39, 128.18, 113.32, 111.00, 75.48, 25.49; ¹⁹F NMR (376 MHz, CD₃CN + drop CF₃CO₂H) δ (ppm), -127.25; HRMS (EI): Calc'd for C₁₅H₁₂F₂O₂: 262.0805. Found: 262.0816.

1-(4-(benzyloxy)-3,5-difluorophenyl)-2-bromoethanone, 126d. Oil, ~95%; IR (NaCl): 3035, 2922, 1692, 1621, 1577, 1516, 1446, 1425, 1369, 1205, 1041, 965, 749, 696; ¹H NMR (400 MHz, CDCl₃) δ (ppm), 7.55 (d, *J* = 6.54, 2H), 7.43 (m, 5H), 5.34 (s, 2H) 4.41 (s, 3H); ¹⁹F NMR (376 MHz, CDCl₃ + drop CF₃CO₂H) δ (ppm), -127.88.

2-(4-(benzyloxy)-3,5-difluorophenyl)-2-oxoethyl-4-(tert-butoxycarbonyl-amino) butanoate, 126e. Adhesive ppt., 93%; IR (KBr) 3302, 3230, 3100-2800, 1742, 1700,

1660, 1621, 1518, 1426, 1407, 1202, 1152, 951, 748, 698, 672 cm^{-1} ; ^1H NMR (400 MHz, CD_3CN) δ (ppm), 7.56 (d, $J = 6.32$, 2H), 7.43 (m, 5H), 5.32 (s, 2H), 5.08 (s, 2H), 3.09 (t, $J = 6.83$, 2H), 2.45 (t, $J = 7.58$, 2H), 1.76 (m, 2H), 1.40 (s, 9H); ^{13}C NMR (125 MHz, $\text{d}^6\text{-DMSO}$) δ (ppm), 193.45, 172.21, 160.02, 156.10, 151.72, 149.22, 146.32, 135.30, 128.76, 128.18, 115.54, 113.99, 105.01, 76.91, 69.95, 68.01, 39.30, 30.61, 28.20, 24.85; ^{19}F NMR (376 MHz, CD_3CN) δ (ppm), -127.82; HRMS (M + Na): Calc'd for $\text{C}_{24}\text{H}_{27}\text{F}_2\text{NO}_6\text{Na}$: 486.1704. Found: 486.1700.

4-(2-(3,5-difluoro-4-hydroxyphenyl)-2-oxoethoxy)-4-oxobutan-1-aminium2,2,2-trifluoroacetate, 126. White ppt., 82%, Mp: 85–87 °C; IR (KBr): 3435, 3238, 3100–2800, 1740, 1695, 1608, 1524, 1420, 1399, 1310, 1270, 1200, 1165, 1050, 823, 800, 759, 720. cm^{-1} ; ^1H NMR (400 MHz, MeOD) δ (ppm), 7.63 (d, $J = 7.41$, 2H), 5.39 (d, 2H), 3.07 (t, $J = 7.33$, 2H), 2.64 (t, $J = 7.09$, 2H), 2.05 (m, 2H); ^{13}C NMR (125 MHz, MeOD) δ (ppm), 194.16, 175.94, 157.12, 155.17, 155.12, 144.00, 132.59, 128.13, 115.39, 69.88, 42.47, 33.93, 26.42; ^{19}F NMR (376 MHz, MeOD) δ (ppm), -133.62; HRMS (M+): Calc'd for $\text{C}_{12}\text{H}_{14}\text{F}_2\text{NO}_4$: 274.0891. Found: 274.0884.

1-(4-benzyloxy)-2,6-difluorophenyl)ethanone, 127c. 5-(benzyloxy)-2-bromo-1,3-difluorobenzene, **127b**, was generated by the same method as for **122b**, determined to be pure by ^1H NMR and GC/MS and utilized in the synthesis of **127c**. Oil, 97%; IR (NaCl): 3035, 2930, 1696, 1610, 1571, 1500, 1451, 1433, 1360, 1199, 1043, 978, 748, 695; ^1H NMR (400 MHz, CDCl_3) δ (ppm), 7.39 (m, 5H), 6.62 (dt, $J = 8.07$, $J = 5.08$, 2H), 5.08 (s, 2H) 2.56 (dd, $J = 1.85$, 3H); ^{13}C NMR (125 MHz, CDCl_3) δ (ppm), 193.78, 163.12, 162.20, 161.02, 134.26, 128.74, 127.74, 111.05, 99.54; ^{19}F NMR

(376 MHz, CD₃CN + drop CF₃CO₂H) δ (ppm), -108.33; HRMS (EI): Calc'd for C₁₅H₁₂F₂O₂: 262.0805. Found: 262.0812.

1-(4-benzyloxy)-2,6-difluorophenyl)-2-bromoethanone, 127d. Oil, ~95%; ¹H NMR (400 MHz, CDCl₃) δ (ppm), 7.45 (m, 5H), 6.61 (dt, *J* = 10.47, *J* = 5.32, 2H), 5.10 (s, 2H), 4.35 (s, 2H).

2-(4-(benzyloxy)-2,6-difluorophenyl)-2-oxoethyl-4-(tert-butoxycarbonyl-amino)-butanoate, 127e. White ppt., 90%, Mp: 69–71 °C; IR (KBr): 3304, 3100-2800, 1742, 1703, 1652, 1630, 1437, 1407, 1201, 1153, 1133, 1049, 953, 750, 699, 667, cm⁻¹; ¹H NMR (400 MHz, d⁶-DMSO) δ (ppm), 7.43 (m, 5H), 6.97 (dd, *J* = 11.14, *J* = 4.46, 1H), 6.89 (t, *J* = 5.95, 1H), 5.22 (s, 2H), 5.08 (s, 2H), 2.95 (t, *J* = 6.80, 2H), 2.41 (t, *J* = 7.59, 2H), 1.65 (m, 2H), 1.37 (s, 9H); ¹³C NMR (125 MHz, d⁶-DMSO) δ (ppm), 188.75, 172.12, 163.10, 162.68, 160.75, 155.59, 135.51, 128.88, 128.33, 128.06, 106.77, 106.49, 100.06, 76.33, 69.63, 67.69, 38.01, 29.40, 24.70; ¹⁹F NMR (376 MHz, d⁶-DMSO) δ (ppm), -108.41; HRMS (M + Na): Calc'd for C₂₄H₂₇F₂NO₆Na: 486.1704. Found: 486.1682.

4-2-(2,6-difluoro-4-hydroxyphenyl)-2-oxoethoxy)-4-oxobutan-1-aminium 2,2,2-trifluoroacetate, 127. White ppt., 86%, Mp: 85–87 °C; IR (KBr): 3438, 3245, 3100-2800, 1741, 1694, 1610, 1525, 1420, 1400, 1310, 1268, 1200, 1165, 1050, 825, 800, 758, 720. cm⁻¹; ¹H NMR (400 MHz, MeOD) δ (ppm) 7.41 (d, 1H), 6.54 (d, *J* = 13.06, 2H), 5.10 (s, 2H), 3.09 (t, *J* = 7.59, 2H), 2.59 (t, *J* = 7.05, 2H), 2.00 (m, 2H); ¹³C NMR (125 MHz, D₂O) δ (ppm) 188.59, 171.98, 163.70, 162.48, 161.56, 128.75,

117.38, 99.68, 68.98, 38.52, 30.07, 22.45; ^{19}F NMR (376 MHz, D_2O) δ (ppm) - 109.55; HRMS (M^+): Calc'd for $\text{C}_{12}\text{H}_{14}\text{F}_2\text{NO}_4$: 274.0891. Found: 274.08879.

2-(benzyloxy)-5-bromo-1,3,4-trifluorobenzene, 128b. Oil, 94%; IR (NaCl): 3033, 2952, 1629, 1598, 1487, 1475, 1456, 1190, 1089, 1018, 821, 744, 696 cm^{-1} ; ^1H NMR (400 MHz, CDCl_3) δ 7.38 (m, 5H), 7.11-7.09 (qd, $J = 2.54$, 1H), 5.22 (s, 2H); ^{13}C NMR (125 MHz, CDCl_3) δ 152.73, 150.75, 135.53, 129.06, 128.65, 128.45, 115.38, 114.56, 113.11, 102.41, 98.93, 66.31; ^{19}F NMR (376 MHz, $\text{CDCl}_3 + \text{drop CF}_3\text{CO}_2\text{H}$) δ -131.82, -133.66, -147.45; HRMS (EI): Calc'd for $\text{C}_{13}\text{H}_8\text{F}_3\text{BrO}$: 315.9711. Found: 315.9712.

1-(4-(benzyloxy)-2,3,5-trifluorophenyl)ethanone, 128c. White ppt., 84%, Mp: 45–47 °C; IR (CHCl_3): 3002, 2943, 1691, 1627, 1500, 1375, 1346, 1081, 1039, 918, 750, 702 cm^{-1} ; ^1H NMR (400 MHz, CDCl_3) δ 7.45 (m, 6H), 5.37 (s, 2H), 2.68 (s, 3H); ^{13}C NMR (125 MHz, CDCl_3) δ 194.74, 152.20, 150.23, 147.94, 143.62, 135.58, 128.77, 119.68, 118.10, 115.83, 113.56, 66.45, 31.39; ^{19}F NMR (376 MHz, $\text{CDCl}_3 + \text{drop CF}_3\text{CO}_2\text{H}$) δ -131.10, -136.69, -149.56. HRMS (EI): Calc'd for $\text{C}_{15}\text{H}_{11}\text{F}_3\text{O}_2$: 280.0711. Found: 280.0717.

1-(4-(benzyloxy)-2,3,5-trifluorophenyl)-2-bromoethanone, 128d. Oil, ~94%; IR (CHCl_3): 3000, 2945, 1698, 1624, 1502, 1369, 1352, 1081, 1045, 921, 750, 699. ^1H NMR (400 MHz, CDCl_3) δ (ppm) 7.53–7.51 (qd, $J = 2.30$, 1H), 7.40 (m, 5H), 5.25 (d, 2H), 4.45 (s, 2H).

2-(4-(benzyloxy)-2,3,5-trifluorophenyl)-2-oxoethyl-4-(tert-butoxy-carbonyl-amino)butanoate, 128e. White ppt., 93%, Mp: 110–112 °C; IR (KBr) 3302, 3100-

2800, 1743, 1703, 1651, 1629, 1437, 1407, 1202, 1170, 1147, 950, 748, 698, 667 cm^{-1} ; ^1H NMR (400 MHz, d^6 -DMSO) δ (ppm), 7.62-7.60 (qd, $J = 2.30$, 1H), 7.41 (m, 5H), 6.88, (t, $J = 6.00$, 1H), 5.40 (s, 2H), 5.26 (s, 2H), 2.96 (t, $J = 6.82$, 2H), 2.44 (t, $J = 7.60$, 2H), 1.67 (m, 2H), 1.38 (s, 9H); ^{13}C NMR (125 MHz, d^6 -DMSO) δ (ppm), 188.33, 172.09, 155.60, 151.48, 149.53, 148.47, 146.44, 144.63, 142.83, 140.05, 128.55, 116.87, 110.58, 77.46, 75.71, 68.22, 30.53, 28.21, 24.89; HRMS (M + Na): Calc'd for $\text{C}_{24}\text{H}_{26}\text{F}_3\text{NO}_6\text{Na}$: 504.1610. Found: 504.1593.

4-oxo-4-(2-oxo-2-(2,3,5-trifluoro-4-hydroxyphenyl) ethoxy) butan-1-aminium 2,2,2-trifluoroacetate, 128. White ppt., 90%, Mp: 131–133 $^{\circ}\text{C}$; IR (KBr): 3434, 3244, 3100-2800, 1738, 1695, 1610, 1523, 1420, 1400, 1309, 1267, 1199, 1166, 1049, 824, 800, 759, 720 cm^{-1} ; ^1H NMR (400 MHz, D_2O) δ (ppm), 7.52-7.50 (qd, $J = 2.35$, 1H), 5.37 (d, 2H), 3.14 (t, $J = 7.06$, 2H), 2.72 (t, $J = 6.71$, 2H), 2.07 (m, 2H); ^{13}C NMR (125 MHz, D_2O) δ (ppm), 190.89, 174.05, 163.12, 149.21, 147.28, 141.03, 139.81, 117.19, 115.16, 109.89, 69.88, 42.47, 33.93, 26.42; ^{19}F NMR (376 MHz, D_2O) δ (ppm), -136.48, -137.81, -156.79; HRMS (M⁺): Calc'd for $\text{C}_{12}\text{H}_{13}\text{F}_3\text{NO}_4$: 292.0797. Found: 292.0794.

1-(benzyloxy)-4-bromo-2,3,5,6-tetrafluorobenzene, 129b. White ppt., 96%, Mp: 43–45 $^{\circ}\text{C}$; IR (CHCl_3): 3002, 2943, 1560, 1458, 1442, 1407, 1380, 1039, 918, 750; ^1H NMR (400 MHz, CDCl_3) δ (ppm) 7.39 (m, 5H), 5.28 (s, 2H); ^{13}C NMR (125 MHz, CDCl_3) δ (ppm) 146.18, 144.22, 144.11, 140.70, 135.25, 129.04, 128.72, 93.26, 76.51; ^{19}F NMR (376 MHz, CDCl_3 + drop $\text{CF}_3\text{CO}_2\text{H}$) δ (ppm) -131.37, -155.12. HRMS (EI): Calc'd for $\text{C}_{13}\text{H}_7\text{F}_4\text{BrO}$: 333.9616. Found: 333.9606.

1-(4-(benzyloxy)-2,3,5,6-tetrafluorophenyl)ethanone, 129c. A solution of **129b** (1.00g 2.98 mmol), tributyl(1-ethoxyvinyl)stannane (1.44 ml, 4.27 mmol) and 25 ml toluene was degassed for 30 min while stirring. Tetrakis(triphenylphosphine) palladium (0) (205 mg, 0.178 mmol) was then added and the solution heated to 100 °C overnight with stirring. Fifty ml of 50% HCl (aq) were added and the solution stirred for 6 h, followed by filtration through Celite that effectively removed the palladium black. The resulting toluene filtrate was charged with 50 ml of saturated aqueous potassium fluoride and continuously stirred for 12 h. The insoluble tributylfluorostannane was then filtered, the aqueous layer removed, and the organic layer concentrated. Flash column chromatography (6:1 Hex/Et₂O) afforded 1-(4-(benzyloxy)-2,3,5,6-tetrafluorophenyl)ethanone, **129c**, in 85% yield (755 mg) as a faint yellow solid. Mp: 47–49 °C; IR (CDCl₃): 2921, 2852, 1712, 1643, 1461, 1377, 1190, 1100, 742, 723, 696 cm⁻¹; ¹H NMR (400 MHz, CDCl₃) δ (ppm) 7.38 (m, 5H), 5.27 (s, 2H), 2.59 (t, *J* = 1.90, 3H); ¹³C NMR (125 MHz, CDCl₃) δ (ppm) 192.07, 146.39, 143.95, 142.52, 139.89, 135.28, 129.27, 128.46, 66.07, 32.70; ¹⁹F NMR (376 MHz, CDCl₃ + drop CF₃CO₂H) δ (ppm) -144.22, -161.88; HRMS (M + H): Calc'd for C₁₅H₁₁F₄O₂: 299.0695. Found: 299.0702.

1-(4-(benzyloxy)-2,3,5,6-tetrafluorophenyl)-2-bromoethanone, 129d. Oil, ~99%; IR (CHCl₃): 2919, 2856, 1721, 1645, 1453, 1379, 1190, 1107, 745, 715, 696; ¹H NMR (400 MHz, CDCl₃) δ (ppm) 7.40 (m, 5H), 5.35 (s, 2H), 4.32 (t, *J* = 1.20, 2H).

2-(4-(benzyloxy)-2,3,5,6-tetrafluorophenyl)-2-oxoethyl-4-(tert-butoxycarbonyl-amino)butanoate, 129e. White ppt., 87%, Mp: 106–108 °C; IR (KBr) 3301, 3100-

2800, 1744, 1703, 1655, 1615, 1487, 1437, 1407, 1210, 1153, 1050, 749, 700, 667 cm^{-1} ; ^1H NMR (400 MHz, d^6 -DMSO) δ (ppm) 7.42 (m, 5H), 6.88, (t, $J = 5.92$, 1H), 5.43 (s, 2H), 5.02 (t, $J = 1.43$, 2H), 2.93 (t, $J = 6.74$, 2H), 2.41 (t, $J = 7.57$, 2H), 1.65 (m, 2H), 1.37 (s, 9H); ^{13}C NMR (125 MHz, d^6 -DMSO) δ (ppm), 188.04, 172.14, 155.59, 145.97, 143.96, 141.32, 139.47, 135.39, 128.64, 128.39, 109.10, 77.46, 76.14, 68.81, 30.39, 28.82, 24.82; HRMS (M + Na): Calc'd for $\text{C}_{24}\text{H}_{25}\text{F}_4\text{NO}_6\text{Na}$: 522.1516. Found: 522.1493.

4-oxo-4-(2-oxo-2-(2,3,5,6-tetrafluoro-4-hydroxyphenyl)ethoxy)butan-1-aminium-2,2,2-trifluoroacetate, 129. White ppt., 83%, Mp: 107–109 °C; IR (KBr): 3440, 3241, 3100-2800, 1735, 1690, 1610, 1525, 1420, 1400, 1310, 1265, 1200, 1166, 1050, 824, 800, 759, 720. cm^{-1} ; ^1H NMR (400 MHz, D_2O) δ (ppm), 5.25 (t, $J = 1.67$, 2H), 3.07 (t, $J = 7.61$, 2H), 2.66 (t, $J = 7.06$, 2H), 2.01 (m, 2H); ^{13}C NMR (125 MHz, D_2O) δ (ppm), 189.10, 173.25, 162.36, 147.43, 139.18, 129.31, 117.78, 113.12, 104.46, 69.40, 38.59, 30.13, 22.22; ^{19}F NMR (376 MHz, D_2O) δ (ppm), -142.76, -163.05; HRMS (M⁺): Calc'd for $\text{C}_{12}\text{H}_{12}\text{F}_4\text{NO}_4$: 310.0702. Found: 310.0701.

1-benzyloxy-4-bromo-2-trifluoromethylbenzene, 130b. Oil, 93%; IR (NaCl): 3033, 2935, 1602, 1490, 1454, 1139, 1053, 908, 811, 732 cm^{-1} ; ^1H NMR (400 MHz, CDCl_3) δ (ppm), 7.71 (d, $J = 2.56$, 1H), 7.56 (d, $J = 2.56$, 1H), 7.38 (m, 5H), 6.90 (d, $J = 8.91$, 1H), 5.19 (s, 2H); ^{13}C NMR (125 MHz, CDCl_3) δ (ppm), 155.66, 135.89, 130.29, 129.19, 128.58, 127.02, 124.31, 121.59, 120.81, 115.22, 112.45; ^{19}F NMR (376 MHz, CDCl_3 + drop $\text{CF}_3\text{CO}_2\text{H}$) δ (ppm), -63.49; HRMS (EI): Calc'd for $\text{C}_{14}\text{H}_{10}\text{F}_3\text{BrO}$: 329.9867. Found: 329.9850.

1-(4-benzyloxy-3-trifluoromethylphenyl)ethanone, 130c. White ppt., 84%, Mp: 119-121 °C; IR (CHCl₃): 3055, 2987, 2829, 1685, 1610, 1421, 1265, 1141, 896, 738, 696 cm⁻¹; ¹H NMR (400 MHz, CDCl₃) δ (ppm), 8.23 (d, *J* = 2.10, 1H), 8.11 (dd, *J* = 8.78, *J* = 2.29, 1H), 7.44 (m, 5H), 7.09 (d, *J* = 8.80, 1H), 5.29 (s, 2H), 2.59 (s, 3H); ¹³C NMR (125 MHz, CDCl₃) δ (ppm), 201.19, 159.89, 135.05, 129.10, 128.5, 127.04, 124.49, 121.78, 119.35, 116.09, 113.26, 110.42, 71.02, 26.11; ¹⁹F NMR (376 MHz, CDCl₃ + drop CF₃CO₂H) δ (ppm), -63.77; HRMS (EI): Calc'd for C₁₆H₁₄F₃O₂: 295.0946. Found: 295.0927.

1-(4-benzyloxy-3-trifluoromethylphenyl)-2-bromoethanone, 130d. Oil, ~93%; IR (CHCl₃): 3058, 2989, 2821, 1687, 1605, 1421, 1255, 1139, 892, 740, 690 cm⁻¹; ¹H NMR (400 MHz, CDCl₃) δ (ppm), 7.90 (dd, *J* = 8.96, *J* = 2.15, 2H), 7.43 (m, 5H), 7.06 (d, *J* = 8.90, 1H), 5.31 (s, 2H), 4.39 (s, 2H); ¹⁹F NMR (376 MHz, CDCl₃ + drop CF₃CO₂H) δ (ppm), -63.81.

2-(4-benzyloxy-3-trifluoromethylphenyl)-2-oxoethyl-4-(tert-butoxycarbonyl-amino)butanoate, 130e. White ppt., 87%, Mp: 112-114°C; IR (KBr) 3304, 3100-2800, 1741, 1701, 1659, 1612, 1508, 1437, 1407, 1218, 1167, 1137, 1053, 1008, 741, 699, 667; ¹H NMR (400 MHz, d⁶-DMSO) δ (ppm), 8.26 (dd, *J* = 8.64, *J* = 2.20, 1H), 8.15 (d, *J* = 1.50, 1H), 7.43 (m, 5H), 7.34 (t, *J* = 7.15, 1H), 6.88 (t, *J* = 7.25, 1H), 5.48 (s, 2H), 5.41 (s, 2H), 2.98 (t, *J* = 6.74, 2H), 2.44 (t, *J* = 7.63, 2H), 1.70 (m, 2H), 1.38 (s, 9H); ¹³C NMR (125 MHz, d⁶-DMSO) δ(ppm), 190.79, 172.18, 159.87, 155.60, 135.73, 133.10, 132.00, 131.42, 128.69, 127.94, 126.44, 124.27, 122.10, 119.93, 117.63, 114.27, 77.45, 70.21, 66.16, 38.97, 28.22, 26.47, 24.96; ¹⁹F NMR (376 MHz,

CD₃CN + drop CF₃CO₂H) δ (ppm), -61.41; HRMS (M + Na): Calc'd for C₂₅H₂₈F₃NO₆Na: 518.1766. Found 518.1756.

2-(4-hydroxy-3-(trifluoromethyl)phenyl)-2-oxoethyl4-(tert-butoxy-carbonyl)-aminobutanoate, 130e'. The general method of Theodorakis¹⁴⁶ was employed. To a solution of **130e** (1.10g, 2.22 mmol) in 25 ml EtOAc was added 220 mg of 10% Pd/C, and the heterogenous mixture stoppered with a septum. While stirring, hydrogen (H₂) was infused through a needle into the solution. The reaction was completed ~ 2h as indicated by TLC. The residual Pd/C was filtered off through Celite and the organic phase concentrated under reduced pressure to yield 875 mg of **130e'** as an adhesive precipitate (97%); ¹H NMR (400 MHz, d⁶-DMSO) δ (ppm), 11.60 (s, 1H), 8.10 (dd, $J = 8.80, J = 2.10$, 1H), 7.25 (t, $J = 8.00$, 1H), 7.15 (d, $J = 7.70$, 1H), 6.90 (t, $J = 7.20$, 1H), 5.48 (s, 2H) 2.96 (t, $J = 6.90$, 2H), 2.42 (t, $J = 7.50$, 2H), 1.66 (m, 2H), 1.38 (s, 9H).

4-(2-(4-hydroxy-3-trifluoromethylphenyl)-2-oxoethoxy)-4-oxobutan-1-amonium 2,2,2-trifluoroacetate, 130. A modified preparation of Marsh's¹³ technique was utilized. To a round bottomed flask containing **130e'** (800 mg, 1.97 mmol) was added 20 ml of 1:1 TFA/CH₂Cl₂. The reaction persisted for 15 min while stirring and at room temperature. At this time, excess solvent was removed under reduced pressure, washed with 50 ml of 1:1 CH₂Cl₂/H₂O and the water layer retained and lyophilized to afford **130** as a white solid, (72%); Mp: 129-131 °C; IR (KBr): 3439, 3271, 3100-2800, 1742, 1692, 1605, 1516, 1431, 1380, 1311, 1253, 1222, 1200, 1166, 1057, 822, 760 cm⁻¹; ¹H NMR (400 MHz, D₂O) δ (ppm), 8.25 (d, $J = 2.10$, 1H),

8.12 (d, $J = 9.29$, 1H), 7.20 (d, $J = 8.98$, 1H), 5.55 (s, 2H), 3.15 (t, $J = 8.05$, 2H), 2.73 (t, $J = 9.29$, 2H), 2.06, (m, 2H); ^{13}C NMR (125 MHz, MeOD) δ (ppm), 191.05, 172.35, 161.92, 161.05, 133.82, 128.25, 125.01, 122.32, 120.16, 117.42, 115.71, 65.97, 38.51, 30.09, 22.38; HRMS (M⁺): Calc'd for C₁₃H₁₅F₃NO₄: 306.0953. Found 306.0953.

The same steps were utilized to make **131** and **132**.

1-(benzyloxy)-4-bromo-2-(trifluoromethoxy)benzene, 131b. Oil, 93%; IR (NaCl): 3033, 2916, 1595, 1500, 1454, 1382, 1190, 1135, 1024, 804, 736, 696. ^1H NMR (400 MHz, CDCl₃) δ 7.36 (m, 8H), 6.88 (d, $J = 8.9$, 1H), 5.15 (s, 2H); ^{13}C NMR (125 MHz, CDCl₃) δ 150.33, 138.80, 135.79, 129.06, 127.13, 121.61, 119.55, 117.49, 115.45, 112.36, 110.92, 71.13; ^{19}F NMR (376 MHz, CDCl₃ + drop CF₃CO₂H) δ -59.08; HRMS (EI): Calc'd for C₁₄H₁₀F₃BrO₂: 345.9816. Found: 345.9812.

1-(4-(benzyloxy)-3-(trifluoromethoxy)phenyl)ethanone, 131c. Oil, 92%; IR (NaCl): 3035, 2929, 1681, 1606, 1581, 1514, 1454, 1427, 1380, 1205, 1170, 1135, 813, 738, 696; ^1H NMR (400 MHz, CDCl₃) δ 7.87 (dd, $J = 8.88$, $J = 2.01$, 2H), 7.43 (m, 5H), 7.26 (d, $J = 8.57$, 1H), 5.25 (s, 2H) 2.56 (s, 3H); ^{13}C NMR (125 MHz, CDCl₃) δ 195.65, 154.73, 137.40, 135.84, 129.34, 127.44, 122.68, 119.53, 117.49, 115.74, 113.85, 111.20, 70.64, 25.56; ^{19}F NMR (376 MHz, CDCl₃ + drop CF₃CO₂H) δ -58.69; HRMS (EI): Calc'd for C₁₆H₁₃F₃O₃: 310.0817. Found: 310.0828.

1-(4-benzyloxy-3-trifluoromethoxyphenyl)-2-bromoethanone, 131d. Oil, ~93%; IR (CDCl₃): 3035, 2928, 1680, 1606, 1580, 1516, 1444, 1423, 1371, 1215, 1150, 1125, 827, 730, 692; ^1H NMR (400 MHz, CDCl₃) δ (ppm), 8.26 (d, $J = 2.00$, 1H),

8.14 (dd, $J = 8.74$, $J = 2.20$, 1H), 7.41 (m, 5H), 7.12 (d, $J = 8.58$, 1H), 5.26 (s, 2H)
4.37 (s, 2H); ^{19}F NMR (376 MHz, CDCl_3 + drop $\text{CF}_3\text{CO}_2\text{H}$) δ (ppm), -58.73.

2-(4-benzyloxy-3-trifluoromethoxy)phenyl-2-oxoethyl-4-(tert-butoxycarbonyl-amino)butanoate, 131e. White ppt., 85%, Mp: 112-114°C; IR (KBr): 3307, 3100-2800, 1742, 1701, 1659, 1606, 1437, 1407, 1209, 1167, 955, 743, 700, 667; ^1H NMR (400 MHz, d^6 -DMSO) δ (ppm), 8.03 (dd, $J = 8.98$, $J = 2.20$, 1H), 7.89 (t, $J = 2.63$, 1H), 7.42 (m, 5H), 6.88 (t, $J = 6.30$, 1H), 5.44 (s, 2H) 5.35 (s, 2H) 2.98 (t, $J = 6.79$, 2H), 2.44 (t, $J = 7.59$, 2H), 1.68 (m, 2H), 1.38 (s, 9H); ^{13}C NMR (125 MHz, d^6 -DMSO) δ (ppm), 190.79, 172.18, 159.87, 155.60, 134.40, 133.10, 132.00, 128.91, 127.23, 126.44, 124.27, 122.10, 119.93, 117.38, 114.27, 77.45, 70.32, 66.16, 39.47, 30.62, 28.22, 24.96; ^{19}F NMR (376 MHz, CD_3CN + drop $\text{CF}_3\text{CO}_2\text{H}$) δ (ppm), -61.14; HRMS (M + Na): Calc'd for $\text{C}_{25}\text{H}_{28}\text{F}_3\text{NO}_7\text{Na}$: 534.1716. Found 534.1712.

2-(4-hydroxy-3-(trifluoromethoxy)phenyl)-2-oxoethyl-4-(tert-butoxycarbonyl-amino)butanoate, 131e'. Adhesive ppt., 97%; ^1H NMR (400 MHz, d^6 -DMSO) δ (ppm), 7.87 (dd, $J = 8.60$, $J = 2.20$, 1H), 7.81 (s, 1H), 7.11 (d, $J = 8.62$, 1H), 6.89 (t, $J = 5.50$, 1H), 5.38 (s, 2H), 2.97 (t, $J = 6.80$, 2H), 2.42 (t, $J = 7.65$, 2H), 1.70 (m, 2H), 1.38 (s, 9H).

4-(2-(4-hydroxy-3-trifluoromethoxyphenyl)-2-oxoethoxy)-4-oxobutan-1-ammonium-2,2,2-trifluoroacetate, 131. White ppt., 96%, Mp: 121-123 °C. IR (KBr): 3439, 3271, 3100-2800, 1742, 1692, 1605, 1516, 1431, 1380, 1311, 1253, 1222, 1200, 1166, 1057, 822, 760 cm^{-1} ; ^1H NMR (400 MHz, D_2O) δ (ppm), 7.90 (t, $J = 1.50$, 1H), 7.85 (dd, $J = 8.82$, $J = 2.13$, 1H), 7.14 (d, $J = 8.80$, 1H), 5.47 (s, 2H),

3.08 (t, $J = 7.65$, 2H), 2.68 (t, $J = 7.08$, 2H), 2.02 (m, 2H); ^{13}C NMR (125 MHz, D_2O) δ (ppm), 193.76, 174.15, 163.12, 154.43, 136.51, 132.19, 129.16, 125.96, 123.47, 121.99, 119.37, 117.73, 66.67, 38.53, 30.23, 21.96; HRMS (M^+): Calc'd for $\text{C}_{13}\text{H}_{15}\text{F}_3\text{NO}_5$: 322.0902. Found: 322.0905.

1-(4-(benzyloxy)-3-nitrophenyl)ethanone, 132c. 3-nitro-4-hydroxyacetophenone is commercially available. 96%. *This compound is known.* ^1H NMR (400 MHz, CDCl_3) δ (ppm), 8.45 (dd, $J = 9.22$, $J = 2.38$, 1H), 8.14 (dd, $J = 9.15$, $J = 1.69$, 1H), 7.42 (m, 6H), 5.34 (s, 2H), 2.60 (s, 2H).

1-(4-(benzyloxy)-3-nitrophenyl)-2-bromoethanone, 132d. Oil, ~97%; ^1H NMR (400 MHz, CDCl_3) δ (ppm), 8.34 (s, 1H), 8.00 (d, 1H), 7.28 (m, 6H), 5.20 (s, 2H), 4.23 (s, 2H).

2-(4-(benzyloxy)-3-nitrophenyl)-2-oxoethyl-4-(tert-butoxycarbonyl-amino)

butanoate, 132e. White ppt., 67%, Mp: 144-146°C. IR (KBr): 3310, 3100-2800, 1740, 1700, 1655, 1603, 1433, 1400, 1204, 1170, 955, 745, 697, 665; ^1H NMR (400 MHz, CD_3CN) δ (ppm), 8.37 (dd, $J = 7.12$, $J = 2.57$, 1H), 8.12 (d, $J = 1.50$, 1H), 7.43 (m, 6H), 6.85 (t, $J = 7.21$, 1H), 5.34 (s, 2H), 3.09 (t, $J = 6.79$, 2H), 2.46 (t, $J = 7.60$, 2H), 1.77 (m, 2H), 1.40 (s, 9H); ^{13}C NMR (125 MHz, CD_3CN) δ (ppm), 195.22, 173.42, 160.65, 158.77, 139.23, 136.54, 135.40, 133.98, 131.78, 128.36, 125.89, 119.24, 116.82, 66.72, 38.44, 30.51, 29.11, 21.88; HRMS ($\text{M} + \text{Na}$): Calc'd for $\text{C}_{24}\text{H}_{28}\text{N}_2\text{O}_8\text{Na}$: 495.1743. Found: 495.1755

4-(2-(4-hydroxy-3-nitrophenyl)-2-oxoethoxy)-4-oxobutan-1-aminium-2,2,2-

trifluoroacetate, 132. White ppt., 78%, Mp: 76-78°C; IR (KBr): 3441, 3265, 3100-

2800, 1740, 1690, 1605, 1520, 1430, 1377, 1309, 1252, 1225, 1199, 1166, 1055, 820, 760. cm^{-1} ; ^1H NMR (400 MHz, D_2O) δ (ppm), 8.72 (d, $J = 2.16$, 1H), 8.20 (d, $J = 9.29$, 1H), 7.32 (d, $J = 8.85$, 1H), 5.56 (s, 2H), 3.14 (t, $J = 7.80$, 2H), 2.72 (t, $J = 9.18$, 2H), 2.08 (m, 2H); ^{13}C NMR (125 MHz, D_2O) δ (ppm), 193.16, 174.10, 163.13, 157.81, 135.75, 134.33, 126.61, 120.50, 117.44, 115.12, 66.69, 38.54, 30.23, 21.96; HRMS (M^+): Calc'd for $\text{C}_{12}\text{H}_{15}\text{N}_2\text{O}_6$: 283.0925. Found: 283.0914.

4-(2-(4-hydroxy-3,5-dimethoxyphenyl)-2-oxoethoxy)-4-oxobutan-1-aminium

2,2,2-trifluoroacetate, 133. The synthesis of **133** was accomplished from use of the procedure by Conrad, et. al.⁹⁷

4-(2-(4-hydroxy-3-methoxyphenyl)-2-oxoethoxy)-4-oxobutan-1-aminium-2,2,2-

trifluoroacetate, 134. The synthesis of **134** was accomplished from use of the procedure by Conrad, et. al.⁹⁷

1-(2,4-bis(benzyloxy)phenyl)ethanone, 135b. 2,4-dihydroxyacetophenone is commercially available. Benzylation of this utilized the same procedure as in the synthesis of **122b**. White ppt., 97%. This compound is known. ^1H NMR (400 MHz, CDCl_3) δ (ppm), 7.86 (t, $J = 7.63$, 1H), 7.39 (m, 11H), 6.64 (dd, $J = 8.71$, $J = 2.33$, 1H), 5.12 (s, 2H), 5.10 (s, 2H), 2.57 (s, 3H).

1-(2,4-bis(benzyloxy)phenyl)-2-bromoethanone, 135c. An identical procedure was used as to construct **122d**. ~ 94%. ^1H NMR (400 MHz, CDCl_3) δ (ppm), 7.78 (s, 1H), 7.35 (m, 10H), 6.60 (d, 2H), 5.12 (s, 2H), 5.09 (s, 2H), 4.51 (s, 1H), 4.46 (1H).

2-(2,4-bis(benzyloxy)phenyl)-2-oxoethyl 4-(tert-butoxycarbonylamino)butanoate, 135d. The same procedure was utilized as to synthesize **122e**. Adhesive ppt, 48%; IR

(KBr): 3310, 3100-2800, 1743, 1700, 1658, 1601, 1436, 1400, 1200, 1165, 955, 745, 742, 700, 697, 665, 651; ¹H NMR (400 MHz, d⁶-DMSO) δ (ppm), 7.93 (t, *J* = 8.79, 1H), 7.43 (m, 10H), 7.14 (dd, *J* = 8.74, *J* = 2.15, 1H), 6.88 (t, *J* = 5.70, 1H), 6.62 (d, *J* = 4.66, 1H), 5.37 (s, 2H), 5.29 (s, 1H), 5.21 (s, 1H), 5.10 (s, 2H), 2.94 (t, *J* = 6.63, 2H), 2.37 (t, *J* = 7.51, 2H), 1.76 (m, 2H), 1.37 (s, 9H); ¹³C NMR (125 MHz, d⁶-DMSO) δ (ppm), 190.50, 172.15, 164.65, 159.78, 155.58, 135.99, 132.04, 128.35, 127.51, 118.10, 107.59, 103.90, 100.33, 77.43, 70.72, 69.19, 39.95, 30.68, 28.22, 24.88; HRMS (M + H): Calc'd for C₃₁H₃₆NO₇: 534.2492. Found: 534.2504.

2-(2,4-dihydroxyphenyl)-2-oxoethyl-4-(tert-butoxycarbonylamino)butanoate,

135e. An identical procedure was used as to engender **130'e**. Adhesive ppt., 97%; ¹H NMR (400 MHz, d⁶-DMSO) δ (ppm), 11.43, (s, 1H), 11.34 (s, 1H), 7.88 (s, 1H), 7.70 (d, 1H), 6.87 (t, 1H), 6.38 (d, 1H), 5.28 (s, 1H), 2.96 (t, 2H), 2.40 (t, 2H), 1.67 (m, 2H), 1.38 (s, 9H).

4-(2-(2,4-dihydroxyphenyl)-2-oxoethoxy)-4-oxobutan-1-aminium-2,2,2-

trifluoroacetate, 135. An identical procedure was used as to produce **130**. White ppt., 85%, Mp: 136-138 °C; IR (KBr): 3432, 3274, 3100-2800, 1739, 1691, 1602, 1520, 1421, 1377, 1309, 1298, 1201, 1178, 1128, 1055, 1027, 1008, 823, 762, 717, 613 cm⁻¹; ¹H NMR (400 MHz, D₂O) δ (ppm), 7.97 (d, *J* = 6.81, 1H), 7.72 (d, *J* = 8.84, 1H), 6.53 (d, *J* = 7.63, 1H), 5.48 (s, 1H), 5.43 (s, 1H), 3.14 (t, *J* = 7.64, 2H), 2.72 (t, *J* = 7.05, 2H), 2.08 (m, 2H); ¹³C NMR (125 MHz, D₂O) δ (ppm), 193.77, 174.15, 162.75, 151.02, 144.22, 125.92, 122.70, 119.65, 117.37, 115.58, 66.60, 38.51, 30.28, 22.00; HRMS (M +): Calc'd for C₁₂H₁₆NO₅: 254.1028. Found: 254.1038.

The same methodology was utilized to assemble **136-141**.

1-(3,4-bis(benzyloxy)phenyl)ethanone, 136b. 3,4-dihydroxyacetophenone is commercially available. Benzylation of this utilized the same procedure as in the synthesis of **127b**. 98%. This compound is known. ¹H NMR (400 MHz, CDCl₃) δ (ppm), 7.63 (dd, *J* = 8.77, *J* = 2.32, 1H), 7.40 (m, 11H), 6.94 (dd, *J* = 9.10, *J* = 1.90, 1H), 5.25 (s, 2H), 5.22 (s, 2H), 2.52 (s, 3H).

1-(3,4-bis(benzyloxy)phenyl)-2-bromoethanone, 136c. Oil ~96%; ¹H NMR (400 MHz, CDCl₃) δ (ppm), 7.68 (s, 1H), 7.41 (m, 11H), 6.96 (d, 1H), 5.24 (s, 2H), 5.22 (s, 2H), 4.46 (s, 2H).

2-(3,4-bis(benzyloxy)phenyl)-2-oxoethyl-4-(tert-butoxy-carbonyl-amino)-butanoate, 136d. White ppt., 90%, Mp: 112-114°C; IR (KBr): 3310, 3100-2800, 1743, 1700, 1658, 1601, 1436, 1400, 1200, 1165, 955, 745, 742, 700, 697, 665, 651; ¹H NMR (400 MHz, d⁶-DMSO) δ (ppm), 7.62 (dd, *J* = 7.25, *J* = 2.38, 1H), 7.56 (d, *J* = 1.72, 1H), 7.38 (m, 10H), 7.19 (d, *J* = 8.13, 1H), 6.92 (t, *J* = 7.21, 1H), 5.40 (s, 2H), 5.27 (s, 2H), 5.21 (s, 2H), 2.97 (t, *J* = 6.78, 2H), 2.40 (t, *J* = 7.70, 2H), 1.70 (m, 2H), 1.38 (s, 9H); ¹³C NMR (125 MHz, d⁶-DMSO) δ (ppm), 197.09, 171.80, 155.60, 152.85, 147.98, 136.85, 128.41, 127.94, 127.58, 126.84, 122.64, 113.04, 112.51, 77.47, 70.00, 66.07, 39.61, 30.67, 28.22, 24.54; HRMS (M + H): Calc'd for C₃₁H₃₆NO₇: 534.2492. Found: 534.2484.

2-(2,4-dihydroxyphenyl)-2-oxoethyl-4-(tert-butoxycarbonylamino)butanoate, 136e. Adhesive ppt., 98%; ¹H NMR (400 MHz, d⁶-DMSO) δ (ppm), 7.32 (d, 2H),

6.93 (s, 1H), 6.89 (t, 1H), 5.39 (s, 2H), 2.98 (t, 2H), 2.38 (t, 2H), 1.68 (m, 2H), 1.40 (s, 9H).

4-(2-(3,4-dihydroxyphenyl)-2-oxoethoxy)-4-oxobutan-1-aminium-2,2,2-

trifluoroacetate, 136. White ppt., 92%, Mp: 56-58°C; IR (KBr): 3432, 3274, 3100-2800, 1739, 1691, 1602, 1520, 1421, 1377, 1309, 1298, 1201, 1178, 1128, 1055, 1027, 1008, 823, 762, 717, 613 cm^{-1} ; ^1H NMR (400 MHz, D_2O) δ (ppm), 7.35 (s, 1H), 7.33 (s, 1H), 6.91 (d, $J = 7.10$, 1H), 5.36 (s, 2H), 3.07 (t, $J = 6.80$, 2H), 2.65 (t, $J = 7.76$, 2H), 2.00 (m, 2H); ^{13}C NMR (125 MHz, D_2O) δ (ppm), 194.29, 174.13, 163.06, 150.88, 144.11, 125.88, 122.69, 119.74, 117.42, 115.10, 66.56, 38.30, 30.23, 21.95; HRMS (M^+): Calc'd for $\text{C}_{12}\text{H}_{16}\text{NO}_5$: 254.1028. Found: 254.1032.

1-(4-(benzyloxy)-3-methylphenyl)ethanone, 137b. 3-methyl-4-dihydroxyacetophenone is commercially available. Benzylation of this comprised the same procedure as in the synthesis of **122b**. white ppt., 95%. *This compound is known.* ^1H NMR (400 MHz, CDCl_3) δ (ppm), 7.82 (s 1H), 7.80 (s, 1H), 7.40 (m, 5H), 6.90 (d, $J = 8.75$, 1H), 5.17 (s, 2H), 2.56 (s, 3H), 2.33 (s, 3H).

1-(4-(benzyloxy)-3-methylphenyl)-2-bromoethanone, 137c. Oil, ~97%; ^1H NMR (400 MHz, CDCl_3) δ (ppm), 7.82 (d, 2H), 7.40 (m, 5H), 6.88 (d, $J = 8.80$, 1H), 5.19 (s, 2H), 4.33 (s, 2H), 2.33 (s, 3H).

2-(4-(benzyloxy)-3-methylphenyl)-2-oxoethyl-4-(tert-butoxycarbonyl-amino)

butanoate, 137d. White ppt., 94%, Mp: 105-106 °C; IR (KBr): 3307, 3100-2800, 1742, 1701, 1659, 1606, 1437, 1407, 1209, 1167, 955, 743, 700, 667; ^1H NMR (400 MHz, $\text{d}^6\text{-DMSO}$) δ (ppm), 7.82 (d, $J = 9.14$, 2H), 7.40 (m, 5H), 7.14 (d, $J = 8.10$,

1H), 6.87 (t, $J = 7.40$, 1H), 5.39 (s, 2H), 5.25 (s, 2H), 2.96 (t, $J = 6.81$, 2H), 2.42 (t, $J = 7.62$, 2H), 2.24 (s, 3H), 1.70 (m, 2H), 1.38 (s, 9H); ^{13}C NMR (125 MHz, d^6 -DMSO) δ (ppm), 191.14, 172.20, 161.40, 155.60, 136.67, 131.00, 130.10, 129.26, 128.50, 127.34, 126.45, 125.07, 111.62, 77.45, 69.55, 66.03, 39.33, 30.68, 28.18, 24.98, 16.04; HRMS (M + Na): Calc'd for $\text{C}_{25}\text{H}_{31}\text{NO}_6\text{Na}$: 464.2049. Found: 464.2017.

2-(4-hydroxy-3-methylphenyl)-2-oxoethyl-4-(tert-butoxycarbonyl-amino)-butanoate, 137e. Adhesive ppt., 98%; ^1H NMR (400 MHz, d^6 -DMSO) δ (ppm), 10.76 (s, 1H), 7.86 (d, $J = 9.26$, 2H), 7.66 (d, $J = 8.04$, 1H), 6.89 (t, 1H), 5.38 (s, 2H), 2.96 (t, $J = 6.94$, 2H), 2.42 (t, $J = 7.88$, 2H), 2.24 (s, 3H), 1.70 (m, 2H), 1.38 (s, 9H).

4-(2-(4-hydroxy-3-methylphenyl)-2-oxoethoxy)-4-oxobutan-1-aminium-2,2,2-trifluoroacetate, 137. White ppt., 89%, Mp: 118-120°C. IR (KBr): 3432, 3274, 3100-2800, 1739, 1691, 1602, 1520, 1421, 1377, 1309, 1298, 1201, 1178, 1128, 1055, 1027, 1008, 823, 762, 717, 613. cm^{-1} ; ^1H NMR (400 MHz, d^6 -DMSO) δ (ppm), 7.86 (s, 3H), 7.72 (d, $J = 6.22$, 1H), 7.67 (dd, $J = 9.03$, $J = 1.79$, 1H), 5.39 (s, 1H), 2.88 (t, $J = 6.97$, 2H), 2.56 (t, $J = 7.55$, 2H), 2.16 (s, 3H), 1.87 (m, 2H); ^{13}C NMR (125 MHz, d^6 -DMSO) δ (ppm), 190.67, 171.72, 160.98, 158.27, 130.76, 127.76, 125.10, 120.30, 117.94, 114.76, 66.11, 38.09, 30.15, 22.10, 15.80; HRMS (M⁺): Calc'd for $\text{C}_{13}\text{H}_{18}\text{NO}_4$: 252.1230. Found: 252.1212.

1-(4-(benzyloxy)-3,5-dimethylphenyl)ethanone, 138b. 4-hydroxy-3,3-dimethylacetophenone is commercially available. Benzylation of this involve the same procedure as in the synthesis of **135b**. Oil, 95%. *This compound is known.* GC/MS

(EI): One peak, retention time, 8.38 min (initial temp 50°C, ramp 25°C/min until 300°C), MS; 254.0 m/z.

1-(4-(benzyloxy)-3,5-dimethylphenyl)-2-bromoethanone, 138c. White ppt., ~95%.

This compound is known. GC/MS (EI): One peak, retention time, 9.87 min (initial temp 50°C, ramp 25°C/min until 300°C), MS; 331.9, 333.9 m/z.

2-(4-(benzyloxy)-3,5-dimethylphenyl)-2-oxoethyl-4-(tert-butoxycarbonylamino)-

butanoate, 138d. Adhesive ppt., 96%; IR (KBr): 3307, 3100-2800, 1742, 1701, 1659, 1606, 1437, 1407, 1209, 1167, 955, 743, 700, 667; ¹H NMR (400 MHz, d⁶-DMSO) δ (ppm), 7.70 (d, *J* = 8.60, 1H), 7.50-7.40 (m, 5H), 6.89 (t, *J* = 7.20, 1H), 5.42 (s, 2H), 4.88 (s, 2H), 2.97 (t, *J* = 6.90, 2H), 2.43 (t, *J* = 7.80, 2H), 2.29 (s, 6H), 1.68 (m, 2H), 1.36 (s, 9H); ¹³C NMR (125 MHz, d⁶-DMSO) δ (ppm), 191.84, 172.19, 160.04, 155.60, 137.06, 131.49, 129.59, 128.68, 128.36, 128.13, 127.85, 77.45, 73.52, 66.20, 38.97, 30.50, 28.18, 24.97, 16.20; HRMS (M + Na): Calc'd for C₂₆H₃₃NO₆Na: 478.2206; Found: 478.2191. (M + H): Calc'd for C₂₆H₃₄NO₆: 456.2386. Found: 456.2388.

2-(4-hydroxy-3,5-dimethylphenyl)-2-oxoethyl-4-(tert-butoxycarbonylamino)-

butanoate, 138e. Adhesive ppt., 99%; IR (KBr): 3548, 3301, 3100-2800, 1739, 1702, 1661, 1606, 1437, 1407, 1209, 1167, 955, 743, 700, 667; ¹H NMR (400 MHz, d⁶-DMSO) δ (ppm), 9.40 (s, 1H), 7.59 (d, *J* = 8.60, 2H), 6.89 (t, *J* = 7.15, 1H), 5.36 (s, 2H), 2.98 (t, *J* = 7.00, 2H), 2.55 (t, *J* = 7.50, 2H), 2.20 (s, 6H), 1.92 (m, 2H); ¹³C NMR (125 MHz, d⁶-DMSO) δ (ppm), 190.91, 172.20, 159.67, 155.59, 128.60,

125.25, 123.74, 77.44, 65.91, 38.96, 30.90, 28.18, 24.98, 16.52; HRMS (M + Na): Calc'd for C₁₉H₂₇NO₆Na: 388.1736. Found: 388.1735.

4-(2-(4-hydroxy-3,5-dimethylphenyl)-2-oxoethoxy)-4-oxobutan-1-aminium-2,2,2-trifluoroacetate, 138. White ppt., 92%, Mp: 125-127°C; IR (KBr): 3550, 3301, 3100-2800, 1739, 1702, 1661, 1606, 1437, 1407, 1209, 1167, 955, 743, 700, 667; ¹H NMR (400 MHz, d⁶-DMSO) δ (ppm), 9.36 (s, 1H), 7.86 (s, 3H), 7.62 (d, *J* = 8.60, 2H), 5.36 (s, 2H), 2.98 (t, *J* = 7.00, 2H), 2.43 (m, 5H), 2.22 (s, 6H), 1.69 (m, 2H), 1.37 (s, 9H); ¹³C NMR (125 MHz, d⁶-DMSO) δ (ppm), 189.74, 170.61, 157.71, 156.71, 127.72, 124.97, 123.15, 116.95, 65.02, 37.10, 28.88, 21.48, 15.55; HRMS (M+): Calc'd for C₁₄H₂₀NO₄: 266.1392. Found: 266.1389.

1-(4-(benzyloxy)-2-methylphenyl)ethanone, 139b. 4-hydroxy-2-methylacetophenone is commercially available. Benzylation of this entailed the same procedure as in the synthesis of **135b**. White ppt., 93%, *This compound is known*. GC/MS (EI): One peak, retention time, 8.24 min (initial temp 50°C, ramp 25°C/min until 300°C), MS; 240.0 m/z.

1-(4-(benzyloxy)-2-methylphenyl)-2-bromoethanone, 139c. White ppt., ~92%. *This compound is known*. GC/MS (EI): One peak, retention time, 9.77 min (initial temp 50°C, ramp 25°C/min until 300°C), MS; 317.9, 319.9 m/z.

2-(4-(benzyloxy)-2-methylphenyl)-2-oxoethyl-4-(tert-butoxycarbonyl-amino)-butanoate, 139d. Adhesive ppt., 91%; IR (KBr): 3307, 3100-2800, 1742, 1701, 1659, 1606, 1437, 1407, 1209, 1167, 955, 743, 700, 667; ¹H NMR (400 MHz, d⁶-DMSO) δ (ppm), 7.86 (d, *J* = 9.10, 1H), 7.47-7.40 (m, 5H), 6.97 (t, *J* = 6.50, 2H),

6.87 (t, $J = 7.35$, 1H), 5.28 (s, 2H), 5.19 (s, 2H), 2.97 (t, $J = 6.70$, 2H), 2.42 (m, 5H), 1.68 (m, 2H), 1.37 (s, 9H); ^{13}C NMR (125 MHz, $\text{d}^6\text{-DMSO}$) δ (ppm), 193.63, 172.21, 161.05, 155.60, 141.48, 136.40, 132.04, 128.47, 127.42, 125.06, 118.30, 111.85, 107.74, 77.45, 69.30, 67.05, 38.83, 30.68, 28.22, 24.54, 21.11; HRMS (M + Na): Calc'd for $\text{C}_{25}\text{H}_{31}\text{NO}_6\text{Na}$: 464.2049. Found: 464.2040.

2-(4-hydroxy-2-methylphenyl)-2-oxoethyl-4-(tert-butoxycarbonyl-amino)-butanoate, 139e. Adhesive ppt., 98%; IR (KBr): 3460, 3300, 3100-2800, 1740, 1699, 1662, 1606, 1437, 1407, 1209, 1167, 955, 743, 700, 667; ^1H NMR (400 MHz, $\text{d}^6\text{-DMSO}$) δ (ppm), 10.30 (d, 1H), 7.78 (d, $J = 9.10$, 1H), 6.89 (t, $J = 7.50$, 1H), 6.71 (t, $J = 6.30$, 1H), 5.26 (s, 2H), 2.98 (t, $J = 6.70$, 2H), 2.41 (m, 5H), 1.69 (m, 2H), 1.39 (s, 9H); ^{13}C NMR (125 MHz, $\text{d}^6\text{-DMSO}$) δ (ppm), 192.91, 172.21, 160.96, 155.60, 141.83, 131.87, 125.29, 118.74, 112.51, 77.45, 66.86, 38.97, 30.46, 28.22, 24.95, 21.68; HRMS (M + Na): Calc'd for $\text{C}_{18}\text{H}_{25}\text{NO}_6\text{Na}$: 374.1580. Found: 374.1577.

4-(2-(4-hydroxy-2-methylphenyl)-2-oxoethoxy)-4-oxobutan-1-aminium-2,2,2-trifluoroacetate, 139. White ppt., 95%, Mp: 110-112°C; IR (KBr): 3460, 3300, 3100-2800, 1740, 1699, 1662, 1606, 1437, 1407, 1209, 1167, 955, 743, 700, 667; ^1H NMR (400 MHz, $\text{d}^6\text{-DMSO}$) δ (ppm), 7.86 (s, 3H), 7.80 (d, $J = 9.00$, 1H), 6.74 (t, $J = 6.20$, 1H), 5.28 (s, 2H), 2.96 (t, $J = 6.70$, 2H), 2.54 (t, $J = 7.60$, 2H), 2.40 (s, 3H), 1.87 (m, 2H); ^{13}C NMR (125 MHz, $\text{d}^6\text{-DMSO}$) δ (ppm), 192.71, 171.72, 161.19, 158.64, 141.88, 131.90, 124.55, 118.81, 117.56, 112.58, 67.02, 37.84, 30.14, 22.54, 20.34; HRMS (M +): Calc'd for $\text{C}_{13}\text{H}_{18}\text{NO}_4$: 252.1236. Found: 252.1227.

2-(4-(benzyloxy)phenyl)-2-oxoethyl propionate, 140b. 2-(4-(benzyloxy)phenyl)-2-oxoethyl propionate is commercially available. Benzylation of this involved the same procedure as in the synthesis of **135b**. *This compound is known.* 97%, GC/MS (EI): One peak, retention time, 7.63 min (initial temp 50°C, ramp 25°C/min until 300°C), MS; 262.0 m/z.

2-(4-(benzyloxy)phenyl)-2-oxoethyl 2-bromopropanoate, 140c (racemic). ~94%. GC/MS (EI): One peak, retention time, 8.10 min (initial temp 50°C, ramp 25°C/min until 300°C), MS; 317.0, 319.0, m/z.

(S)-tert-butyl 5-(4-(benzyloxy)phenyl)-4-methyl-5-oxopentylcarbamate and (R)-tert-butyl-5-(4-(benzyloxy)phenyl)-4-methyl-5-oxopentylcarbamate, (R,S)-140d. Adhesive ppt., 95%; IR (KBr): 3307, 3100-2800, 1742, 1701, 1659, 1606, 1437, 1407, 1209, 1167, 955, 743, 700, 667; ¹H NMR (400 MHz, d⁶-DMSO) δ (ppm), 7.98 (d, *J* = 8.89, 2H), 7.40 (m, 5H), 7.14 (d, *J* = 9.03, 2H), 6.87 (t, *J* = 7.35, 1H), 5.95 (m, 1H), 5.21 (s, 2H), 2.93 (t, *J* = 7.00, 2H), 2.37 (t, *J* = 7.51, 2H), 1.63 (m, 2H), 1.39 (s, 9H), 1.17 (d, *J* = 7.20, 3H); ¹³C NMR (125 MHz, d⁶-DMSO) δ (ppm), 194.93, 172.10, 162.61, 155.61, 136.31, 130.67, 128.48, 128.03, 127.53, 126.38, 114.93, 77.47, 69.89, 63.47, 36.16, 30.12, 28.18, 20.70, 17.08; HRMS (M + Na): Calc'd for C₂₅H₃₁NO₆Na: 464.2049. Found: 464.2049.

(S)-tert-butyl-5-(4-hydroxyphenyl)-4-methyl-5-oxopentylcarbamate and (R)-tert-butyl-5-(4-hydroxyphenyl)-4-methyl-5-oxopentylcarbamate, (R,S)-140e. Adhesive ppt., 92%; ¹H NMR (400 MHz, d⁶-DMSO) δ (ppm), 7.87 (d, *J* = 9.05, 2H), 6.88 (m, 3H), 5.90 (m, 1H), 2.94 (t, *J* = 6.86, 2H), 2.34 (t, *J* = 7.72, 2H), 2.24 (s, 3H),

1.63 (m, 2H), 1.39 (s, 9H), 1.18 (d, $J = 6.88$, 3H); ^{13}C NMR (125 MHz, $\text{d}^6\text{-DMSO}$) δ (ppm), 195.55, 173.02, 163.50, 157.24, 132.90, 128.93, 115.54, 78.43, 71.95, 40.00, 31.57, 29.14, 25.82, 16.81; HRMS (M + Na): Calc'd for $\text{C}_{18}\text{H}_{25}\text{NO}_6\text{Na}$: 374.1567. Found: 374.1567.

(R)-4-(1-(4-hydroxyphenyl)-1-oxopropan-2-yloxy)-4-oxobutan-1-aminium-2,2,2-trifluoroacetate and (S)-4-(1-(4-hydroxyphenyl)-1-oxopropan-2-yloxy)-4-oxobutan-1-aminium-2,2,2-trifluoroacetate, (R,S)-140. Adhesive ppt., 83%; IR (KBr): 3448, 3274, 3100-2800, 1739, 1691, 1602, 1520, 1421, 1377, 1309, 1298, 1201, 1178, 1128, 1055, 1027, 1008, 823, 762, 717, 613 cm^{-1} ; ^1H NMR (400 MHz, D_2O) δ (ppm), 7.99 ($J = 8.69$, 2H), 7.00 (d, $J = 8.10$, 2H), 6.06 (m, 1H), 3.06 ($J = 7.10$, 2H), 2.64 (t, $J = 7.70$, 2H), 2.00 (m, 2H), 1.54 (d, $J = 7.05$, 3H); ^{13}C NMR (125 MHz, $\text{d}^6\text{-DMSO}$) δ (ppm), 190.67, 171.72, 160.98, 158.27, 130.76, 127.76, 125.10, 120.30, 117.94, 114.76, 66.11, 38.09, 30.15, 22.10, 15.80; HRMS (M +): Calc'd for $\text{C}_{13}\text{H}_{18}\text{NO}_4$: 252.1230. Found: 252.1236.

1-(4-(benzyloxy)phenyl)butan-1-one, 141b. 1-(4-(benzyloxy)phenyl)butan-1-one is commercially available. Benzylation of this involved the same procedure as in the synthesis of **122b**. *This compound is known.* White ppt., 97%. ^1H NMR (400 MHz, CDCl_3) δ (ppm), 7.96 (d, $J = 8.64$, 2H), 7.40 (m, 5H), 7.02 (d, $J = 8.50$, 2H), 5.14 (s, 2H), 2.90 (t, $J = 7.43$, 2H), 1.76 (m, 2H), 1.01 (t, $J = 6.73$, 3H).

1-(4-(benzyloxy)phenyl)-3-bromobutan-1-one, 141c. Racemic, 88%; GC/MS (EI): One peak, retention time, 9.58 min (initial temp 50°C , ramp $25^\circ\text{C}/\text{min}$ until 300°C), MS; 331.8, 333.9 m/z.

(R)-tert-butyl 4-(4-(benzyloxy)benzoyl)hexylcarbamate and (S)-tert-butyl 4-(4-(benzyloxy)benzoyl)hexylcarbamate (R,S)-141d. Adhesive ppt., 89%; IR (KBr): 3307, 3100-2800, 1742, 1701, 1659, 1606, 1437, 1407, 1209, 1167, 955, 743, 700, 667; ¹H NMR (400 MHz, d⁶-DMSO) δ (ppm), 7.99 (d, *J* = 8.62, 2H), 7.39 (m, 5H), 7.13 (d, *J* = 8.88, 2H), 6.87 (t, *J* = 7.21, 1H), 5.88 (m, 1H), 5.22 (s, 2H), 2.94 (t, *J* = 6.88, 2H), 2.39 (t, *J* = 7.51, 2H), 1.70-1.60 (m, 4H), 1.37 (s, 9H), 0.94 (t, *J* = 7.05, 3H); ¹³C NMR (125 MHz, d⁶-DMSO) δ (ppm), 194.42, 172.51, 162.60, 155.58, 136.23, 130.63, 128.49, 128.03, 127.85, 127.10, 115.45, 77.77, 75.64, 70.45, 39.14, 30.77, 28.21, 24.91, 20.73, 9.49; HRMS (M + Na): Calc'd for C₂₆H₃₃NO₆Na: 478.2206. Found: 464.2189.

(R)-tert-butyl 4-(4-hydroxybenzoyl)hexylcarbamate and (S)-tert-butyl 4-(4-hydroxybenzoyl)hexylcarbamate, (R,S)-141e. Adhesive ppt., 98%; ¹H NMR (400 MHz, d⁶-DMSO) δ (ppm), 10.66 (s, 1H), 7.89 (d, *J* = 8.75, 2H), 6.88 (m, 3H), 5.80 (m, 1H), 2.94 (t, *J* = 6.95, 2H), 2.37 (t, *J* = 7.33, 2H), 1.70-1.60 (m, 4H), 1.38 (s, 9H), 0.94 (t, *J* = 6.85, 3H); ¹³C NMR (125 MHz, d⁶-DMSO) δ (ppm), 194.04, 172.26, 162.52, 155.58, 130.86, 125.29, 115.45, 77.59, 75.59, 39.13, 30.95, 28.35, 24.92, 21.02, 9.54; HRMS (M + Na): Calc'd for C₁₇H₂₇NO₆Na: 388.1736. Found: 388.1721.

(R)-4-(1-(4-hydroxyphenyl)-1-oxopropan-2-yloxy)-4-oxobutan-1-aminium 2,2,2-trifluoroacetate and (S)-4-(1-(4-hydroxyphenyl)-1-oxopropan-2-yloxy)-4-oxobutan-1-aminium 2,2,2-trifluoroacetate, (R,S)-141. Adhesive ppt., 80%; IR (KBr): 3450, 3274, 3100-2800, 1739, 1691, 1602, 1520, 1421, 1377, 1309, 1298,

1201, 1178, 1128, 1055, 1027, 1008, 823, 762, 717, 613. cm^{-1} ; ^1H NMR (400 MHz, d^6 -DMSO) δ (ppm), 7.88 ($J = 8.23$, 2H), 6.88 (d, $J = 7.75$, 2H), 5.83 (m, 1H), 2.85 ($J = 7.01$, 2H), 2.40 (t, $J = 7.62$, 2H), 1.82-1.68 (m, 4H), 0.91 (d, $J = 6.82$, 3H); ^{13}C NMR (125 MHz, d^6 -DMSO) δ (ppm), 193.38, 171.76, 162.69, 158.41, 130.87, 125.42, 117.47, 115.50, 75.82, 38.08, 30.17, 24.57, 22.55, 9.48; HRMS (M^+): Calc'd for $\text{C}_{14}\text{H}_{20}\text{NO}_4$: 266.1392. Found: 266.1389.

2-bromo-1-(4-fluorophenyl)ethanone, 142b. 4-fluoroacetophenone is commercially available. The same conditions were used as in the synthesis of **141c**. This compound is known. Oil, ~95% yield by GC/MS (EI): One peak, retention time, 4.79 min (initial temp 50°C , ramp $25^\circ\text{C}/\text{min}$ until 300°C), MS; 215.9, 217.9 m/z .

2-(4-fluorophenyl)-2-oxoethyl 4-(tert-butoxycarbonylamino)butanoate, 142c. The same general procedure to make **122e** was followed. White ppt., 82%, Mp: 85 - 87°C ; IR (KBr): 3307, 3100-2800, 1742, 1701, 1659, 1606, 1437, 1407, 1209, 1167, 955, 743, 700, 667; ^1H NMR (400 MHz, d^6 -DMSO) δ (ppm), 8.04 (m, 2H), 7.39 (t, $J = 8.80$, 2H), 6.87 (t, $J = 7.40$, 1H), 5.46 (s, 2H), 2.96 (dd, $J = 6.82$, $J = 6.65$, 2H), 2.42 (t, $J = 7.94$, 2H), 1.68 (m, 2H), 1.38 (s, 9H); ^{13}C NMR (125 MHz, d^6 -DMSO) δ (ppm), 191.51, 172.19, 166.35, 164.34, 155.60, 130.63, 116.09, 77.46, 66.26, 39.14, 30.62, 28.22, 24.95; HRMS ($\text{M} + \text{Na}$): Calc'd for $\text{C}_{17}\text{H}_{22}\text{FNO}_5\text{Na}$: 362.1380. Found: 362.1377

4-(2-(4-fluorophenyl)-2-oxoethoxy)-4-oxobutan-1-aminium 2,2,2-trifluoroacetate 142. The same general method to make **130** was followed. Adhesive ppt., 93%; IR (KBr): 3460, 3307, 3100-2800, 1742, 1701, 1659, 1606, 1437, 1407, 1209, 1167,

955, 743, 700, 667. ^1H NMR (400 MHz, D_2O) δ (ppm), 8.06 (m, 2H), 7.32 (t, $J = 8.80$, 2H), 5.56 (s, 2H), 3.12 (dd, $J = 6.82$, $J = 6.65$, 2H), 2.72 (t, $J = 7.94$, 2H), 2.06 (m, 2H); ^{19}F NMR (376 MHz, D_2O) δ (ppm), -104.12. ^{13}C NMR (125 MHz, d^6 -DMSO) δ (ppm), 191.46, 171.72, 166.40, 164.39, 158.67, 130.91, 116.12; HRMS (M^+): Calc'd for $\text{C}_{12}\text{H}_{15}\text{FNO}_3$: 240.1030. Found: 240.0998.

5-(2-(4-(benzyloxy)-2-fluorophenyl)-2-oxoethyl)-1-tert-butyl-2-(tert-butoxycarbonylamino)pentanedioate, 143e. The series to construct **143e** paralleled those for **122e**. Adhesive ppt., 91%; IR (KBr): 3307, 3100-2800, 1742, 1701, 1659, 1606, 1437, 1407, 1209, 1167, 955, 743, 700, 667; ^1H NMR (400 MHz, d^6 -DMSO) δ (ppm), 7.85 (t, $J = 8.88$, 1H), 7.40 (m, 5H), 7.22 (d, $J = 7.64$, 1H), 7.10 (d, $J = 10.50$, 1H), 7.01 (d, $J = 6.61$, 1H), 5.24 (s, 2H), 5.22 (s, 2H), 3.89 (m, 1H), 2.45 (t, $J = 6.69$, 2H), 1.99 (m, 1H), 1.89 (m, 1H), 1.39 (s, 18H); ^{13}C NMR (125 MHz, d^6 -DMSO) δ (ppm), 198.83, 171.32, 170.32, 164.28, 162.14, 154.64, 135.99, 131.42, 128.63, 127.95, 115.84, 112.37, 111.80, 102.83, 80.42, 78.11, 70.18, 68.41, 59.74, 30.73, 29.76, 28.15, 25.91; HRMS ($\text{M} + \text{Na}$): Calc'd for $\text{C}_{29}\text{H}_{36}\text{FNO}_8\text{Na}$: 568.2323. Found: 568.2296.

1-tert-butyl-5-(2-(2-fluoro-4-hydroxyphenyl)-2-oxoethyl)-2-(tert-butoxycarbonylamino)pentanedioate, 143e'. An identical procedure was followed to compose **130e'**. Adhesive ppt., 94%; IR (KBr): 3460, 3100-2800, 1742, 1701, 1659, 1606, 1437, 1407, 1209, 1167, 955, 743, 700, 667; ^1H NMR (400 MHz, MeOD) δ (ppm), δ 7.86 (t, $J = 8.24$, 1H), 6.90 (t, $J = 6.55$, 1H), 6.73 (d, $J = 7.70$, 1H), 6.64 (d, $J = 9.10$, 1H), 5.24 (s, 2H), 3.99 (m, 1H), 2.56 (t, $J = 7.05$, 2H), 2.10 (m, 1H), 1.97 (m, 1H),

1.51 (s, 18H); ^{13}C NMR (125 MHz, MeOD) δ (ppm), 189.27, 172.44, 171.59, 165.31, 163.29, 158.70, 131.71, 115.88, 113.74, 102.51, 81.28, 79.14, 68.50, 54.80, 47.10, 29.73, 27.33, 26.47; HRMS (M + Na): Calc'd for $\text{C}_{22}\text{H}_{31}\text{FNO}_8$: 456.2034. Found: 456.2034. Calc'd for $\text{C}_{22}\text{H}_{30}\text{FNO}_8\text{Na}$: 478.1853. Found: 478.1866.

1-carboxy-4-(2-(2-fluoro-4-hydroxyphenyl)-2-oxoethoxy)-4-oxobutan-1-aminium 2,2,2-trifluoroacetate, 143. The same procedure was used as in the synthesis of **130**. Adhesive ppt., 68%; IR (KBr): 3460, 3274, 3100-2800, 1739, 1691, 1602, 1520, 1421, 1377, 1309, 1298, 1201, 1178, 1128, 1055, 1027, 1008, 823, 762, 717, 613 cm^{-1} ; ^1H NMR (400 MHz, MeOD) δ (ppm), δ 7.84 (t, $J = 8.20$, 1H), 6.75 (d, $J = 7.52$, 1H), 6.62 (d, $J = 9.22$, 1H), 5.22 (s, 2H), 3.96 (m, 1H), 2.53 (t, $J = 6.92$, 2H), 2.09 (m, 1H), 1.97 (m, 1H); ^{13}C NMR (125 MHz, MeOD) δ (ppm), 189.55, 172.46, 169.99, 163.47, 161.33, 130.12, 117.24, 115.37, 114.10, 112.03, 103.37, 68.81, 54.27, 29.33, 26.48; HRMS (M⁺): Calc'd for $\text{C}_{13}\text{H}_{15}\text{FNO}_6$: 300.0878. Found 300.0859.

The same sequence of steps was followed to generate **144** and **145**.

5-(2-(4-(benzyloxy)-3-fluorophenyl)-2-oxoethyl)-1-tert-butyl-2-(tert-butoxy-carbonylamino)pentanedioate, 144e. Adhesive ppt., 82%; IR (KBr): 3307, 3100-2800, 1742, 1701, 1659, 1606, 1437, 1407, 1209, 1167, 955, 743, 700, 667; ^1H NMR (400 MHz, CD_3OD) δ (ppm), δ 7.82 (t, $J = 8.85$, 1H), 7.44 (m, 6H), 7.21 (d, $J = 12.02$, 1H), 5.43 (s, 2H), 5.31 (d, 2H), 3.89 (m, 1H), 2.49 (t, $J = 6.88$, 2H), 1.99 (m, 1H), 1.89 (m, 1H), 1.39 (s, 18H); ^{13}C NMR (125 MHz, $\text{d}^6\text{-DMSO}$) δ (ppm), 190.58, 171.74, 170.32, 155.53, 152.29, 150.89, 150.34, 135.82, 128.56, 127.93, 126.91,

125.61, 115.29, 114.83, 80.42, 78.11, 70.36, 66.23, 53.45, 29.75, 27.90, 27.60, 25.92;
HRMS (M + Na): Calc'd for C₂₉H₃₆FNO₈Na: 568.2323. Found: 568.2275.

1-tert-butyl-5-(2-(3-fluoro-4-hydroxyphenyl)-2-oxoethyl)-2-(tert-butoxy-carbonylamino)pentanedioate, 144e'. Adhesive ppt., 94%; IR (KBr): 3460, 3100-2800, 1742, 1701, 1659, 1606, 1437, 1407, 1209, 1167, 955, 743, 700, 667; ¹H NMR (400 MHz, d⁶-DMSO) δ (ppm), δ 7.72 (t, *J* = 8.52, 1H), 7.67 (d, *J* = 8.63, 1H), 7.22 (d, *J* = 7.64, 1H), 7.05 (t, *J* = 8.14, 1H), 5.39 (s, 2H), 3.82 (m, 1H), 2.48 (t, *J* = 6.88, 2H), 1.95 (m, 1H), 1.82 (m, 1H), 1.40 (s, 18H); ¹³C NMR (125 MHz, d⁶-DMSO) δ (ppm), 190.30, 171.74, 171.33, 155.53, 151.56, 150.50, 148.63, 125.62, 117.23, 115.70, 80.41, 78.10, 66.11, 54.37, 29.70, 28.15, 27.90, 25.79; HRMS (M + Na): Calc'd for C₂₂H₃₁FNO₈: 456.2034. Found: 456.2034. Calc'd for C₂₂H₃₀FNO₈Na: 478.1853. Found: 478.1815.

1-carboxy-4-(2-(3-fluoro-4-hydroxyphenyl)-2-oxoethoxy)-4-oxobutan-1-aminium 2,2,2-trifluoroacetate, 144. Adhesive ppt., 84%; IR (KBr): 3455, 3269, 3100-2800, 1741, 1693, 1610, 1553, 1420, 1201, 1050, 823, 759, 719 cm⁻¹; ¹H NMR (400 MHz, D₂O) δ (ppm), 7.72 (d, *J* = 8.98, 2H), 7.08 (t, *J* = 9.52, 1H), 5.41 (s, 2H), 4.57 (t, *J* = 7.42, 1H), 2.65 (t, *J* = 7.14, 2H), 2.34 (m, 1H), 2.12 (m, 1H); ¹³C NMR (125 MHz, D₂O) δ (ppm), 190.12, 172.06, 170.06, 161.44, 152.57, 150.54, 131.17, 126.14, 119.58, 117.22, 115.40, 67.74, 53.99, 30.02, 23.51; HRMS (M⁺): Calc'd for C₁₃H₁₅FNO₆: 300.0878. Found 300.0892.

5-(2-(4-(benzyloxy)-3-(trifluoromethyl)phenyl)-2-oxoethyl)-1-tert-butyl-2-(tert-butoxycarbonylamino)pentanedioate, 145e. This was synthesized in the same

manner as **143e** by a laboratory associate. However, no characterization was done preceding the next synthetic step.

1-tert-butyl-5-(2-(4-hydroxy-3-(trifluoromethyl)phenyl)-2-oxoethyl)-2-(tert-butoxycarbonylamino)pentanedioate, 145e'. Adhesive ppt., 91%; ^1H NMR (400 MHz, $\text{d}^6\text{-DMSO}$) δ (ppm), 11.73 (s, 1H), 8.08 (s, 1H), 8.06 (s, 1H), 7.21 (d, $J = 7.52$, 1H), 7.13 (d, $J = 9.50$), 5.55 (s, 2H), 3.91 (dd, $J = 8.40$, $J = 5.80$, 1H), 2.49 (t, $J = 9.05$, 2H), 1.94, (m, 2H), 1.82 (m, 1H), 1.40 (s, 9H), 1.36 (s, 9H).

1-carboxy-4-(2-(4-hydroxy-3-(trifluoromethyl)phenyl)-2-oxoethoxy)-4-oxobutan-1-aminium 2,2,2-trifluoroacetate, 145. White ppt., 55%, Mp: 59-61°C; IR (KBr): 3405, 3310, 3100-2800, 1735, 1710, 1690, 1595, 1520, 1430, 1370, 1248, 1200, 1165, 1050, 818, 760, 710 cm^{-1} ; ^1H NMR (400 MHz, MeOD) δ (ppm), 8.13 (d, $J = 1.50$, 1H), 8.06 (dd, $J = 8.70$, $J = 2.10$, 1H), 7.06 (d, $J = 8.50$, 1H), 5.41 (s, 2H), 4.55 (d, $J = 9.10$, 1H), 2.61 (t, $J = 7.70$, 2H), 2.36, (m, 1H), 2.12 (m, 1H); ^{13}C NMR (125 MHz, MeOD) δ (ppm), 192.31, 173.69, 162.42, 159.48, 159.19, 134.81, 128.68, 126.79, 123.89, 118.70, 118.07, 116.42, 67.78, 53.46, 31.21, 27.19; HRMS (M^+): Calc'd for $\text{C}_{14}\text{H}_{15}\text{F}_3\text{NO}_6$: 350.0851. Found 350.0863.

1-(4-(benzyloxy)phenyl)ethanone, 146b. The same procedure to construct **135b** was utilized but only one equivalent of benzyl bromide was required. White ppt, 96%. This compound is known. GC/MS (EI): One peak, retention time, 7.43 min (initial temp 50°C, ramp 25°C/min until 300°C), MS; 226.09 m/z.

1-(4-(benzyloxy)phenyl)-2-bromoethanone, 146c. The same method to generate **135c** was used. Oil, ~94%. *This compound is known*. GC/MS (EI): One peak,

retention time, 8.22 min (initial temp 50°C, ramp 25°C/min until 300°C), MS; 304.01, 306.01 m/z.

2-(4-(benzyloxy)phenyl)-2-oxoethyl-2-(tert-butoxycarbonylamino)acetate, 146d.

The same general method to produce **135d** was used but with N-Boc-Gly. White ppt., 95%, Mp: 100-102°C; IR (KBr): 3307, 3100-2800, 1742, 1701, 1659, 1606, 1437, 1407, 1209, 1167, 955, 743, 700, 667; ¹H NMR (400 MHz, CDCl₃) δ (ppm), 7.90 (d, *J* = 8.49, 2H), 7.41 (m, 5H), 7.05 (d, *J* = 8.82, 2H), 5.37 (s, 2H), 5.15 (s, 2H), 5.04 (s, 1H), 4.12 (d, *J* = 7.02, 2H), 1.45 (s, 9H); ¹³C NMR (125 MHz, CDCl₃) δ (ppm), 189.94, 170.09, 163.32, 155.72, 135.92, 132.28, 130.12, 128.77, 128.04, 127.15, 114.99, 80.10, 70.25, 66.30, 42.31, 28.33; HRMS (M + Na): Calc'd for C₂₂H₂₅NO₆Na: 422.1580. Found: 422.1559.

2-(4-hydroxyphenyl)-2-oxoethyl 2-(tert-butoxycarbonylamino)acetate, 146e.

The same general method to produce **135e** was used. White ppt., 94%, Mp: 125-127 °C; ¹H NMR (400 MHz, d⁶-DMSO) δ (ppm), 10.48 (s, 1H), 7.85 (d, *J* = 8.66, 2H), 7.27 (t, *J* = 5.63, 1H), 6.88 (d, *J* = 8.23, 2H), 5.42 (s, 2H), 3.82 (d, *J* = 6.95, 2H), 1.38 (s, 9H); ¹³C NMR (125 MHz, d⁶-DMSO) δ (ppm), 190.36, 170.15, 162.87, 155.75, 130.55, 125.32, 115.41, 78.48, 66.25, 41.58, 28.04; HRMS (M + Na): Calc'd for C₁₅H₁₉NO₆Na: 332.1110. Found: 332.1101.

2-(2-(4-hydroxyphenyl)-2-oxoethoxy)-2-oxoethanaminium-2,2,2-trifluoroacetate,

146. The same general method to produce **135** was followed. Adhesive ppt, 79%; IR (KBr): 3405, 3310, 3100-2800, 1735, 1710, 1690, 1595, 1520, 1430, 1370, 1248, 1200, 1165, 1050, 818, 760, 710 cm⁻¹; ¹H NMR (400 MHz, MeOD) δ (ppm), 7.88 (d,

$J = 8.42$, 2H), 6.88 (d, $J = 8.06$, 2H), 5.57 (s, 1H), 5.47 (s, 1H), 4.24 (s, 1H), 4.04 (s, 1H); ^{13}C NMR (125 MHz, MeOD) δ (ppm), 191.21, 168.34, 167.11, 163.54, 130.40, 125.88, 117.38, 115.41, 66.63, 40.52; HRMS (M⁺): Calc'd for $\text{C}_{10}\text{H}_{12}\text{NO}_4$: 210.0766. Found: 210.0764.

The same succession of steps was followed to produce **147-149**. The amino acids all were N-Boc protected.

2-(4-(benzyloxy)phenyl)-2-oxoethyl-2-(tert-butoxycarbonylamino)-3-methyl-

butanoate, 147d. White ppt., 95%, Mp: 119-120°C; IR (KBr): 3307, 3100-2800, 1742, 1701, 1659, 1606, 1437, 1407, 1209, 1167, 955, 743, 700, 667; ^1H NMR (400 MHz, d^6 -DMSO) δ (ppm), 7.96 (d, $J = 8.60$, 2H), 7.40 (m, 5H), 7.13 (m, 3H), 5.49 (d, $J = 8.24$, 1H), 5.42 (d, $J = 8.20$, 1H), 5.15 (s, 2H), 4.05 (t, $J = 6.75$, 1H), 2.14 (m, 1H), 1.39 (s, 9H), 0.97 (d, $J = 7.05$, 6H); ^{13}C NMR (125 MHz, d^6 -DMSO) δ (ppm), 190.88, 171.51, 162.60, 155.73, 136.37, 130.15, 128.89, 128.03, 127.79, 126.89, 114.97, 78.19, 69.53, 66.34, 59.07, 29.78, 27.91, 19.03; HRMS (M + Na): Calc'd for $\text{C}_{25}\text{H}_{31}\text{NO}_6\text{Na}$: 464.2049. Found: 464.2061.

2-(4-hydroxyphenyl)-2-oxoethyl-2-(tert-butoxycarbonylamino)-3-methyl-

butanoate, 147e. Adhesive ppt., 75%; ^1H NMR (400 MHz, MeOD) δ (ppm), 7.90 (d, $J = 8.75$, 2H), 6.88 (m, 3H), 5.50 (d, $J = 8.22$, 1H), 5.46 (d, $J = 8.15$, 1H), 4.22 (t, $J = 6.85$, 1H), 2.25 (m, 1H), 1.48 (s, 9H), 1.05 (d, $J = 7.10$, 6H); ^{13}C NMR (125 MHz, MeOD) δ (ppm), 191.03, 171.84, 163.00, 156.88, 130.73, 125.81, 114.80, 79.19, 66.02, 59.08, 30.58, 27.17, 18.26; HRMS (M + Na): Calc'd for $\text{C}_{18}\text{H}_{25}\text{NO}_6\text{Na}$: 374.1580. Found: 374.1592.

1-(2-(4-hydroxyphenyl)-2-oxoethoxy)-3-methyl-1-oxobutan-2-aminium-2,2,2-trifluoroacetate, 147. Adhesive ppt, 72%; IR (KBr): 3405, 3310, 3100-2800, 1735, 1710, 1690, 1595, 1520, 1430, 1370, 1248, 1200, 1165, 1050, 818, 760, 710 cm^{-1} ; ^1H NMR (400 MHz, MeOD) δ (ppm), 7.86 (d, $J = 8.29$, 2H), 6.88 (d, $J = 8.02$, 2H), 5.59 (d, $J = 8.22$, 1H), 5.42 (d, $J = 8.15$, 1H), 4.09 (t, $J = 6.72$, 1H), 2.49 (m, 1H), 1.06 (d, $J = 7.15$, 6H); ^{13}C NMR (125 MHz, MeOD) δ (ppm), 188.64, 167.78, 161.50, 158.73, 129.15, 123.81, 115.85, 113.58, 65.78, 61.36, 27.84, 16.29; HRMS (M⁺): Calc'd for $\text{C}_{13}\text{H}_{18}\text{NO}_4$: 252.1230. Found: 252.1222.

1-(2-(4-hydroxyphenyl)-2-oxoethoxy)-3-(1H-indol-3-yl)-1-oxopropan-2-aminium 2,2,2-trifluoroacetate, 148. The precursor, **148e**, was obtained from an associate, without characterization. White ppt., 92%, Mp: 75-77°C; IR (KBr): 3405, 3310, 3100-2800, 1735, 1710, 1690, 1595, 1520, 1430, 1370, 1248, 1200, 1165, 1050, 818, 760, 710 cm^{-1} ; ^1H NMR (400 MHz, $\text{d}^6\text{-DMSO}$) δ (ppm), 11.11 (s, 1H), 10.70, (s, 1H), 8.46, (s, 3H), 7.87 (d, $J = 12.1$, 2H), 7.60 (d, $J = 8.10$, 1H), 7.41, (d, $J = 8.04$, 1H), 7.33 (d, $J = 4.23$, 1H), 7.10 (t, $J = 7.95$, $J = 1\text{H}$), 7.05 (t, $J = 7.85$, 1H), 6.92 (d, $J = 8.20$, 2H), 5.61 (dd, $J = 16.30$, $J = 12.20$, 2H), 4.45 (t, $J = 7.05$, 1H), 3.32 (m, 2H); ^{13}C NMR (125 MHz, $\text{d}^6\text{-DMSO}$) δ (ppm), 189.81, 169.06, 162.96, 158.82, 136.25, 130.50, 128.10, 126.90, 125.12, 125.01, 121.20, 118.89, 117.96, 115.52, 111.57, 106.37, 67.29, 52.53, 26.36; HRMS (M⁺): Calc'd for $\text{C}_{19}\text{H}_{19}\text{N}_2\text{O}_4$: 339.1345. Found: 339.1345.

1-(2-(4-hydroxyphenyl)-2-oxoethoxy)-1-oxo-3-phenylpropan-2-aminium-2,2,2-trifluoroacetate, 149. The precursor, **149e**, was obtained from an associate, without

characterization. White ppt., 74%, Mp: 64-66°C; IR (KBr): 3405, 3310, 3100-2800, 1735, 1710, 1690, 1595, 1520, 1430, 1370, 1248, 1200, 1165, 1050, 818, 760, 710 cm^{-1} ; ^1H NMR (400 MHz, d^6 -DMSO) δ (ppm), 10.86, (s, 1H), 8.58, (s, 3H), 7.87 (d, $J = 8.04$, 2H), 7.31 (m, 5H), 6.92 (d, $J = 8.15$, 2H), 5.61 (dd, $J = 16.15$, $J = 4.00$, 2H), 4.45 (t, $J = 4.20$, 1H), 3.30 (dd, $J = 15.88$, $J = 8.03$, 1H), 3.18 (dd, $J = 12.10$, $J = 4.05$, 1H); ^{13}C NMR (125 MHz, d^6 -DMSO) δ (ppm), 189.73, 168.75, 163.00, 158.66, 134.66, 130.50, 129.55, 128.60, 127.26, 124.95, 117.95, 115.51, 67.27, 53.01, 36.03; HRMS (M⁺): Calc'd for $\text{C}_{17}\text{H}_{18}\text{NO}_4$: 300.1230. Found: 300.1244.

(4R)-2-(4-(benzyloxy)phenyl)-2-oxoethyl-4-((3R,5R,8R,10S,12S,13R,17R)-3,12-dihydroxy-10,13-dimethylhexadecahydro-1H-cyclopenta[a]phenanthren-17-yl)pentanoate, 150d. The reaction was patterned after the one to synthesize **146d** but used DMF instead of CH_3CN as the solvent. White ppt., 84%, Mp: 77-79°C; ^1H NMR (400 MHz, CDCl_3) δ (ppm), 7.90 (d, $J = 8.47$, 2H), 7.40 (m, 5H), 7.01 (d, $J = 9.00$, 2H), 5.28 (s, 2H), 5.14 (s, 2H), 3.99 (s, 1H), 3.67 (s, 1H), 2.56 (m, 1H), 2.46 (m, 1H), 2.00-1.00 (m, 26 H), 1.01 (s, 3H), 0.91 (s, 3H), 0.67 (s, 3H); ^{13}C NMR (125 MHz, d^6 -DMSO) δ (ppm), 197.78, 173.72, 163.16, 135.98, 130.11, 128.75, 128.34, 127.51, 127.48, 114.89, 73.18, 71.88, 70.21, 65.89, 65.62, 53.46, 48.28, 47.37, 46.54, 42.10, 36.46, 36.31, 36.06, 35.23, 35.05, 34.14, 33.69, 30.92, 30.82, 30.54, 28.66, 27.44, 26.14, 23.66, 23.19, 17.39, 17.29, 15.30, 12.79.

(4R)-2-(4-hydroxyphenyl)-2-oxoethyl-4-((3R,5R,8R,10S,12S,13R,17R)-3,12-dihydroxy-10,13-dimethylhexadecahydro-1H-cyclopenta[a]phenanthren-17-yl)pentanoate, 150. The same method to produce **130e'** was used. White ppt., 93%,

Mp: 97-99°C; ¹H NMR (400 MHz, d⁶-DMSO) δ (ppm), 7.84 (d, *J* = 8.42, 2H), 6.88 (d, *J* = 8.95, 2H), 5.35 (s, 2H), 4.21, (s, 1H), 3.81, (s, 1H), 2.52 (m, 1H), 2.40 (m, 1H), 2.00-1.00 (m, 26 H), 0.96 (s, 3H), 0.85 (s, 3H), 0.62 (s, 3H); ¹³C NMR (125 MHz, d⁶-DMSO) δ (ppm), 190.91, 173.97, 160.98, 130.46, 127.41, 115.72, 73.29, 71.98, 65.90, 65.65, 60.46, 53.45, 48.29, 47.10, 42.08, 36.37, 36.02, 35.20, 34.13, 33.70, 30.73, 30.43, 28.61, 27.45, 26.12, 23.65, 23.17, 21.10, 17.37, 15.29, 14.22, 12.75; HRMS (M + H): Calc'd for C₃₂H₄₇O₆: 527.3373. Found: 527.3397. (M + Na): Calc'd for C₃₂H₄₆O₆Na: 549.3192. Found: 549.3191. (M + NH₄): Calc'd for C₃₂H₅₀O₆N: 544.3639. Found: 544.3634.

diethyl 2-(4-(benzyloxy)phenyl)-2-oxoethylphosphonate, 151d. The general method of De Borggraeve¹⁴⁷ was utilized. An Argon purged solution of 1-(4-(benzyloxy)phenyl)-2-bromoethanone (**146d**, 2.44 g (7.99 mmol)) in 10 ml of neat triethylphosphite was heated to 100°C, where it was maintained with stirring and under Argon for 17h. After cooling to room temperature, most of the surfeit CH₃CN/Triethylphosphite was removed under reduced pressure. The mixture was then flash chromatographed on silica with gradients of ethyl acetate/hexanes mixtures, until **151d** eluted at 100% ethyl acetate. After 1 day of vacuum, viscous oil was observed, 2.48 g (86%). *This compound is known.* ¹H NMR (400 MHz, d⁶-DMSO) δ (ppm), 8.00 (d, *J* = 9.25, 2H), 7.40 (m, 5H), 7.13 (d, *J* = 9.56, 2H), 5.22 (s, 2H), 4.00 (m, 4H), 1.24 (t, *J* = 8.33, 6H).

diethyl 2-(4-hydroxyphenyl)-2-oxoethylphosphonate, 151. The same general method to produce **130e'** was used. White ppt., 96%, Mp: 108-110°C; IR (KBr):

3460, 3310, 3100-2800, 1735, 1710, 1690, 1595, 1520, 1430, 1370, 1248, 1200, 1165, 1050, 818, 760, 710 cm^{-1} ; ^1H NMR (400 MHz, d^6 -DMSO) δ (ppm), 10.45 (s, 1H), 7.89 (d, $J = 9.31$, 2H), 6.85 (d, $J = 9.40$, 2H), 5.09 (s, 2H), 4.00 (m, 4H), 1.24 (t, $J = 8.47$, 6H); ^{13}C NMR (125 MHz, d^6 -DMSO) δ (ppm), 190.28, 162.46, 131.89, 127.80, 115.07, 60.88, 37.66, 16.10; HRMS (M + Na): Calc'd for $\text{C}_{12}\text{H}_{17}\text{PO}_5\text{Na}$: 295.0711; Found: 295.0698; (M + H): Calc'd for $\text{C}_{12}\text{H}_{18}\text{PO}_5$: 273.0892. Found: 273.0877.

1-(4-(benzyloxy)phenyl)-2-fluoroethanone, 152d. To a solution of 1-(4-(benzyloxy)phenyl)-2-bromoethanone (analog of **146d**, 820 mg (2.69 mmol)) in 100 ml CH_3CN was added cesium fluoride (1.63 g, 10.7 mmol). The heterogenous mixture was refluxed for 1.5 h at which time the reaction was deemed complete as indicated by GC/MS. Excess CH_3CN was removed under reduced pressure, equal volumes of EtOAc/ H_2O added (50 ml), the organic phase retained and flash chromatographed on silica gel (1:1 Et₂O, Hex), affording 590 mg of **152d** as a white ppt, 90%, Mp: 106-108°C; IR (KBr): 3460, 3310, 3100-2800, 1735, 1710, 1690, 1595, 1520, 1430, 1370, 1248, 1200, 1165, 1050, 818, 760, 710 cm^{-1} ; ^1H NMR (400 MHz, CDCl_3) δ (ppm), 7.98 (d, $J = 8.67$, 2H), 7.40 (m, 5H), 7.06 (d, $J = 9.10$, 2H), 5.54 (s, 1H), 5.43 (s, 1H), 5.16 (s, 2H); ^{13}C NMR (125 MHz, CDCl_3) δ (ppm), 192.01, 163.37, 135.91, 131.58, 130.30, 128.77, 127.50, 126.45, 114.80, 84.22, 70.24; HRMS (FAB +): Calc'd for $\text{C}_{15}\text{H}_{13}\text{FO}_2$: 245.0978. Found: 245.0978.

2-fluoro-1-(4-hydroxyphenyl)ethanone, 152. White ppt., 92%. *This compound is known.* ^1H NMR (400 MHz, MeOD) δ (ppm), 7.91 (d, $J = 8.50$, 2H), 6.91 (d, $J =$

9.15, 2H), 5.72 (s, 1H), 5.61 (s, 1H); HRMS (M - H): Calc'd for C₈H₆FO₂: 153.0352. Found: 153.0326. (M + Na): Calc'd for C₈H₇FO₂Na: 177.0328. Found: 177.0327.

benzyl 5-acetyl-2-(benzyloxy)benzoate, 153b. The reaction conditions to produce **153c** were amenable to those to create **153b**. White ppt., 93%, Mp: 98-100 °C; IR (KBr): 3325, 3100-2800, 1726, 1697, 1676, 1598, 1500, 1452, 1370, 1269, 1230, 1176, 1060, 1030, 1008, 821, 757, 721, 698 cm⁻¹; ¹H NMR (400 MHz, CDCl₃) δ (ppm), 8.46 (d, *J* = 2.10, 1H), 8.08 (dd, *J* = 9.00, *J* = 2.34, 1H), 7.44-7.33 (m, 10H), 7.09 (d, *J* = 8.85, 2H), 5.38 (s, 2H), 5.25 (s, 2H), 2.58 (s, 3H); ¹³C NMR (125 MHz, CDCl₃) δ (ppm), 195.42, 165.04, 160.91, 135.11, 134.24, 133.04, 130.28, 129.16, 128.22, 127.81, 119.35, 117.36, 112.49, 70.08, 68.86, 25.74; HRMS (M + Na): Calc'd for C₂₃H₂₀O₄Na: 383.1259. Found: 383.1262.

benzyl 2-(benzyloxy)-5-(2-bromoacetyl)benzoate, 153c. The synthetic method to generate **122d** was followed. Oil, 95%; IR (KBr): 3325, 3100-2800, 1726, 1697, 1676, 1598, 1500, 1452, 1370, 1269, 1230, 1176, 1060, 1030, 1008, 821, 757, 721, 698 cm⁻¹; ¹H NMR (400 MHz, CDCl₃) δ (ppm), 8.50 (d, *J* = 2.15, 1H), 8.10 (dd, *J* = 9.00, *J* = 2.40, 1H), 7.44-7.33 (m, 10H), 7.10 (d, *J* = 8.90, 2H), 5.38 (s, 2H), 5.25 (s, 2H), 4.41 (s, 2H); ¹³C NMR (125 MHz, CDCl₃) δ (ppm), 189.39, 165.32, 162.18, 135.68, 135.48, 134.52, 133.49, 128.74, 128.26, 127.11, 126.47, 120.87, 113.44, 70.86, 67.21, 30.48; HRMS (M + Na): Calc'd for C₂₃H₁₉BrO₄Na: 461.0365. Found: 461.0372.

benzyl-2-(benzyloxy)-5-(2-(4-(*tert*-butoxycarbonyl-amino)-butanoyloxy)-acetyl)-benzoate, 153d. The synthetic mode to engender **122e** was utilized. White ppt.,

75%, Mp: 75-77°C; IR (KBr): 3271, 3100-2800, 1733, 1701, 1697, 1600, 1577, 1500, 1454, 1415, 1365, 1269, 1251, 1215, 1166, 1056, 1028, 1008, 919, 875, 821, 758, 700 cm⁻¹; ¹H NMR (400 MHz, d⁶-DMSO) δ (ppm), 8.26 (d, *J* = 2.44, 1H), 8.12 (dd, *J* = 9.00, *J* = 2.33, 1H), 7.44-7.33 (m, 11H), 6.89 (t, *J* = 5.51, 2H), 5.45 (s, 2H), 5.33 (s, 2H), 2.97 (t, *J* = 7.20, 2H), 2.42 (t, *J* = 7.00, 2H), 1.68 (m, 2H), 1.38 (s, 9H); ¹³C NMR (125 MHz, CDCl₃) δ (ppm), 190.85, 172.13, 165.28, 161.01, 155.90, 135.82, 133.51, 130.81, 128.42, 128.04, 127.89, 127.33, 126.27, 113.95, 77.78, 70.10, 64.96, 59.73, 39.30, 30.64, 28.22, 25.24; HRMS (M + Na): Calc'd for C₃₂H₃₅NO₈Na: 584.2260. Found: 584.2239.

5-(2-(4-(*tert*-butoxycarbonylamino)butanoyloxy)acetyl)-2-hydroxybenzoic acid,

153e. The reaction conditions to produce **130e'** were abided. Adhesive ppt., 96%; ¹H NMR (400 MHz, d⁶-DMSO) δ (ppm), 8.37 (d, *J* = 2.35, 1H), 8.08 (dd, *J* = 9.15, *J* = 2.30, 1H), 7.10 (d, *J* = 8.90, 2H) 6.90 (t, *J* = 5.51, 2H), 5.43 (s, 2H), 2.98 (t, *J* = 7.15, 2H), 2.44 (t, *J* = 7.05, 2H), 1.68 (m, 2H), 1.36 (s, 9H).

4-(2-(3-carboxy-4-hydroxyphenyl)-2-oxoethoxy)-4-oxobutan-1-aminium-2,2,2-

trifluoroacetate, 153. The method used to produce **130** was followed. Adhesive ppt., 94%; IR (KBr): 3440, 3274, 3100-2800, 1733, 1741, 1692, 1649, 1631, 1596, 1500, 1450, 1416, 1299, 1201, 1184, 1124, 1053, 1006, 823, 800, 760, 707, 680 cm⁻¹; ¹H NMR (400 MHz, D₂O) δ (ppm), 8.36 (s, 1H), 8.00 (d, *J* = 8.93, 1H), 7.08 (d, *J* = 8.10), 5.46 (s, 2H), 3.12 (t, *J* = 7.20, 2H), 2.68 (t, *J* = 7.00, 2H), 2.06 (m, 2H); ¹³C NMR (125 MHz, D₂O) δ (ppm), 193.77, 174.11, 171.62, 165.14, 163.06, 134.87,

131.89, 119.72, 117.89, 115.09, 113.41, 66.60, 38.55, 30.45, 21.97; HRMS (M⁺): Calc'd for C₁₃H₁₆NO₆: 282.0978. Found: 282.0967.

4-(2-(4-hydroxy-3-(methoxycarbonyl)phenyl)-2-oxoethoxy)-4-oxobutan-1-

aminium 2,2,2-trifluoroacetate, 154. The precursor, methyl-5-(2-(4-(*tert*-butoxycarbonylamino)butanoyloxy)acetyl)-2-hydroxybenzoate, was received from an associate. Adhesive ppt., 79%; IR (KBr): 3440, 3274, 3100-2800, 1733, 1741, 1692, 1649, 1631, 1596, 1500, 1450, 1416, 1299, 1201, 1184, 1124, 1053, 1006, 823, 800, 760, 707, 680 cm⁻¹; ¹H NMR (400 MHz, D₂O) δ (ppm), 8.40 (s, 1H), 8.03 (d, *J* = 9.05, 1H), 7.05 (d, *J* = 8.00, 1H), 5.48 (s, 2H), 3.96 (s, 3H), 3.10 (t, *J* = 7.15, 2H), 2.70 (t, *J* = 7.00, 2H), 2.05 (m, 2H); ¹³C NMR (125 MHz, D₂O) δ (ppm), 193.33, 174.36, 169.84, 165.22, 162.84, 133.99, 132.18, 121.01, 117.44, 115.87, 113.73, 66.88, 51.10, 39.02, 29.97; HRMS (M⁺): Calc'd for C₁₄H₁₈NO₆: 298.1134. Found: 298.1123.

benzyl 2-(benzyloxy)-5-(2-(dodecanoyloxy)acetyl)benzoate, 155d. The same method to produce **153d** was used but with dodecanoic acid. Oil, 79%; IR (KBr): 3271, 3100-2800, 1733, 1701, 1697, 1600, 1577, 1500, 1454, 1415, 1365, 1269, 1251, 1215, 1166, 1056, 1028, 1008, 919, 875, 821, 758, 700 cm⁻¹; ¹H NMR (400 MHz, d⁶-DMSO) δ (ppm), 8.26 (d, *J* = 2.30, 1H), 8.14 (dd, *J* = 8.85, *J* = 2.25, 1H), 7.44-7.33 (m, 11H), 5.42 (s, 2H), 5.32 (s, 4H), 2.42 (t, *J* = 7.15, 2H), 1.55 (m, 2H), 1.26-1.15 (m, 16), 0.84 (t, *J* = 5.95, 3H); ¹³C NMR (125 MHz, d⁶-DMSO) δ (ppm), 190.35, 173.29, 165.34, 162.09, 135.67, 133.62, 132.43, 130.80, 128.33, 127.10, 126.76, 120.77, 113.49, 70.82, 67.20, 65.60, 33.94, 31.80, 30.51, 29.64, 29.37, 29.29,

29.13, 24.93, 22.72, 21.09, 14.23; HRMS (M + Na): Calc'd for C₃₅H₄₂O₆Na: 581.2879. Found: 581.2850. (M + H): Calc'd for C₃₅H₄₃O₆: 559.3060. Found: 559.3055. (M + NH₄): Calc'd for C₃₅H₄₆O₆N: 576.3325. Found: 576.3337.

5-(2-(dodecanoyloxy)acetyl)-2-hydroxybenzoic acid, 155. The same method to generate **153e** was followed. White ppt., 92%, Mp: 58-60°C; IR (KBr): 3271, 3100-2800, 1733, 1701, 1697, 1600, 1577, 1500, 1454, 1415, 1365, 1269, 1251, 1215, 1166, 1056, 1028, 1008, 919, 875, 821, 758, 700 cm⁻¹; ¹H NMR (400 MHz, CDCl₃) δ (ppm), 11.02, (s, 1H), 8.51 (d, *J* = 2.05, 1H), 8.11 (dd, *J* = 4.80, *J* = 4.10, 1H), 7.10 (d, *J* = 7.95, 1H), 5.32 (s, 2H), 2.25 (t, *J* = 7.20, 2H), 1.70 (m, 2H), 1.39-1.27 (m, 16H), 0.88 (t, *J* = 6.00, 3H); ¹³C NMR (125 MHz, CDCl₃) δ (ppm), 190.34, 173.82, 172.53, 166.28, 135.87, 128.91, 126.16, 118.74, 111.25, 65.67, 35.44, 33.99, 31.93, 31.00, 29.63, 29.36, 29.12, 24.93, 22.71, 14.15; HRMS (M - H): Calc'd for C₂₁H₂₉O₆: 377.1964. Found: 377.1959.

The same procedures were utilized to synthesize **156**.

benzyl 2-(benzyloxy)-5-(2-(tetradecanoyloxy)acetyl)benzoate, 156d. White ppt., 71%, Mp: 55-57°C; IR (KBr): 3271, 3100-2800, 1733, 1701, 1697, 1600, 1577, 1500, 1454, 1415, 1365, 1269, 1251, 1215, 1166, 1056, 1028, 1008, 919, 875, 821, 758, 700 cm⁻¹; ¹H NMR (400 MHz, d⁶-DMSO) δ (ppm), 8.26 (d, *J* = 2.30, 1H), 8.14 (dd, *J* = 8.85, *J* = 2.25, 1H), 7.44-7.33 (m, 11H), 5.42 (s, 2H), 5.33 (s, 4H), 2.40 (t, *J* = 7.10, 2H), 1.56 (m, 2H), 1.26-1.22 (m, 20H), 0.84 (t, *J* = 6.00, 3H); ¹³C NMR (125 MHz, CDCl₃) δ (ppm), 190.955, 174.49, 165.34, 162.09, 135.67, 133.62, 132.43, 130.80, 128.33, 127.10, 126.76, 120.77, 113.49, 70.82, 67.20, 65.60, 33.94, 31.80,

30.51, 29.64, 29.37, 29.29, 29.13, 28.66, 28.31, 24.93, 22.72, 21.09, 14.23; HRMS (M + Na): Calc'd for C₃₇H₄₆O₆Na: 609.3192. Found: 609.3201.

2-hydroxy-5-(2-(tetradecanoyloxy)acetyl)benzoic acid, 156. White ppt., 94%, Mp: 60-62°C; IR (KBr): 3271, 3100-2800, 1733, 1701, 1697, 1600, 1577, 1500, 1454, 1415, 1365, 1269, 1251, 1215, 1166, 1056, 1028, 1008, 919, 875, 821, 758, 700 cm⁻¹; ¹H NMR (400 MHz, d⁶-DMSO) δ (ppm), 8.30 (d, *J* = 2.30, 1H), 7.92 (dd, *J* = 8.80, *J* = 2.20, 1H), 6.88 (d, *J* = 8.60, 1H), 5.36 (s, 2H), 2.40 (t, *J* = 7.05, 2H), 1.56 (m, 2H), 1.26-1.22 (m, 20H), 0.85 (t, *J* = 6.00, 3H); ¹³C NMR (125 MHz, CDCl₃) δ (ppm), 190.40, 174.49, 172.42, 170.63, 133.28, 130.85, 123.29, 117.31, 116.06, 65.78, 33.62, 31.27, 29.04, 28.99, 28.95, 28.86, 28.69, 28.51, 28.33, 26.23, 24.47, 22.08, 13.94; HRMS (M + Na): Calc'd for C₂₃H₃₄O₆Na: 429.2253. Found: 429.2250.

5-acetyl-2-(benzyloxy)benzoic acid, 157b. The general benzylation method as **122b** was followed. To a solution of methyl-5-acetyl-2-hydroxybenzoate (**157a**, 3.06 g, 15.7 mmol) in 50 ml of DMF was added potassium carbonate (6.53 g, 47.3 mmol) and benzyl bromide (4.68 ml, 39.4 mmol). The reaction was stirred at room temperature for 2 days. At this time, the mixture was diluted with 200 ml of 1:1 EtOAc/H₂O, the organic phase retained, concentrated, and flash chromatographed on silica gel (4:1 Hex/EtOAc) to obtain an oil, 4.40 g (98%) that was then dissolved in 100 ml of CH₃OH with 25 ml of aqueous 6 M KOH. The mixture was stirred for 3 h, at which time, conc. HCl was added slowly until an acidic solution was manifest by pH paper. The profuse solid material (KCl) was filtered off, 150 ml of CHCl₃ added, the organic phase extracted, dried with MgSO₄, and inspissated *in vacuo* to produce

157b as a white precipitate, 3.50 g (92%). *This compound is known.* ^1H NMR (400 MHz, CDCl_3) δ (ppm), 8.77 (d, $J = 2.00$, 1H), 8.23 (dd, $J = 8.68$, $J = 2.20$, 1H), 7.45 (m, 5H), 7.22 (d, $J = 8.75$, 1H), 5.38 (s, 2H), 2.63 (s, 3H).

5-acetyl-N-(4-benzoylphenyl)-2-(benzyloxy)benzamide, 157c. The general approach utilized by Fairbanks, et. al.¹⁴⁸ was applied. To a solution comprised of **157b** (614 mg, 2.27 mmol) in 25 ml of dry CH_2Cl_2 was added DCC (469 mg, 2.27 mmol) and DMAP (69 mg, 0.568 mmol). This admixture was immured in an ice/saturated NaCl solution ($\sim 0^\circ\text{C}$). While stirring, a solution of 4-aminophenyl-(phenyl)methanone (448 mg, 2.27 mmol) in 10 ml of CH_2Cl_2 was slowly added dropwise. Once added, the reaction mixture was removed from the ice bath and persisted at room temperature overnight. At this time, the excess DCU was filtered off and remaining solution flash chromatographed ($\text{CH}_2\text{Cl}_2/\text{EtOAc}$) to afford **157c** as a white precipitate, 58%. Mp: 185-187 $^\circ\text{C}$; IR (KBr): 3271, 3100-2800, 1685, 1670, 1649, 1593, 1535, 1500, 1323, 1311, 1200, 1054, 1028, 1008, 927, 823, 760 cm^{-1} ; ^1H NMR (400 MHz, CDCl_3) δ (ppm), 10.10 (s, 1H), 8.94 (d, $J = 2.32$, 1H), 8.24 (dd, $J = 8.94$, $J = 2.32$, 1H), 7.77-7.46 (m, 14H), 6.69 (d, $J = 8.28$, 1H), 5.33 (s, 2H), 2.68 (s, 3H); ^{13}C NMR (125 MHz, CDCl_3) δ (ppm), 196.50, 195.64, 162.29, 159.96, 150.90, 142.07, 138.86, 135.49, 134.25, 133.63, 132.88, 132.19, 131.30, 129.78, 129.55, 128.98, 128.29, 127.20, 120.98, 118.92, 113.65, 72.48, 26.62; HRMS (M + H): Calc'd for $\text{C}_{29}\text{H}_{24}\text{NO}_4$: 450.1705. Found: 450.1700.

N-(4-benzoylphenyl)-2-(benzyloxy)-5-(2-bromoacetyl)benzamide, 157d. The synthetic method paralleled that for **122d**. Oil, $\sim 92\%$; ^1H NMR (400 MHz, CDCl_3) δ

(ppm), 10.10 (s, 1H), 8.95, (d, $J = 2.32$, 1H), 8.24 (dd, $J = 8.94$, $J = 2.32$, 1H), 7.77-7.46 (m, 15H), 5.35 (s, 2H), 4.53 (s, 2H).

2-(3-(4-benzoylphenylcarbamoyl)-4-(benzyloxy)phenyl)-2-oxoethyl-4-(tert-butoxycarbonylamino)butanoate, 157e. The same reaction conditions were utilized as those to produce **122e**. White ppt., 48%, Mp: 199-201°C; IR (KBr): 3271, 3100-2800, 1685, 1670, 1649, 1593, 1535, 1500, 1323, 1311, 1200, 1054, 1028, 1008, 927, 823, 760 cm^{-1} ; ^1H NMR (400 MHz, d^6 -DMSO) δ (ppm), 10.69 (s, 1H), 8.20, (d, $J = 2.10$, 1H), 8.14 (dd, $J = 9.00$, $J = 2.40$, 1H), 7.77-7.46 (m, 14H), 6.89 (t, $J = 5.95$, 1H), 5.48 (s, 2H), 5.35 (s, 2H), 2.97 (t, $J = 6.80$, 2H), 2.40 (t, $J = 7.80$, 2H), 1.70 (m, 2H), 1.38 (s, 9H); ^{13}C NMR (125 MHz, d^6 -DMSO) δ (ppm), 194.56, 191.01, 172.23, 164.29, 159.60, 155.61, 142.90, 137.45, 136.00, 132.32, 132.08, 131.12, 131.73, 131.12, 129.48, 129.41, 128.50, 128.15, 127.71, 126.59, 125.80, 118.68, 113.41, 77.47, 70.35, 66.17, 30.65, 28.22, 24.95; HRMS (M + Na): Calc'd for $\text{C}_{38}\text{H}_{38}\text{N}_2\text{O}_8\text{Na}$: 673.2526. Found: 673.2534.

2-(3-(4-benzoylphenylcarbamoyl)-4-hydroxyphenyl)-2-oxoethyl-4-(tert-butoxycarbonylamino)butanoate, 157f. The same reaction conditions were utilized as those to produce **130'**. Adhesive ppt., 86%; ^1H NMR (400 MHz, CD_3CN) δ (ppm), 9.21 (s, 1H), 8.45, (d, $J = 2.20$, 1H), 8.03 (dd, $J = 9.00$, $J = 2.40$, 1H), 7.56 (d, $J = 8.65$, 2H), 7.31-7.24 (m, 7H), 7.05 (d, $J = 7.20$, 1H), 5.48 (s, 2H), 5.35 (s, 2H), 3.09 (t, $J = 7.00$, 2H), 2.45 (t, $J = 7.80$, 2H), 1.78 (m, 2H), 1.40 (s, 9H).

4-(2-(3-(4-benzoylphenylcarbamoyl)-4-hydroxyphenyl)-2-oxoethoxy)-4-oxobutan-1-aminium 2,2,2-trifluoroacetate, 157. The same reaction conditions

were utilized as those to generate **130**. Adhesive ppt., 74%; IR (KBr): 3271, 3100-2800, 1685, 1670, 1649, 1593, 1535, 1500, 1323, 1311, 1200, 1054, 1028, 1008, 927, 823, 760 cm^{-1} ; ^1H NMR (400 MHz, d^6 -DMSO) δ (ppm), 12.75 (s, 1H), 10.57 (s, 1H), 8.56 (d, $J = 2.00$, 1H), 8.08 (dd, $J = 8.80$, $J = 2.10$, 1H), 7.87 (s, 3H), 7.69 (d, $J = 8.20$, 2H), 7.35 (t, $J = 7.68$, 2H), 7.30 (m, 4H), 7.25 (t, $J = 7.30$, 1H), 7.18 (d, $J = 8.69$, 1H), 5.56 (s, 2H), 2.96 (t, $J = 6.80$, 2H), 2.65 (t, $J = 7.80$, 2H), 1.96 (m, 2H); ^{13}C NMR (125 MHz, d^6 -DMSO) δ (ppm), 190.68, 171.77, 165.31, 162.69, 157.90, 157.65, 141.35, 137.96, 135.97, 132.78, 130.02, 129.00, 128.61, 128.41, 125.94, 125.12, 121.06, 118.60, 117.61, 116.05, 66.28, 38.11, 30.12, 22.59; HRMS (M⁺): Calc'd for $\text{C}_{26}\text{H}_{25}\text{N}_2\text{O}_6$: 461.1707. Found: 461.1715.

The same reaction conditions were utilized to produce 159-165.

3,5-difluorophenyl-5-acetyl-2-(benzyloxy)benzoate, 158c. White ppt., 82%, Mp: 115-117 $^{\circ}\text{C}$; IR (KBr): 3275, 3100-2800, 1751, 1731, 1677, 1606, 1502, 1465, 1363, 1271, 1208, 1122, 1056, 1028, 1008, 822, 760 cm^{-1} ; ^1H NMR (400 MHz, CDCl_3) δ (ppm), 8.60 (d, $J = 2.20$, 1H), 8.19 (dd, $J = 9.00$, $J = 2.20$, 1H), 7.50 (d, $J = 8.10$, 2H), 7.38 (m, 3H), 7.18 (d, $J = 8.2$, 2H), 6.77 (m, 3H), 5.30 (s, 2H), 2.63 (s, 3H); ^{13}C NMR (125 MHz, CDCl_3) δ (ppm), 195.82, 164.05, 162.93, 161.95, 152.16, 135.34, 134.81, 133.67, 132.84, 128.91, 128.19, 127.09, 118.69, 113.33, 106.19, 101.78, 70.63, 26.42; HRMS (M + H): Calc'd for $\text{C}_{22}\text{H}_{24}\text{F}_2\text{O}_4\text{Na}$: 405.0914. Found: 405.0918.

3,5-difluorophenyl-2-(benzyloxy)-5-(2-bromoacetyl)benzoate, 158d. Oil, ~93%; ^1H NMR (400 MHz, CDCl_3) δ (ppm), 8.63 (d, $J = 2.20$, 1H), 8.20 (dd, $J = 9.00$, $J =$

2.20, 1H), 7.50 (d, $J = 8.10$, 2H), 7.38 (m, 3H), 7.18 (d, $J = 8.2$, 2H), 6.77 (m, 3H), 5.32 (s, 2H), 4.44 (s, 2H).

3,5-difluorophenyl-2-(benzyloxy)-5-(2-(4-(*tert*-butoxycarbonylamino)-butanoyloxy)acetyl)benzoate, 158e. Oil, 44%; IR (KBr): 3271, 3100-2800, 1685, 1670, 1649, 1593, 1535, 1500, 1323, 1311, 1200, 1054, 1028, 1008, 927, 823, 760 cm^{-1} ; ^1H NMR (400 MHz, d^6 -DMSO) δ (ppm), 8.50, (d, $J = 2.10$, 1H), 8.24 (dd, $J = 9.00$, $J = 2.40$, 1H), 7.53-7.49 (m 6H), 7.39 (d, $J = 5.60$, 1H), 7.13 (dd, $J = 8.20$, $J = 2.10$, 2H), 6.89 (t, $J = 5.95$, 1H), 5.49 (s, 2H), 5.40 (s, 2H), 2.98 (t, $J = 6.80$, 2H), 2.42 (t, $J = 7.80$, 2H), 1.70 (m, 2H), 1.37 (s, 9H); ^{13}C NMR (125 MHz, d^6 -DMSO) δ (ppm), 190.88, 172.44, 170.36, 164.36, 162.80, 161.74, 155.55, 151.39, 135.99, 134.59, 131.77, 128.44, 127.65, 126.97, 118.45, 114.22, 106.30, 102.18, 77.44, 70.32, 66.16, 59.75, 39.50, 30.42, 28.71, 24.33; HRMS (M + Na): Calc'd for $\text{C}_{31}\text{H}_{31}\text{F}_2\text{NO}_8\text{Na}$: 606.1916. Found: 606.1899. (M + H): Calc'd for $\text{C}_{31}\text{H}_{32}\text{F}_2\text{NO}_8$: 584.2096. Found: 584.2078.

3,5-difluorophenyl-5-(2-(4-(*tert*-butoxycarbonylamino)butanoyloxy)acetyl)-2-hydroxybenzoate, 158f. Adhesive ppt., 86%; ^1H NMR (400 MHz, d^6 -DMSO) δ (ppm), 8.56, (d, $J = 2.10$, 1H), 8.22 (dd, $J = 9.00$, $J = 2.40$, 1H), 7.22 (d, $J = 9.60$, 1H), 7.39 (d, $J = 5.60$, 1H), 7.08 (dd, $J = 8.20$, $J = 1.90$, 1H), 7.02 (m, 2H), 5.49 (s, 2H), 2.97 (t, $J = 6.80$, 2H), 2.42 (t, $J = 7.80$, 2H), 1.69 (m, 2H), 1.39 (s, 9H).

4-(2-(3-((3,5-difluorophenoxy)carbonyl)-4-hydroxyphenyl)-2-oxoethoxy)-4-oxobutan-1-aminium 2,2,2-trifluoroacetate, 158. Adhesive ppt., 82%; IR (KBr): 3271, 3100-2800, 1685, 1670, 1649, 1593, 1535, 1500, 1323, 1311, 1200, 1054,

1028, 1008, 927, 823, 760 cm^{-1} ; ^1H NMR (400 MHz, MeOD) δ (ppm), 8.68, (d, $J = 2.10$, 1H), 8.22 (dd, $J = 9.10$, $J = 2.40$, 1H), 7.19 (d, $J = 9.10$, 1H), 7.07 (d, $J = 5.42$, 1H), 7.00 (m, 2H), 5.51 (s, 2H), 3.08 (t, $J = 6.80$, 2H), 2.66 (t, $J = 7.80$, 2H), 2.04 (m, 2H). ^{19}F NMR (376 MHz, MeOD) δ (ppm), -109.79; ^{13}C NMR (125 MHz, MeOD) δ (ppm), 190.89, 172.05, 166.59, 165.62, 164.08, 162.23, 161.54, 151.63, 135.33, 131.31, 126.05, 118.20, 112.15, 106.07, 101.66, 66.00, 38.80, 28.69, 22.50; HRMS (M⁺): Calc'd for $\text{C}_{19}\text{H}_{18}\text{F}_2\text{NO}_6$: 394.1102. Found: 394.1101.

2-(trifluoromethyl)phenyl-5-acetyl-2-(benzyloxy)benzoate, 159c. White ppt., 51%. Mp: 83-85 °C; IR (KBr): 3271, 3100-2800, 1755, 1681, 1598, 1502, 1494, 1456, 1409, 1361, 1323, 1197, 1168, 1132, 1112, 1056, 1028, 1009, 822, 760, 698 cm^{-1} ; ^1H NMR (400 MHz, CDCl_3) δ (ppm), 8.72, (d, $J = 2.20$, 1H), 8.20 (dd, $J = 9.00$, $J = 2.20$, 1H), 7.75 (d, $J = 8.20$, 1H), 7.65 (dd, $J = 12.05$, $J = 8.00$, 1H), 7.52 (d, $J = 8.20$, 2H), 7.43-7.32 (m, 5H), 7.17 (dd, $J = 8.50$, $J = 2.20$, 1H), 5.35 (s, 2H), 2.63 (s, 3H); ^{13}C NMR (125 MHz, CDCl_3) δ (ppm), 195.95, 162.59, 162.39, 148.22, 135.63, 134.63, 133.14, 129.88, 128.72, 128.13, 127.04, 126.37, 124.61, 124.20, 123.36, 122.03, 119.86, 118.21, 113.36, 70.76, 26.31; HRMS (M + Na): Calc'd for $\text{C}_{23}\text{H}_{17}\text{F}_3\text{O}_4\text{Na}$: 437.0977. Found: 437.0966.

2-(trifluoromethyl)phenyl-2-(benzyloxy)-5-(2-bromoacetyl)benzoate, 159d. Oil, ~93%. ^1H NMR (400 MHz, CDCl_3) δ (ppm), 8.72, (d, $J = 2.20$, 1H), 8.20 (dd, $J = 9.00$, $J = 2.20$, 1H), 7.75 (d, $J = 8.20$, 1H), 7.65 (dd, $J = 12.05$, $J = 8.00$, 1H), 7.51 (d, $J = 8.20$, 2H), 7.43-7.32 (m, 5H), 7.17 (dd, $J = 8.50$, $J = 2.20$, 1H), 5.35 (s, 2H), 4.45 (s, 2H).

2-(trifluoromethyl)phenyl-2-(benzyloxy)-5-(2-(4-(tert-butoxycarbonyl-amino)-butanoyloxy)acetyl)benzoate, 159e. White ppt., 44%, Mp: 117-119 °C; IR (KBr): 3271, 3100-2800, 1753, 1697, 1666, 1600, 1529, 1494, 1456, 1415, 1380, 1367, 1321, 1272, 1195, 1166, 1143, 1112, 1055, 1028, 1009, 821, 760 cm⁻¹; ¹H NMR (400 MHz, d⁶-DMSO) δ (ppm), 8.52, (d, *J* = 2.20, 1H), 8.37 (dd, *J* = 9.00, *J* = 2.20, 1H), 7.85 (m, 2H), 7.58-7.50 (m, 5H), 7.37 (t, *J* = 9.00, 2H), 7.31 (d, *J* = 8.10, 1H), 6.89 (t, *J* = 5.80, 1H), 5.48 (s, 2H), 5.42 (s, 2H), 2.98 (t, *J* = 6.80, 2H), 2.42 (t, *J* = 7.80, 2H), 1.68 (m, 2H), 1.37 (s, 9H); ¹³C NMR (125 MHz, d⁶-DMSO) δ (ppm), 190.80, 172.23, 162.09, 155.61, 147.63, 135.99, 134.90, 134.22, 131.55, 128.41, 127.88, 127.06, 126.84, 126.34, 125.10, 124.11, 121.95, 121.20, 119.78, 117.98, 114.35, 77.46, 70.19, 66.09, 39.43, 30.62, 28.20, 20.73; HRMS (M + Na): Calc'd for C₃₂H₃₂F₃O₈Na: 638.1978. Found: 638.1960.

2-(trifluoromethyl)phenyl-5-(2-(4-(tert-butoxycarbonyl-amino)-butanoyloxy)-acetyl)-2-hydroxybenzoate, 159f. Adhesive ppt., 90%; ¹H NMR (400 MHz, d⁶-DMSO) δ (ppm), 11.43, (s, 1H), 8.51, (d, *J* = 2.20, 1H), 8.17 (dd, *J* = 9.00, *J* = 2.20, 1H), 7.62 (d, *J* = 8.40, 2H), 7.56 (m, 2H), 7.19 (d, *J* = 8.10, 1H), 6.89 (t, *J* = 5.80, 1H), 5.44 (s, 2H), 2.98 (t, *J* = 6.80, 2H), 2.43 (t, *J* = 7.80, 2H), 1.68 (m, 2H), 1.37 (s, 9H).

4-(2-(4-hydroxy-3-((2-(trifluoromethyl)phenoxy)carbonyl)phenyl)-2-oxoethoxy)-4-oxobutan-1-aminium 2,2,2-trifluoroacetate, 159. Adhesive ppt., 81%; IR (KBr): 3442, 3271, 3100-2800, 1741, 1691, 1645, 1600, 1494, 1454, 1417, 1380, 1323, 1269, 1199, 1172, 1130, 1053, 1026, 821, 800, 760, 717 cm⁻¹; ¹H NMR (400 MHz,

d^6 -DMSO) δ (ppm), 11.43 (s, 1H), 8.51, (d, $J = 2.20$, 1H), 8.17 (dd, $J = 9.00$, $J = 2.20$, 1H), 7.88-7.83 (m, 5H), 7.62-7.58 (m, 2H), 7.19 (d, $J = 8.20$, 1H), 5.49 (s, 2H), 2.90 (t, $J = 6.80$, 2H), 2.42 (t, $J = 7.80$, 2H), 1.86 (m, 2H); ^{19}F NMR (376 MHz, d^6 -DMSO) δ (ppm), -63.07; ^{13}C NMR (125 MHz, d^6 -DMSO) δ (ppm), 190.46, 171.74, 165.18, 163.73, 159.43, 158.27, 147.48, 134.97, 134.20, 131.86, 128.46, 126.94, 125.21, 124.13, 121.61, 118.11, 115.73, 114.45, 66.16, 38.10, 30.15, 22.32; HRMS (M⁺): Calc'd for $\text{C}_{20}\text{H}_{19}\text{NF}_3\text{O}_6$: 426.1165. Found: 426.1140.

2-fluorophenyl 5-acetyl-2-(benzyloxy)benzoate, 160c. White ppt., 57%, Mp: 91-93°C; IR (KBr): 3271, 3100-2800, 1755, 1681, 1598, 1502, 1494, 1456, 1409, 1361, 1323, 1197, 1168, 1132, 1112, 1056, 1028, 1009, 822, 760, 698 cm^{-1} ; ^1H NMR (400 MHz, CDCl_3) δ (ppm), 8.73, (d, $J = 2.20$, 1H), 8.23 (dd, $J = 9.00$, $J = 2.20$, 1H), 7.40 (t, $J = 7.50$, 2H), 7.38-7.33 (m, 3H), 7.28-7.20 (m, 5H), 5.34 (s, 2H), 2.71 (s, 3H); ^{19}F NMR (376 MHz, CDCl_3) δ (ppm), -128.93; ^{13}C NMR (125 MHz, CDCl_3) δ (ppm), 190.82, 172.10, 169.24, 161.98, 155.77, 154.92, 151.67, 138.03, 136.08, 134.43, 131.67, 128.55, 127.00, 124.36, 124.87, 118.09, 116.78, 115.42, 77.01, 26.87; HRMS (M + Na): Calc'd for $\text{C}_{22}\text{H}_{17}\text{FO}_4\text{Na}$: 387.1009. Found: 387.1015.

2-fluorophenyl-2-(benzyloxy)-5-(2-bromoacetyl)benzoate, 160d. Oil, ~ 84%; ^1H NMR (400 MHz, CDCl_3) δ (ppm), 8.78, (d, $J = 2.20$, 1H), 8.22 (dd, $J = 9.00$, $J = 2.20$, 1H), 7.40 (t, $J = 7.50$, 2H), 7.38-7.33 (m, 3H), 7.28-7.20 (m, 5H), 5.36 (s, 2H), 4.44 (s, 2H).

3-fluorophenyl-2-(benzyloxy)-5-(2-(4-(*tert*-butoxycarbonyl-amino)-butanoyloxy)-acetyl)benzoate, 160e. White ppt., 74%, Mp: 114-116 °C; IR (KBr): 3271, 3100-

2800, 1755, 1681, 1598, 1502, 1494, 1456, 1409, 1361, 1323, 1197, 1168, 1132, 1112, 1056, 1028, 1009, 822, 760, 698 cm^{-1} ; ^1H NMR (400 MHz, d^6 -DMSO) δ (ppm), 8.51, (d, $J = 2.20$, 1H), 7.51 (m, 3H), 7.38-7.33 (m, 3H), 7.28-7.20 (m, 5H), 6.88 (t, $J = 6.90$, 1H), 5.49 (s, 2H), 5.41 (s, 2H), 2.98 (t, $J = 6.80$, 2H), 2.42 (t, $J = 7.80$, 2H), 1.68 (m, 2H), 1.37 (s, 9H); ^{19}F NMR (376 MHz, CDCl_3) δ (ppm), -128.98; ^{13}C NMR (125 MHz, d^6 -DMSO) δ (ppm), 190.91, 172.24, 170.37, 161.92, 155.62, 154.57, 152.61, 137.66, 136.01, 134.74, 131.67, 128.41, 127.65, 127.06, 126.39, 125.21, 124.23, 118.09, 116.79, 114.37, 77.49, 70.23, 66.18, 59.75, 30.64, 28.21, 24.96; HRMS (M + Na): Calc'd for $\text{C}_{31}\text{H}_{32}\text{FNO}_8\text{Na}$: 588.2010. Found: 588.2021.

2-fluorophenyl-5-(2-(4-(*tert*-butoxycarbonylamino)butanoyloxy)acetyl)-2-hydroxybenzoate, 160f. White ppt., 74%, Mp: 114-116 $^\circ\text{C}$; IR (KBr): 3271, 3100-2800, 1755, 1681, 1598, 1502, 1494, 1456, 1409, 1361, 1323, 1197, 1168, 1132, 1112, 1056, 1028, 1009, 822, 760, 698 cm^{-1} ; ^1H NMR (400 MHz, d^6 -DMSO) δ (ppm), 8.52, (d, $J = 2.20$, 1H), 8.13 (dd, $J = 9.00$, $J = 2.20$, 1H), 7.45-7.29 (m, 5H), 7.19 (d, $J = 8.10$, 1H), 5.44 (s, 2H), 2.96 (t, $J = 6.80$, 2H), 2.42 (t, $J = 7.80$, 2H), 1.68 (m, 2H), 1.37 (s, 9H); ^{19}F NMR (376 MHz, d^6 -DMSO) δ (ppm), -130.36; ^{13}C NMR (125 MHz, d^6 -DMSO) δ (ppm), 190.67, 172.24, 163.53, 163.22, 155.62, 154.56, 152.59, 137.42, 134.88, 132.08, 127.91, 125.37, 124.35, 118.15, 116.76, 114.20, 77.49, 66.06, 59.75, 30.64, 28.21, 24.96; HRMS (M + Na): Calc'd for $\text{C}_{24}\text{H}_{26}\text{FNO}_8\text{Na}$: 498.1540. Found: 498.1533.

4-(2-(3-((2-fluorophenoxy)carbonyl)-4-hydroxyphenyl)-2-oxoethoxy)-4-oxobutan-1-aminium 2,2,2-trifluoroacetate, 160. Adhesive ppt., 92%; IR (KBr):

3271, 3100-2800, 1755, 1681, 1598, 1502, 1494, 1456, 1409, 1361, 1323, 1197, 1168, 1132, 1112, 1056, 1028, 1009, 822, 760, 698 cm^{-1} ; ^1H NMR (400 MHz, d^6 -DMSO) δ (ppm), 11.55 (s, 1H), 8.55, (d, $J = 2.20$, 1H), 8.14 (dd, $J = 9.00$, $J = 2.20$, 1H), 7.86 (s, 3H), 7.47-7.39 (m, 4H), 7.21 (d, $J = 8.10$, 1H), 5.51 (s, 2H), 2.89 (t, $J = 6.80$, 2H), 2.59 (t, $J = 7.80$, 2H), 1.86 (m, 2H), 1.37 (s, 9H); ^{19}F NMR (376 MHz, d^6 -DMSO) δ (ppm), -130.75; ^{13}C NMR (125 MHz, d^6 -DMSO) δ (ppm), 190.58, 171.73, 163.63, 163.14, 158.23, 154.56, 152.60, 137.45, 134.83, 132.11, 127.88, 125.22, 124.35, 118.17, 116.76, 115.64, 114.34, 66.26, 38.08, 30.10, 22.57; HRMS (M⁺): Calc'd for $\text{C}_{19}\text{H}_{19}\text{FNO}_6$: 376.1191. Found: 376.1197.

3-nitrophenyl 5-acetyl-2-(benzyloxy)benzoate, 161c. White ppt., 46%, Mp: 106-108°C; IR (KBr): 3271, 3100-2800, 1728, 1712, 1677, 1604, 1502, 1454, 1392, 1353, 1321, 1284, 1209, 1168, 1051, 1024, 1004, 902, 823, 761, 725 cm^{-1} ; ^1H NMR (400 MHz, CDCl_3) δ (ppm), 8.69, (d, $J = 2.20$, 1H), 8.17-8.15 (m, 2H), 8.10 (d, $J = 8.20$, 1H), 7.59-7.49 (m, 4H), 7.41-7.35 (m, 3H), 7.20 (d, $J = 8.60$, 1H), 5.31 (s, 2H), 2.64 (s, 3H); ^{13}C NMR (125 MHz, CDCl_3) δ (ppm), 196.02, 163.13, 162.36, 151.09, 148.85, 135.49, 133.36, 131.40, 130.10, 128.35, 127.20, 121.97, 120.93, 118.48, 117.64, 115.45, 113.39, 112.19, 71.02, 26.63; HRMS (M + Na): Calc'd for $\text{C}_{22}\text{H}_{17}\text{NO}_6\text{Na}$: 414.0954. Found: 414.0966.

3-nitrophenyl 2-(benzyloxy)-5-(2-bromoacetyl)benzoate, 161d. Oil, ~65%; ^1H NMR (400 MHz, CDCl_3) δ (ppm), 8.71, (d, $J = 2.20$, 1H), 8.17-8.15 (m, 2H), 8.10 (d, $J = 8.20$, 1H), 7.59-7.49 (m, 4H), 7.41-7.35 (m, 3H), 7.22 (d, $J = 8.60$, 1H), 5.35 (s, 2H), 4.46 (s, 2H).

3-nitrophenyl-2-(benzyloxy)-5-(2-(4-(*tert*-butoxycarbonyl-amino)butanoyloxy)-acetyl)benzoate, 161e. Adhesive ppt., 39%; IR (KBr): 3271, 3100-2800, 1728, 1712, 1677, 1604, 1502, 1454, 1392, 1353, 1321, 1284, 1209, 1168, 1051, 1024, 1004, 902, 823, 761, 725 cm^{-1} ; ^1H NMR (400 MHz, d^6 -DMSO) δ (ppm), 8.56, (d, $J = 2.30$, 1H), 8.20 (m, 3H), 7.75 (d, $J = 8.00$, 2H), 7.52-7.48 (m, 3H), 7.37-7.34 (m, 3H), 6.89 (t, $J = 7.10$, 1H), 5.49 (s, 2H), 5.40 (s, 2H), 2.96 (t, $J = 6.90$, 2H), 2.43 (t, $J = 7.70$, 2H), 1.67 (m, 2H), 1.36 (s, 9H); ^{13}C NMR (125 MHz, d^6 -DMSO) δ (ppm), 190.67, 172.34, 164.67, 161.54, 155.80, 150.84, 148.34, 136.36, 134.51, 131.82, 129.85, 128.84, 128.13, 127.96, 127.66, 126.94, 121.11, 118.24, 117.48, 114.27, 78.77, 70.42, 66.13, 39.72, 30.34, 28.14, 24.27; HRMS (M + Na): Calc'd for $\text{C}_{31}\text{H}_{32}\text{N}_2\text{O}_{10}\text{Na}$: 615.1955. Found: 615.1971.

3-nitrophenyl-5-(2-(4-(*tert*-butoxycarbonylamino)butanoyloxy)acetyl)-2-hydroxybenzoate, 161f. Adhesive ppt., 87%; ^1H NMR (400 MHz, d^6 -DMSO) δ (ppm), 8.52, (d, $J = 2.30$, 1H), 8.13 (dd, $J = 8.40$, $J = 2.30$, 1H), 7.70 (d, $J = 8.00$, 1H), 7.59-7.51 (m, 2H), 7.19 (dd, $J = 7.90$, $J = 1.90$, 2H), 6.88 (t, $J = 7.10$, 1H), 5.49 (s, 2H), 2.97 (t, $J = 6.90$, 2H), 2.44 (t, $J = 7.70$, 2H), 1.67 (m, 2H), 1.36 (s, 9H).

4-(2-(4-hydroxy-3-((3-nitrophenoxy)carbonyl)phenyl)-2-oxoethoxy)-4-oxobutan-1-aminium 2,2,2-trifluoroacetate, 161. White ppt., 80%, Mp: 58-60°C; IR (KBr): 3271, 3100-2800, 1728, 1712, 1677, 1604, 1502, 1454, 1392, 1353, 1321, 1284, 1209, 1168, 1051, 1024, 1004, 902, 823, 761, 725 cm^{-1} ; ^1H NMR (400 MHz, d^6 -DMSO) δ (ppm), 8.51, (d, $J = 2.30$, 1H), 8.13 (dd, $J = 8.40$, $J = 2.30$, 1H), 7.84 (s, 3H), 7.71 (d, $J = 8.00$, 1H), 7.59-7.51 (m, 2H), 7.19 (dd, $J = 7.90$, $J = 1.90$, 2H), 5.52

(s, 2H), 2.91 (t, $J = 6.90$, 2H), 2.60 (t, $J = 7.70$, 2H), 1.86 (m, 2H); ^{13}C NMR (125 MHz, $\text{d}^6\text{-DMSO}$) δ (ppm), 190.60, 171.74, 164.55, 158.22, 157.77, 154.78, 150.11, 137.46, 134.55, 131.87, 130.01, 125.16, 122.46, 120.44, 118.68, 116.79, 115.89, 114.49, 66.29, 38.09, 30.08, 22.57; HRMS (M⁺): Calc'd for $\text{C}_{19}\text{H}_{19}\text{N}_2\text{O}_8$: 403.1136. Found: 403.1145.

4-nitrophenyl 5-acetyl-2-(benzyloxy)benzoate, 162c. White ppt., 91%. Mp: 93-95°C; IR (KBr): 3250, 3100-2800, 1751, 1728, 1677, 1649, 1598, 1523, 1411, 1348, 1269, 1195, 1165, 1055, 1026, 1007, 905, 860, 823, 760 cm^{-1} ; ^1H NMR (400 MHz, CDCl_3) δ (ppm), 8.64, (d, $J = 2.20$, 1H), 8.30 (d, $J = 9.20$, 2H), 8.21 (d, $J = 8.40$, 1H), 7.50 (dd, $J = 8.40$, $J = 2.10$, 2H), 7.41-7.35 (m, 5H), 7.20 (d, $J = 8.65$, 1H), 5.31 (s, 2H), 2.63 (s, 3H); ^{13}C NMR (125 MHz, CDCl_3) δ (ppm), 196.07, 171.26, 162.79, 155.58, 145.43, 135.47, 133.55, 131.44, 130.17, 128.79, 127.57, 126.76, 125.53, 122.70, 118.48, 115.67, 71.02, 26.44; HRMS (M + Na): Calc'd for $\text{C}_{22}\text{H}_{17}\text{NO}_6\text{Na}$: 414.0954. Found: 414.0969.

4-nitrophenyl-2-(benzyloxy)-5-(2-bromoacetyl)benzoate, 162d. Oil, ~84%; ^1H NMR (400 MHz, CDCl_3) δ (ppm), 8.70, (d, $J = 2.20$, 1H), 8.33 (d, $J = 9.20$, 2H), 8.23 (d, $J = 8.40$, 1H), 7.51 (dd, $J = 8.40$, $J = 2.10$, 2H), 7.41-7.35 (m, 5H), 7.24 (d, $J = 8.65$, 1H), 5.35 (s, 2H), 4.46 (s, 2H).

4-nitrophenyl-2-(benzyloxy)-5-(2-(4-(tert-butoxycarbonyl-amino)butanoyloxy)acetyl)benzoate, 162e. White ppt., 57%, Mp: 105-107 °C; IR (KBr): 3275, 3100-2800, 1745, 1697, 1658, 1602, 1523, 1413, 1348, 1271, 1195, 1165, 1051, 1026, 1007, 860, 823, 761 cm^{-1} ; ^1H NMR (400 MHz, $\text{d}^6\text{-DMSO}$) δ (ppm), 8.55, (d, J

= 2.20, 1H), 8.36 (d, $J = 9.20$, 2H), 8.26 (d, $J = 8.40$, 1H), 7.58 (dd, $J = 8.40$, $J = 2.10$, 2H), 7.53-7.50 (m, 3H), 7.41-7.37 (m, 2H), 7.33 (d, $J = 8.65$, 1H), 6.89 (t, $J = 7.10$, 1H), 5.50 (s, 2H), 5.42 (s, 2H), 2.97 (t, $J = 6.90$, 2H), 2.44 (t, $J = 7.70$, 2H), 1.70 (m, 2H), 1.38 (s, 9H); ^{13}C NMR (125 MHz, $\text{d}^6\text{-DMSO}$) δ (ppm), 190.88, 172.22, 162.33, 161.89, 156.56, 155.31, 145.18, 136.02, 134.64, 131.89, 128.46, 127.66, 127.18, 126.35, 125.34, 123.32, 118.44, 114.28, 77.46, 70.30, 66.19, 40.06, 30.64, 28.22, 24.44; HRMS (M + Na): Calc'd for $\text{C}_{31}\text{H}_{32}\text{N}_2\text{O}_{10}\text{Na}$: 615.1955. Found: 615.1937.

4-nitrophenyl-5-(2-(4-(*tert*-butoxycarbonylamino)butanoyloxy)acetyl)-2-

hydroxybenzoate, 162f. White ppt., 87%, Mp: 144-146°C; IR (KBr): 3275, 3100-2800, 1745, 1697, 1658, 1602, 1523, 1413, 1348, 1271, 1195, 1165, 1051, 1026, 1007, 860, 823, 761 cm^{-1} ; ^1H NMR (400 MHz, $\text{d}^6\text{-DMSO}$) δ (ppm), 11.30 (s, 1H), 8.54 (d, $J = 2.20$, 2H), 8.38 (d, $J = 9.20$, 2H), 8.18 (d, $J = 8.40$, 1H), 7.65 (dd, $J = 8.40$, $J = 2.10$, 2H), 7.20 (d, $J = 8.65$, 1H), 6.89 (t, $J = 7.10$, 1H), 5.47 (s, 2H), 2.98 (t, $J = 6.90$, 2H), 2.43 (t, $J = 7.70$, 2H), 1.68 (m, 2H), 1.38 (s, 9H); ^{13}C NMR (125 MHz, $\text{d}^6\text{-DMSO}$) δ (ppm), 190.63, 172.00, 165.08, 156.94, 145.21, 142.34, 134.78, 132.13, 130.99, 126.12, 125.31, 123.44, 118.08, 114.64, 77.45, 66.08, 39.96, 30.64, 28.21, 24.95; HRMS (M + Na): Calc'd for $\text{C}_{24}\text{H}_{26}\text{N}_2\text{O}_{10}\text{Na}$: 525.1485. Found: 525.1487.

4-(2-(4-hydroxy-3-((4-nitrophenoxy)carbonyl)phenyl)-2-oxoethoxy)-4-oxobutan-1-aminium 2,2,2-trifluoroacetate, 162. White ppt., 91%, Mp: 88-90°C; IR (KBr): 3275, 3100-2800, 1745, 1697, 1658, 1602, 1523, 1413, 1348, 1271, 1195, 1165, 1051, 1026, 1007, 860, 823, 761 cm^{-1} ; ^1H NMR (400 MHz, $\text{d}^6\text{-DMSO}$) δ (ppm), 11.48

(s, 1H), 8.54, (d, $J = 2.20$, 2H), 8.38 (d, $J = 9.20$, 2H), 8.15 (d, $J = 8.40$, 1H), 7.80 (s, 3H), 7.63 (dd, $J = 8.40$, $J = 2.10$, 2H), 7.19 (d, $J = 8.65$, 1H), 5.51 (s, 2H), 2.89 (t, $J = 6.90$, 2H), 2.59 (t, $J = 7.70$, 2H), 1.86 (m, 2H); ^{13}C NMR (125 MHz, $\text{d}^6\text{-DMSO}$) δ (ppm), 190.59, 171.78, 163.55, 157.99, 157.75, 155.18, 145.23, 134.76, 132.19, 125.34, 125.19, 123.44, 118.38, 115.99, 114.76; HRMS (M⁺): Calc'd for $\text{C}_{19}\text{H}_{19}\text{N}_2\text{O}_8\text{Na}$: 403.1141. Found: 403.1131.

3,5-bis(trifluoromethyl)phenyl 5-acetyl-2-(benzyloxy)benzoate, 163c. White ppt., 90%, Mp: 73-75°C; IR (KBr): 3270, 3100-2800, 1753, 1731, 1679, 1629, 1598, 1500, 1413, 1371, 1282, 1205, 1180, 1137, 1056, 1029, 1008, 844, 821, 760, 700 cm^{-1} ; ^1H NMR (400 MHz, CDCl_3) δ (ppm), 8.65, (d, $J = 2.20$, 1H), 8.23 (dd, $J = 8.80$, $J = 2.40$, 1H), 7.80 (d, $J = 2.20$, 1H), 7.67 (d, $J = 8.80$, 2H), 7.50 (dd, $J = 8.40$, $J = 2.10$, 2H), 7.42-7.36 (m, 3H), 7.20 (d, $J = 8.65$, 1H), 5.31 (s, 2H), 2.64 (s, 3H); ^{13}C NMR (125 MHz, CDCl_3) δ (ppm), 195.71, 171.20, 162.94, 162.40, 151.27, 135.28, 133.45, 132.55, 130.01, 128.81, 127.35, 126.03, 123.86, 121.69, 119.84, 118.15, 113.41, 71.13, 26.42; HRMS (M + Na): Calc'd for $\text{C}_{24}\text{H}_{16}\text{F}_6\text{O}_4\text{Na}$: 505.0850. Found: 505.0866.

3,5-bis(trifluoromethyl)phenyl-2-(benzyloxy)-5-propionylbenzoate, 163d. Oil, ~92%. ^1H NMR (400 MHz, CDCl_3) δ (ppm), 8.69, (d, $J = 2.20$, 1H), 8.25 (dd, $J = 8.80$, $J = 2.40$, 1H), 7.81 (d, $J = 2.20$, 1H), 7.68 (d, $J = 8.80$, 2H), 7.51 (dd, $J = 8.40$, $J = 2.10$, 2H), 7.43-7.37 (m, 3H), 7.23 (d, $J = 8.65$, 1H), 5.33 (s, 2H), 4.45 (s, 2H).

3,5-bis(trifluoromethyl)phenyl-2-(benzyloxy)-5-(2-(4-(*tert*-butoxycarbonyl-amino)butanoyloxy)acetyl)benzoate, 163e. Adhesive ppt., 58%; IR (KBr): 3270,

3100-2800, 1745, 1697, 1602, 1529, 1500, 1460, 1371, 1282, 1253, 1174, 1139, 1054, 1029, 1008, 823, 760, 680 cm^{-1} ; ^1H NMR (400 MHz, d^6 -DMSO) δ (ppm), 8.60, (d, $J = 2.20$, 1H), 8.29 (dd, $J = 8.80$, $J = 2.40$, 1H), 8.11 (m, 3H), 7.54-7.50 (m, 3H), 7.39-7.34 (m, 3H), 7.20 (d, $J = 8.65$, 1H), 6.89 (t, $J = 7.10$, 1H), 5.50 (s, 2H), 5.41 (s, 2H), 2.97 (t, $J = 6.90$, 2H), 2.44 (t, $J = 7.70$, 2H), 1.70 (m, 2H), 1.38 (s, 9H); ^{13}C NMR (125 MHz, d^6 -DMSO) δ (ppm), 190.86, 172.24, 162.38, 161.99, 155.60, 151.32, 135.98, 134.72, 132.09, 131.66, 128.40, 128.00, 127.32, 126.30, 123.91, 121.72, 119.98, 118.22, 114.19, 77.46, 70.40, 66.17, 39.63, 30.64, 28.21, 24.97; HRMS ($\text{M} + \text{Na}$): Calc'd for $\text{C}_{33}\text{H}_{31}\text{F}_6\text{NO}_8\text{Na}$: 706.1852. Found: 706.1844; ($\text{M} + \text{H}$): Calc'd for $\text{C}_{33}\text{H}_{32}\text{F}_6\text{NO}_8$: 684.2032. Found: 684.2028.

3,5-bis(trifluoromethyl)phenyl-5-(2-(4-(*tert*-butoxycarbonyl-amino)butanoyloxy)acetyl)-2-hydroxybenzoate, 163f. Adhesive ppt., 35%; ^1H NMR (400 MHz, CD_3CN) δ (ppm), 8.70, (d, $J = 2.20$, 1H), 8.16 (dd, $J = 8.80$, $J = 2.40$, 1H), 8.01 (m, 3H), 7.15 (d, $J = 8.65$, 1H), 5.36 (s, 2H), 3.08 (t, $J = 6.90$, 2H), 2.44 (t, $J = 7.70$, 2H), 1.79 (m, 2H), 1.39 (s, 9H).

4-(2-(3-((3,5-bis(trifluoromethyl)phenoxy)carbonyl)-4-hydroxyphenyl)-2-oxoethoxy)-4-oxobutan-1-aminium-2,2,2-trifluoroacetate, 163. White ppt., 93%, Mp: 77-79°C; IR (KBr): 3438, 3270, 3100-2800, 1741, 1691, 1600, 1460, 1413, 1373, 1282, 1201, 1176, 1130, 1054, 1029, 1008, 823, 761, 717, 680 cm^{-1} ; ^1H NMR (400 MHz, d^6 -DMSO) δ (ppm), 11.49, (s, 1H), 8.58, (d, $J = 2.20$, 1H), 8.21 (d, $J = 8.80$, 2H), 8.14 (d, $J = 6.10$, 2H), 7.85 (s, 3H), 7.20 (d, $J = 8.65$, 1H), 5.51 (s, 2H), 2.88 (t, $J = 6.90$, 2H), 2.59 (t, $J = 7.70$, 2H), 1.88 (m, 2H); ^{13}C NMR (125 MHz, d^6 -

DMSO) δ (ppm), 190.55, 171.76, 163.68, 157.97, 157.48, 151.23, 134.81, 132.35, 131.34, 125.14, 124.07, 121.75, 119.97, 118.24, 115.88, 114.51, 66.26, 38.08, 30.10, 22.57; HRMS (M⁺): Calc'd for C₂₁H₁₈F₆NO₆: 494.1038. Found: 494.1021.

quinolin-8-yl 5-acetyl-2-(benzyloxy)benzoate, 164c. White ppt., 86%, Mp: 179-181°C; IR (KBr): 3275, 3100-2800, 1745, 1670, 1598, 1581, 1496, 1467, 1448, 1382, 1276, 1238, 1199, 1163, 1056, 1028, 1007, 873, 821, 760, 692, 680 cm⁻¹; ¹H NMR (400 MHz, CDCl₃) δ (ppm), 8.92, (m, 2H), 8.23 (m, 2H), 7.78 (dd, $J = 7.20$, $J = 2.47$, 1H), 7.59-7.52 (m, 4H), 7.46 (dd, $J = 8.28$, $J = 4.25$, 1H), 7.32-7.28 (m, 3H), 7.18 (d, $J = 8.70$, 1H), 5.34 (s, 2H), 2.65 (s, 3H); ¹³C NMR (125 MHz, CDCl₃) δ (ppm), 196.24, 163.86, 162.41, 156.72, 150.62, 147.60, 136.00, 135.87, 134.29, 134.06, 129.92, 129.63, 128.59, 128.42, 128.10, 127.07, 126.82, 126.29, 121.79, 119.54, 113.41, 70.71, 24.96; HRMS (M + H): Calc'd for C₂₅H₂₀NO₄: 398.1392. Found: 398.1389.

quinolin-8-yl 2-(benzyloxy)-5-(2-bromoacetyl)benzoate, 164d. Oil, ~84%. ¹H NMR (400 MHz, CDCl₃) δ (ppm), 8.96, (m, 2H), 8.23 (m, 2H), 7.80 (dd, $J = 7.20$, $J = 2.47$, 1H), 7.63-7.58 (m, 4H), 7.55 (dd, $J = 8.28$, $J = 4.25$, 2H), 7.49-7.30 (m, 3H), 7.21 (d, $J = 8.70$, 1H), 5.37 (s, 2H), 4.52 (s, 2H).

quinolin-8-yl-2-(benzyloxy)-5-(2-(4-(tert-butoxycarbonyl-amino)-butanoyloxy)-acetyl)benzoate, 164e. Adhesive ppt., 48%; IR (KBr): 3275, 3100-2800, 1745, 1670, 1598, 1581, 1496, 1467, 1448, 1382, 1276, 1238, 1199, 1163, 1056, 1028, 1007, 873, 821, 760, 692, 680 cm⁻¹; ¹H NMR (400 MHz, d⁶-DMSO) δ (ppm), 8.91, (d, $J = 8.05$, 1H), 8.89 (d, $J = 7.60$, 1H), 8.70 (d, $J = 9.40$, 1H), 8.50 (d, $J = 8.75$, 1H), 7.97 (dd, J

= 7.50, $J = 2.10$, 1H), 7.69 (d, $J = 8.20$, 2H), 7.64 (dd, $J = 8.28$, $J = 4.25$, 1H), 7.53 (m, 3H), 7.33 (m, 3H), 6.89 (d, $J = 7.10$, 1H), 5.52 (s, 2H), 5.43 (s, 2H), 2.98 (t, $J = 6.90$, 2H), 2.44 (t, $J = 7.70$, 2H), 1.68 (m, 2H), 1.37 (s, 9H); ^{13}C NMR (125 MHz, d^6 -DMSO) δ (ppm), 190.98, 172.24, 170.32, 162.74, 162.04, 155.59, 150.76, 146.93, 140.45, 136.27, 135.06, 134.55, 131.92, 129.17, 128.34, 127.76, 127.06, 126.47, 126.20, 122.30, 121.71, 119.02, 114.27, 77.49, 70.09, 66.19, 39.14, 33.32, 30.65, 28.21, 24.44; HRMS (M + H): Calc'd for $\text{C}_{34}\text{H}_{35}\text{N}_2\text{O}_8$: 592.2393. Found: 599.2347. (M + Na): Calc'd for $\text{C}_{34}\text{H}_{34}\text{N}_2\text{O}_8\text{Na}$: 621.2213. Found: 621.2204.

quinolin-8-yl-5-(2-(4-(*tert*-butoxycarbonylamino)butanoyloxy)acetyl)-2-

hydroxybenzoate, 164f. White ppt., 92%, Mp: 137-139°C; IR (KBr): 3469, 3298, 3274, 3100-2800, 1743, 1697, 1664, 1631, 1604, 1500, 1421, 1365, 1299, 1249, 1232, 1199, 1166, 1056, 1027, 1009, 875, 821, 760 cm^{-1} ; ^1H NMR (400 MHz, d^6 -DMSO) δ (ppm), 11.34 (s, 1H), 8.92, (d, $J = 8.05$, 1H), 8.67 (d, $J = 7.60$, 1H), 8.52 (d, $J = 9.40$, 1H), 8.21 (d, $J = 8.75$, 1H), 8.01 (dd, $J = 7.50$, $J = 2.10$, 1H), 7.76 (d, $J = 8.20$, 2H), 7.71 (dd, $J = 8.28$, $J = 4.25$, 1H), 7.21 (d, $J = 8.40$, 1H), 6.89 (d, $J = 7.10$, 1H), 5.48 (s, 2H), 2.96 (t, $J = 6.90$, 2H), 2.43 (t, $J = 7.70$, 2H), 1.68 (m, 2H), 1.37 (s, 9H); ^{13}C NMR (125 MHz, d^6 -DMSO) δ (ppm), 190.76, 172.24, 164.92, 163.64, 155.59, 150.85, 146.45, 140.05, 136.53, 134.94, 131.91, 129.14, 128.34, 126.98, 125.60, 122.34, 121.88, 118.31, 114.49, 77.45, 66.10, 39.47, 30.65, 28.21, 24.95; HRMS (M + H): Calc'd for $\text{C}_{27}\text{H}_{29}\text{N}_2\text{O}_8$: 509.1924. Found: 509.1910. (M + Na): Calc'd for $\text{C}_{27}\text{H}_{28}\text{N}_2\text{O}_8\text{Na}$: 531.1743. Found: 531.1739.

4-(2-(4-hydroxy-3-((quinolin-8-yloxy)carbonyl)phenyl)-2-oxoethoxy)-4-oxobutan-1-aminium 2,2,2-trifluoroacetate, 164. Adhesive ppt., 92%; IR (KBr): 3469, 3298, 3274, 3100-2800, 1743, 1697, 1664, 1631, 1604, 1500, 1421, 1365, 1299, 1249, 1232, 1199, 1166, 1056, 1027, 1009, 875, 821, 760 cm^{-1} ; ^1H NMR (400 MHz, $\text{d}^6\text{-DMSO}$) δ (ppm), 11.34 (s, 1H), 8.91, (d, $J = 8.05$, 1H), 8.67 (d, $J = 7.60$, 1H), 8.52 (d, $J = 9.40$, 1H), 8.21 (d, $J = 8.75$, 1H), 8.01 (dd, $J = 7.50$, $J = 2.10$, 1H), 7.80 (s, 3H), 7.76 (d, $J = 8.20$, 2H), 7.71 (dd, $J = 8.28$, $J = 4.25$, 1H), 7.21 (d, $J = 8.40$, 1H), 5.53 (s, 2H), 2.89 (t, $J = 6.90$, 2H), 2.60 (t, $J = 7.70$, 2H), 1.87 (m, 2H); ^{13}C NMR (125 MHz, $\text{d}^6\text{-DMSO}$) δ (ppm), 190.70, 171.76, 164.82, 163.69, 158.09, 157.84, 150.83, 146.43, 140.03, 136.57, 134.91, 131.96, 129.14, 126.56, 125.44, 122.35, 121.90, 118.33, 117.98, 115.55, 66.30, 38.09, 30.09, 22.55; HRMS (M^+): Calc'd for $\text{C}_{22}\text{H}_{21}\text{N}_2\text{O}_6$: 409.1400. Found: 409.1394.

Naphthalen-1-yl 5-acetyl-2-(benzyloxy)benzoate, 165c. White ppt., 39%, Mp: 134-136°C; IR (KBr): 3275, 3100-2800, 1745, 1670, 1598, 1581, 1496, 1467, 1448, 1382, 1276, 1238, 1199, 1163, 1056, 1028, 1007, 873, 821, 760, 692, 680 cm^{-1} ; ^1H NMR (400 MHz, CDCl_3) δ (ppm), 8.75, (d, $J = 2.36$, 1H), 8.22 (dd, $J = 8.79$, $J = 2.36$, 1H), 7.97 (d, $J = 8.66$, 1H), 7.91 (d, $J = 8.73$, 1H), 7.81 (d, $J = 8.53$, 1H), 7.54-7.49 (m, 4H), 7.41-7.34 (m, 5H), 7.23 (d, $J = 8.93$, 1H), 5.36 (s, 2H), 2.65 (s, 3H); ^{13}C NMR (125 MHz, CDCl_3) δ (ppm), 196.03, 164.30, 162.08, 146.86, 135.52, 134.72, 134.39, 134.15, 133.30, 130.03, 128.74, 128.59, 128.24, 127.99, 127.22, 126.48, 126.23, 125.46, 121.57, 119.77, 118.28, 113.37, 70.97, 26.48; HRMS ($\text{M} + \text{H}$): Calc'd for $\text{C}_{26}\text{H}_{20}\text{O}_4\text{Na}$: 419.1259. Found: 419.1268.

Naphthalen-1-yl 2-(benzyloxy)-5-(2-bromoacetyl)benzoate, 165d. Oil, ~88%; ¹H NMR (400 MHz, CDCl₃) δ (ppm), 8.77, (d, *J* = 2.36, 1H), 8.25 (dd, *J* = 8.79, *J* = 2.36, 1H), 8.01 (d, *J* = 8.66, 1H), 7.93 (d, *J* = 8.73, 1H), 7.82 (d *J* = 8.53, 1H), 7.56-7.50 (m, 4H), 7.41-7.34 (m, 5H), 7.27 (d, *J* = 8.93, 1H), 5.36 (s, 2H), 4.45 (s, 2H).

Naphthalen-1-yl-2-(benzyloxy)-5-(2-(4-(*tert*-butoxycarbonyl-amino)-butanoyloxy)acetyl)benzoate, 165e. This compound was manufactured by an associate and was not characterized prior to further reactivity.

Naphthalen-1-yl-5-(2-(4-(*tert*-butoxycarbonylamino)butanoyloxy)acetyl)-2-hydroxybenzoate, 165f. Yellow, adhesive ppt, 96%; IR (KBr): 3450, 3275, 3100-2800, 1745, 1670, 1598, 1581, 1496, 1467, 1448, 1382, 1276, 1238, 1199, 1163, 1056, 1028, 1007, 873, 821, 760, 692, 680 cm⁻¹; ¹H NMR (400 MHz, d⁶-DMSO) δ (ppm), 11.54 (s, 1H), 8.62, (d, *J* = 2.36, 1H), 8.14 (dd, *J* = 8.79, *J* = 2.36, 1H), 8.02 (m, 2H), 7.93 (d, *J* = 8.73, 1H), 7.62-7.58 (m, 3H), 7.49 (d, *J* = 8.10, 1H), 7.16 (d, *J* = 8.93, 1H), 6.89 (t, *J* = 5.90, 1H), 5.36 (s, 2H), 2.98 (t, *J* = 6.90, 2H), 2.43 (t, *J* = 7.70, 2H), 1.70 (m, 2H), 1.37 (s, 9H); ¹³C NMR (125 MHz, CDCl₃) δ (ppm), 190.50, 172.24, 165.18, 164.27, 155.60, 146.19, 134.52, 134.17, 132.18, 129.71, 128.48, 127.99, 126.85, 126.36, 125.75, 124.80, 121.22, 119.75, 118.70, 115.02, 77.45, 66.07, 39.47, 30.67, 28.22, 24.97; HRMS (M + Na): Calc'd for C₂₈H₂₉NO₈Na: 530.1791. Found: 530.1794.

4-(2-(4-hydroxy-3-((naphthalen-1-yloxy)carbonyl)phenyl)-2-oxoethoxy)-4-oxobutan-1-aminium 2,2,2-trifluoroacetate, 165. White ppt., 91%, Mp: 63-65°C; IR (KBr): 3450, 3275, 3100-2800, 1745, 1670, 1598, 1581, 1496, 1467, 1448, 1382,

1276, 1238, 1199, 1163, 1056, 1028, 1007, 873, 821, 760, 692, 680 cm^{-1} ; ^1H NMR (400 MHz, d^6 -DMSO) δ (ppm), 11.55, (s, 1H), 8.65, (d, $J = 2.36$, 1H), 8.17 (d, $J = 7.60$, 2H), 8.05 (d, $J = 8.20$, 1H), 7.95 (s, 3H), 7.84 (d, $J = 8.55$, 1H), 7.63 (m, 3H), 7.51 (d, $J = 8.10$, 1H), 7.27 (d, $J = 8.93$, 1H), 6.89 (t, $J = 5.90$, 1H), 5.56 (s, 2H), 2.90 (t, $J = 6.90$, 2H), 2.60 (t, $J = 7.70$, 2H), 1.88 (m, 2H); ^{13}C NMR (125 MHz, d^6 -DMSO) δ (ppm), 190.64, 171.75, 165.04, 163.52, 158.02, 157.54, 146.12, 134.63, 132.21, 129.73, 128.65, 127.67, 126.88, 125.76, 122.10, 121.15, 119.74, 118.59, 118.11, 116.03, 115.17, 66.32, 38.09, 30.11, 22.58; HRMS (M^+): Calc'd for $\text{C}_{23}\text{H}_{22}\text{NO}_6\text{Na}$: 408.1447. Found: 408.1447.

(R)-((R)-1-(4-(benzyloxy)phenyl)-1-oxopropan-2-yl)-2-acetoxy-2-phenylacetate + (R)-((S)-1-(4-(benzyloxy)phenyl)-1-oxopropan-2-yl)-2-acetoxy-2-phenylacetate

166a, 167a. A parallel process as described for the synthesis of **122e** was utilized. Viscous oil, 94%; IR (KBr): 3275, 3100-2800, 1745, 1697, 1658, 1602, 1523, 1413, 1348, 1271, 1195, 1165, 1051, 1026, 1007, 860, 823, 761 cm^{-1} ; ^1H NMR (400 MHz, d^6 -DMSO) δ (ppm), 7.96 (d, $J = 8.17$, 2H), 7.88 (d, $J = 8.95$, 2H), 7.48-7.35 (m, 20H), 7.11 (d, $J = 8.17$, 2H), 7.07 (d, $J = 8.20$, 2H), 6.07, (d, $J = 3.00$, 2H), 6.04 (d, $J = 2.90$, 2H), 5.22 (s, 2H), 5.21, (s, 2H), 2.13 (s, 3H), 2.10 (s, 3H), 1.39 (d, $J = 7.00$, 3H), 1.33 (d, $J = 6.75$, 3H); ^{13}C NMR (125 MHz, d^6 -DMSO) δ (ppm), 193.85, 193.83, 170.33, 169.79, 169.70, 167.77, 167.74, 162.69, 162.58, 161.99, 136.49, 136.34, 133.59, 133.11, 130.91, 130.81, 130.70, 130.05, 129.67, 129.26, 129.19, 128.71, 128.58, 128.50, 128.37, 128.11, 128.04, 127.97, 127.80, 127.78, 127.58, 127.43, 127.41, 126.43, 126.38, 115.08, 114.92, 114.84, 114.61, 73.82, 73.68, 72.43,

72.16, 69.54, 69.52, 20.74, 20.32, 16.95, 16.89; HRMS (M + Na): Calc'd for C₂₆H₂₄O₆Na: 455.1471. Found: 455.1474. (M + H): Calc'd for C₂₆H₂₅O₆: 433.1651. Found: 433.1670.

(R)-((R)-1-(4-hydroxyphenyl)-1-oxopropan-2-yl)-2-acetoxy-2-phenylacetate +
(R)-((S)-1-(4-hydroxyphenyl)-1-oxopropan-2-yl)-2-acetoxy-2-phenylacetate, 166,

167. A parallel process as described for the synthesis of **130e'** was utilized. Viscous oil, 99%; IR (KBr): 3455, 3100-2800, 1745, 1697, 1658, 1602, 1523, 1413, 1348, 1271, 1195, 1165, 1051, 1026, 1007, 860, 823, 761 cm⁻¹; ¹H NMR (400 MHz, d⁶-DMSO) δ (ppm), 10.53 (s, 2H), 7.84 (d, *J* = 8.17, 2H), 7.80 (d, *J* = 8.95, 2H), 7.53-7.42 (m, 10H), 6.85 (d, *J* = 8.17, 2H), 6.82 (d, *J* = 8.20, 2H), 6.07, (d, *J* = 3.00, 2H), 6.04 (d, *J* = 2.90, 2H), 2.12 (s, 3H), 2.10 (s, 3H), 1.38 (d, *J* = 7.00, 3H), 1.32 (d, *J* = 6.75, 3H); ¹³C NMR (125 MHz, d⁶-DMSO) δ (ppm), 193.49, 193.46, 169.78, 169.69, 167.76, 167.73, 162.68, 162.57, 133.64, 133.57, 131.07, 130.96, 130.28, 129.26, 129.19, 129.07, 128.88, 128.70, 128.62, 128.57, 128.13, 127.99, 127.83, 127.74, 124.88, 124.83, 115.62, 115.47, 114.91, 114.43, 74.83, 74.18, 72.34, 72.03, 20.38, 20.32, 17.08, 17.00; HRMS (M + Na): Calc'd for C₁₉H₁₈O₆Na: 365.1001. Found: 365.0996.

6-((R)-4-((3R,5R,8R,9S,10S,12S,13R,14S,17R)-3,12-dihydroxy-10,13-dimethylhexadecahydro-1H-cyclopenta[a]phenanthren-17-yl)pentan-amido)hexan-1-aminium, 168c. A solution of deoxycholic acid **168a**, (DOC, 503 mg, 1.28 mmol), N-hydroxybenzotriazole (HOBT, 173 mg, 1.28 mmol), and 1-ethyl-3-(3-dimethylaminopropyl) carbodiimide hydrochloride (EDCI, 368 mg, 1.92 mmol) in 10 ml of

DMF was stirred for 30 min to ensure complete dissolution. While stirring, *tert*-butyl 6-aminohexylcarbamate (277 mg, 1.28 mmol) in 5 ml DMF was slowly added over 5 minutes. The reaction proceeded for 22 h under ambient conditions. After this time, the solution was diluted with ethyl acetate and 100 ml of water was added. An extraction of the organic layer then was performed, followed by addition of anhydrous magnesium sulfate. After concentration, 15 ml of 4 M HCl in 1,4-dioxane was added. Stirring of this solution, under ambient conditions, occurred for 1 h. Excess solution was removed under reduced pressure for 2 days to afford **168c** as a white, adhesive precipitate, 456 mg (75%). IR (KBr): 3584, 3226, 2950, 2846, 1657, 1569, 1448, 1419, 1390, 1340, 1157, 1100, 1062, 1016; ¹H NMR (400 MHz, MeOD) δ 7.98 (s, 1H), 3.61 (m, 2H), 3.19 (t, 2H), 2.94 (t, 2H), 2.31 (m, 4H), 1.61-1.33 (m, 31H), 1.23 (s, 3H), 0.99 (s, 3H), 0.88 (s, 3H); ¹³C NMR (125 MHz, MeOD), δ 177.97, 74.17, 72.68, 48.83, 48.15, 47.72, 43.75, 40.89, 40.80, 37.61, 37.44, 37.34, 37.13, 36.57, 35.46, 34.98, 33.66, 32.08, 31.22, 30.96, 30.09, 30.01, 28.87, 28.63, 27.49, 27.15, 25.02, 23.86, 17.74, 13.33; HRMS (M⁺): Calc'd for C₃₀H₅₅N₂O₃: 491.4213. Found: 491.4209.

(R)-4-((3R,5R,8R,9S,10S,12S,13R,14S,17R)-3,12-dihydroxy-10,13-dimethylhexadecahydro-1H-cyclopenta[a]phenanthren-17-yl)-N-(6-(3-(3',6'-dihydroxy-3-oxo-3H-spiro[isobenzofuran-1,9'-xanthene]-5-yl)thioureido)hexyl)pentanamide, 168. A solution of **168c** (238 mg, 0.484 mmol) and fluorescein-4-isothiocyanate (FITC, 226 mg, 0.581 mmol) in 20 ml of MeOH was stirred for 30 min. While stirring at 0° C, triethylamine (TEA, 67 mL (0.484 mmol)) was added over a period of

5 minutes. The reaction proceeded under ambient conditions for 16 h. Inspissation under reduced pressure followed to yield a dark red/brown precipitate. Flash column chromatography (100% Ethyl acetate, then 1:1 Ethyl acetate/Acetone, then 1:1 Acetone/Methanol furnished 227 mg of **168** (53%) as a yellowish, waxy precipitate. IR (KBr): 3580, 3278, 2933, 2856, 1757, 1712, 1614, 1587, 1504, 1452, 1365, 1334, 1220, 1180, 1118, 1081, 871, 850, 786, 711, 673; ¹H NMR (400 MHz, MeOD) δ 8.22 (s, 1H), 7.76 (m, 2H), 7.16 (d, 1H), 6.68 (m, 3H), 6.55 (m, 3H), 3.61 (m, 2H), 3.19 (t, 2H), 2.94 (t, 2H), 2.31 (m, 4H), 1.61-1.33 (m, 31H), 1.23 (s, 3H), 0.99 (s, 3H), 0.88 (s, 3H); ¹³C NMR (125 MHz, MeOD), δ 182.84, 176.96, 171.68, 154.70, 142.76, 131.75, 130.66, 126.28, 126.11, 126.02, 120.22, 118.83, 114.35, 112.29, 112.04, 74.17, 72.68, 48.83, 48.15, 47.72, 43.75, 40.89, 40.80, 37.58, 37.34, 36.96, 36.58, 35.45, 34.96, 34.38, 33.60, 31.22, 30.49, 30.05, 30.00, 29.69, 28.88, 28.55, 27.75, 27.62, 25.03, 23.91, 17.83, 13.43, 9.38. HRMS (M + H): Calc'd for C₅₁H₆₅N₃O₈S: 880.4571. Found: 880.4578.

References

- ¹ Faworskii, J. *Russ. Chem. Soc.*, **26**, 559 (1894).
- ² Harmata, M.; Wacharasindhu, S. *Org. Lett.*, **2005**, *7*, 2563-2565.
- ³ Zhang, L.; Koreeda, M. *Org. Lett.*, **2002**, *4*, 3755-3758.
- ⁴ January 2008.
- ⁵ Bordwell, F.G.; Strong, J.G. *J. Org. Chem.*, **1973**, *38*(3), 579-585.
- ⁶ Hamblin, G.D.; Jimenez, R.P.; Sorensen, T.S. *J. Org. Chem.*, **2007**, *72*, 8033-8045.
- ⁷ Moliner, V.; Castillo, R.; Safont, V.S.; Oliva, M.; Bohn, S.; Tunon, I.; Andres, I. *J. Am. Chem. Soc.*, **1997**, *119*, 1941-1947.
- ⁸ Aston, E.A. *J. Am. Chem. Soc.*, **1940**, *62*, 2590.
- ⁹ Stevens, C.L.; Malik, W.; Pratt, W. *J. Am. Chem. Soc.*, **1950**, *72*, 4578.
- ¹⁰ Kende, A.S. *Organic Reactions*; 1960: Vol. 11, 261-316.
- ¹¹ Richard. *Compt. Rend.*, **1933**, *197*, 1943.
- ¹² McPhee, W.; Klingsberg, E. *J. Am. Chem. Soc.*, **1944**, *66*, 1132.
- ¹³ Loftfield, R.B. *J. Am. Chem. Soc.*, **1950**, *72*, 632.
- ¹⁴ Bordwell, F.G.; Frame, R.R.; Scamehorn, R.G.; Strong, J.G.; Meyerson, S. *J. Am. Chem. Soc.*, **1967**, *89*, 6704-6711.
- ¹⁵ Fohlisch, B.; Franz, T.; Kreiselmeier, G. *Eur. J. Org. Chem.*, **2005**, 4687-4698.
- ¹⁶ Castillo, R.; Andres, J.; Moliner, V. *J. Phys. Chem. A.*, **2001**, *105*, 2453-2460.
- ¹⁷ Schamp, N.; De Kimpe, N.; Coppens, W. *Tetrahedron*, **1975**, *31*, 2081-2087.
- ¹⁸ Stork, G., Borowitz, I.J. *J. Am. Chem. Soc.*, **1960**, *82*, 4307-4315.
- ¹⁹ Loftfield, R.B. *J. Am. Chem. Soc.*, **1951**, *73*, 4707.
- ²⁰ Burr, J.G.; Dewar, M.J.S. *J. Chem. Soc.*, **1951**, 1201.
- ²¹ Chenier, P.J. *J. Chem. Ed.*, **1978**, *55*, 286-291.
- ²² F.G. Bordwell is the Clare Hamilton Hall Professor Emeritus of the Department of Chemistry at Northwestern University.
- ²³ Bordwell, F.G.; Scamehorn, R.G. *J. Am. Chem. Soc.*, **1968**, *90*, 6751-6758.
- ²⁴ Bordwell, F.G.; Almy, J. *J. Org. Chem.*, **1973**, *38*, 575-579.
- ²⁵ Bordwell, F.G.; Carlson, M.W.; Knipe, A.C. *J. Am. Chem. Soc.*, **1969**, *91*, 3949-3950.
- ²⁶ Bordwell, F.G.; Carlson, M.W.; *J. Am. Chem. Soc.*, **1970**, *92*, 3370-3377.
- ²⁷ Bordwell, F.G.; Scamehorn, R.G.; Springer, W.R. *J. Am. Chem. Soc.*, **1969**, *91*, 2087-2093.
- ²⁸ Bordwell, F.G.; Scamehorn, R.G.; Knipe, A.C. *J. Am. Chem. Soc.*, **1970**, *92*, 2172-2173.
- ²⁹ Bordwell, F.G.; Scamehorn, R.G. *J. Am. Chem. Soc.*, **1971**, *93*, 3410-3415.
- ³⁰ Bordwell, F.G.; Strong, J.G. *J. Org. Chem.*, **1973**, *38*, 579-585.
- ³¹ Jones, J.R. *Trans. Faraday Soc.*, **1965**, *61*, 95.
- ³² Bell, R.P.; Lidwell, O.M. *Proc. Roy. Soc. (London)*, **1940**, *A176*, 88,
- ³³ Streitwieser, A. Jr. *Chem Rev.*, **1956**, *56*, 571.

-
- ³⁴ Lofftfield, R.B.; Schaad, L. *J. Am. Chem. Soc.*, **1954**, *76*, 35.
- ³⁵ Skrobek, A.; Tchoubar, B. *C.R. Acad. Sci., Paris*, **1966**, *80*, 263.
- ³⁶ Ingold, C.K. "Structure and Mechanism in Organic Chemistry," Cornell University Press, Ithaca, N.Y., **1953**, p365.
- ³⁷ Grunwald, E.; Winstein, S. *J. Am. Chem. Soc.*, **1948**, *70*, 846.
- ³⁸ Brown, H.C.; Okamoto, Y. *J. Am. Chem. Soc.*, **1958**, *80*, 4979.
- ³⁹ Bordwell, F.G.; Williams, J.M. *J. Am. Chem. Soc.*, **1968**, *90*, 435.
- ⁴⁰ Smith, A.C.B.; Wilson, W. *J. Chem. Soc.* **1955**, 1342.
- ⁴¹ Hoffmann, R. *J. Am. Chem. Soc.*, **1968**, *90*, 1475.
- ⁴² Bodor, N.; Dewar, M.J.S.; Harget, A. *J. Am. Chem. Soc.*, **1970**, *92*, 3854.
- ⁴³ Liberles, A.; Greenberg, A.; Lest, A. *J. Am. Chem. Soc.*; **1972**, *94*, 8685-8688.
- ⁴⁴ House, H.O.; Gilmore, W.F. *J. Am. Chem. Soc.*, **1961**, *83*, 3980-3985.
- ⁴⁵ Moliner, V.; Castillo, R.; Safont, V.S.; Oliva, M.; Bohn, S.; Tunon, I.; Andres, J. *J. Am. Chem. Soc.*, **1997**, *119*, 1941-1947.
- ⁴⁶ Smissman, E.E.; Hite, G. *J. Am. Chem. Soc.*, **1959**, *81*, 1201-1203.
- ⁴⁷ Wenkert, E.; Bakuzis, P.; Baumgarten, R.J.; Leicht, C.L.; Schenk, H.P. *J. Am. Chem. Soc.*, **1971**, *93*, 3208-3216.
- ⁴⁸ Strachan, A.N.; Blacet, F.E. *J. Am. Chem. Soc.*, **1955**, *77*, 5254-5257.
- ⁴⁹ Modern Molecular Photochemistry, ed. Turro, N.J., Benjamin/Cummings, Reading, 1978.
- ⁵⁰ Anderson, J.C.; Reese, C.B. *Tetrahedron*, **1962**, *1*, 1-4.
- ⁵¹ Sheehan, J.C.; Umezawa, K. *J. Org. Chem.*, **1973**, *38*, 3771-3774.
- ⁵² Sonawane, H.R.; Bellur, N.S.; Kulkarni, D.G.; Ayyangar, N.R. *Tetrahedron*, **1994**, *50*, 1243.
- ⁵³ Sonowane, H.R.; Bellur, N.S.; Nazeruddin, G.M. *Tetrahedron*, **1995**, *51*, 11281-11294.
- ⁵⁴ Givens, R.S.; Oettle, W.F. *Chem. Comm.*, **1969**, 1164.
- ⁵⁵ Givens, R.S.; Streckowski, L. *J. Am. Chem. Soc.*, **1975**, *97*, 5867-5873.
- ⁵⁶ Kropp, P.J.; Jones, T.H.; Poindexter, G.S. *J. Am. Chem. Soc.*, **1973**, *95*, 5420.
- ⁵⁷ Walling, C.; Walts, H.P.; Milovanovic, J.; Papplannou, C.G. *J. Am. Chem. Soc.*, **1970**, *92*, 4927.
- ⁵⁸ Sheehan, J.C.; Wilson, R.M. *J. Am. Chem. Soc.*, **1964**, *86*, 5277.
- ⁵⁹ Givens, R.S.; Matuszewski, B. *J. Am. Chem. Soc.*, **1984**, *106*, 6860-6861.
- ⁶⁰ Givens, R.S.; Athey, P.S.; Kueper, L.W. III.; Matuszewski, B.; Xue, J-Y. *J. Am. Chem. Soc.*, **1992**, *114*, 8708-8710.
- ⁶¹ Creary, X.; Geiger, C.C. *J. Am. Chem. Soc.*, **1982**, *104*, 4151.
- ⁶² Givens, R.S.; Athey, P.S.; Kueper, L.W. III.; Matuszewski, B.; Xue, J-Y.; Fister, T. *J. Am. Chem. Soc.*, **1993**, *115*, 6001-6010.
- ⁶³ Givens, R.S.; Park, C.H. *Tett. Lett.*, **1996**, *37*, 6259-6262.
- ⁶⁴ Givens, R.S.; Park, C.H. *J. Am. Chem. Soc.*, **1997**, *119*, 2453-2463.
- ⁶⁵ Hilborn, J.W.; MacKnight, E.; Pincock, J.A.; Wedge, P.J. *J. Am. Chem. Soc.*, **1994**, *116*, 3337-3346.
- ⁶⁶ Lipson, M.; Deniz, A.A.; Peters, K.S. *J. Am. Chem. Soc.*, **1996**, *118*, 2992-2997.

-
- ⁶⁷ Givens, R.S.; Jung, A.; Park, C.H.; Weber, J.; Bartlett, W. *J. Am. Chem. Soc.*, **1997**, *119*, 8369-8370.
- ⁶⁸ Givens, R.S.; Weber, J.F.; Conrad, P.G. III.; Orosz, G.; Donahue, S.L.; Thayer, S.A. *J. Am. Chem. Soc.*, **2000**, *122*, 2687-2697
- ⁶⁹ Banerjee, A.; Falvey, D.E. *J. Am. Chem. Soc.*, **1998**, *120*, 2965-2966.
- ⁷⁰ DeCosta, D.P.; Pincock, J.A. *J. Am. Chem. Soc.*, **1989**, *111*, 8948.
- ⁷¹ Lutz, H.; Breheret, E.; Lindqvist, L. *J. Phys. Chem.*, **1973**, *77*, 1758.
- ⁷² Demeter, A.; Berces, T. *Photochem. Photobiol., A*. **1989**, *46*, 27.
- ⁷³ Zhang, K.; Corrie, J.T.; Munasinghe, V.R.N.; Wan, P. *J. Am. Chem. Soc.*, **1999**, *121*, 5625-5632.
- ⁷⁴ Ireland, J.F.; Wyatt, P.A.H. *Adv. Phys. Org. Chem.*, **1976**, *12*, 131.
- ⁷⁵ Mukaihata, H.; Nakagawa, T.; Kohtani, S.; Itoh, M. *J. Am. Chem. Soc.*, **1994**, *116*, 10612.
- ⁷⁶ Leary, G. *J. Chem. Soc., Perkin Trans. 2*, **1972**, 640.
- ⁷⁷ Fischer, M.; Wan, P. *J. Am. Chem. Soc.*, **1998**, *120*, 2680.
- ⁷⁸ Conrad, P.G. III; Givens, R.S.; Hellrung, B.; Rajesh, C.S.; Ramseier, M.; Wirz, J. *J. Am. Chem. Soc.*, **2000**, *122*, 9346-9347.
- ⁷⁹ Kearns, D.R.; Case, W.A. *J. Am. Chem. Soc.*, **1966**, *88*, 5087-5097.
- ⁸⁰ Ma, C.; Zuo, P.; Kwok, W.M.; Chan, W.S.; Kan, J.T.W.; Toy, P.H.; Phillips, D.L. *J. Org. Chem.*, **2004**, *69*, 6641-6657.
- ⁸¹ Ma, C.; Chan, W.S.; Kwok, W.M.; Zuo, P.; Phillips, D.L. *J. Phys. Chem. B*, **2004**, *108*, 9264-9276.
- ⁸² Ma, C.; Kwok, W.M.; Chan, W.S.; Zuo, P.; Kan, J.T.W.; Toy, P.H.; Phillips, D.L. *J. Am. Chem. Soc.*, **2005**, *127*, 1463-1472.
- ⁸³ Case, W.A.; Kearns, D.R. *J. Chem. Phys.*, **1970**, *52*, 2175-2191.
- ⁸⁴ Wagner, P.J.; Kempenninen, A.E.; Schott, H.N. *J. Am. Chem. Soc.*, **1973**, *95*, 5604-5614.
- ⁸⁵ Ohmori, N.; Suzuki, T.; Ito, M. *J. Phys. Chem.*, **1988**, *92*, 1086-1093.
- ⁸⁶ Zuo, P.; Ma, C.; Kwok, W.M.; Chan, W.S.; Phillips, D.L. *J. Org. Chem.*, **2005**, *70*, 8661-8675.
- ⁸⁷ Chan, W.S.; Ma, C.; Kwok, W.M.; Phillips, D.L. *J. Phys. Chem. A*, **2005**, *109*, 3454-3469.
- ⁸⁸ Ma, C.; Kwok, W.M.; Chan, W.S.; Du, Y.; Kan, J.T.W.; Toy, P.H.; Phillips, D.L. *J. Am. Chem. Soc.*, **2006**, *128*, 2558-2570.
- ⁸⁹ Creary, X.; Geiger, C.C. *J. Am. Chem. Soc.*, **1982**, *104*, 4151-4162.
- ⁹⁰ Chen, X.; Ma, C.; Kwok, W.M.; Guan, X.; Du, Y.; Phillips, D.L. *J. Phys. Chem. A*, **2006**, *110*, 12406-12413.
- ⁹¹ Chen, X.; Ma, C.; Kwok, W.M.; Guan, X.; Du, Y.; Phillips, D.L. *J. Phys. Chem. B*, **2007**, *111*, 11832-11842.
- ⁹² Givens, R.S.; Heger, D.; Hellrung, B.; Kamdzhilov, Y.; Mac, M.; Conrad, P.G. II.; Cope, E.; Lee, J.I.; Mata-Segreda, J.F.; Schowen, R.L.; Wirz, J. *J. Am. Chem. Soc.*, **2008**, *130*, 3307-3309.

-
- ⁹³ Radziszewski, J.G.; Gil, M.; Gorski, A.; Spanget-Larsen, J.; Waluk, J.; Mroz, B.J. *J. Phys. Chem.* **2001**, *115*, 9733-9738.
- ⁹⁴ Gisin, M.; Wirz, J. *Helv. Chim. Acta* **1983**, *66*, 1556-1568.
- ⁹⁵ Chiang, Y.; Kresge, A.J.; Zhu, Y. *J. Am. Chem. Soc.*, **2002**, *124*, 6349-6356.
- ⁹⁶ Hegazi, M.; Mata-Segreda, J.F.; Schowen, R.L. *J. Org. Chem.*, **1980**, *45*, 307-310.
- ⁹⁷ Conrad, P.G. II; Givens, R.S.; Weber, J.; Kandler, K. *Org. Lett.*, **2000**, *2*, 1545-1547.
- ⁹⁸ Alen, J.; Dobrzanska, L.; De Borggraeve, W.M.; Compennolle, F. *J. Am. Chem. Soc.*, **2007**, *72*, 1055-1057.
- ⁹⁹ Gensini, M.; de Meijere, A. *Chem. Eur. J.*, **2004**, *10*, 785-790.
- ¹⁰⁰ Norris, J.L.; Hangauer, M.J.; Porter, N.A.; Caprioli, R.M. *J. Mass. Spectrom.*, **2005**, *40*, 1319-1326.
- ¹⁰¹ Ge, M.; Cline, E.; Yang, L. *Tetrahedron Letters*, **2006**, *47*, 5797-5799.
- ¹⁰² Balzani, V.; Bolletta, F.; Scandola, F. *J. Am. Chem. Soc.*, **1980**, *102*, 2152-2163.
- ¹⁰³ Winstein, S.; Clippinger, E.; Fainberg, A.H.; Heck, R.; Robinson, G.C. *J. Am. Chem. Soc.*, **1956**, *78*, 328-335.
- ¹⁰⁴ Goeldner, M.G.; Givens, R.S. *Dynamic studies in Biology, Phototriggers, Photoswitches, and Caged Compounds*, Wiley-VCH, Weinheim, 2005.
- ¹⁰⁵ Ghose, A.K.; Viswanadhan, V. N.; Wendoloski, J.J. *J. Phys. Chem. A.*, **1998**, *102*, 3762-3772.
- ¹⁰⁶ Leo, A., Weininger, D. CLogP version 3.4, Pomona Medicinal Chemistry Project, Pomona College, Claremont, CA, 1988.
- ¹⁰⁷ SYBYL 7.3, The Tripos Associates, St. Louis, MO, 2007.
- ¹⁰⁸ Dr. Gerry Lushington, University of Kansas
- ¹⁰⁹ IUPAC definition, 1994
- ¹¹⁰ Prof. J. Wirz; Dr. D. Heger; Dr. P. Sebej.
- ¹¹¹ Yousef, A. Dissertation 2005.
- ¹¹² Tsushima, M.; Tokuda, K.; Ohsaka, T. *Anal. Chem.*, **1994**, *66*, 4551-4556.
- ¹¹³ Conrad, P.G. II. Dissertation, 2001.
- ¹¹⁴ Pincock, J.A. *Acc. Chem. Res.*, **1997**, *30*, 43-49.
- ¹¹⁵ Turro, Nicholas J. *Modern Molecular Photochemistry*. University Science Books, New York, 1991.
- ¹¹⁶ Provided in the Chem Draw® 3D software package
- ¹¹⁷ Wagner, P.J. *Acc. Chem. Res.*, **1971**, *4*, 168-177.
- ¹¹⁸ Gillard, R.E.; Stoddart, J.F.; White, A.J.P.; Williams, B.J.; Williams, D.J. *J. Org. Chem.*, **1996**, *61*, 4504-4505.
- ¹¹⁹ Cope, Elizabeth. Dissertation 2008
- ¹²⁰ Anslyn, E.V.; Dougherty, D.A. *Modern Physical Organic Chemistry*. University Science Books: Sausalito 2006.
- ¹²¹ Dr. Chicheng Ma, unpublished results
- ¹²² Professor Emeritus, Department of Chemistry, UCLA.

-
- ¹²³ Winstein, S.; Klinedinst, P.E.; Robinson, G.C. Jr. *J. Am. Chem. Soc.*, **1961**, *83*, 885-895.
- ¹²⁴ Winstein, S.; Robinson, G.C. *J. Am. Chem. Soc.*, **1958**, *80*, 169-181.
- ¹²⁵ Winstein, S.; Klinedinst, P.E. Jr.; Clippinger, E. *J. Am. Chem. Soc.*, **1961**, *83*, 4986-4989.
- ¹²⁶ Allen, A.D.; Tidwell, T.T.; Tee, O.S. *J. Am. Chem. Soc.*, **1993**, *115*, 10091-10096.
- ¹²⁷ Stensrud, K.; Givens, R.S.; Noh, J.; Kandler, K. Manuscript in Progress.
- ¹²⁸ Kim, G.; Kandler, K. *Nature Neuroscience*, **2003**, *6*, 282-290.
- ¹²⁹ Prof's Wendy and Bill Picking, Molecular Biosciences, University of Kansas.
- ¹³⁰ Stensrud, K.; Adam, P.; La Mar, C.; Sudharsan, R.; Lushington, G.H.; Shelton, N.; Olive, A.H.; Givens, R.S.; Picking, W.L.; Picking, W.D. *J. Biol. Chem.*, **2008**, submitted.
- ¹³¹ Chan Ho Park, Dissertation 1996.
- ¹³² Desilets, D.J.; Kissinger, P.T.; Lytle, F.E., *Anal. Chem.*, **1987**, *59*, 1244-1246.
- ¹³³ SYBYL 7.2, The Tripos Associates, St. Louis, MO, 2007.
- ¹³⁴ Clark, M.; Cramer, R.D.; Van Opdenbosch, N. *J. Comput. Chem.*, **1989**, *10*, 982-1012.
- ¹³⁵ M. J. Frisch, G.W. Trucks, H.B. Schlegel, G.E. Scuseria, M.A. Robb, J.R. Cheeseman, J.A. Montgomery Jr., T. Vreven, K.N. Kudin, J.C. Burant, J.M. Millam, S.S. Iyengar, J. Tomasi, V. Barone, B. Menucci, M.Cossi, G. Scalamani, N. Rega, G.A. Peterson, H. Nakatsuji, M. Hada, M. Ehara, K. Toyota, R. Fukuda, H. Hasegawa, M. Ishida, T. Nakajima, Y. Honda, O. Kitao, H. Nakai, M. Kleine, X. Li, J.E. Knox, H.P. Hratchian, J.B. Cross, V. Bakken, C. Adamo, J. Jaramillo, R. Gomperts, R.E. Stratmann, O. Yazyev, A.J. Austin, R. Cammi, C. Pomelli, J.W. Ochterski, P.Y. Ayala, K. Morokuma, G.A. Voth, P. Salvador, J.J. Dannenberg, V.G. Zakrzewski, S. Dapprich, A.D. Daniels, M.C. Strain, O. Farkas, D.K. Malick, A.D. Rabuck, K. Raghavachari, J.B. Foresman, J.V. Ortiz, Q. Cui, A.G. Baboul, S. Clifford, J. Cioslowski, B.B. Stefanov, G. Liu, A. Liashenko, P. Piskorz, I. Komaromi, R.L. Martin, D.J. Fox, T. Keith, M.A. Al-Laham, C.Y. Peng, A. Nanayakkara, M. Challacombe, P.M.W. Gill, B. Johnson, W. Chen, M.W. Wong, C. Gonzalez, J.A. Pople, Gaussian 03, Revision C.02. Gaussian Inc., Wallingford, CT, 2004.
- ¹³⁶ Becke, A.D.; *J. Chem. Phys.*, **1993**, *98*, 5648-5652.
- ¹³⁷ Ditchfield, R.; Hehre, W.J.; Pople, J.A. *J. Chem. Phys.* **1971**, *54*, 724-728.
- ¹³⁸ Pople, J.A.; Seeger, R.; Krishan, R. *Int. J. Quant. Chem. Symp.* **1977**, *11*, 149-163.
- ¹³⁹ Hawker, C.J.; Lee, R.; Frechet, J.M. *J. Am. Chem. Soc.*, **1991**, *113*, 4583-4588.
- ¹⁴⁰ Machin, P.J.; Hurst, D.N.; Bradshaw, R.M.; Blaber, L.C.; Burden, D.T.; Fryer, A.D.; Melarange, R.A.; Shivdasani, C. *J. Med. Chem.*, **1983**, *26*, 1570-1576.
- ¹⁴¹ Kosugi, M.; Sumiya, T.; Obara, Y.; Suzuki, M.; Sano, H.; Migita, T. *Bull. Chem. Soc. Jpn.*, **1987**, *60*, 767-768.
- ¹⁴² Paul, S.; Gupta, V.; Gupta, R.; Loupy, A. *Tetrahedron Lett.* **2003**, *44*, 439-442.
- ¹⁴³ Hiyama, T.; Fujita, M. *J. Org. Chem.*, **1988**, *53*, 5405-5415.

-
- ¹⁴⁴ Marsh, J.P.; Goodman, L. *J. Org. Chem.*, **1965**, *30*, 2491-2492.
- ¹⁴⁵ Combi-Blocks, LLC. 7949 Silverton Avenue, Suite 915, San Diego, CA, 92126 USA.
- ¹⁴⁶ Guizzunti, G.; Brady, T.P.; Malhotra, V.; Theodorakis, E.A. *J. Am. Chem. Soc.*, **2006**, *128*, 4190-4191.
- ¹⁴⁷ Alen, J.; Dobrzanska, L.; De Borggraeve, W.M.; Compennolle, F. *J. Org. Chem.*, **2007**, *72*, 1055-1057.
- ¹⁴⁸ Chambers, D.J.; Evans, G.R.; Fairbanks, A.J. *Tetrahedron: Asymmetry*, **2005**, *16*, 45-55.